

1. Report No. FHWA/TX-09/0-5505-1		2. Government Accession No.		3. Recipient's Catalog No.	
4. Title and Subtitle SIMPLIFIED METHOD FOR ESTIMATING SCOUR AT BRIDGES				5. Report Date February 2009 Published: August 2009	
				6. Performing Organization Code	
7. Author(s) Jean-Louis Briaud, Anand V. Govindasamy, Dongkyun Kim, Paolo Gardoni, Francisco Olivera, Hamn-Ching Chen, Christopher Mathewson, and Kenneth Elsbury				8. Performing Organization Report No. Report 0-5505-1	
9. Performing Organization Name and Address Texas Transportation Institute The Texas A&M University System College Station, Texas 77843-3135				10. Work Unit No. (TRAIS)	
				11. Contract or Grant No. Project 0-5505	
12. Sponsoring Agency Name and Address Texas Department of Transportation Research and Technology Implementation Office P.O. Box 5080 Austin, Texas 78763-5080				13. Type of Report and Period Covered Technical Report: September 2005-August 2008	
				14. Sponsoring Agency Code	
15. Supplementary Notes Project performed in cooperation with the Texas Department of Transportation and the Federal Highway Administration. Project Title: Simplified Method for Estimating Scour URL: http://tti.tamu.edu/documents/0-5505-1.pdf					
16. Abstract This research proposes a new method to assess a bridge for scour. It is made up of three levels of assessments. The first level is termed Bridge Scour Assessment 1 (BSA 1). The second and third levels are termed BSA 2 and BSA 3, respectively. BSA 1 overcomes the qualitative nature of current initial evaluation procedures by extrapolating present scour measurements to obtain the scour depth corresponding to a specified future flood event. It utilizes computer-generated extrapolation charts based on a large combination of hypothetical bridges, which relate the future scour depth/maximum observed scour depth ratio to the future flood velocity/maximum observed flood velocity ratio. BSA 2 has to be carried out if BSA 1 does not conclude with a specific plan of action for the bridge. BSA 2 determines the maximum scour depth. Though conservative, BSA 2 was introduced due to its simplicity. BSA 3 has to be carried out if BSA 2 does not conclude with a specific plan of action. BSA 3 involves the calculation of time-dependent scour depth rather than simply using the maximum scour depth. BSA 3 is valuable in the case of highly erosion-resistant materials that do not achieve the maximum scour depth within the lifetime of a bridge. Both BSA 2 and BSA 3 utilize erosion classification charts that replace site-specific erosion testing for preliminary evaluations. The scour vulnerability depends on the comparison of the predicted scour depth and the allowable scour depth of the foundation. Hydrologic and hydraulic computer programs were developed to obtain the flow parameters. These programs generate maps of the maximum previous flood recurrence interval experienced by a specified bridge in Texas and converts flow into flow velocities. The 11 case histories used as validation showed good agreement between predicted and measured values. BSA 1 was then applied to 16 bridges. In this process, 6 out of 10 scour-critical bridges were found to be stable in terms of scour. The proposed bridge scour assessment procedure allows for the economical and relatively simple evaluation of scour-critical bridges. It also overcomes the over-conservatism in current methods.					
17. Key Words Scour, Bridges, Bridge Scour Assessment, Erodibility, Scour-Critical Bridges, Flood, Recurrence Interval			18. Distribution Statement No restrictions. This document is available to the public through NTIS: National Technical Information Service Springfield, Virginia 22161 http://www.ntis.gov		
19. Security Classif.(of this report) Unclassified		20. Security Classif.(of this page) Unclassified		21. No. of Pages 482	22. Price

SIMPLIFIED METHOD FOR ESTIMATING SCOUR AT BRIDGES

by

Jean-Louis Briaud
Research Engineer, Texas A&M University

Anand V. Govindasamy and Dongkyun Kim
Graduate Students, Texas A&M University

Paolo Gardoni
Assistant Professor, Texas A&M University

Francisco Olivera
Associate Professor, Texas A&M University

Hamn-Ching Chen and Christopher Mathewson
Professors, Texas A&M University

and

Kenneth Elsbury
Graduate Student, Texas A&M University

Report 0-5505-1

Project 0-5505

Project Title: Simplified Method for Estimating Scour

Performed in cooperation with the
Texas Department of Transportation
and the
Federal Highway Administration

February 2009

Published: August 2009

TEXAS TRANSPORTATION INSTITUTE
The Texas A&M University System
College Station, Texas 77843-3135

DISCLAIMER

The contents of this report reflect the views of the authors, who are responsible for the facts and the accuracy of the data presented herein. The contents do not necessarily reflect the official view or policies of the Federal Highway Administration (FHWA) or the Texas Department of Transportation (TxDOT). This report does not constitute a standard, specification, or regulation. This report is not intended for construction, bidding, or permit purposes. The engineer in charge of the project was Jean-Louis Briaud PE #48690.

ACKNOWLEDGMENTS

This project was conducted in cooperation with TxDOT and FHWA. The authors thank the Project Director John G. Delphia and the members of TxDOT's Project Monitoring Committee George R. Herrmann and Mark McClelland. The result of this project is truly a team effort and John G. Delphia, George R. Herrmann, and Mark McClelland did much more than monitor the project. Their contribution was extremely valuable to the research team. We also wish to thank all the district engineers who sent us information on the bridges; Keyvon Jahedkar in the Bryan District was particularly helpful.

TABLE OF CONTENTS

	Page
List of Figures	xii
List of Tables	xix
Executive Summary	1
Background.....	1
Approach Taken to Solve the Problem.....	1
Outcome of the Study	2
Significance of the Study.....	3
1. Introduction	5
1.1. Bridge Scour	5
1.2. Geomaterials: A Definition.....	5
1.3. Erodibility of Geomaterials.....	8
1.4. The Problem Addressed.....	8
1.5. Why This Problem Was Addressed	9
1.6. Approach Selected to Solve the Problem.....	11
1.7. Validation of the Proposed Assessment Method	11
1.8. Application to Scour-Critical Bridges	12
2. Background	13
2.1. Introduction.....	13
2.2. Current Assessment Methods In Practice	14
2.2.1. FHWA Guidelines for Evaluating Scour at Bridges.....	14
2.2.2. Bridge Scour Evaluation Practice in Texas	15
2.2.3. Tennessee Level 1 Assessment.....	22
2.2.4. The Idaho Plan of Action for Scour-Critical Bridges	25
2.2.5. USGS Method for Rapid Estimation of Scour Based on Limited Site Data.....	25

2.2.6. Other Bridge Scour Assessment Procedures.....	28
2.2.7. Limitations of Current Assessment Methods.....	33
2.2.8. The SRICOS-EFA Method for Bridge Piers	35
2.2.9. The SRICOS-EFA Method for Bridge Contractions	36
2.2.10. The SRICOS-EFA Method for Bridge Abutments.....	39
2.2.11. Concept of Equivalent Time	39
2.3. The HEC-18 Abutment Scour Equations.....	43
2.3.1. Froehlich’s Live-Bed Abutment Scour Equation	43
2.3.2. The HIRE Live-Bed Abutment Scour Equation	45
3. Erodibility Charts	47
3.1. Introduction.....	47
3.2. Factors Influencing Erosion Resistance.....	48
3.3. Critical Shear Stress–Critical Velocity Relationship.....	50
3.4. The Erosion Function Charts	52
3.4.1. Overview.....	52
3.4.2. Relationship between Selected Geomaterials and the Erosion Function Charts	55
3.5. The Erosion Threshold Charts	68
3.5.1. Overview.....	68
3.5.2. The Use of a Riprap Design Equation for Scour in Fractured Rock.....	69
3.5.3. The Erosion Threshold–Mean Grain Size Chart.....	69
4. Hydrology	75
4.1. Introduction.....	75
4.2. Types of Bridge-Gage Relationships	76
4.2.1. Bridge-Gage Relationship Type I: Bridge with Flow Gage	76
4.2.2. Bridge-Gage Relationship Type II—Bridge with Gages Nearby, Either Upstream or Downstream	77
4.2.3. Bridge-Gage Relationship Type III—Bridge with a Gage at a Nearby and Hydrologically Similar Watershed	78

4.2.4. Bridge-Gage Relationship Type IV—Bridges with No Flow Gage at All	79
4.3. Obtaining Hydraulic Information from Bridge-Gage Relationships	79
4.3.1. Obtaining Hydraulic Information for BSA 1	79
4.3.2. Obtaining Hydraulic Information for BSA 2 and BSA 3.....	80
4.4. Special Case of Bridge-Gage Relationship Type IV	80
4.4.1. Approach 1: Rainfall-Flow Correlation Approach	80
4.4.2. Approach 2: Recurrence Interval Mapping Approach.....	101
4.5. Flood Frequency Analysis	118
4.5.1. Types of Flood Frequency Analysis	118
4.5.2. Probability Distributions.....	119
4.5.3. Parameter Estimation	120
4.5.4. Types of Distributions and Parameter Estimation Methods	121
4.5.5. Application of the Methods to the Texas Data and Results.....	126
4.5.6. Discussion of Flood Frequency Analysis	145
4.6. USGS Regional Regression Equation.....	147
4.7. Step-by-Step Procedure	149
5. Bridge Scour Assessment 1	153
5.1. Introduction.....	153
5.2. The Z-Future Charts.....	155
5.2.1. Case 1: $V_{\text{fut}} > V_{\text{mo}}$	165
5.2.2. Case 2: $V_{\text{fut}} < V_{\text{mo}}$	165
5.3. The BSA 1 Flowchart	166
5.3.1. The BSA 1 (Uniform Deposit) Flowchart and Procedure	166
5.3.2. The BSA 1 (Multilayer Analysis) Flowchart and Procedure.....	169
5.4. Step-by-Step Procedure for BSA 1	177
5.5. BSA 1 (Uniform Deposit) Example.....	181

6. Bridge Scour Assessment 2	187
6.1. Introduction.....	187
6.2. The BSA 2 Flowchart and Procedure	187
6.3. Step-by-Step Procedure for BSA 2.....	190
6.4. Example of BSA 2 Analysis	192
7. Bridge Scour Assessment 3	197
7.1. Introduction.....	197
7.2. The BSA 3 Flowchart and Procedure	197
7.3. Step-by-Step Procedure for BSA 3.....	199
7.4. Example of BSA 3 Analysis	202
8. Case Histories and Validation.....	207
8.1. Introduction.....	207
8.2. Criteria for Selection.....	207
8.3. The Bridges Selected as Case Histories.....	208
8.3.1. Overview and Location.....	208
8.3.2. Case-by-Case Description of Bridges.....	209
8.4. Validation of the Simplified Method	212
8.4.1. Validation of BSA 1.....	212
8.4.2. Validation of BSA 2.....	215
8.4.3. Validation of BSA 3.....	216
8.5. Schoharie Creek Revisited.....	217
9. Application to Scour-Critical Bridges.....	227
9.1. Introduction.....	227
9.1.1. Case-by-Case Description of Bridges.....	227
9.1.2. Results of Application.....	233

10. Conclusions.....	241
10.1. General.....	241
10.2. Erodibility of Geomaterials	241
10.3. Bridge Scour Assessment 1	242
10.4. Bridge Scour Assessment 2	242
10.5. Bridge Scour Assessment 3	243
10.6. Hydraulic Parameter for BSA 1 from Hydrologic Analysis.....	244
10.7. Hydraulic Parameters for BSA 2 and BSA 3 from Hydrologic Analysis.....	245
10.8. Validation of the Proposed Assessment Method	245
10.9. Application to Scour-Critical Bridges	246
10.10. Recommendations.....	246
11. References.....	247
Appendix A: Data on Z-Future Charts.....	253
Appendix B: BSA 1 (Multilayer Analysis) Calculation Flowchart	271
Appendix C: Data on Case Histories.....	275
Appendix D: Data on EFA Curves	305
Appendix E: TAMU-FLOW User’s Manual.....	391
Appendix F: TAMU-FLOOD User’s Manual	419

LIST OF FIGURES

	Page
Figure 1-1. General Illustration of How a Bridge Affects River Flow.....	6
Figure 1-2. The Three Components of Scour (after Briaud et al. 2005).....	7
Figure 1-3. The Location of Scour-Critical Bridges in Texas.	10
Figure 2-1. Map Showing the 25 Districts of Texas (after Haas et al. 1999).	18
Figure 2-2. The SVEAR Screening Process Flow Chart (after Haas et al. 1999).	19
Figure 2-3. Secondary Screening Flowchart (after Texas Department of Transportation 1993)..	21
Figure 2-4. Comparison of Contraction Scour Depth by the Rapid Estimation Method and by Level 2 Method (after Holnbeck and Parrett 1997).	27
Figure 2-5. Comparison of Pier Scour Depth by the Rapid Estimation Method and by Level 2 Method (Holnbeck and Parrett 1997).	27
Figure 2-6. Comparison of Abutment Scour Depth by the Rapid Estimation Method and by Level 2 Method (Holnbeck and Parrett 1997).	28
Figure 2-7. General Conditions Scour Vulnerability Ranking Flowchart (after Colorado Highway Department 1990).....	29
Figure 2-8. Abutment Scour Vulnerability Ranking Flowchart (after Colorado Highway Department 1990).	30
Figure 2-9. Pier Scour Vulnerability Ranking Flowchart (after Colorado Highway Department 1990).	31
Figure 2-10. Comparison between HEC-18 and the SRICOS Method.	34
Figure 2-11. Initial Erosion Rate.	36
Figure 2-12. Contracted and Uncontracted Widths (after Briaud et al. 2005).....	39
Figure 2-13. Comparison of Pier Scour Depth Using Extended SRICOS and Simple SRICOS Methods (after Briaud et al. 2001b).....	41
Figure 2-14. Comparison of Contraction Scour Depth Using SRICOS-EFA and Simple SRICOS-EFA Methods (after Wang 2004).	42
Figure 2-15. Some Abutment Scour Parameters.....	44
Figure 2-16. Abutment Shapes (after Richardson and Davis 2001).	44

Figure 3-1. Failed Attempts at Correlating the Critical Shear Stress and Initial Slope with Water Content (Cao et al. 2002).	49
Figure 3-2. Failed Attempts at Correlating the Critical Shear Stress and Initial Slope with Undrained Shear Strength (Cao et al. 2002).	50
Figure 3-3. Critical Shear Stress–Critical Velocity Relationship.	51
Figure 3-4. Erosion Categories Based on Velocity.....	53
Figure 3-5. Erosion Categories Based on Shear Stress.....	54
Figure 3-6. EFA Test Data on Low Plasticity Clays Plotted on the Erosion Function Charts.	56
Figure 3-7. EFA Test Data on High Plasticity Clays Plotted on the Erosion Function Charts.	57
Figure 3-8. EFA Test Data on Low Plasticity Silts Plotted on the Erosion Function Charts.	58
Figure 3-9. EFA Test Data on High Plasticity Silt Plotted on the Erosion Function Charts.	59
Figure 3-10. EFA Test Data on Samples Intermediate between Low Plasticity Clay and Low Plasticity Silt Plotted on the Erosion Function Charts.	60
Figure 3-11. EFA Test Data on Clayey Sands Plotted on the Erosion Function Charts.	61
Figure 3-12. EFA Test Data on Samples Intermediate between Silty Sand and Clayey Sand Plotted on the Erosion Function Charts.	62
Figure 3-13. EFA Test Data on Poorly Graded Sands Plotted on the Erosion Function Charts.	63
Figure 3-14. EFA Test Data on Gravel Plotted on the Erosion Function Charts.....	64
Figure 3-15. Zone for Low Plasticity Clay.	65
Figure 3-16. Zone for High Plasticity Clay.	66
Figure 3-17. Zone for Clayey Sands.	67
Figure 3-18. Zone for Poorly Graded Sand	68
Figure 3-19. Critical Velocity as a Function of Mean Grain Size.	71
Figure 3-20. Critical Velocity as a Function of Mean Grain Size Including Data Points from Simulation Using United States Army Corps of Engineers EM 1601 Riprap Design Equation.....	72
Figure 3-21. Critical Shear Stress as a Function of Mean Grain Size.	73

Figure 4-1. Map Showing the Bridge-Gage Relationship Type II—Gage Upstream/Downstream of Bridge.	78
Figure 4-2. Location of the USGS Flow Gage and NCDC Rainfall Gage Pairs Chosen for the Investigation.	83
Figure 4-3. Illustration of the Methodology through Which the Rainfall Accumulation Time Window Is Determined.	85
Figure 4-4. Relationship between Yearly Instantaneous Flow Peaks (y) and the Concurrent Rainfall Depth (x) at USGS Gage 08037050.	86
Figure 4-5. Relationship between Yearly Instantaneous Flow Peaks (y) and the Concurrent Rainfall Depth (x) at USGS Gage 08039100.	87
Figure 4-6. Relationship between Yearly Instantaneous Flow Peaks (y) and the Concurrent Rainfall Depth (x) at USGS Gage 08103900.	87
Figure 4-7. Relationship between Yearly Instantaneous Flow Peaks (y) and the Concurrent Rainfall Depth (x) at USGS Gage 08131400.	88
Figure 4-8. Relationship between Yearly Instantaneous Flow Peaks (y) and the Concurrent Rainfall Depth (x) at USGS Gage 08154700.	88
Figure 4-9. Relationship between Yearly Instantaneous Flow Peaks (y) and the Concurrent Rainfall Depth (x) at USGS Gage 08155300.	89
Figure 4-10. Relationship between Yearly Instantaneous Flow Peaks (y) and the Concurrent Rainfall Depth (x) at USGS Gage 08165300.	89
Figure 4-11. Relationship between Yearly Instantaneous Flow Peaks (y) and the Concurrent Rainfall Depth (x) at USGS Gage 08200000.	90
Figure 4-12. Relationship between Yearly Instantaneous Flow Peaks (y) and the Concurrent Rainfall Depth (x) at USGS Gage 08201500.	90
Figure 4-13. Relationship between Yearly Instantaneous Flow Peaks (y) and the Concurrent Rainfall Depth (x) at USGS Gage 08211520.	91
Figure 4-14. Relationship between Yearly Instantaneous Flow Peaks (y) and the Concurrent Rainfall Depth (x) at USGS Gage 08365800.	91
Figure 4-15. Relationship between Yearly Instantaneous Flow Peaks (y) and the Concurrent Rainfall Depth (x) at USGS Gage 08431700.	92
Figure 4-16. Relationship between Yearly Instantaneous Flow Peaks (y) and the Concurrent Rainfall Depth (x) at USGS Gage 08365800.	92
Figure 4-17. Relationship between the Recurrence Interval of the Rainfall and the Flow. The Non-parameteric Approach to Flood Frequency Analysis Was Used to Estimate the Recurrence Intervals.	94

Figure 4-18. Relationship between the Recurrence Interval of the Rainfall and the Flow. The Parametric Approach to Flood Frequency Analysis Was Used to Estimate the Recurrence Intervals.	95
Figure 4-19. Histogram of the Difference between the Recurrence Interval of the Precipitation and That of Flow. The Plotting Position Formula Was Used When Estimating Recurrence Intervals of Flow and Precipitation.	97
Figure 4-20. Histogram of the Difference between the Recurrence Interval of the Precipitation and That of Flow. The GLO and GEV Distribution Was Used to Estimate the Recurrence Interval of Precipitation and Flow, Respectively.....	98
Figure 4-21. Hydrograph (USGS Gage 08030750) and Hyetograph (NCDC TX-6177) of the Year 1979. The Distance between the Two Gages Is 0.3 Miles.	100
Figure 4-22. Hydrograph (USGS Gage 08154700) and Hyetograph (NCDC TX-0428) of the Year 1998. Distance between the Two Gages Is 3.9 Miles.	102
Figure 4-23. Hydrograph (USGS Gage 08200000) and Hyetograph (NCDC TX-8845) of the Year 1998. Distance between the Two Gages Is 7.4 Miles.	103
Figure 4-24. Relationship between the Recurrence Interval of the Maximum Flow Peak and the Ratio Q_{mo}/Q_{100}	106
Figure 4-25. Location of the USGS Gages Used to Find Relationship between Recurrence Interval of Flow Peaks and Ratio of Flow.	107
Figure 4-26. Wide Channel.	109
Figure 4-27. Narrow Channel.	111
Figure 4-28. Relationship between Observed versus Cross-Validated V_{mo}/V_{100} . The Slope of the Regression Equation and the Correlation Coefficient of the Two Variables Indicate Regional Tendency.	115
Figure 4-29. Histogram of the Error between the Cross-Validated V_{mo}/V_{100} and the Observed V_{mo}/V_{100}	116
Figure 4-30. Location of All USGS flow Gages in Texas and the Surrounding States.....	127
Figure 4-31. Location of the 744 USGS flow Gages Used to Generate the Map of the Flow Recurrence Interval.....	127
Figure 4-32. Schematic of the Triangle-Based Linear Interpolation.	129
Figure 4-33. Map Showing the Interpolated Recurrence Interval Color Shading (Upper) and the Value of the Recurrence Intervals of the Flow Peaks Observed (Lower) in Year 2001.....	130
Figure 4-34. Result of the Flood Frequency Analysis for USGS Gage 08019500.....	131

Figure 4-35. Result of the Flood Frequency Analysis for USGS Gage 08028500.....	132
Figure 4-36. Result of the Flood Frequency Analysis for USGS Gage 08033500.....	133
Figure 4-37. Recurrence Interval Map of the Maximum Flood That Was Observed between the Year 1990 and 2006.....	134
Figure 4-38. Recurrence Interval Map of the Maximum Flood That Was Observed between the Year 1970 and 2006.....	135
Figure 4-39. Recurrence Interval Map of the Maximum Flood That Was Observed between the Year 1920 and 2006.....	136
Figure 4-40. Location of the 244 NCDC rain gages that were used to produce the rainfall recurrence interval maps.....	138
Figure 4-41. Maps Showing the Interpolated Recurrence Interval Color Shading and the Value of the Recurrence Intervals of the 6-hr Maximum Rainfall Observed in Year 2003.....	139
Figure 4-42. Recurrence Interval Map of the Maximum Rainfall That Was Observed between the Year 1995 and 2003.....	140
Figure 4-43. Comparison of the Recurrence Interval of Yearly Flow Peaks Estimated by GEV-MLE (x) and GEV-LMOM (y).	142
Figure 4-44. Comparison of the Recurrence Interval of Yearly Flow Peaks Estimated by GEV-MLE and Log-Pearson Type III-MOM.....	143
Figure 4-45. Comparison of the Recurrence Interval of Yearly Flow Peaks Estimated by GEV-LMOM and Log-Pearson Type III-MOM.....	144
Figure 4-46. Weight Factor of GEV-MLE versus Proportion of the Stations at Which the Recurrence Interval of the Maximum Flow Peak Does Not Exceed the Length of the Record of the Station.....	146
Figure 4-47. Map of regional characteristic parameter Ω across Texas (Asquith and Roussel, 2009).....	148
Figure 4-48. Flowchart of the Hydrology Part.....	149
Figure 5-1. Definition of the reference surface for Z_{thresh}	154
Figure 5-2. BSA 1 (Uniform Deposit) Flowchart.....	155
Figure 5-3. Z-Future Chart for Category I and II Materials	156
Figure 5-4. Z-Future Chart for Category III Materials (Pier Diameter: 0.1 m to 1.0 m).....	157
Figure 5-5. Z-Future Chart for Category III Materials (Pier Diameter: 1 m to 10 m).....	158
Figure 5-6. Z-Future Chart for Category IV Materials.	159

Figure 5-7. Z-Future Chart for Category V Materials.	160
Figure 5-8. Scour Due to Sequence of Two Flood Events: $V_{fut} > V_{mo}$ (after Briaud et al. 2001b).....	163
Figure 5-9. Scour Due to Sequence of Two Flood Events: $V_{fut} < V_{mo}$ (after Briaud et al. 2001).....	164
Figure 5-10. A General Illustration for BSA 1 (Multilayer Analysis).....	170
Figure 5-11. Case 1(a) for BSA 1 (Multilayer Analysis).....	174
Figure 5-12. Case 1(b) for BSA 1 (Multilayer Analysis).....	175
Figure 5-13. Case 1(c) for BSA 1 (Multilayer Analysis).....	175
Figure 5-14. Case 2(a) for BSA 1 (Multilayer Analysis).....	176
Figure 5-15. Case 2(b) for BSA 1 (Multilayer Analysis).....	176
Figure 5-16. Case 2(c) for BSA 1 (Multilayer Analysis).....	177
Figure 5-17. TAMU-FLOOD Input and Output for BSA 1 Example.	184
Figure 5-18. Recurrence Interval Map Generated from TAMU-FLOOD for the BSA 1 Example.	185
Figure 6-1. The BSA 2 Flowchart.....	188
Figure 6-2. Definition of Length of Active Flow Obstructed by the Abutment and Angle of Embankment Flow.....	193
Figure 7-1. The BSA 3 (Time Analysis) Flowchart	198
Figure 8-1. Location of the 11 Case Histories Selected for Validation.....	209
Figure 8-2. Comparison between Z_{fut} Values Predicted by BSA 1 and Corresponding Field Measurements.....	214
Figure 8-3. Comparison of Maximum Scour Depth Obtained Using EFA Test Data and the Erosion Function Chart.	216
Figure 8-4. The 1987 Schoharie Creek Bridge Failure.....	218
Figure 8-5. One of the Schoharie Creek Bridge Spans Plunging into the River.	219
Figure 8-6. Flow-Velocity Relationship for Schoharie Creek Pier 3.....	220
Figure 8-7. Schoharie Creek Pier 3 (after NTSB 1987).....	221
Figure 8-8. Photo of Pier 2 Taken in 1956.....	222
Figure 8-9. Photo of Pier 2 Taken in 1977.....	222

Figure 8-10. Photo of Pier 2 Taken in 1987 after the Failure.....	222
Figure 8-11. Photo of Pier 3 Taken in 1987 after the Failure.....	223
Figure 8-12. Estimated Erosion Functions for the Schoharie Creek Riprap and Glacial Till.....	225

LIST OF TABLES

	Page
Table 2-1. Codes in FHWA Item 113 (modified after Richardson and Davis 2001).	16
Table 2-2. TxDOT District Identification (after Haas et al. 1999).	17
Table 2-3. Application of Priority Rankings to Scour-Critical Bridges (after Ayres Associates 2004).	25
Table 2-4. Abutment Shape Coefficients (after Richardson and Davis 2001).	45
Table 3-1. Some Soil Properties Influencing Erodibility (after Briaud 2008).	48
Table 3-2. Erosion Categories in the Erosion Function Charts.	54
Table 4-1. Properties of the Rainfall-Flow Gage Pairs Used for the Analysis.	82
Table 4-2. The Regional Regression Equations of Asquith and Roussel (2009).	147
Table 4-3. Description of the Flowchart of the Hydrology Part.	150
Table 5-1. Rock Mass Erosion (after Briaud 2008).	167
Table 5-2. Definition of Terms in BSA 1 (Multilayer Analysis).	171
Table 5-3. Sub-cases within Case 1 and Case 2.	174
Table 5-4. Step-by-Step Procedure for BSA 1 (Uniform Deposit).	178
Table 5-5. Step-by-Step Procedure for BSA 1 (Multilayer Analysis).	180
Table 6-1. Step-by-Step Procedure for BSA 2.	190
Table 7-1. Step-by-Step Procedure for BSA 3 (Time Analysis).	200
Table 8-1. Summary of the 11 Case Histories Selected for Validation.	208
Table 8-2. Results of BSA 3 Validation.	217
Table 8-3. Peak Discharge versus WSPRO Mean Velocity at Schoharie Creek Pier 3 (after NTSB 1987).	219
Table 9-1. Bridges Selected for Application Using the Proposed Bridge Scour Assessment Method.	228
Table 9-2. Comparison between BSA 1 Outcome and the Current TxDOT Scour Designation for the 18 Bridges.	240

EXECUTIVE SUMMARY

BACKGROUND

Bridge scour is the term describing the loss of geomaterials due to water flowing around bridge supports. There are two major categories of scour: general scour and local scour. General scour involves the general accumulation or removal of sediments in the riverbed (termed aggradation and degradation) and is not due to the bridge. Local scour is the erosion of geomaterials around flow obstacles posed by bridge. There are three types of local scour: pier, abutment, and contraction scour. Pier and abutment scour are the removal of geomaterials around the pier foundation and bridge abutment, respectively. Contraction scour is the removal of geomaterials from the riverbed due to the narrowing of the river channel created by the approach embankments and piers of a bridge. Current standard bridge scour assessment methods are either qualitative initial evaluations or quantitative scour depth evaluations using equations based on experiments in sand. The first method does not provide realistic results in many cases because of its qualitative nature. The second method is often conservative in the case of clays, which are known to erode at a much slower rate than sand.

There are approximately 600 bridges in Texas that are deemed scour critical by the use of methods that predict excessive scour depths in erosion resistant materials. To overcome this over-conservatism, researchers at Texas A&M University developed the Scour Rate in Cohesive Soils (SRICOS-EFA method to calculate the time dependent scour depth in clays. This method requires site-specific erosion testing. However, carrying out soil sampling at the 600 scour critical bridges, testing them, and performing scour analyses would be uneconomical. Therefore, there was a need to develop a relatively simple and economical method that does not require site-specific erosion testing.

APPROACH TAKEN TO SOLVE THE PROBLEM

The approach selected to solve the problem was based on a combination of a review of existing knowledge, soil erosion tests, study of case histories, computer simulations, verification of the method against available data, and application to a few scour critical and non scour critical

bridges. The review of existing knowledge helped establish a solid foundation. The erosion tests provided a database of erodibility properties according to soil type, which led to erosion categories presented in a standard erosion chart. The case histories gave an idea of the data that are currently available. The computer simulations were used for hydrologic and hydraulic analyses aimed at obtaining relevant flow parameters. A parametric analysis was carried out to generate scour depth extrapolation charts. The method validation was based on comparisons between case histories that were subjected to the proposed assessment procedure and actual field measurements. The method was then applied to 10 scour critical and 3 non scour critical bridges in Texas to check its impact on their current scour designation.

OUTCOME OF THE STUDY

The researchers developed a three-level Bridge Scour Assessment (BSA) procedure which is simple, economical, and does not require site-specific erosion testing. The first level, BSA 1, consists of obtaining the maximum observed scour depth Z_{mo} during the bridge life and the maximum flood velocity V_{mo} during the bridge life. Z_{mo} is gathered from bridge records while V_{mo} is obtained from a simple computer program that generates maps of maximum floods in Texas for a given period. These maps are based on interpolation between records collected at United States Geological Survey (USGS) flow gages during the last century. The values of V_{mo} and Z_{mo} are used together with a specified future flood velocity V_{fut} to predict the corresponding future scour depth Z_{fut} . Z_{fut} is then compared to the scour depth that is tolerable for the foundation Z_{thresh} . Z_{thresh} is often taken as one-half of the pile length in Texas. If Z_{fut} is less than Z_{thresh} , the bridge is not scour critical. Otherwise, one needs to proceed to BSA2, which involves more calculations including maximum scour depths Z_{max} . If BSA2 also fails to conclude that the bridge is not scour critical, one needs to proceed to BSA3, which involves more calculations including the time dependent scour depth Z_{fin} based on the standard erosion charts. The BSA1 method was evaluated against 11 case histories by comparing the predicted and measured Z_{fut} values. The comparison was very good. BSA 1 was then applied to 10 scour critical and 3 non scour critical bridges. In this process, 6 of the 10 scour critical bridges were found to be stable and could be removed from the scour critical list and the 3 non scour critical bridges were confirmed as non scour critical. Out of the 4 bridges that remained scour critical after BSA 1, 2

bridges did not have sufficient information for BSA 2 or BSA 3 to be carried out. The remaining 2, having sufficient information, remained scour critical after BSA 2 and BSA 3 were carried out.

SIGNIFICANCE OF THE STUDY

The proposed bridge scour assessment procedure allows for the economical and simple evaluation of scour critical bridges. It also overcomes the over-conservatism in current methods. This method will lead to a more realistic bridge scour evaluation and stands to remove many bridges from the scour critical list at a great saving to the State of Texas.

1. INTRODUCTION

1.1. BRIDGE SCOUR

Bridge scour is the term used to describe the loss of geomaterials (soils, rocks, and intermediate geomaterials) due to water flowing around bridge supports. There are two major categories of scour, general scour and local scour. General scour refers to the aggradation or degradation of geomaterials in the riverbed that is not due to the local obstacles present at a bridge. Aggradation is the gradual and general accumulation of sediments at the bottom of the river, and degradation is the gradual and general removal of sediments from the riverbed (Briaud et al. 2004). Local scour refers to the erosion of geomaterials around flow obstacles posed by the presence of the bridge. Figure 1-1 gives a general illustration of how river flow is affected by a bridge. There are three types of local scour: pier scour, abutment scour, and contraction scour. Pier scour is the removal of geomaterials around the foundation of a pier; abutment scour is the removal of geomaterials around an abutment at the junction between a bridge and an embankment; contraction scour is the removal of geomaterials from the bottom of the river due to the narrowing of the river channel created by the approach embankments and piers of a bridge (Briaud et al. 2004). Figure 1-2 illustrates the three components of scour.

1.2. GEOMATERIALS: A DEFINITION

Geomaterials can be classified into three categories: soils, rocks, and intermediate geomaterials such as cobbles and boulders. Briaud (2008) defines soil as an earth element that can be classified by the Unified Soil Classification System (USCS). The classification tests for soils are the grain size analysis (sieve analysis and hydrometer analysis) and the Atterberg limits. The grain size analysis leads to the determination of the mean grain size D_{50} of a material, which is the grain size corresponding to 50 percent of the soil weight passing a sieve with an opening size that is equal to D_{50} . The first major division in soils is the classification between coarse-grained soils and fine-grained soils. Soils that have a D_{50} greater than 0.075 mm are the coarse-grained soils. Conversely, soils with a D_{50} smaller than 0.075 mm are the fine-grained soils. Coarse-grained soils include gravels and sands and are identified by their grain size. Fine-grained soils

include silts and clays and are identified on the basis of Atterberg limits (Briaud et al. 2004). Briaud (2008) defines rock as an earth element that has a joint spacing of more than 0.3 ft (0.1 m) and an unconfined compressive strength of the intact rock core of more than 10445 psf (500 kPa). Intermediate geomaterials are materials whose behavior is intermediate between soils and rocks, such as cobbles, boulders, and riprap.

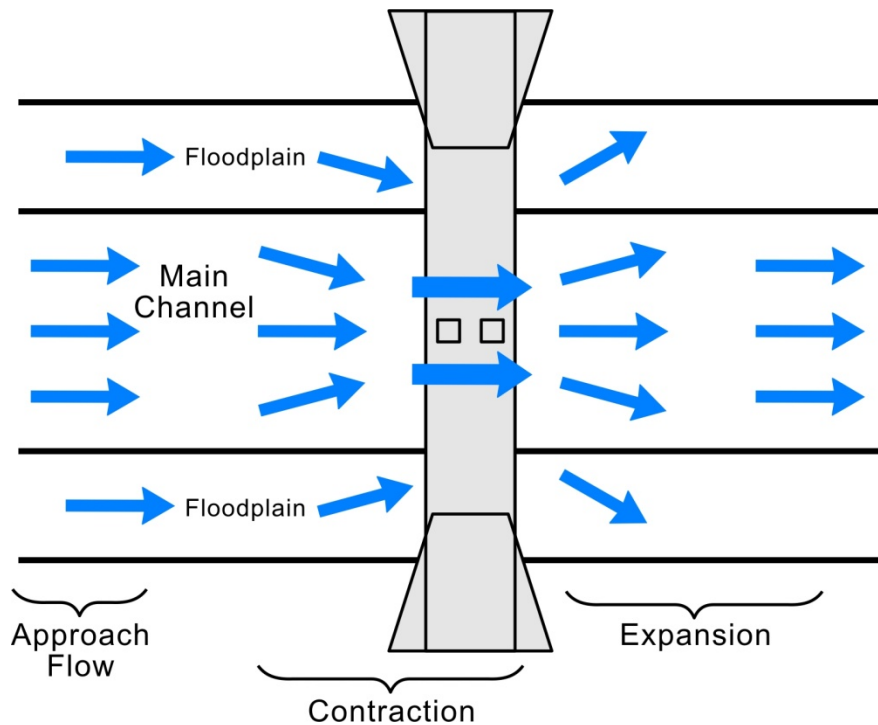


Figure 1-1. General Illustration of How a Bridge Affects River Flow.

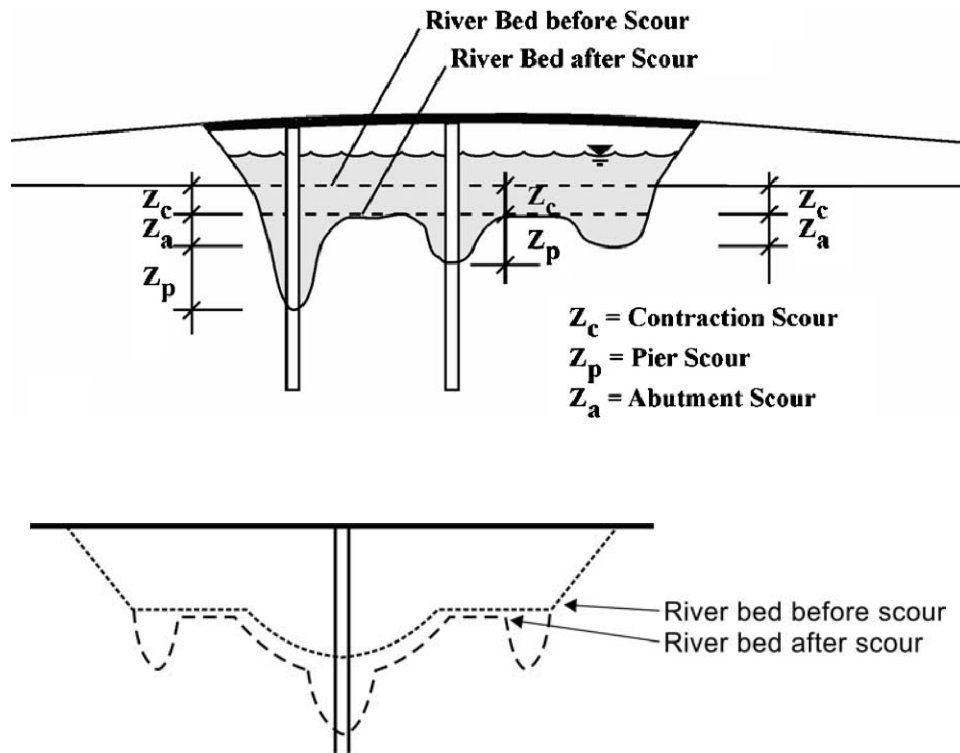


Figure 1-2. The Three Components of Scour (after [Briaud et al. 2005](#)).

1.3. ERODIBILITY OF GEOMATERIALS

The erodibility of soil or rock is defined as the relationship between the erosion rate, \dot{Z} , and the velocity of water, V , at the soil/rock–water interface. This definition, however, is not very satisfactory because the velocity varies in direction and intensity in the flow field (Briaud 2008). To be exact, the velocity of water is zero at the soil/rock interface. A more adequate definition is the relationship between erosion rate \dot{Z} and shear stress at the soil/rock interface. However, the velocity is often used because it is easier to gauge an erosion problem from a velocity standpoint.

One of the most important material parameters in soil erosion is the threshold of erosion (Briaud 2008). Below the threshold value, erosion does not take place. Once the applied hydraulic shear stress (or more simply, the velocity) exceeds the threshold value, erosion is initiated until the equilibrium scour depth is obtained. The threshold value for erosion in terms of shear stress is the critical shear stress τ_c and in terms of velocity is the critical velocity V_c . Important parameters that assist in describing the erosion function include the threshold value, the initial rate of scour, and the equilibrium scour depth. The erosion rate in clays and rocks can be many times smaller than the erosion rate in sands.

1.4. THE PROBLEM ADDRESSED

This project deals with the development of a bridge scour assessment procedure that is relatively simple and economical EFA and does not require site-specific erosion testing. Previously, TxDOT in a project with Texas A&M University developed the Erosion Function Apparatus EFA to measure the erosion function of soils and rocks. In conjunction with that research project, a method to determine the scour rate in cohesive soils at bridge piers was developed. This method is termed the SRICOS-EFA Method for bridge piers. This method predicts the scour depth as a function of time when a cylindrical pier in layered soil is subjected to a long-term deepwater flow velocity hydrograph. Subsequently, Texas A&M University in collaboration with National Cooperative Highway Research Program (NCHRP) developed the SRICOS-EFA Method for bridge contractions. This method predicts the scour depth as a function of time when a bridge contraction in layered soil is subjected to a long-term deepwater flow velocity hydrograph. For each of these two methods, two levels of complexity were developed by the

Texas A&M University scour research group. The first level is termed the Extended SRICOS Method, which requires the testing of soil samples and the use of a velocity hydrograph and a computer program. The second level is termed the Simple SRICOS-EFA Method, which also requires the testing of soil samples but does not require a computer program and instead relies on simple hand calculations (Briaud et al. 2004). In this TxDOT project, the Simple SRICOS-EFA Method was employed in simulations that led to a more simple and economical method for bridge scour assessment that does not require site-specific erosion testing.

1.5. WHY THIS PROBLEM WAS ADDRESSED

The reason for solving this problem is that there are approximately 600 bridges in Texas that have been deemed scour critical. The locations of these bridges are shown in [Figure 1-3](#). However, many of them are so labeled because of the use of over-conservative scour calculation methods that predict excessive scour depths under a design flood event. Currently available methods of bridge scour evaluation rely upon three categories of assessment methods. The first category, termed Level 1 analysis, is a preliminary scour evaluation procedure that is based on field observations and primarily qualitative in nature, but could also rely on simplified scour depth–hydraulic parameter relationships that are mainly based on flume tests in sand. This category does not utilize actual measured scour data. The second and third categories, termed Level 2 and Level 3 analysis, involve more detailed calculations of maximum scour depth based on flume tests in sand. The difference between the second and third categories is that a Level 2 analysis consists of hydraulic modeling and the computation of the estimated depth of maximum potential scour resulting from a design flood event; a Level 3 analysis consists of a fluvial computer model simulation or a laboratory model study of a site to assess complex conditions that are beyond the scope of the Level 2 analysis procedures. The first method does not provide realistic results in many cases due to its reliance on a more qualitative form of assessment. The second and third methods are often conservative in the case of clays, which are known to erode at a much slower rate than sand.

In order to overcome the over-conservative nature of these methods, [Briaud et al. \(1999, 2005\)](#) at Texas A&M University developed the SRICOS-EFA Method to calculate scour depths due to pier and contraction scour that are capable of accounting for time-dependent scour in

clays. However, these methods require site-specific erosion testing. Sampling soils at the 600 scour-critical bridges and subsequently testing them would represent a huge cost and is therefore uneconomical in addressing the bridge scour problem in Texas.

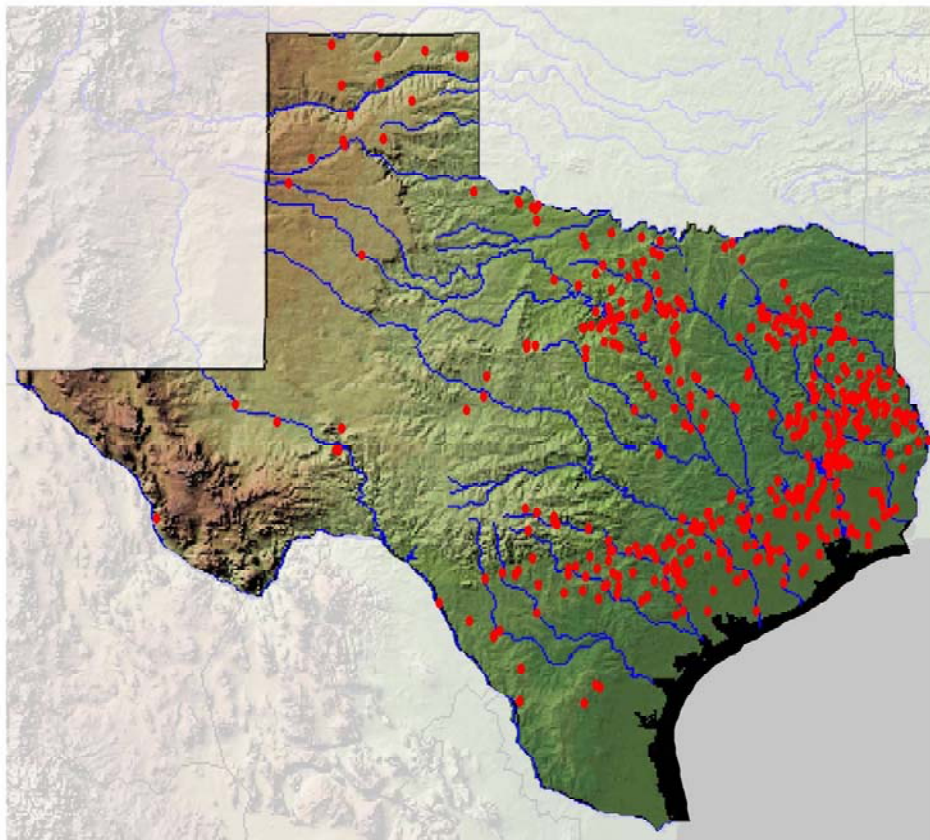


Figure 1-3. The Location of Scour-Critical Bridges in Texas.

Therefore, for geomaterials that erode at much slower rates than sands (e.g., clays and some rocks), a more realistic method that is relatively cheap and economical is required to replace the calculation methods based on sand. In order to overcome the qualitative nature of current initial evaluation procedures, a method that utilizes actual scour measurements and compares them with the foundation's load-carrying capacity is also required.

1.6. APPROACH SELECTED TO SOLVE THE PROBLEM

The approach selected to solve the problem of assessing a bridge more realistically for scour is based on a combination of a review of existing knowledge, EFA tests, a study of case histories, computer simulation, and verification of the method against available data. The review of existing knowledge avoided duplication of effort and helped establish a solid foundation. The EFA tests provided a database of erodibility properties according to soil type, which led to the development of erosion categories. These categories were plotted on an either a velocity versus erosion rate or shear stress versus erosion rate graph. The dividing lines for the various categories were determined using a conservative approach (i.e., using straight lines). The advantage of this approach is that it eliminates the need for site-specific erosion testing. The case histories gave an idea of the data that bridge inspectors have and use. It was also a good overview of bridges in Texas. The computer simulations were used to carry out hydrologic and hydraulic analysis to obtain relevant flow parameters. The simulations were also used to simulate a very large number of combinations of bridge scour parameters, which enabled the development of bridge scour assessment charts, termed Z-Future Charts. Verification was based on comparison of case histories that were subjected to the proposed assessment procedure and actual field measurements.

1.7. VALIDATION OF THE PROPOSED ASSESSMENT METHOD

Several full case histories were selected for the validation of the proposed bridge scour assessment procedure. The required information was soil data, flow data, age of the bridge, foundation type and dimensions, and scour depths. There were 11 cases that were considered adequate and suitable, and were used in the validation process.

The bridge records for the case histories had limited bridge scour measurements. In fact, there were no bridge scour measurements taken before the year 1991. Since most of the bridges were reasonably old (up to approximately 80 years old), they had experienced the largest flow velocity prior to the first bridge scour measurement. This resulted in all the cases having a $V_{\text{fut}}/V_{\text{mo}}$ ratio equal to or less than unity for the BSA 1 validation. It should be noted that all of the bridge records had the ground line for the “as-built” condition, which we used as a reference

point for evaluation using BSA-1. Results of the BSA 1 validation show good agreement between predicted and measured values. However, this validation is only for $V_{\text{fut}}/V_{\text{mo}}$ ratios equal to or less than unity. The results of the validation of BSA 2 show good agreement between the BSA 2 method and the SRICOS-EFA Method. The validation of BSA 3 indicates that BSA 3 tends to overestimate the scour depth when compared to field measurements. This could be due to the fact that the selection of erosion categories on the basis of soil type is very conservative (by design). However, BSA 3 does improve on the over-estimation of scour depth by 2 ft to 4 ft when compared to maximum scour depths.

1.8. APPLICATION TO SCOUR-CRITICAL BRIDGES

BSA 1 was applied to 10 scour critical and 3 non scour critical bridges. In this process, 6 of the 10 scour critical bridges were found to be stable and could be removed from the scour critical list and the 3 non scour critical bridges were confirmed as non scour critical. Out of the 4 bridges that remained scour critical after BSA 1, 2 bridges did not have sufficient information for BSA 2 or BSA 3 to be carried out. The remaining 2, having sufficient information, remained scour critical after BSA 2 and BSA 3 were carried out.

2. BACKGROUND

2.1. INTRODUCTION

Currently available methods of bridge scour evaluation rely upon three categories of assessment methods. The first category, termed Level 1 analysis, is a preliminary scour evaluation procedure that is based on field observations and is primarily qualitative in nature, but could also rely on simplified scour depth–hydraulic parameter relationships that are mainly based on flume tests in sand. This category does not utilize actual measured scour data. The second and third categories, termed Level 2 and Level 3 analysis, involve more detailed calculations of maximum scour depth based on flume tests in sand. The difference between the second and third categories is that a Level 2 analysis consists of hydraulic modeling and the computation of the estimated depth of maximum potential scour resulting from a design flood event; a Level 3 analysis consists of a fluvial computer model simulation or a laboratory model study of a site to assess complex conditions that are beyond the scope of the Level 2 analysis procedures. The first method does not provide realistic results in many cases due to its reliance on a more qualitative form of assessment. The second and third methods are often conservative in the case of clays, which are known to erode at a much slower rate than sand. [Briaud et al. \(1999, 2005\)](#) at Texas A&M University developed models to calculate scour depths due to pier and contraction scour that are capable of accounting for time-dependent scour in clays. These methods, collectively called the SRICOS method ([Briaud et al. 1999, 2005](#)) require site-specific erosion testing ([Govindasamy et al. 2008](#)).

Preliminary scour evaluation procedures have been developed by or for several state departments of transportation (DOTs). For example, the Montana DOT, in collaboration with USGS, developed a rapid scour evaluation process that relies upon calculated scour depth–measured hydraulic parameter relationships ([Holnbeck and Parrett 1997](#)). A similar method has also been adopted by the Missouri DOT ([Huizinga and Rydlund 2004](#)). The Tennessee DOT uses an initial evaluation process that utilizes a qualitative index based on field observations to describe the potential problems resulting from scour ([Simon et al. 1989](#)). Similar qualitative methods have been adopted by the California, Idaho, and Texas DOTs and the Colorado Highway Department for their initial assessment of bridges for scour. [Johnson \(2005\)](#) developed

a preliminary assessment procedure that individually rates 13 stream channel stability indicators, which are then summed to provide an overall score that places a bridge in one of four categories: excellent, good, fair, and poor (Govindasamy et al. 2008).

Current practice for more detailed scour evaluation is heavily influenced by two Federal Highway Administration (FHWA) hydraulic engineering circulars (HECs) called HEC-18 and HEC-20 (Richardson and Davis 2001, Lagasse et al. 1995). These methods are known to be overly conservative in the case of clays and some types of rock since they are based on flume tests in sand and do not account for time-dependent scour (Govindasamy et al. 2008).

2.2. CURRENT ASSESSMENT METHODS IN PRACTICE

2.2.1. FHWA Guidelines for Evaluating Scour at Bridges

On October 28, 1991, FHWA issued Technical Advisory T5140.23 titled “Evaluating Scour at Bridges,” which detailed recommendations for developing and implementing scour evaluations for bridges over waterways. Jones and Ortiz (2002) define a scour-critical bridge as one with foundation elements that are determined to be unstable for the calculated and/or observed stream stability or scour conditions. To monitor the conditions of bridges throughout the nation, FHWA maintains a database called the National Bridge Inventory (NBI) (Jones and Ortiz 2002). In the NBI database, FHWA codes bridges in terms of scour and stream stability according to Technical Advisory T5140.23 (Federal Highway Administration 1991), which categorizes the evaluation of these issues according to the following items:

- Item 61 for channel and channel protection, and
- Item 113 for scour-critical bridges.

For Item 61, the bridge being evaluated is rated from the number 0 to 9 or the letter “N.” For Item 113, the bridge being evaluated is rated from the number 0 to 9 or the letter “U” or “N.” For example, in Item 113, a ranking of “0” would indicate that a bridge is scour critical, has failed, and is closed to traffic. A ranking of “9” would indicate that the bridge foundations are on dry land, well above flood water elevation. The ranking “U” indicates that the bridge is supported by unknown foundations. The ranking “N” indicates that the bridge is not over a

waterway (Richardson and Davis 2001). A detailed description of the codes used can be found in Appendix J of HEC-18 (Richardson and Davis 2001). Table 2-1 shows the codes in FHWA Item 113.

2.2.2. Bridge Scour Evaluation Practice in Texas

Launched in 1991, the TxDOT bridge scour evaluation and mitigation program consists of the use of a bridge inventory database, scour inspection procedures, and several levels of screening processes (Haas et al. 1999). The TxDOT bridge inventory database, called the Bridge Inventory, Inspection, and Appraisal Program (BRINSAP) database, is devised to meet the inventory system requirements of Section 650.311(a) of the National Bridge Inspection Standards (NBIS) (Federal Highway Administration 2004). In the BRINSAP database, Item 113 provides the scour rating while Item 113.1 provides a scour vulnerability assessment for each bridge. TxDOT's inspection procedures comprise initial inspections, routine inspections, and special inspections. Under certain circumstances, damage inspections and in-depth inspections are also conducted. Bridges that have a low vulnerability to scour are excluded from extensive hydraulic analyses to reduce costs. These mechanisms are used by TxDOT to meet NBIS regulations and establish procedures to ensure the safety of bridges. Additionally, these mechanisms provide data that indicate the risk of scour-related damage for each bridge, which would then enable the prioritization of bridge sites to receive scour countermeasures.

Table 2-1. Codes in FHWA Item 113 (modified after Richardson and Davis 2001).

Codes	Description
N	Bridge is not over waterway.
U	Unknown foundation that has not been evaluated for scour. Until risk is determined, POA should be developed.
9	Bridge foundations on dry land well above flood water elevations.
8	Bridge foundations determined to be stable for the assessed or calculated scour condition. Scour is determined to be above top of footing by assessment, calculation, or installation of properly designed countermeasures.
7	Countermeasures have been installed to mitigate an existing problem with scour and to reduce the risk of bridge failure during flood event.
6	Scour calculations/evaluation has not been made. (Use only to describe case where bridge has not yet been evaluated for scour potential.)
5	Bridge foundations determined to be stable for assessed or calculated scour condition. Scour is determined to be within the limits of footings or piles by assessment, calculations, or installation of properly designed countermeasures.
4	Bridge foundations determined to be stable for assessed or calculated scour conditions; field review indicates action is required to protect exposed foundations.
3	Bridge is scour critical; bridge foundations determined to be unstable for assessed or calculated scour conditions: scour within limits of footings or piles, or scour below spread-footing base or pile tips.
2	Bridge is scour critical; field review indicates that extensive scour has occurred at bridge foundations, which are determined to be unstable by: a comparison of calculated scour and observed scour during the bridge inspection or an engineering evaluation of the observed scour reported by the bridge inspector.
1	Bridge is scour critical; field review indicates that failure of piers/abutments is imminent. Bridge is closed to traffic. Failure is imminent based on: a comparison of calculated and observed scour during the bridge inspection or an engineering evaluation of the observed scour condition reported by the bridge inspector.
0	Bridge is scour critical. Bridge has failed and is closed to traffic.

Note: Modification after Richardson and Davis (2001) is the removal of the code “T,” which is for bridges over tidal waters.

2.2.2.1. The BRINSAP Database

TxDOT has a state-level equivalent of NBI called the BRINSAP database. The BRINSAP database comprises 135 fields for each bridge record and gives a comprehensive account of the

physical and functional characteristics of each bridge. The database categorizes bridges into two major groups of structures, the on-system and off-system bridges. On-system bridges generally are structures that belong to the state highway department or other state or federal agencies, which are responsible for their maintenance. Off-system structures in general belong to local municipalities. The State of Texas comprises 25 districts, which are divided into 254 counties (Haas et al. 1999). The BRINSAP database includes entries for the district and county where each structure is located. TxDOT's 25 districts are shown in Table 2-2 and Figure 2-1.

Table 2-2. TxDOT District Identification (after Haas et al. 1999).

District	No.	District	No.	District	No.	District	No.	District	No.
Paris	1	Odessa	6	Lufkin	11	Corpus Christi	16	Pharr	21
Ft. Worth	2	San Angelo	7	Houston	12	Bryan	17	Laredo	22
Wichita Falls	3	Abilene	8	Yoakum	13	Dallas	18	Brownwood	23
Amarillo	4	Waco	9	Austin	14	Atlanta	19	El Paso	24
Lubbock	5	Tyler	10	San Antonio	15	Beaumont	20	Childress	25

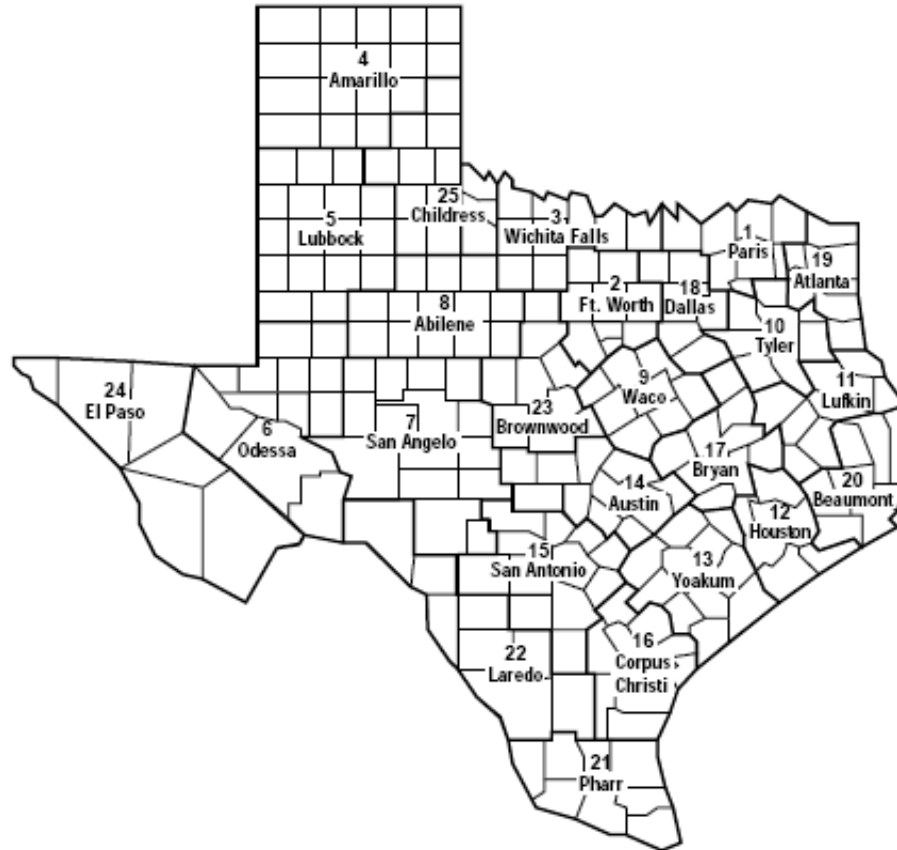


Figure 2-1. Map Showing the 25 Districts of Texas (after Haas et al. 1999).

2.2.2.2. Initial Screening Method for Scour Evaluation

The FHWA Technical Advisory T5140.23 requirement for evaluating bridges for scour prompted TxDOT to develop an initial scour screening process aimed at detecting bridges that may require further scour evaluation. In 1991, TxDOT developed an initial screening process that comprised a cursory geomorphic survey of bridges over waterways. The evaluation of the bridges is performed by carrying out a field survey of the hydraulic and physical characteristics of the bridge site. The results of the survey were then used to complete the Scour Vulnerability Examination and Ranking Format (SVEAR) shown in Figure 2-2, which leads to a scour susceptibility ranking of the bridges (Haas et al. 1999). The objective of the program was to identify the bridges with scour problems and the extent of the associated problem and

subsequently provide a means of prioritizing bridges to receive further evaluation. The SVEAR process categorizes bridges into those having known scour problems, those highly susceptible to scour, those with medium susceptibility to scour, and those having low risk. The prioritization procedure for the bridges relies on the outcome of the SVEAR process and data in the BRINSAP database (Olona 1992).

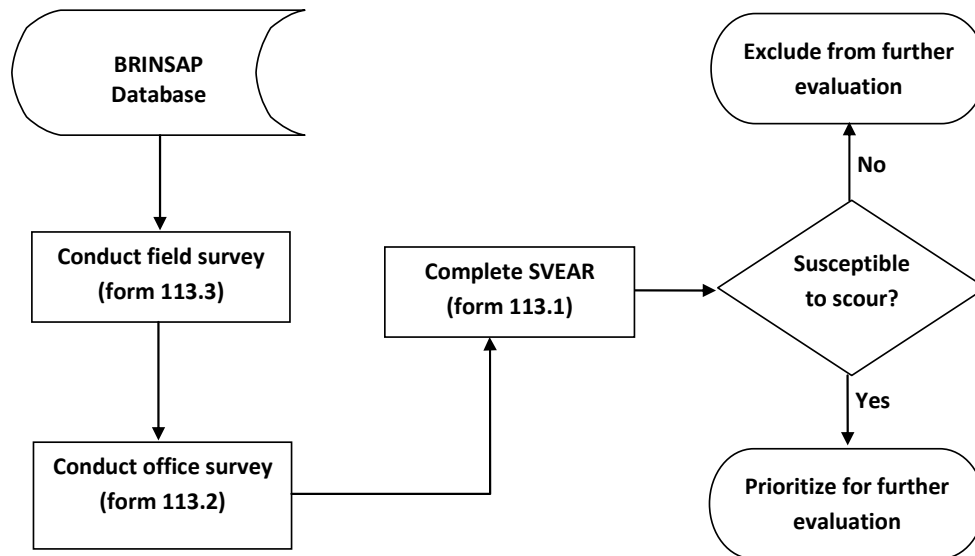


Figure 2-2. The SVEAR Screening Process Flow Chart (after Haas et al. 1999).

Due to the fact that the initial screening process (SVEAR) yielded a large number of bridges that were designated as vulnerable to scour, there was a need to refine the evaluation process to better assess and understand the bridges. To achieve this, TxDOT developed the Texas Secondary Evaluation and Analysis for Scour (TSEAS) (Haas et al. 1999). TSEAS consists of two distinct parts. The first part is a question-and-answer process termed Secondary Screening and is rather similar to the initial screening process. The Secondary Screening process is aimed at determining risk factors and differentiating between stream stability and bridge scour factors. The second part, termed Concise Analysis (or Detailed Analysis), is a simplified bridge scour analysis procedure that is performed depending on the outcome of the Secondary Screening. It should be noted that the TSEAS process was used primarily during the initial categorization of bridges for scour and has not really been used since.

2.2.2.3. Secondary Screening

TxDOT developed a secondary screening procedure in 1993, which contains 11 questions that need to be answered by the bridge inspector. The issues covered in the questions are as follows (Texas Department of Transportation 1993):

1. the presence of non-erodible rock or cohesive materials with Texas Cone Penetration TCP-N values greater than 100 blows/ft as the foundation material;
2. the presence of existing scour countermeasures;
3. the presence of sand as the foundation material;
4. evidence of general channel degradation, local bridge scour, or both;
5. the impact of stream migration;
6. historical scour damage at the bridge;
7. the effects of mining or mining-related operations on the bridge site;
8. the impact of skewed bents on scour at the bridge site;
9. the impact of dams and other control structures on the bridge site;
10. the presence of spread footings that are not supported by piles or embedded in rock; and
11. the impact of debris.

The response to some of the issues mentioned above may require a field visit if documentation established during the initial screening process was insufficient (Texas Department of Transportation 1993). Figure 2-3 shows the secondary screening flowchart, where BS refers to bridge scour problems and SS refers to stream stability problems. In the figure, the definitions of Item 113 and Item 113.1 and the associated numeric code have been explained in the preceding section.

the design phase of the structure (and in the construction plans) or can be estimated based on historic and/or nominal additional field data. If neither of these techniques yields reasonable hydraulic parameters for a Concise Analysis, a Detailed Analysis is recommended ([Texas Department of Transportation 1993](#)).

The following is an outline of the steps required for the Detailed and Concise Analyses as presented in TSEAS ([Texas Department of Transportation 1993](#)):

1. determination of hydraulic variables such as natural channel and through-bridge velocities, wetted perimeter, and Manning's n values;
2. determination of maximum allowable scour based on estimated foundation bearing capacity and lateral stability;
3. estimation of maximum pier scour;
4. determination of potential pier scour;
5. determination of maximum allowable flow contraction ratio;
6. determination of channel geometry contraction ratio;
7. estimation of actual flow contraction ratio;
8. comparison of allowable scour depths with estimated scour depths; and
9. recommendations for BRINSAP coding and/or further handling.

2.2.3. Tennessee Level 1 Assessment

The Tennessee Level 1 Assessment ([United States Geological Survey 1993](#)) procedure, which is an initial bridge scour assessment technique, is designed to provide a qualitative index indicating the potential for problems due to localized scour and general stream instability. In this procedure, a bridge inspector makes basic scour or stream stability-related measurements or visually estimates them. These and other qualitative measurements provide information on the general stability of the stream reach in which the bridge is located. The data include observations of land use in the watershed, bed and bank material, bank slope, bank vegetation, meander and point bar locations, debris production, channel constriction, and observable bank-erosion processes. Additionally, the data include more detailed information on the structural components of the

bridge that could influence local scour such as the number of piers in the main channel, skew angle of the piers with respect to flow, the skew angle and placement of abutments, observable localized scour at piers and abutments, and debris accumulation at the bridge. Two indices (the potential scour index and observed scour index) are produced by the Tennessee Level 1 analysis. As a follow-up to the Level 1 analysis, the Tennessee DOT employs a Level 2 analysis, which adopts the HEC-18 ([Richardson and Davis 2001](#)) methods to estimate the maximum scour depth.

2.2.3.1. Potential Scour Index

The potential scour index is used to identify and rank bridges with significant potential scour problems. The potential scour index is computed by summing a collection of variables that have been assigned a ranking and is used to indicate problems for local scour and channel instability. Sites with a potential scour index greater than 20 have substantial potential for scour problems. The potential scour index comprises the following variables ([United States Geological Survey 1993](#)):

- erodibility of bed material,
- bed protection and bank protection,
- stage of channel evolution,
- percent of channel constriction,
- number of piers in channel,
- percent horizontal and vertical blockage,
- bank erosion,
- meander impact point from bridge,
- pier skew,
- mass wasting at pier, and
- high flow angle of approach.

While the rankings of the above variables are not weighted for relative importance, certain variables can be weighted higher than others if deemed appropriate by local transportation departments.

2.2.3.2. Observed Scour Index

The observed scour index is used to identify bridges with immediate scour problems. It can also provide additional insight into the potential for scour at a site. The observed scour index only considers local scour problems and does not account for general stream stability problems.

The observed scour index is computed using the following variables ([United States Geological Survey 1993](#)):

- signs of observed pier scour,
- exposure of abutment piling,
- failed riprap at the bridge,
- movement of bed riprap,
- presence of blow holes, and
- mass wasting at pier.

2.2.3.3. Relationship between Potential Scour Index and Observed Scour Index

Since they are not comparable values, the potential scour index and observed scour index should not be compared directly. There is neither a theoretical relationship nor a correlation implied between the two indices. The observed scour index only captures scour observable by the inspector and may not necessarily affect the bridge's structural stability. For example, exposed piling at several bridge piers can produce a high observed scour index even though very little localized scour or general channel degradation has occurred. The observed scour index should supplement the potential scour index to identify bridges requiring a more detailed analysis.

2.2.4. The Idaho Plan of Action for Scour-Critical Bridges

The Idaho Plan of Action is a prioritizing mechanism for Idaho’s scour-critical bridges and bridges with unknown foundation. The method used to prioritize these bridges is based on the lifetime risk, which by definition is the lifetime cost of failure multiplied by the lifetime probability of failure and, for scour-critical bridges, the estimated probability of failure (Ayres Associates 2004). Ayres Associates (2004) go on to state that the lifetime risk is the expected cost of scour-related bridge failure, which is obtained by combining the cost of failure with the probability of failure. The values of probability of failure and failure cost are based on the expanded HYRISK method, which is detailed in Pearson et al. (2000). As a simple illustration, a bridge with a high failure cost due to heavy traffic volume may still have a lifetime risk that is relatively low due to a low probability of failure. The application of the Idaho POA to scour-critical bridges is shown in Table 2-3.

Table 2-3. Application of Priority Rankings to Scour-Critical Bridges (after Ayres Associates 2004).

Category	Scour Vulnerability	Number of Bridges	Lifetime Risk (L_r)	Annual Probability of Failure (P_f)
A	Vital	37	$L_r > \$5,000,000$ (lifetime cut-off value set in consultation with Idaho DOT Scour Committee)	-
B	Extreme	12	$L_r < \$5,000,000$	$P_f \geq 10\%$
C	Severe	109	$L_r < \$5000,000$	$P_f < 10\%$ (for bridges founded on spread footings)
D	Moderate	37	-	$P_f < 1\%$ (for bridges on driven pile foundation)

2.2.5. USGS Method for Rapid Estimation of Scour Based on Limited Site Data

In 1997, Holnbeck and Parrett developed a method for the rapid estimation of scour at highway bridges for USGS. This procedure was initially developed for the state of Montana for the

purpose of aiding the Montana DOT in meeting the national bridge scour program requirements. The method was developed based on the following requirements:

1. requirement of only limited site data;
2. provides estimates of scour depth that would be reasonably comparable to estimates from more detailed methods, for example the Level 2 scour analysis; and
3. provides estimates at each site in a few hours or less.

[Holnbeck and Parrett \(1997\)](#) developed this method from Level 2 scour analyses performed by the USGS in 10 states, namely Montana, Colorado, Indiana, Iowa, Mississippi, Missouri, New Mexico, South Carolina, Texas, and Vermont. The components of bridge scour that were considered in both the Level 2 analysis and the proposed rapid estimation method are contraction scour and local scour at piers and abutments. Based on the Level 2 analysis, they presented the components of scour as a function of more easily estimated parameters during a bridge inspection. The contraction scour was expressed as a function of discharge at the contracted section, approach water depth, and D_{50} . The pier scour was expressed as a function of flow attack angle, Froude number, and pier width. Abutment scour was expressed as a function of abutment shape and flow depth at the abutment. [Holnbeck and Parrett \(1997\)](#) provide a detailed description of these relationships. The outcome of the rapid method was compared with its corresponding Level 2 analysis for several bridge sites and is shown in [Figure 2-4](#), [Figure 2-5](#), and [Figure 2-6](#).

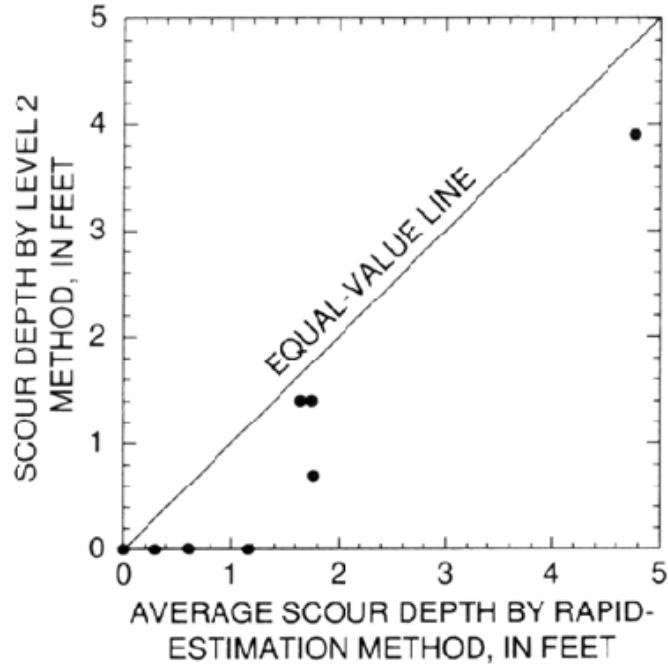


Figure 2-4. Comparison of Contraction Scour Depth by the Rapid Estimation Method and by Level 2 Method (after [Holnbeck and Parrett 1997](#)).

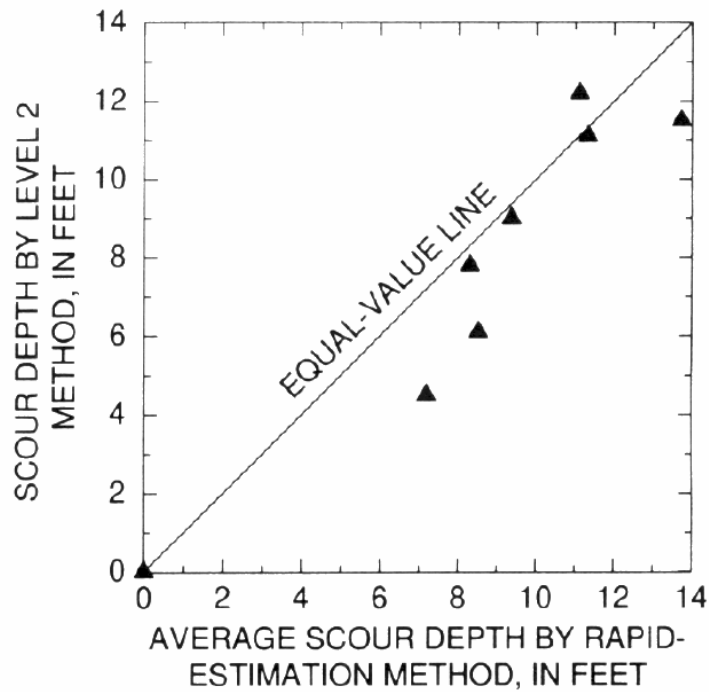


Figure 2-5. Comparison of Pier Scour Depth by the Rapid Estimation Method and by Level 2 Method ([Holnbeck and Parrett 1997](#)).

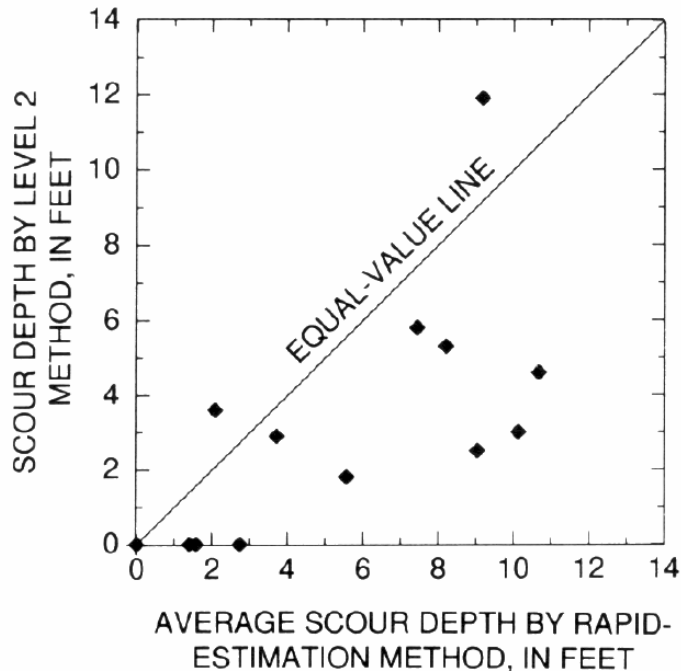


Figure 2-6. Comparison of Abutment Scour Depth by the Rapid Estimation Method and by Level 2 Method (Holnbeck and Parrett 1997).

2.2.6. Other Bridge Scour Assessment Procedures

Several state DOTs and government agencies have developed techniques for assessing scour at bridges. For example, the [Colorado Highway Department \(1990\)](#) developed a scour vulnerability assessment procedure based on the geology, hydraulics, river conditions, and foundations of bridges that enables scour prioritizing in scour susceptibility categories. This procedure incorporates three flowcharts (shown in [Figure 2-7](#), [Figure 2-8](#), and [Figure 2-9](#)), which are for general scour and stream stability issues, abutment scour, and pier scour, respectively. The numerical values included in the flowchart were selected to emphasize the relative effect of each parameter on the potential to produce scour. Note that the values of each parameter are such that the most scour-vulnerable bridge has the largest value. As evident from the flowcharts, this procedure is highly qualitative.

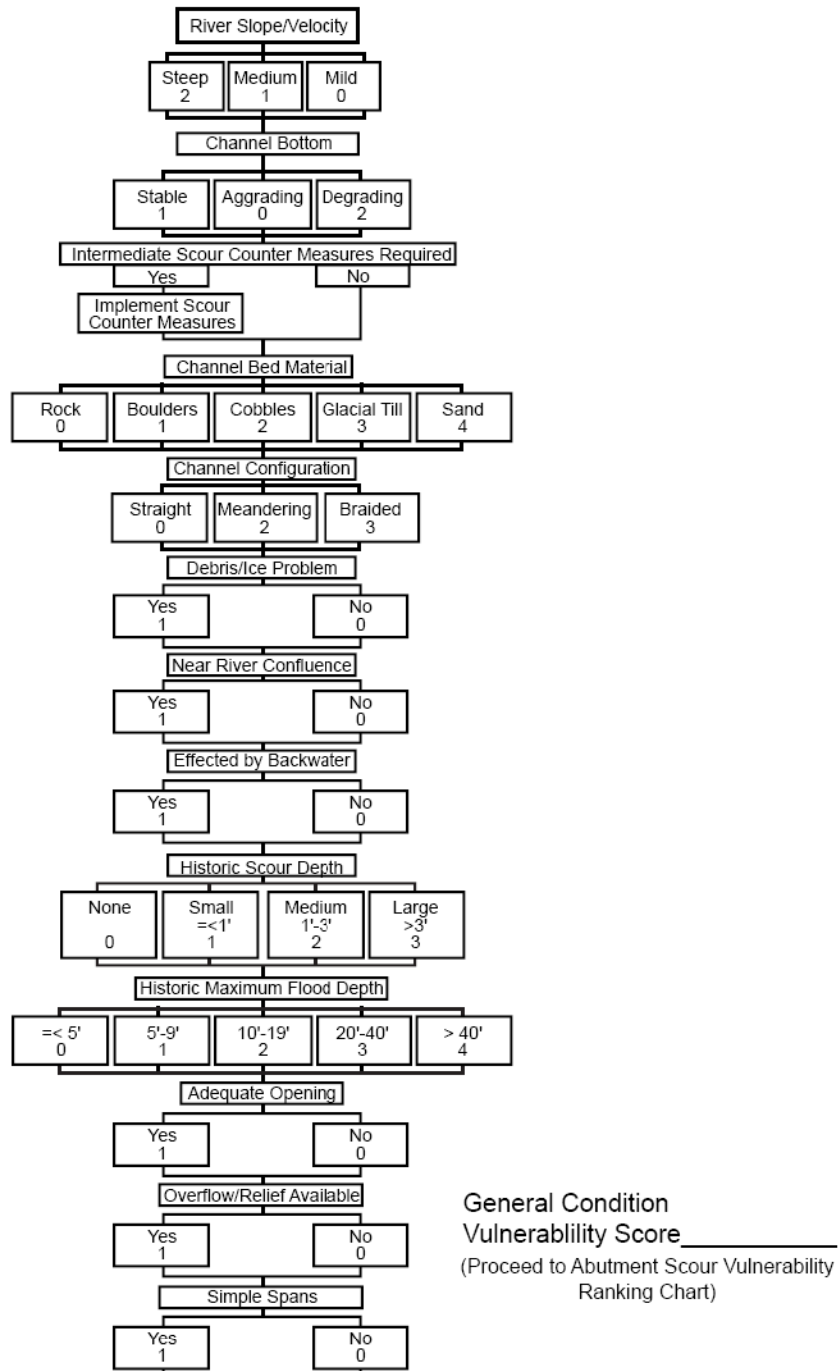
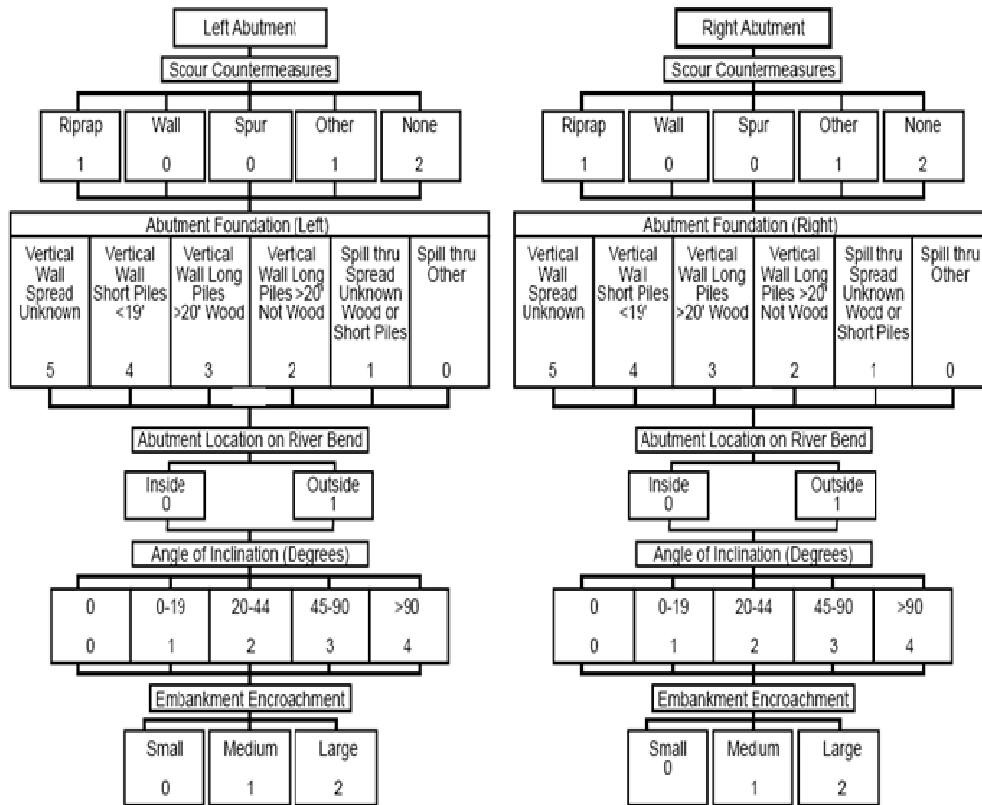


Figure 2-7. General Conditions Scour Vulnerability Ranking Flowchart (after Colorado Highway Department 1990).



Left Abutment
Vulnerability Score _____

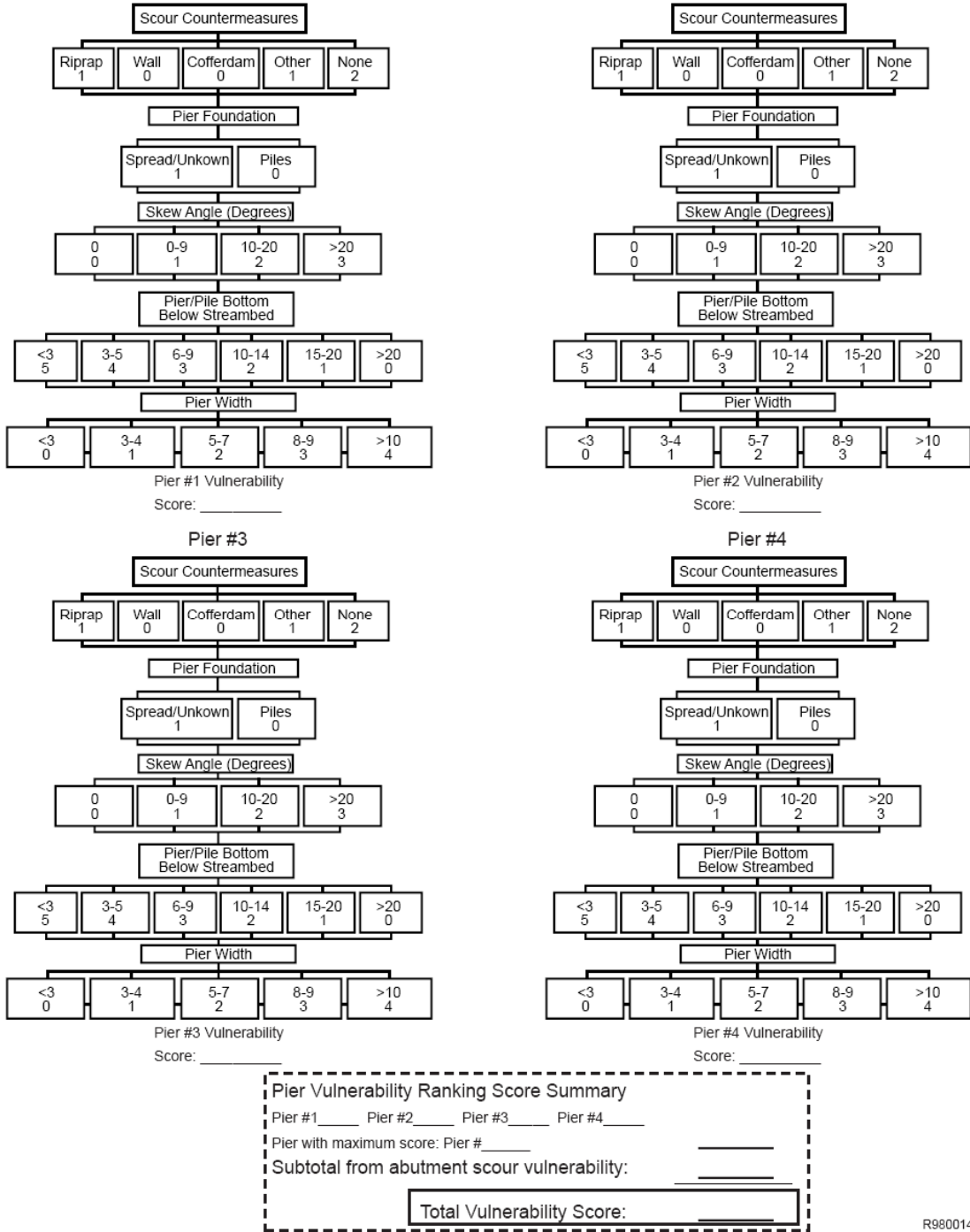
Right Abutment
Vulnerability Score _____

Left and Right are established looking downstream

Abutment Scour Vulnerability
 Left Abutment _____ Right Abutment _____ Total _____
 General Conditions Vulnerability Score _____ Total _____
 Subtotal _____
 (Final score if there are points)

Proceed to Pier Scour Vulnerability Ranking Flow Chart if Necessary

Figure 2-8. Abutment Scour Vulnerability Ranking Flowchart (after Colorado Highway Department 1990).



R9800148

Figure 2-9. Pier Scour Vulnerability Ranking Flowchart (after Colorado Highway Department 1990).

[Kattell and Eriksson \(1998\)](#) developed a bridge scour evaluation procedure for the United States Department of Agriculture Forest Service, which covered a screening process, scour analysis, and countermeasures. This procedure has four steps as indicated below:

1. office screening and management priority analysis;
2. field review, scour vulnerability analysis, and prioritizing;
3. detailed scour evaluation; and
4. plan of action.

Steps 1 and 2 are similar to the more qualitative assessment procedures as described in the preceding sections. In fact, the method proposed by [Kattell and Eriksson \(1998\)](#) utilizes the Colorado Highway Department flowcharts and also recommends the USGS rapid estimation procedure. Step 3 in the method follows the guidelines in HEC-18 ([Richardson and Davis 2001](#)).

[Palmer et al. \(1999\)](#) at the University of Washington developed an expert system for evaluation of scour and stream stability. Their method, termed Cataloging and Expert Evaluation of Scour Risk and River Stability at Bridge Sites (CAESAR), is a field-deployable decision support system that helps bridge inspectors identify probable scour risks and assess the bridge sites economically ([Harmsen et al. 2001](#)). [Harmsen et al. \(2001\)](#) go on to state that the purpose of the expert system is to:

1. determine the scour risk of a bridge based on site observations and history; and
2. catalog, store, and retrieve information pertaining to the bridge site conditions.

The CAESAR expert system is based on user input information such as the presence of bank countermeasures and associated damage, evidence of localized erosion, accumulation of debris, and bed cross-section profile. The system relies on a rule base that determines if measures to mitigate scour damage are required. It uses knowledge and expertise obtained from existing literature including HEC-18 ([Richardson and Davis 2001](#)) and HEC-20 ([Lagasse et al. 1995](#)), and from experienced professionals in the field of bridge inspection, river hydraulics, and geomorphology to draw conclusions about the site based upon bridge construction information and characteristics, and inspection records ([Harmsen et al. 2001](#)). This knowledge base was

developed mainly through surveys and extensive interviews with experts (Adams et al. 1995). The key feature of the CAESAR expert system is the logic that is employed to reach a conclusion describing the scour risk of the bridge. As mentioned above, existing literature and the views of scour experts were used to develop this logic, which has been encoded in a Bayesian network to account for the lack of confidence in the qualitative input of the bridge inspector. Harmsen et al. (2001) and Palmer et al. (1997) give more detailed descriptions of the logic and Bayesian network in the CAESAR expert system.

Other states, such as Missouri (Huizinga and Rydlund 2004) and California (California Department of Transportation 2007) have adopted similar scour assessment procedures. These methods either are similar to the more qualitative forms of assessments described in the preceding sections or use detailed maximum scour depth calculations based on HEC-18 (Richardson and Davis 2001). The Massachusetts Highway Department uses a bridge inspection data collection, storage, and distribution system called the Integrated Bridge Inspection Information System (IBIIS), which was not initially developed for the purpose of scour risk determination (Harmsen et al. 2001, Leung and Albert 1996).

2.2.7. Limitations of Current Assessment Methods

The current methods of bridge scour assessment have several limitations. The procedures that fall within the category of a Level 1 analysis are qualitative in nature and dependent upon the inspector that is carrying out the inspection. Additionally, these methods, including those assigning a scour index to bridges, do not actually assess the current scour condition and probable future state of the bridge against the capacity of the bridge foundations. This could be dangerous because a qualitative inspection may not identify the bridge foundation in terms of its safety factor against failure. For procedures falling within the category of a Level 2 and Level 3 analysis, the most evident limitation is the use of the HEC-18 (Richardson and Davis 2001) method for the determination of maximum scour depth in clays and some rocks. The sole use of the maximum scour depth tends to be overly conservative and lead to the designation of actually stable bridges as scour-critical bridges. The method proposed by Briaud et al. (1999, 2005) termed the SRICOS Method, which will be discussed in the next section, overcomes this shortcoming by introducing a time-dependent scour depth. This method, however, requires site-specific erosion testing. Note that this methodology applies to clear-water scour and does not

simulate live bed scour. Furthermore it does not include infilling. In this sense, this is a conservative prediction of scour depth. A comparison between pier scour depths obtained from the HEC-18 method, which considers the soil at the bridge site as fine sand, and the SRICOS Method for poorly graded sand (SP), low plasticity clay (CL) and high plasticity clay (CH) is shown in Figure 2-10. In this case, the pier being considered is 5 ft (1.5 m) and the upstream velocity is 10 ft/s (3.1 m/s).

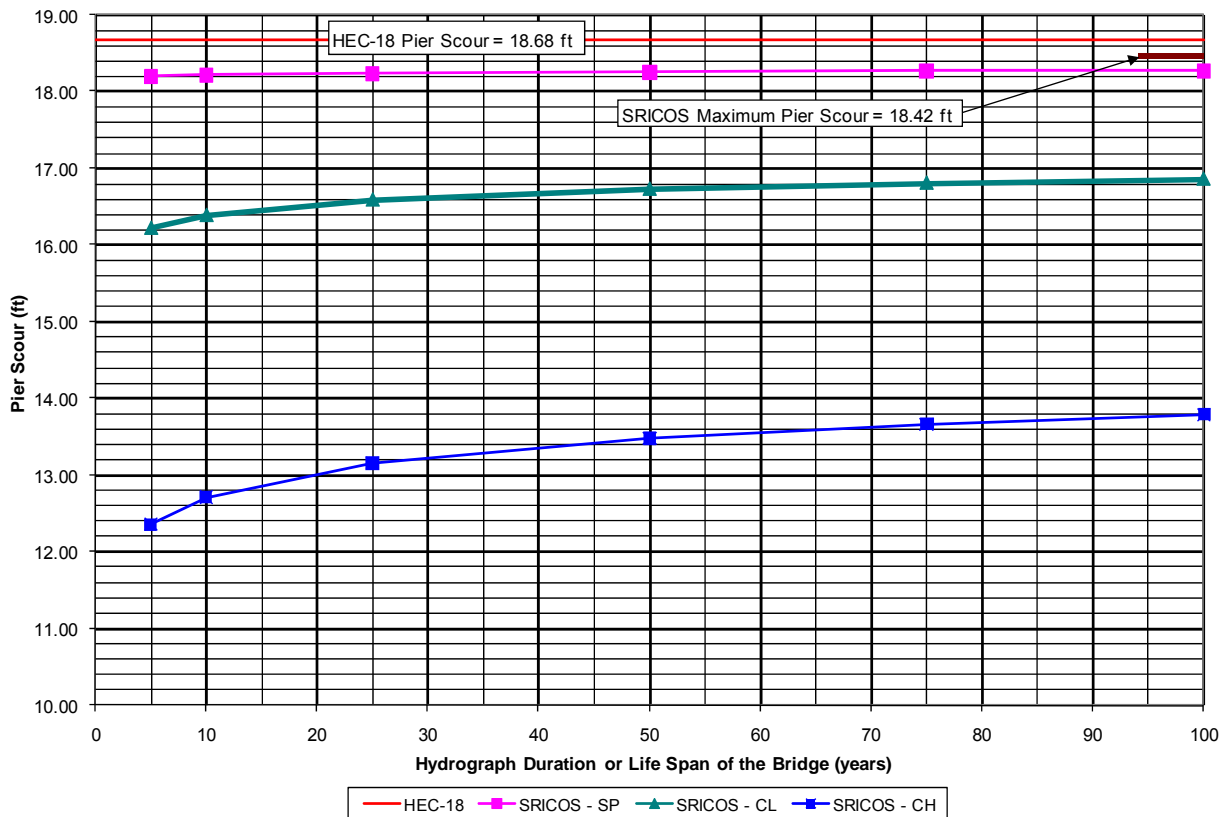


Figure 2-10. Comparison between HEC-18 and the SRICOS Method.

If it is assumed that the scour process is stopped when the critical shear stress is reached at the bottom of the hole, then it is clear that sands and clays do not scour to the same depth and that a soil property must be included in any maximum depth of scour equation. This is why the initial work of Briaud et al. 2001 has been revised in projects NCRHP 24-15 (NCHRP Report 516, Briaud et al. 2004) and NCHRP 24-15(2) (upcoming report, Briaud et al. 2009).

2.2.8. The SRICOS-EFA Method for Bridge Piers

Briaud et al. (1999) developed a method to predict the scour depth versus time curve around a cylindrical pier founded in clay. This method, termed the SRICOS-EFA Method for bridge piers, is employed in development and application of BSA 2 and BSA 3. The procedure involves obtaining soil samples at the bridge site and testing it in the EFA to obtain the erosion function (Briaud et al. 2001a). Further analysis is carried out based on the erosion function to determine the scour depth versus time curve around the bridge pier. This procedure is described as follows (Briaud et al. 1999):

1. Obtain samples at the bridge site, as close as possible to the pier and within the estimated maximum scour depth, $Z_{\max,p}$.
2. Test the samples in the EFA to obtain the erosion function, i.e., the scour rate \dot{Z} , versus the applied hydraulic shear stress, τ . In addition to this, the EFA test also provides the scour rate \dot{Z} versus velocity V curve.
3. Predict the maximum shear stress, τ_{\max} , which will be induced around the pier by the flowing water, prior to the initiation of scour at the pier. The maximum pier scour depth is the maximum scour that can take place at the pier under the given flow condition and is independent of time. It is given by:

$$\tau_{\max,p} = 0.094\rho V_{\text{appr}}^2 \left(\frac{1}{\log R_e} - \frac{1}{10} \right) \quad (2.1)$$

where the Reynolds Number, R_e , is defined as $V_{\text{appr}}D/\nu$, V_{appr} is the mean upstream approach velocity, D is the pier diameter, and ν is the kinematic viscosity of water ($10^{-6} \text{ m}^2/\text{s}$ at 20° C). Equation (2.1) is obtained from numerical simulations and is detailed in Wei et al. (1997).

4. Use the measured \dot{Z} versus τ (or V) curve to obtain the initial scour rate, \dot{Z}_i , corresponding to τ_{\max} . This is illustrated in Figure 2-10.

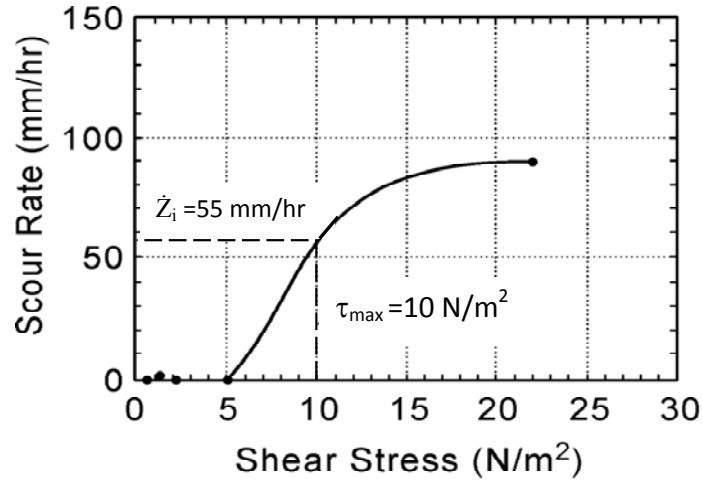


Figure 2-11. Initial Erosion Rate.

5. Predict the maximum depth of per scour, $Z_{\max,p}$, using the following equation:

$$Z_{\max,p}(\text{mm}) = 0.18 \text{Re}^{0.635} \quad (2.2)$$

Equation (2.2) is obtained from a series of flume tests in clay and is described in detail in Gudavalli et al. (1997).

6. Use \dot{Z}_i and $Z_{\max,p}$ to develop the hyperbolic function describing the scour depth Z versus time t curve. The hyperbolic function is:

$$Z_{\text{fin},p} = \frac{t}{\frac{1}{\dot{Z}_i} + \frac{t}{Z_{\max,p}}} \quad (2.3)$$

where $Z_{\text{fin},p}$ is the pier scour depth corresponding to a given time t and is termed the final pier scour depth.

2.2.9. The SRICOS-EFA Method for Bridge Contractions

Briaud et al. (2005) developed a method to predict the scour depth versus time curve in a contracted channel when water flows at a constant velocity. This method, termed the SRICOS-EFA Method for bridge contractions, is employed in BSA 2 and BSA 3. Similar to the SRICOS-EFA Method for bridge piers, this procedure also involves obtaining soil samples at the

bridge site and testing them in the EFA to obtain the erosion function (Briaud et al. 2001a). Further analysis is carried out based on the erosion function to determine the scour depth versus time curve in the contracted channel. This procedure is described as follows (Briaud et al. 2005):

1. Obtain samples at the contracted bridge section within the estimated maximum scour depth, $Z_{\max,c}$.
2. Test the samples in the EFA to obtain the erosion function, i.e., the scour rate \dot{Z} , versus the applied hydraulic shear stress, τ . In addition to this, the EFA test also provides the scour rate \dot{Z} versus velocity V curve.
3. Calculate the maximum contraction scour depth, $Z_{\max,c}$, for a given velocity using the following equation:

$$Z_{\max,c} = 1.90H_1 \left(1.38 \frac{B_1}{B_2} F - F_c \right) \quad (2.4)$$

where H_1 is the upstream water depth, B_1 is the uncontracted channel width, B_2 is the contracted channel width (Figure 2-11), F is the Froude Number defined as $V_{\text{appr}}/(gH_1)^{0.5}$, F_c is the critical Froude Number defined as $V_c/(gH_1)^{0.5}$, V_{appr} is the mean approach velocity, V_c is the critical velocity of the soil, and g is the acceleration due to gravity.

4. Calculate the maximum shear stress, $\tau_{\max,c}$, which will be induced at the contracted section by the flowing water, prior to the initiation of contraction scour. The maximum contraction scour depth is the maximum scour that can take place at the contracted section under the given flow condition and is independent of time. It is given by:

$$\tau_{\max,c} = k_R k_\theta k_H k_L \gamma_w n^2 V_{\text{appr}}^2 R_h^{-0.33} \quad (2.5)$$

where k_R = contraction ratio factor = $0.62 + 0.38\left(\frac{B_1}{B_2}\right)^{1.75}$

k_θ = transition angle factor = $1 + 0.9\left(\frac{\theta_1}{90}\right)^{1.5}$

k_L = contraction length factor

$$= \begin{cases} 1 & , \text{for } \left(\frac{L}{B_1 - B_2}\right) \geq 0.35 \\ 0.77 + 1.36\left(\frac{L}{B_1 - B_2}\right) - 2\left(\frac{L}{B_1 - B_2}\right)^2 & , \text{for } \left(\frac{L}{B_1 - B_2}\right) < 0.35 \end{cases}$$

k_H = water depth factor = 1

R_h = hydraulic radius

$$= \frac{A}{P}$$

where A is the flow area and P the wetted perimeter in the uncontracted zone

γ_w = unit weight of water

5. Use the measured \dot{Z} versus τ (or V) curve to obtain the initial scour rate, \dot{Z}_i , corresponding to $\tau_{\max,c}$. This is illustrated in [Figure 2-11](#).
6. Use \dot{Z}_i and $Z_{\max,p}$ to develop the hyperbolic function describing the scour depth Z versus time t curve. The hyperbolic function is:

$$Z_{\text{fin},c} = \frac{t}{\frac{1}{\dot{Z}_i} + \frac{t}{Z_{\max,c}}} \quad (2.6)$$

where $Z_{\text{fin},c}$ is the contraction scour depth corresponding to a given time t and is termed the final contraction scour depth.

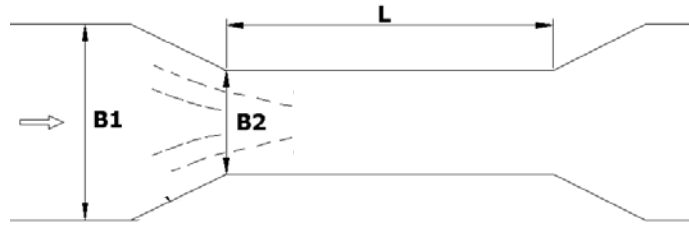


Figure 2-12. Contracted and Uncontracted Widths (after Briaud et al. 2005).

2.2.10. The SRICOS-EFA Method for Bridge Abutments

The SRICOS-EFA Method for bridge abutments is being finalized at Texas A&M University under a recently concluded NCHRP research project (Briaud et al. 2009, in progress).

2.2.11. Concept of Equivalent Time

2.2.11.1. Equivalent Time for Bridge Piers

The concept of equivalent time (t_e) was first developed for pier scour by Briaud et al. (2001b), who define it as the time required for the maximum velocity in the hydrograph, V_{max} , to create the same scour depth as the one created by the complete hydrograph. The equivalent time concept was needed to enable a simple calculation of time-dependent scour depth, rather than carrying out more complex hydrograph-based scour analysis. The steps in the development of equivalent time for bridge piers are as follows (after Briaud et al. 2004):

1. Soil samples were collected at each bridge site in Shelby tubes and tested in the EFA to obtain the erosion function, \dot{Z} versus τ .
2. The hydrograph from the nearest gage station was obtained, and the SRICOS program (Briaud et al. 1999, 2005) was used to calculate the scour depth.
3. The scour depth using the SRICOS program was entered into Equation (2.6) with the corresponding \dot{Z}_i and Z_{max} values in order to obtain $t_{e,p}$. The value for \dot{Z}_i was obtained from the average \dot{Z} versus τ curve within the final scour depth by reading the \dot{Z} value corresponding to τ_{max} , which was obtained from Equation (2.1). In Equation (2.1) the pier

diameter, B , and the maximum velocity appearing in the hydrograph, V_{\max} , over the period of interest was used. The value for Z_{\max} was obtained from Equation (2.2), using the same values for pier diameter and velocity that were used in Equation (2.1).

4. The single hydrograph at a bridge site was further broken down into smaller units that themselves were considered hydrographs. This process was done for all eight bridge sites investigated. This process generated 55 cases. The equivalent time for the bridge piers, $t_{e,p}$, was developed utilizing the various cases obtained.
5. The equivalent time obtained from the steps described above was then correlated to the duration of the hydrograph (t_{hyd}), the maximum hydrograph velocity (V_{\max}), and the initial erosion rate (\dot{Z}_i). A multiple regression was performed on the data and yielded the following relationship:

$$t_{e,p}(\text{hr})=73\left[t_{\text{hyd}}(\text{years})\right]^{0.126}\left[V_{\max}(\text{m/s})\right]^{1.706}\left[\dot{Z}_i(\text{mm/hr})\right]^{-0.20} \quad (2.7)$$

The regression coefficient for Equation (2.7) was 0.77. A comparison between the pier scour depth using the complete hydrograph input (termed Extended SRICOS) and the pier scour depth obtained from the equivalent time method (Simple SRICOS) was compared and is presented in Figure 2-13.

The equivalent time as presented in Equation (2.7) can be used to calculate the pier scour depth at the end of a given hydrograph just by applying the maximum velocity, initial scour rate, and hydrograph duration. The equivalent time equation for pier scour is limited to the database from which it was derived. This database included hydrographs that were anywhere from 3 to 50 years in duration and for 7 Texas rivers.

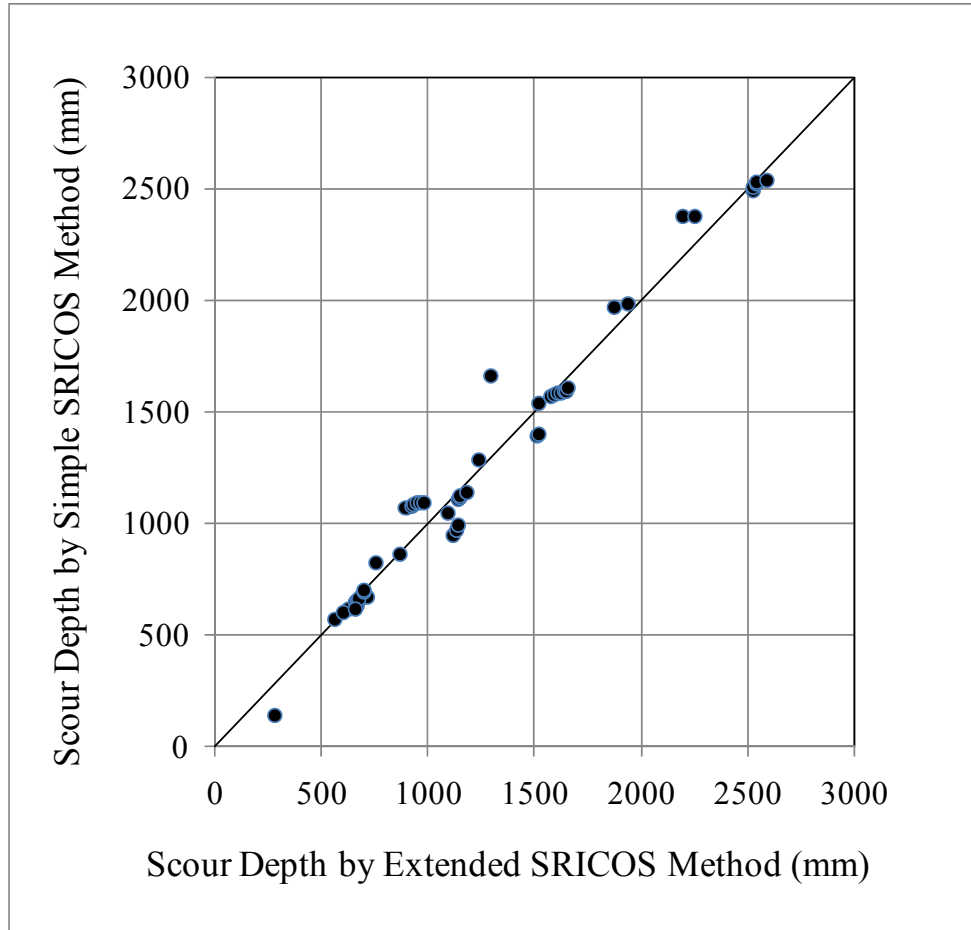


Figure 2-13. Comparison of Pier Scour Depth Using Extended SRICOS and Simple SRICOS Methods (after Briaud et al. 2001b).

2.2.11.2. Equivalent Time for Bridge Contractions

The equivalent time for contraction scour, $t_{e,c}$, was developed by Wang (2004). It was developed using a method similar to the one used for the development of equivalent time for bridge piers. Wang (2004) used 6 bridge sites, which generated 28 cases by segmenting the hydrographs for the 6 bridges, in addition to using the complete hydrograph. The initial rate of scour (\dot{Z}_i) was determined from the erosion function at a shear stress corresponding to τ_{max} obtained from Equation (2.5). Multiple regression was performed on the data, and the following equation was obtained:

$$t_{e,c} \text{ (hr)} = 644.32 [t_{\text{hyd}} \text{ (years)}]^{0.4242} [V_{\text{max}} \text{ (m/s)}]^{1.648} [\dot{Z}_i \text{ (mm/hr)}]^{-0.605} \quad (2.8)$$

The regression coefficient for Equation (2.8) was 0.965. A comparison between the contraction scour depth using the complete hydrograph input (termed SRICOS-EFA) and the contraction scour depth obtained from the equivalent time method (Simple SRICOS-EFA) was compared and is presented in Figure 2-14.

The equivalent time as presented in Equation (2.8) can be used to calculate the contraction scour depth at the end of a given hydrograph just by applying the maximum velocity and initial scour rate and hydrograph duration. The equivalent time equation for contraction scour is limited to the database from which it was derived. This database included hydrographs which were anywhere from 2 to 35 years in duration and for 6 Texas rivers.

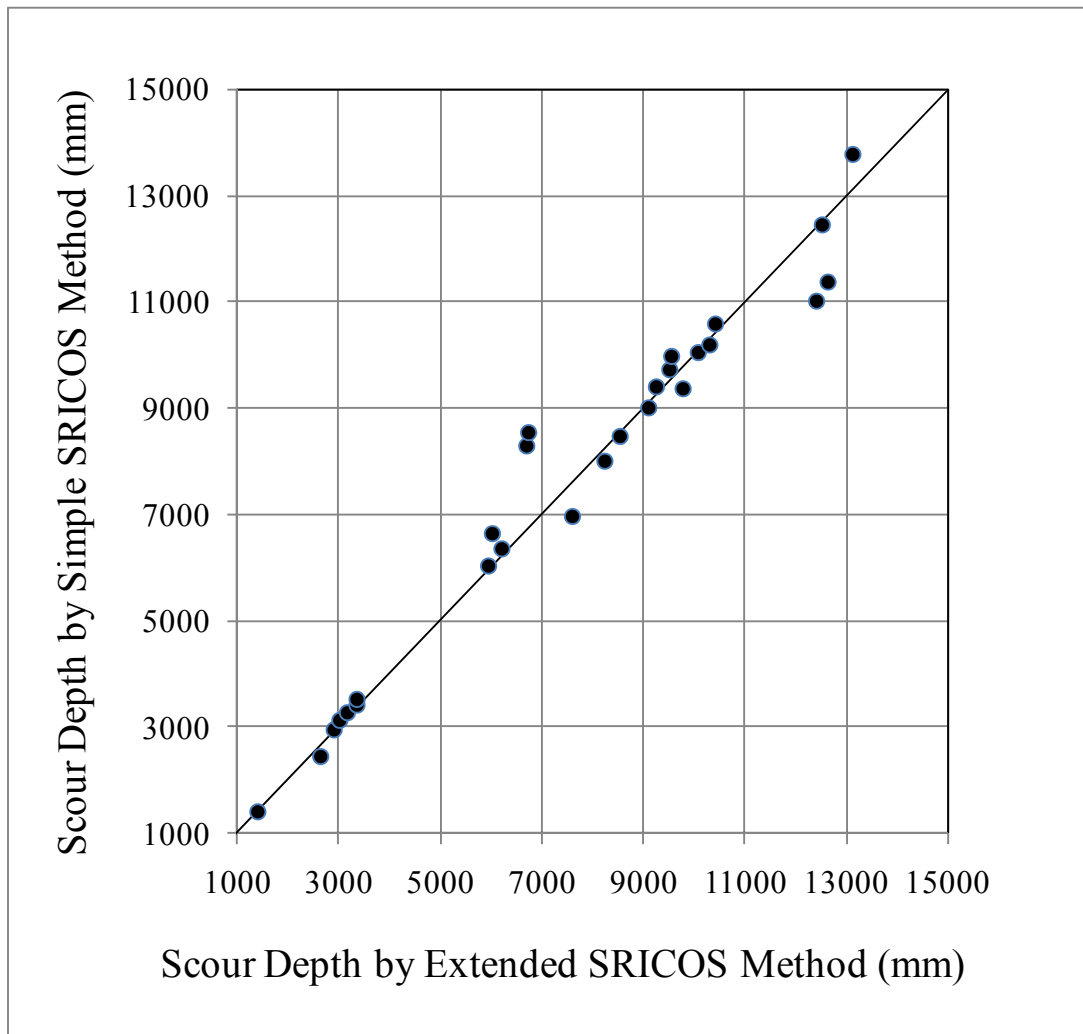


Figure 2-14. Comparison of Contraction Scour Depth Using SRICOS-EFA and Simple SRICOS-EFA Methods (after Wang 2004).

2.3. THE HEC-18 ABUTMENT SCOUR EQUATIONS

Two types of abutment scour equations are employed in BSA 2 to compute the maximum abutment scour depth, $Z_{\max,a}$. These equations are Froehlich's live-bed abutment scour equation (Froehlich 1989a,) and the HIRE live-bed abutment scour equation (Richardson and Davis 2001). Richardson and Davis (2001) recommend these equations for both live-bed and clear-water abutment scour conditions.

2.3.1. Froehlich's Live-Bed Abutment Scour Equation

The Froehlich's equation was developed based on a compilation of measurements from several laboratory studies of local scour at bridge abutments. A total of 170 live-bed measurements compiled for maximum depth of local scour at model bridge abutments were assembled and analyzed (Froehlich 1989, Richardson and Davis 2001). The equation proposed by Froehlich (1989) is as follows:

$$z_{\max, a} / y_a = 2.27K_1K_2(L' / y_a)^{0.43} F^{0.61} \quad (2.9)$$

where L' is the length of active flow obstructed by the embankment, y_a is the average depth of flow on the floodplain defined as A_e/L , A_e is the flow area of the approach cross section obstructed by the embankment, L is the length of embankment projected normal to the flow (Figure 2-15), and F is the Froude number of approach flow upstream of the abutment. K_1 is the abutment shape coefficient (Figure 2-16 and Table 2-4), and K_2 is the coefficient for angle of embankment to flow defined as $(\theta/90)^{0.13}$ (Figure 2-15).

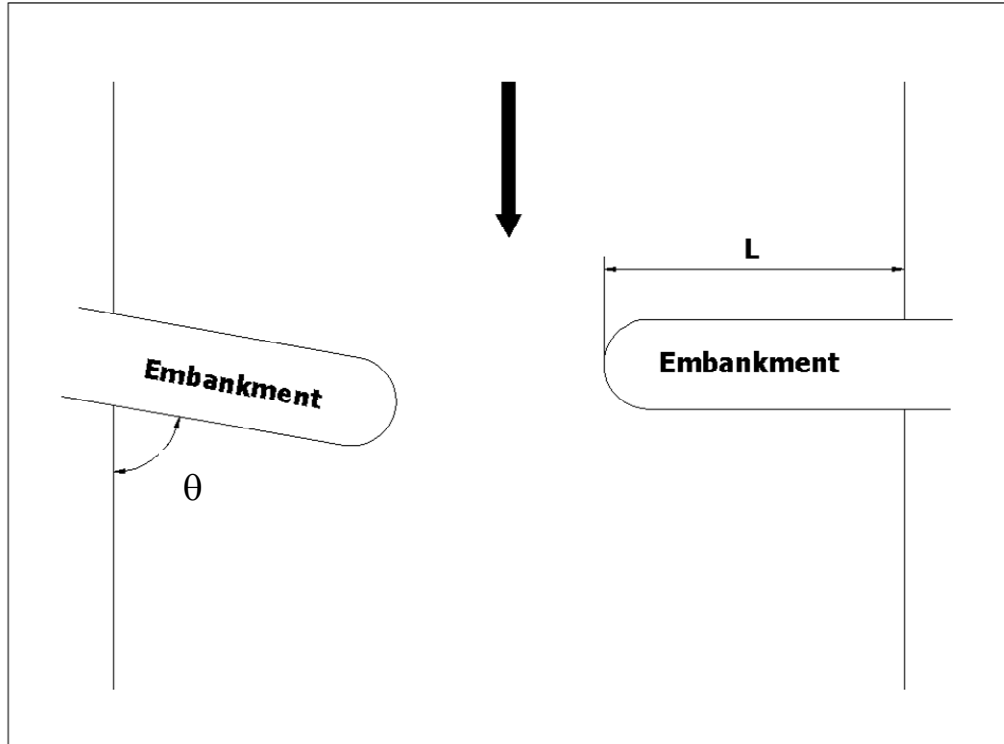


Figure 2-15. Some Abutment Scour Parameters.

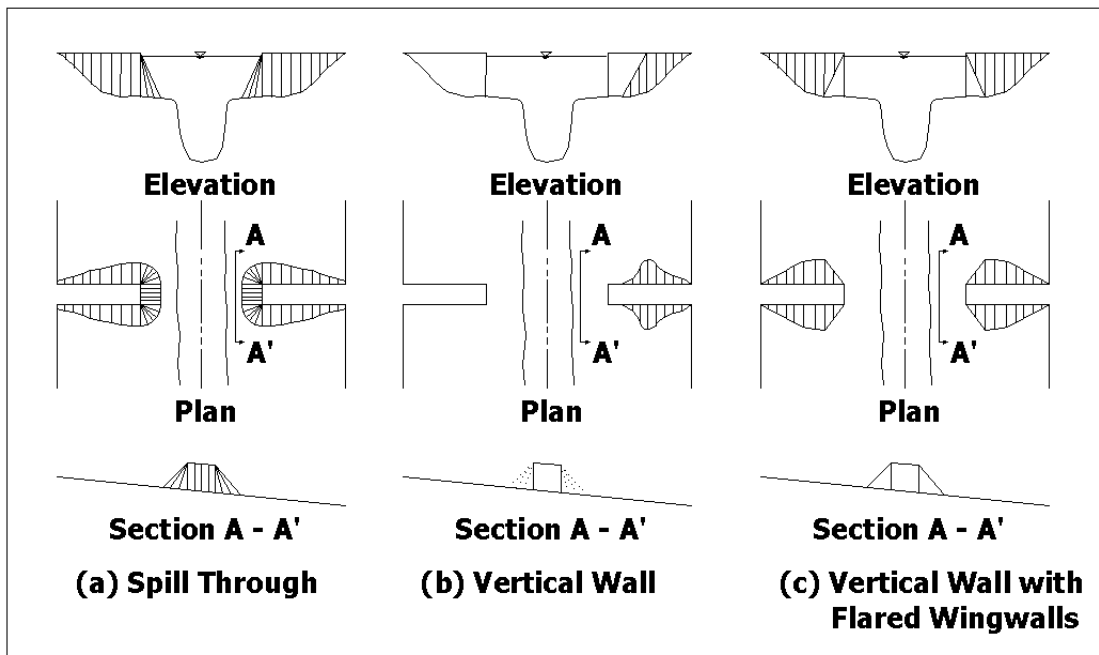


Figure 2-16. Abutment Shapes (after Richardson and Davis 2001).

Table 2-4. Abutment Shape Coefficients (after Richardson and Davis 2001).

Abutment Shape Coefficients	
Description	K_1
Vertical-wall abutment	1.00
Vertical-wall abutment w/wing walls	0.82
Spill-through abutment	0.55

2.3.2. The HIRE Live-Bed Abutment Scour Equation

The HIRE equation is a modified equation of an equation based on field scour data at the end of spurs in the Mississippi River obtained by the United States Army Corps of Engineers (USACE) (Richardson et al. 2001). The HIRE equation is applicable when the ratio of the projected abutment length, L , to the flow depth, y_1 , is greater than 25. The HIRE equation is given by Richardson and Davis (2001) as follows:

$$z_{\max, a} \text{ (m)} = 4y_1 Fr^{0.33} K_1 K_2 / 0.55 \quad (2.10)$$

where y_1 is the depth of flow at the abutment on the overbank or in the main channel, F is the Froude Number based on the velocity and depth adjacent to and upstream of the abutment, K_1 is the abutment shape coefficient (Figure 2-16 and Table 2-4), and K_2 is the coefficient for skew angle of abutment flow as calculated for Froehlich's equation (Figure 2-15).

3. ERODIBILITY CHARTS

3.1. INTRODUCTION

The erodibility of soil or rock is defined as the relationship between the erosion rate, \dot{Z} , and the velocity of water, V , at the soil/rock–water interface. This definition, however, is not very satisfactory because the velocity varies in direction and intensity in the flow field (Briaud 2008). To be exact, the velocity of water is zero at the soil/rock interface. A more adequate definition is the relationship between erosion rate \dot{Z} and shear stress at the soil/rock interface and is given by:

$$\frac{dZ}{dt} = \dot{Z} = f(\tau) \quad (3.1)$$

$$\frac{dZ}{dt} = \dot{Z} = f(V) \quad (3.2)$$

However, the velocity is often used because it is easier to gauge an erosion problem from a velocity standpoint. In this report, the methods to obtain scour depth are primarily based on velocity. These methods were developed by previous researchers and presented in terms of velocity (Briaud et al. 1999, 2005; Richardson and Davis 2001; Froehlich 1989b).

Briaud (2008) describes erodible materials according to three material categories: soil, rock, and intermediate geomaterials. Here soil is defined as an earth element that can be classified by the USCS, and rock is defined as an earth element that has a joint spacing of more than 0.3 ft (0.1 m) and an unconfined compressive strength of the intact rock core of more than 10445 psf (500 kPa). Intermediate geomaterials are materials whose behavior is intermediate between soils and rocks, such as cobbles, boulders, and riprap. The erosion of rock occurs through two main processes, rock substance erosion and rock mass erosion. Briaud (2008) defines rock substance erosion as the erosion of rock material itself and rock mass erosion as the removal of blocks from the jointed rock mass. In the case of rock mass erosion, the material making up the rock blocks is the one being eroded.

3.2. FACTORS INFLUENCING EROSION RESISTANCE

The erodibility of geomaterials can vary significantly according to their properties as well as the properties of the water flowing over the soil. The soil properties influencing erodibility are listed in [Table 3-1](#).

Table 3-1. Some Soil Properties Influencing Erodibility (after [Briaud 2008](#)).

Soil water content	Soil dispersion ratio
Soil unit weight	Soil cation exchange capacity
Soil plasticity index	Soil sodium absorption rate
Soil undrained shear strength	Soil pH
Soil void ratio	Soil temperature
Soil swell	Water temperature
Soil mean grain size	Water salinity
Soil percent passing #200 sieve	Water pH
Soil clay minerals	

As mentioned above, erodibility is a function, and therefore attempts at correlating conventional soil properties such as plasticity index, undrained shear strength, percent passing #200 sieve, water content, and unit weight with the erosion resistance can only be made for elements of the erosion function such as the critical shear stress (and critical velocity) and the initial slope of the erosion function. Such correlations were attempted by [Cao et al. \(2002\)](#) and are presented in [Figure 3-1](#) and [Figure 3-2](#).

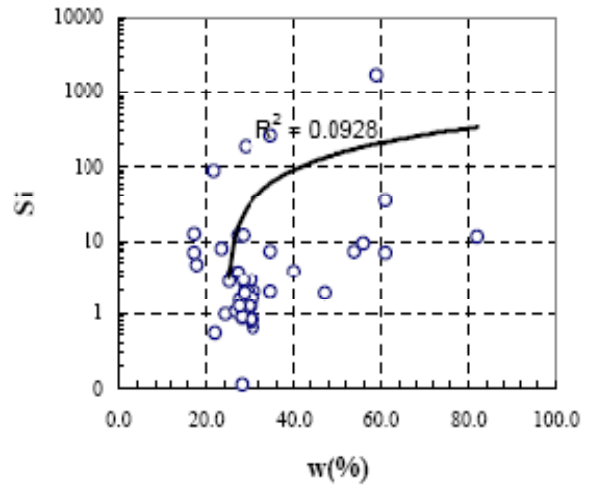
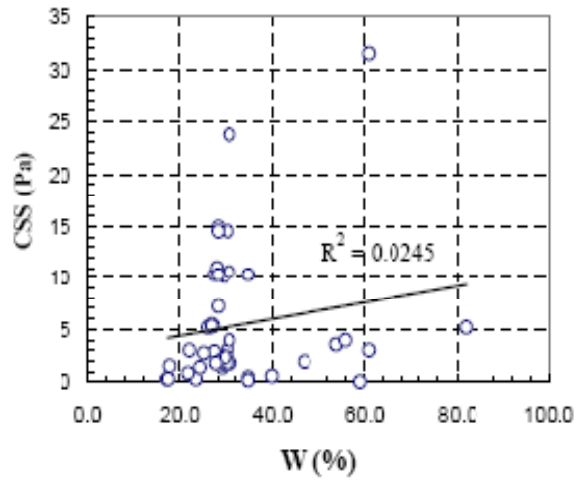


Figure 3-1. Failed Attempts at Correlating the Critical Shear Stress and Initial Slope with Water Content (Cao et al. 2002).

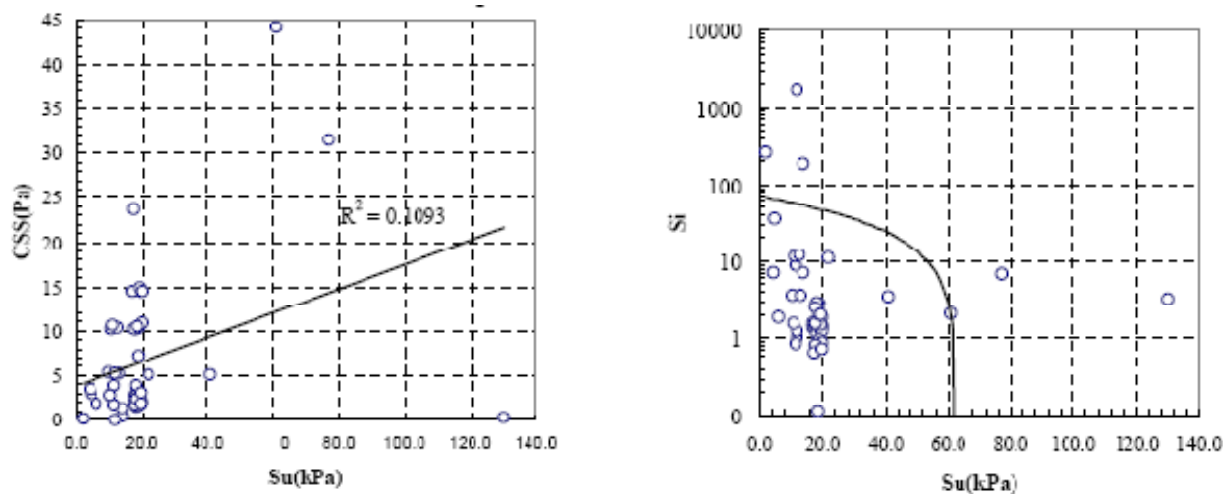


Figure 3-2. Failed Attempts at Correlating the Critical Shear Stress and Initial Slope with Undrained Shear Strength (Cao et al. 2002).

Since attempts at obtaining a reasonable correlation between erosion resistance and soil properties failed, it is most preferable to measure the erosion function directly in an apparatus such as the Erosion Function Apparatus (Briaud et al. 2001a). The EFA is a test apparatus that measures the erosion function of a soil, which is the relationship between the soil erosion rate and the applied hydraulic shear stress or velocity. However, direct measurements require soil sampling at the bridge site and can create substantial costs in a bridge scour assessment. Therefore, several charts collectively termed the Erodibility Charts were developed for the purpose of this report. The Erodibility Charts comprise the Erosion Function Charts and the Erosion Threshold Charts. These charts will be introduced and detailed in the remaining sections of this chapter.

3.3. CRITICAL SHEAR STRESS–CRITICAL VELOCITY RELATIONSHIP

The critical shear stress (τ_c) – critical velocity (V_c) relationship was investigated to provide a useful means of interchanging known values of either one of these values with the other. A database comprising 81 EFA tests was used to investigate this relationship. τ_c values were plotted against V_c values and are presented in Figure 3-3. This resulted in a very reasonable relationship

with an R^2 value of 0.96. For simplicity, the relationship between these two parameters is proposed as:

$$\tau_c \text{ (N/m}^2\text{)} = 5[V_c \text{ (m/s)}]^2 \quad (3.3)$$

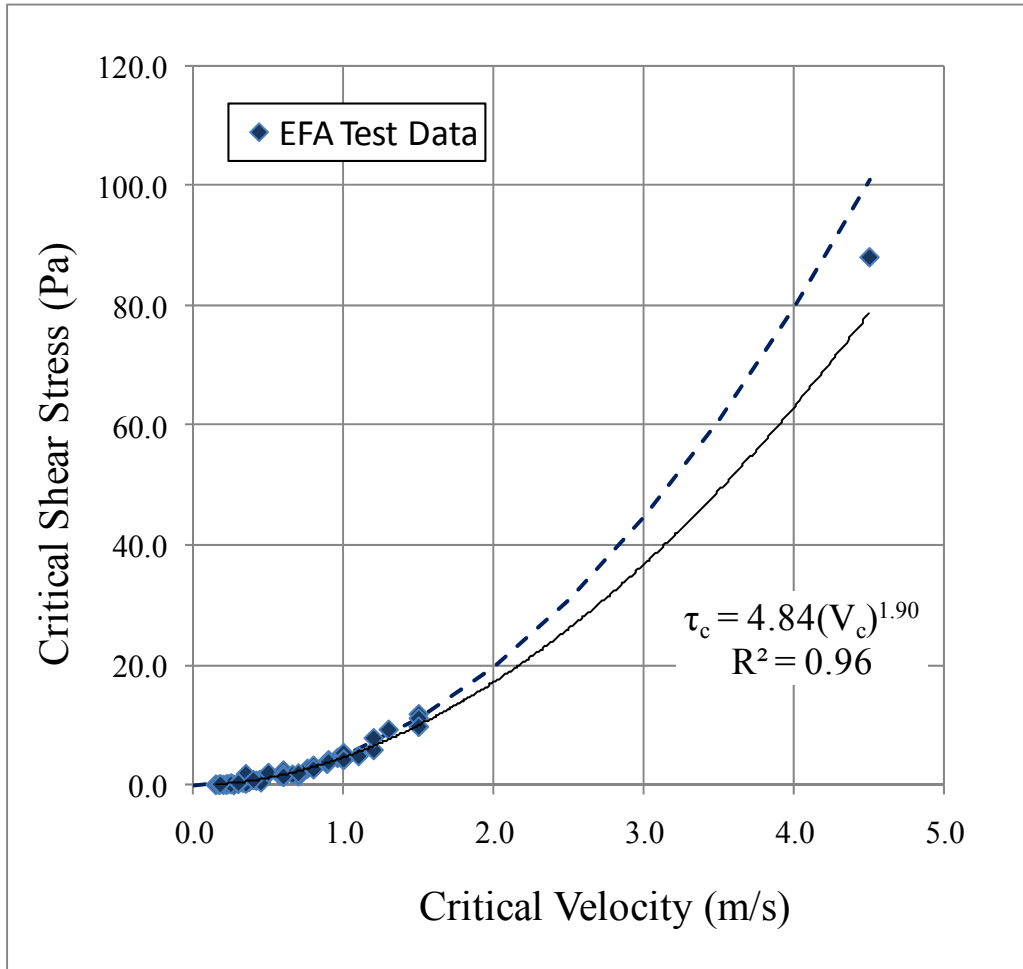


Figure 3-3. Critical Shear Stress–Critical Velocity Relationship.

While τ_c depends mostly on the soil properties, V_c depends also on the water depth in an open channel. The above equation comes from tests in the EFA, which creates a pipe flow. In this case, the water depth is not involved. Calculations using the United States Army Corps of Engineers EM 1601 equation show that ignoring the water depth in calculating the critical

velocity may create a ± 20 percent error for common values of water depth (3.3 ft to 82 ft or 1 m to 25 m).

3.4. THE EROSION FUNCTION CHARTS

3.4.1. Overview

The Erosion Function Charts are charts that show erosion categories demarcated on the \dot{Z} - τ and \dot{Z} - V charts (Figure 3-4 and Figure 3-5). The erosion categories are shown in Table 3-2. These charts were developed on the basis of EFA tests and the experience of the authors. The Erosion Function Charts essentially eliminate the need for site-specific erosion testing for preliminary investigation (Govindasamy et al. 2008). These charts are one way to represent the EFA test data, which is based on erosion categories. Another means of representing the data would be to do so based on the Unified Soil Classification System (USCS). Each of these representations has advantages and disadvantages, because the erosion rate of the soil is a function of many properties (see Table 3-1). Based on the material category in question or the USCS classification of the soil, the user can use the boundaries of these erosion categories or classifications to determine the critical velocity τ_c or critical velocity V_c of the material. The definition of τ_c is the hydraulic shear stress corresponding to an erosion rate of 0.1 mm/hr, and the definition of V_c is the water velocity corresponding to an erosion rate of 0.1 mm/hr. The user can also use these boundaries or the space between them to arbitrarily determine the erosion function of a geomaterial based on engineering judgment. Table 3-2 also shows the values of τ_c and V_c according to erosion categories.

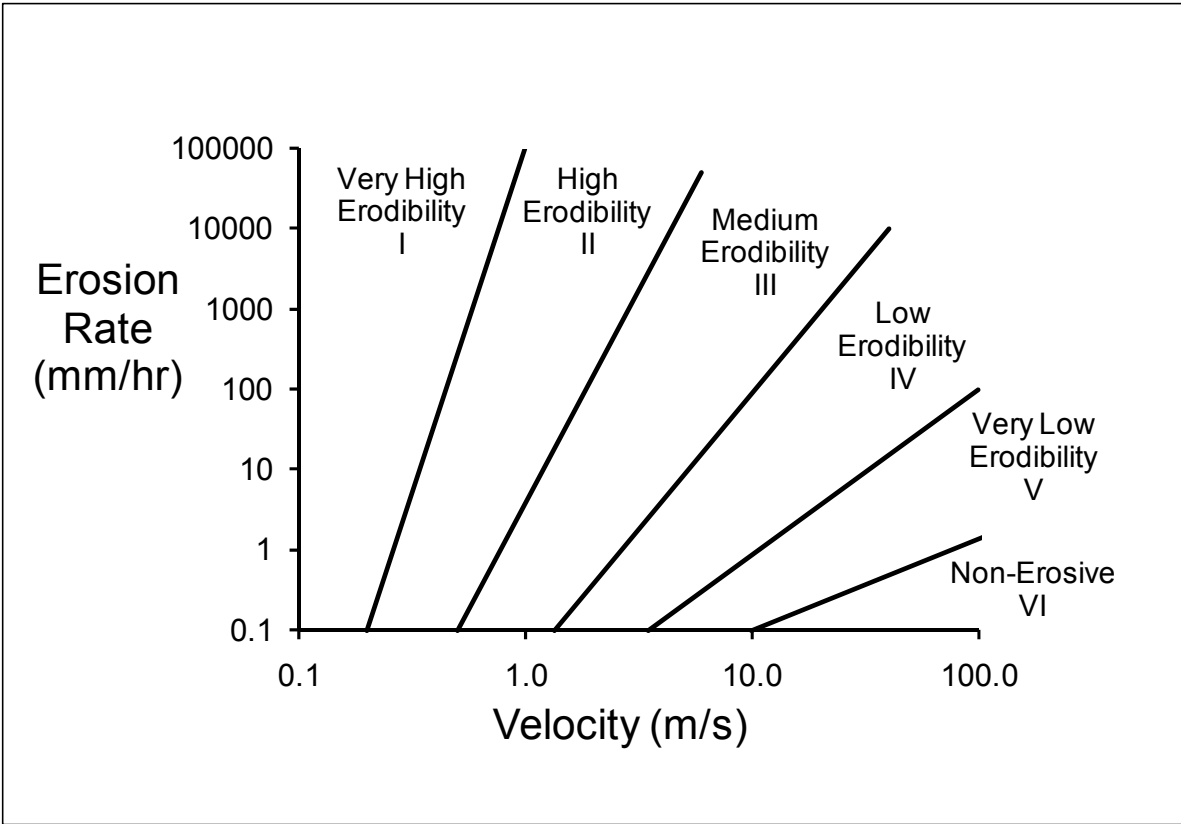


Figure 3-4. Erosion Categories Based on Velocity.

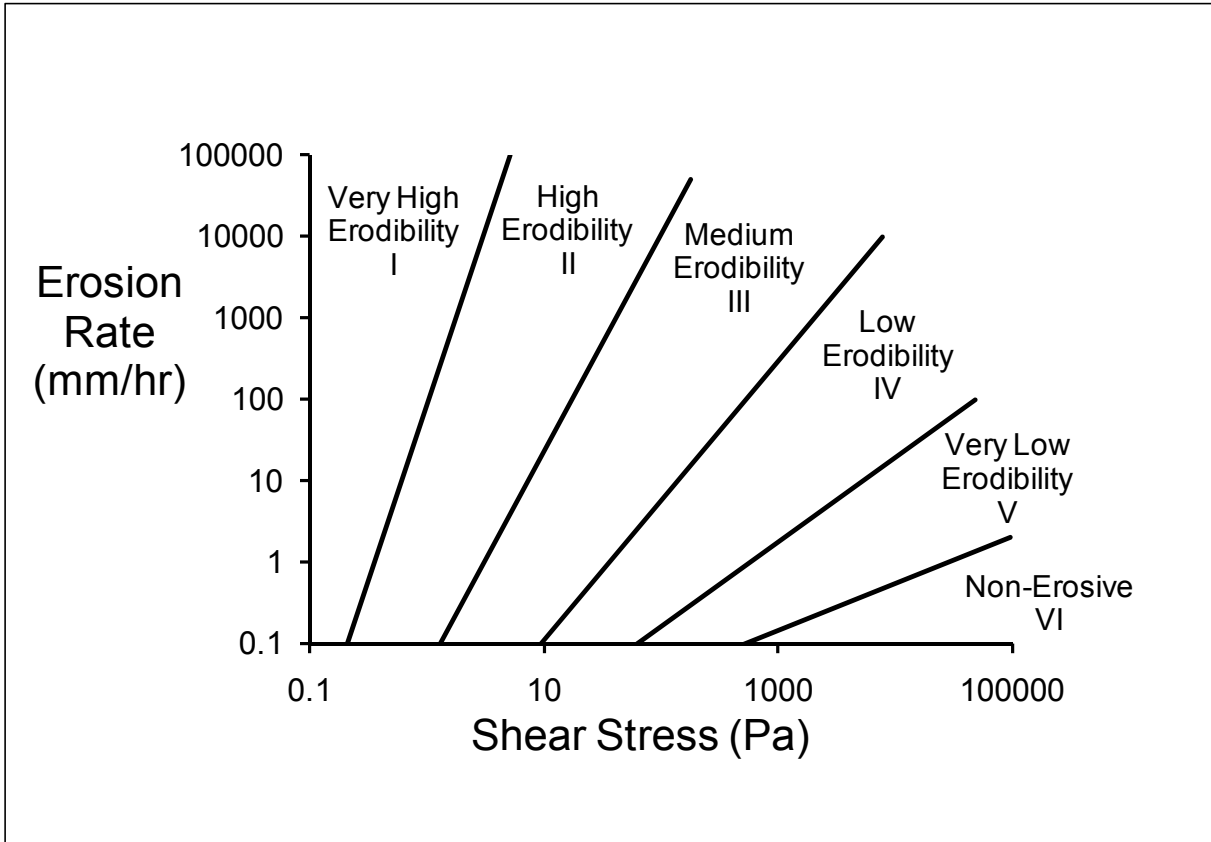


Figure 3-5. Erosion Categories Based on Shear Stress.

Table 3-2. Erosion Categories in the Erosion Function Charts.

Erosion Category	Description	Critical Shear Stress, τ_c (Pa)	Critical Velocity, V_c (m/s)
Category I	Very high erodibility geomaterials	0.1	0.1
Category II	High erodibility geomaterials	0.2	0.2
Category III	Medium erodibility geomaterials	1.3	0.5
Category IV	Low erodibility geomaterials	9.3	1.35
Category V	Very low erodibility geomaterials	62.0	3.5
Category VI	Non-erosive materials	500	10

Note: τ_c and V_c here are defined as the low-end shear stress and velocity of the erosion categories.

3.4.2. Relationship between Selected Geomaterials and the Erosion Function Charts

This report incorporates 81 erosion function tests that were carried out at Texas A&M University and TxDOT laboratories. A summary table of these samples with EFA data and routine soil properties (e.g., index properties, unit weight, undrained shear strength, percent passing #200 sieve, and mean grain size) is presented in [Appendix D](#). These samples were classified using the USCS. From the 81 samples, the following soil categories were obtained:

- low plasticity clay (CL),
- high plasticity clay (CH),
- low plasticity silt (ML),
- high plasticity silt (MH),
- soil intermediate between low plasticity clay and low plasticity silt (CL-ML),
- clayey sand (SC),
- soil intermediate between silty sand and clayey sand (SM-SC),
- poorly graded sand (SP), and
- fine gravel.

These samples were grouped according to their USCS categories and plotted separately on the Erosion Function Charts ([Figure 3-6](#) through [Figure 3-14](#)). This was done to provide a suitable erosion function of a particular material type based on USGS classification on the Erosion Function Charts. It should be noted that the materials do not generally fall distinctly into a single erosion category. The materials generally seem to plot approximately across two categories. The mean and coefficient of variation of the material critical velocity (μ_{V_c} and COV_{V_c}) are indicated in the top right corner of these figures. The remaining five figures do not have this information due to insufficient test data for the corresponding material type. For the CL materials, one data set, i.e., the San Jacinto Layer 2 sample, was ignored in the calculation of the mean and COV since this was considered to be an outlier. For the CH materials, three data sets, i.e., the samples B3-(30-32), EFA-38, and B3-(48-50), were not considered in the calculation of the mean and COV since these were considered to be outliers.

Care should be exercised while selecting the erosion function for a material being investigated. As explained earlier in this chapter, there are many factors that impact erodibility. In cases when these are unknown, it is recommended that the user exercise some caution when selecting the erosion category by selecting conservative values.

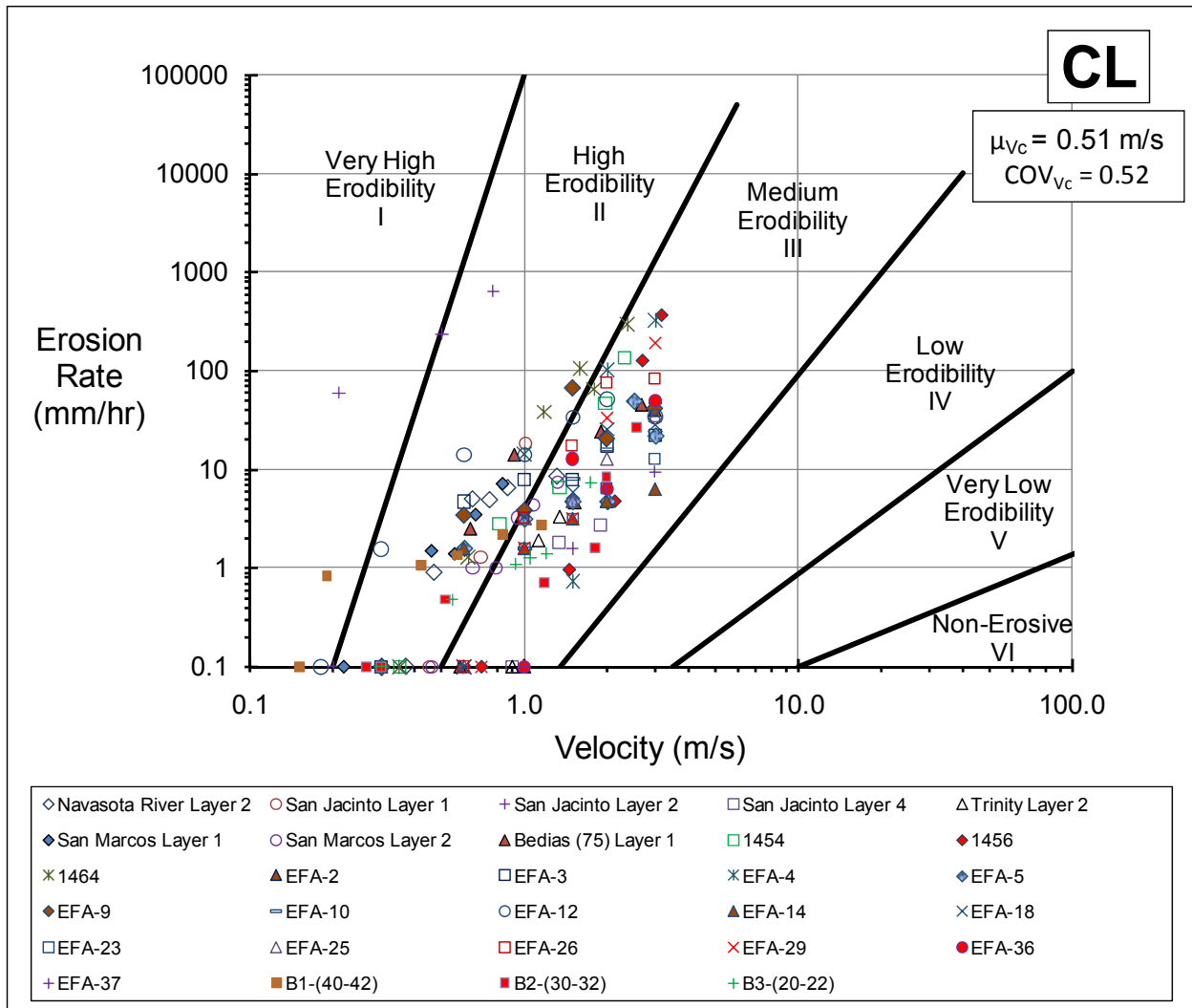


Figure 3-6. EFA Test Data on Low Plasticity Clays Plotted on the Erosion Function Charts.

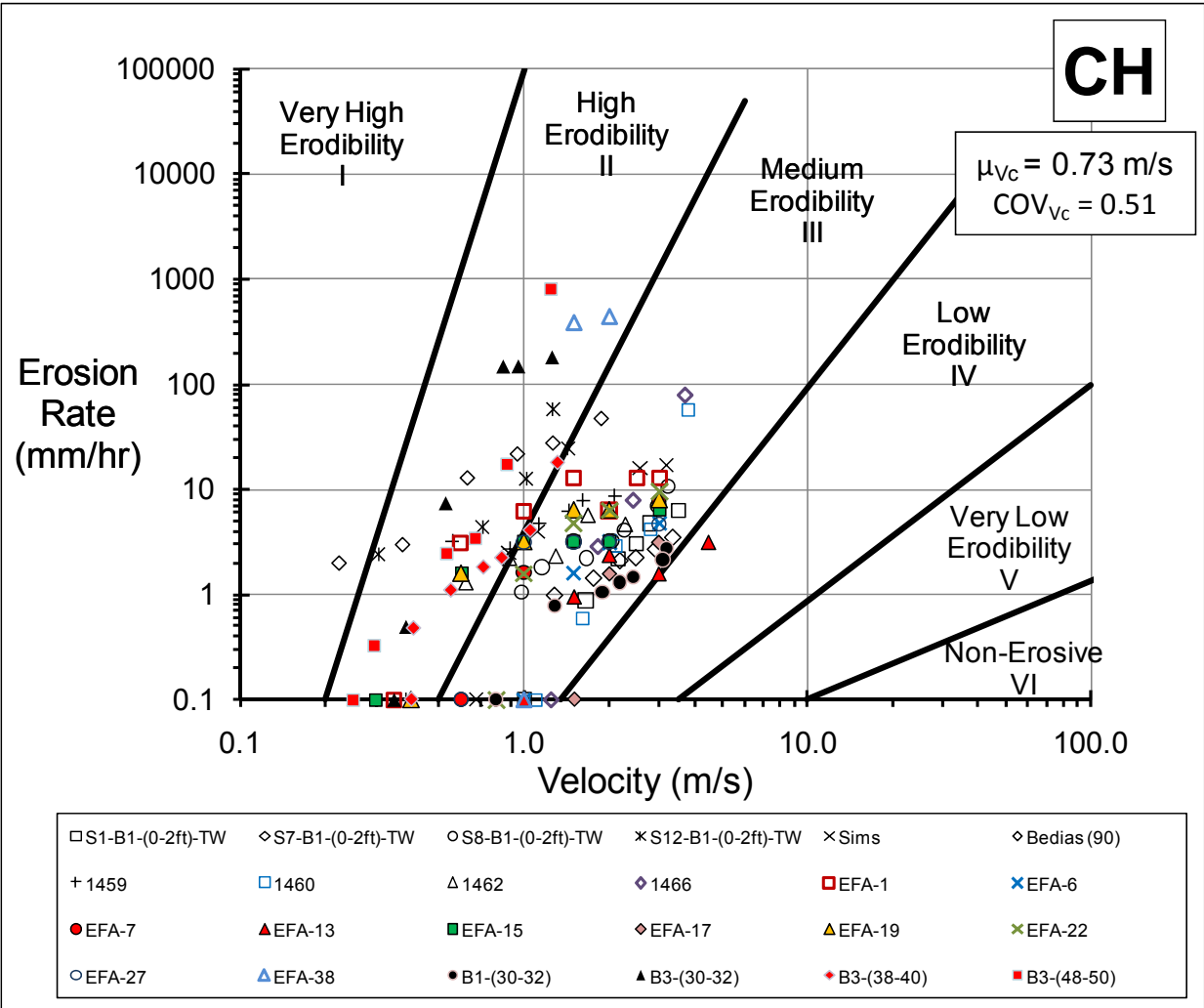


Figure 3-7. EFA Test Data on High Plasticity Clays Plotted on the Erosion Function Charts.

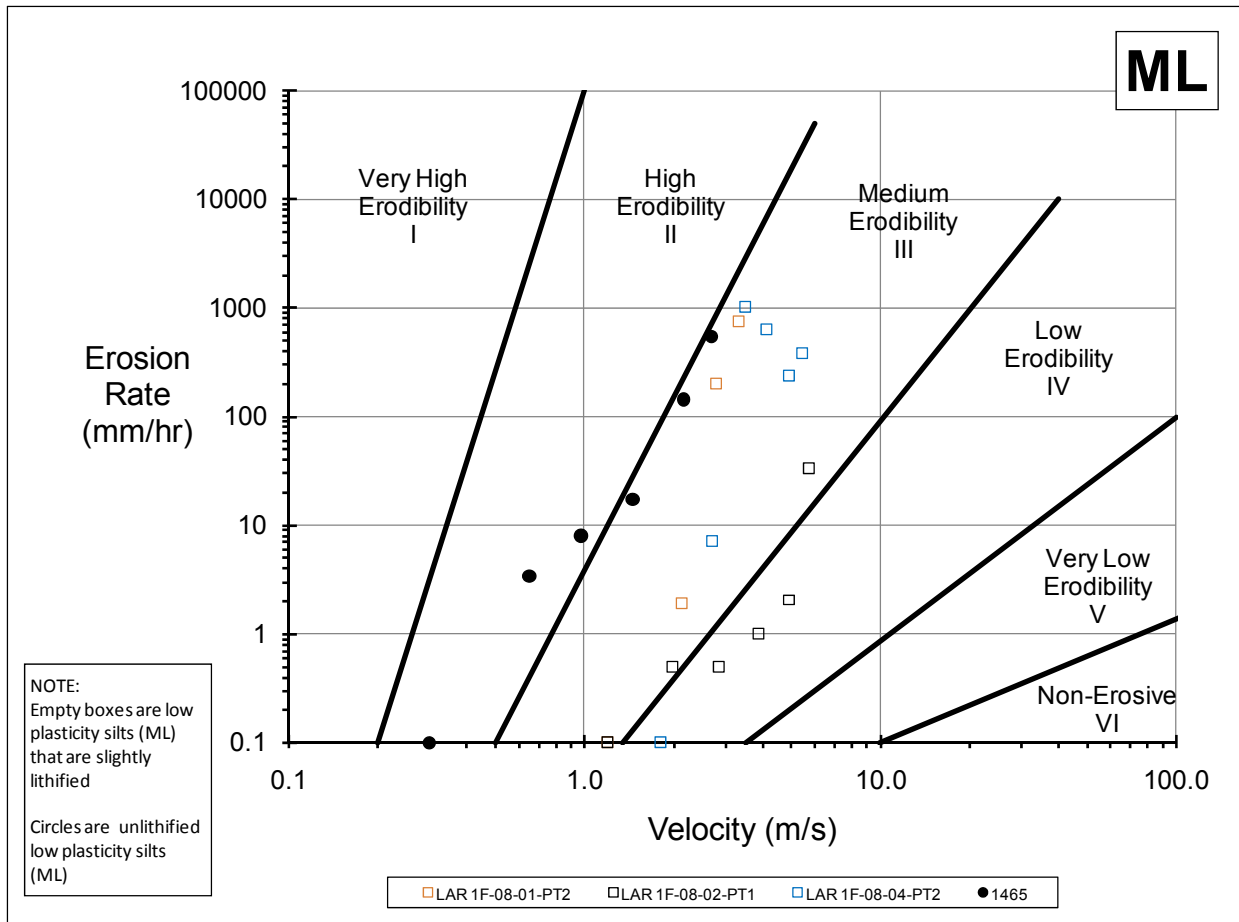


Figure 3-8. EFA Test Data on Low Plasticity Silts Plotted on the Erosion Function Charts.

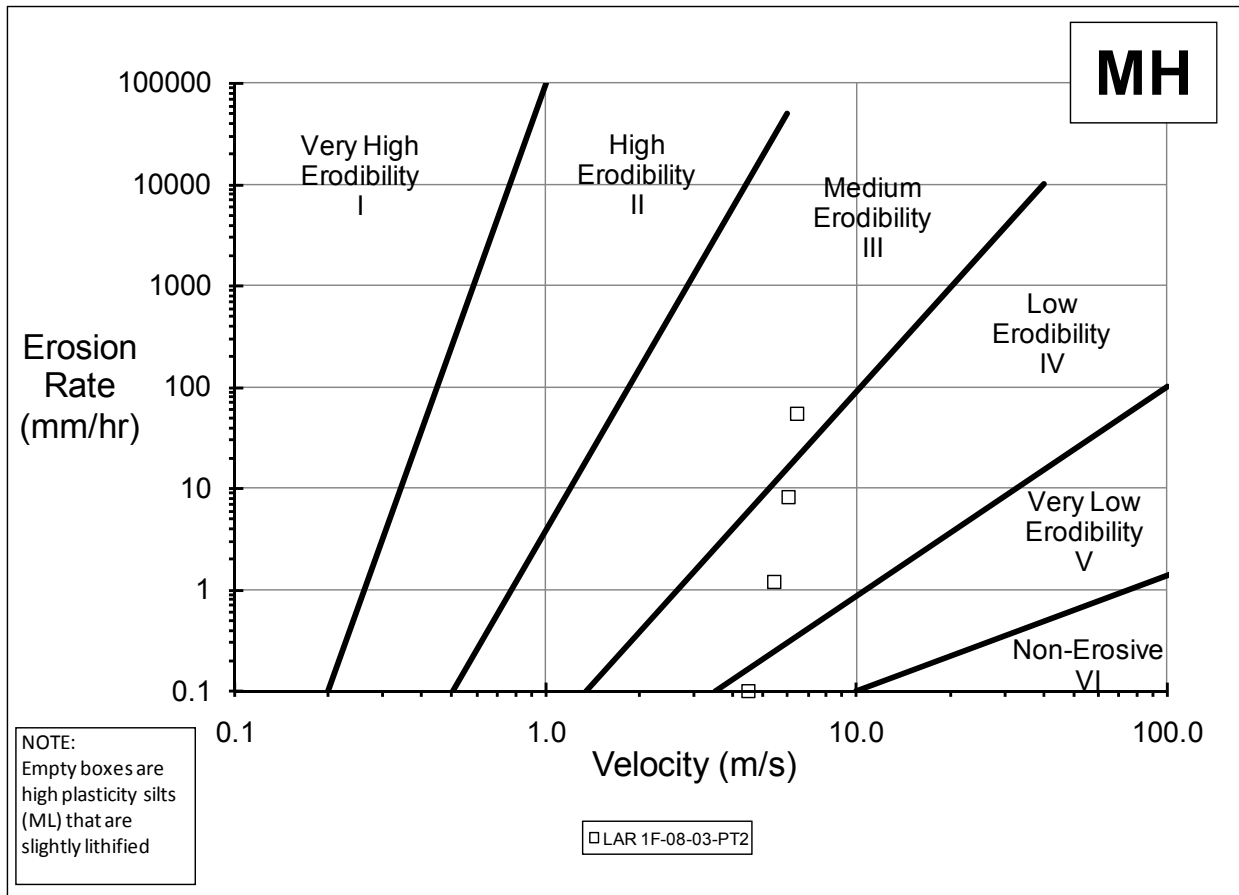


Figure 3-9. EFA Test Data on High Plasticity Silt Plotted on the Erosion Function Charts.

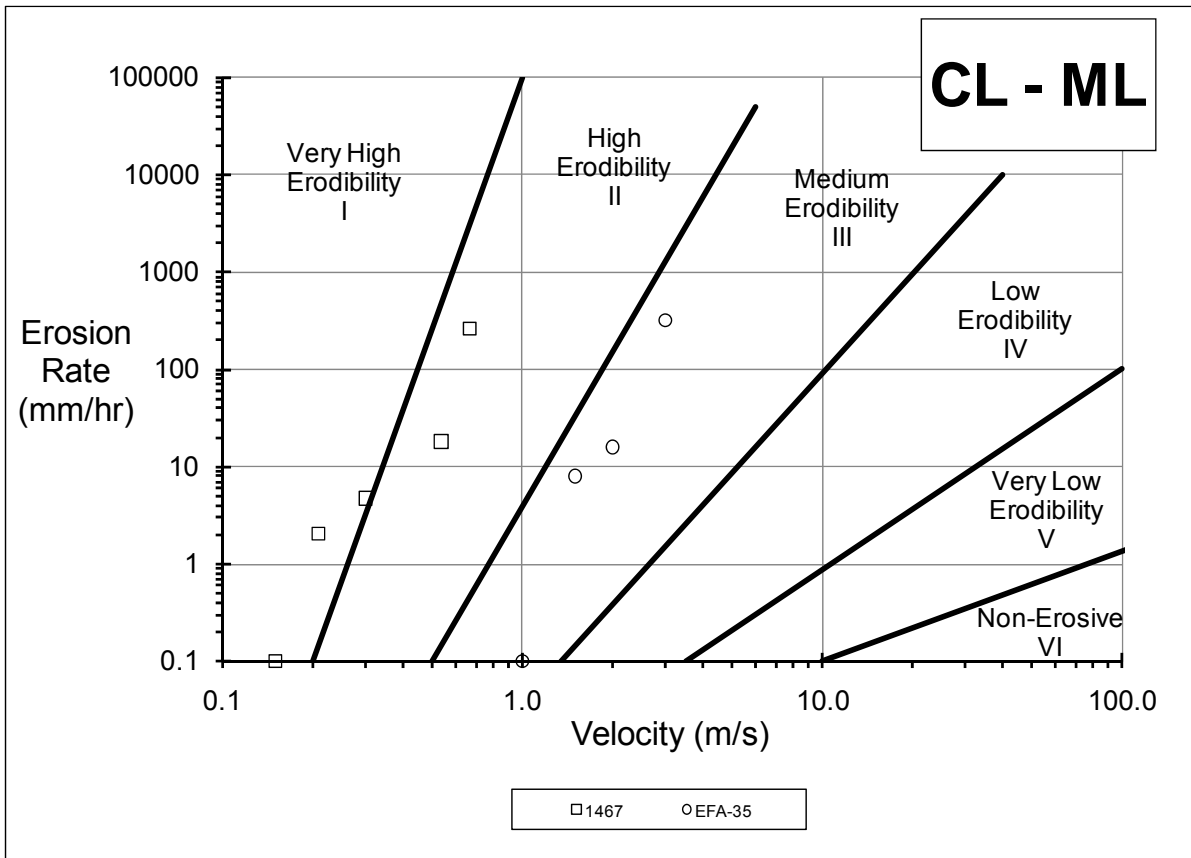


Figure 3-10. EFA Test Data on Samples Intermediate between Low Plasticity Clay and Low Plasticity Silt Plotted on the Erosion Function Charts.

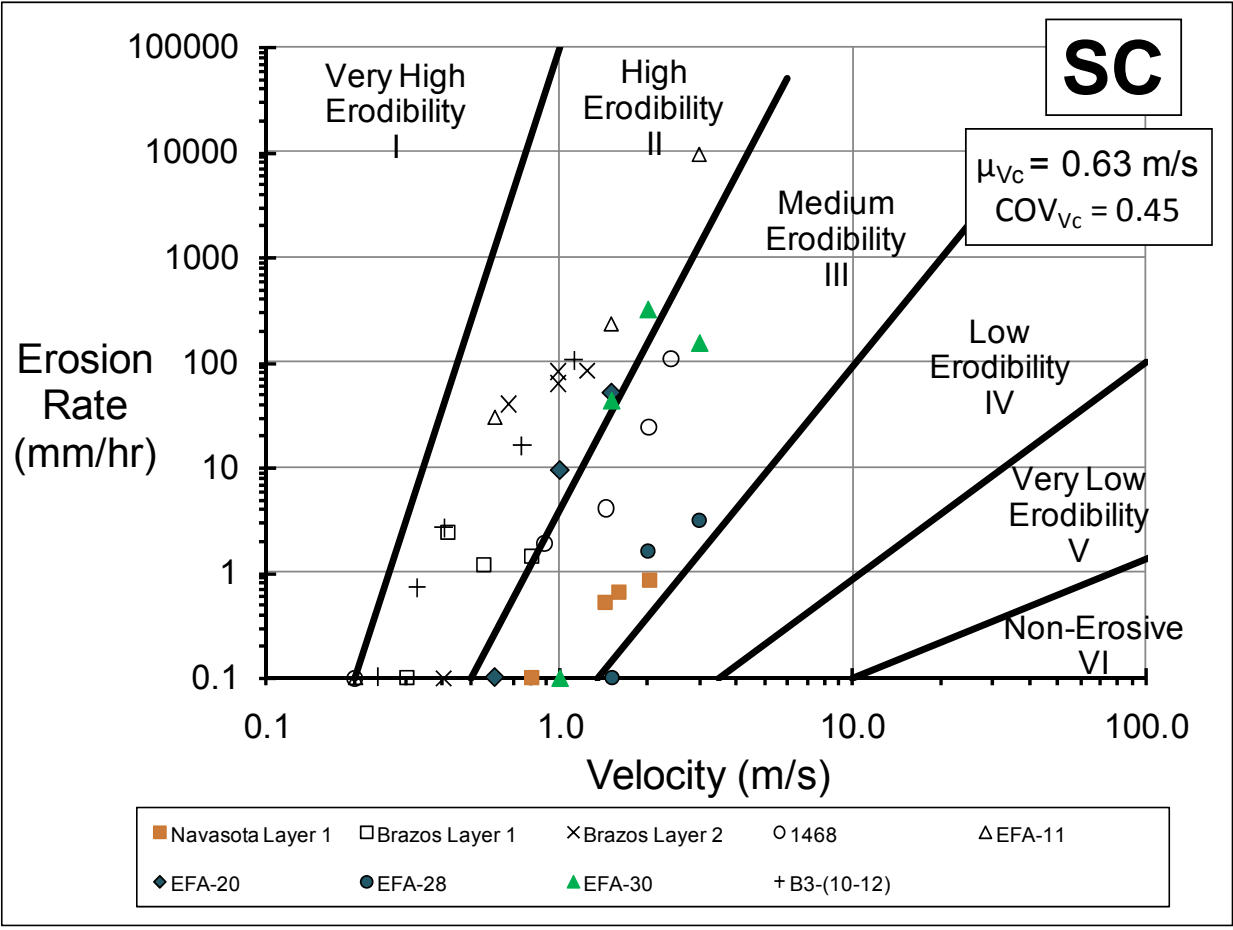


Figure 3-11. EFA Test Data on Clayey Sands Plotted on the Erosion Function Charts.

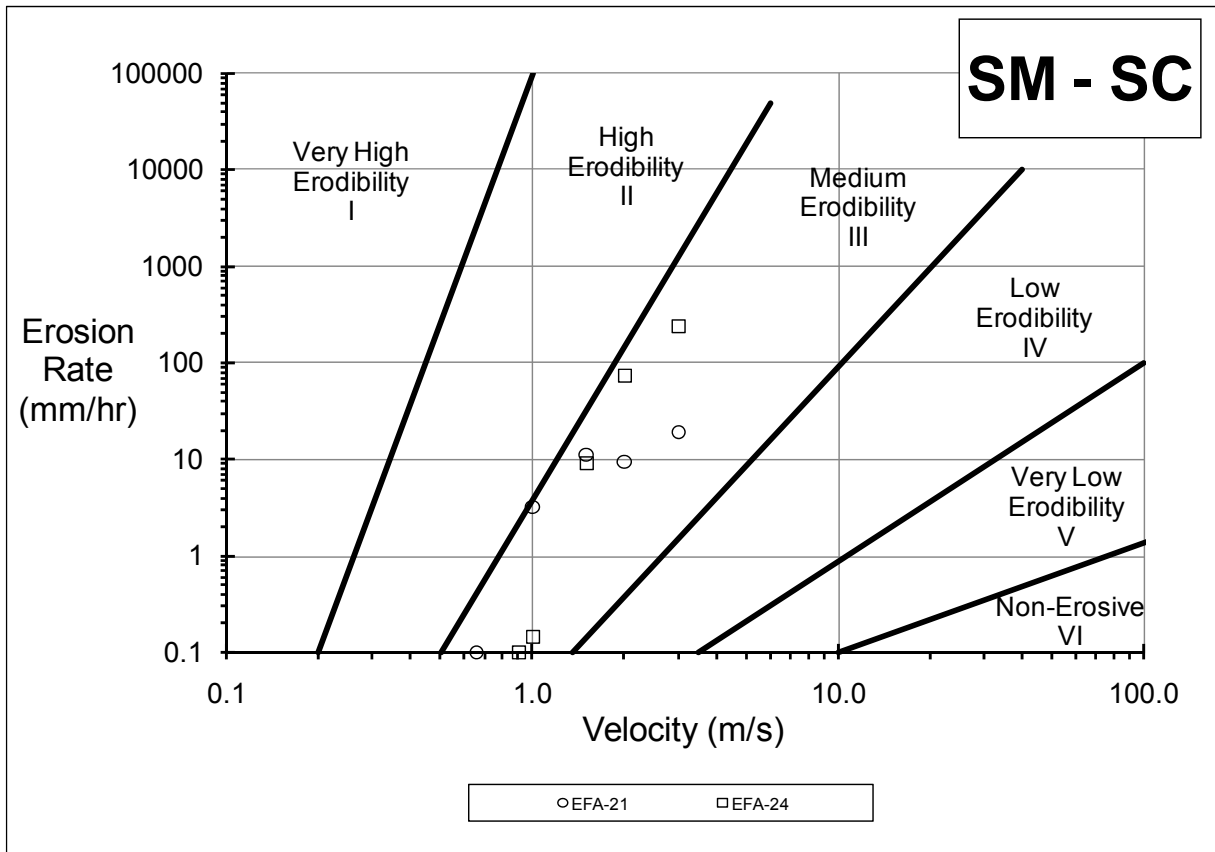


Figure 3-12. EFA Test Data on Samples Intermediate between Silty Sand and Clayey Sand Plotted on the Erosion Function Charts.

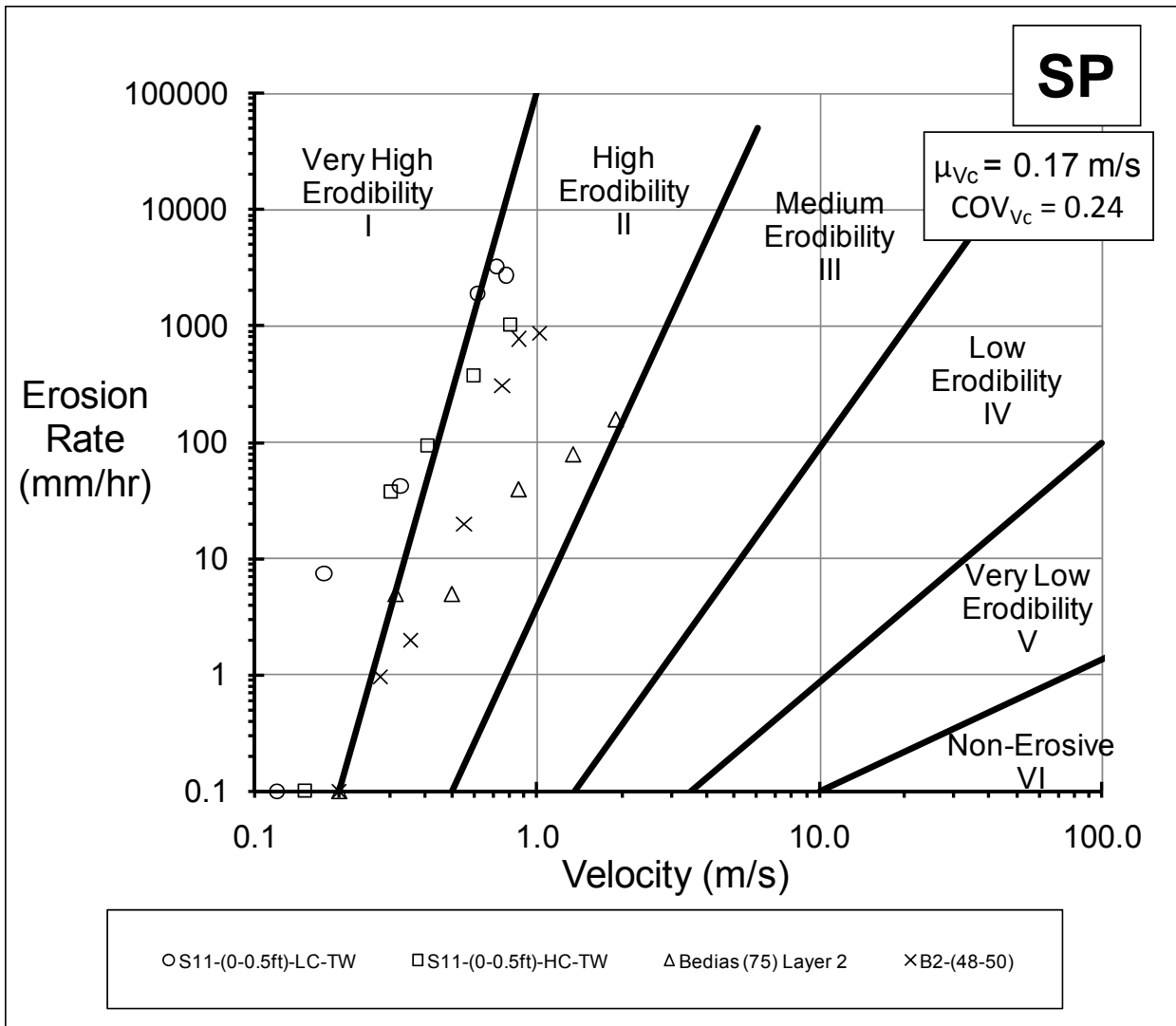


Figure 3-13. EFA Test Data on Poorly Graded Sands Plotted on the Erosion Function Charts.

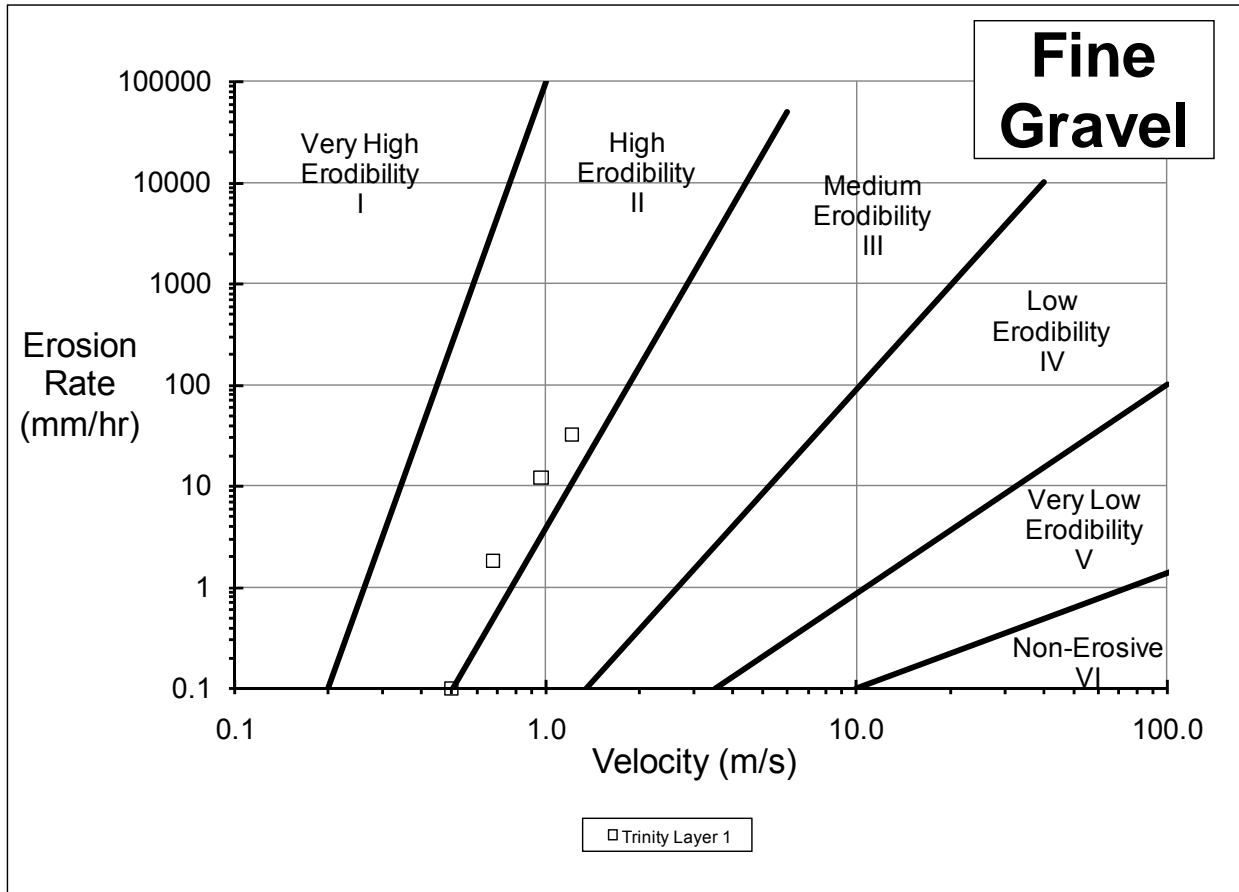


Figure 3-14. EFA Test Data on Gravel Plotted on the Erosion Function Charts.

Figure 3-15 through Figure 3-18 show the approximate zones for CL, CH, SC, and SP materials. These zones are based on the EFA test data that were presented in Figure 3-6, Figure 3-7, Figure 3-10, Figure 3-11, Figure 3-12, and Figure 3-13. The rest of the materials were not zoned on the Erosion Function Charts due to lack of test data.

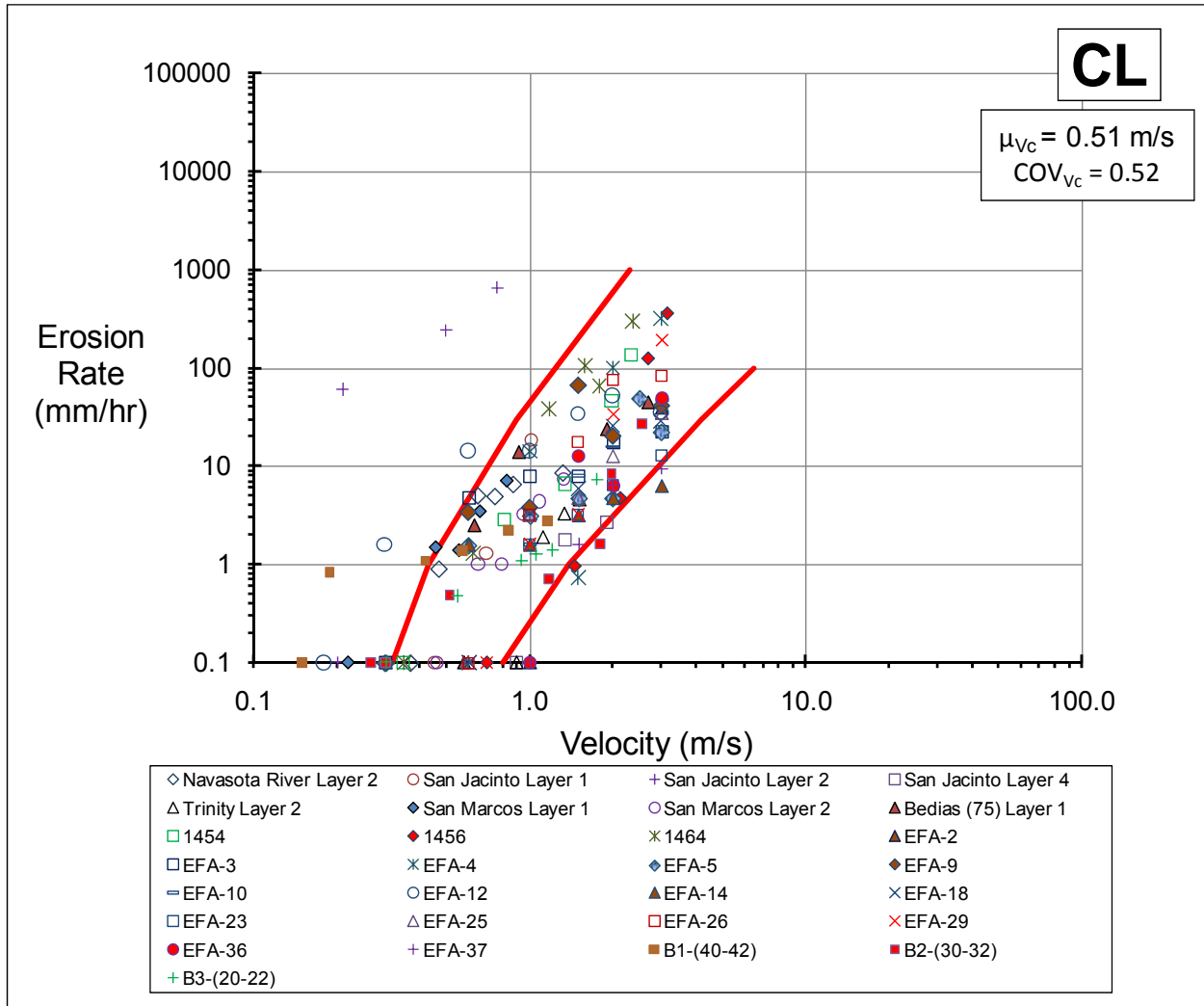


Figure 3-15. Zone for Low Plasticity Clay.

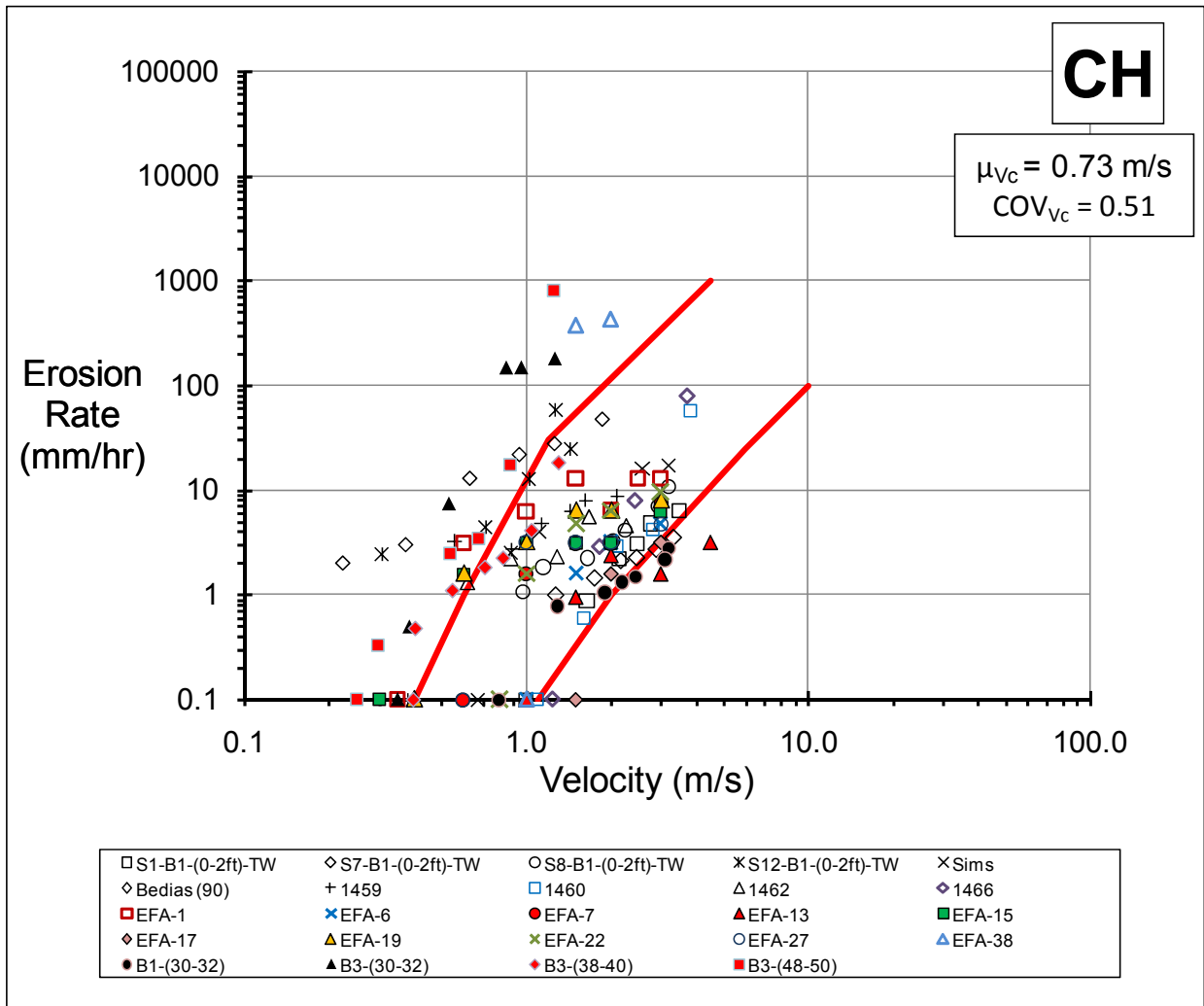


Figure 3-16. Zone for High Plasticity Clay.

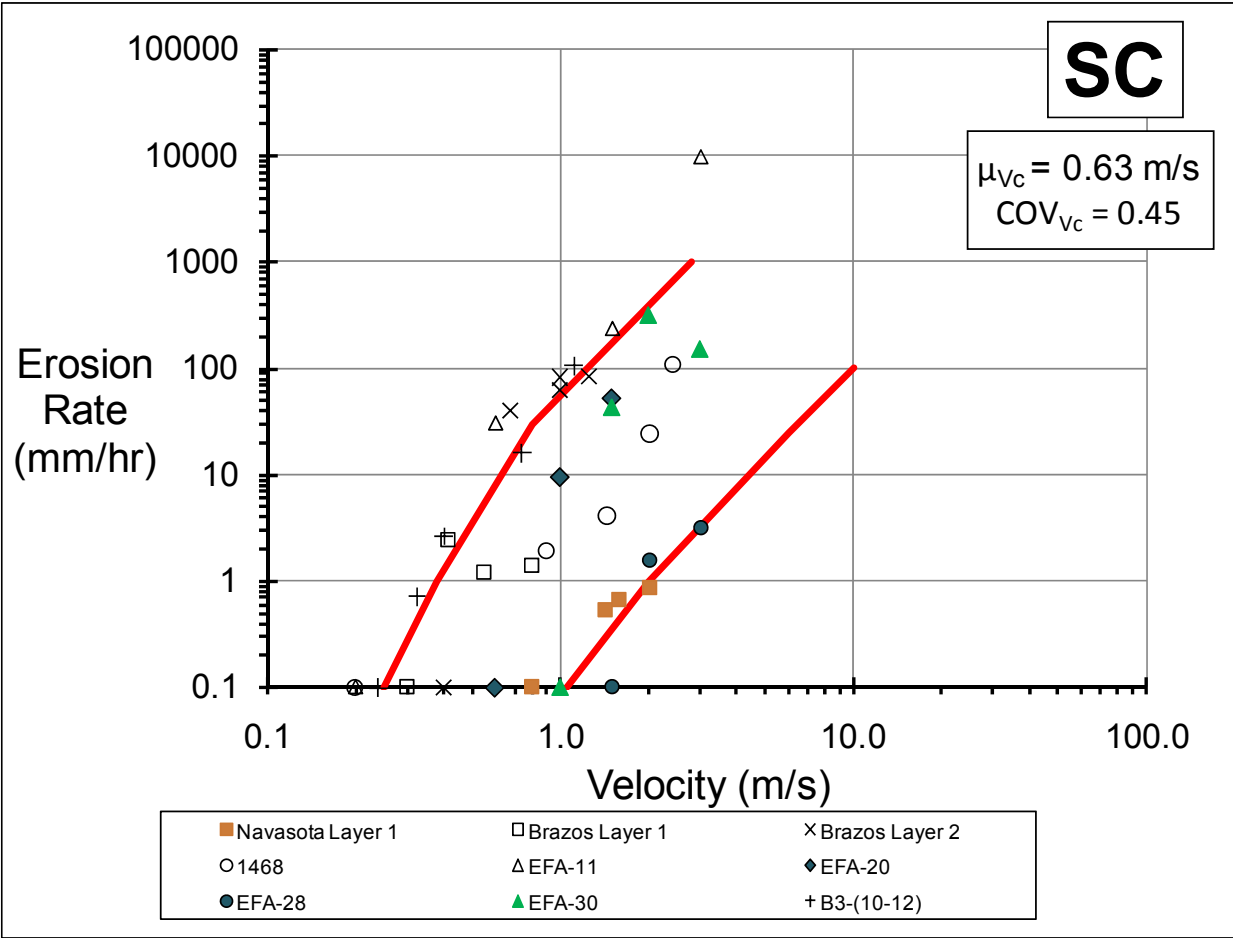


Figure 3-17. Zone for Clayey Sands.

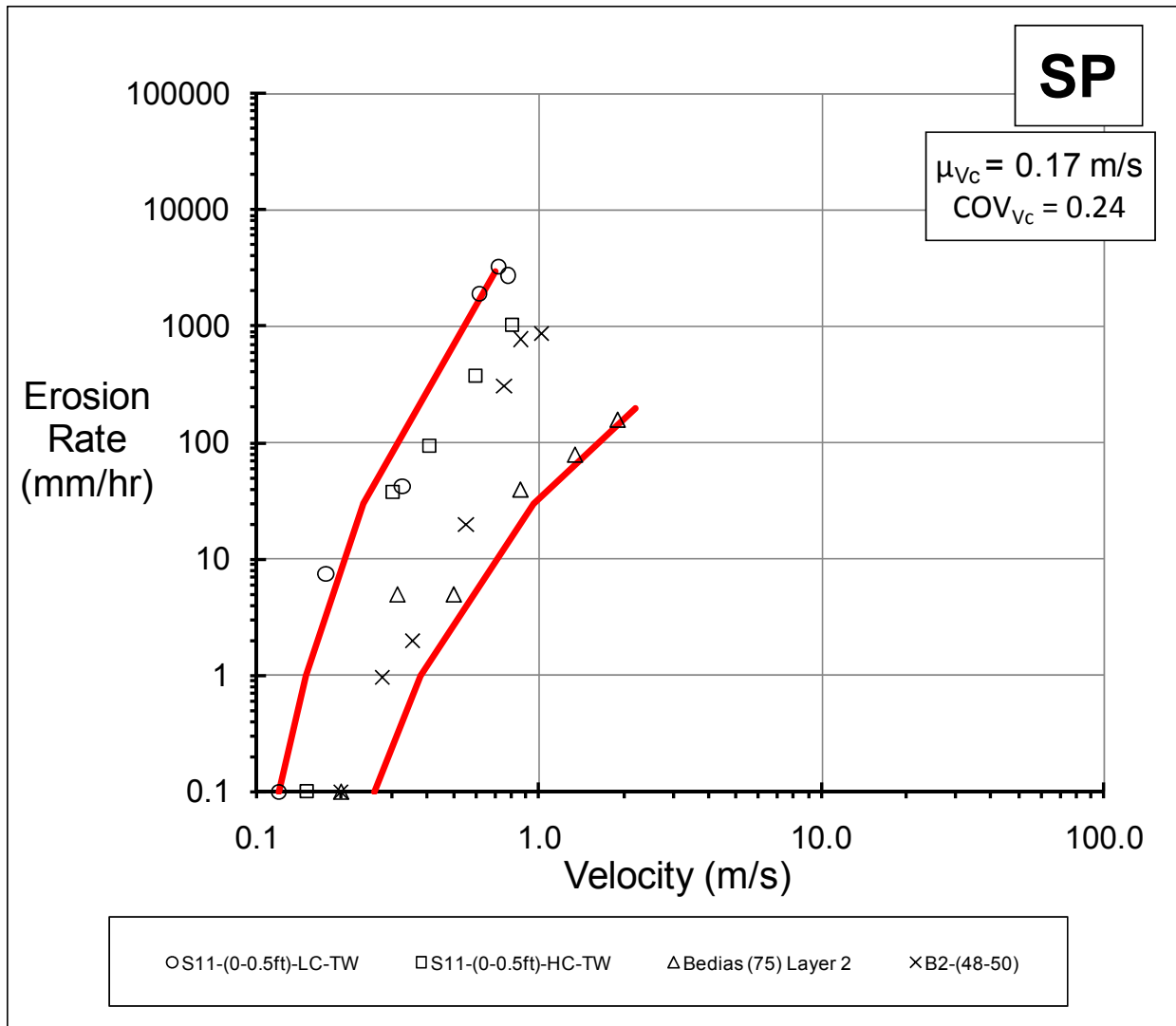


Figure 3-18. Zone for Poorly Graded Sand

3.5. THE EROSION THRESHOLD CHARTS

3.5.1. Overview

Briaud (2008) suggests that the threshold of erosion is one of the most important soil parameters in erosion. Below the threshold value, erosion does not take place. Once the applied hydraulic stress exceeds the threshold value, erosion is initiated until the equilibrium scour depth is achieved. As mentioned in Chapter 2, the threshold value for erosion in terms of shear stress is the critical shear stress τ_c and in terms of velocity is the critical velocity V_c . Due to their importance, the threshold values were investigated and charts were developed to aid engineers in

estimating them. Essentially, these are charts that show the relationship between the erosion threshold values and the particle size of the geomaterial. Collectively, these charts are termed the Erosion Threshold Charts, presented in terms of τ_c and V_c .

3.5.2. The Use of a Riprap Design Equation for Scour in Fractured Rock

In order to include fractured rock in Erosion Threshold Charts, a study was done by employing a riprap design equation to estimate the threshold velocity that would cause a block of riprap with a certain size (particle diameter) to move. The design equation employed was the United States Army Corps of Engineers EM 1601 riprap design equation (United States Army Corps of Engineers 1995). The EM 1601 equation is as follows:

$$\frac{d_{30}}{y} = 0.30 \left[\frac{V}{\sqrt{(S_g - 1)gy}} \right]^{2.5} \quad (3.4)$$

where d_{30} is the particle diameter corresponding to 30 percent passing by weight, V is the mean depth velocity of flow, y is the water depth, g is the acceleration of gravity, and S_g is the particle specific gravity. Equation 3.3 was rearranged to determine the velocity as a function of grain size as follows:

$$V = \left[\frac{3.33d_{30}}{y} \right]^{0.4} \sqrt{(S_g - 1)gy} \quad (3.5)$$

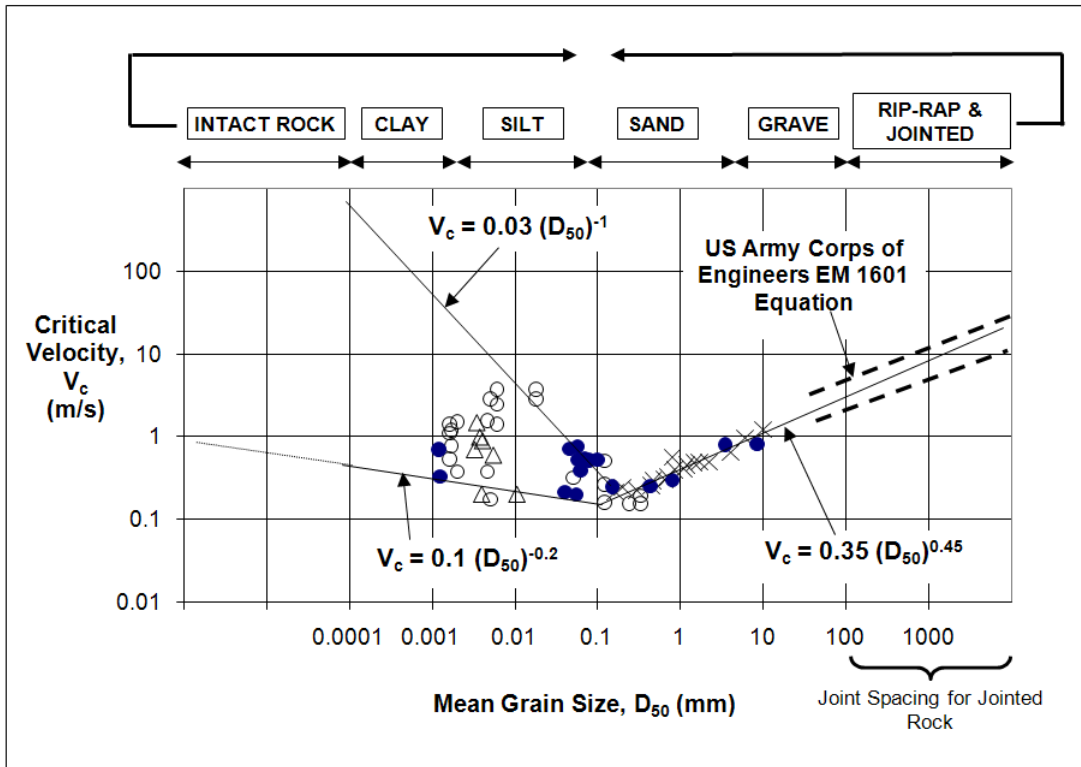
Subsequently, the velocity corresponding to a specified range for both particle size, d_{30} , and water depth, y , was computed for a fixed $S_g = 2.65$. The range of particle diameter was between 100 and 10,000 mm. The range of water depth was between 1 and 25 m. This resulted in 300 combinations of these parameters. The results of these simulations will be shown when the Erosion Threshold Charts are present below.

3.5.3. The Erosion Threshold–Mean Grain Size Chart

The erosion threshold–mean grain size charts are shown in Figure 3-19, Figure 3-20, and Figure 2-21. Figure 3-19 presents the erosion threshold in terms of velocity, and Figure 3-20 shows the data points from the simulation of the riprap design equation. Figure 3-21 presents the erosion threshold in terms of shear stress. This chart was essentially developed using EFA test

results as well as data in the literature to relate the critical velocity of the geomaterial to its mean grain size. As can be observed in the charts, the critical value and the grain size displays a “V” shape. The most erodible materials are the fine sands. The charts also point out that particle size controls the erosion threshold in coarse-grained soils and does not provide a correlation with the threshold value for fine-grained soils. The curve proposed by [Shields \(1936\)](#) has been presented on the charts as well. Also, [Hjulström \(1935\)](#) proposed a similar curve for both fine-grained and coarse-grained soils, but his method turned out to be too simple ([Briaud 2008](#)) because the erosion of fine grained soils is not related to the size of the soil grains only.

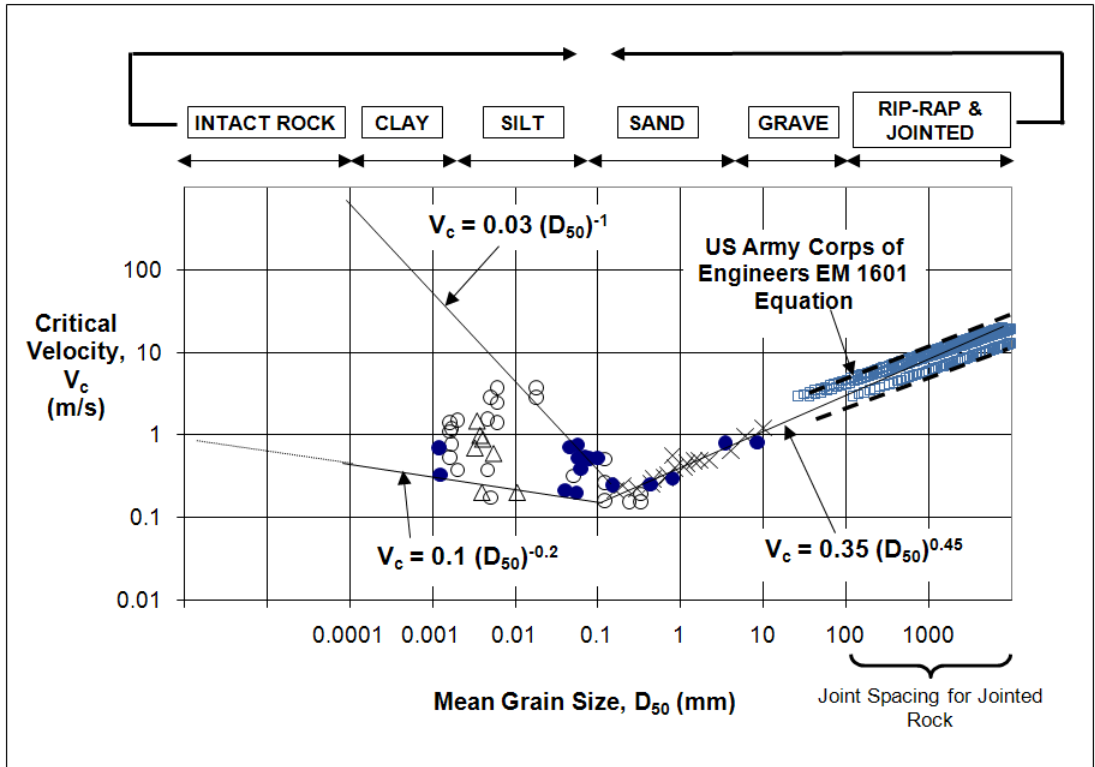
The range of threshold velocities V_c obtained using the riprap design equation ([Equation \[3.4\]](#)) is shown in [Figure 3-20](#). For fractured rock, the particle diameter is assumed to be the rock fracture spacing, which seems to be a reasonable assumption because one can expect a piece of fractured rock with a certain fracture spacing to have similar critical erosion properties as a piece of riprap with a diameter that is equal to the fracture spacing.



Legend:

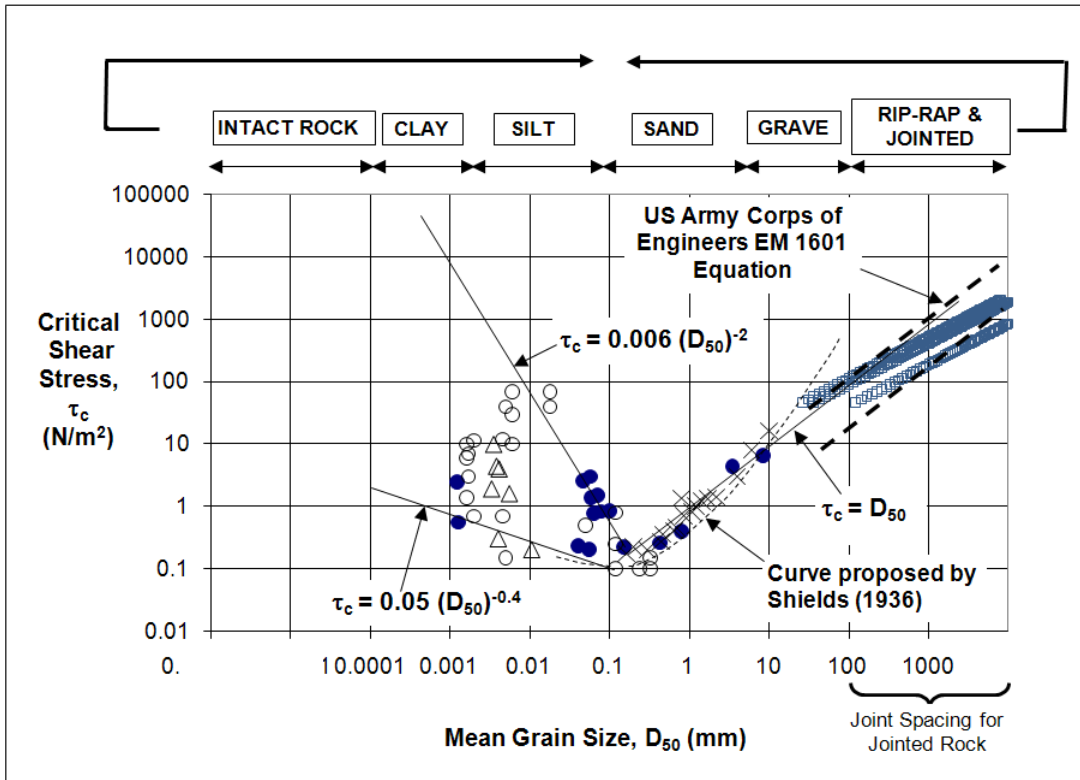
- TAMU Data as reported by Briaud, J.-L. et. al. (2001). "Erosion Function Apparatus for Scour Rate Predictions." *J. Geotech. and Geoenviron. Engrg.*, ASCE, 127(2), 105-113.
- TAMU Data as reported by Briaud, J.-L. (2006). "Erosion Tests on New Orleans Levee Samples." *Texas A&M University Internal Report*.
- × Data from Shields, Casey, US.WES, Gilbert, White as reported by Vanoni, V.A., ed. (1975). "Sedimentation Engineering." *ASCE manuals and reports on engineering practice*, ASCE, New York.
- Data points from simulation using U.S. Army Corps of Engineers EM 1601 Riprap Design Equation (U.S. Army Corps of Engineers 1995). In this case, the mean grain size plotted is D_{30} .
- △ TxDOT EFA Data (tests performed in 2008)

Figure 3-19. Critical Velocity as a Function of Mean Grain Size.



- Legend:
- TAMU Data as reported by Briaud, J.-L. et. al. (2001). "Erosion Function Apparatus for Scour Rate Predictions." *J. Geotech. and Geoenviron. Engrg.*, ASCE, 127(2), 105-113.
 - TAMU Data as reported by Briaud, J.-L. (2006). "Erosion Tests on New Orleans Levee Samples." *Texas A&M University Internal Report*.
 - × Data from Shields, Casey, US.WES, Gilbert, White as reported by Vanoni, V.A., ed. (1975). "Sedimentation Engineering." *ASCE manuals and reports on engineering practice*, ASCE, New York.
 - Data points from simulation using U.S. Army Corps of Engineers EM 1601 Riprap Design Equation (U.S. Army Corps of Engineers 1995). In this case, the mean grain size plotted is D_{30} .
 - △ TxDOT EFA Data (tests performed in 2008)

Figure 3-20. Critical Velocity as a Function of Mean Grain Size Including Data Points from Simulation Using United States Army Corps of Engineers EM 1601 Riprap Design Equation.



Legend:

- TAMU Data as reported by Briaud, J.-L. et. al. (2001). "Erosion Function Apparatus for Scour Rate Predictions." *J. Geotech. and Geoenviron. Engrg.*, ASCE, 127(2), 105-113.
- TAMU Data as reported by Briaud, J.-L. (2006). "Erosion Tests on New Orleans Levee Samples." *Texas A&M University Internal Report*.
- × Data from Shields, Casey, US.WES, Gilbert, White as reported by Vanoni, V.A., ed. (1975). "Sedimentation Engineering." *ASCE manuals and reports on engineering practice*, ASCE, New York.
- Data points from simulation using U.S. Army Corps of Engineers EM 1601 Riprap Design Equation (U.S. Army Corps of Engineers 1995). In this case, the mean grain size plotted is D_{30} .
- △ TxDOT EFA Data (tests performed in 2008)

Figure 3-21. Critical Shear Stress as a Function of Mean Grain Size.

4. HYDROLOGY

4.1. INTRODUCTION

As explained in [Chapter 1](#), the proposed scour assessment procedure requires the velocity of the flow at the bridge cross section. This chapter explains how this is done.

In Bridge Scour Assessment 1, the required hydraulic information is the ratio $V_{\text{fut}}/V_{\text{mo}}$, where V_{fut} represents the velocity of a flow with a high recurrence interval that may happen in the future and V_{mo} represents the velocity of the maximum observed flow at the bridge. These velocities represent the mean velocities for the flow cross section. The ratio $V_{\text{fut}}/V_{\text{mo}}$ is required for the engineer to use the Z-Future Charts, which will be explained in [Chapter 5](#). V_{fut} corresponds to the flood with a 100-year recurrence interval and is regarded as a standard design flood for major hydraulic structures and, most importantly, scour depth evaluation. Throughout this chapter the term V_{100} (mean velocity corresponding to the 100-year flood) will replace V_{fut} . However, one could choose a V_{fut} that is different from V_{100} .

In BSA 1, the ratio V_{100}/V_{mo} can be directly acquired without having to calculate the explicit values of V_{100} and V_{mo} . This study explored and verified that there is a strong relationship between the recurrence interval of the observed maximum flow at the bridge (Q_{mo}) and ratio V_{100}/V_{mo} . Thus, knowing the recurrence interval of the Q_{mo} will yield a reasonable estimate of V_{100}/V_{mo} . The recurrence interval of Q_{mo} can be obtained using various approaches based on the availability of the flow data at the bridge being investigated, as described later.

In Bridge Scour Assessment 2 and Bridge Scour Assessment 3, the procedure to determine hydraulic information from the hydrology part is composed of two major steps: obtaining Q_{100} and Q_{mo} , and converting flow into velocity, i.e., conversion of Q_{100} and Q_{mo} into V_{100} and V_{mo} . The first step is broken down into four different cases that depend on the relationship between the location of the bridge and the location of the gage.

4.2. TYPES OF BRIDGE-GAGE RELATIONSHIPS

The bridge-gage relationships represent the spatial association of the bridge and the flow data recorded by a gage. In other words, these categories of bridge-gage relationships involve availability of flow data directly at the bridge, upstream/downstream of the bridge, in a hydrologically similar and nearby watershed, or where there is no inferable flow information. The bridge-gage relationships are aimed at determining hydraulic information required for bridge scour assessment, i.e., V_{100} and V_{mo} . The bridge-gage relationships are as follows.

4.2.1. Bridge-Gage Relationship Type I: Bridge with Flow Gage

Some bridges have a flow gage installed on them. The flow record for these gages can be obtained from the website of the National Water Information System of USGS ([United States Geological Survey 2008](#)). The geographical information (longitude and latitude) and site name of the flow gages are also provided by USGS. Therefore, matching the flow records from this website and the bridge being investigated is straightforward.

Even though the flow record is available from USGS at the bridge location in this case, the length of the record should also be sufficient to perform a flood frequency analysis (FFA). FFA is used to determine Q_{100} , which is then converted into V_{100} . A short duration of flow record is not sufficiently representative of unknown long-term series of flow peaks and may lead to an FFA that yields inaccurate estimates of Q_{100} and V_{100} . This investigation suggests that engineers should use a flow record greater than or equal to 20 years. This is a safer value compared to the 10 years suggested by [Dingman \(2001\)](#) as an absolute minimum.

In the case of Bridge-Gage Relationship Type I, the required hydraulic information for scour assessment and how to obtain it are explained as follows:

6. Flow velocity corresponding to 100-year flood (V_{100})
 - a. Obtain the time series of annual instantaneous flow peaks $Q(t)$ for a period of at least 20 years.
 - b. Ignore the flow records influenced by human intervention (i.e., regulated flow records).

- c. Perform FFA on the unregulated flow records to obtain Q_{100} .
 - d. Convert Q_{100} into V_{100} using TAMU-FLOW. TAMU-FLOW is a software tool provided with this report that converts the discharge into velocity of a stream channel specified by the user.
7. Flow velocity corresponding to the greatest flow observed by the bridge (V_{mo})
- a. Obtain the time series of annual instantaneous flow peaks $Q(t)$ for a period of at least 20 years.
 - b. Find the maximum flow value out of the time series ignoring the data recorded before the bridge was constructed (Q_{mo}).
 - c. Convert Q_{mo} into V_{mo} using TAMU-FLOW.
8. Ratio of V_{100} to V_{mo} (V_{100}/V_{mo})
- a. Divide V_{100} by V_{mo} estimated from above.

4.2.2. Bridge-Gage Relationship Type II—Bridge with Gages Nearby, Either Upstream or Downstream

If a flow gage is not available directly at the bridge, the data measured from flow gages located nearby, either upstream or downstream of the bridge, can be utilized. In this case, the flow records can be transformed based on the ratio of drainage area of the bridge being investigated to the drainage area of the upstream/downstream gage. [Figure 4-1](#) shows an example of this case. This figure shows the watershed for the bridge on FM 541 crossing Cibolo Creek. It also shows a downstream gage that shares the same watershed as the bridge. The measured area of the watershed of the gage and the bridge is 827 miles² and 769 miles², respectively. The flow record at the gage can be transformed into that of the bridge by using the ratio of drainage area as follows using the equation suggested by [Asquith and Thompson \(2008\)](#).

$$\text{Flow record at the bridge} = \text{Flow record at the gage} \times \left[\frac{769 \text{ miles}^2}{827 \text{ miles}^2} \right]^{0.5} \quad (4-1)$$

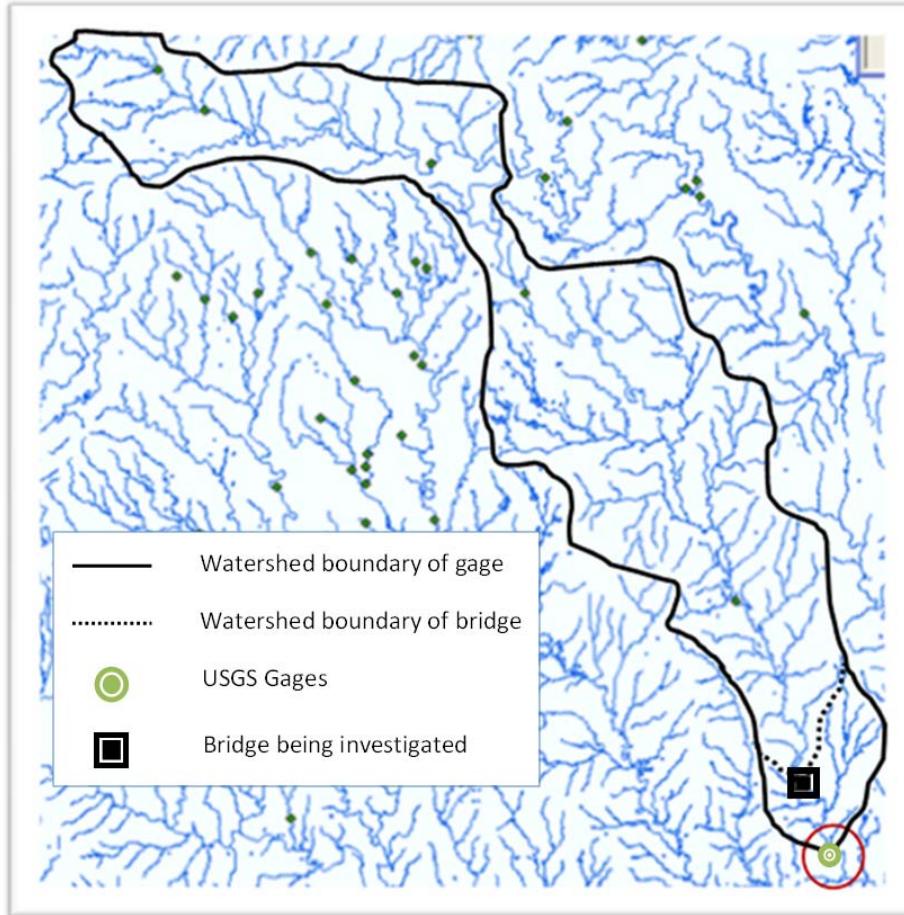


Figure 4-1. Map Showing the Bridge-Gage Relationship Type II—Gage Upstream/Downstream of Bridge.

Once the flow record at the bridge becomes available through this process, all other procedures to acquire the ratio (V_{100}/V_{m0}) for BSA 1 or explicit values of V_{100} and V_{m0} for BSA 2 are the same as the ones for Bridge-Gage Relationship Type I.

4.2.3. Bridge-Gage Relationship Type III—Bridge with a Gage at a Nearby and Hydrologically Similar Watershed

When there is no flow gage at the bridge or no flow gage upstream or downstream of the bridge, a flow gage at a nearby watershed can be used to obtain the flow records at the bridge if the hydrological properties (i.e., land use, land cover, and average slope) of both watersheds are similar. The ratio of the drainage area can be used to obtain the flow data at the watershed of the

bridge. Again, all other procedures to acquire the ratio (V_{100}/V_{mo}) for BSA 1 or explicit values of V_{100} and V_{mo} for BSA 2 are the same as the ones for Bridge-Gage Relationship Type I.

4.2.4. Bridge-Gage Relationship Type IV—Bridges with No Flow Gage at All

In the case where there is no flow gage at or near the bridge for the scour analysis, the recurrence interval of Q_{mo} is presented on a map of the state of Texas. This map, termed the recurrence interval map, was obtained by spatial interpolation of the recurrence interval of Q_{mo} values estimated at flow gages in Texas. This procedure will be explained later in this chapter. By using the map and the latitude-longitude coordinates of the bridge, the user gets the recurrence intervals of Q_{mo} for the bridge being investigated. These values are then used to acquire the ratio (V_{100}/V_{mo}) for BSA 1 or explicit values of V_{100} and V_{mo} for BSA 2 and BSA 3.

4.3. OBTAINING HYDRAULIC INFORMATION FROM BRIDGE-GAGE RELATIONSHIPS

The transformation of the recurrence interval of Q_{mo} into a velocity V_{mo} depends on the level of scour assessment.

4.3.1. Obtaining Hydraulic Information for BSA 1

The ratio V_{100}/V_{mo} (as opposed to the explicit value of V_{100} and V_{mo}) is required for BSA 1. This value is obtained using the following methodology:

9. Obtain the recurrence interval of the Q_{mo} at the bridge. (For Type IV, spatially interpolate the recurrence interval of the Q_{mo} observed at nearby gages.) This procedure can be automated by using the software tool TAMU-FLOOD, which is provided with this report. The user's manual of TAMU-FLOOD is available in [Appendix F](#) of this report.
10. Obtain the ratio Q_{100}/Q_{mo} using the relationship between the recurrence interval of Q_{mo} and the ratio Q_{100}/Q_{mo} , presented in [section 4.4.2.1](#).
11. Convert Q_{100}/Q_{mo} into V_{100}/V_{mo} using Manning's equation.

A detailed description of each of these steps including the theoretical background is provided later in this chapter.

4.3.2. Obtaining Hydraulic Information for BSA 2 and BSA 3

The explicit values of V_{100} and V_{m0} are required for the BSA 2 and BSA 3 stage of the scour analysis. The following methodology can be used to obtain these values:

12. Obtain the recurrence interval of Q_{m0} at the bridge by using TAMU-FLOOD.
13. Using the regional regression equation ([Asquith and Slade 1996](#)) and the recurrence interval of Q_{m0} , acquire Q_{m0} . Obtain Q_{100} from the same equation.
14. Convert Q_{m0} and Q_{100} into V_{m0} and V_{100} using channel geometry and properties (i.e., Manning's coefficients and channel slope). HEC-RAS ([HEC-RAS 2008](#)) and TAMU-FLOW ([Appendix E](#)) can be used to acquire these values.

4.4. SPECIAL CASE OF BRIDGE-GAGE RELATIONSHIP TYPE IV

As explained earlier, if the bridge has no inferable flow information available at or near it, flow information should be inferred based on other hydrological information. Two approaches were tried to obtain the flow data for the bridge with no inferable flow information. The first approach investigates the correlation between flow and rainfall data. The second approach investigates the spatial variation of flow data at gages and uses an interpolation technique to obtain the hydraulic information at a bridge with no flow data. These approaches are termed Approach 1 and 2 and are described as follows.

4.4.1. Approach 1: Rainfall-Flow Correlation Approach

The assumption of this approach is that rainfall with a high recurrence interval causes a flood with a recurrence interval that is similar to that of the rainfall. If the magnitude of the rainfall is over a given threshold, the impact of the rainfall on the processes that generate the flood is significantly greater than that of other hydrologic factors such as soil type, land use, and soil moisture condition prior to the flood event. Thus, inferring flood information from rainfall magnitude while ignoring other hydrologic factors was considered to be a possible approach. Then, the information required for the scour analysis, such as the ratio V_{100}/V_{m0} or the individual value of V_{100} and V_{m0} , could be obtained.

4.4.1.1. Approach 1 Methodology

To investigate the rainfall-flow correlation, 13 rain gage–flow gage pairs were chosen across Texas. The properties and the location of the pairs are given in [Table 4-1](#) and shown in [Figure 4-2](#), respectively. Column 7 of [Table 4-1](#) is the length of the flow path starting from the flow gage to the hydrologically furthest location in the watershed. Columns 8 and 9 are the minimum and maximum, respectively, of the possible time of concentration of the watershed that is calculated by the following Kirpich formula:

$$\text{Time of concentration} = 0.0078 L^{0.77} S^{-0.385} \quad (4-2)$$

where L [ft] is the longest flow path (column 7) and S [ft/mile] is the average watershed slope.

Table 4-1. Properties of the Rainfall-Flow Gage Pairs Used for the Analysis.

1	2	3	4	5	6	7	8	9
USGS Flow Gage ID	NCDC(National Climate Data Center) Rain Gage ID	Drainage Area (Mile²)	Distance between Gages (Mile)	Overlapping Period (Year)	Rain Gage Centered at the Watershed	Longest Flow Path (Mile)	Tc_Kirpich (1) (Hour)	Tc_Kirpich (2) (Hour)
08037050	6177	31	0.3	28	yes	18	6.7	15
08039100	7951	89	8.2	16	yes	23	8.1	18
08077600	4307	122	11	29	yes	N/A	N/A	N/A
08103900	1068	33	7.4	35	no	16	6.1	14
08131400	7943	81	4.4	39	no	30	9.9	22
08154700	428	22	3.9	22	no	16	6.1	14
08155300	428	116	6.0	25	no	35	11	25
08165300	4375	169	9.3	25	yes	40	12	28
08200000	8845	96	7.4	48	yes	25	8.6	19
08201500	8845	45	10	39	no	22	7.8	17
08211520	2015	90	4.3	28	no	30	9.9	22
08365800	2797	6	5.1	19	no	N/A	N/A	N/A
08431700	6104	52	6.5	20	no	20	7.2	16

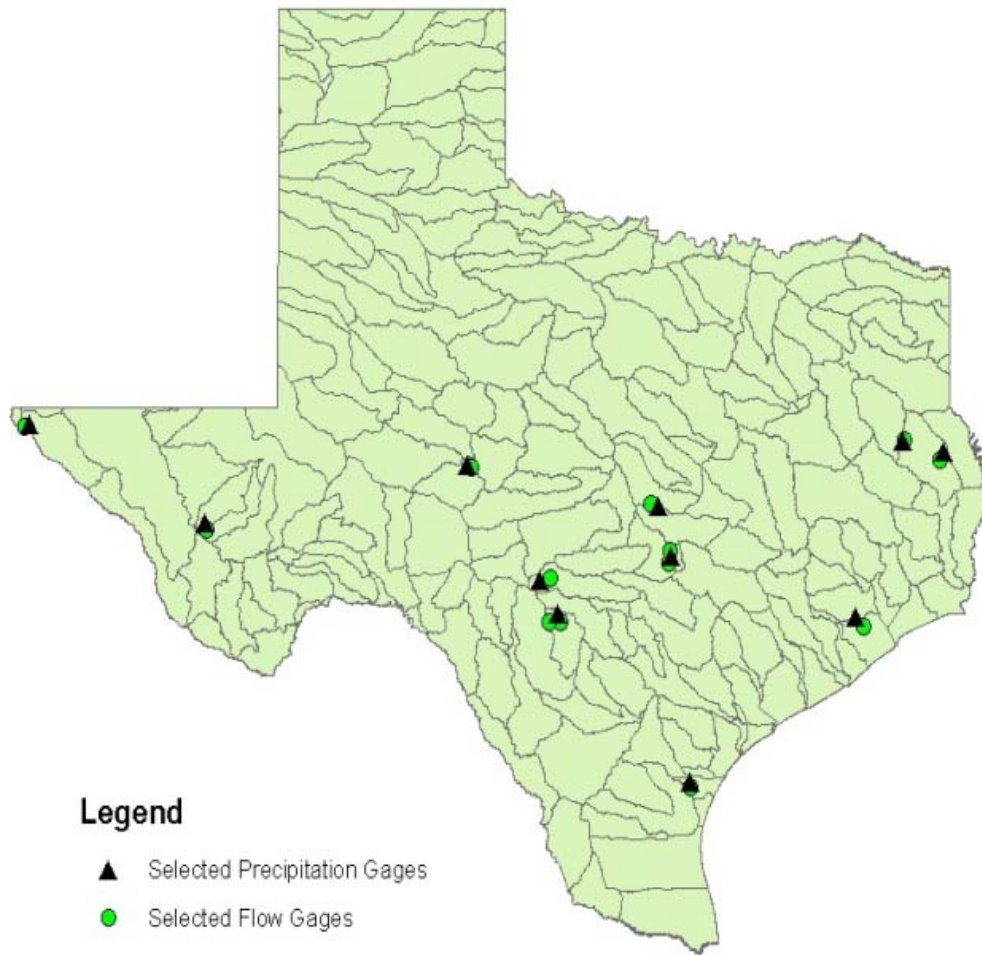


Figure 4-2. Location of the USGS Flow Gage and NCDC Rainfall Gage Pairs Chosen for the Investigation.

The yearly instantaneous peak flow (YIPF) was available at all 13 flow gages. Hourly precipitation is available at all chosen precipitation gages. Gage pairs were chosen based on the following criteria:

1. The drainage area of the flow gage should be less than 200 miles². The area that can be represented by a single rain gage has a limit; as the drainage area becomes large, the spatial variability of the rainfall plays an important role in flow generation and the relationship between rainfall and flow becomes weak.

2. The length of the flow record should be longer than 15 years. Since the purpose of the study was the flood frequency analysis to obtain Q_{100} and V_{100} , a minimal length of the recording period was necessary. The period of rainfall and flow record may not be identical. For example, the flow data may be available from 1950 to 2006 and the rainfall data from 1970 to 2003. In such a case, the analysis was based on the overlapping period. For this example, it would be from 1970 to 2003.
3. The distance between two gages should be less than 12 miles. The spatial variation of the rainfall plays an important role in the generation of flow. Therefore, as the distance between the flow gage and the rainfall gage increases, the uncertainty in predicting flow from rainfall increases. Thus, only the gage pairs separated by less than 12 miles were used.

The following procedure was used to investigate the possible relationship between an extreme rainfall event and the recorded flow corresponding to that event:

15. Acquire the YIPF and the date at which YIPF occurred for every overlapping year of flow and rainfall records.
16. Acquire the “concurrent” precipitation from the hourly precipitation records. Here, concurrent precipitation means the rainfall event that happened over a given time of concentration of the watershed (column 8 and 9 of [Table 4.1](#)) right before or during the day on which YIPF occurred. The starting time of the concurrent precipitation and the time of concentration of the watershed are adjusted so that the relationship between YIPF and rainfall volume can be optimized ([Figure 4-3](#)).
17. Calculate the volume of the rainfall that occurred within the watershed by multiplying the value that is obtained in step 2 by the drainage area of the flow gage.
18. Compare the YIPF and the volume of rainfall that occurred within the watershed.
19. Perform a frequency analysis for the flow and rainfall data that were obtained in steps 1 and 2. Compare the recurrence intervals of the YIPF and the concurrent precipitation.

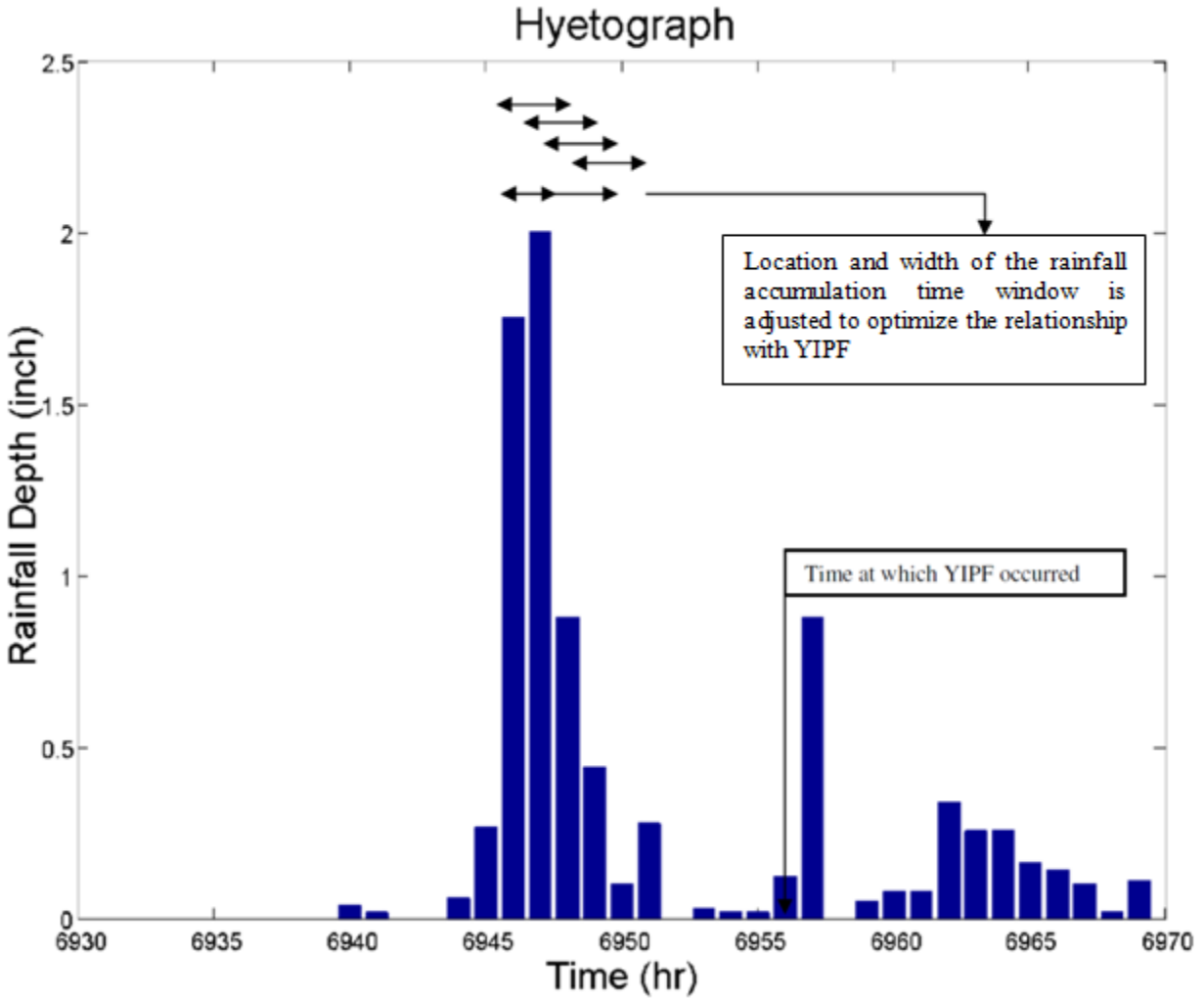


Figure 4-3. Illustration of the Methodology through Which the Rainfall Accumulation Time Window Is Determined.

4.4.1.2. Approach 1 Results

Relationship between the YIPF and the Concurrent Precipitation.

Figure 4-4 through Figure 4-16 shows the scatter plots between the YIPF and the concurrent precipitation at each of the gage pairs. Each data point on the plot reflects a year; thus the number of points in each scatter plot represents the total number of overlapping years between precipitation and flow records. The R^2 of the minimum squared error regression line for each scatter plot ranged from 0.003 to 0.58. Because there are many other hydrological variables that

affect the generation of flood other than precipitation, the poor relationship is not surprising. One would think that the correlation would improve for larger floods. However, this is not obvious as only 6 out of the 13 plots show this tendency. Furthermore, many cases give low flow events for high rainfall volume. Conversely, there were also cases with low rainfall events that resulted in high flow events. Also, for the station pair USGS08103900-NCDC1068 (Figure 4-6) and USGS08165300-NCDC4375 (Figure 4-10), the greatest flood was caused by zero rainfall depth. If the rainfall gauge during the flood time was working properly, this suggests that the spatial variation of the rainfall measurement should be considered an important factor affecting the generation of a flood. A more detailed description regarding the sources of poor relationship between rainfall and flow will be discussed in the following section of this chapter.

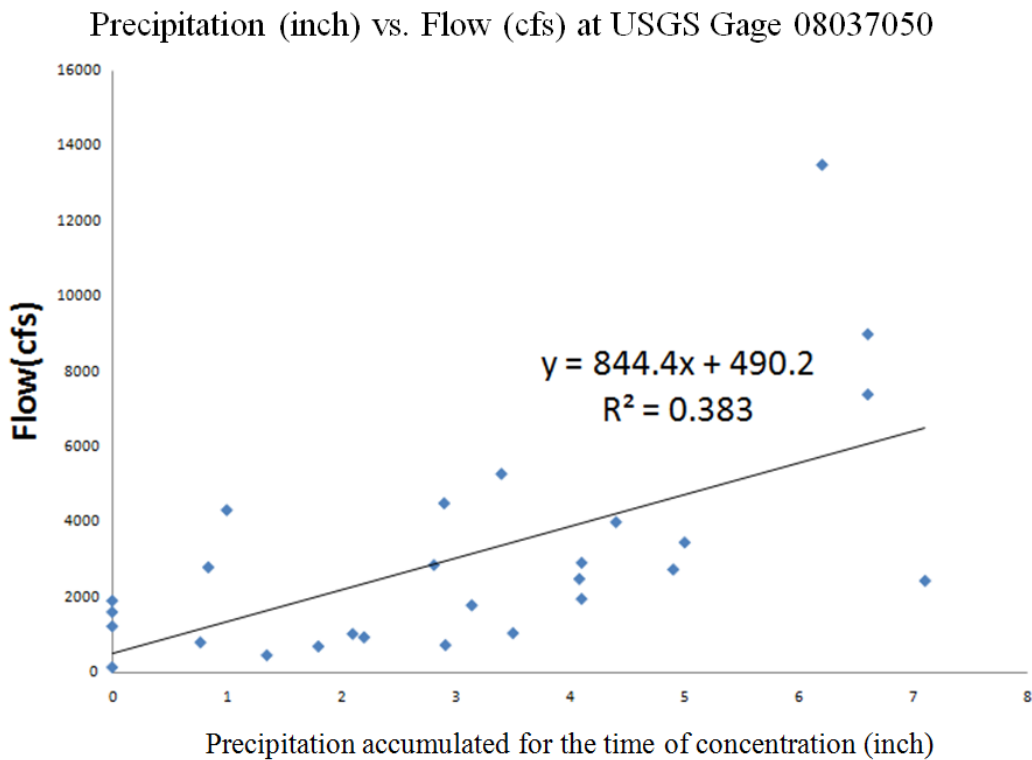


Figure 4-4. Relationship between Yearly Instantaneous Flow Peaks (y) and the Concurrent Rainfall Depth (x) at USGS Gage 08037050.

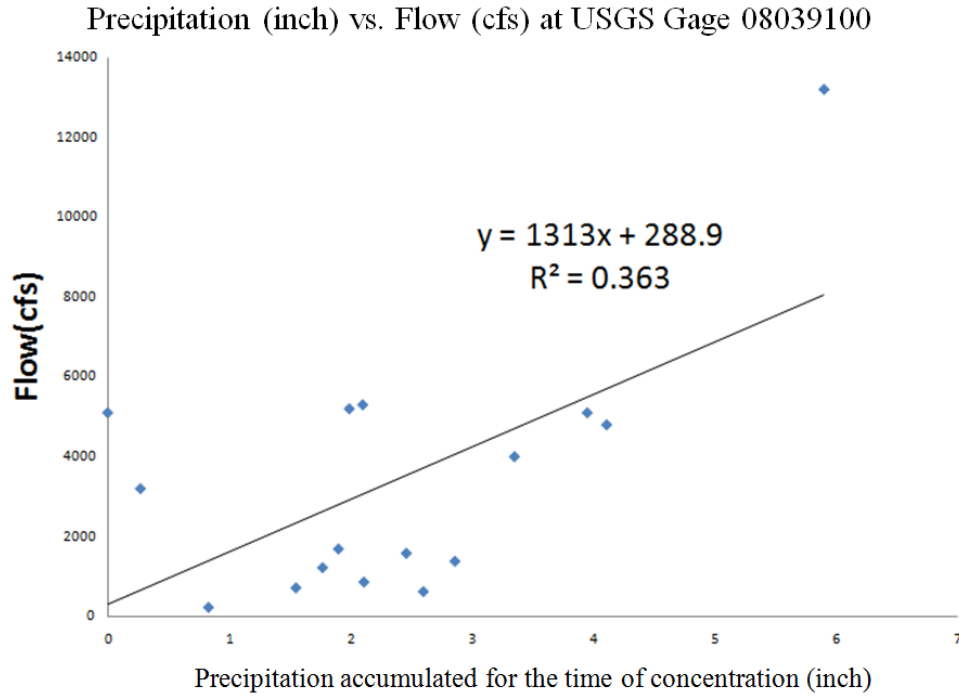


Figure 4-5. Relationship between Yearly Instantaneous Flow Peaks (y) and the Concurrent Rainfall Depth (x) at USGS Gage 08039100.

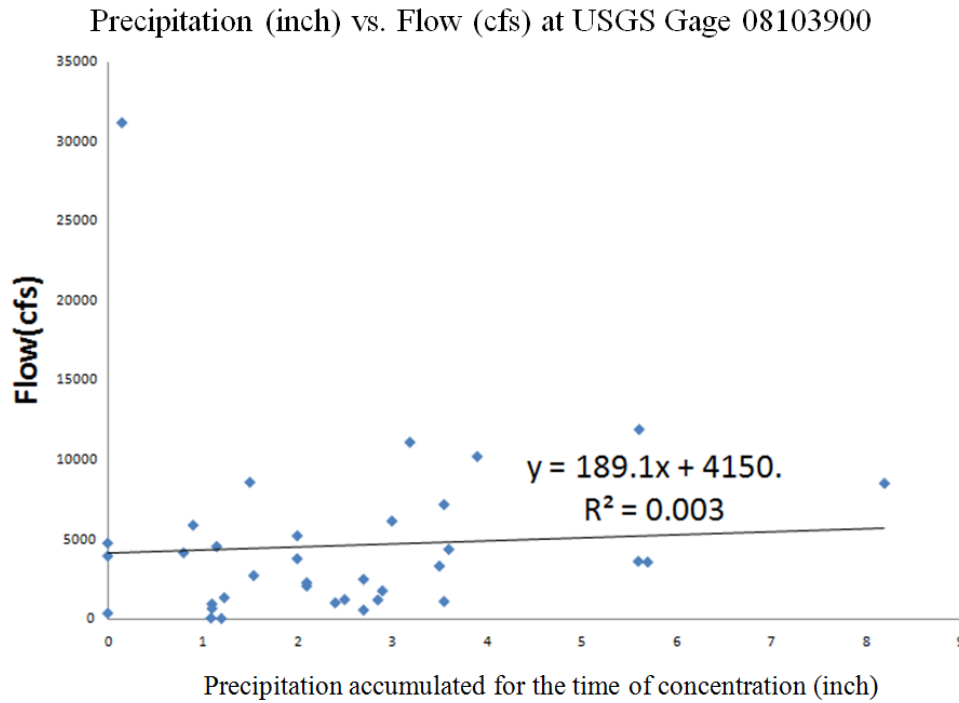


Figure 4-6. Relationship between Yearly Instantaneous Flow Peaks (y) and the Concurrent Rainfall Depth (x) at USGS Gage 08103900.

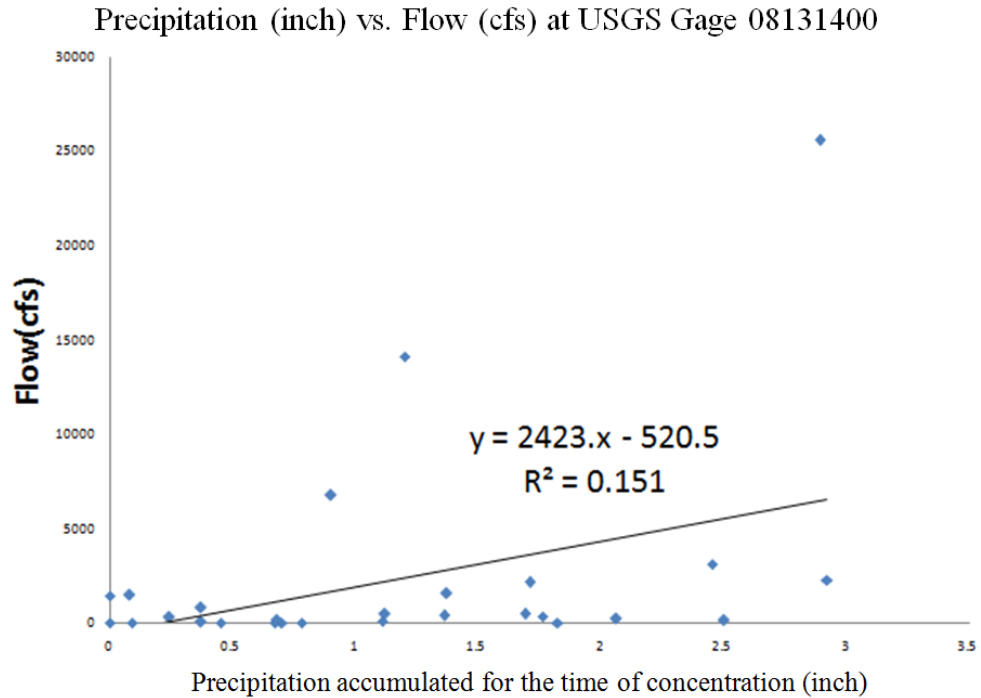


Figure 4-7. Relationship between Yearly Instantaneous Flow Peaks (y) and the Concurrent Rainfall Depth (x) at USGS Gage 08131400.

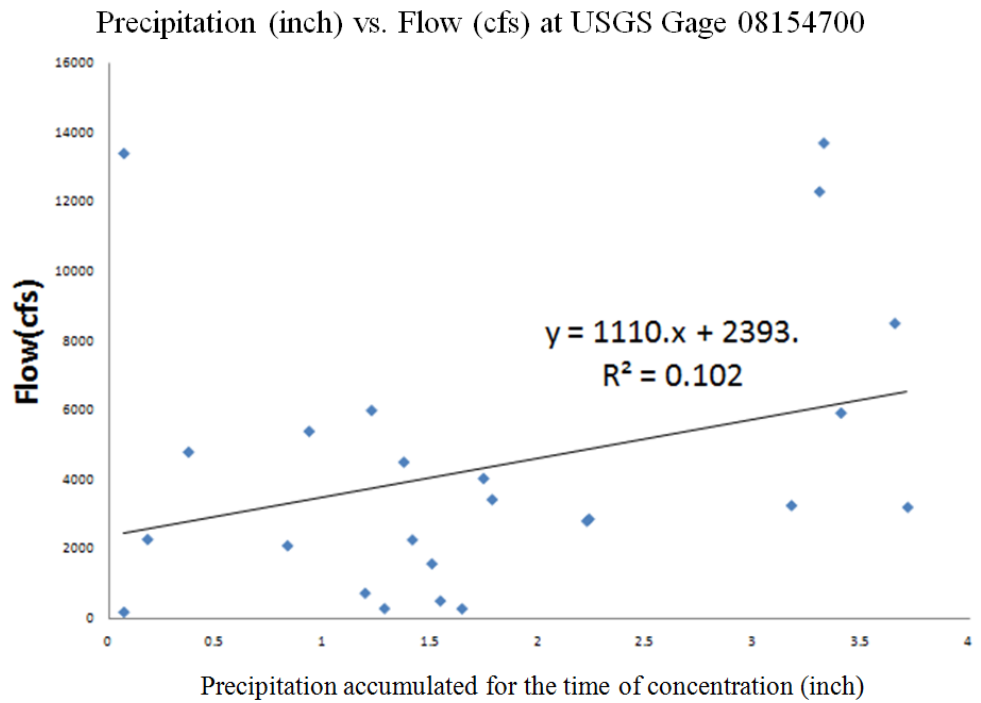


Figure 4-8. Relationship between Yearly Instantaneous Flow Peaks (y) and the Concurrent Rainfall Depth (x) at USGS Gage 08154700.

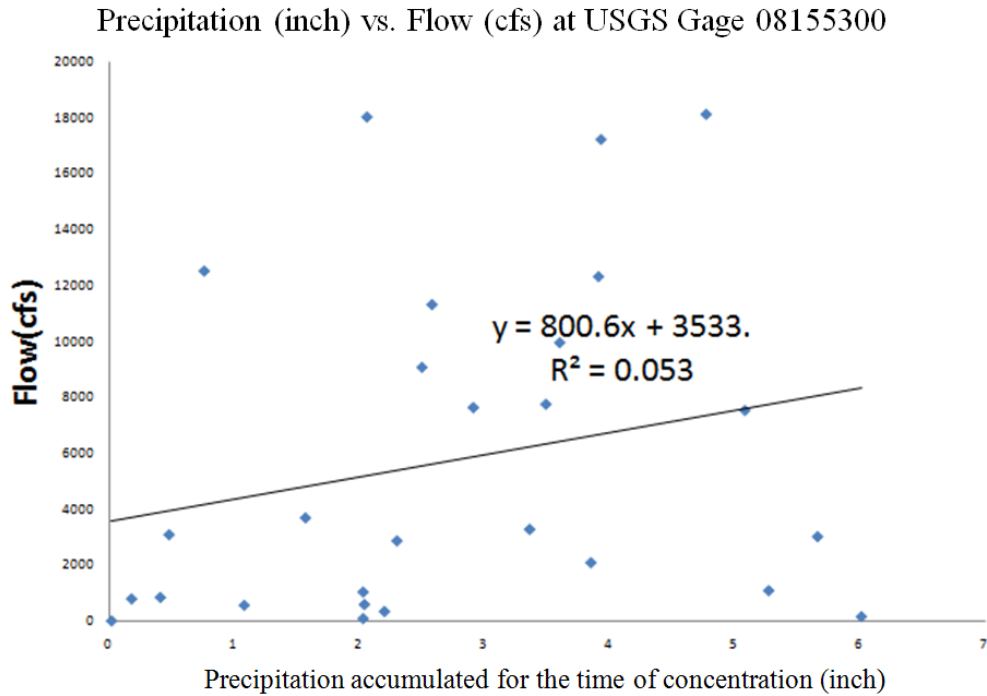


Figure 4-9. Relationship between Yearly Instantaneous Flow Peaks (y) and the Concurrent Rainfall Depth (x) at USGS Gage 08155300.

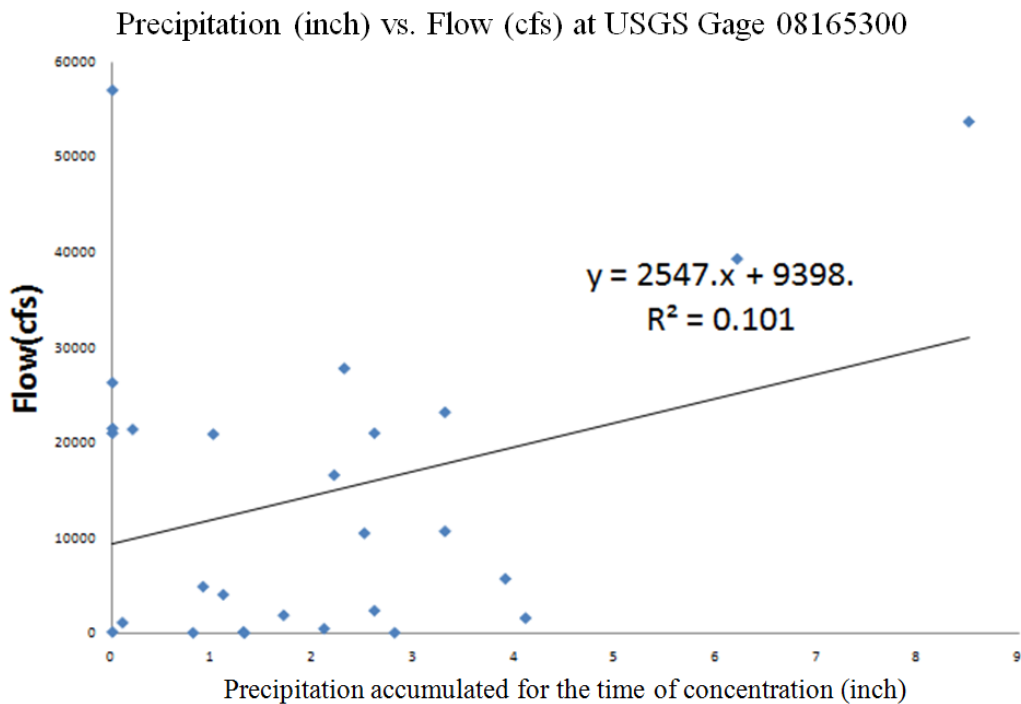


Figure 4-10. Relationship between Yearly Instantaneous Flow Peaks (y) and the Concurrent Rainfall Depth (x) at USGS Gage 08165300.

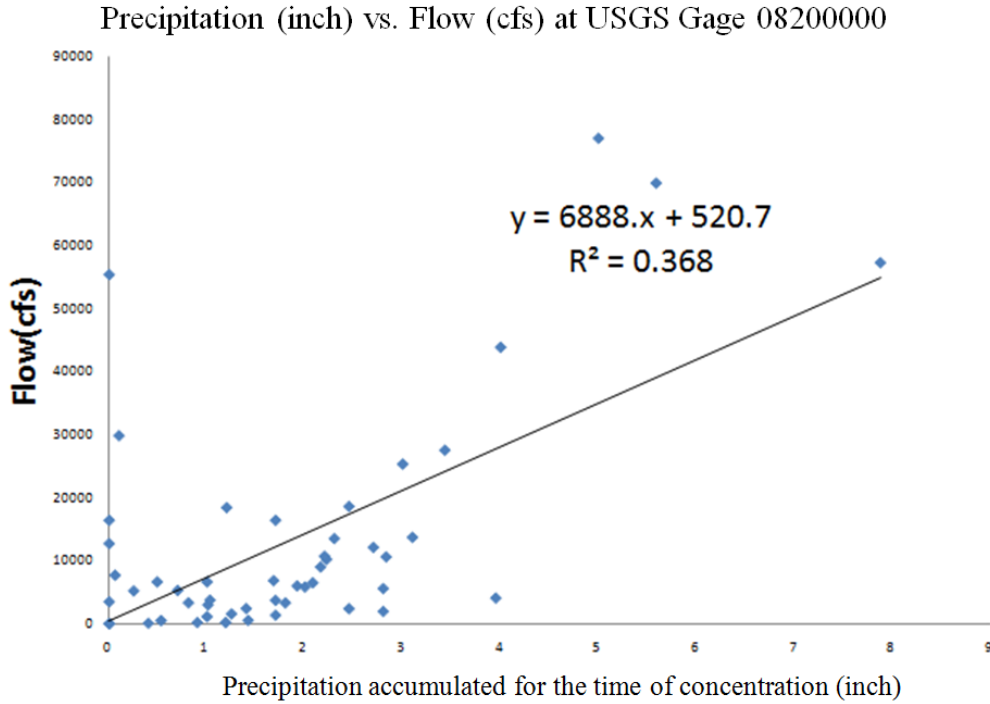


Figure 4-11. Relationship between Yearly Instantaneous Flow Peaks (y) and the Concurrent Rainfall Depth (x) at USGS Gage 08200000.

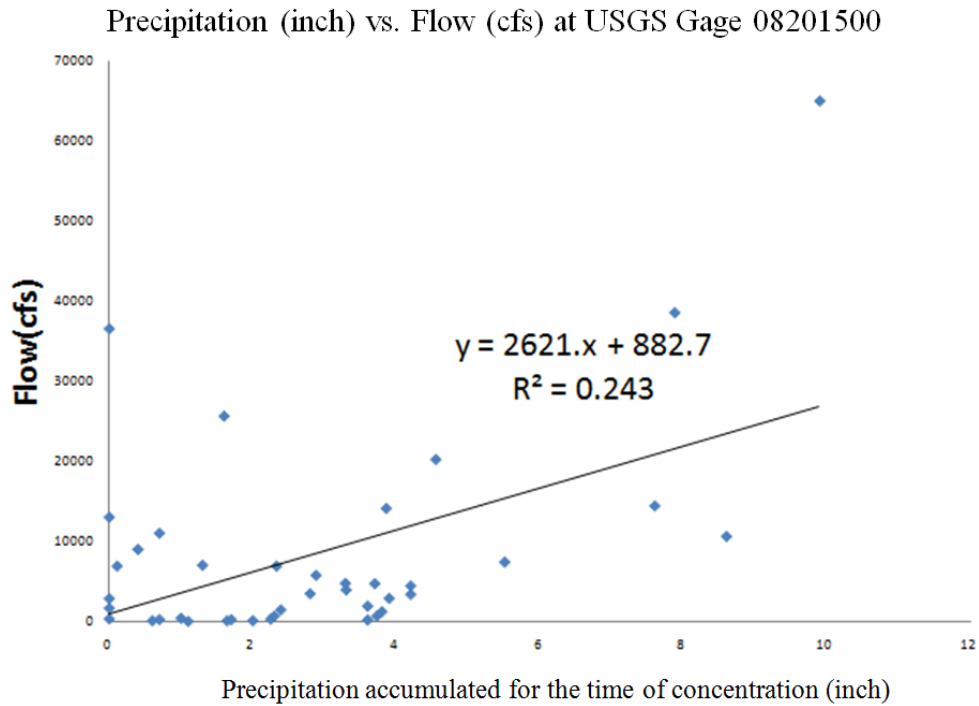


Figure 4-12. Relationship between Yearly Instantaneous Flow Peaks (y) and the Concurrent Rainfall Depth (x) at USGS Gage 08201500.

Precipitation (inch) vs. Flow (cfs) at USGS Gage 08211520

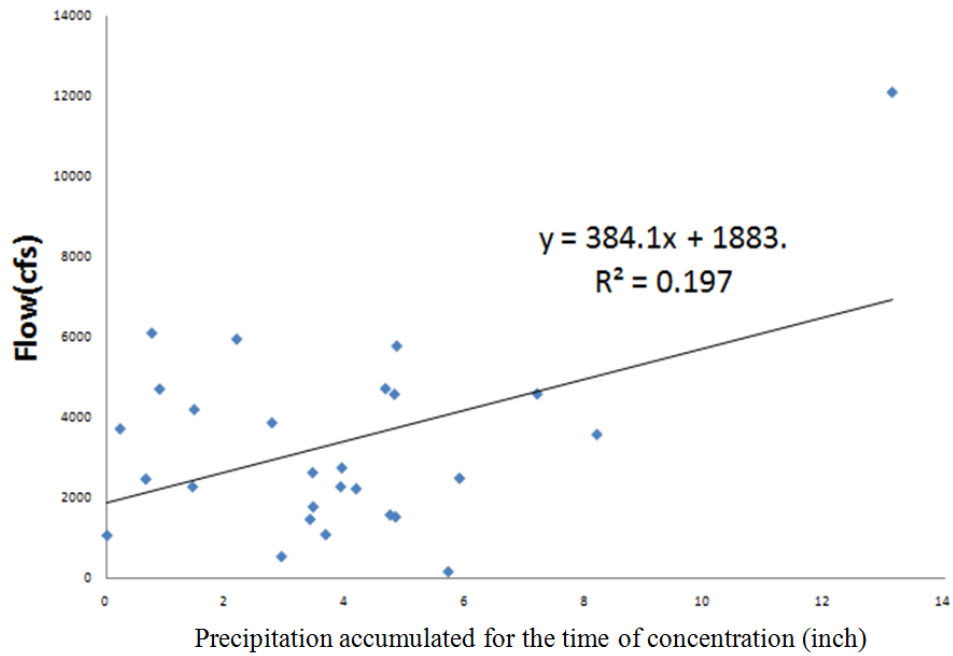


Figure 4-13. Relationship between Yearly Instantaneous Flow Peaks (y) and the Concurrent Rainfall Depth (x) at USGS Gage 08211520.

Precipitation (inch) vs. Flow (cfs) at USGS Gage 08365800

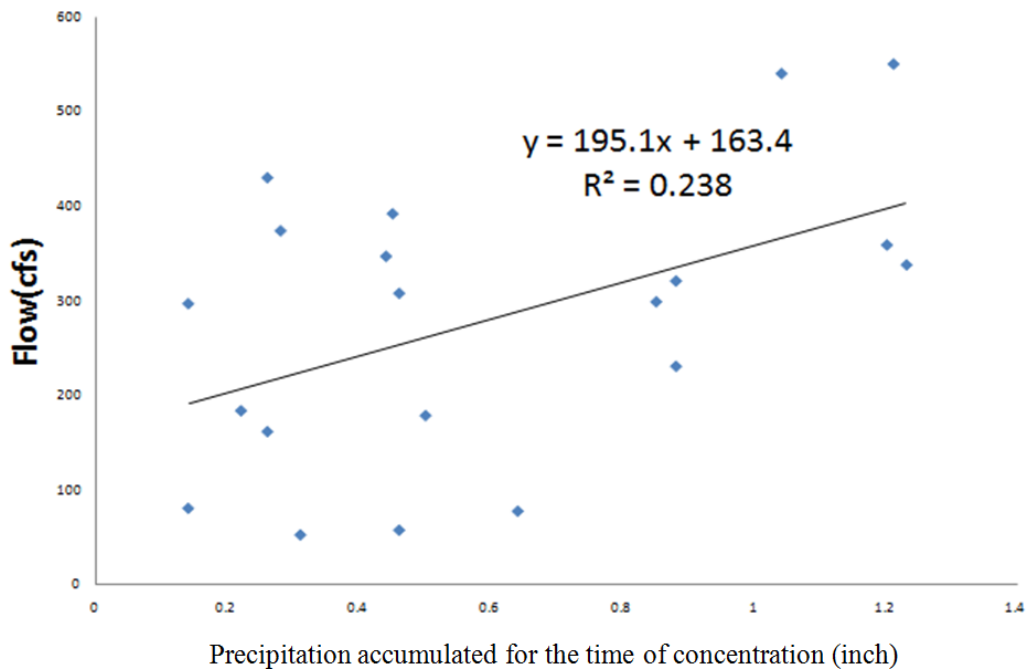


Figure 4-14. Relationship between Yearly Instantaneous Flow Peaks (y) and the Concurrent Rainfall Depth (x) at USGS Gage 08365800.

Precipitation (inch) vs. Flow (cfs) at USGS Gage 08431700

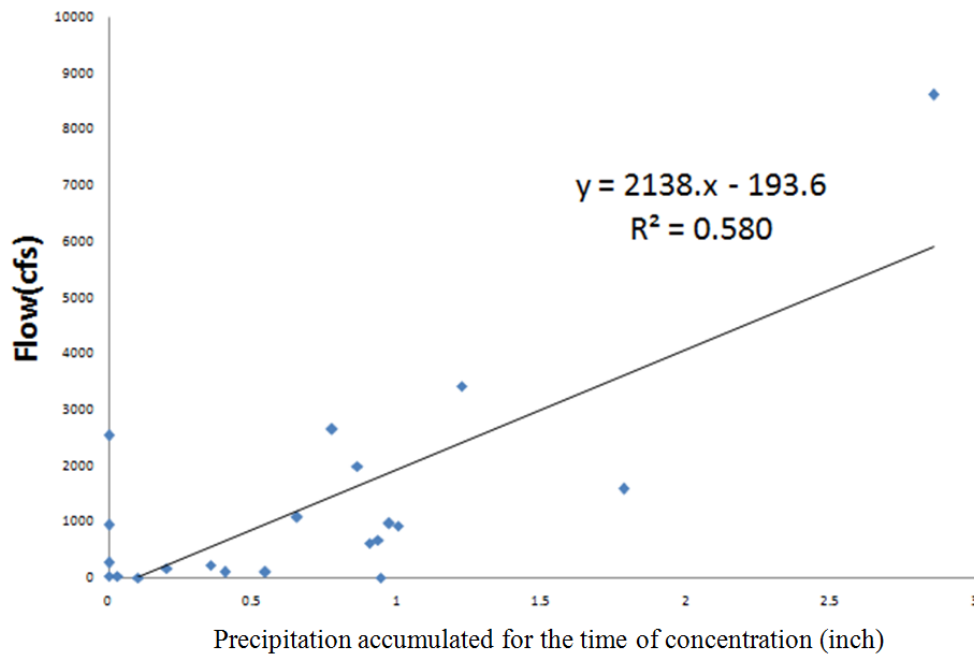


Figure 4-15. Relationship between Yearly Instantaneous Flow Peaks (y) and the Concurrent Rainfall Depth (x) at USGS Gage 08431700.

Precipitation (inch) vs. Flow (cfs) at USGS Gage 08365800

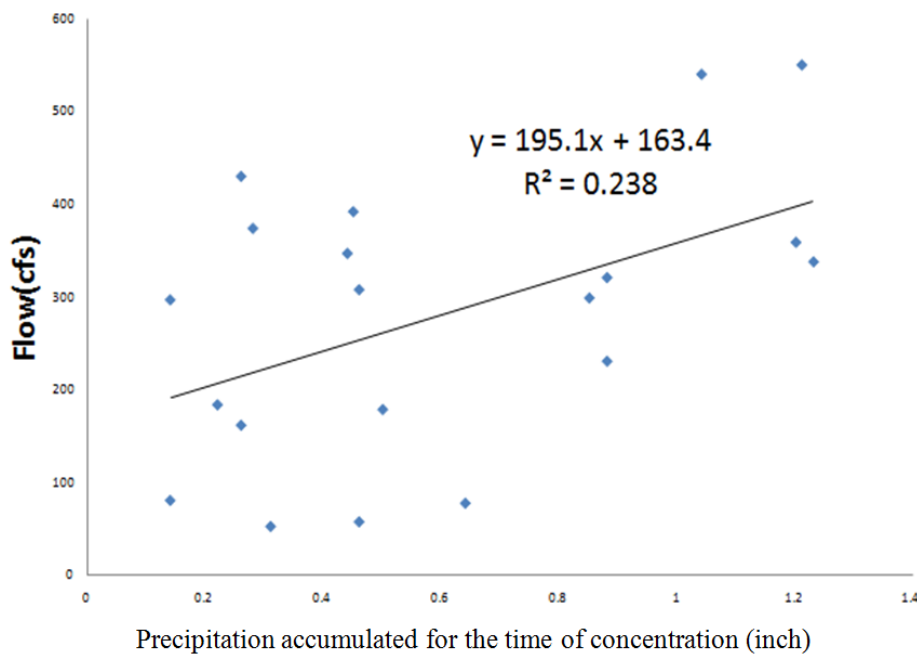


Figure 4-16. Relationship between Yearly Instantaneous Flow Peaks (y) and the Concurrent Rainfall Depth (x) at USGS Gage 08365800.

Relationship between the Recurrence Intervals of the YIPF and the Concurrent Precipitation.

The recurrence interval of the YIPF and the concurrent precipitation were also compared. Both parametric and non-parametric flood frequency analyses explained later in this chapter were attempted to acquire the recurrence interval of the flow and rainfall. [Figure 4-17](#) (the non-parametric approach) and [Figure 4-18](#) (the parametric approach) show the comparison of the recurrence interval of both variables. In the parametric approach of flood frequency analysis, flow records were assumed to have a generalized extreme value (GEV) distribution, and the parameters of the distribution were determined by the method of L-moments. The generalized logistic distribution (GLO) was used to capture the probability distribution of the precipitation records. The parameters were also determined using the method of L-moments. No clear relationship between the two variables was identified. There are many points indicating significant discrepancy between the recurrence interval of flow and rainfall. Based on the non-parametric approach of flood frequency analysis, most floods with a recurrence interval over 100 years were associated with the rainfall events with a return period of 30 years or less. Conversely, rainfall events with a return period of 120 years or more had a flood with a return period of 40 years or less. A similar trend was observed from the approach that used parametric frequency analysis. Explanations are given in the next section.

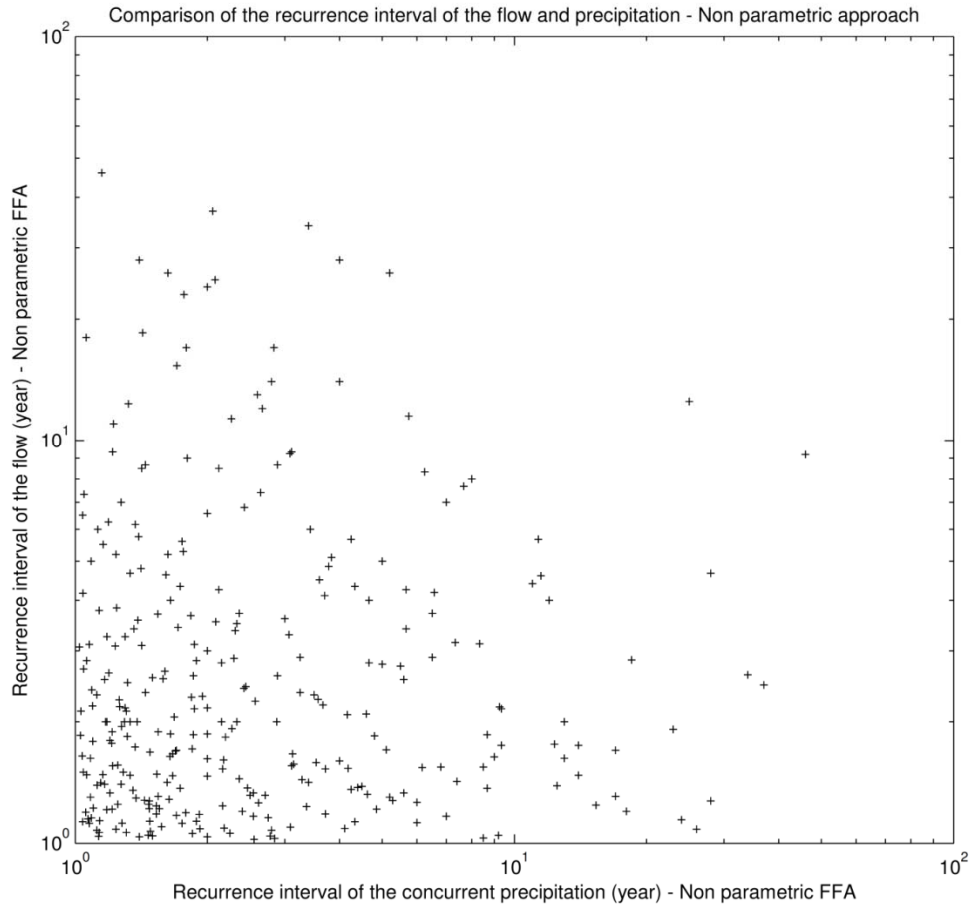


Figure 4-17. Relationship between the Recurrence Interval of the Rainfall and the Flow. The Non-parametric Approach to Flood Frequency Analysis Was Used to Estimate the Recurrence Intervals.

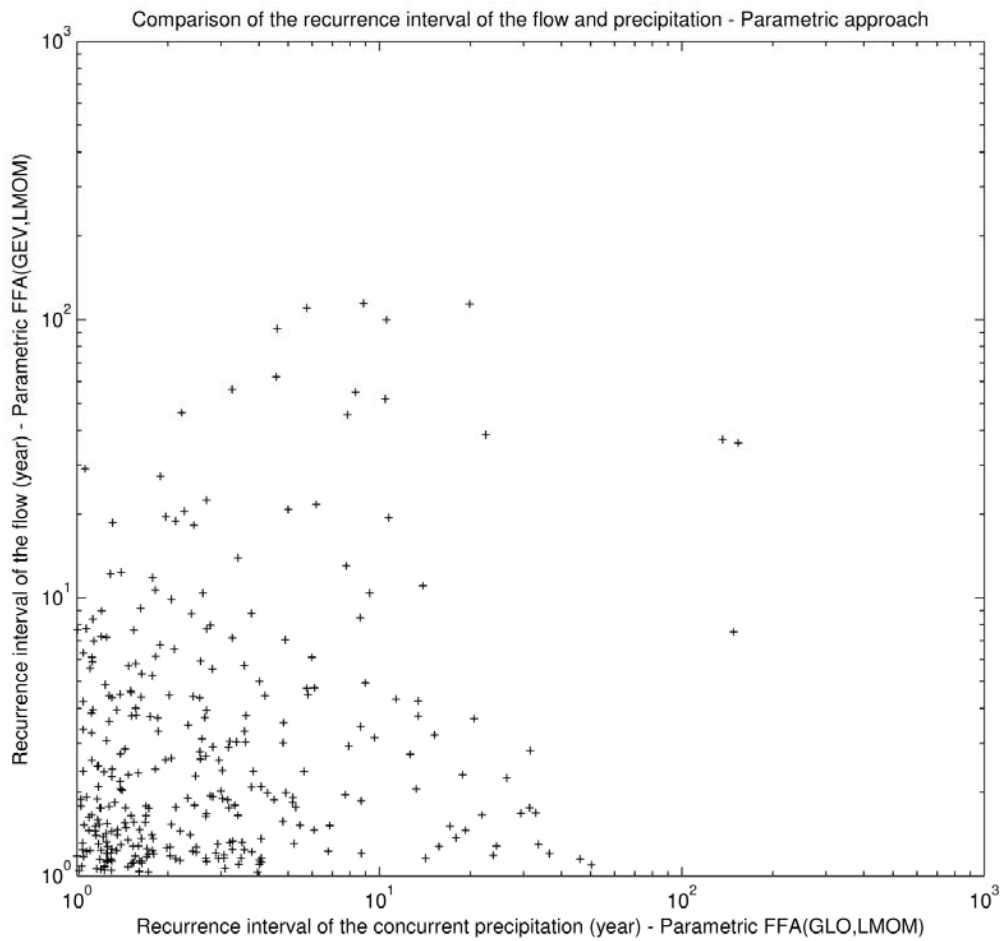


Figure 4-18. Relationship between the Recurrence Interval of the Rainfall and the Flow. The Parametric Approach to Flood Frequency Analysis Was Used to Estimate the Recurrence Intervals.

Uncertainty Analysis of Approach 1.

The histogram of the difference between the recurrence interval of flow and precipitation normalized by the sum of both was produced to analyze the uncertainty of Approach 1. A total of 311 values of the difference between flow and precipitation for 13 gages was used for the analysis. In [Figure 4-19](#), the plotting position formula was used to obtain the recurrence interval of the flow and of the precipitation. In [Figure 4-20](#), the GLO distribution was used to estimate the recurrence interval of precipitation, whereas the GEV distribution was used to estimate the

recurrence interval of the YIPF. Both histograms have means and modes that are approximately 0. The mean and the standard deviation of the first histogram was -0.0012 and 0.4474, respectively. The mean and standard deviation for the second histogram were -0.0152 and 0.4672, respectively. It is difficult to draw clear and conclusive remarks about these results because the values used to produce the histogram were normalized by the sum of the dependent variable (recurrence interval of flow) and independent variable (recurrence interval of precipitation). However, the following possible outcomes are expected in an effort to predict the recurrence interval of flow from the recurrence interval of the precipitation: (1) the recurrence interval of the flow has a tendency to approach to the recurrence interval of precipitation regardless of the magnitude of the recurrence interval of the precipitation. This is because the mean and mode of both histograms are close to 0; (2) while the tendency explained in (1) will be observed in many cases, there are also many chances that the recurrence interval of the flow is predicted to be significantly different from that of precipitation regardless of the magnitude of the recurrence interval of the precipitation. This is because the histograms have large standard deviations.

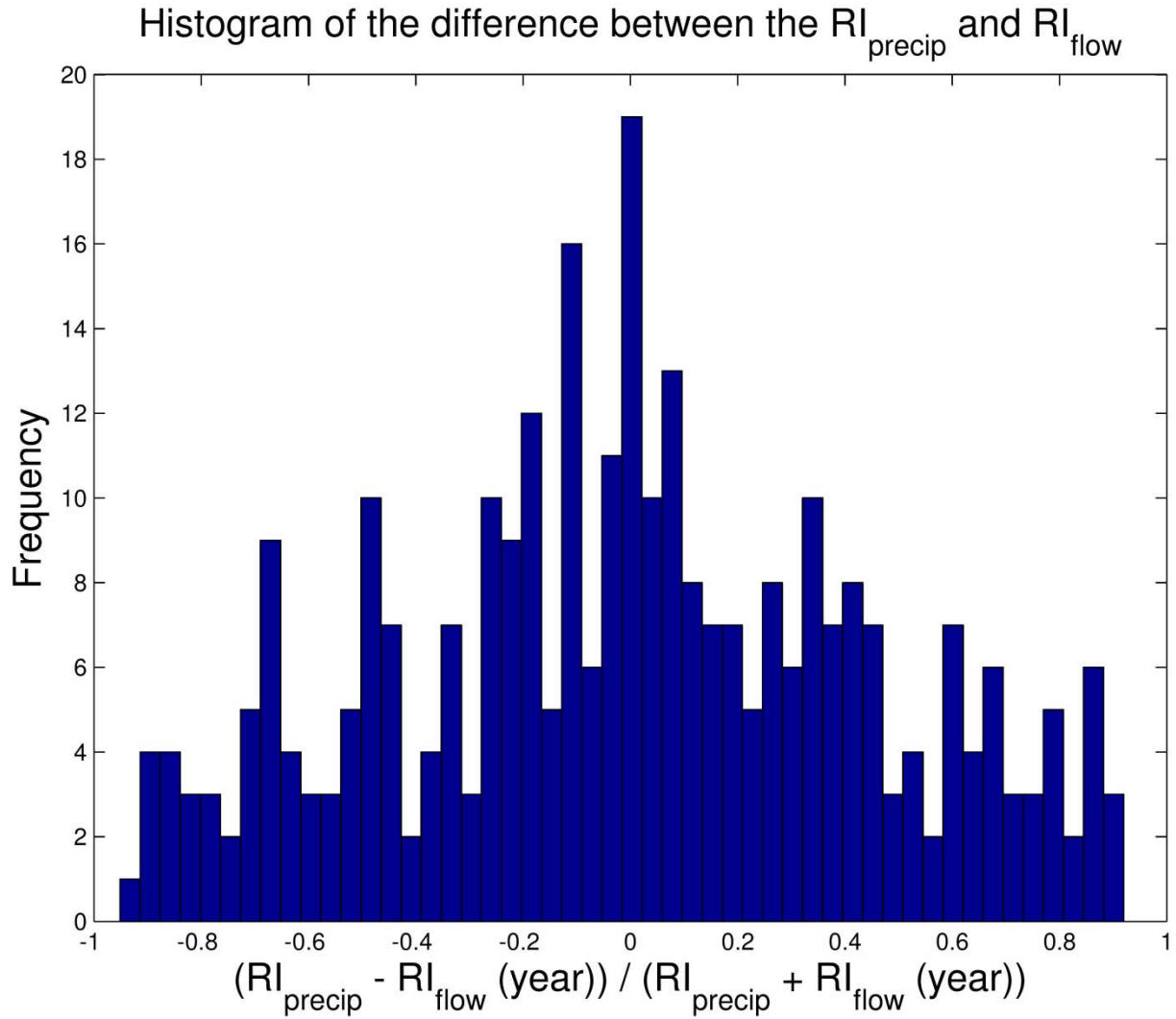


Figure 4-19. Histogram of the Difference between the Recurrence Interval of the Precipitation and That of Flow. The Plotting Position Formula Was Used When Estimating Recurrence Intervals of Flow and Precipitation.

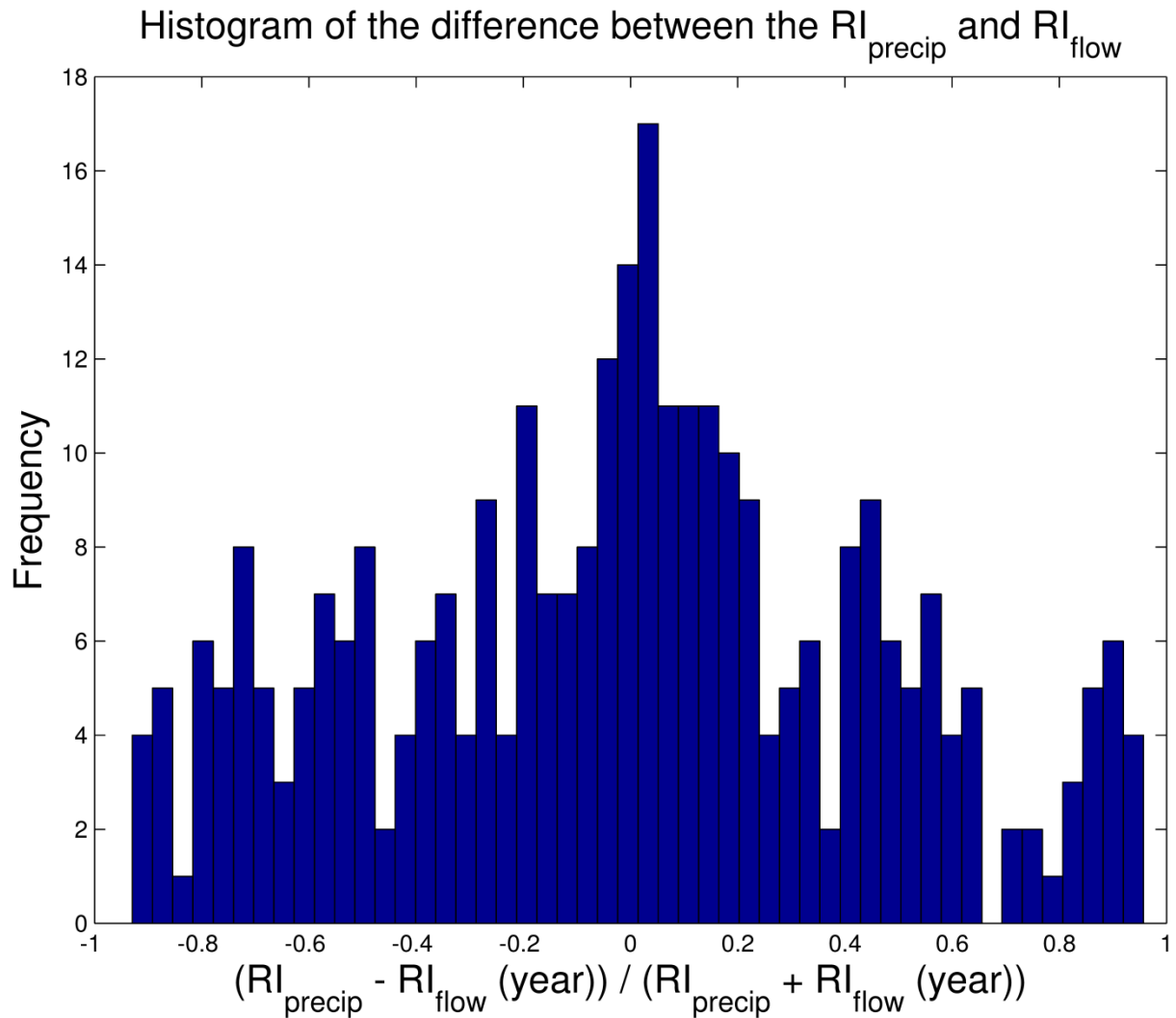


Figure 4-20. Histogram of the Difference between the Recurrence Interval of the Precipitation and That of Flow. The GLO and GEV Distribution Was Used to Estimate the Recurrence Interval of Precipitation and Flow, Respectively.

4.4.1.3. Approach 1 Discussion

According to the results of Approach 1, the assumption that the rainfall event with a high return period over a given threshold would cause a flood with a similar return period is not verified. Some important explanations for the poor relationship between rainfall and flow are proposed below.

Spatial Variability of the Rainfall.

The spatial coverage within which a single rainfall gage has uniform depth is about 10 miles² (Wurbs and James 2001). The assumption that the measured precipitation at one gage can represent the spatial variability of the rainfall over the entire watershed is very crude. Even for the case in which the rain gage was located near the center of the watershed, the relationship between the rainfall and flow did not show any distinct improvement. For example, NCDC rainfall gage 4375 was centered at USGS flow gage 08165300, but the highest flow measured in this gage was associated with zero rainfall. If the rain gages were working properly during the flood time, this indicates that a rainfall event that occurs on a small local part of the watershed away from a rain gage can cause a large flood without being detected by a rain gage nearby at the center of the watershed. Figure 4-21 illustrates this example. The plot shows the hyetograph (NCDC Gage ID TX-6177) and hydrograph (USGS 08030750) of the year 1979, in which the historical maximum YIPF was detected. Specific information about this gage pair is given in Table 4-1. A portion of the hydrograph that is indicated by the arrow is associated with zero rainfall. Only the spatial variability of the rainfall can explain the flow detected during this period. Conversely, there were many cases in which a rainfall event with an extremely high return period was associated with a flood of low recurrence interval. One possible reason for this phenomenon is that the detected rainfall event was limited to a small local part of the watershed. For example, in Figure 4-21, the highest recorded hourly precipitation is associated with low value of flow.

Hydrograph (USGS Gage 08030750) and Hyetograph (NCDC TX-6177) of the Year 1979

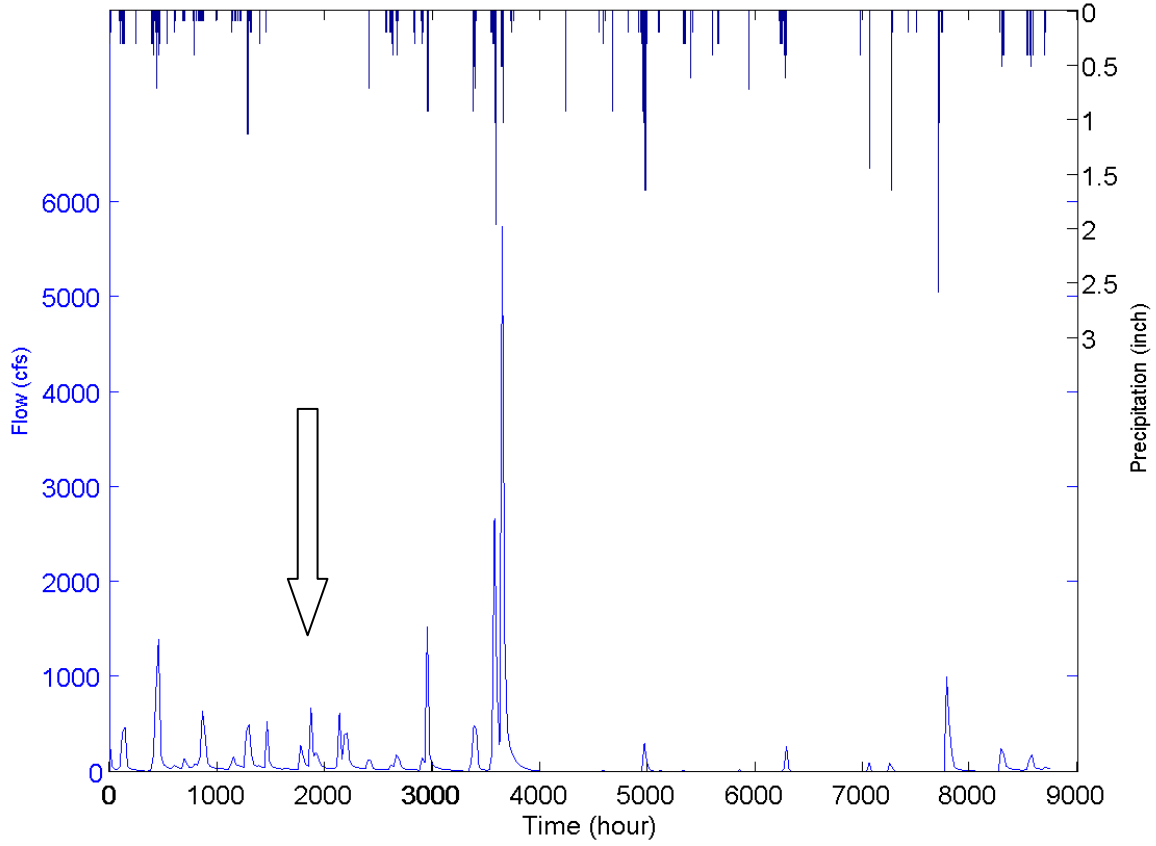


Figure 4-21. Hydrograph (USGS Gage 08030750) and Hyetograph (NCDC TX-6177) of the Year 1979. The Distance between the Two Gages Is 0.3 Miles.

Impact of the Other Factors Influencing Runoff Generation and Their Spatial Variability.

Other hydrologic factors such as initial soil-moisture condition, types of land cover, and land use have an impact on the rainfall to flow relationship. The spatial variability of these other factors will also adversely affect the assumption that the rainfall can be correlated to flows in rivers. There may be a threshold of rainfall amount beyond which the impact of these factors becomes insignificant, but it was not found in this study. The case event with a rainfall event with a high return period associated with a flood low recurrence interval can also be explained as follows: The soil could have been dry before these extreme rainfall events, or the land cover of the watershed could have been relatively more permeable than that of other watersheds. [Figure 4-21](#) through [Figure 4-23](#) show the hydrograph and hyetograph of adjacent flow gage–precipitation gage pairs obtained during a given year. The highest flood of the year is associated not only with the intensive precipitation event that occurred right before the flood but also with many rainfall events before it, which indicates the importance of the antecedent soil moisture condition.

4.4.2. Approach 2: Recurrence Interval Mapping Approach

Since the result of Approach 1 indicated that inferring flow information solely based on precipitation will yield highly inaccurate estimates, an alternative was investigated for acquiring the flow information at ungaged basins (Bridge-Gage Relationship Type IV). In this approach, the recurrence interval of the observed flow at flow gages in Texas was organized in a map, and an interpolation technique was used to acquire the recurrence interval of the flow at ungaged basins.

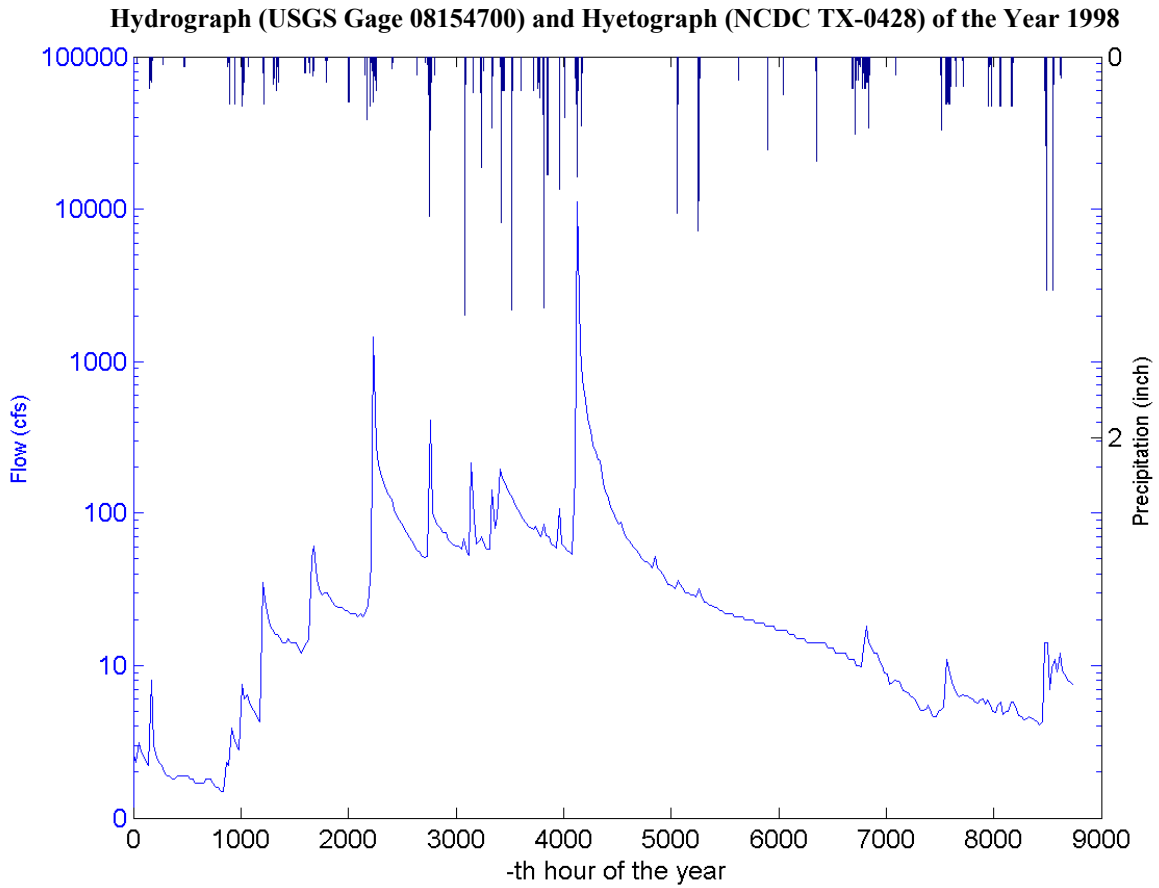


Figure 4-22. Hydrograph (USGS Gage 08154700) and Hyetograph (NCDC TX-0428) of the Year 1998. Distance between the Two Gages Is 3.9 Miles.

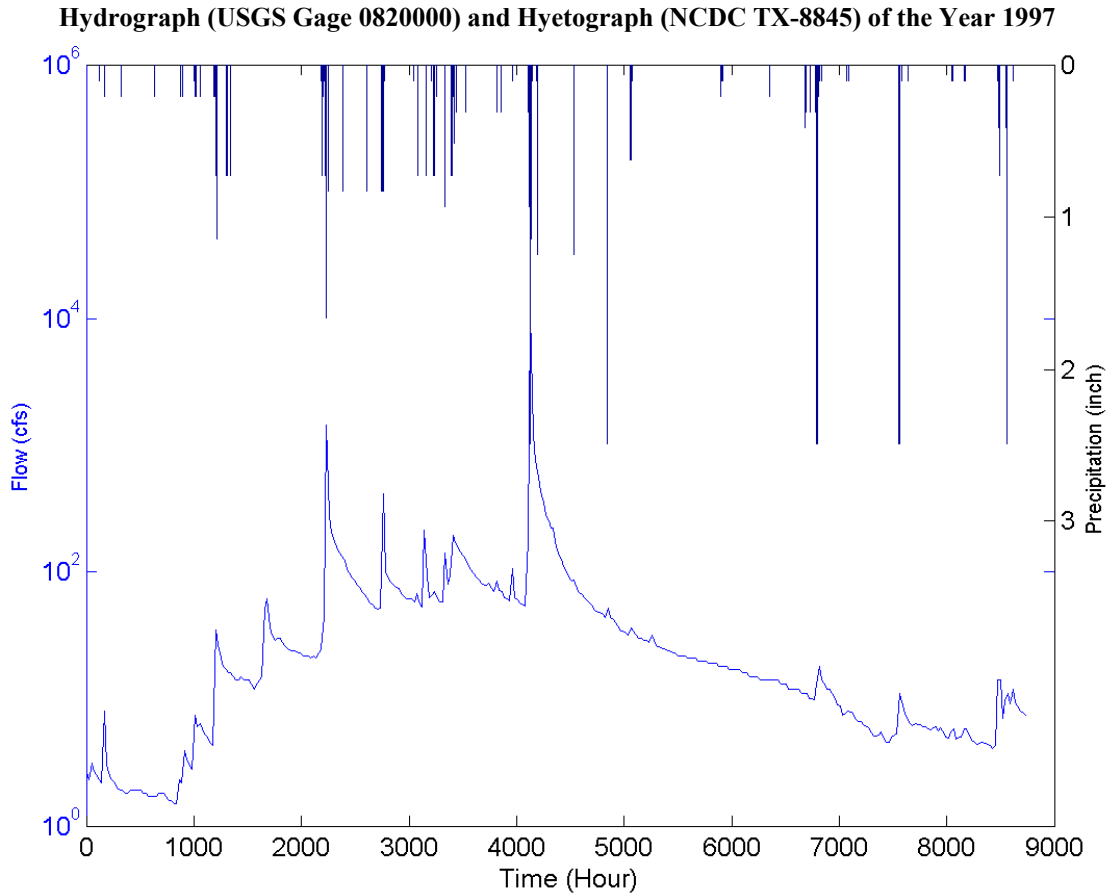


Figure 4-23. Hydrograph (USGS Gage 0820000) and Hyetograph (NCDC TX-8845) of the Year 1998. Distance between the Two Gages Is 7.4 Miles.

The following assumption is the basis for this approach: If an extreme flood event with a high recurrence interval is observed in one basin, a similar magnitude flood should happen as well at nearby locations. This is because of the following reasons:

20. The factors influencing the mechanisms of flood generation (i.e., watershed characteristics such as land cover, land use, and initial soil-moisture condition) are similar for adjacent basins.
21. Large rainfall events that cause large floods in one location are likely to have a spatial coverage large enough to cover nearby regions.

Once the recurrence interval of the Q_{mo} (maximum observed flow) is obtained by the aforementioned approach, it should be converted into Q_{100}/Q_{mo} (for BSA 1) or the explicit values of Q_{100} and Q_{mo} (for BSA 2 and BSA 3). For BSA 1, this study found a relationship between the recurrence interval of Q_{mo} and the value Q_{mo}/Q_{100} based on the flow data of 101 flow gages in Texas. The ratio Q_{100}/Q_{mo} is then converted into the ratio V_{100}/V_{mo} based on channel geometry. The method for this procedure based on Manning's equation is explained in a later section of this chapter. For BSA 2 and BSA 3, regional regression equations (Asquith and Roussel, 2009) are used to acquire Q_{100} and Q_{mo} first; then it is converted into V_{100} and V_{mo} based on channel geometry and properties. HEC-RAS (Hydrologic Engineering Center – River Analysis System) or TAMU-FLOW can be used for this process.

4.4.2.1. Approach 2 Methodology

Here, the methodology for developing the recurrence interval map is explained, including:

22. the process where the recurrence interval of the maximum flow experienced by the bridge is spatially interpolated from the nearby flow gages,
23. the process where the recurrence interval of Q_{mo} is converted into the ratio Q_{mo}/Q_{100} , and
24. the process where the ratio of the discharge (Q_1/Q_2) is converted into the ratio of velocity (V_1/V_2).

The steps of these processes are as follows:

25. Acquire the recurrence interval of the maximum flow experienced by a bridge. Estimating the recurrence interval of the maximum flow experienced by a bridge is the first step to obtain the required hydraulic information for this bridge scour analysis. The following step-by-step procedure was used to obtain this value:
 - a. Obtain the yearly flow peak data from flow gages that are close to the ungaged basin of concern.
 - b. Perform a flood frequency analysis for all those gages to obtain the recurrence interval of the YIPF at all gage locations during the years of concern (i.e., starting from the year in which the bridge was built to the year of the last bridge inspection).

- c. For each year, spatially interpolate the recurrence intervals of the YIPF at the nearby gages to acquire the recurrence interval at the ungaged location. Here, a linear interpolation method was used.
 - d. Acquire the recurrence interval of the maximum flood at the ungaged location during the period of concern by choosing the highest recurrence interval calculated in step c during that period.
26. Determine the relationship between the maximum recurrence interval and Q_{mo}/Q_{100} . Once the maximum recurrence interval (RI) is obtained, it should be converted into the ratio Q_{mo}/Q_{100} to be used in BSA 1. This value can be obtained through the relationship between the recurrence interval of the maximum observed flow and the ratio Q_{mo}/Q_{100} as shown in [Figure 4-24](#). Then, Q_{mo}/Q_{100} can be converted into V_{mo}/V_{100} using the relationship between the ratios of flow and velocity that is derived from Manning's equation. The ratio required by the scour analysis is V_{100}/V_{mo} ; thus the ratio V_{mo}/V_{100} , which is evaluated here, should be inverted before application in BSA 1.

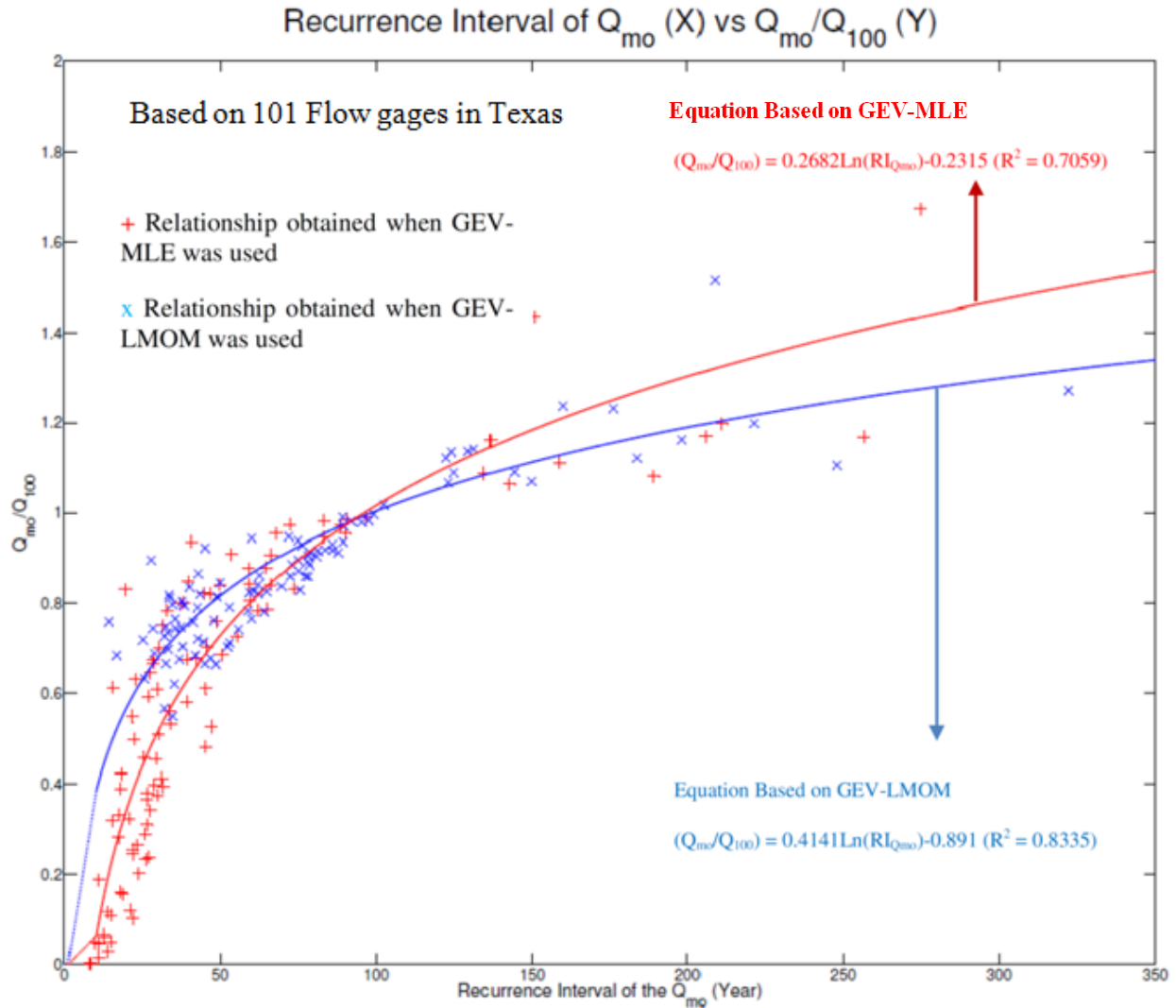


Figure 4-24. Relationship between the Recurrence Interval of the Maximum Flow Peak and the Ratio Q_{mo}/Q_{100} .

Figure 4-24 shows the relationship between the recurrence interval of Q_{mo} ($\text{RI}_{Q_{mo}}$) and the ratio Q_{mo}/Q_{100} based on 101 USGS gages across Texas. The gages were chosen by the following criteria:

- a. The length of record of the unregulated flow should exceed 20 years.
- b. The flow record at the gage should be well distributed so that the parametric approach of flood frequency analysis can be performed.

The locations of the USGS gages that contain such flow data (101 gages) are shown in [Figure 4-25](#). For each gage, a flood frequency analysis was performed to acquire the recurrence interval of the maximum of the yearly peak discharges and the 100-year flood. In [Figure 4-24](#), the recurrence interval of the maximum observed flow at each station is plotted on the x-axis, and the ratio Q_{mo}/Q_{100} on the y-axis. The scatter of x is the result from the flood frequency analysis based on the FFA method in which the generalized extreme value distribution and the L-moments (GEV-LMOM) were applied. The results scatter, plus correspond to the FFA method in which the generalized extreme value distribution and the maximum likelihood (GEV-MLE) were used. Detailed descriptions on GEV-LMOM and GEV-MLE are given later when the flood frequency analysis is discussed.

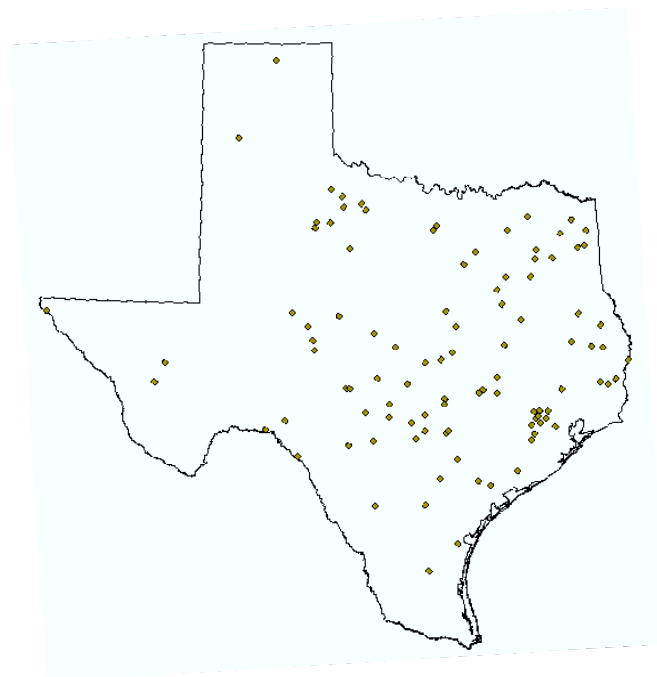


Figure 4-25. Location of the USGS Gages Used to Find Relationship between Recurrence Interval of Flow Peaks and Ratio of Flow.

The relationship between the two variables is apparent with R^2 of 0.71 (GEV-LMOM) and 0.83 (GEV-MLE). Thus, this study suggests the following regression equations to obtain the ratio Q_{mo}/Q_{100} from the recurrence interval estimate of the maximum flow peak:

When GEV-LMOM is preferred:

$$\frac{Q_{mo}}{Q_{100}} = 0.4141 \ln(RI_{Q_{mo}}) - 0.89, \text{ if } RI_{Q_{mo}} > 10 \quad (4-3)$$

$$\frac{Q_{mo}}{Q_{100}} = \frac{0.0635}{9} (RI_{Q_{mo}} - 1), \text{ if } RI_{Q_{mo}} \leq 10 \quad (4-4)$$

When GEV-MLE is preferred:

$$\frac{Q_{mo}}{Q_{100}} = 0.2682 \ln(RI_{Q_{mo}}) - 0.2315, \text{ if } RI_{Q_{mo}} > 10 \quad (4-5)$$

$$\frac{Q_{mo}}{Q_{100}} = \frac{0.3861}{9} (RI_{Q_{mo}} - 1), \text{ if } RI_{Q_{mo}} \leq 10 \quad (4-6)$$

In Equation (4-3) through Equation (4-6), $RI_{Q_{mo}}$ is the recurrence interval of the YIPF. Both equations can yield a negative value of Q_{mo}/Q_{100} for a small recurrence interval (i.e., less than 2 years). To prevent the equations from yielding a negative value, the portion of the equation that yields the negative recurrence interval was linearly interpolated as Equation (4-4) and Equation (4-6).

27. Determine the relationship between Q_{mo}/Q_{100} and V_{mo}/V_{100} . Once the ratio Q_{mo}/Q_{100} is obtained using the methods suggested in the previous sections, it should be converted into V_{100}/V_{mo} to be applied in BSA 1. The ratio V_{mo}/V_{100} can be obtained without having to know the explicit values of V_{mo} and V_{100} by using Manning's equation. The equation that converts one ratio to the other depends on the shape of the channel cross section. The shapes of the channel are categorized according to a wide channel and a narrow channel:

- a. Wide channel. If the depth of the channel is significantly smaller than the width of the channel (Figure 4-26), the area and the wetted parameter of the channel can be approximated by the following equations:

$$A = dw \quad (4-7)$$

$$P = w + 2d \cong w \quad (4-8)$$

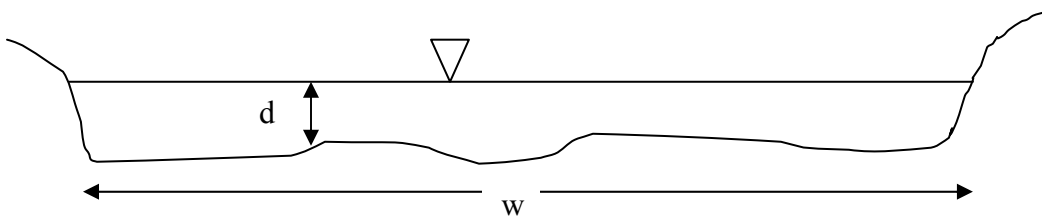


Figure 4-26. Wide Channel.

Thus, the hydraulic radius, R_h , of the channel can be approximated as follows:

$$R_h = \frac{A}{P} = \frac{dw}{w} = d \quad (4-9)$$

Here, we introduce two hypothetical flow values in the wide channel, Q_1 and Q_2 , and the corresponding velocity values V_1 and V_2 . By Manning's equation:

$$Q_1 = \frac{1}{n} A_1 R_{h1}^{\frac{2}{3}} S_1^{\frac{1}{2}} \quad (4-10)$$

$$Q_2 = \frac{1}{n} A_2 R_{h2}^{\frac{2}{3}} S_2^{\frac{1}{2}} \quad (4-11)$$

where A_1 , R_{h1} , and S_1 represent the area, the hydraulic radius, and the slope of the channel for Q_1 , respectively; and A_2 , R_{h2} , and S_2 represent the same values for Q_2 , respectively.

The ratio $\frac{Q_1}{Q_2}$ is:

$$\frac{Q_1}{Q_2} = \frac{\frac{1}{n} A_1 R_{h_1}^{\frac{2}{3}} S_1^{\frac{1}{2}}}{\frac{1}{n} A_2 R_{h_2}^{\frac{2}{3}} S_2^{\frac{1}{2}}} \quad (4-12)$$

Because $S_1 = S_2$:

$$\frac{Q_1}{Q_2} = \frac{A_1 R_{h_1}^{\frac{2}{3}}}{A_2 R_{h_2}^{\frac{2}{3}}} \quad (4-13)$$

Here, from Equation (4-7) and Equation (4-9):

$$A_1 = d_1 w \quad (4-14)$$

$$A_2 = d_2 w \quad (4-15)$$

$$R_{h_1} = d_1 \quad (4-16)$$

$$R_{h_2} = d_2 \quad (4-17)$$

Thus:

$$\frac{Q_1}{Q_2} = \frac{d_1 w d_1^{\frac{2}{3}}}{d_2 w d_2^{\frac{2}{3}}} = \frac{d_1^{\frac{5}{3}}}{d_2^{\frac{5}{3}}} \quad (4-18)$$

The ratio $\frac{V_1}{V_2}$ is given by:

$$\frac{V_1}{V_2} = \frac{\frac{1}{n} R_{h_1}^{\frac{2}{3}} S_1^{\frac{1}{2}}}{\frac{1}{n} R_{h_2}^{\frac{2}{3}} S_2^{\frac{1}{2}}} \quad (4-19)$$

In a similar manner:

$$\frac{V_1}{V_2} = \frac{R_{h_1}^{\frac{2}{3}}}{R_{h_2}^{\frac{2}{3}}} = \frac{d_1^{\frac{2}{3}}}{d_2^{\frac{2}{3}}} \quad (4-20)$$

From Equation (4-17) and Equation (4-19):

$$\frac{V_1}{V_2} = \frac{R_{h_1}^{\frac{2}{3}}}{R_{h_2}^{\frac{2}{3}}} = \left[\frac{d_1^{\frac{5}{3}}}{d_2^{\frac{5}{3}}} \right]^{\frac{2}{5}} = \left[\frac{Q_1}{Q_2} \right]^{\frac{2}{5}} = \left[\frac{Q_1}{Q_2} \right]^{0.4} \quad (4-21)$$

- b. Narrow channel. The triangular channel shown in [Figure 4-27](#) is the case in which the depth of the channel is larger than the width. In such a case, the width and the depth of the flow area can be expressed as follows:

$$w = 2a \cdot \sin\theta \quad (4-22)$$

$$d = a \cdot \cos\theta \quad (4-23)$$

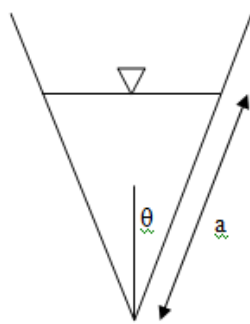


Figure 4-27. Narrow Channel.

The ratio $\frac{Q_1}{Q_2}$ is:

$$\frac{Q_1}{Q_2} = \frac{\frac{1}{n} A_1 R_{h1}^{\frac{2}{3}} S_1^{\frac{1}{2}}}{\frac{1}{n} A_2 R_{h2}^{\frac{2}{3}} S_2^{\frac{1}{2}}} \quad (4-24)$$

Because $S_1 = S_2$:

$$\frac{Q_1}{Q_2} = \frac{A_1 R_{h1}^{\frac{2}{3}}}{A_2 R_{h2}^{\frac{2}{3}}} \quad (4-25)$$

where:

$$A_1 = a_1^2 \cos\theta \sin\theta \quad (4-26)$$

$$A_2 = a_2^2 \cos\theta \sin\theta \quad (4-27)$$

$$R_{h1} = \frac{a_1^2 \cos\theta \sin\theta}{2a_1} = \frac{a_1 \cos\theta}{2}$$

$$R_{h2} = \frac{a_2^2 \cos\theta \sin\theta}{2a_2} = \frac{a_2 \cos\theta}{2}$$

Thus:

$$\frac{Q_1}{Q_2} = \frac{a_1^2 \cos\theta \sin\theta \left(\frac{a_1 \cos\theta}{2}\right)^{\frac{2}{3}}}{a_2^2 \cos\theta \sin\theta \left(\frac{a_2 \cos\theta}{2}\right)^{\frac{2}{3}}} = \left(\frac{a_1}{a_2}\right)^{\frac{8}{3}} \quad (4-28)$$

The ratio $\frac{V_1}{V_2}$ is given by:

$$\frac{V_1}{V_2} = \frac{\frac{1}{n} R_{h1}^{\frac{2}{3}} S_1^{\frac{1}{2}}}{\frac{1}{n} R_{h2}^{\frac{2}{3}} S_2^{\frac{1}{2}}} \quad (4-29)$$

In a similar manner:

$$\frac{V_1}{V_2} = \frac{R_{h1}^{\frac{2}{3}}}{R_{h2}^{\frac{2}{3}}} = \frac{\left(\frac{a_1 \cos \theta}{2}\right)^{\frac{2}{3}}}{\left(\frac{a_2 \cos \theta}{2}\right)^{\frac{2}{3}}} = \left(\frac{a_1}{a_2}\right)^{\frac{2}{3}} \quad (4-30)$$

From Equation (4-28) and Equation (4-30):

$$\frac{V_1}{V_2} = \left(\frac{a_1}{a_2}\right)^{\frac{2}{3}} = \left[\left(\frac{a_1}{a_2}\right)^{\frac{8}{3}}\right]^{\frac{1}{4}} = \left[\frac{Q_1}{Q_2}\right]^{\frac{1}{4}} = \left[\frac{Q_1}{Q_2}\right]^{0.25} \quad (4-31)$$

Assuming that the flow cross section falls between the two extremes of a wide and a narrow section, it can be concluded that:

$$\left[\frac{Q_1}{Q_2}\right]^{\frac{1}{4}} < \frac{V_1}{V_2} < \left[\frac{Q_1}{Q_2}\right]^{\frac{2}{5}} \quad (4-32)$$

The choice of the exponent (0.25 – 0.4) can be made based on the shape of the cross section of the channel. If the depth of the flow is small compared to the width, one can choose an exponent that is close to 0.4. If the depth of flow is large compared to the width, one can choose an exponent close to 0.25. Most rivers fall in the category of wide and shallow, and an exponent of 0.35 may be a reasonable approximation on the average:

$$\frac{V_1}{V_2} \cong \left[\frac{Q_1}{Q_2}\right]^{0.35} \quad (4-33)$$

4.4.2.2. Approach 2 Validation

To see if the estimated ratio V_{mo}/V_{100} is close to the observed ratio V_{mo}/V_{100} , the following approach was used:

28. Obtain the recurrence interval of an observed flood at a gage.
29. Assume that the flow gage is nonexistent and estimate the recurrence interval at the gage by spatially interpolating the recurrence intervals of the flow observed at nearby gages. This value is the cross-validated recurrence interval (CVRI).
30. Calculate Q_{mo}/Q_{100} for both the observed and cross-validated recurrence interval using Equation (4-3), Equation (4-4), Equation (4-5), or Equation (4-6).
31. Convert the ratio Q_{mo}/Q_{100} into V_{mo}/V_{100} using Equation (4-33).
32. Compare V_{mo}/V_{100} calculated from the observed recurrence interval and the cross-validated recurrence interval in step 4.

This procedure is called cross validation. A match between the observed and cross-validated value is an indicator of spatial tendency. The cross validation of V_{mo}/V_{100} was performed for all observed flow peaks that happened in Texas during the period 1950 to 2006. A total of 27,070 flow peaks were cross validated. Among these flow peaks, the ones observed at gages that were less than 120 miles from other gages were chosen for further analysis (a total of 3845 flow peaks). This filtering criterion was used because even the largest storm observed at one location in a given year has a limited spatial coverage, which was assumed to be 120 miles in this study. The result of the cross validation is shown in [Figure 4-28](#). The correlation coefficient between the two variables is 0.61. This means that V_{mo}/V_{100} at the bridge location without a flow gage can be predicted, with a certain accuracy, by spatially interpolating the results from the gages located less than 120 miles from the bridge location. The slope and the intercept of the regression equation was 0.58 and 0.2, respectively. The 1:1 line and the regression equation meet when V_{mo}/V_{100} equals 0.45. This suggests that the predicted V_{mo}/V_{100} greater than 0.45 is generally under-estimates, which puts the result of the scour analysis on a safer side, and vice versa.

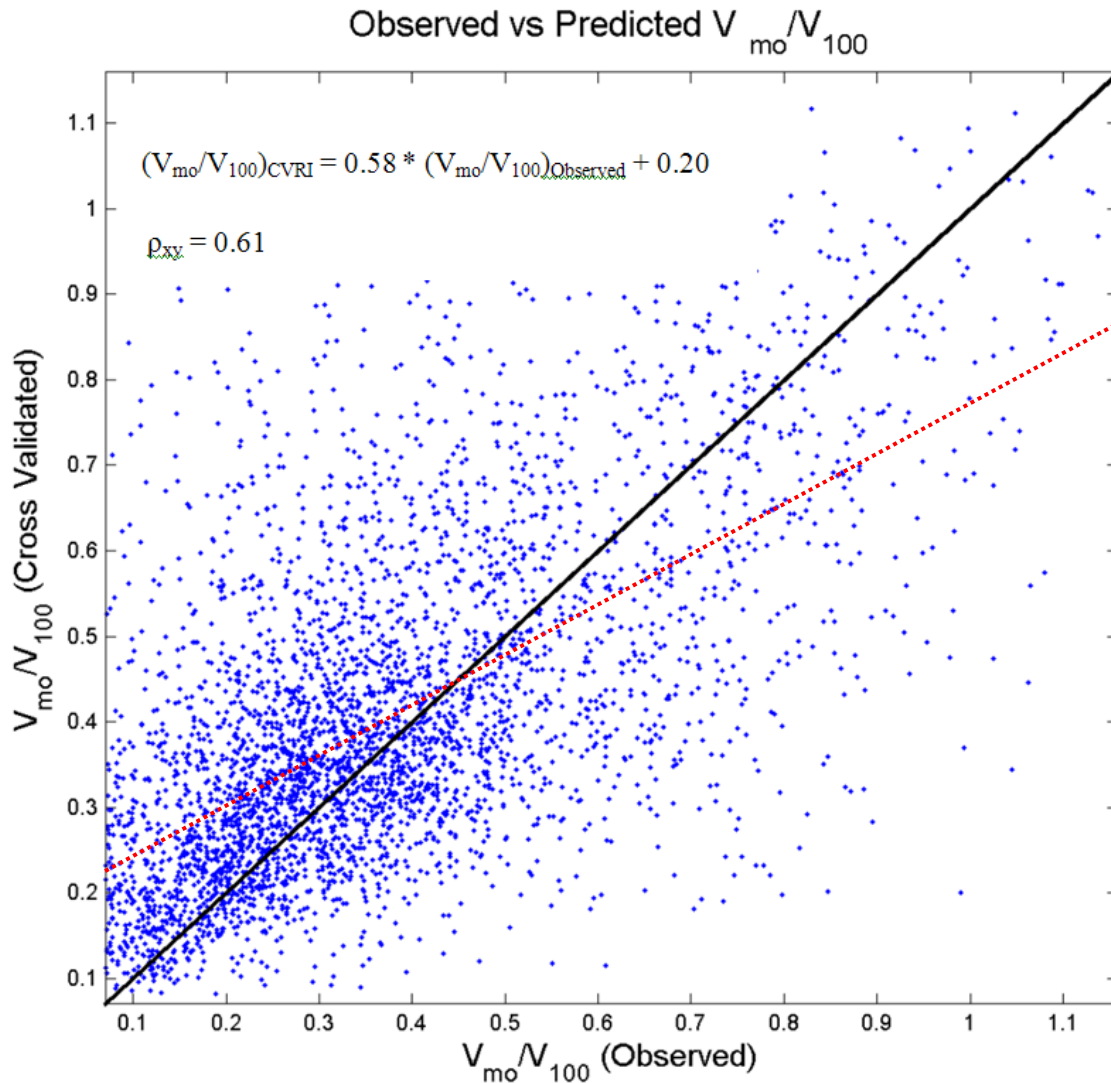


Figure 4-28. Relationship between Observed versus Cross-Validated V_{mo}/V_{100} . The Slope of the Regression Equation and the Correlation Coefficient of the Two Variables Indicate Regional Tendency.

Figure 4-17 shows the histogram of the error between the cross-validated and observed velocity ratio. The histogram was produced to quantify the level of error that can be induced by using the suggested approach. The discrepancy between the two variables is distributed in a bell shape with a mean of $\mu = -0.04$ and a standard deviation of $\sigma = 0.18$. Assuming that the error can be modeled with a normal distribution, the predicted V ratio using Approach 2 would be such that:

$$P(\mu - \sigma < \frac{V_{mo}}{V_{100 (obs)}} - \frac{V_{mo}}{V_{100 (CV)}} < \mu + \sigma) = P(-0.22 < \frac{V_{mo}}{V_{100 (obs)}} - \frac{V_{mo}}{V_{100 (CV)}} < 0.16) = 0.68 \quad (4-34)$$

$$P(\mu - 2\sigma < \frac{V_{mo}}{V_{100 (obs)}} - \frac{V_{mo}}{V_{100 (CV)}} < \mu + 2\sigma) = P(-0.40 < \frac{V_{mo}}{V_{100 (obs)}} - \frac{V_{mo}}{V_{100 (CV)}} < 0.32) = 0.95 \quad (4-35)$$

Histogram of the error between the cross-validated V_{mo}/V_{100} and the observed V_{mo}/V_{100}

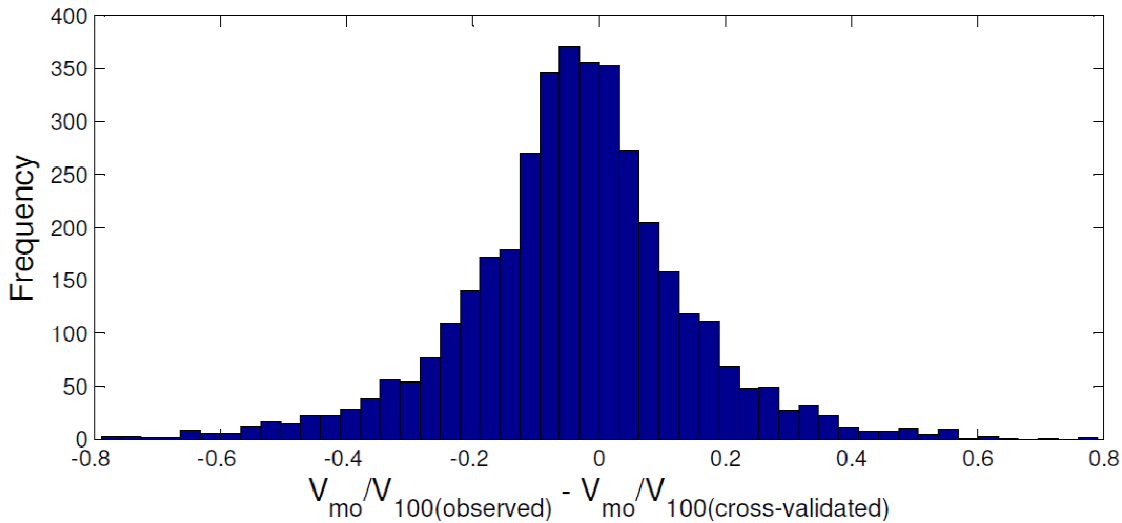


Figure 4-29. Histogram of the Error between the Cross-Validated V_{mo}/V_{100} and the Observed V_{mo}/V_{100} .

4.4.2.3. Approach 2 Discussion

The procedures through which the hydrologic information required for the scour analysis can be obtained for ungaged basins have been explained. The process by which the recurrence interval of the maximum flow is converted into the ratio V_{100}/V_{mo} does not incorporate the uncertainties that significantly affect the accuracy of the produced result. However, the methodology suggested for the first process by which the recurrence interval at the ungaged basin is obtained based on the recurrence interval of the nearby gages has not been suggested by any previous studies and therefore required further close analysis of its validity. As an effort to validate the process, cross-validation analysis was performed on the value V_{mo}/V_{100} . The result of the

analysis revealed that the recurrence interval of the observed flow peaks can be spatially interpolated to predict the value V_{mo}/V_{100} with a reasonable accuracy by hydrologic standards (see [Figure 4-17](#)). However, engineers should be fully aware of the uncertainties induced by each of the steps that Approach 2 uses to obtain the ratio V_{mo}/V_{100} from the recurrence interval of the flow. Particularly, the recurrence interval value read from the interpolated surface, which is automatically given by TAMU-FLOOD, should not be accepted without caution because it contains uncertainty that can significantly affect the results of the scour analysis. The following questions should be asked when making an engineering judgment before using the interpolated recurrence interval read from TAMU-FLOOD:

33. Is the location of the bridge close enough to the flow gages from which the recurrence interval is interpolated?
34. What is the size of the watershed defined by the bridge location? Is it reasonable to accept the interpolated recurrence interval if it comes from watersheds of significantly different size?
35. Was the flood measured at the nearby gages regional or localized? Are there any resources that can help in answering that question?
36. Were the descriptions of all major floods that occurred around the bridge identified and considered? The descriptions of the floods are given by TAMU-FLOOD. Is there any other evidence of large floods in the area (i.e., newspaper articles)?
37. What recurrence interval value would be obtained by intuition and engineering judgment without the aid of color shading of the interpolated map? Is it significantly different from the value given by TAMU-FLOOD?
38. Were all available data used to obtain the flood history of the bridge? Are there any flow gages upstream/downstream of (Bridge-Gage Relationship Type II) or near (Bridge-Gage Relationship Type III) the bridge?

It has to be noted that more accurate flow and velocity values can be obtained with a more intensive hydrologic analysis. However, no further in-depth analysis was pursued because of the following reasons:

39. The original purpose of the current project was to develop a “simple” method of scour evaluation for engineers.
40. Incorporation of further hydrologic concepts that can produce more certain and accurate result requires a much larger amount of data.
41. The precipitation data are not sufficiently dense (one station each 1550 km², [NCDC 2008](#)) and temporally consistent.

Therefore, the following is the suggested approach:

42. Locate the bridge by longitude and latitude.
43. Inspect the map of maximum recurrence intervals from nearby gages.
44. Use engineering judgment, intuition, and any additional local information to predict the recurrence interval of the highest flood experienced by the bridge, $RI_{Q_{mo}}$.
45. Use the interpolation map option and obtain the interpolated value of $RI_{Q_{mo}}$.
46. Decide on a value of $RI_{Q_{mo}}$.
47. Obtain Q_{mo}/Q_{100} from $RI_{Q_{mo}}$, and then V_{mo}/V_{100} from Q_{mo}/Q_{100} .

4.5. FLOOD FREQUENCY ANALYSIS

Flood frequency analysis is a procedure to estimate the return period of the flow peaks and the magnitude of the flow for a given return period. FFA is an essential part of the bridge scour assessment procedures presented in this report. BSA 1 requires the ratio (V_{100}/V_{mo}), while both BSA 2 and BSA 3 require explicit values of V_{100} and V_{mo} . This chapter explains the methods of the flood frequency analysis that are used in this study.

4.5.1. Types of Flood Frequency Analysis

In general, there are two types of flood frequency analysis. The first one is called the non-parametric approach, and the second one is called the parametric approach. In the non-parametric approach, the YIPFs for N years are ranked in descending order, with the highest value assigned a rank 1 and the smallest assigned a rank N. Then, the probability P_m that the observation with

rank m is equaled or exceeded is estimated based on the suggested equations shown in Table 1 of [Cuanne \(1978\)](#). One example of the equations is Weibull plotting formula as follows:

$$P_m = \frac{m}{N+1} \quad (4-36)$$

Then P_m and the corresponding flow value are plotted on the probability graph paper to find the general tendency of the flow records. The plot is used to obtain, by extrapolating and interpolating, the flow corresponding to a given probability P_m . The non-parametric approach can provide reasonably accurate estimates of the flow with a given recurrence interval (or the recurrence interval of a given flow) within the range covered by the observations, but the estimated values located outside of the observed range can be inaccurate ([Wurbs and James 2001](#)).

In the parametric approach, the record of observed flow is assumed to behave according to a given probability distribution. Based on this assumption, the parameters of the distribution are estimated using the recorded flow peaks. Then, the recurrence interval of a given flow or the flow with a given recurrence interval is estimated based on the distribution. As opposed to the non-parametric approach, the parametric approach of frequency analysis can provide more accurate estimates of the flow of the recurrence interval located beyond the observed data range.

4.5.2. Probability Distributions

Since the parametric approach of flood frequency analysis assumes that the flow records behave based on a given probability distribution, the type of probability distribution to model the flow frequency must be chosen. Numerous generalized extreme value distributions and Log-Pearson Type III distributions are most widely used to model the frequency of river flows. Numerous studies have shown that generalized extreme value distribution can successfully model the distribution of river flow peaks ([Hosking 1985](#), [Hosking and Wallis 1996](#), [Rosbjerg and Madsen 1995](#), [Smith 1987](#), [Stedinger and Lu 1995](#)). The Log-Pearson Type III distribution is suggested by the U.S. government document “Bulletin 17B—Guidelines for Determining Flood Flow Frequency” ([United States Internal Geological Survey, 1982](#)). The document was created to prevent the discordance of analysis results caused by the use of various frequency analysis methods. It requests that federal agencies use the suggested methods based on the Log-Pearson

Type III distribution and encourages state, local, and private organizations to do so to assure more uniformity, compatibility, and comparability in the frequency values. Thus, the Log-Pearson Type III distribution can be regarded as the standard distribution to model the frequency of peak flows.

Since the performance of both distributions in modeling peak flow frequency has been proven through numerous previous studies, it is difficult to choose between the two distributions. This study provides flow frequency estimates based on both distributions. Other distributions that are used to model the frequency of floods include Log-normal distribution, Gumbel distribution, Exponential distribution, Generalized Pareto distribution, and Generalized logistic distribution (page 565, [Dingman, 2001](#)).

4.5.3. Parameter Estimation

Once the distribution is chosen, the parameters of the distribution should be determined. The three most common methods of parameter estimation are the method of moments, the method of L-moments, and the method of maximum likelihood.

In the method of moments (MOM), the moments of the sample (in this case, the observed yearly instantaneous peak flows) are equated to the moments of the model distribution, which gives a set of equations that can be solved for the parameter values. In a similar manner, the method of L-moments (LMOM) matches the L-moments of the sample and model moments. The method of maximum likelihood (MLE) finds the parameter set $\vec{\theta}$ that maximizes the following likelihood function:

$$L(\theta)=f(x_1;\vec{\theta}) \cdot f(x_2;\vec{\theta}) \cdot f(x_3;\vec{\theta}) \cdots \cdot f(x_n;\vec{\theta}) \quad (4-37)$$

where f is the probability density function and x_i is the observed sample value.

Each method has its distinctive advantages and disadvantages. The method of moments is straightforward, making it easy to derive the parameter estimates. However, oftentimes the equation representing the moments of the model probability distribution is unavailable, which makes it impossible to use the method of moments. Furthermore, it lacks some optimality properties such as unbiasedness and minimum variance, which basically means that the

estimated parameters contain more uncertainty than the ones estimated by using the other two methods. The method of maximum likelihood has the following disadvantages: oftentimes it is impossible to derive the analytical form of the equations solving for the parameter values making the use of a numerical approach necessary; and oftentimes the numerical optimization algorithm used to find the optimum parameter sets maximizing the likelihood function fails and yields unreasonable parameter estimates. However, when the size of the sample is large enough, the estimated parameters are expected to have unbiasedness and minimum variance. The method of L-moments has the advantage of being robust with respect to outliers and its bias tends to be small. Also, L-moment estimators can often be used when the maximum likelihood estimates are unavailable, are difficult to compute, or have undesirable properties. In summation, when the size of the sample is large enough, the MLE can provide the most accurate estimates of the parameters. The LMOM can be successfully used when the sample size is not large enough. The method of moments does not have a distinctive advantage compared to the other two methods except that it is easy to apply. However, the governmental standard Bulletin 17B uses MOM for the estimation of parameters.

4.5.4. Types of Distributions and Parameter Estimation Methods

To acquire the recurrence interval of flow peaks, parameters of a given distribution (Log-Pearson Type III or generalized extreme value distribution) should be calculated using a given parameter estimation method (MOM, MLE, or LMOM). The following combination of the probability distribution and the parameter estimation methods are used in this study:

48. Log-Pearson Type III–method of moments,
49. generalized extreme value distribution–method of maximum likelihood, and
50. generalized extreme value distribution–method of L-moments.

The first combination was adopted because it is the federal government standard. The second and third combinations were chosen based on the findings of studies indicating that the generalized extreme value distribution can successfully model the flow peaks regardless of the variability of climates ([Aranda 2001](#), [Farquharson et al. 1992](#), [Hosking 1985](#), [Hosking and Wallis 1996](#), [Kumar and Chatterjee 2005](#), [Rosbjerg and Madsen 1995](#), [Smith 1987](#), [Stedinger](#)

and Lu 1995, Vogel et al. 1993, Wang 1997, Zaidman et al. 2003). A detailed description of each method is provided.

4.5.4.1. Log-Pearson Type III–Method of Moments

This method models the natural log of the flow peaks using the Pearson Type III distribution. Thus, it has to be kept in mind that “x” in the following set of equations represents the natural log of the flow peaks. The probability density function and the cumulative density function of the Pearson Type III distribution are defined as follows by three parameters, i.e., μ (location), σ (scale), and γ (shape).

If $\gamma \neq 0$, let:

$$\alpha=4/\gamma^2, \beta=\frac{1}{2}\sigma|\gamma|, \text{ and } \xi = \mu - 2\sigma/\gamma \quad (4-38)$$

If $\gamma > 0$:

$$f(x)=\frac{(x-\xi)^{\alpha-1}e^{-\frac{x-\xi}{\beta}}}{\beta^{\alpha}\Gamma(\alpha)} \quad (4-39)$$

$$F(x) = \Gamma(\alpha, \frac{x-\xi}{\beta})/\Gamma(\alpha) \quad (4-40)$$

If $\gamma < 0$:

$$f(x)=\frac{(\xi-x)^{\alpha-1}e^{-\frac{\xi-x}{\beta}}}{\beta^{\alpha}\Gamma(\alpha)} \quad (4-41)$$

$$F(x) = 1 - \Gamma(\alpha, \frac{x-\xi}{\beta})/\Gamma(\alpha) \quad (4-42)$$

If $\gamma = 0$, then the distribution is normal as follows:

$$f(x) = \phi\left(\frac{x-\mu}{\sigma}\right) \quad (4-43)$$

$$F(x) = \Phi\left(\frac{x-\mu}{\sigma}\right) \quad (4-44)$$

Here $\Gamma(\cdot)$ is the gamma function and $G(a, x) = \int_0^x t^{a-1} e^{-t} dt$

The three parameters should be determined using a given parameter estimation method. In this study, these are estimated using the method of moments as suggested by Bulletin 17B.

The moments of samples can be calculated by using the following equations:

$$\hat{\mu} = \frac{1}{n} \sum_{i=1}^n X_i \quad (4-45)$$

$$\hat{\sigma} = \sqrt{\frac{1}{n-1} \sum_{i=1}^n (X_i - \hat{\mu})^2} \quad (4-46)$$

$$\hat{\gamma} = \frac{n}{(n-1)(n-2)\hat{\sigma}^3} \sum_{i=1}^n (X_i - \hat{\mu})^3 \quad (4-47)$$

Once the sample moments are calculated by Equation (4-45), Equation (4-46), and Equation (4-47), they are plugged into Equation (4-38) to acquire the value of α , β , and ξ . The calculated α , β , and ξ are then plugged into Equation (4-40) or Equation (4-42). The recurrence interval of the peak flow can be estimated by the following equation:

$$RI_{\text{peak}} = \frac{1}{1-F(\log_e \text{Flow})} (\text{year}) \quad (4-48)$$

4.5.4.2. Generalized Extreme Value Distribution–Method of Maximum Likelihood

The probability density function and cumulative density function of the generalized extreme value distribution is defined as follows.

The distribution has three parameters: ξ (location), α (scale), and k (shape).

$$f(x) = \alpha^{-1} e^{-(1-k)y - e^{-y}} \quad (4-49)$$

$$F(x) = e^{-e^{-y}} \quad (4-50)$$

where:

$$y = -k^{-1} \log \left(1 - \frac{k(x - \xi)}{\alpha} \right), \quad k \neq 0 \quad (4-51)$$

$$y = \frac{(x - \xi)}{\alpha}, \quad k = 0 \quad (4-52)$$

In the method of maximum likelihood, the following likelihood function is formulated first:

$$L(\theta) = f(x_1; \bar{\theta}) \cdot f(x_2; \bar{\theta}) \cdot f(x_3; \bar{\theta}) \cdots f(x_n; \bar{\theta}) \quad (4-53)$$

Here, $\bar{\theta}$ is a vector representing parameter sets (i.e., $\bar{\theta} = (\xi, \alpha, k)$) and x_i represents the observed flow peaks at a given station. Because the x_i values are known constants, $L(\theta)$ becomes the function of only three parameters. Then, any numerical optimization algorithm can be applied to obtain $\bar{\theta}$ that maximizes Equation (4-53). In this study, a search algorithm based on the numerical partial derivative of the likelihood function was used.

4.5.4.3. Generalized Extreme Value Distribution–Method of L-Moments

Here, the L-moments of samples are calculated first and are equated to the L-moments of the generalized extreme value distribution. The first, second, and third L-moments of the sample and the model distribution are used to obtain three equations to solve the three unknown parameters. Sample L-moments are calculated by the following equations.

First, the observation x_i 's are ranked such that $x_1 \leq x_2 \leq \dots \leq x_n$.

$$b_0 = \frac{1}{n} \sum_{i=1}^n x_i \quad (4-54)$$

$$b_1 = \frac{1}{n(n-1)} \sum_{i=2}^n (i-1) x_i \quad (4-55)$$

$$b_2 = \frac{1}{n(n-1)(n-2)} \sum_{i=3}^n (i-1)(i-2) x_i \quad (4-56)$$

$$b_3 = \frac{1}{n(n-1)(n-2)(n-3)} \sum_{i=4}^n (i-1)(i-2)(i-3)x_i \quad (4-57)$$

$$\hat{\lambda}_1 = b_0 \quad (4-58)$$

$$\hat{\lambda}_2 = 2b_1 - b_0 \quad (4-59)$$

$$\hat{\lambda}_3 = 6b_2 - 6b_1 + b_0 \quad (4-60)$$

$$\hat{\tau}_3 = \frac{\hat{\lambda}_3}{\hat{\lambda}_2} \quad (4-61)$$

Then, Equation (4-58), Equation (4-59), and Equation (4-61) are equated to Equation (4-62), Equation (4-63), and Equation (4-64) representing the L-moments of the generalized extreme value distribution:

$$\lambda_1 = \xi + \alpha \{1 - \Gamma(1+k)\} / k \quad (4-62)$$

$$\lambda_2 = \alpha(1 - 2^{-k})\Gamma(1+k) / k \quad (4-63)$$

$$\tau_3 = 2 \frac{(1-3^{-k})}{(1-2^{-k})} - 3 \quad (4-64)$$

where $\Gamma(\cdot)$ is the gamma function.

By equating Equation (4-58), Equation (4-59), and Equation (4-61) to Equation (4-62), Equation (4-63), and Equation (4-64), respectively, the three equations that are function of the three parameters are obtained. This system of equations can be solved using numerical methods. This study applied the Newton-Rhapson algorithm to find the parameter sets.

4.5.5. Application of the Methods to the Texas Data and Results

4.5.5.1. Data Description

The three methods of flood frequency analysis were applied to all available USGS gages in Texas and surrounding states. The gages in the states neighboring Texas were considered for the analysis to obtain higher accuracy of the interpolated return periods in areas near the border of Texas. A total of 3116 USGS gages were considered for the flood frequency analysis. The record of the earliest gage dates back to the year 1828, and the latest records were obtained in the year 2006. To maximize the accuracy of the analysis, only ages with 20 years or more of unregulated flow peak records were considered for the analysis. The number of such stations was 1650. Among these stations, there were several where the numerical algorithm for MLE failed to obtain parameters. This reflects that the flow record is not well represented by statistical distribution suggesting that the parameters estimated by the other two methods would also be inaccurate. Thus, these stations were excluded from the data set that was used for the generation of the surface map of the return period of YIPFs. The total number of stations used for the generation of the surface map was 744. [Figure 4-30](#) shows the location of all 3116 gages located in Texas and its surrounding states, among which 744 were used for the generation of a map of the flow recurrence interval ([Figure 4-31](#)).

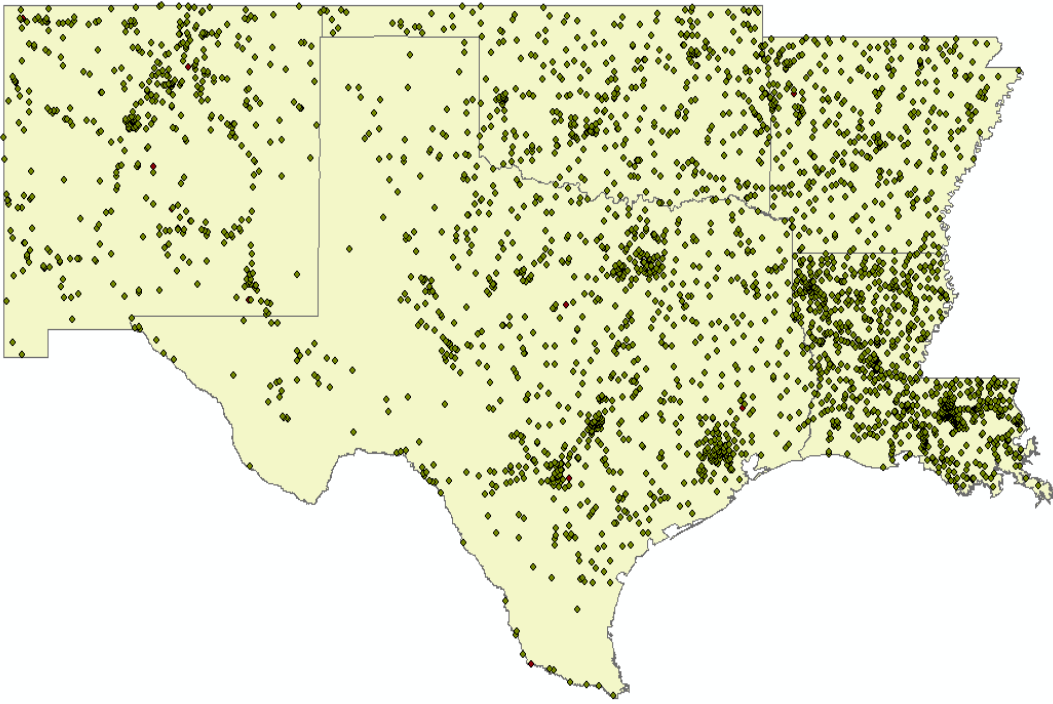


Figure 4-30. Location of All USGS flow Gages in Texas and the Surrounding States.

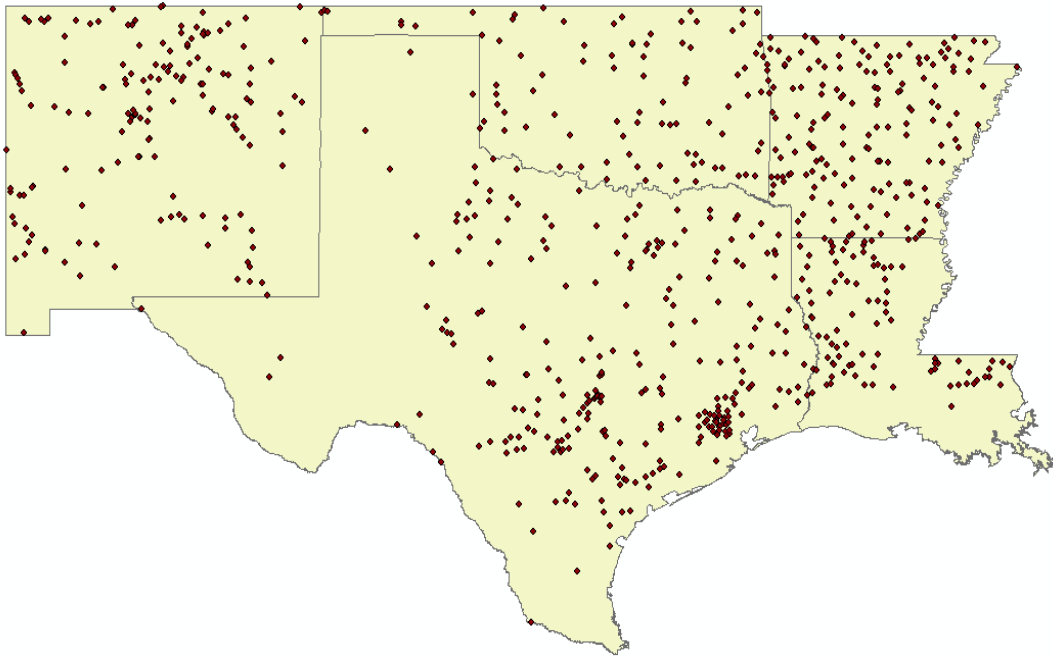


Figure 4-31. Location of the 744 USGS flow Gages Used to Generate the Map of the Flow Recurrence Interval.

4.5.5.2. Regulated Flow Peaks

Flow peaks at some gages were regulated by upstream hydraulic structures constructed to prevent flooding in downstream areas. Such flow peaks were excluded from the data set used to estimate the parameters. However, it is still possible to assign frequency to the regulated flow gages based on the parameter sets estimated using the unregulated flow peaks collected prior to the flow becoming regulated. For example, USGS flow gage 07339000 has unregulated flow records from 1930 to 1968 and regulated flow peaks from 1969 to 2006. In this case, only the flow peaks recorded between 1930 and 1968 are used to estimate the parameters of the probability distribution. Then, the frequency of all recorded flow peaks (1930 to 2006) are determined based on the distribution with the estimated parameter sets.

4.5.5.3. Recurrence Interval of the Yearly Flow Peaks at the Gage

The recurrence interval of the YIPF (the highest flow observed in a given year) was estimated using the three methods to analyze flow frequency. The estimated recurrence interval of the yearly flow peaks at each station is spatially interpolated to produce the surface map of the recurrence intervals over Texas. Here, the triangle-based linear interpolation technique was used to obtain the surface of the flow recurrence interval. In the triangle-based linear interpolation, the value v_u at an unknown location with the coordinate (x', y') , is estimated in the following manner.

Let $f(x, y)$ be the equation of the flat surface of the recurrence interval that encompasses the point (x', y') . The general equation for the surface can be written as:

$$f(x, y) = Ax + By + C \quad (4-65)$$

where A, B, and C are the constants to be determined. Because the equation $f(x, y)$ has three unknown constants to be calculated, it requires at least three points in space where the recurrence interval is known (p_0 , p_1 , and p_2 in [Figure 4-32](#)). Using the known coordinates and recurrence interval at p_0 , p_1 , and p_2 , a system of three equations is obtained and can be solved for A, B, and C. Once the constants of Equation (4-65) are determined, the recurrence interval at point (x', y') can be determined by the following equation:

$$f(x', y') = Ax' + By' + C \quad (4-66)$$

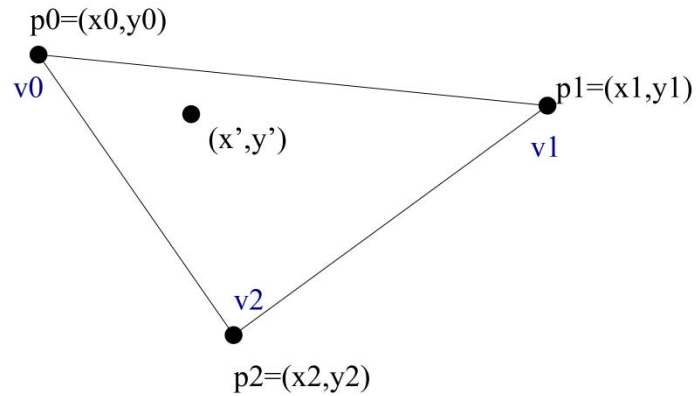


Figure 4-32. Schematic of the Triangle-Based Linear Interpolation.

A map was generated for each year and can be retrieved using the software TAMU-FLOOD ([Appendix F](#)). An example of such a map is shown in [Figure 4-33](#). The map is for the year 2001. The empty circles in the map represent the location of USGS gages where the flood frequency analysis was performed. The numbers beside the empty circles represent the recurrence interval of the flow peak observed in the year 2001 at the location of the empty circle. The color shadings in the map represent the interpolated values of the recurrence interval estimated from the recurrence intervals observed at nearby locations.

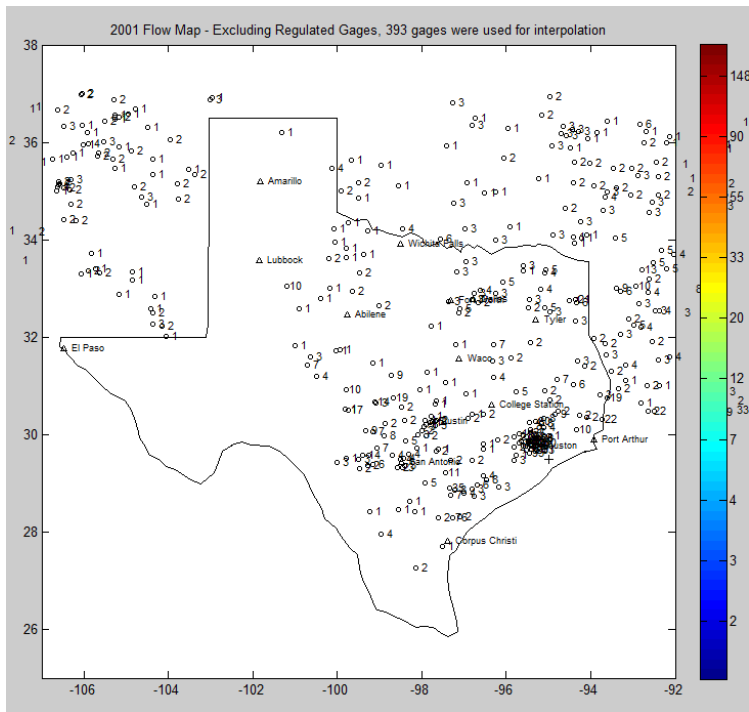
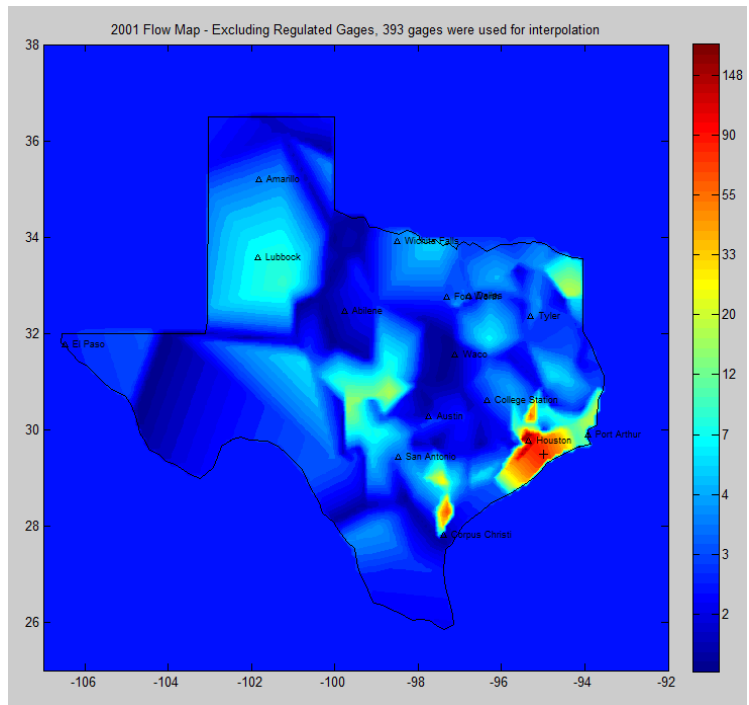


Figure 4-33. Map Showing the Interpolated Recurrence Interval Color Shading (Upper) and the Value of the Recurrence Intervals of the Flow Peaks Observed (Lower) in Year 2001.

The recurrence interval shown in Figure 4-33 is the one estimated using Log-Pearson Type III and the method of moments. TAMU-FLOOD has an option to switch from one method of frequency analysis to another, so one can see the map of the same year using different frequency analysis methods. In general, the method of frequency analysis does not cause a significant difference in the estimated recurrence interval of flow peaks and design flood if sufficient length of data is provided. Figure 4-34 through Figure 4-36 show the results of the frequency analysis for some selected USGS flow gages. The discrepancy of return period caused by the use of different FFA methods and its impact on the scour analysis result will be discussed in Section 4.5.5.6.

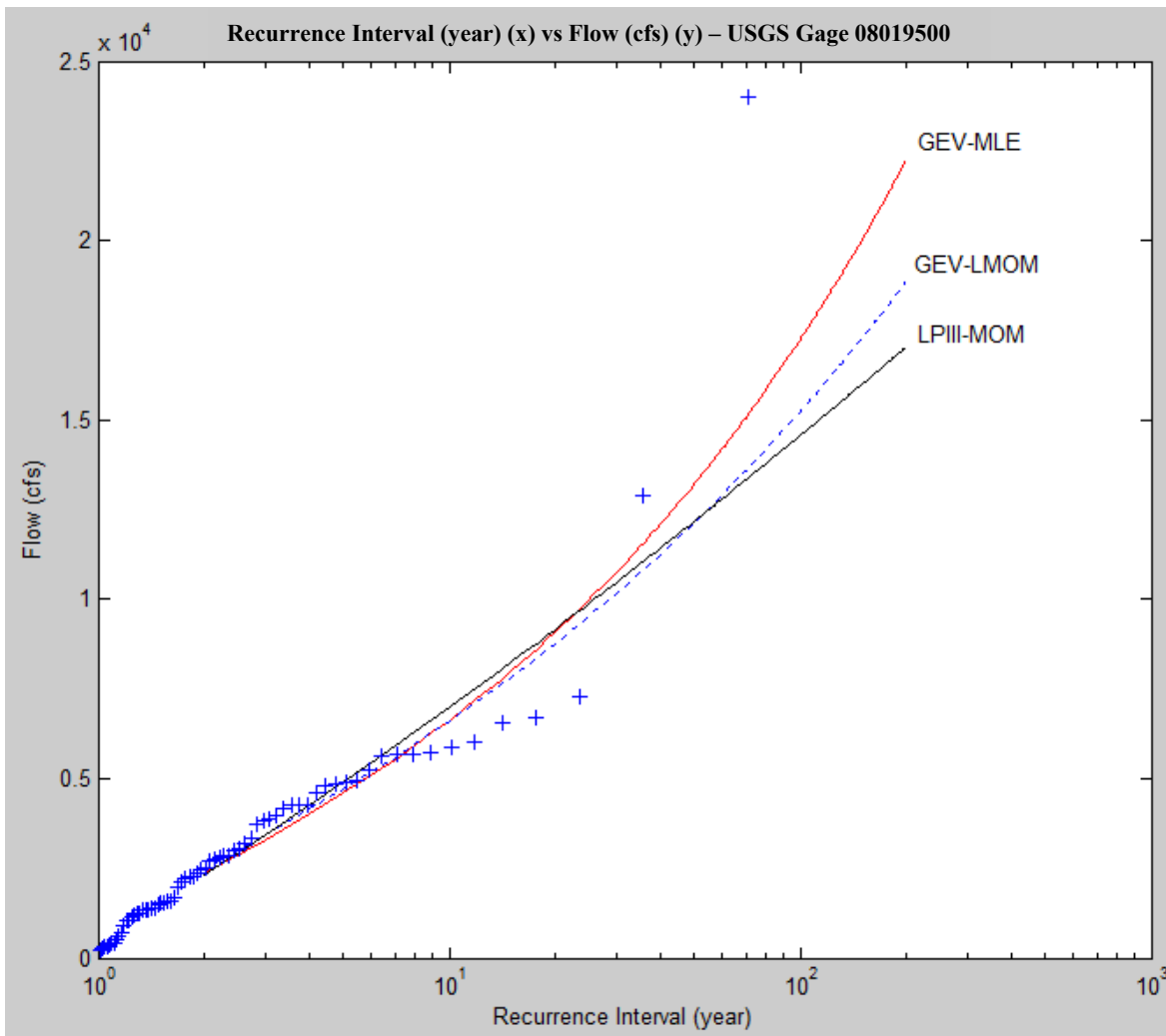


Figure 4-34. Result of the Flood Frequency Analysis for USGS Gage 08019500.

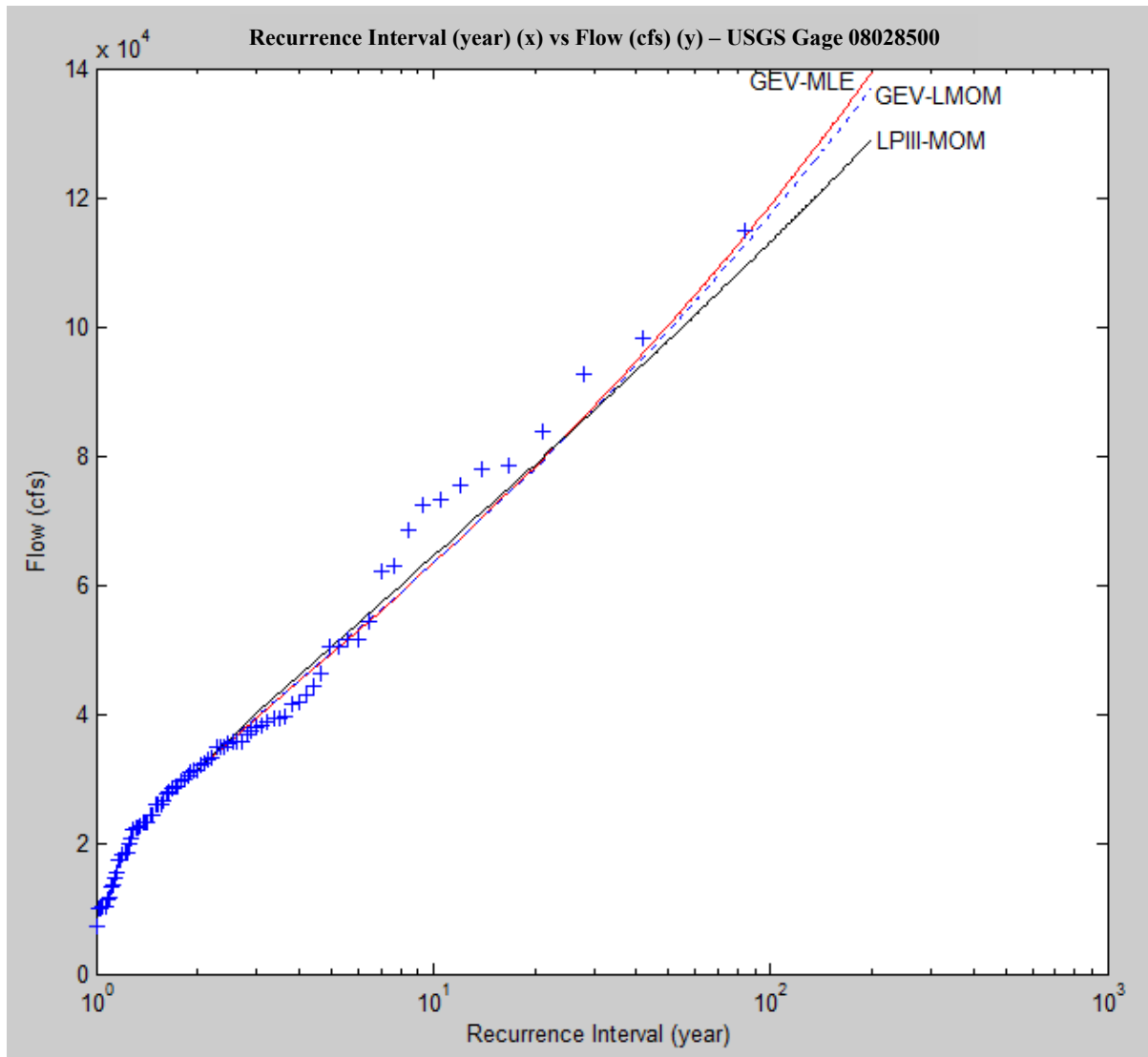


Figure 4-35. Result of the Flood Frequency Analysis for USGS Gage 08028500.

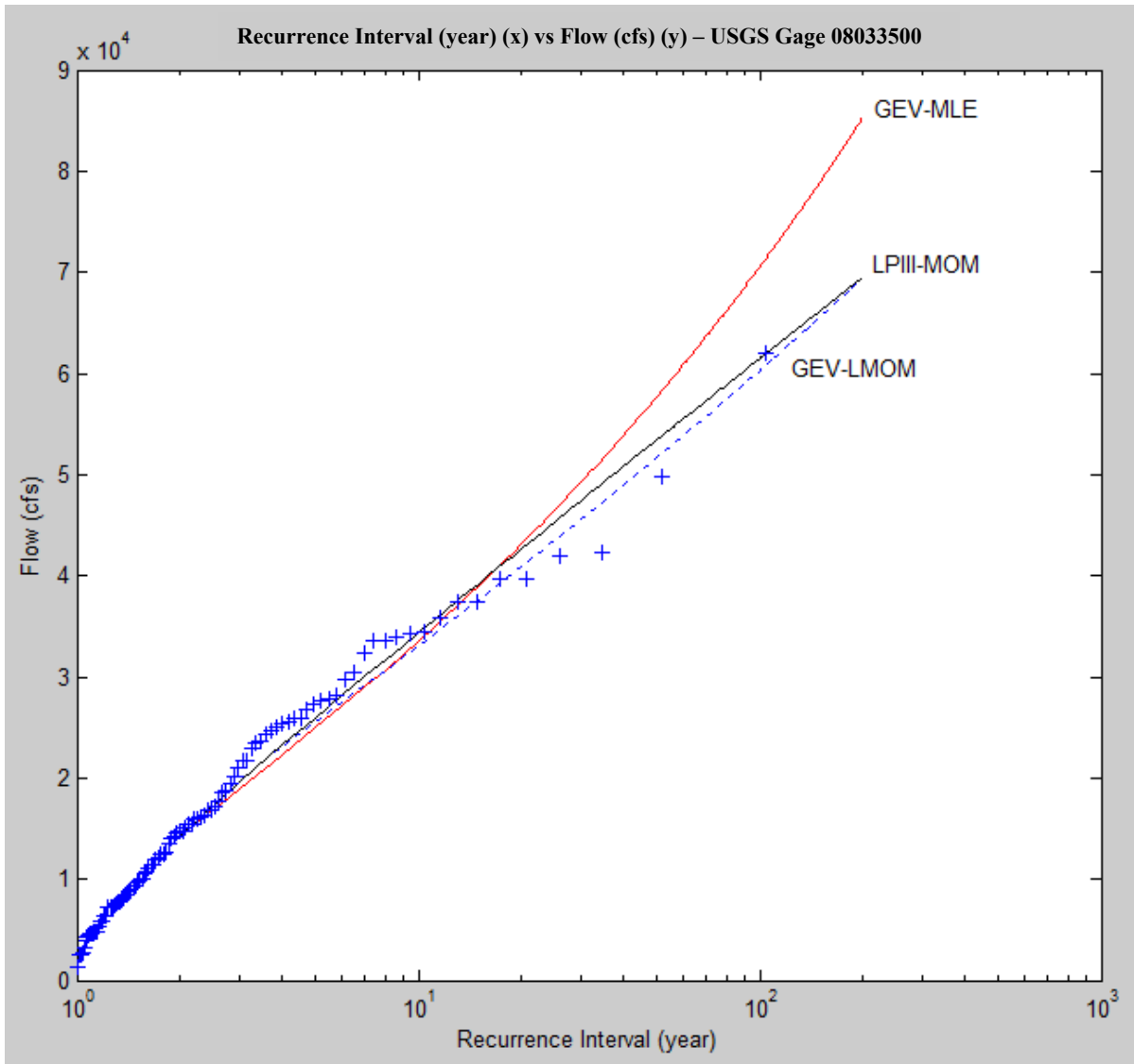


Figure 4-36. Result of the Flood Frequency Analysis for USGS Gage 08033500.

4.5.5.4. Recurrence Interval of the Maximum Flood over a Given Period

The scour analysis model applied in this study assumes that the maximum flood that the bridge has experienced causes the major portion of the bridge scour. Thus, it is essential to determine the recurrence interval of the maximum flood that the bridge has experienced. This value is obtained by overlapping the recurrence interval map of each year during a given period (i.e., starting from the year in which the bridge was constructed to the year of the latest inspection), and retaining the maximum recurrence interval among the overlapped maps. [Figure 4-37](#) through

Figure 4-39 show such maps. The color shading in the maps shows the interpolated recurrence interval of the maximum flow peaks observed between the year 1990 and 2006 (Figure 4-37), 1970 and 2006 (Figure 4-38), and 1920 to 2006 (Figure 4-39) according to the color scale. TAMU-FLOOD has an option to adjust the starting and ending year so that they match the year of construction and the year of last inspection of the bridge, respectively.

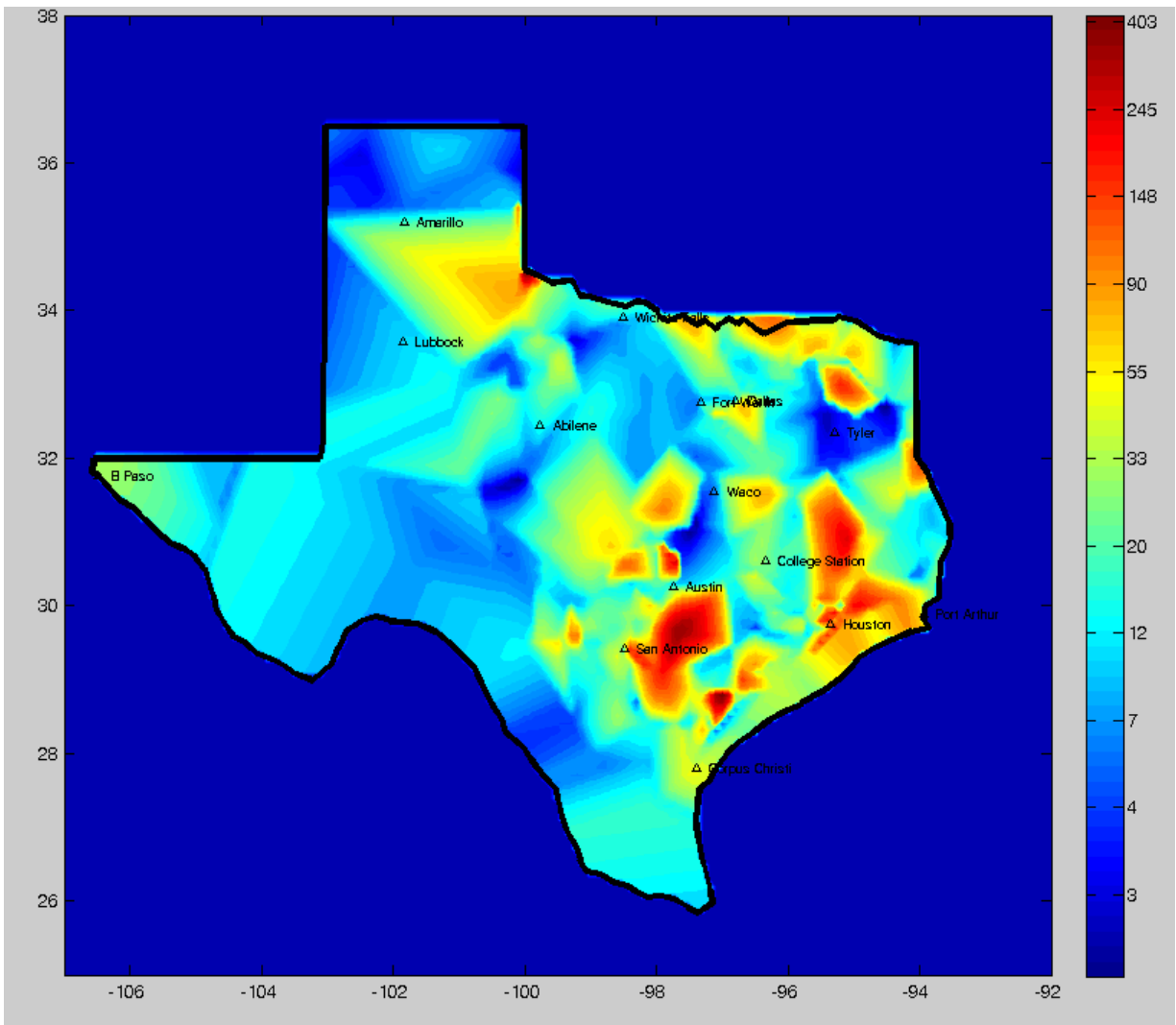


Figure 4-37. Recurrence Interval Map of the Maximum Flood That Was Observed between the Year 1990 and 2006.

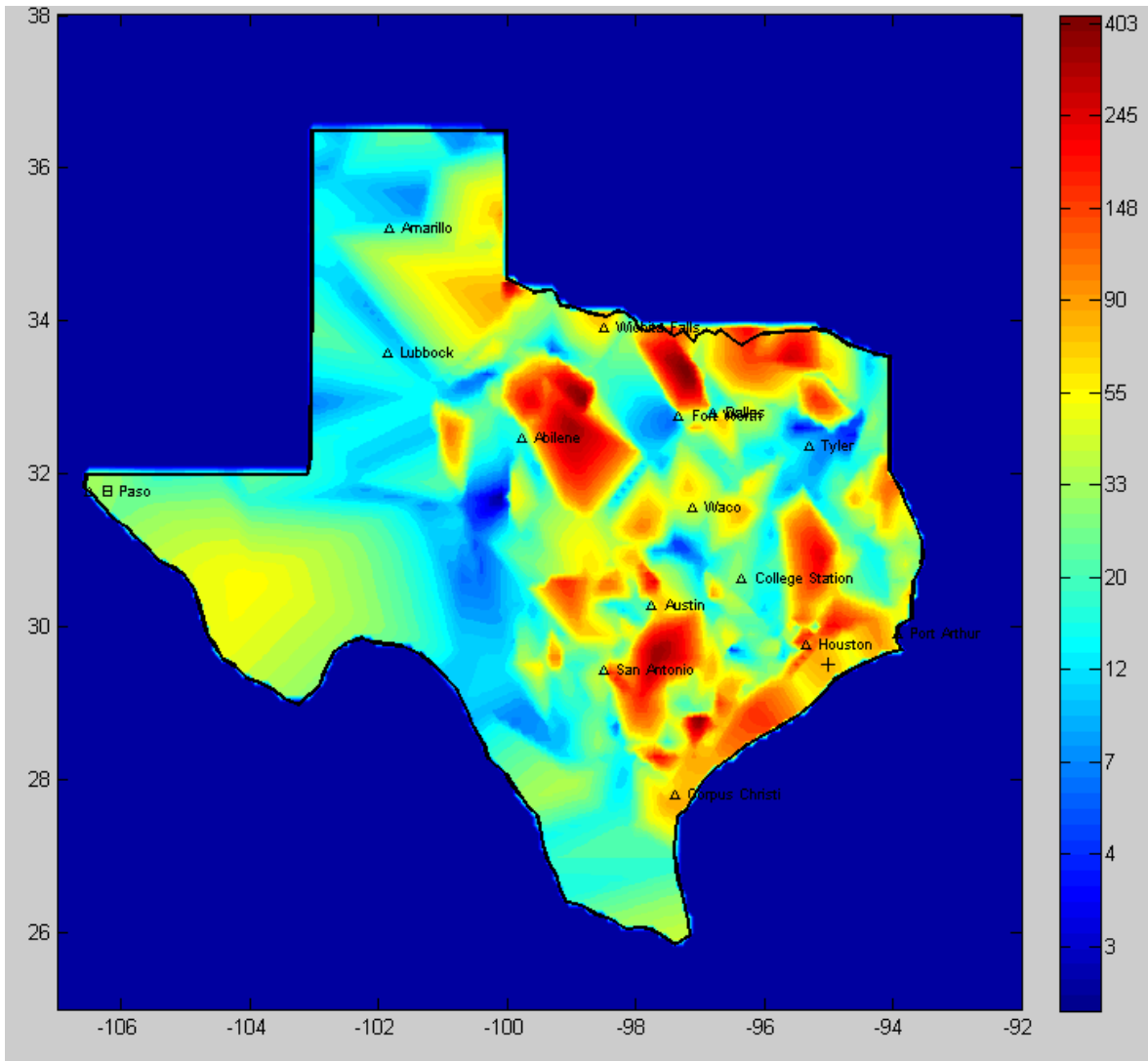


Figure 4-38. Recurrence Interval Map of the Maximum Flood That Was Observed between the Year 1970 and 2006.

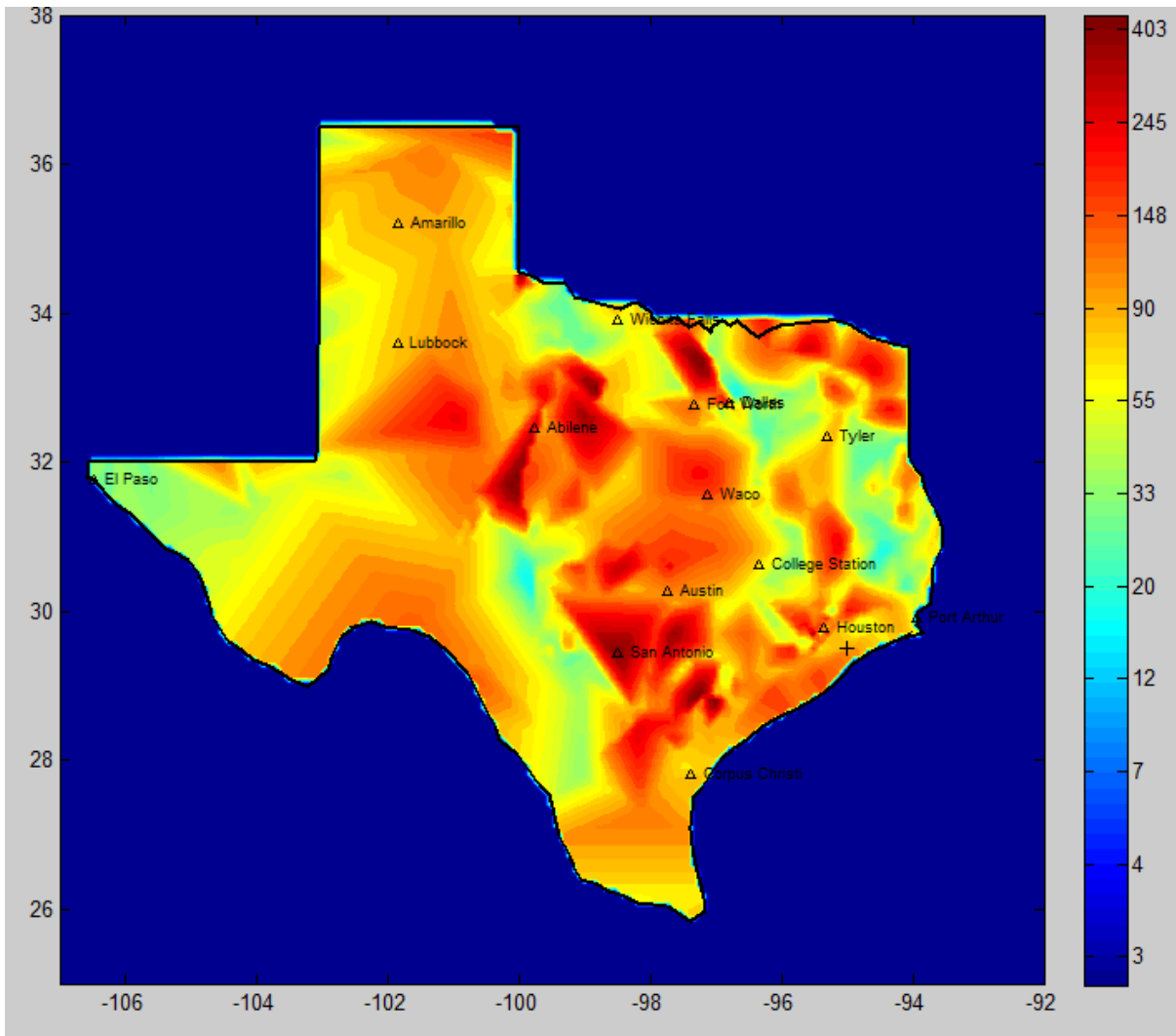


Figure 4-39. Recurrence Interval Map of the Maximum Flood That Was Observed between the Year 1920 and 2006.

4.5.5.5. *Recurrence Interval Maps of Rainfall*

To assist the user in applying engineering judgment for the determination of the maximum flood that the bridge has experienced, TAMU-FLOOD provides the recurrence interval maps of the annual maximum rainfall along with those of floods. The maps of the rainfall recurrence interval are produced using a similar method applied to obtain the maps of the flow recurrence interval. First, the yearly maximum rainfall observed at each rainfall gage in Texas (Figure 4-40) during a given year is obtained based on a given rainfall duration (i.e., 1-hr yearly maximum rainfall, 3-hr yearly maximum rainfall, etc.). Then, the recurrence interval of the yearly maximum rainfall is estimated through frequency analysis. Then, the surface of the recurrence interval is interpolated using the triangle-based linear interpolation technique to produce the recurrence interval map of a given year (e.g. Figure 4-41). These maps are overlapped to obtain the recurrence interval of maximum rainfall during a given period (e.g. Figure 4-42). These rainfall maps are especially useful when the network of flood gages is not dense enough to make a reasonable conclusion on the maximum recurrence interval that the bridge has experienced. For example, Figure 4-17, which provides a measure of uncertainty expected in the prediction of V_{mo}/V_{100} when using the flood recurrence interval map, is generated using the flow gages that are less than 120 miles away from the adjacent gages. If the bridge is located further than this threshold value from flow gages, the uncertainty in the predicted V_{mo}/V_{100} cannot be measured. In such cases, comparing the rainfall recurrence interval map with the flow recurrence interval map can help users make a judgment.

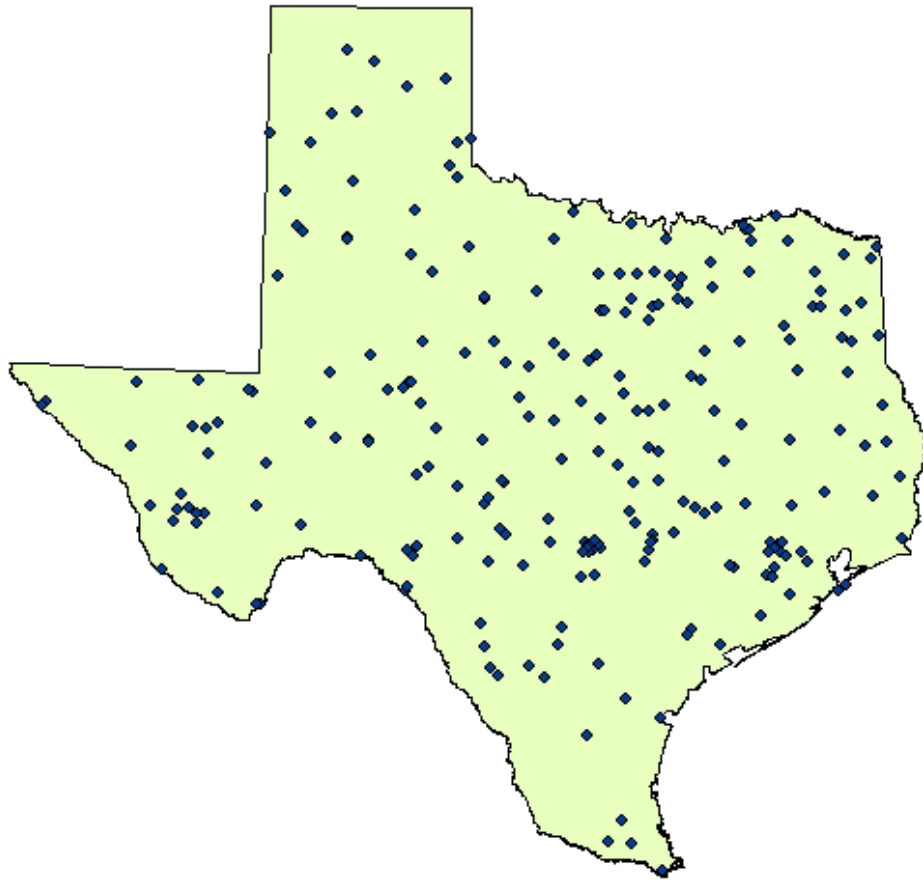


Figure 4-40. Location of the 244 NCDC rain gages that were used to produce the rainfall recurrence interval maps.

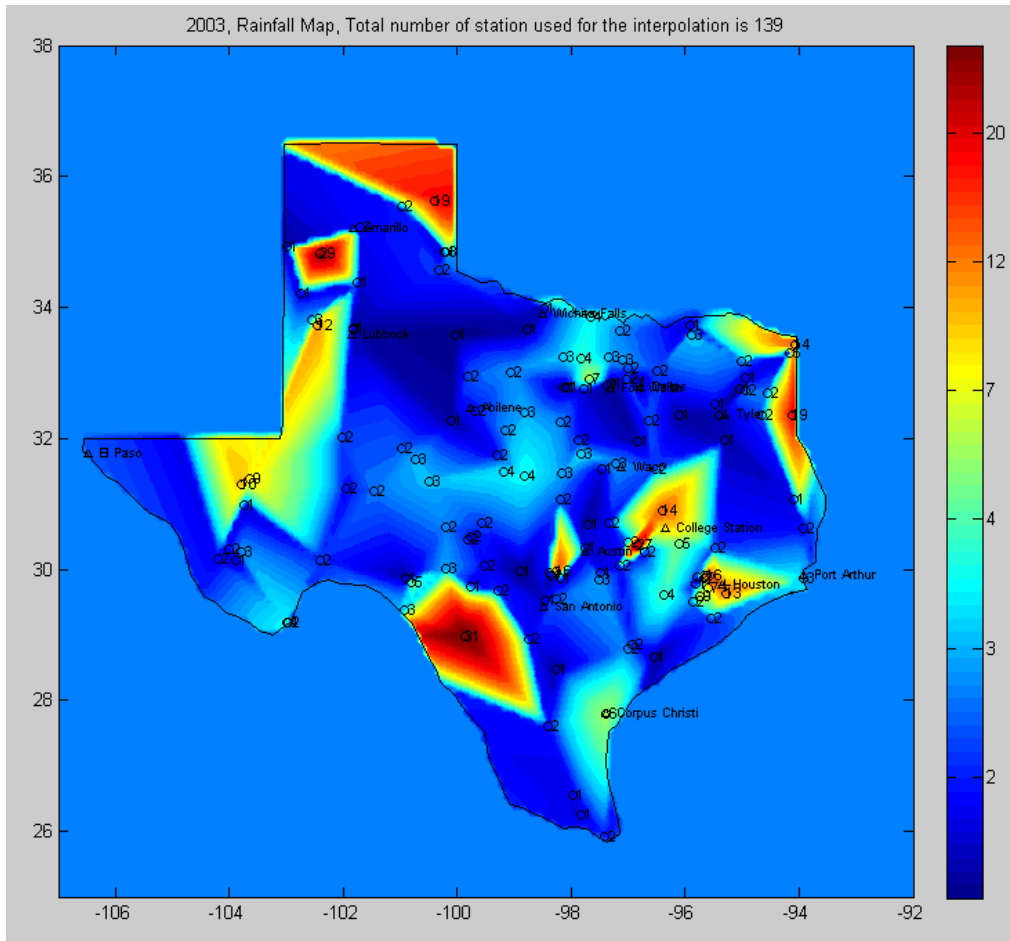


Figure 4-41. Maps Showing the Interpolated Recurrence Interval Color Shading and the Value of the Recurrence Intervals of the 6-hr Maximum Rainfall Observed in Year 2003.

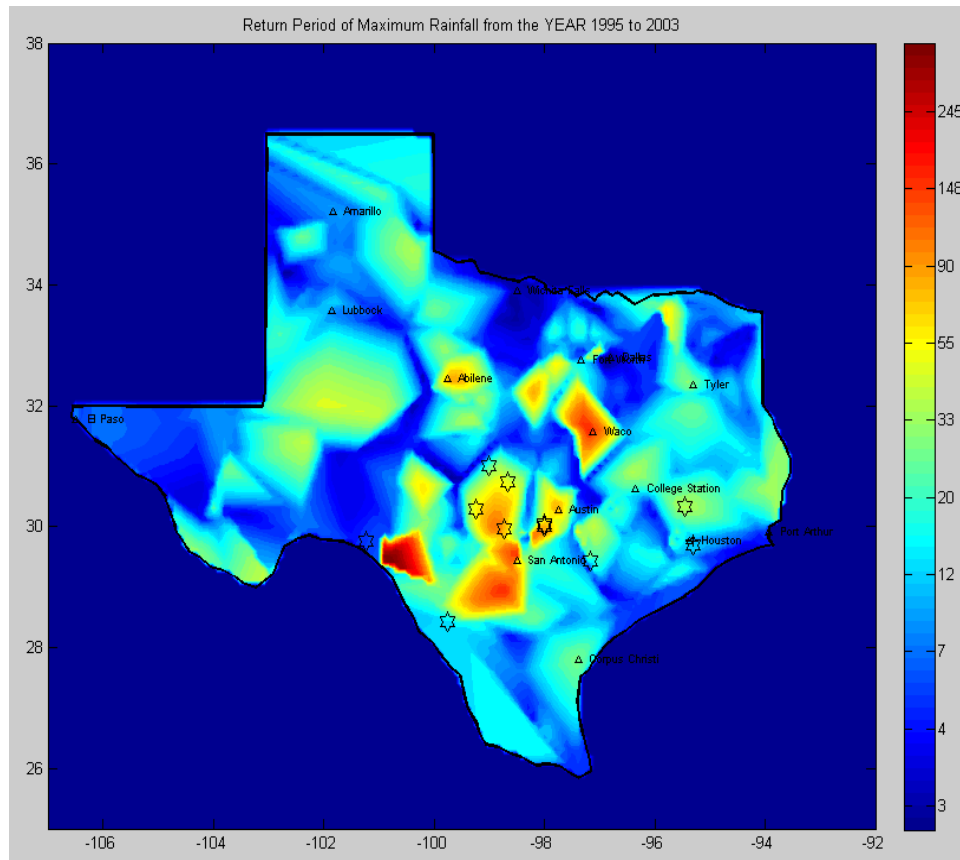


Figure 4-42. Recurrence Interval Map of the Maximum Rainfall That Was Observed between the Year 1995 and 2003.

4.5.5.6. Comparison of the Methods Applied

Because all three methods of flood frequency analysis have verified performance by numerous previous studies, it is difficult to choose a specific methodology. This study compared the recurrence interval estimates by the three methodologies to check if one method has a consistent difference from the others independent of the observed flow peaks at gages. [Figure 4-43](#) to [Figure 4-45](#) show the comparison of the estimated recurrence intervals between GEV-MLE and GEV-LMOM, GEV-MLE and Log-Pearson Type III-MOM, and GEV-LMOM and Log-Pearson Type III-MOM, respectively. To generate the plots, flood frequency analysis was performed on 262 USGS gages in Texas that meet the following criteria:

- The length of the unregulated flow peaks at the gage should be more than 20.

- The numerical algorithm for GEV-MLE flood frequency analysis should yield stable analysis results.

A total of 14,796 flow peaks from 262 USGS gages were available between 1900 and 2006. Among these flow peaks, 8708 were unregulated. Return periods were assigned to all 14,796 flow peaks based on the parameters estimated from 8708 unregulated flow peaks. The comparison indicates that the return period estimates by GEV-MLE are approximately 18 percent and 20 percent lower than those estimated by GEV-LMOM and Log-Pearson Type III-MOM, respectively. This also means that a flood with a given return period estimated by GEV-MLE will be higher than the one estimated by GEV-LMOM or by Log-Pearson Type III-MOM. The recurrence interval estimates by GEV-LMOM were approximately 9 percent lower than those estimated by Log-Pearson Type III-MOM. It can be noted from these comparisons that the flood frequency analysis by GEV-MLE is the most conservative method in scour analysis because it gives the lowest recurrence interval for the observed maximum flow compared to the other two methods. For example, saying that a given observed depth of scour was caused by a 10-year flood is a more conservative statement than saying that the same depth of scour is caused by a 50-year flood. In other words, the predicted scour depth corresponding to 100-year flood will be greater according to the first case than the second case, which will make engineers conclude that the bridge is more susceptible to scour.

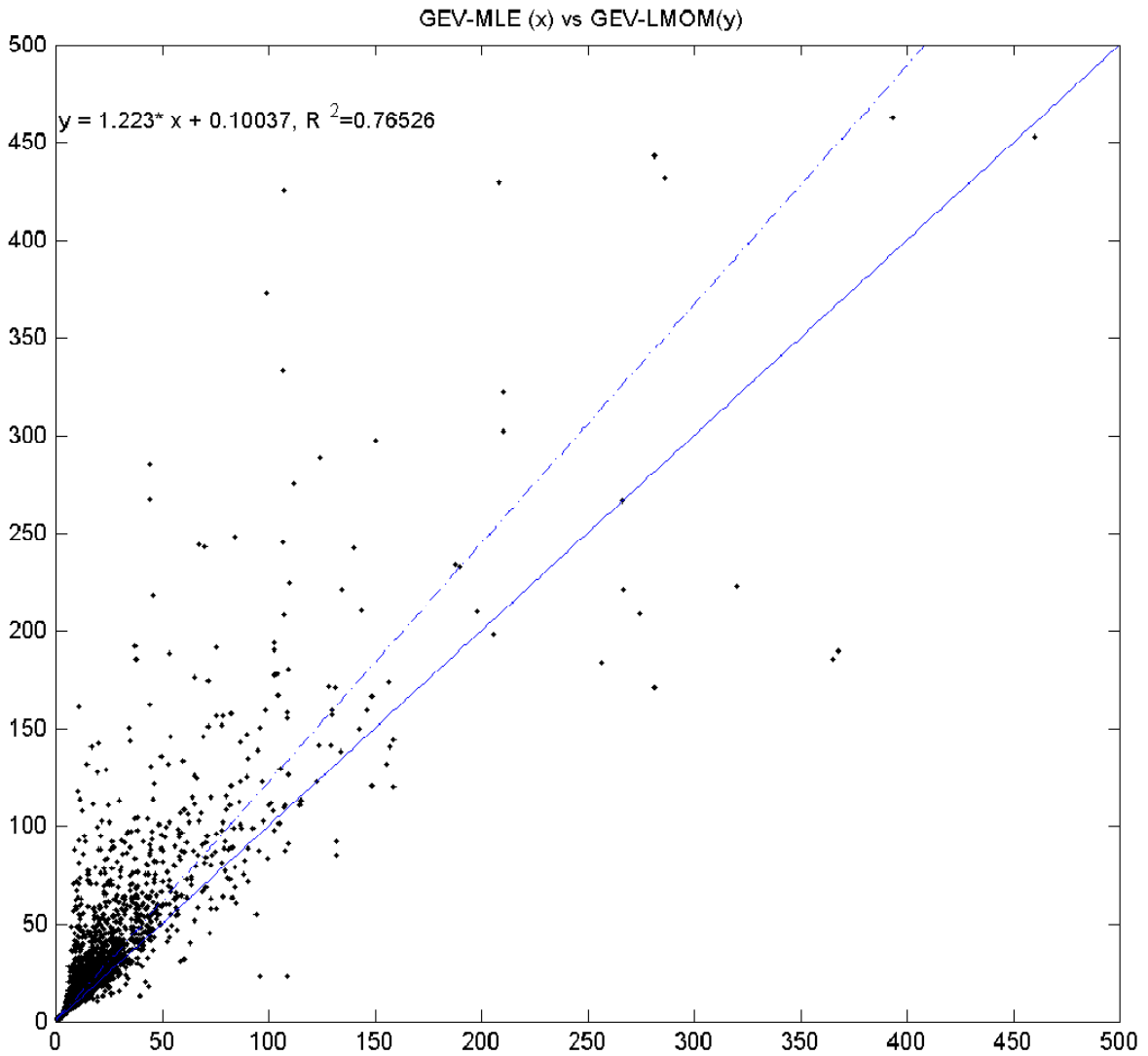


Figure 4-43. Comparison of the Recurrence Interval of Yearly Flow Peaks Estimated by GEV-MLE (x) and GEV-LMOM (y).

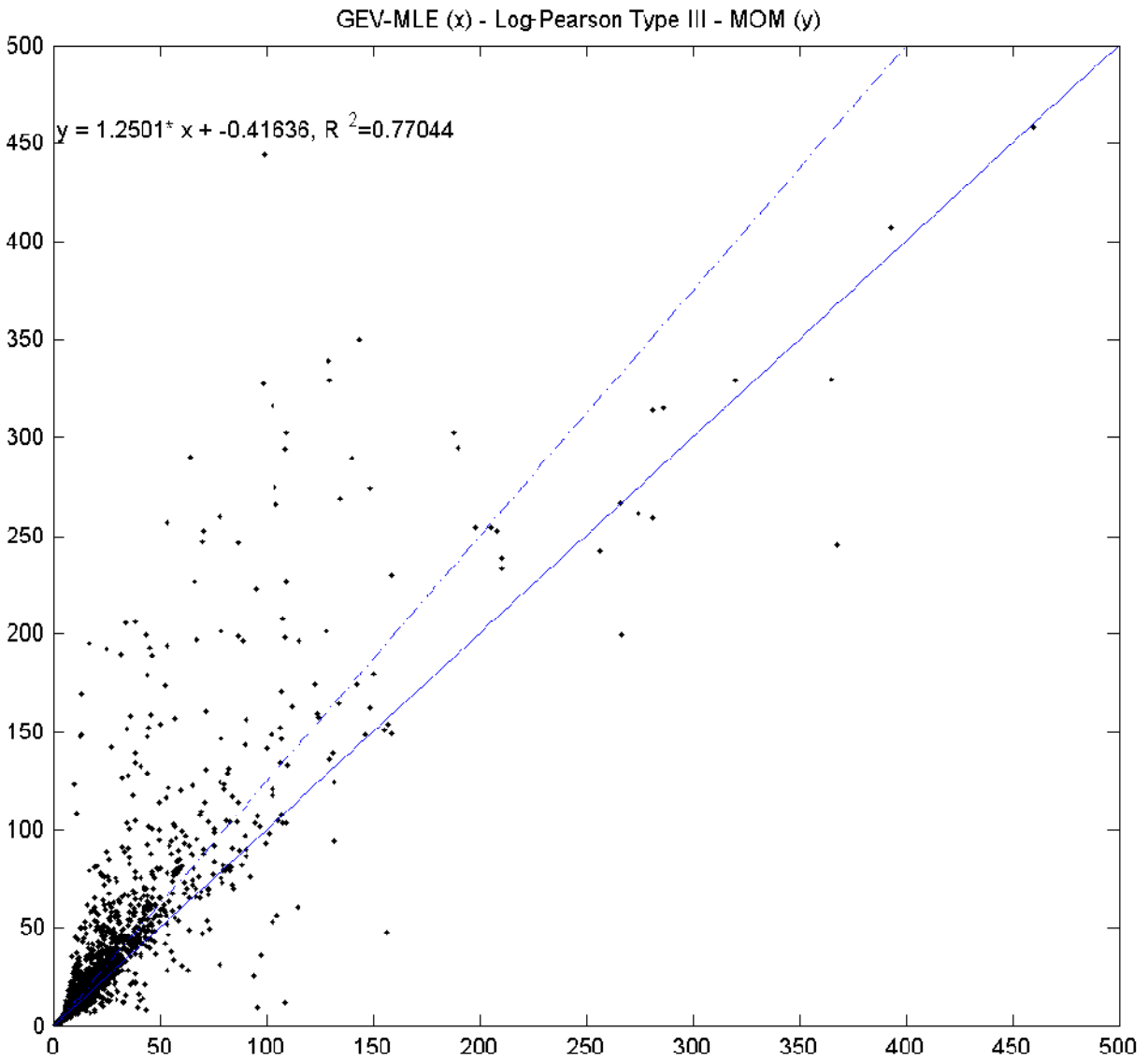


Figure 4-44. Comparison of the Recurrence Interval of Yearly Flow Peaks Estimated by GEV-MLE and Log-Pearson Type III-MOM.

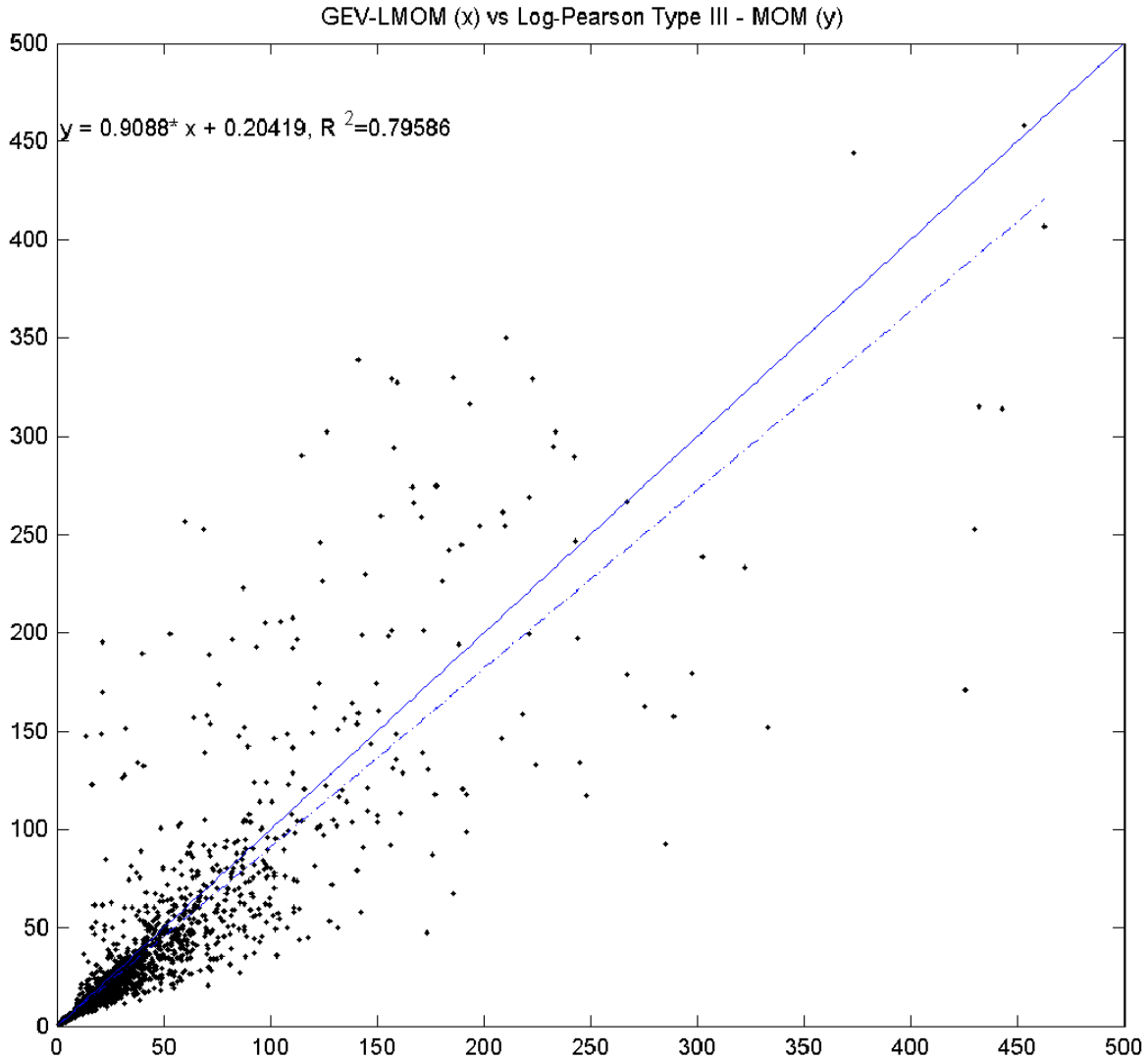


Figure 4-45. Comparison of the Recurrence Interval of Yearly Flow Peaks Estimated by GEV-LMOM and Log-Pearson Type III-MOM.

4.5.5.7. Composite of the Recurrence Interval by GEV-MLE and GEV-LMOM

Because the upper and lower boundaries of the recurrence interval for a given flow can generally be captured by the estimates based on GEV-MLE and GEV-LMOM, this study suggests a composite recurrence interval by a combination of both GEV-MLE and GEV-LMOM. By definition, the probability that an x -year flood or a flood higher than the x -year flood can happen in any one year is $\frac{1}{x}$. Then, the probability that the x -year flood is not equaled or not exceeded

during the x -year period becomes $(1 - \frac{1}{x})^x$. As x increases, this value converges to 0.37. This means that there is at least a 0.37 probability that the recurrence interval of the maximum flow peak recorded at a gage does not exceed the length of the record at the gage. If this principle is applied to the 262 gages in Texas where flood frequency analysis was performed, approximately 37 percent of the gages (97 gages) should have a maximum observed flow peak where the recurrence interval does not exceed the length of the record. GEV-MLE and GEV-LMOM provided 46 percent and 16 percent of such gages, respectively. If the recurrence interval of the maximum flow peak at each gage is taken as a linear combination of the estimates by GEV-MLE and GEV-LMOM (i.e., $RI = a \cdot RI_{GEV-MLE} + b \cdot RI_{GEV-LMOM}$), the proportion of such stations can match the 0.37 target value. [Figure 4-46](#) shows the relationship between the weight factor of the recurrence interval estimate by GEV-MLE (in the above equation) and the proportion of the stations where the recurrence interval of the maximum flow peak does not exceed the length of the record. The weight factor of the GEV-MLE estimate that makes the proportion 0.37 is 0.81. Thus, the composite recurrence interval is suggested as the following equation:

$$RI = 0.81 \cdot RI_{GEV-MLE} + 0.19 \cdot RI_{GEV-LMOM} \quad (4-64)$$

4.5.6. Discussion of Flood Frequency Analysis

In this chapter, the methods of FFA that were applied in this study were explained. Then, the recurrence interval of the yearly floods observed at the gages in and around Texas was estimated by each FFA method and compared. The result of the comparison indicates that GEV-LMOM gives the highest recurrence interval for a given magnitude of flood while GEV-MLE gives the lowest recurrence interval estimates. Estimates by Log-Pearson Type III-MOM were in between GEV-LMOM and GEV-MLE. Overall, there is a systematic bias in the estimated recurrence interval based on the choice of probability distribution and parameter estimation method. This bias seems to come from the fact that there are many gages that do not have enough length of data for the frequency analysis. The accuracy of the extrapolated recurrence interval of a flood with a recurrence interval greater than the length of the gage record has always been an issue in flood frequency analysis. However, this study provides the recurrence intervals for a given flood based on various FFA methods and lets the user choose the most appropriate one based on engineering judgment. Also, a composite recurrence interval was suggested for the users that

need one simple answer for the scour analysis. Even though TAMU-FLOOD ([Appendix F](#)) provides the user with a simple answer that can be directly applied to a bridge scour assessment, users should be cautious about the uncertainties inherent in their choice of flood frequency methods.

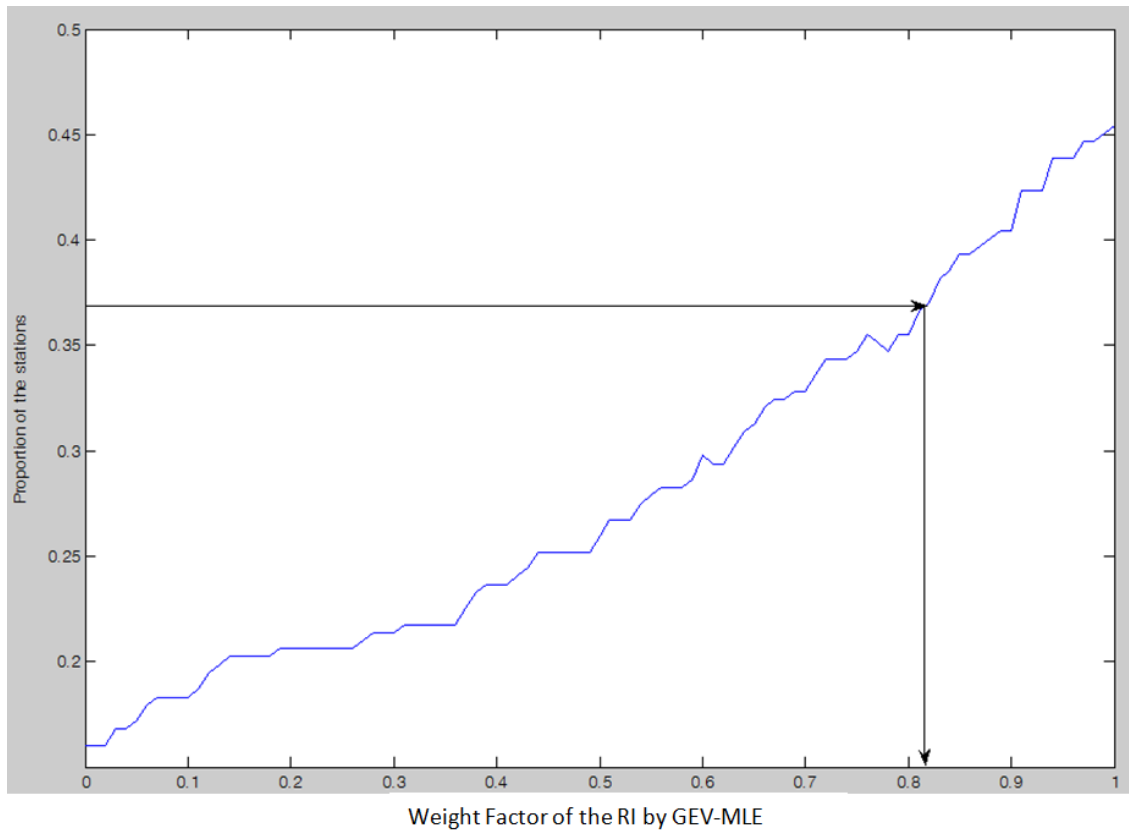


Figure 4-46. Weight Factor of GEV-MLE versus Proportion of the Stations at Which the Recurrence Interval of the Maximum Flow Peak Does Not Exceed the Length of the Record of the Station.

4.6. USGS REGIONAL REGRESSION EQUATION

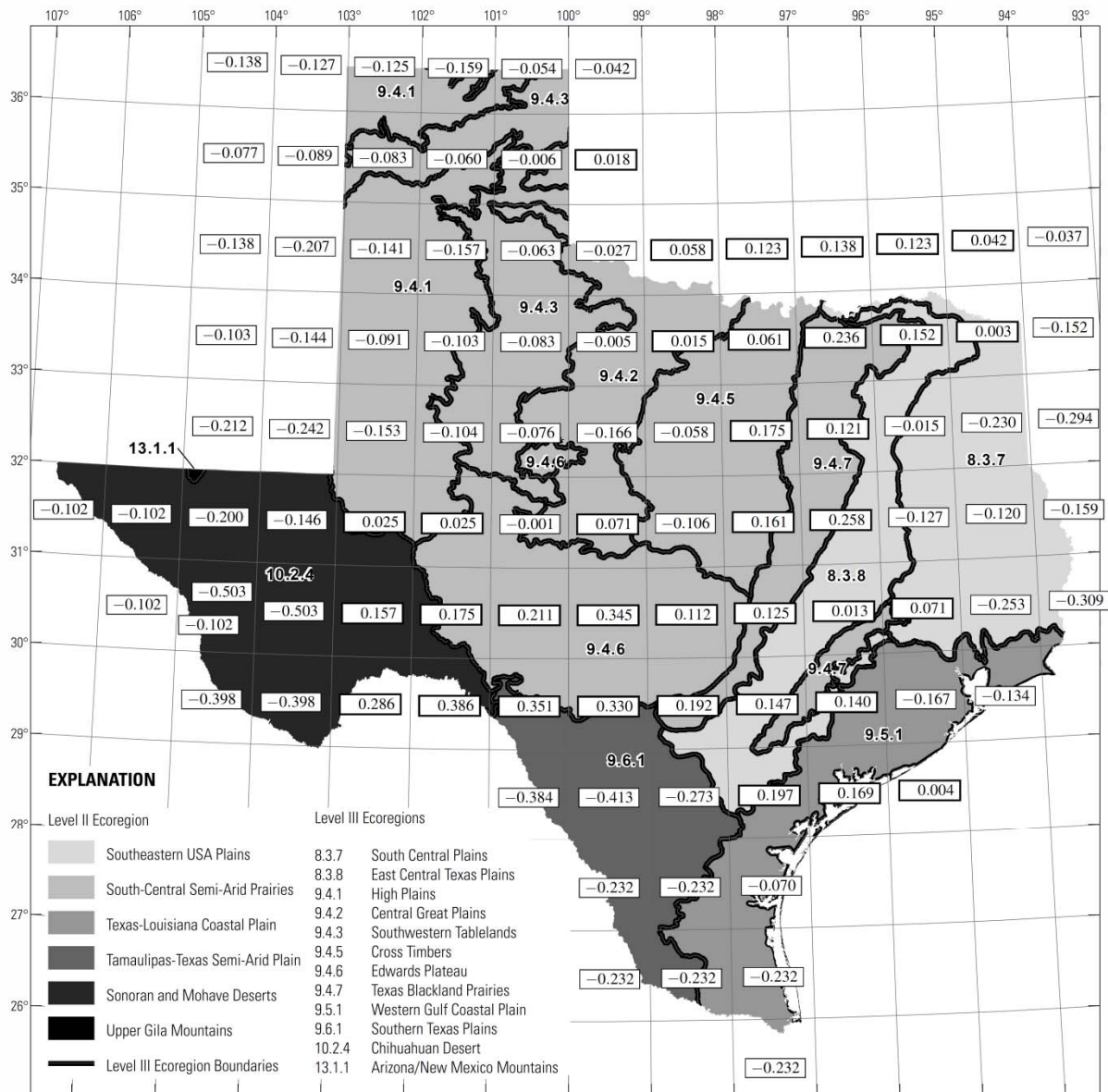
Asquith and Roussel (2009), in cooperation with the Texas Department of Transportation, suggested sets of equations that relate the basin characteristics to the design flow (e.g., 50-year flood, 100-year flood) of the basin. These equations are typically referred to as the regional regression equations. The regional regression equations are used in BSA 2 and BSA 3 when the estimated recurrence intervals are converted into flow values.

Asquith and Roussel (2009) replaces USGS (1996). Thus, the further use of the equations in USGS (1996) is not recommended. Also, the regional regression equations are developed for “natural basins,” where human development does not significantly affect the rainfall-runoff generation process. Thus, the equations should be used with higher caution when estimating the design floods in a basin with human development.

Table 4-2 shows the regional regression equations of Asquith and Roussel (2009). The equation relate the flood with a given recurrence interval [cfs] to mean annual precipitation (P, [inch]), dimensionless average channel slope (S, [L/L]), Drainage Area (A [mi²]), and a parameter Ω that reflects the characteristics of the watershed. The value of Ω can be read from the map of Texas shown in Figure 4-47

Table 4-2. The Regional Regression Equations of Asquith and Roussel (2009).

P: mean annual precipitation [inch], S: dimensionless average channel slope [L/L], A: Drainage Area [mi²], Ω: Basin characteristic parameter (Figure 4-47)		
Recurrence Interval of the Flood	Equation	Adjusted R-Squared
5	$Q_5 = P^{1.308} S^{0.372} \cdot 10^{[0.885\Omega + 16.62 - 15.43A^{-0.0215}]}$	0.88
10	$Q_{10} = P^{1.105} S^{0.476} \cdot 10^{[0.961\Omega + 11.17 - 8.997A^{-0.0424}]}$	0.89
25	$Q_{25} = P^{1.140} S^{0.446} \cdot 10^{[0.945\Omega + 11.79 - 9.819A^{-0.0374}]}$	0.89
50	$Q_{50} = P^{1.105} S^{0.476} \cdot 10^{[0.961\Omega + 11.17 - 8.997A^{-0.0424}]}$	0.87
100	$Q_{100} = P^{1.071} S^{0.507} \cdot 10^{[0.969\Omega + 10.82 - 8.448A^{-0.0467}]}$	0.86



Base from Texas Natural Resources Information System digital data
 Ecoregions from Commission for Environmental Cooperation, 1997
 Scale 1:7,920,000
 Albers equal-area projection, datum NAD 83
 Standard parallels 27°30' and 35°00', latitude of origin 31°00', central meridian -100°00'
 Horizontal coordinate information is referenced to the North American Datum of 1983 (NAD 83).

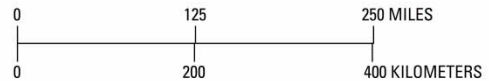


Figure 4-47. Map of regional characteristic parameter Ω across Texas (Asquith and Roussel, 2009).

4.7. STEP-BY-STEP PROCEDURE

In this section, the step-by-step procedures of the hydrology part of the bridge scour analysis is explained. Figure 4-48 and Table 4-3 describe the flowchart of the hydrology part, which can be used as a guideline to obtain the hydrologic information for the bridge scour analysis.

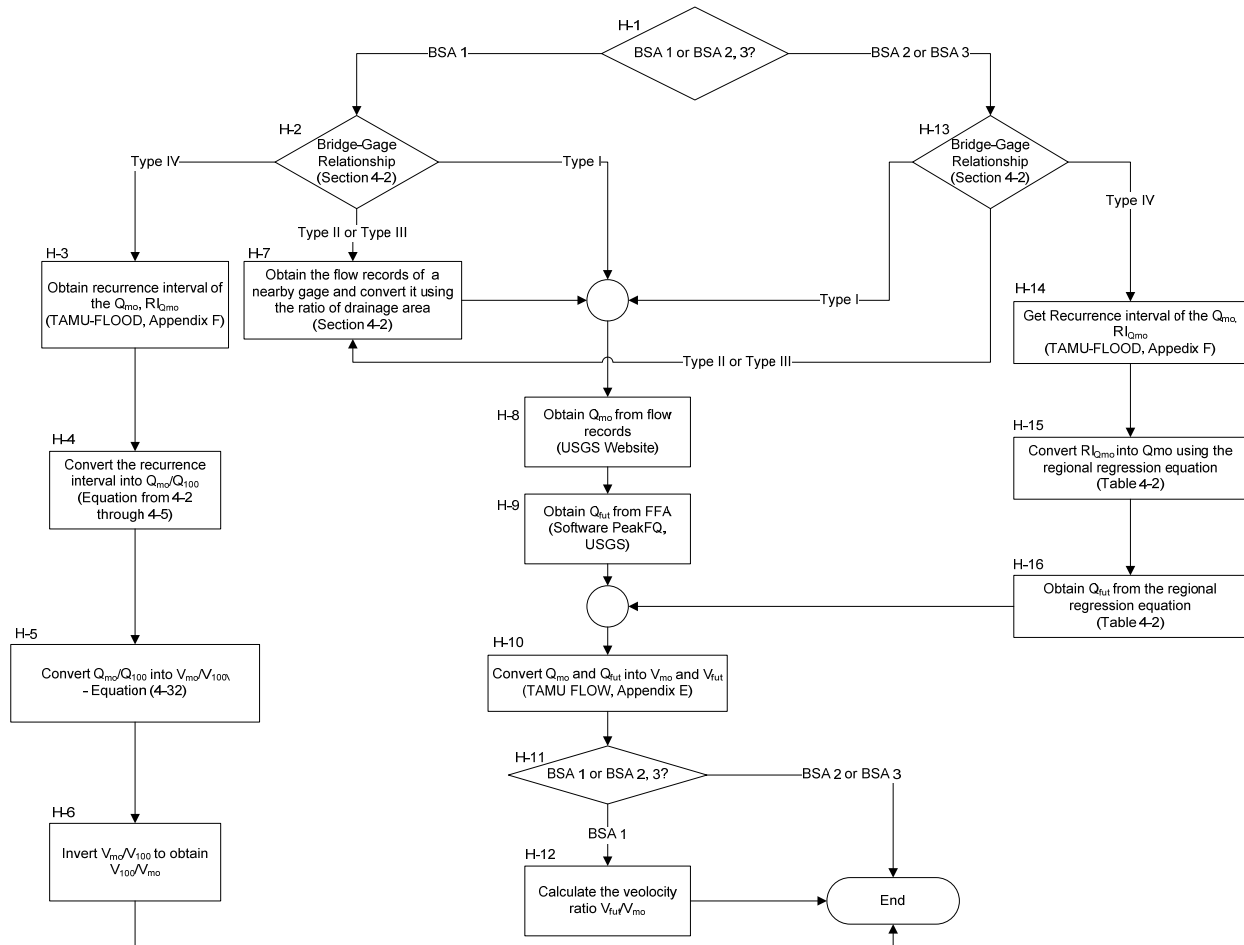


Figure 4-48. Flowchart of the Hydrology Part.

Table 4-3. Description of the Flowchart of the Hydrology Part.

Box No.	Description
H-1	Decision box that determines the types of bridge scour analysis. Choose between BSA 1, BSA 2, and BSA 3. BSA 1 requires the flow velocity ratio $V_{\text{fut}}/V_{\text{mo}}$ whereas BSA 2 and BSA 3 require the explicit value of V_{fut} and V_{mo} .
H-2	Decision box that determines the bridge-gage relationship. If the flow gage is located at the bridge, follow the arrow of Type I. If the flow gage is located upstream/downstream close to the bridge or if the flow gage is located close to a hydrologically similar watershed, follow the arrow of Type II or III. If the flow record cannot be obtained by any measure, follow the arrow of Type IV.
H-3	Box that explains how to obtain the recurrence interval of the maximum flood ($RI_{Q_{\text{mo}}}$) that the bridge has experienced. TAMU-FLOOD (Appendix F) can be used for this process.
H-4	Box that explains how to convert $RI_{Q_{\text{mo}}}$ into the flow ratio Q_{mo}/Q_{100} . This study explored and found the relationship between the two variables using 101 USGS gages across Texas. Equation (4-2) through Equation (4-5) describe this relationship.
H-5	Box that explains how to convert the ratio of flow (Q_{mo}/Q_{100}) into the ratio of velocity (V_{mo}/V_{100}). Manning's equation is used for this step. The conversion equation that is derived by this study is given in Equation (4-32).
H-6	BSA 1 requires the inversion (V_{100}/V_{mo}) of the velocity ratio (V_{mo}/V_{100}) calculated from the previous step.
H-7	Box that explains how to obtain flow records for a bridge that has a gage upstream or downstream (Bridge-Gage Relationship Type II), and for a bridge that has a gage in a nearby hydrologically similar watershed (Bridge-Gage Relationship Type III). The detailed description for this step is provided in Section 4.2 .
H-8	Box that explains the first step to be performed after obtaining the flow record at the bridge. From the record, pick the greatest flood that happened after the bridge was built (Q_{mo}).

Table 4-3. Description of the Flowchart of the Hydrology Part (Continued).

Box No.	Description
H-9	Box that explains how to obtain the future flood to be considered by BSA. Typically this value is a design flood such as Q_{100} . This value can be obtained through the FFA. One of the most typical software tools that does FFA is PeakFQ provided by the USGS website (http://water.usgs.gov/software/PeakFQ/).
H-10	Box that explains how to convert the flow (cfs) into velocity (ft/s). This step can be done by typical river analysis software such as HEC-RAS. This study also provides a software tool TAMU-FLOW (Appendix E), a simplified version of HEC-RAS that specifically focuses on converting flow into velocity.
H-11	Decision box that determines the types of bridge scour analysis. Choose between BSA 1, BSA 2, and BSA 3. BSA 1 requires the flow velocity ratio V_{fut}/V_{mo} whereas BSA 2 and 3 require the explicit value of V_{fut} and V_{mo} .
H-12	Box that explains how to obtain the ratio of velocity. Simply divide V_{fut} by V_{mo} to obtain the input variable for BSA 1.
H-13	Decision box that determines the bridge-gage relationship. If the flow gage is located at the bridge, follow the arrow of Type I. If the flow gage is located upstream/downstream of the bridge or the flow gage is located close to a hydrologically similar watershed, follow the arrow of Type II or III. If the flow record cannot be obtained by any measure, follow the arrow of Type IV.
H-14	Box that explains how to obtain the recurrence interval of the maximum flood ($RI_{Q_{mo}}$) that the bridge has experienced. TAMU-FLOOD (Appendix F) can be used for this process.
H-15	Box that explains how to convert $RI_{Q_{mo}}$ into Q_{mo} . This step is done by using the regional regression equations. The equations are given at http://pubs.usgs.gov/wri/wri964307/pdf/wri4307.pdf . Plot the recurrence interval (x) against the flow value obtained from the regional regression equation (y). Then, visually estimate $RI_{Q_{mo}}$ from Q_{mo} .
H-16	Box that explains how to obtain Q_{fut} . Typically, Q_{fut} is Q_{100} , which can be estimated by using the regional regression equations (Table 4-2).

5. BRIDGE SCOUR ASSESSMENT 1

5.1. INTRODUCTION

Bridge Scour Assessment 1 is a bridge scour assessment procedure that makes use of existing data collected either from bridge records maintained by the authorities or by site visit (Govindasamy et al. 2008). Figure 5-1 Reference Surface for Z_{thresh} and Figure 5-2 show the BSA 1 flowchart.

The main idea behind the BSA 1 procedure is that the scour depth corresponding to a specified future flood event is obtained through extrapolation charts that relate the scour depth ratio ($Z_{\text{fut}}/Z_{\text{mo}}$) to the velocity ratio ($V_{\text{fut}}/V_{\text{mo}}$). Here, Z_{fut} is the scour depth corresponding to a specified future flood, Z_{mo} is the maximum observed scour at the bridge, V_{fut} is the velocity corresponding to the specified future flood, and V_{mo} is the maximum velocity observed at the bridge until the time Z_{mo} is measured. The extrapolation charts, termed the Z-Future Charts, are presented in Figure 5-3 through Figure 5-7. The vulnerability of the bridge associated with scour depends on the comparison between Z_{fut} and the allowable scour depth of the foundation, Z_{thresh} . In the case of this report, Z_{thresh} is defined relative to the initial as-built ground line (Figure 5-1). There are two flowcharts for BSA 1; the first one is an assessment procedure for a bridge site that is underlain by a uniform deposit or for a scour depth being investigated that is not expected to exceed the top layer in a non-uniform deposit. This assessment procedure is termed BSA 1 (Uniform Deposit) and is shown in Figure 5-2. The second flowchart is called BSA 1 (Multilayer Analysis) and is used for layered deposits when the scour depth being investigated extends beyond the top layer. The BSA 1 (Multilayer Analysis) flowchart is shown in Figure 5-2. Both analyses are explained in detail in this chapter.

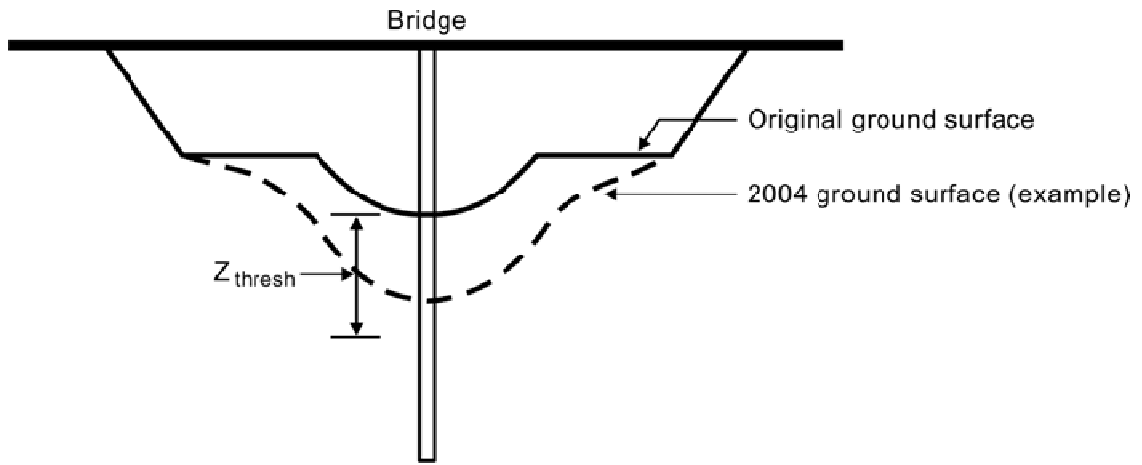


Figure 5-1. Definition of the Reference Surface for Z_{thresh} .

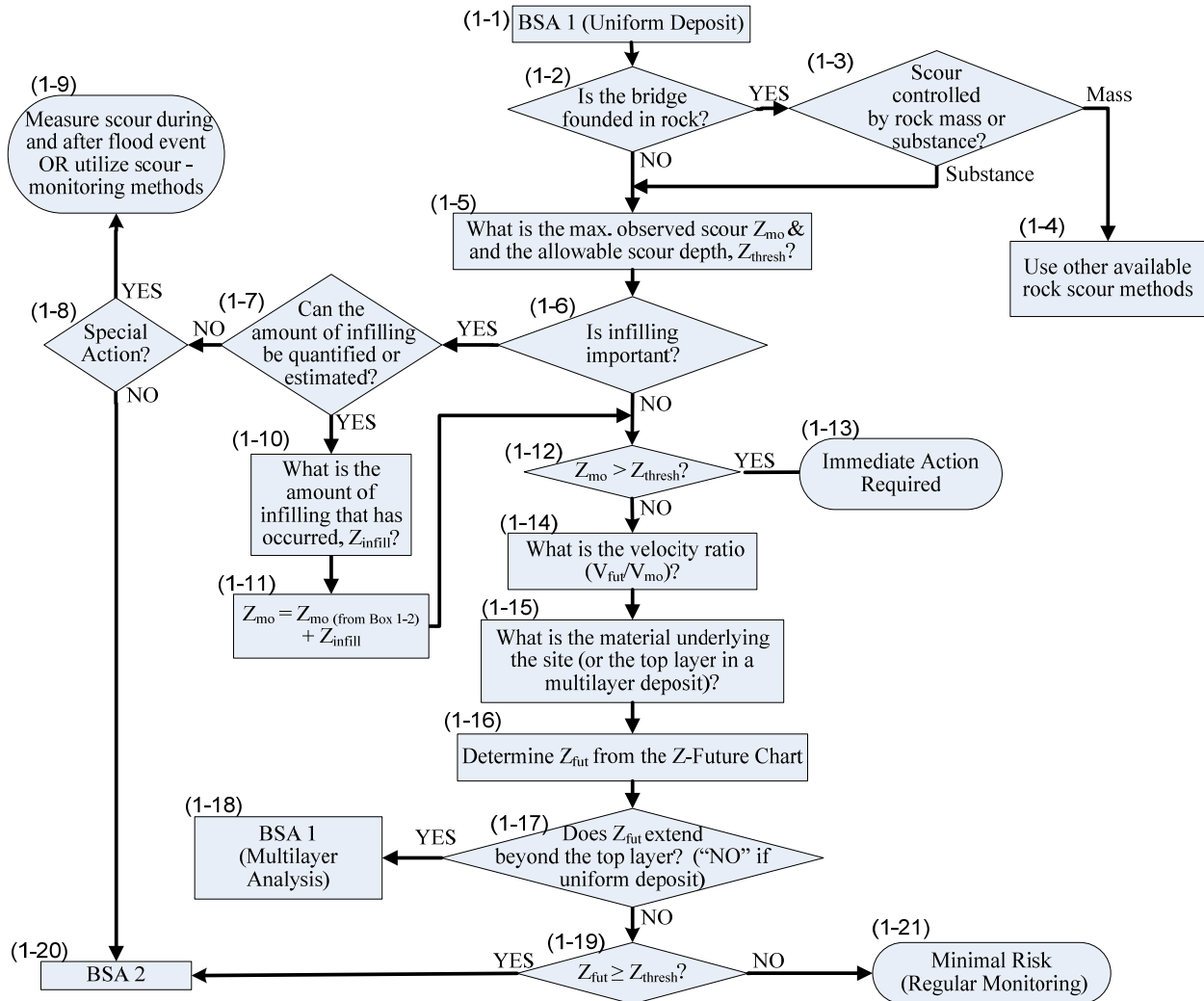


Figure 5-2. BSA 1 (Uniform Deposit) Flowchart.

5.2. THE Z-FUTURE CHARTS

The Z-Future Charts (Figure 5-3 through Figure 5-7) are essentially extrapolation charts that determine the scour depth Z_{fut} corresponding to a specified future flood event based on the following information:

- the maximum observed scour depth at the bridge site, termed Z_{mo} ;
- the maximum flow velocity experienced by the bridge from the time it was built to when Z_{mo} is recorded, termed V_{mo} ;

- the velocity of the future flood being considered, termed V_{fut} ;
- the age of the bridge at the time Z_{mo} was recorded, termed t_{hyd} ;
- the pier scour parameter: pier size; and
- the contraction scour parameters: water depth, soil critical velocity, and contraction ratio (B_2/B_1 as shown in Figure 2-12).

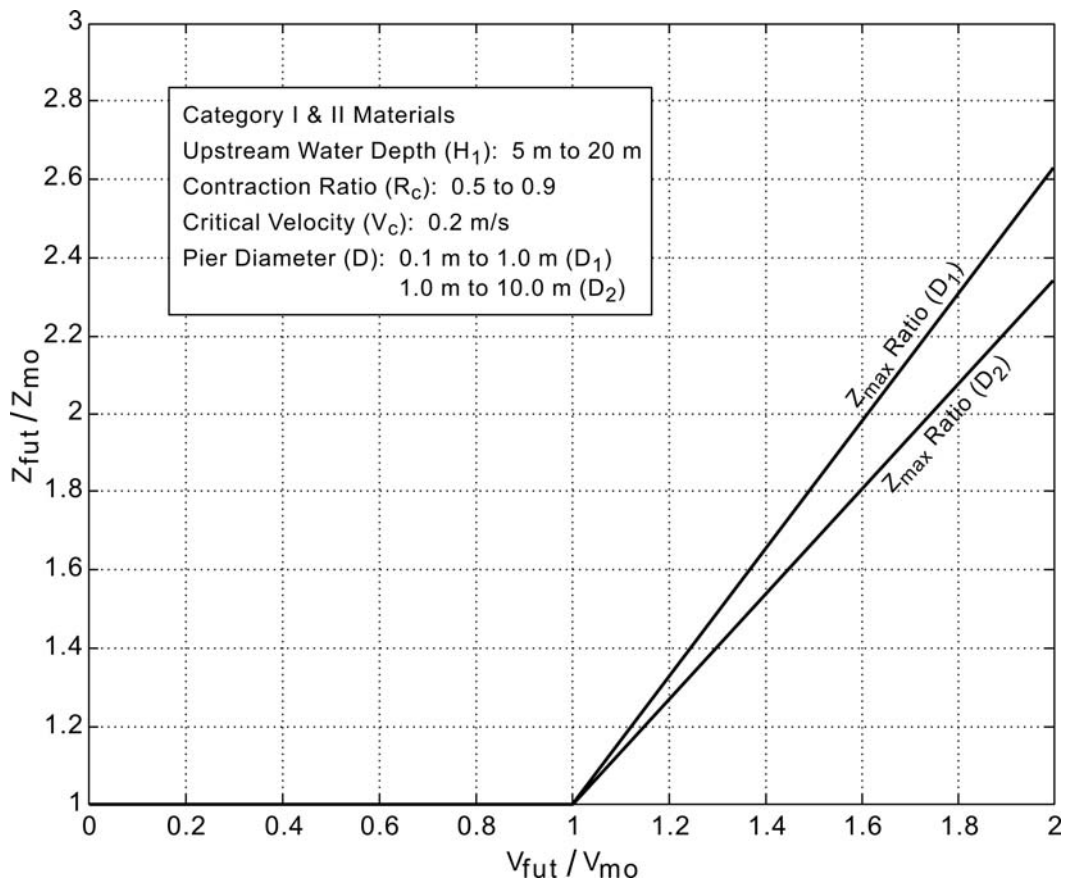


Figure 5-3. Z-Future Chart for Category I and II Materials.

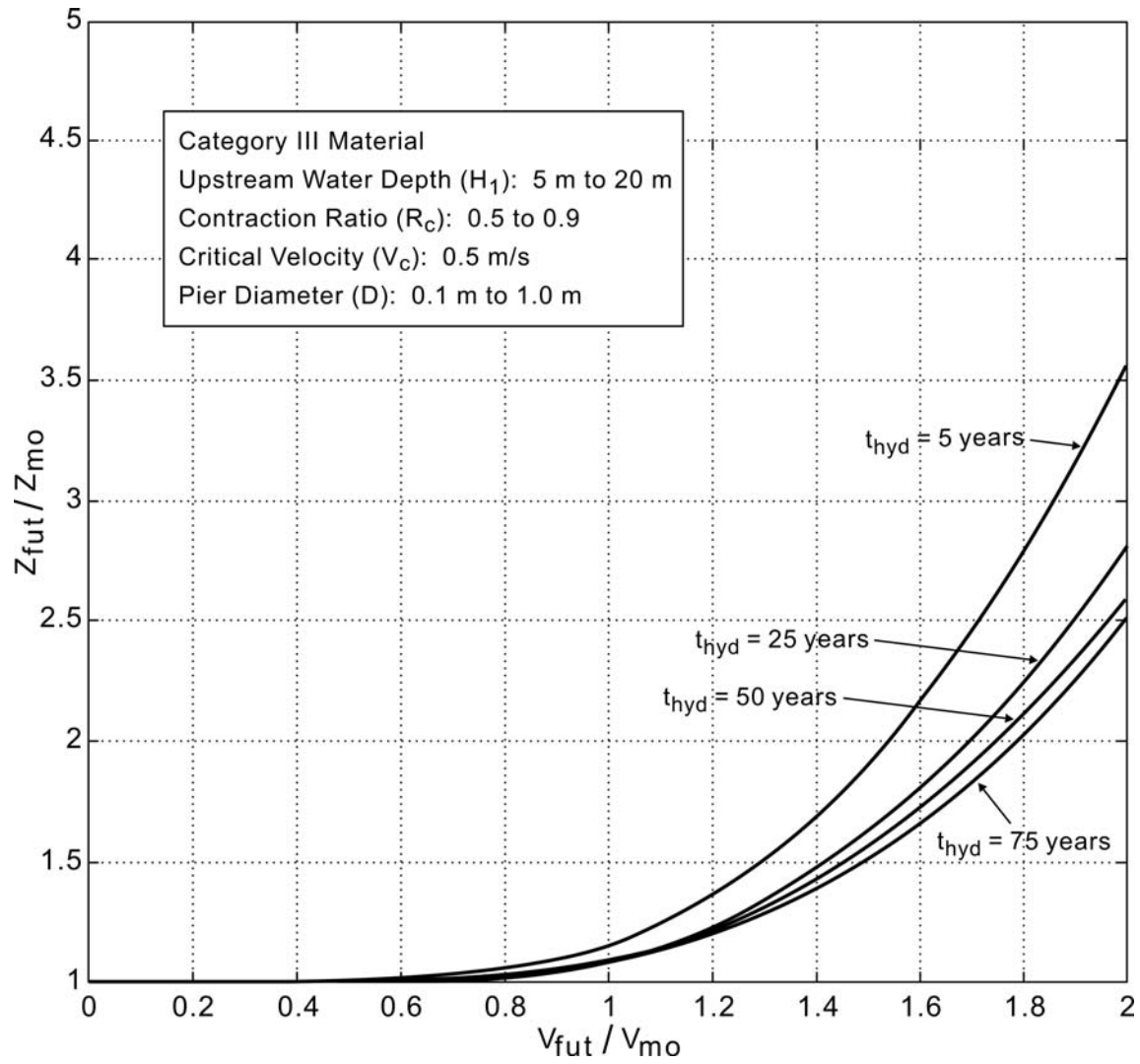


Figure 5-4. Z-Future Chart for Category III Materials (Pier Diameter: 0.1 m to 1.0 m).

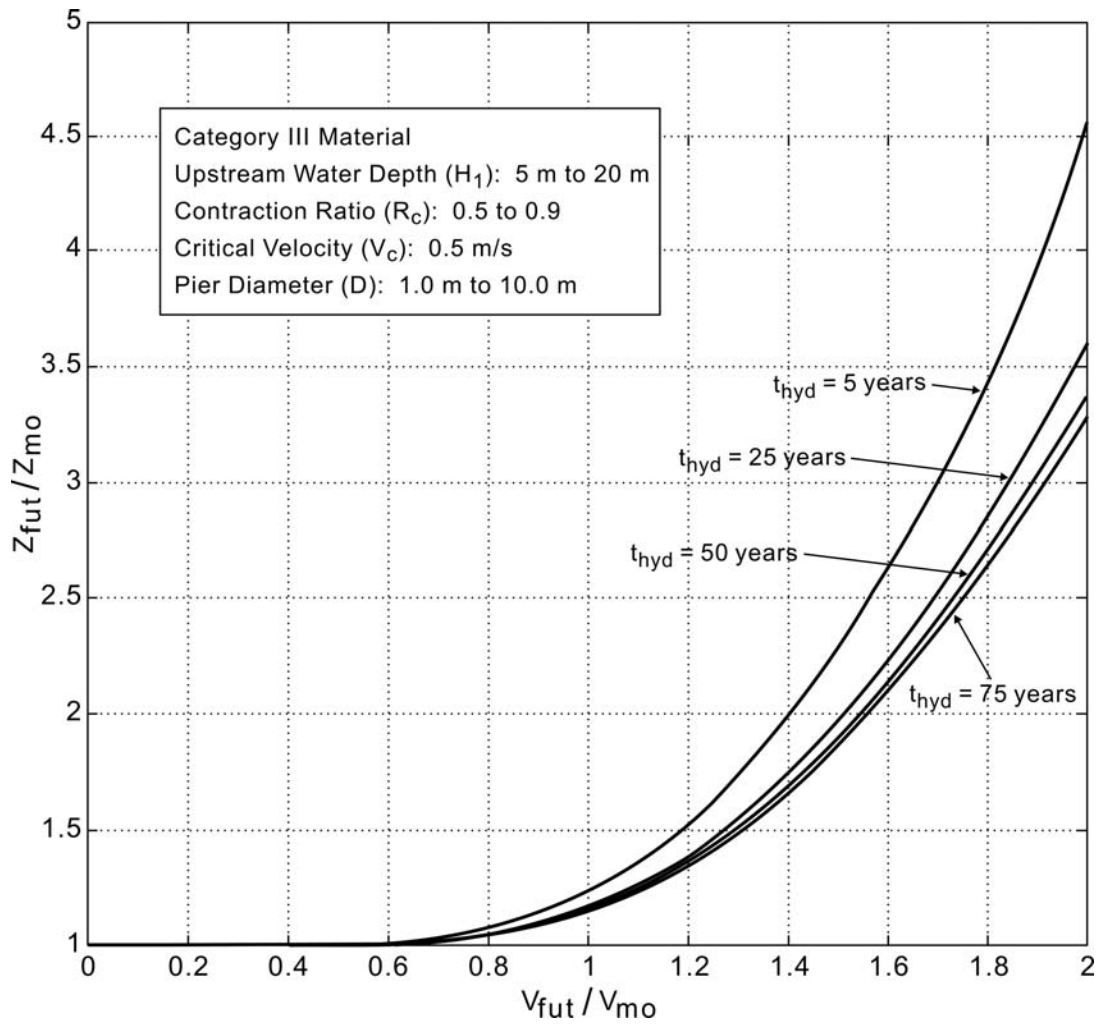


Figure 5-5. Z-Future Chart for Category III Materials (Pier Diameter: 1 m to 10 m).

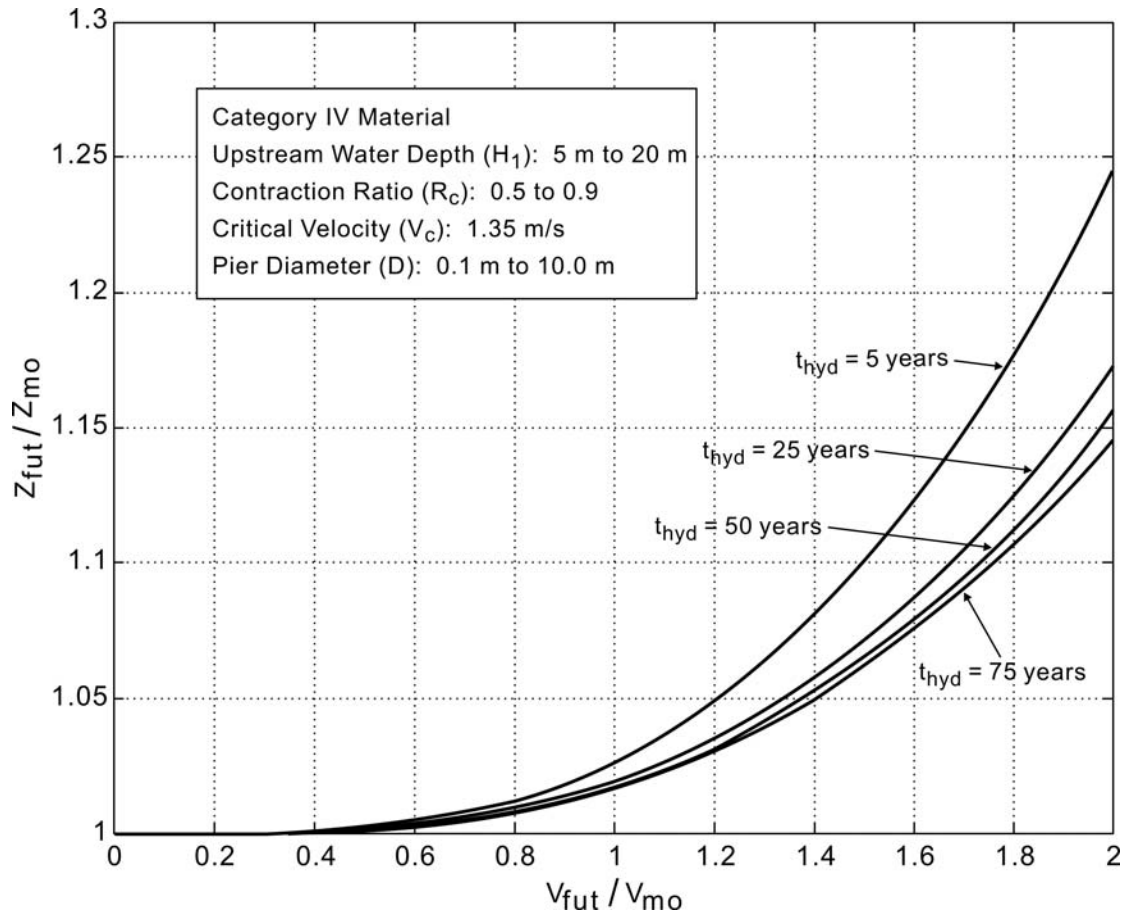


Figure 5-6. Z-Future Chart for Category IV Materials.

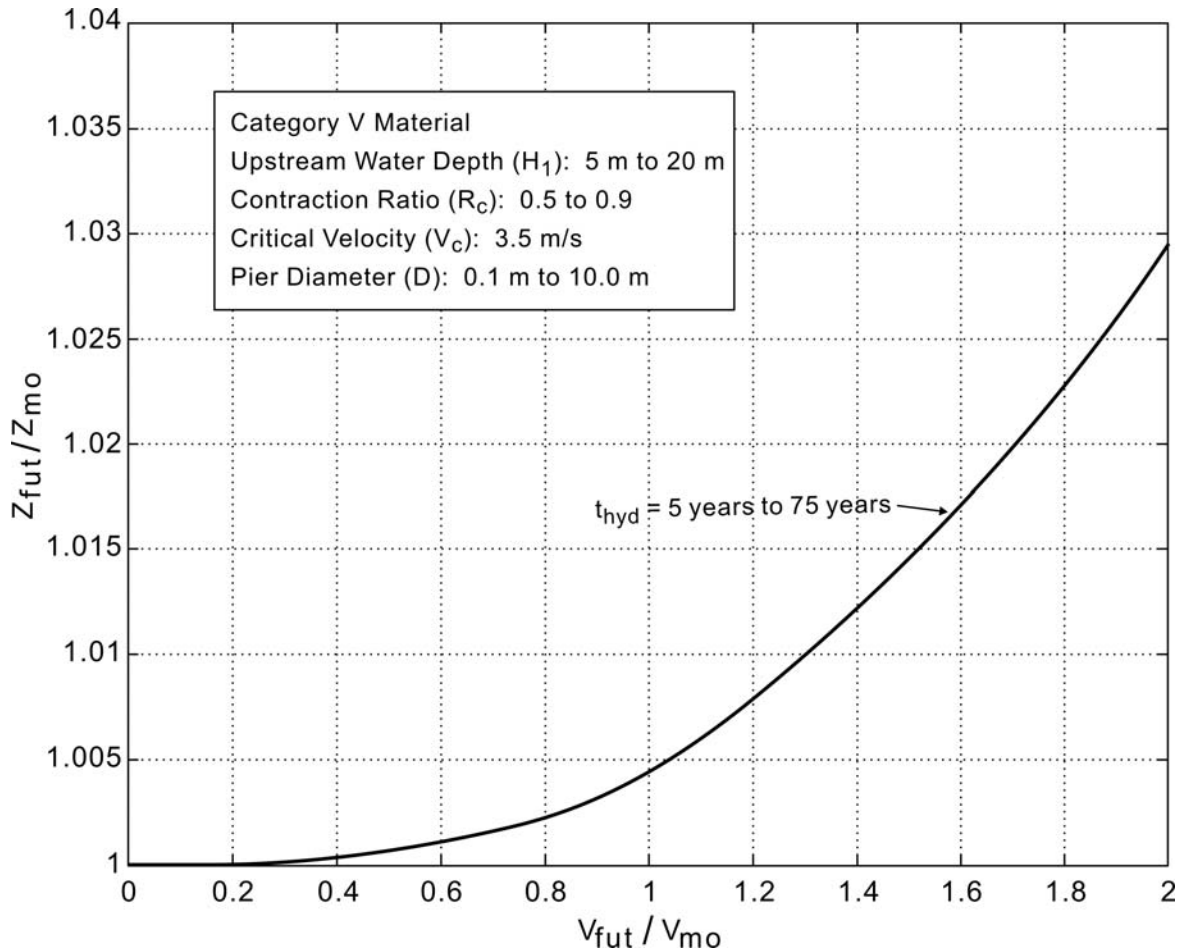


Figure 5-7. Z-Future Chart for Category V Materials.

The Z-Future Charts were developed using the Simple SRICOS-EFA Method for pier and contraction (Briaud et al. 1999, 2005), which was detailed in Chapter 3. Simple SRICOS-EFA simulations were carried out by employing the equivalent time to represent the age of the bridge and varying the pier scour parameter, contraction scour parameters, and material underlying the bridge site. The materials underlying the site are in accordance with five of the six erosion categories in the Erosion Function Charts (Figure 5-3 through Figure 5-7). These simulations computed the time-dependent scour depth as a result of two consecutive flows having velocities V_{mo} and V_{fut} , respectively. The two general cases covered by the simulations are as follows:

1. Case 1: $V_{\text{fut}} \geq V_{\text{mo}}$. This case represents the scenario where the bridge is being assessed for a future flood that is equal to or larger than the maximum flood it has experienced, where the velocity ratio ($V_{\text{fut}}/V_{\text{mo}}$) is equal to or greater than unity.
2. Case 2: $V_{\text{fut}} < V_{\text{mo}}$. This case represents the scenario where the bridge is being assessed for a future flood that is smaller than the maximum flood it has experienced, where the velocity ratio ($V_{\text{fut}}/V_{\text{mo}}$) is less than unity.

The material categories involved in these simulations are Erosion Categories I through V. Category VI was omitted from the simulations since materials that fall under this category are considered non-erosive and a Simple SRICOS-EFA simulation on them would lead to no additional scour.

Simple SRICOS-EFA simulations of pier scour depth and contraction scour depth as described above were carried out by creating various combinations of the following parameters:

1. V_{fut} and V_{mo} ranging from 0.3 ft/s (0.1 m/s) to 11.5 ft/s (3.5 m/s), which is well within the velocity range of flow of rivers in Texas;
2. upstream water depth, H_1 , ranging from 16.4 ft (5 m) to 65.6 ft (20 m);
3. channel contraction ratio, R_c , ranging from 0.5 to 0.9;
4. Soil-critical velocity, V_c , according to the five material categories investigated, i.e., Erosion Categories I through V; and
5. pier diameter, D , ranging from 0.3 ft (0.1 m) to 32.8 ft (10.0 m).

For the case of Category III materials, the Z-Future Charts were separated into two charts, i.e., one for D ranging from 0.1 m to 1.0 m and the other for D ranging from 1.0 m to 10.0 m (Figure 5-4 and Figure 5-5). This was done because there was notable difference between the band of $Z_{\text{fut}}/Z_{\text{mo}}$ ratios from these two ranges of pier diameters. The pier diameters for all other categories were lumped together, i.e., ranging from 0.1 m to 10.0 m since there was no significant difference due to the low erosion rates.

Simulations of pier and contraction scour depth described above were carried out for approximately 360,000 combinations of the above parameters for each material category. The

data points on [Figure 5-3](#) through [Figure 5-7](#) have been omitted to improve the clarity of the curves but are shown in [Appendix A](#). The Z_{fut} values were normalized with the corresponding Z_{mo} values, and the V_{fut} values were normalized with the corresponding V_{mo} values and subsequently plotted against each other to form the Z-Future Charts. It should be noted that Z_{mo} in these simulations are computed values based on a given V_{mo} and other relevant parameters.

[Figure 5-8](#) and [Figure 5-9](#) show how two sequences of floods, i.e., the maximum flood observed at the bridge Q_{mo} (with a corresponding V_{mo}) and the specified future flood Q_{fut} (with a corresponding V_{fut}), are simulated. This procedure is adopted from [Briaud et al. \(2001b\)](#). [Figure 5-8](#) illustrates the approach adopted for Case 1 where V_{fut} is larger than V_{mo} , while [Figure 5-9](#) shows the approach for Case 2 where V_{fut} is smaller than V_{mo} .

In general, the Z-Future Charts lead to the determination of Z_{fut} by employing the following relationship:

$$Z_{\text{fut}} = Z_{\text{mo}} \times f(V_{\text{fut}}/V_{\text{mo}}) \quad (5.1)$$

where f is some function of $(V_{\text{fut}}/V_{\text{mo}})$ obtained from the Z-Future Charts and is always equal to or greater than unity (for the case of clear-water scour, as considered in these simulations). The velocity ratio $(V_{\text{fut}}/V_{\text{mo}})$ is plugged into the chart by the user to obtain the value of the function f , based on the material type, age of the bridge, and pier scour and contraction scour parameters. Z_{mo} is obtained from bridge inspection and measurement records.

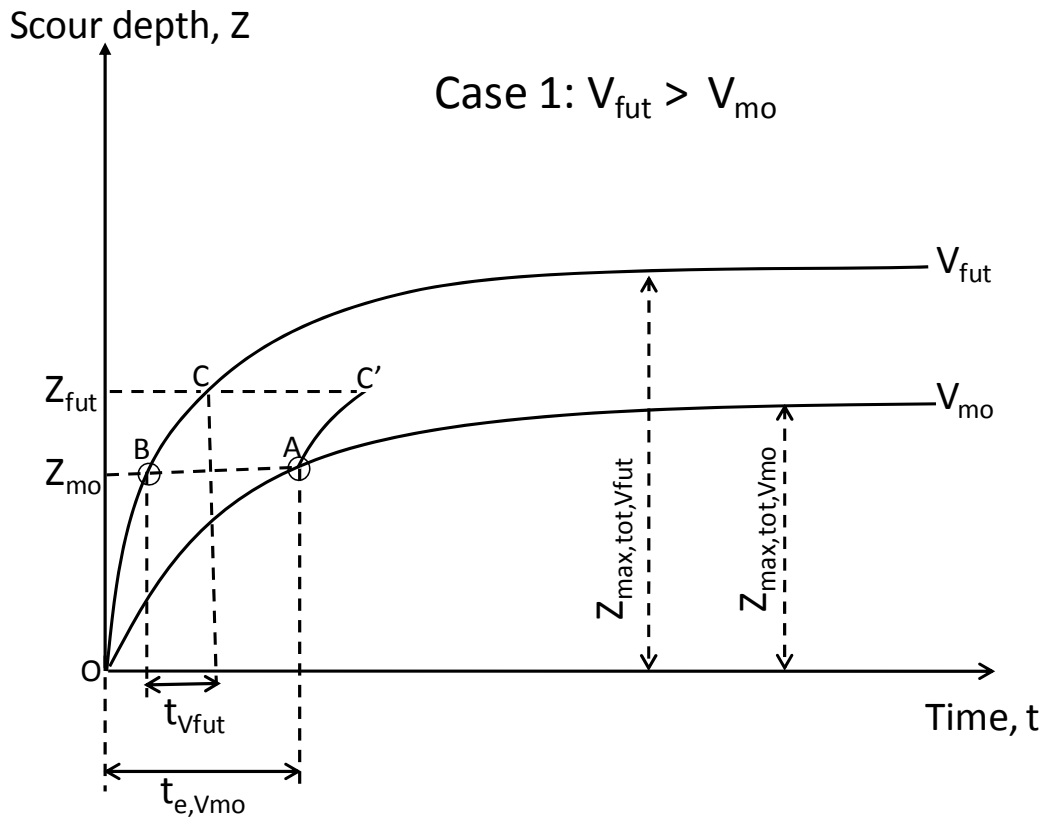


Figure 5-8. Scour Due to Sequence of Two Flood Events: $V_{fut} > V_{mo}$ (after Briaud et al. 2001b).

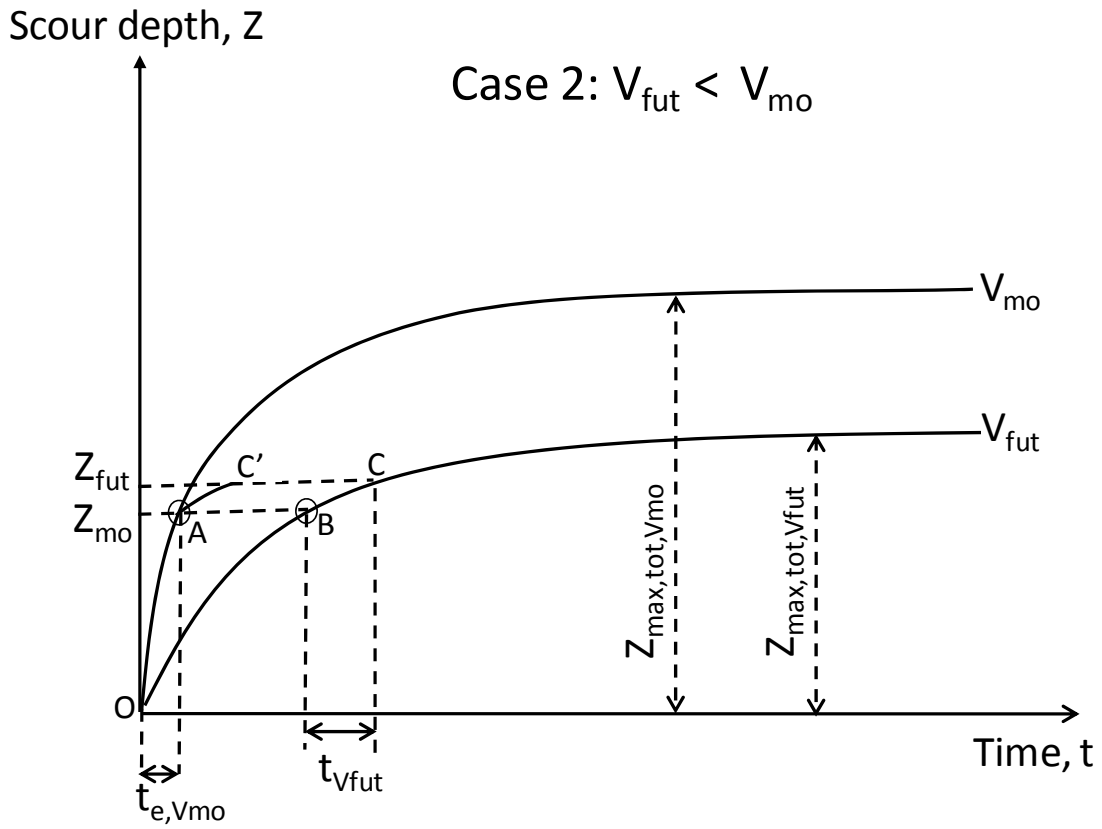


Figure 5-9. Scour Due to Sequence of Two Flood Events: $V_{fut} < V_{mo}$
(after [Briaud et al. 2001](#)).

5.2.1. Case 1: $V_{fut} > V_{mo}$

In Figure 5-8, the scour depth (Z) versus time (t) curve under V_{fut} and V_{mo} are shown. The lower curve represents the Z - t relationship for the lower velocity, V_{mo} , and the upper curve represents the Z - t relationship for the higher velocity, V_{fut} . In this analysis, the velocity hydrograph at the bridge until the most recent scour measurement is converted into an equivalent time, with t_{hyd} as the hydrograph duration and V_{mo} as the maximum hydrograph velocity (Equation [2.7] and Equation [2.8]). At the start of the application of the equivalent time $t_{e,V_{mo}}$ and V_{mo} , the scour depth is zero (point O in Figure 5-8) and progresses to Z_{mo} (point A) at the end of $t_{e,V_{mo}}$. At the start of the future flood, the scour depth is translated to point B where it is still equal to Z_{mo} on the upper curve. In the development of the Z -Future Charts, the duration of the future flood is taken as 72 hr at a constant velocity, V_{fut} . This duration of the future flood is termed $t_{V_{fut}}$ in Figure 5-8 and Figure 5-9. At the end of the future flood ($t_{V_{fut}}$), the scour depth would have progressed to Z_{fut} (point C). This Z_{fut} can be equal to the maximum scour depth under the future flood ($Z_{max,tot,V_{fut}}$) if the time is sufficient to reach this maximum value. The combined scour depth time history for Case 1 is given by points O, A, and C'.

5.2.2. Case 2: $V_{fut} < V_{mo}$

In Figure 5-9, the scour depth (Z) versus time (t) curve under V_{fut} and V_{mo} are shown. The lower curve represents the Z - t relationship for the lower velocity, V_{fut} , and the upper curve represents the Z - t relationship for the higher velocity, V_{mo} . Similar to Case 1, the velocity hydrograph at the bridge until the most recent scour measurement is converted into an equivalent time, with t_{hyd} as the hydrograph duration and V_{mo} as the maximum hydrograph velocity (Equation [2.7] and Equation [2.8]). At the start of the application of the equivalent time $t_{e,V_{mo}}$ and V_{mo} , the scour depth is zero (point O in Figure 5-9) and progresses to Z_{mo} (point A) at the end of $t_{e,V_{mo}}$. If Z_{mo} is larger than $Z_{max,tot,V_{fut}}$, which is the maximum scour depth possible under V_{fut} , the scour hole is already deeper than what is possible under V_{fut} and therefore cannot create additional scour (Briaud et al. 2001b). If Z_{mo} is smaller than $Z_{max,tot,V_{fut}}$, the scour depth at the start of the future flood is translated to point B where it is still equal to Z_{mo} on the lower curve. At the end of the future flood, the scour depth would have progressed to Z_{fut} (point C). This Z_{fut} can be equal to the maximum scour depth under the future flood ($Z_{max,tot,V_{fut}}$) if the time is sufficient to reach this

maximum value. The combined scour depth time history for Case 2 is given by points O, A, and C’.

5.3. THE BSA 1 FLOWCHART

The boxes in the BSA 1 flowcharts [Figure 5-2](#)) are of three shapes: rectangular, diamond, and rounded. Rectangular boxes are data collection and calculation boxes, meaning that the data listed in the box need to be collected by the user for the bridge being analyzed and then equations need to be used. Diamond boxes are “yes-no” decision boxes. Rounded boxes are conclusion boxes. All boxes are numbered for easy reference; the first digit represents the BSA level, and the second digit represents the box number.

As mentioned in the introduction to this chapter, the BSA 1 procedure consists of two flowcharts, BSA 1 (Uniform Deposit) and BSA 1 (Multilayer Analysis) flowcharts. BSA 1 (Uniform Deposit) is an assessment procedure for a bridge site that is underlain by a uniform deposit or for a scour depth being investigated that is not expected to exceed the top layer of a multilayer deposit. BSA 1 (Multilayer Analysis) is used for layered deposits when the scour depth being investigated penetrates beyond the top layer.

5.3.1. The BSA 1 (Uniform Deposit) Flowchart and Procedure

In this procedure, the first step is to identify whether the bridge is founded in rock or not. If the bridge is indeed founded in rock, BSA 1 then separates rock mass and rock substance–controlled erosion. Rock mass–controlled erosion occurs when reactions of rock materials to hydraulic stress are controlled by rock mass properties such as fracture and joint spacing, bedding planes, folding, and spatial orientation ([Cato 1991](#)). In rock mass–controlled erosion, the rock materials are eroded and transported as blocks. The critical velocity in rock mass erosion according to rock fracture spacing is shown in [Table 5-1](#). The erosion categories in this table correspond to the Erosion Function Charts ([Figure 3-4](#)). [Table 5-1](#) is preliminary in nature and should be calibrated against field behavior. The critical velocity and critical shear stress of rock as a function of fracture spacing is also shown in the Erosion Threshold Charts ([Figure 3-18](#) and [Figure 3-20](#)). Rock substance–controlled erosion is the erosion process that is governed by the property of the mineral grains forming the rock. These properties include density, strength, hardness,

permeability, weathering, grain size, and grain shape (Cato 1991). In BSA 1 (Uniform Deposit), scour assessments of rock materials that undergo rock mass–controlled erosion should use other available methods for assessing scour in rock. Rock materials that undergo rock substance–controlled erosion are treated as soils in BSA 1.

Table 5-1. Rock Mass Erosion (after Briaud 2008).

Joint Spacing		Critical Velocity		Erosion Category	Orientation of Joints
in	mm	ft/s	m/s		
< 1.2	< 30	1.6 – 4.4	0.5 - 1.35	III Medium	Not applicable
1.2 – 5.9	30 – 150	1.6 – 11.5	1.35 - 3.5	IV Low	Evaluation needed
5.9 – 58.5	150 – 1500	11.5 – 32.8	3.5 - 10	V Very low	Evaluation needed
> 58.5	> 1500	> 32.8	> 10	VI Non-Erosive	Not applicable

Note: This table is preliminary in nature and should be calibrated against field behavior.

There are two conditions for local scour at a bridge when it concerns the presence of sediments in the flow and deposition of sediments from the flow. The first condition is termed clear-water scour and occurs when there is no movement of the bed material in the flow upstream of the bridge, or when the bed material being transported in the upstream reach is transported in suspension through the scour hole (Richardson and Davis 2001). The second condition is termed live-bed scour and occurs when there is transport of bed material from the upstream reach into the bridge crossing (Richardson and Davis 2001). Live-bed scour is cyclic in nature. The scour hole deepens during the rising stage of the flood. At the falling stage of the flood, the flow recedes, and its sediment-carrying capacity reduces. This results in the deposition of sediments, which could take place in the scour hole. This could lead to infilling of the scour hole, yet it is possible that the relative depth of scour is marginally affected all over the river bottom.

When live-bed scour has taken place, the depth of the scour hole measured during bridge inspections could be the scour depth after infilling has occurred. This would be the case if the bridge inspection is carried out either during the falling stage of the flood or after the flood event altogether. Since the Z-Future Charts are developed for clear-water scour conditions, if the measurements taken during the bridge inspection do not account for possible infilling, Z_{fut} would be under-predicted, as implied by Equation (5.1). This would therefore lead to an unconservative or even erroneous assessment of the bridge for scour. Several options are available in BSA 1 when infilling is expected to occur:

1. Quantifying the amount of infilling that has occurred, Z_{infill} . The amount of infilling can be quantified from performing sediment transport calculations, running model tests, probing into the scour hole and roughly identifying the extent of the infilled material, or simply using engineering judgment and local experience. In this case, the value of Z_{mo} used in Equation (5.1) is the summation of the measured scour depth and Z_{infill} .
2. Taking special action. If the amount of infilling cannot be quantified or estimated, special actions such as measuring the scour depth during and after flood events or utilizing scour-monitoring methods can be adopted.
3. Carrying out BSA 2. If the amount of infilling cannot be quantified or estimated, then BSA 2 could be undertaken to obtain the maximum scour depth.

In order to obtain the scour depth ratio, Z_{fut}/Z_{mo} , from the Z-Future Chart, the velocity ratio, V_{fut}/V_{mo} , is required. Once the scour depth ratio is obtained from the Z-Future Chart, Z_{fut} is obtained from Equation (5.1) by plugging in the value of Z_{mo} measured in the field. If the site is underlain by a multilayer deposit and Z_{fut} extends beyond the top layer, then BSA 1 (Multilayer Analysis) should be carried out. Otherwise, if the site is underlain by a uniform deposit or if Z_{fut} does not extend beyond the top layer in a multilayer deposit, BSA 1 (Uniform Deposit) is continued. If Z_{fut} is equal to or greater than the allowable scour depth, Z_{thresh} , BSA 2 should be undertaken. Otherwise, the bridge is deemed “minimal risk” and should undergo regular monitoring.

5.3.2. The BSA 1 (Multilayer Analysis) Flowchart and Procedure

The BSA 1 (Multilayer Analysis) is carried out if a bridge site with a multilayer deposit is found to have a Z_{fut} value according to BSA 1 (Uniform Deposit) that extends beyond the top layer of the deposit. A multilayer analysis is required because using the maximum observed scour depth Z_{mo} in the top layer and extrapolating the scour depth to a different bottom layer could be unconservative in a case where the top layer is more erosion resistant (strong) than the bottom layer. This is because by doing so, one is expecting the less erosion-resistant (weak) bottom layer to respond to hydraulic stresses in a similar manner as the strong layer. Conversely, a bridge site with a weak top layer over a strong bottom layer would be too conservative and uneconomical.

In BSA 1 (Multilayer Analysis), the calculations involved are more detailed than BSA 1 (Uniform Deposit). The underlying principle of the multilayer analysis is the determination of the time it takes to completely erode the top layer and the corresponding remaining time of the future flood duration and its impact on the bottom layer. [Figure 5-10](#) shows an example of a multilayer analysis where V_{fut} is greater than V_{mo} and the top layer is more erosion resistant than the bottom layer. There are three $Z-t$ curves in this figure. The lowest curve is the $Z-t$ relationship for the top layer under velocity V_{mo} . The middle curve is the $Z-t$ relationship for the top layer under velocity V_{fut} . The upper curve is the $Z-t$ relationship for the bottom layer under V_{fut} . The definitions of the parameters that appear in [Figure 5-10](#) are given in [Table 5-2](#).

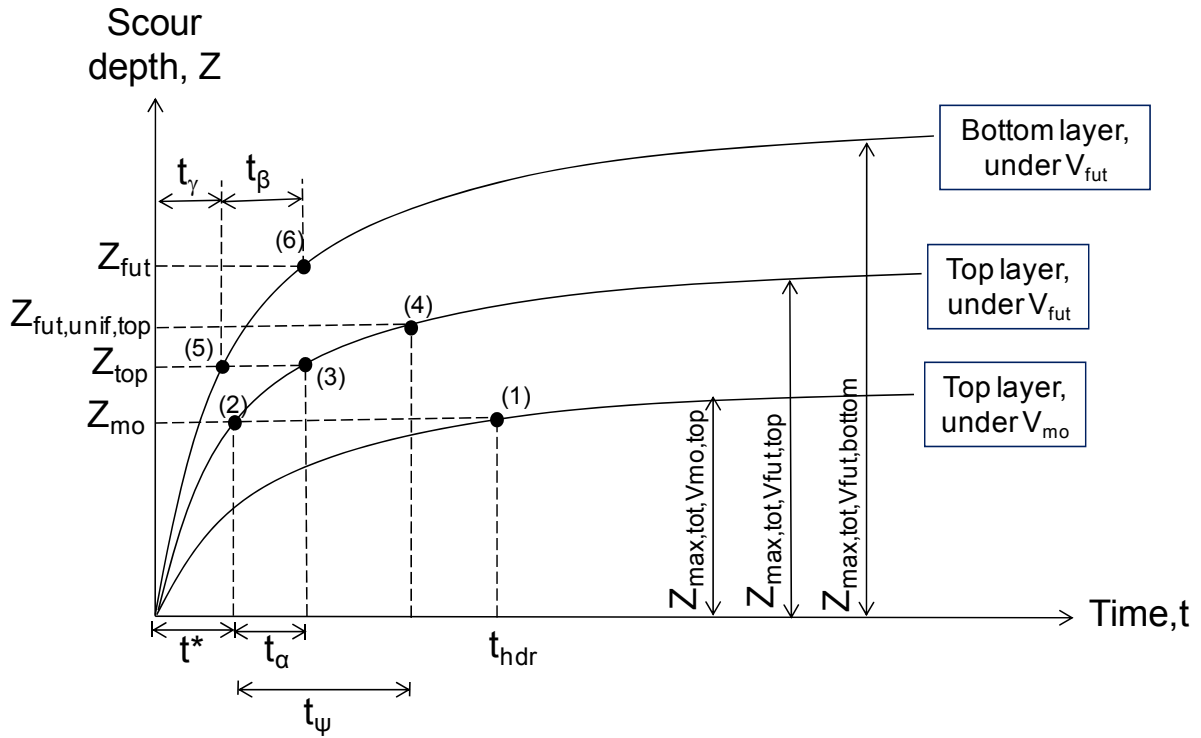


Figure 5-10. A General Illustration for BSA 1 (Multilayer Analysis).

Table 5-2. Definition of Terms in BSA 1 (Multilayer Analysis).

Term	Definition
Z_{mo}	The maximum observed scour depth at the bridge until the time of the most recent scour measurement.
Z_{fut}	The scour depth corresponding to the future flood velocity, V_{fut} .
$Z_{fut,unif,top}$	The scour depth at the end of the future flood assuming the site is made of the top layer material only. This parameter is obtained from the Z-Future Chart based on the material in the top layer and BSA 1 (Uniform Deposit).
Z_{top}	The depth of the lower boundary of the top layer.
$Z_{max,tot,V_{mo},top}$	The maximum total scour depth in a uniform deposit comprised only of the top layer material, under the maximum observed velocity, V_{mo} .
$Z_{max,tot,V_{fut},top}$	The maximum total scour depth in a uniform deposit made of the top layer material, under the future flood velocity, V_{fut} .
$Z_{max,tot,V_{fut},bottom}$	The maximum total scour depth in a uniform deposit made of the bottom layer material, under the future flood velocity, V_{fut} .
t_{hyd}	The age of the bridge at the time Z_{mo} was measured.
t^*	The time for Z_{mo} to be achieved under the future flood velocity, V_{fut} .
t_{ψ}	The duration of the future flood. In the case of this report, the duration of the future flood is chosen as 72 hr under constant velocity, V_{fut} .
t_{α}	The time it takes for the future flood to completely erode the top layer. In other words, it is the time for the scour depth to advance from Z_{mo} to Z_{top} under V_{fut} .
t_{β}	The time between the complete erosion of the top layer due to V_{fut} to the end of the future flood.
t_{γ}	The time required to develop Z_{top} in a uniform deposit made of the bottom layer material, under V_{fut} .

By rearranging the hyperbolic model presented in Equation (2.3), we obtain the time required to achieve a specified final scour depth, Z_{fin} , by the following equation:

$$t = \frac{Z_{fin} Z_{max}}{\dot{Z}_i (Z_{max} - Z_{fin})} \quad (5.2)$$

By using Equation (5.2), t^* , which is time for Z_{mo} to be achieved under V_{fut} , can be determined. Point 2 in Figure 5-10 represents the scour depth Z_{mo} at time t^* and is given by the following equation:

$$t^* = \frac{Z_{mo} Z_{max,tot,V_{fut},top}}{\dot{Z}_{i,V_{fut},top} (Z_{max,tot,V_{fut},top} - Z_{mo})} \quad (5.3)$$

where $Z_{\max,\text{tot},V_{\text{fut},\text{top}}}$ is the maximum total scour that can occur in the top layer under V_{fut} and $\dot{Z}_{i,V_{\text{fut},\text{top}}}$ is the erosion rate for the top layer corresponding to V_{fut} . The value of $\dot{Z}_{i,V_{\text{fut},\text{top}}}$ is obtained from the Erosion Function Charts. The value of $Z_{\max,\text{tot},V_{\text{fut},\text{top}}}$ is obtained by summing the values of maximum pier scour and contraction scour for the top layer material obtained from Equation (2.2) and Equation (2.4).

If Z_{top} is the depth of the lower boundary of the top layer and t_{α} is the time it takes for the scour depth to advance from Z_{mo} to Z_{top} :

$$t^* + t_{\alpha} = \frac{Z_{\text{top}} - Z_{\max,\text{tot},V_{\text{fut},\text{top}}}}{\dot{Z}_{i,V_{\text{fut},\text{top}}}} \quad (5.4)$$

Point 3 in Figure 5-10 represents the scour depth Z_{top} at time $(t^* + t_{\alpha})$. Subsequently, the explicit value of t_{α} can be obtained from Equation (5.3) and Equation (5.4).

Here, t_{ψ} is defined as the duration of the future flood. If it is initially assumed that the bridge site is underlain by a uniform deposit comprising only the top layer material, the scour depth corresponding to the future flood can be obtained from the Z-Future Chart. This scour depth is termed $Z_{\text{fut},\text{unif},\text{top}}$. Then, the value of $(t^* + t_{\psi})$ is given by:

$$t^* + t_{\psi} = \frac{Z_{\text{fut},\text{unif},\text{top}} - Z_{\max,\text{tot},V_{\text{fut},\text{top}}}}{\dot{Z}_{i,V_{\text{fut},\text{top}}}} \quad (5.5)$$

Point 4 in Figure 5-10 represents the scour depth $Z_{\text{fut},\text{unif},\text{top}}$ at time $(t^* + t_{\psi})$. Subsequently, the explicit value of t_{ψ} can be obtained from Equation (5.3) and Equation (5.5).

The duration for which the bottom layer is exposed to the future flood, t_{β} , is given by:

$$t_{\beta} = t_{\psi} - t_{\alpha} \quad (5.6)$$

Here, t_{γ} is defined as the time required to develop Z_{top} in a uniform deposit made of the bottom layer material, under V_{fut} . Then, t_{γ} is given by:

$$t_{\gamma} = \frac{Z_{\text{top}} - Z_{\max,\text{tot},V_{\text{fut},\text{bottom}}}}{\dot{Z}_{i,V_{\text{fut},\text{bottom}}}} \quad (5.7)$$

where $Z_{\max,\text{tot},V_{\text{fut}},\text{bottom}}$ is the maximum total scour that can occur in a uniform deposit comprising the bottom layer material, under V_{fut} . $\dot{Z}_{i,V_{\text{fut}},\text{bottom}}$ is the erosion rate for the bottom layer corresponding to V_{fut} . The value of $\dot{Z}_{i,V_{\text{fut}},\text{bottom}}$ is obtained from the Erosion Function Charts. The value of $Z_{\max,\text{tot},V_{\text{fut}},\text{bottom}}$ is obtained by summing the values of maximum pier scour and contraction scour for the bottom layer material obtained from Equation (2.2) and Equation (2.4). Point 5 in Figure 5-10 represents the scour depth Z_{top} at time t_γ .

The value of Z_{fut} in the multilayer deposit can now be computed using the hyperbolic model with a time input of $(t_\gamma + t_\beta)$. This is represented by point 6 in Figure 5-10. The calculation procedure for BSA 1 (Multilayer Analysis) is presented in a flowchart in Appendix B.

5.3.2.1. Sub-cases in BSA 1 (Multilayer Analysis)

In BSA 1 (Multilayer Analysis), there are three sub-cases within Case 1 and Case 2, which address the variations in the relative positions of the Z-t curves. The variations of the relative positions of the Z-t curves are a result of the variations in the maximum total scour depth that can occur in a particular material. For example, in a situation where the top layer is strong (st) and the bottom layer is weak (w) and V_{fut} is less than V_{mo} , the maximum total scour depth of the two layers have two possible outcomes:

- outcome 1: $Z_{\max,\text{tot},V_{\text{fut}},w} > Z_{\max,\text{tot},V_{\text{mo}},st}$ and
- outcome 2: $Z_{\max,\text{tot},V_{\text{fut}},w} < Z_{\max,\text{tot},V_{\text{mo}},st}$.

where $Z_{\max,\text{tot},V_{\text{fut}},w}$ is the maximum total scour depth in the weak material under V_{fut} and $Z_{\max,\text{tot},V_{\text{mo}},st}$ is the maximum total scour depth in the strong material under V_{mo} . These sub-cases are presented and defined in Table 5-3, and illustrated in Figure 5-11 through Figure 5-16. However, the general concept of BSA 1 (Multilayer Analysis) as presented in Figure 5-10 is applicable to all the sub-cases. The sub-cases are presented to aid the user in understanding the different scenarios that could be encountered while using BSA 1 (Multilayer Analysis).

Table 5-3. Sub-cases within Case 1 and Case 2.

Velocity Ratio	Case	Relative Material Erodibility	Condition
≥ 1 ($V_{fut} \geq V_{mo}$)	1(a)	Strong layer over weak layer	$Z_{max,tot,Vfut,w} > Z_{max,tot,Vmo,st}$
	1(b)	Weak layer over strong layer	$Z_{max,tot,Vfut,w} > Z_{max,tot,Vmo,st}$
	1(c)		$Z_{max,tot,Vfut,w} < Z_{max,tot,Vmo,st}$
< 1 ($V_{fut} < V_{mo}$)	2(a)	Weak layer over strong layer	$Z_{max,tot,Vmo,w} < Z_{max,tot,Vfut,st}$
	2(b)		$Z_{max,tot,Vmo,w} > Z_{max,tot,Vfut,st}$
	2(c)	Strong layer over weak layer	$Z_{max,tot,Vmo,w} > Z_{max,tot,Vfut,st}$

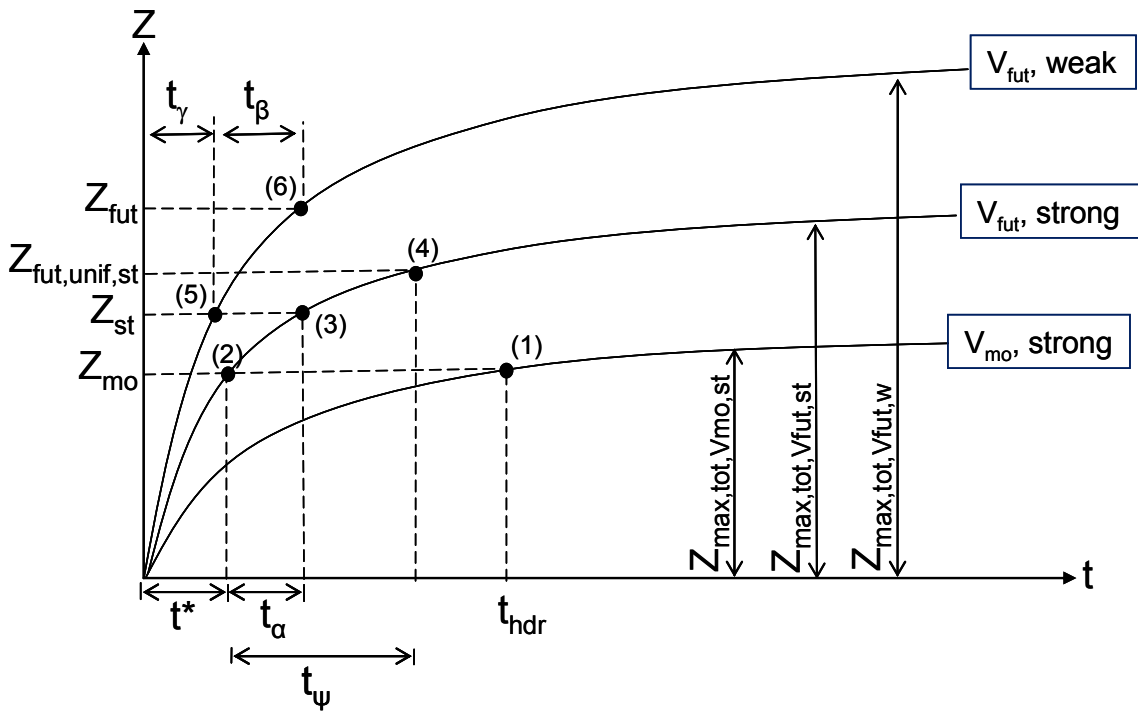


Figure 5-11. Case 1(a) for BSA 1 (Multilayer Analysis).

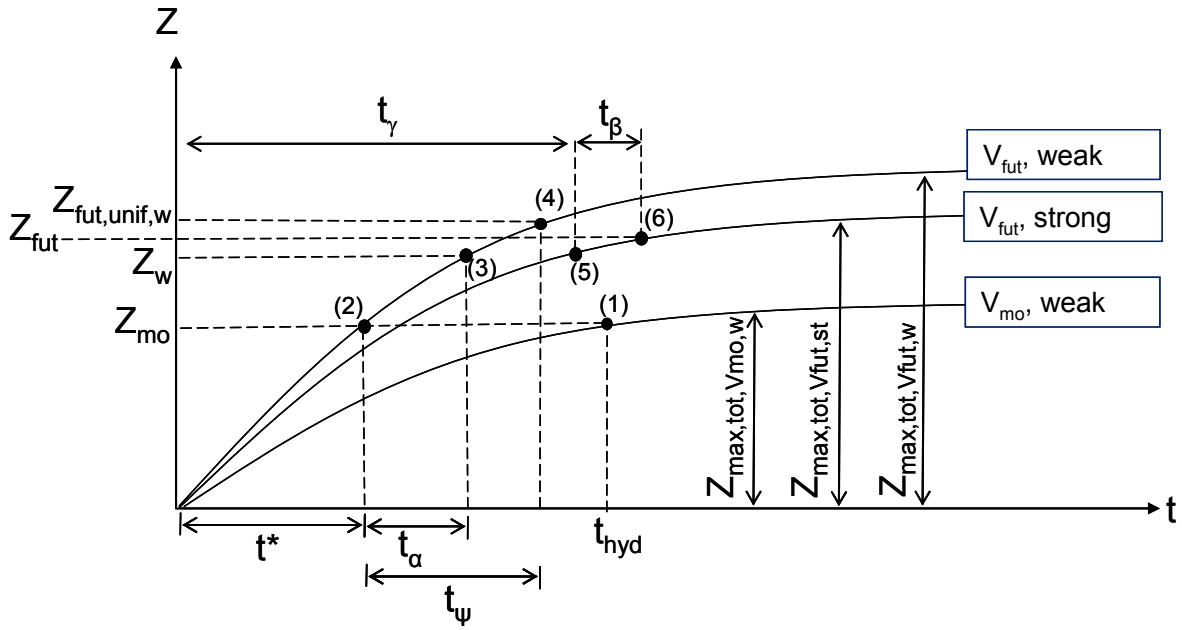


Figure 5-12. Case 1(b) for BSA 1 (Multilayer Analysis).

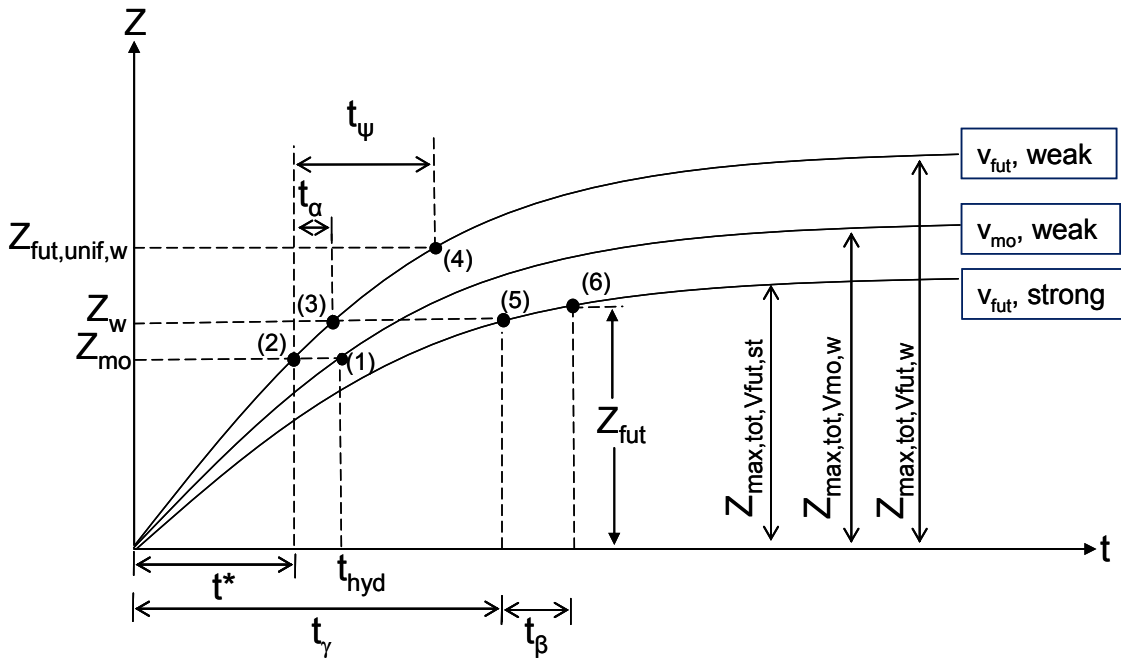


Figure 5-13. Case 1(c) for BSA 1 (Multilayer Analysis).

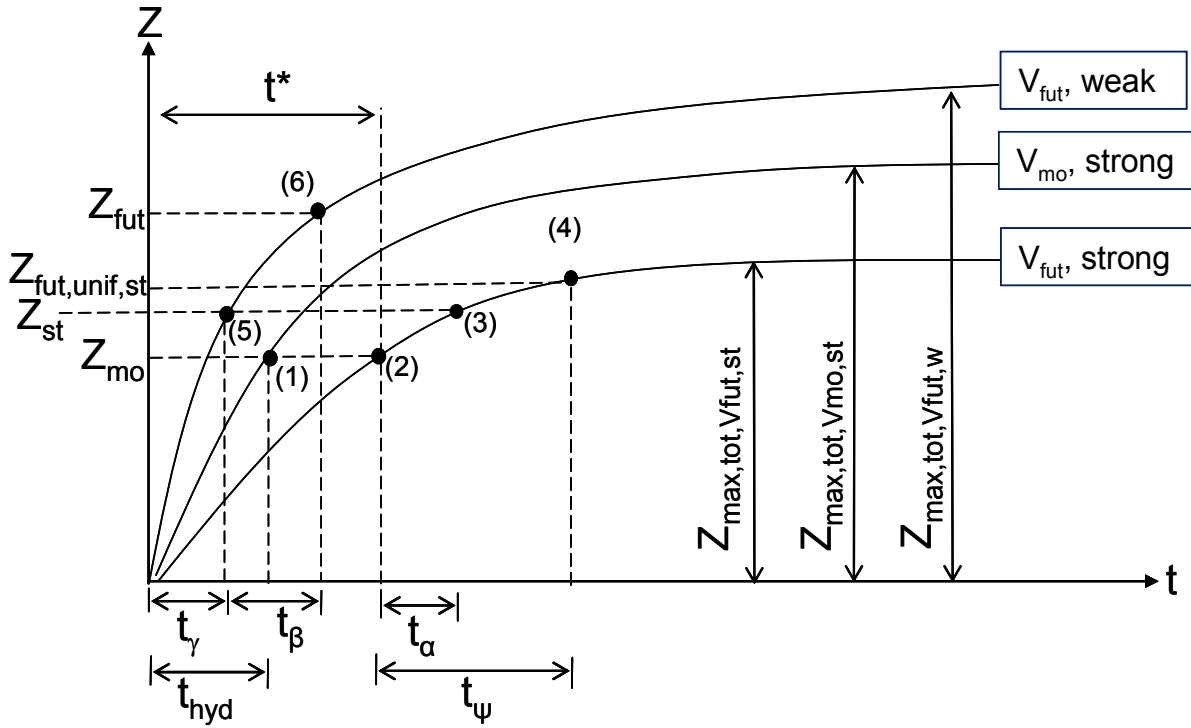


Figure 5-14. Case 2(a) for BSA 1 (Multilayer Analysis).

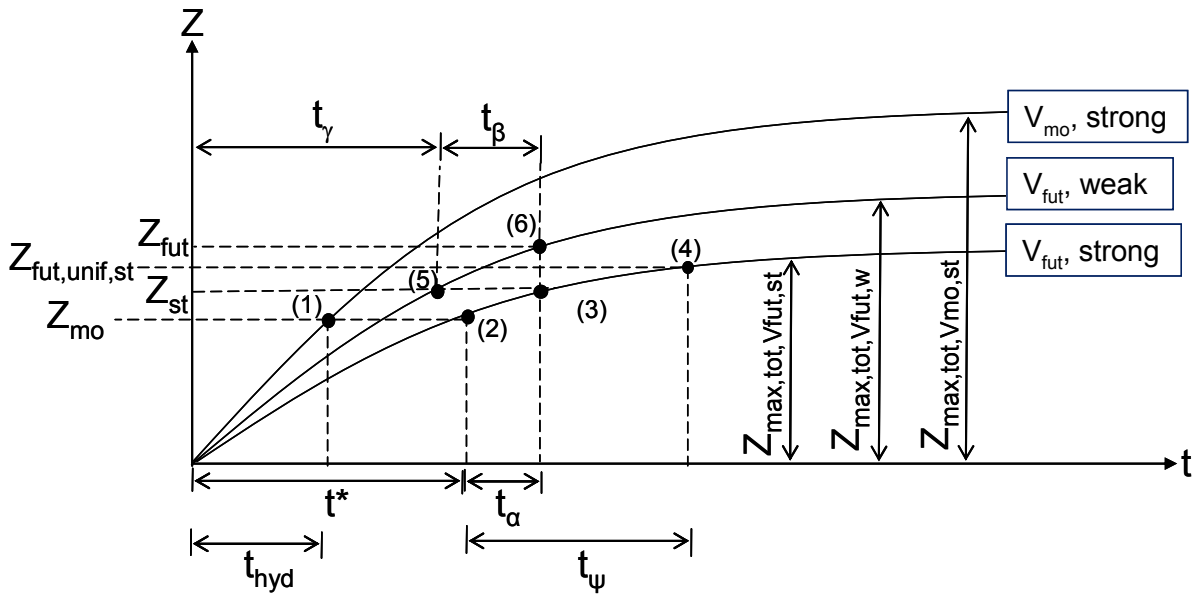


Figure 5-15. Case 2(b) for BSA 1 (Multilayer Analysis).

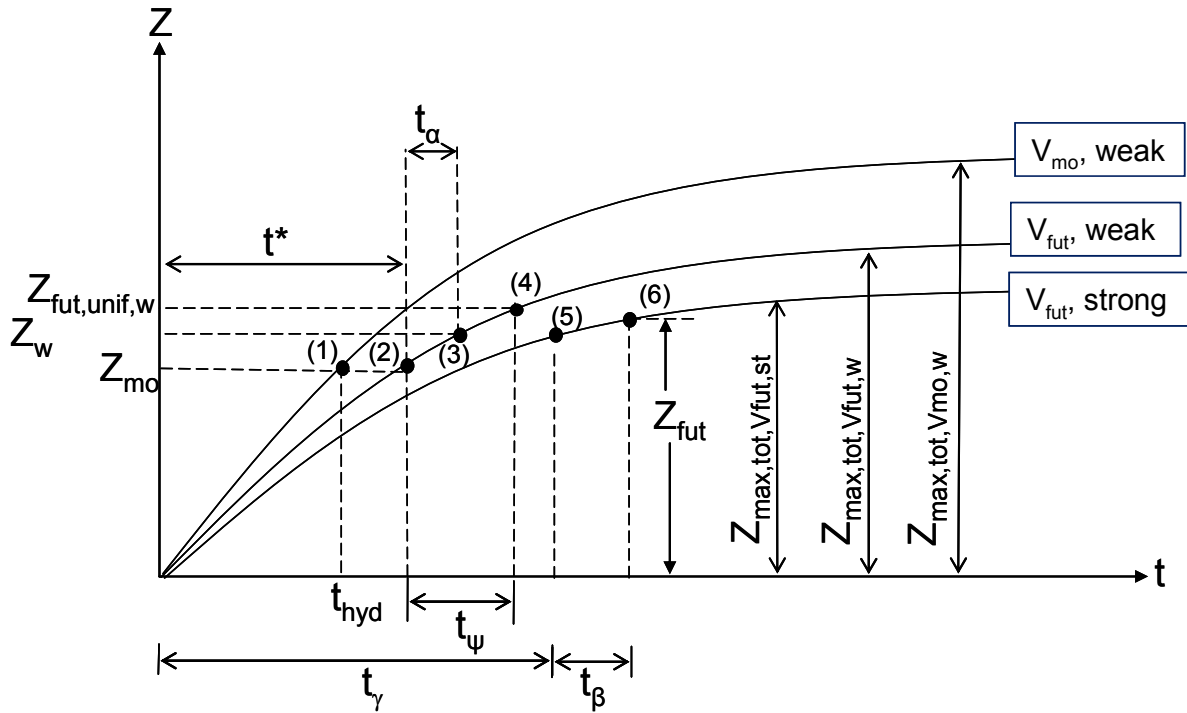


Figure 5-16. Case 2(c) for BSA 1 (Multilayer Analysis).

5.4. STEP-BY-STEP PROCEDURE FOR BSA 1

To assist the user in carrying out a BSA 1 analysis, tables detailing all the steps of the method according to flowchart box number are presented. [Table 5-4](#) is for BSA 1 (Uniform Deposit), and [Table 5-5](#) is for BSA 1 (Multilayer Analysis).

Table 5-4. Step-by-Step Procedure for BSA 1 (Uniform Deposit).

Box No.	Description
1-1	Introduction to BSA 1 (Uniform Deposit).
1-2	The decision box that determines if a bridge is founded in rock. If the bridge is founded in rock, proceed to Box 1-3 . If not, proceed to Box 1-5 .
1-3	<p>The decision box that determines if the erosion of the rock underlying the bridge (if applicable) is rock mass controlled or rock substance controlled:</p> <ul style="list-style-type: none"> • Rock mass controlled: The rock is eroded and transported as blocks that are recognizable and can be identified with the parent material (Cato 1991). • Rock substance controlled: The rock is eroded at the grain level and involves the rock substance properties such as density, strength, hardness, permeability, weathering, grain size, and grain shape (Cato 1991). <p>If the scour process is found to be rock mass controlled, proceed to Box 1-4 where the user is referred to other available methods for assessing rock scour (Table 5-1, Figure 3-4, Figure 3-5, Figure 3-18, and Figure 3-20). If the material is found to be rock substance controlled, it is then treated as a soil. Proceed to Box 1-5.</p>
1-4	The box that refers the user to other available rock scour assessment procedures to address rock mass-controlled erosion (Table 5-1 , Figure 3-4 , Figure 3-5 , Figure 3-18 , and Figure 3-20).
1-5	The data collection box that gathers the maximum observed scour at the bridge, Z_{mo} , and the allowable scour depth of the bridge foundation, Z_{thresh} . Z_{mo} is the largest scour depth ever recorded at the bridge and is usually obtained from bridge inspection records. Z_{thresh} is obtained from foundation bearing capacity or lateral stability analysis. Z_{thresh} is sometimes taken as half the pile embedment length.
1-6	The decision box to determine if infilling of the scour hole is expected to have occurred at the bridge site. Infilling occurs under live-bed scour conditions. If infilling is expected to have occurred, proceed to Box 1-7 .
1-7	The decision box to determine if the amount of infilling can be quantified by several methods including by local experience or engineering judgment. If the amount of infilling can be quantified, proceed to Box 1-10 . If the amount of infilling cannot be quantified, proceed to Box 1-8 .
1-8	The decision box to determine if special action is to be adopted to address the infilling issue. If yes, proceed to Box 1-9 . Otherwise proceed to Box 1-20 .
1-9	<p>Conclusion box that recommends special action options to address infilling. These options are (Delphia 2008):</p> <ul style="list-style-type: none"> • measurement of scour during and after the flood event and • utilization of scour-monitoring methods.
1-10	The data collection box that gathers the amount of infilling, Z_{infill} .
1-11	The calculation box that updates Z_{mo} to account for infilling. This is done by simply adding Z_{infill} to the previous Z_{mo} value that did not account for infilling. Once this process is completed, proceed to Box 1-12 .
1-12	The decision box that determines if Z_{mo} exceeds Z_{thresh} . Sometimes, Z_{thresh} is taken as half the pile embedment length. If yes, proceed to Box 1-13 , which recommends immediate action. Otherwise, proceed to Box 1-14 .

Table 5-4. Step-by-Step Procedure for BSA 1 (Uniform Deposit) (Continued).

Box No.	Description
1-13	Conclusion box that recommends immediate action be taken to protect the bridge against scour-related damage.
1-14	The data collection box that gathers the velocity ratio, V_{fut}/V_{mo} .
1-15	The data collection box that gathers the type of material underlying the bridge site. In the case of a multilayer deposit, this box requires the material of the top deposit.
1-16	The box indicating the determination of Z_{fut} from the Z-Future Charts. The value of the velocity ratio, V_{fut}/V_{mo} or V_{100}/V_{mo} , is plugged into the appropriate chart to obtain the scour depth ratio, Z_{fut}/Z_{mo} . Use Equation (5.1) to obtain Z_{fut} . The Z-Future Charts were developed based on a range of pier scour and contraction scour parameters. These parameters are clearly indicated on the chart. The chart should not be used for cases that <i>do not</i> comply with the range of these parameters. If such a case arises, proceed to BSA 2.
1-17	The decision box that determines if the value of Z_{fut} determined in Box 1-16 extends beyond the top layer of the multilayer deposit, if present. If yes, proceed to BSA 1 (Multilayer Analysis). Otherwise proceed to Box 1-19.
1-18	Leads to BSA 1 (Multilayer Analysis).
1-19	Decision box to determine if the bridge can be designated as “minimal risk.” If Z_{fut} equals or exceeds Z_{thresh} , proceed to BSA 2 to calculate the maximum scour depth. Otherwise, the bridge is deemed “minimal risk” and should undergo regular monitoring.
1-20	Leads to BSA 2.
1-21	Conclusion box that designates the bridge as having minimal risk to scour. The bridge should be subjected to regular monitoring.

Table 5-5. Step-by-Step Procedure for BSA 1 (Multilayer Analysis).

Box No.	Description
1-22	Introduction to BSA 1 (Multilayer Analysis).
1-23	<p>The data collection box that gathers the following parameters:</p> <ul style="list-style-type: none"> • The velocity corresponding to the future flood, V_{fut}. This can be obtained from the hydrologic package that is described in Chapter 4. In this case, V_{fut} is V_{100}. To obtain V_{fut}, obtain the 100-year flood Q_{100} from the USGS Regional Regression Equations. Convert the flow into velocity using TAMU-FLOOD. Steps in this conversion are detailed in the TAMU-FLOW user’s manual (Appendix E). • The maximum flood observed at the bridge, V_{mo}. This is obtained by estimating the recurrence interval of the maximum observed flood, Q_{mo}, using TAMU-FLOOD. The steps to do this are detailed in the TAMU-FLOOD user’s manual (Appendix F). Convert the flow into velocity using TAMU-FLOOD. Steps in this conversion are detailed in the TAMU-FLOW user’s manual (Appendix E). • The maximum observed scour depth, Z_{mo} (including infilling if applicable). • The thickness of the top layer, Z_{top}. • The allowable scour depth, Z_{thresh}, which is obtained from foundation-bearing capacity or lateral stability analysis.
1-24	<p>The data collection box that gathers the following information:</p> <ul style="list-style-type: none"> • The erosion functions of the top and bottom layers. This is done by choosing the upper boundary of the material category in the Erosion Function Charts. • The critical velocity, V_c, of the top and bottom layers. The critical velocity is the velocity that corresponds to an erosion rate of 0.1 mm/hr. • The initial erosion rate of the top and bottom layers corresponding to V_{mo} ($\dot{Z}_{i,V_{mo},top}$ and $\dot{Z}_{i,V_{mo},bottom}$, respectively). • The initial erosion rate of the top and bottom layers corresponding to V_{fut} ($\dot{Z}_{i,V_{fut},top}$ and $\dot{Z}_{i,V_{fut},bottom}$, respectively). • The age of the bridge, t_{hyd}, in terms of equivalent time using V_{mo}. The equivalent time for pier scour, $t_{e,p}$, is obtained from Equation (2.7), and the equivalent time for contraction scour, $t_{e,c}$, is obtained from Equation (2.8). The velocity to be input into the equivalent time equations is V_{mo}, and the rate of scour to be used is obtained from the Erosion Function Chart at velocity V_{mo}.

Table 5-5. Step-by-Step Procedure for BSA 1 (Multilayer Analysis) (Continued).

Box No.	Description
1-25	<p>The data collection box of parameters required to determine the pier and contraction scour parameters. These parameters are as follows:</p> <ul style="list-style-type: none"> • Approach velocity (V_{appr}). • Pier diameter (D). • Kinematic viscosity of water (ν), which is 10^{-6} m²/s at 20° Celsius. • Soil critical velocity (V_c). The critical velocity is the velocity corresponding to an erosion rate of 0.1 mm/hr on the Erosion Function Chart (Figure 3-4 and Figure 3-5). The erosion function is the left boundary curve of the erosion category that best fits the material underlying the bridge site. • Upstream water depth (H_1). • Uncontracted channel width (B_1) and contracted channel width (B_2).
1-26	<p>The calculation box that refers to the BSA 1 (Multilayer Analysis) calculation flowchart presented in Appendix B. The multilayer Z_{fut} is calculated here.</p>
1-27	<p>Decision box to determine if the bridge can be designated as “minimal risk.” If Z_{fut} equals or exceeds Z_{thresh}, proceed to BSA 2 to calculate the maximum scour depth. Otherwise, the bridge is deemed “minimal risk” and should undergo regular monitoring.</p>
1-28	<p>Leads to BSA 2.</p>
1-29	<p>Conclusion box that designates the bridge as having minimal risk to scour. The bridge should be subject to regular monitoring.</p>

5.5. BSA 1 (UNIFORM DEPOSIT) EXAMPLE

Problem: Determine the future scour depth corresponding to the 100-year flood for the following information that characterizes the bridge scour problem:

- Geomaterial type is uniform medium erodibility material (Category III).
- Contraction ratio $R_c = B_2/B_1 = 0.85$, upstream water depth $H_1 = 32.8$ ft (10 m), and pier diameter $D = 3.28$ ft (1.0 m).
- The age of the bridge $t_{hyd} = 25$ years.
- The bridge is not founded in rock.

- The scour conditions are mostly clear-water scour, and a 0.98 ft (0.3 m) infilling is estimated to occur after big floods.
- The maximum observed scour depth $Z_{mo} = 6.56$ ft (2 m).
- The allowable scour depth $Z_{thresh} = 26.3$ ft (8 m).
- The bridge was built in 1981 and assessed in 2006.
- The longitude and latitude of the bridge are -96.0 and 30.0 , respectively.

The following is the solution according to BSA 1 (Uniform Deposit) flowchart box numbers:

- [Box 1-1](#): Start of BSA 1 (Uniform Deposit). Proceed to [Box 1-2](#).
- [Box 1-2](#): The bridge is not founded in rock. Proceed to [Box 1-5](#).
- [Box 1-5](#): $Z_{mo} = 2$ m; $Z_{thresh} = 8$ m. Proceed to [Box 1-6](#).
- [Box 1-6](#): Infilling is estimated at 0.3 m. Proceed to [Box 1-11](#).
- [Box 1-11](#): $Z_{mo} = 2 + 0.3 = 2.3$ m. Proceed to [Box 1-12](#).
- [Box 1-12](#): $Z_{mo} < Z_{thresh}$. Proceed to [Box 1-14](#).
- [Box 1-14](#): To get the velocity ratio $V_{fut}/V_{mo} = V_{100}/V_{mo}$, launch the computer program TAMU-FLOOD and input the following parameters ([Figure 5-17](#)):
 - Input the longitude and latitude of the bridge (-96.0 and 30.0 , respectively).
 - Input the year the bridge was built (1981) and the year of the BSA 1 assessment (2006).
 - Choose the Log-Pearson Type III–MOM flood frequency analysis method.

Run TAMU-FLOOD. The lower portion of [Figure 5-17](#) shows the TAMU-FLOOD output, where the maximum recurrence interval of flow at the bridge is 17 years and V_{mo}/V_{100} is between 0.6 and 0.8. Taking V_{mo}/V_{100} as 0.7, $V_{100}/V_{mo} = 1.4$. The recurrence interval map from 1981 to 2006 is shown in [Figure 5-18](#).

- [Box 1-15](#): Medium erodibility material (Category III). Proceed to [Box 1-16](#).
- [Box 1-16](#): From [Figure 5-4](#), $Z_{fut}/Z_{mo} = 1.5$ for a 25-year-old bridge. In this case, $Z_{fut} = Z_{100}$.

$$\begin{aligned} Z_{fut} = Z_{100} &= 1.5 \times Z_{mo} \\ &= 1.5(7.54 \text{ ft}) = 1.5(2.3 \text{ m}) \\ &= 11.3 \text{ ft (3.5 m)} \end{aligned}$$

Proceed to [Box 1-17](#).

- [Box 1-17](#): The bridge is founded on a uniform soil deposit.
- [Box 1-18](#): $Z_{fut} = Z_{100} = 3.5 \text{ m} = 11.5 \text{ ft}$; $Z_{thresh} = 8 \text{ m} = 26.2 \text{ ft}$. Z_{fut} is less than Z_{thresh} . Proceed to [Box 1-21](#).
- [Box 1-21](#): The bridge is deemed “minimal risk” and should undergo regular monitoring. Although the bridge only experienced a 17-year flood event, the results of the analysis predict that it is stable for the predicted 100-year event superimposed on top of the previous flood events.

TAMU-Flood 1.00

Help

Input Panel

Select the unit of coordinate

Decimals (i.e. -97.3456)

Longitude (Decimals) Latitude (Decimals)

Longitude (DMS) W Latitude (DMS) N

Year Bridge Built Year Last Inspected

Flood Frequency Analysis Methods

Choose a method

Output Format

I want flow map for each year - using only unregulated gages

I want flow map for each year - using all available gages

I want rainfall map for each year

Output

Maximum RI of the bridge(Year) **17**

0.6 < Vmo/V100 < 0.8

Figure 5-17. TAMU-FLOOD Input and Output for BSA 1 Example.

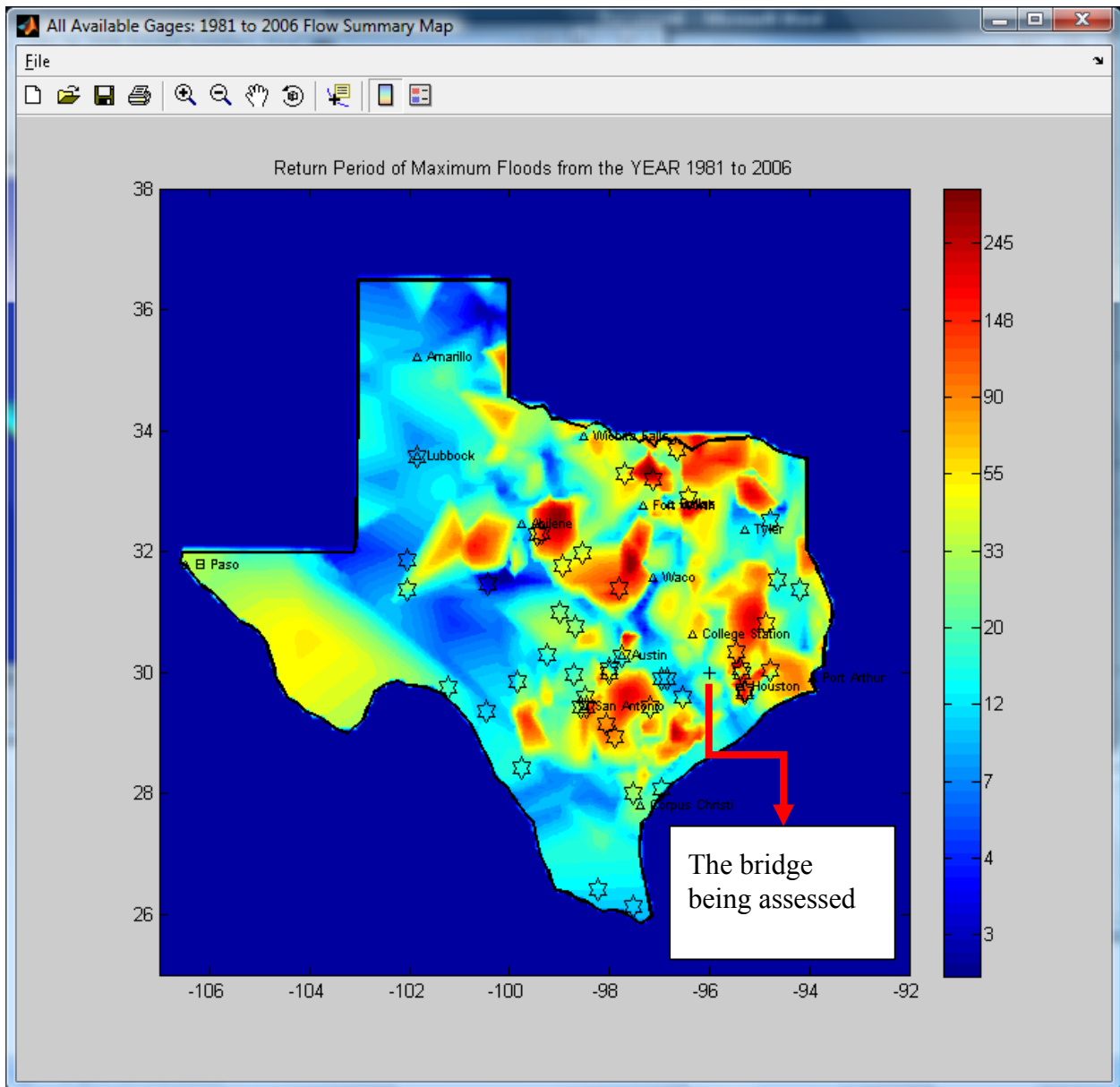


Figure 5-18. Recurrence Interval Map Generated from TAMU-FLOOD for the BSA 1 Example.

6. BRIDGE SCOUR ASSESSMENT 2

6.1. INTRODUCTION

Bridge Scour Assessment 2 is the assessment procedure that has to be carried out if a bridge is not found to have “minimal risk (regular monitoring),” “immediate action required,” or “special action” at the end of BSA 1. BSA 2 is a process that determines the scour vulnerability by applying the maximum scour depth concept. The maximum bridge scour depth concept is based on the assumption that the bridge will experience the maximum possible scour depth (equilibrium scour depth) under V_{fut} within its lifetime. This might not be the case for more erosion-resistant materials such as clays and some rocks. In BSA 2, the maximum scour at the bridge, termed maximum total local scour ($Z_{\text{max,l}}$), is the arithmetic sum of the three components of scour, i.e., maximum pier scour ($Z_{\text{max,p}}$), maximum contraction scour ($Z_{\text{max,c}}$), and maximum abutment scour ($Z_{\text{max,a}}$). The vulnerability associated with scour depends on the comparison between the maximum total local scour depth and the allowable scour depth of the bridge. However, it should be noted that the TxDOT Hydraulics and Geotechnical Manuals do not recommend the use of the current abutment scour equations because they do not yield reasonable results. Instead, TxDOT recommends protecting the abutments to reduce the potential for scour.

6.2. THE BSA 2 FLOWCHART AND PROCEDURE

The BSA 2 flowchart is presented in [Figure 6-1](#). The boxes in the flowchart are of four forms: rectangular, diamond, circle, and rounded. Rectangular boxes are data collection and calculation boxes, meaning that the data listed in the box need to be collected by the user for the bridge being analyzed and, where appropriate, involve the use of equations. Diamond boxes are “yes-no” decision boxes. The circle represents “on page” information. Rounded boxes are conclusion boxes. All boxes are numbered for easy reference; the first digit represents the level of assessment, and the second digit represents the box number.

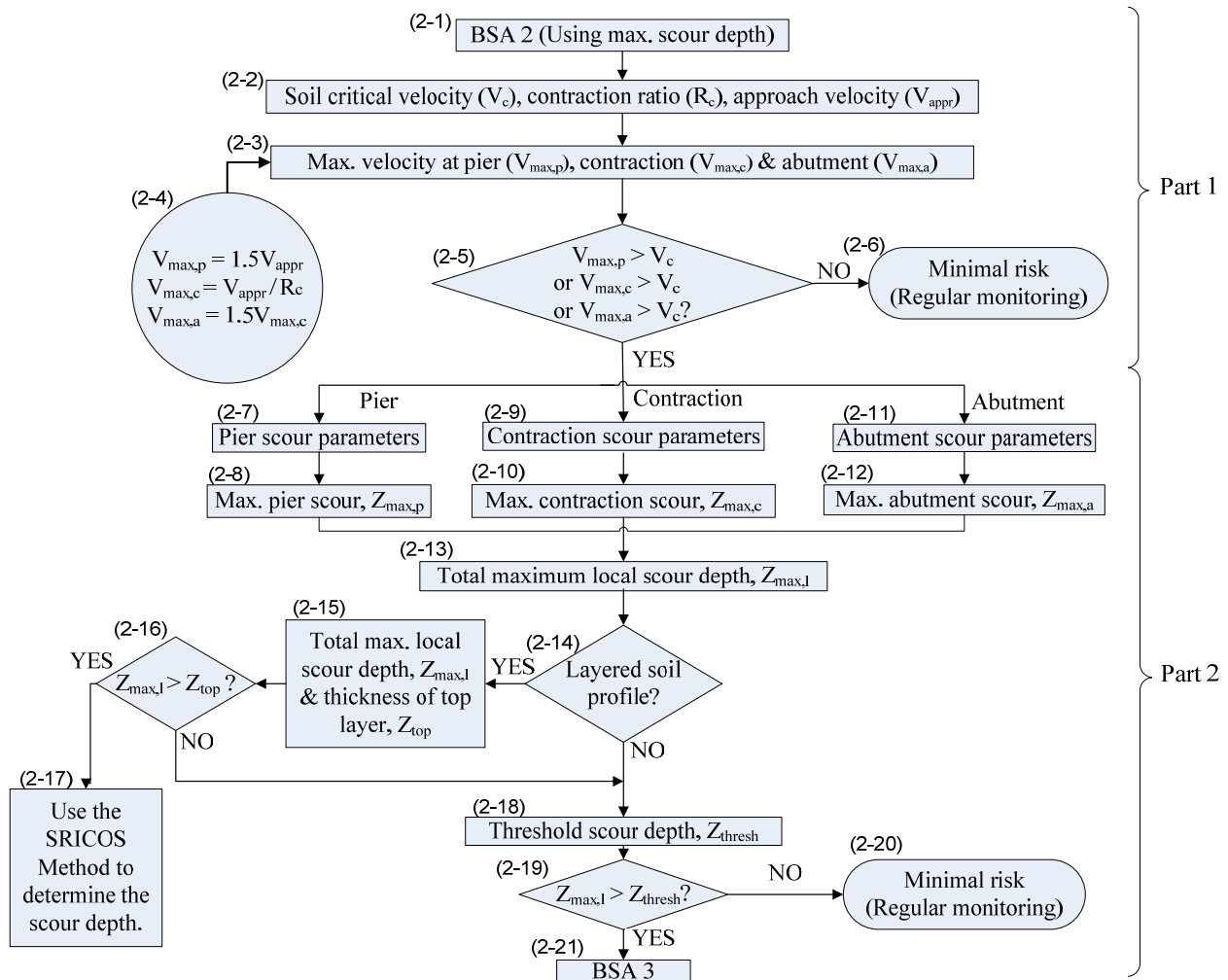


Figure 6-1. The BSA 2 Flowchart.

The BSA 2 flowchart consists of two parts. Part 1 is essentially a simple filtering process that utilizes the critical velocity of the soil present at the bridge (V_c) and local velocities at the pier, contraction, or abutment ($V_{max,p}$, $V_{max,c}$, and $V_{max,a}$, respectively). The critical velocity is obtained by an Erosion Function Chart developed on the basis of a database of EFA tests (Briaud et al. 2001a) and on the experience of the authors (Figure 3-4 and Figure 3-5). The Erosion Function Chart shows erosion categories for various soils, and the bridge inspector can determine the relevant critical velocity. This chart essentially eliminates the need for site-specific erosion testing (Govindasamy et al. 2008). The following equations for local velocities are derived from the authors' experience and numerical simulation results:

$$V_{\max,p} = 1.5 V_{\text{appr}} \quad (6.1)$$

$$V_{\max,c} = V_{\text{appr}} / R_c \quad (6.2)$$

$$V_{\max,a} = 1.5 V_{\max,c} \quad (6.3)$$

where V_{appr} is the approach velocity upstream of the bridge and R_c is the ratio of the contracted width of the channel B_1 to the uncontracted width of the channel B_2 (Figure 2-1).

If any one of the local velocities exceed the soil critical velocity, then part 2 of BSA 2 is required to be carried out. Otherwise, the velocities at the obstruction are less than the velocity required to initiate significant erosion, and the bridge is categorized as “minimal risk (regular monitoring)” (Govindasamy et al. 2008).

In Part 2 of BSA 2, simple calculations for maximum scour depth are carried out. The calculations for maximum pier scour and contraction scour are described in Chapter 2 and detailed in Briaud et al. (1999, 2005). Calculations for maximum abutment scour are also described in Chapter 2 and are based on HEC-18 (Richardson and Davis 2001). The maximum total local scour depth, $Z_{\max,l}$, is a summation of all three scour components:

$$Z_{\max,l} = Z_{\max,p} + Z_{\max,c} + Z_{\max,a} \quad (6.4)$$

where $Z_{\max,p}$, $Z_{\max,c}$, and $Z_{\max,a}$ are the maximum pier scour, contraction scour, and abutment scour, respectively.

The BSA 2 flowchart also addresses the presence of a layered geologic profile at the bridge site. In the case where the maximum total local scour depth, $Z_{\max,l}$, exceeds the thickness of the top layer within the profile, Z_{top} , the maximum scour depth concept is not applicable, requiring analysis using the Extended SRICOS-EFA Method (Briaud et al. 1999, 2003 and 2005). However, if $Z_{\max,l}$ does not exceed Z_{top} , the maximum scour depth concept is applicable. Subsequently, if the value of $Z_{\max,l}$ does not exceed $Z_{\text{threshold}}$, the bridge is deemed “minimal risk (regular monitoring).” Otherwise, BSA 3 needs to be undertaken.

6.3. STEP-BY-STEP PROCEDURE FOR BSA 2

To assist the user in carrying out a BSA 2 analysis, a table detailing all the steps of the method according to the flowchart box numbers is presented in [Table 6-1](#).

Table 6-1. Step-by-Step Procedure for BSA 2.

Box No.	Description
2-1	Introduction to BSA 2. Links BSA 1 to BSA 2.
2-2	<p>The data collection box for the following parameters:</p> <ul style="list-style-type: none"> • Critical velocity (V_c), which is the velocity at which scour is initiated. It is obtained from Erodibility Charts based on the type of material underlying the bridge site. The critical velocity is the velocity corresponding to a scour rate of 0.1 mm/hr. The erosion function is the left boundary curve of the erosion category that fits the material underlying the bridge site. • Contraction ratio (R_c), which is the ratio of the width of the river in the contracted zone, B_2, to the upstream width, B_1 (Figure 2-12). • Approach velocity (V_{appr}), which is the velocity of the water directly upstream of the bridge. The approach velocity is the velocity that corresponds to flow being considered. For example, if the flow being considered is Q_{100}, then the corresponding velocity is V_{100}.
2-3	The data collection box for maximum local velocities at the pier ($V_{max,p}$), contraction ($V_{max,c}$), and abutment ($V_{max,a}$). The relationship between these parameters and the approach velocity, V_{appr} , is given by Equation (6.1) through Equation (6.3) and is also indicated in Box 2-4 for easy reference.
2-4	The “on page” information giving the relationship between local velocities and the approach velocity, as described by Equation (6.1) through Equation (6.3) .
2-5	The decision box that determines if scour would take place at the bridge based on local velocities and critical velocity. If any one of the maximum local velocities as obtained in Box 2-3 exceeds the critical velocity obtained in Box 2-2 , Part 2 of BSA 2 needs to be undertaken. Otherwise, the bridge can be designated as “minimal risk” (Box 2-6).
2-6	Conclusion box indicating that the bridge is deemed as having low scour risk and should undergo regular bridge scour monitoring.

Table 6-1. Step-by-Step Procedure for BSA 2 (Continued).

Box No.	Description
2-7	<p>The data collection box for the parameters required to determine the maximum pier scour. These parameters are as follows:</p> <ul style="list-style-type: none"> • approach velocity (V_{appr}); • pier diameter (D); and • kinematic viscosity of water (ν), which is $10^{-6} \text{ m}^2/\text{s}$ at 20° Celsius.
2-8	<p>The calculation box for the maximum pier scour depth. The maximum pier scour depth is obtained using Equation (2.2).</p>
2-9	<p>The data collection box for the parameters required to determine the maximum contraction scour. These parameters are as follows:</p> <ul style="list-style-type: none"> • Approach velocity (V_{appr}). • Soil critical velocity (V_c). The critical velocity is the velocity corresponding to an erosion rate of 0.1 mm/hr on the Erosion Function Charts (Figure 3-4 and Figure 3-5). The erosion function is the left boundary curve of the erosion category that best fits the material underlying the bridge site. • Upstream water depth (H_1). • Uncontracted channel width (B_1). • Contracted channel width (B_2).
2-10	<p>The calculation box for the maximum contraction scour depth. The maximum contraction scour depth is obtained using Equation (2.4).</p>
2-11	<p>The data collection box for the parameters required to determine the maximum abutment scour. The HIRE equation should be used if the ratio of projected abutment length (L) to the flow depth at the abutment (y_1) is greater than 25. Otherwise the Froehlich equation should be used. The parameters for maximum abutment scour calculation are as follows:</p> <p><i>Froehlich Equation</i></p> <ul style="list-style-type: none"> • Approach velocity (V_{appr}). • Length of active flow obstructed by the embankment (L'). • Average flow depth in the floodplain (y_a). • Abutment shape coefficient (K_1) obtained from Figure 2-16 and Table 2-4. • Coefficient for angle of embankment flow (K_2) as described in Section 2.3.1 and Figure 2-15. <p><i>HIRE Equation</i></p> <ul style="list-style-type: none"> • Approach velocity (V_{appr}). • Abutment shape coefficient (K_1) obtained from Figure 2-16 and Table 2-4. • Coefficient for angle of embankment flow (K_2) as described in Section 2.3.1 and Figure 2-15. • Water depth of flow at the abutment on the overbank or the main channel (y_1).

Table 6-1. Step-by-Step Procedure for BSA 2 (Continued).

Box No.	Description
2-12	The calculation box for the maximum abutment scour depth. The maximum abutment scour depth is obtained using Equation (2.9) or Equation (2.10).
2-13	The calculation box for the maximum local scour depth, $Z_{max,l}$, using Equation 6.4. The maximum total local scour depth is the sum of the maximum pier contraction and abutment scour.
2-14	The decision box to determine if the bridge site is underlain by a layered deposit. If yes, the maximum local scour depth ($Z_{max,l}$) is compared with the thickness of the topmost layer, Z_{top} , in Box 2-16.
2-15	The data collection for the maximum local scour depth, $Z_{max,l}$, and input of the thickness of the topmost soil layer underlying the bridge site, Z_{top} .
2-16	The decision box to determine if the maximum local scour depth ($Z_{max,l}$) is greater than the thickness of the topmost layer, Z_{top} . If yes, the maximum scour depth method is not applicable and the SRICOS Method needs to be used. If not, the maximum scour depth is applicable and BSA 2 is continued in Box 2-18.
2-17	Leads to the SRICOS Method (Briaud et al. 2003).
2-18	The input box for allowable scour depth, Z_{thresh} . This is based on the foundation element being considered.
2-19	The decision box that determines if the bridge is deemed to have a low scour risk or requires BSA 3 analysis. This is done by comparing the values of maximum local scour depth, $Z_{max,l}$, against the allowable scour depth, Z_{thresh} . If $Z_{max,l}$ is greater than Z_{thresh} , the analysis should proceed to BSA 3 (Time Analysis). Otherwise, the bridge is deemed “minimal risk” and should undergo regular monitoring.
2-20	Conclusion box that indicates that the bridge is deemed to have a low scour risk and should undergo regular bridge scour monitoring.
2-21	Leads to BSA 3.

6.4. EXAMPLE OF BSA 2 ANALYSIS

Problem: Determine the maximum scour depth corresponding to the following information that characterizes the bridge scour problem:

- Geomaterial type is uniform medium erodibility material (Category III).
- Contraction ratio $R_c = B_2/B_1 = 0.85$.
- Upstream water depth $H_1 = 32.8$ ft (10 m).

- Pier diameter $D = 3.28$ ft (1.0 m).
- Approach velocity $V_{\text{appr}} = V_{100} = 6.56$ ft (2.0 m/s).
- Water depth directly upstream of abutment $y_0 = 9.84$ ft (3.0 m).
- Length of active flow obstructed by the abutment $L = 13.12$ ft (4.0 m) (Figure 6-2).
- Angle of embankment flow $\theta = 30^\circ$ (Figure 6-2).
- Abutment type is vertical-wall abutment.
- Kinematic viscosity of water at 68°F (20°C), $\nu = 1.05 \times 10^{-5}$ ft^2/s (10^{-6} m^2/s).
- Allowable scour depth $Z_{\text{thresh}} = 32.8$ ft (10 m).

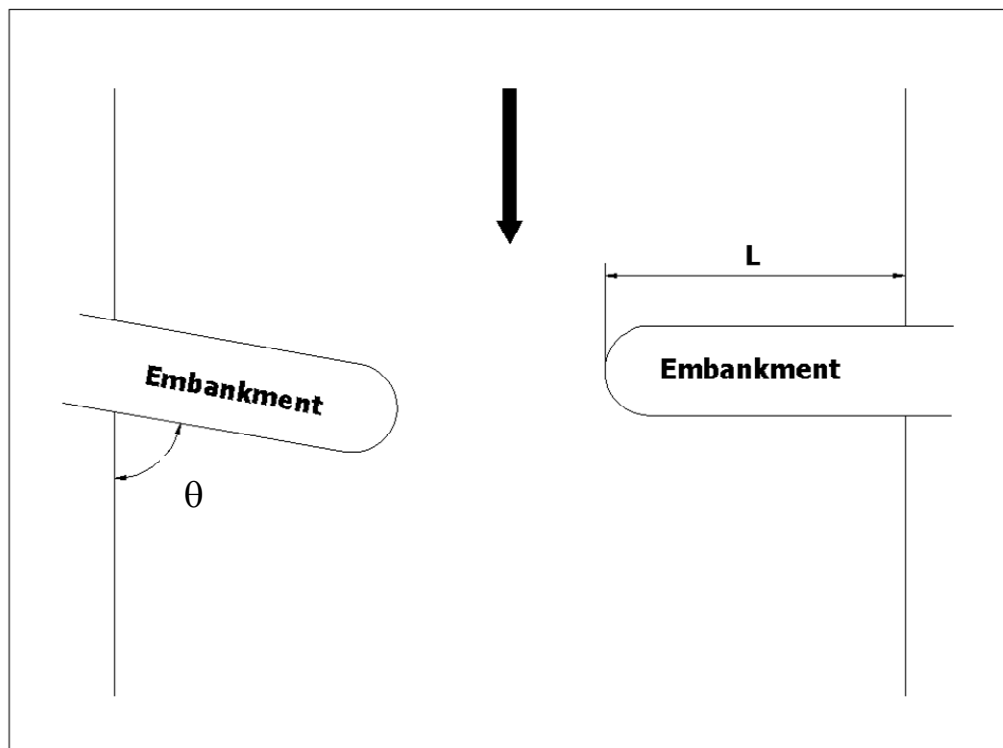


Figure 6-2. Definition of Length of Active Flow Obstructed by the Abutment and Angle of Embankment Flow.

The following is the solution according to BSA 2 flowchart box numbers:

- **Box 2-1:** Start of BSA 2.
- **Box 2-2:** From **Table 3-2**, $V_c = 1.64$ ft/s (0.5 m/s), $R_c = 0.85$, and $V_{\text{appr}} = V_{100} = 6.56$ ft/s (2.0 m/s). Proceed to **Box 2-3**.

- **Box 2-3:** From **Box 2-4**:

$$V_{\text{max,p}} = 1.5V_{\text{appr}} = 1.5(6.56 \text{ ft/s}) = 9.84 \text{ ft/s (3.0 m/s)}$$

$$V_{\text{max,c}} = 1.5V_{\text{appr}} = \frac{V_{\text{appr}}}{R_c} = \frac{6.56}{0.85} = 7.72 \text{ ft/s (2.4 m/s)}$$

$$V_{\text{max,a}} = 1.5(V_{\text{max,c}}) = 1.5(7.72 \text{ ft/s}) = 11.6 \text{ ft/s (3.6 m/s)}$$

Proceed to **Box 2-5**.

- **Box 2-5:**

$V_{\text{max,p}}$ is greater than V_c .

$V_{\text{max,c}}$ is greater than V_c .

$V_{\text{max,a}}$ is greater than V_c .

Proceed to **Box 2-7**.

- **Box 2-7:** Pier scour parameters.

$$D = 3.28 \text{ ft (1.0 m)}, V_{\text{appr}} = V_{100} = 6.56 \text{ ft/s (2.0 m/s)}, \nu = 1.1 \times 10^{-5} \text{ ft}^2/\text{s (10}^{-6} \text{ m}^2/\text{s)}.$$

Proceed to **Box 2-8**.

- **Box 2-8:**

$$Z_{\text{max,p}} \text{ (mm)} = 0.18 \left(\frac{V_{\text{appr}} D}{\nu} \right)^{0.635} = 1804.8$$

$$Z_{\text{max,p}} = 5.91 \text{ ft (1.8 m)}.$$

Proceed to [Box 2-9](#).

- [Box 2-9](#): Contraction scour parameters.

$$R_c = 0.85, H_1 = 32.8 \text{ ft (10.0 m)}, V_{\text{appr}} = V_{100} = 6.56 \text{ ft/s (2.0 m/s)}, V_c = 1.64 \text{ ft/s (0.5 m/s)}.$$

Proceed to [Box 2-10](#).

- [Box 2-10](#):

$$\begin{aligned} Z_{\text{max,c}} &= 1.9H_1 \left[\frac{1.38V_{\text{appr}}}{R_c\sqrt{gH_1}} - \frac{V_c}{\sqrt{gH_1}} \right] \\ &= 1.9(10.0) \left[\frac{1.38(2.0)}{0.85\sqrt{9.81 \times 10.0}} - \frac{0.5}{\sqrt{9.81 \times 10.0}} \right] \\ &= 17.4 \text{ ft (5.3 m)} \end{aligned}$$

Proceed to [Box 2-11](#).

- [Box 2-11](#): Abutment scour parameters.

$$y_a = 9.84 \text{ ft (3.0 m)}, V_{\text{appr}} = V_{100} = 6.56 \text{ ft/s (2.0 m/s)}, L = 13.1 \text{ ft (4.0 m)}, \theta = 30^\circ$$

Abutment type = vertical-wall abutment

Proceed to [Box 2-12](#).

- [Box 2-12](#):

$$\frac{L}{y_a} = \frac{4.0}{3.0} = 1.33 > 2.5$$

Since $\frac{L}{y_a} > 2.5$, use the Froehlich equation.

$$\frac{Z_{\text{max,a}}}{y_a} = 2.27 K_1 K_2 \left(\frac{L}{y_a} \right)^{0.43} F^{0.61}$$

From [Table 2-4](#), $K_1 = 1.00$.

$$K_2 = \left(\frac{\theta}{90}\right)^{0.13} = \left(\frac{30}{90}\right)^{0.13} = 0.87$$

$$\begin{aligned} Z_{\max,a} &= 2.27 y_a K_1 K_2 \left(\frac{L}{y_a}\right)^{0.43} \left(\frac{V_{\text{appr}}}{\sqrt{g y_a}}\right)^{0.61} \\ &= 2.27 (3.0) (1.00) (0.87) \left(\frac{4.0}{3.0}\right)^{0.43} \left(\frac{2.0}{\sqrt{9.81 \times 3.0}}\right)^{0.61} \\ &= 11.8 \text{ ft (3.6 m)} \end{aligned}$$

Proceed to [Box 2-13](#).

- [Box 2-13](#):

$$\begin{aligned} Z_{\max,l} &= Z_{\max,p} + Z_{\max,c} + Z_{\max,a} \\ &= 1.8 + 5.3 + 3.6 \\ &= 10.7 \text{ m} = 35.1 \text{ ft.} \end{aligned}$$

Proceed to [Box 2-14](#).

- [Box 2-14](#): The bridge is not underlain by a layered profile. Proceed to [Box 2-18](#).
- [Box 2-18](#): $Z_{\text{thresh}} = 10 \text{ m} = 32.8 \text{ ft}$. Proceed to [Box 2-19](#).
- [Box 2-19](#): Z_{\max} is greater than Z_{thresh} . Proceed to [Box 2-21](#).
- [Box 2-21](#): BSA 3 needs to be carried out.

7. BRIDGE SCOUR ASSESSMENT 3

7.1. INTRODUCTION

Bridge Scour Assessment 3 is the assessment procedure that has to be carried out if a bridge is not found as “minimal risk (regular monitoring)” at the end of Bridge Scour Assessment 2. BSA 3 involves the calculation of time-dependent scour depth, which is the scour depth after a specified time, rather than simply using the maximum scour depth. This method is valuable in the case of clays and rocks that have high erosion resistance (low erosion rate) and do not achieve the maximum scour depth as computed in BSA 2 within the lifetime of the bridge. The time-dependent scour depth is termed the final scour depth, Z_{fin} . In BSA 3, the total final local scour depth at the bridge, termed the final local scour ($Z_{fin,l}$), is the arithmetic sum of the three components of scour, i.e., final pier scour ($Z_{fin,p}$), final contraction scour ($Z_{fin,c}$), and final abutment scour ($Z_{fin,a}$). Similar to BSA 2, the vulnerability associated with scour depends on the comparison between the total final scour depth, $Z_{fin,l}$, and the allowable scour depth of the bridge, Z_{thresh} .

7.2. THE BSA 3 FLOWCHART AND PROCEDURE

The BSA 3 flowchart is shown in [Figure 7-1](#). The boxes in the flowchart are of three forms: rectangular, diamond, and rounded. Rectangular boxes are data collection and calculation boxes, meaning that the data listed in the box need to be collected by the user for the bridge being analyzed and, where appropriate, involve the use of equations. Diamond boxes are “yes-no” decision boxes. Rounded boxes are conclusion boxes. All boxes are numbered for easy reference; the first digit represents the BSA level, and the second digit represents the box number.

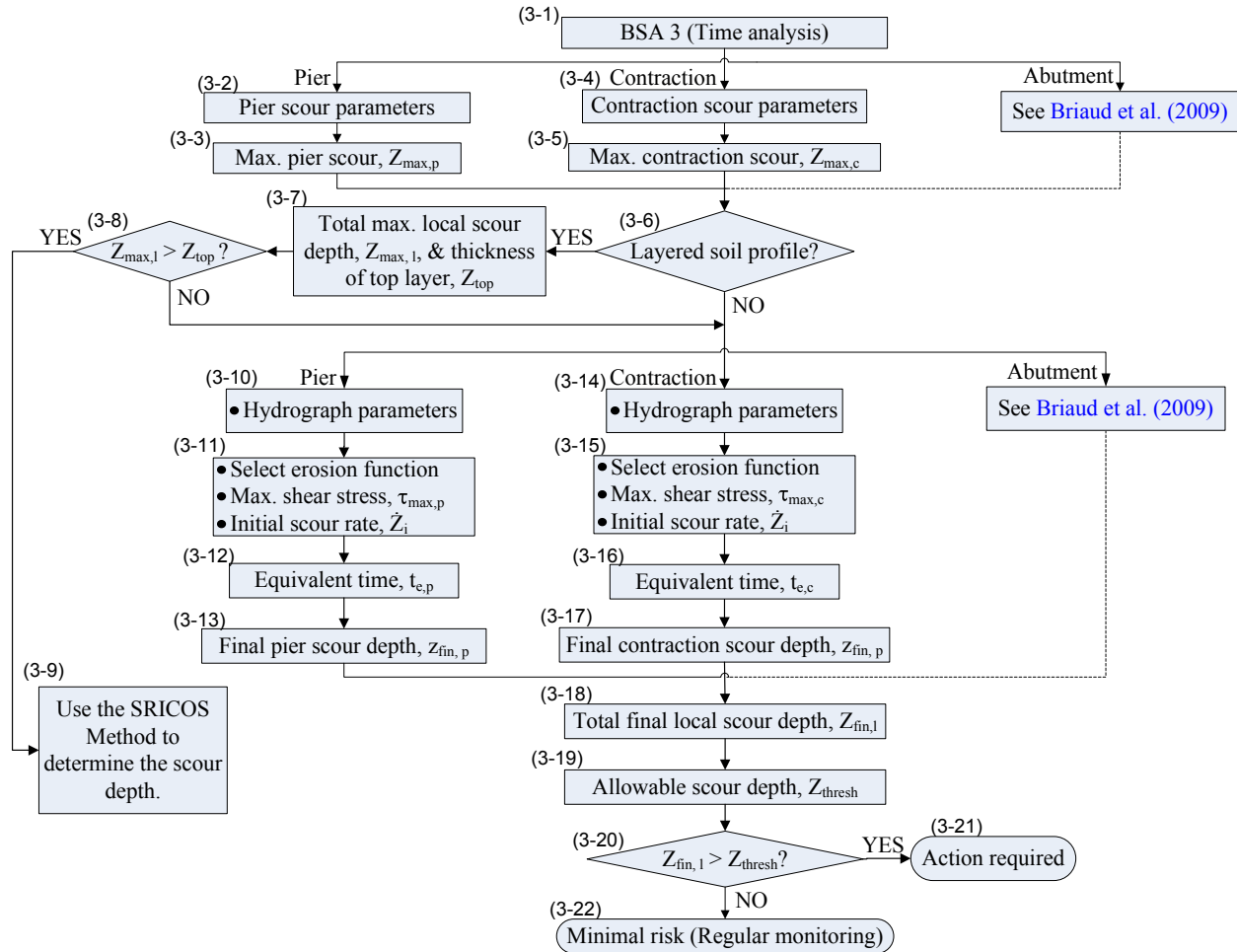


Figure 7-1. The BSA 3 (Time Analysis) Flowchart.

In the BSA 3 analysis, the scour depth versus time is modeled as a hyperbola. Equation (2.3) and Equation (2.6) show the hyperbolic model for pier and contraction scour, respectively (Briaud et al. 1999, 2005). These models have been described in Chapter 2 under the section on SRICOS methods for pier and contraction scour. Similar to the total maximum local scour depth in BSA 2, the time-dependent scour local depth at the end of a specified time, termed the total final local scour depth, $Z_{fin,l}$, is the summation of the final scour depths of the three components of time-dependent scour:

$$Z_{fin,l} = Z_{fin,p} + Z_{fin,c} + Z_{fin,a} \quad (7.1)$$

where $Z_{fin,p}$, $Z_{fin,c}$, and $Z_{fin,a}$ are the pier scour, contraction scour, and abutment scour after a specified time, respectively. The process of determining the time-dependent abutment scour, $Z_{fin,a}$, is ongoing at Texas A&M University, under the leadership of Dr. Jean-Louis Briaud. The procedure to determine final abutment scour depth is being published as [Briaud et al. \(2009\)](#).

The first step in BSA 3 is the determination of the maximum scour depth of the various components of scour, i.e., pier scour, contraction scour, and abutment scour. The calculations could have been carried out in BSA 2. The calculations for maximum pier and contraction scour are described in [Chapter 2](#) and detailed by [Briaud et al. \(1999, 2005\)](#). Calculations for abutment scour are being published as [Briaud et al. \(2009\)](#). If the geologic profile underlying the bridge is layered, the topmost layer is used in the calculation of maximum scour depth. If the total maximum scour depth based on the topmost layer extends beyond that layer, then the Extended SRICOS-EFA Method should be used to determine the time-dependent scour depth ([Briaud et al. 1999, 2003, and 2005](#)). Otherwise, BSA 3 (Time Analysis) is continued.

In BSA 3 (Time Analysis), the hydrograph parameters, i.e., the duration of the hydrograph (t_{hyd}) and the maximum hydrograph velocity (V_{max}), are obtained to determine the equivalent time, as detailed in [Chapter 2](#) and defined by [Equation \(2.7\)](#) and [Equation \(2.8\)](#). In addition to this, the initial rate of scour, \dot{Z}_i , is obtained from the appropriate erosion function selected from the Erodibility Charts ([Figure 3-4](#) and [Figure 3-5](#)). The initial rate of scour, \dot{Z}_i , is the scour rate that corresponds to the approach velocity being considered. The total final pier and contraction scour depths ($Z_{fin,p}$ and $Z_{fin,c}$, respectively) are obtained using [Equations \(2.3\)](#) and [Equation \(2.6\)](#), respectively. If the final local scour depth, $Z_{fin,l}$, does not exceed the allowable scour depth, Z_{thresh} , the bridge is designated as “minimal risk” and should undergo regular monitoring. Otherwise, immediate action is required.

7.3. STEP-BY-STEP PROCEDURE FOR BSA 3

To assist the user in carrying out a BSA 3 analysis, [Table 7-1](#) details all the steps of the method according to flowchart box number.

Table 7-1. Step-by-Step Procedure for BSA 3 (Time Analysis).

Box No.	Description
3-1	Introduction to BSA 3 (Time Analysis). Links BSA 2 to BSA 3.
3-2	<p>The data collection box of parameters required to determine the maximum pier scour. These parameters are as follows:</p> <ul style="list-style-type: none"> • approach velocity (V_{appr}); • pier diameter (D); and • kinematic viscosity of water (ν), which is 10^{-6} m²/s at 20° Celsius.
3-3	The calculation box for the maximum pier scour depth using Equation (2.2) .
3-4	<p>The data collection box of parameters required to determine the maximum contraction scour. These parameters are as follows:</p> <ul style="list-style-type: none"> • Approach velocity (V_{appr}). • Soil critical velocity (V_c). The critical velocity is the velocity corresponding to an erosion rate of 0.1 mm/hr on the Erosion Function Chart (Figure 3-4 and Figure 3-5). The erosion function is the left boundary curve of the erosion category that best fits the material underlying the bridge site. • Upstream water depth (H_1). • Uncontracted channel width (B_1). • Contracted channel width (B_2).
3-5	The calculation box for the maximum contraction scour depth using Equation (2.4) .
3-6	Decision box to determine if the bridge site is underlain by a layered geologic profile. If yes, the maximum local scour depth ($Z_{max,l}$) is compared with the thickness of the topmost layer, Z_{top} , in Box 3.8 .
3-7	The calculation box for the maximum local scour depth, $Z_{max,l}$, and input of the thickness of the topmost soil layer underlying the bridge site, Z_{top} .
3-8	Decision box to determine if the maximum local scour depth ($Z_{max,l}$) is greater than the thickness of the topmost layer, Z_{top} . If yes, the SRICOS Method needs to be used (Briaud et al. 1999, 2003, and 2005).
3-9	Leads to the SRICOS Method.
3-10	<p>The collection box for hydrograph parameters. These parameters are as follows:</p> <ul style="list-style-type: none"> • hydrograph duration (t_{hyd}) and • maximum velocity appearing in the hydrograph (V_{appr}).

Table 7-1. Step-by-Step Procedure for BSA 3 (Time Analysis) (Continued).

Box No.	Description
3-11	<p>The determination of the initial scour rate, \dot{Z}_i, that is to be used in computing the equivalent time for pier scour, $t_{e,p}$ (Equation [2.7]). This is done by carrying out the following steps:</p> <ul style="list-style-type: none"> • Select the erosion function for the material underlying the bridge site using the Erosion Function Chart (Figure 3-4 and Figure 3-5). The erosion function is the left boundary curve of the erosion category that best fits the material. • Get the erosion rate corresponding to the maximum hydrograph velocity, V_{appr}, (or V_{max}) on the selected erosion function. This erosion rate is the initial scour rate, \dot{Z}_i.
3-12	<p>Computation of the equivalent time for pier scour ($t_{e,p}$) using Equation (2.7). The equivalent time is defined as the time required for the maximum velocity of the hydrograph, V_{max}, to create the same scour depth as the one created by the complete hydrograph (Briaud et al. 2004).</p>
3-13	<p>Determination of the final pier scour depth using the hyperbolic model (Equation [2.3]).</p>
3-14	<p>Collection of hydrograph parameters. These parameters are as follows:</p> <ul style="list-style-type: none"> • hydrograph duration (t_{hyd}) and • maximum velocity appearing in the hydrograph (V_{appr}).
3-15	<p>The determination of the initial scour rate, \dot{Z}_i, that is to be used in computing the equivalent time for contraction scour, $t_{e,c}$ (Equation [2.8]). This is done by carrying out the following steps:</p> <ul style="list-style-type: none"> • Select the erosion function for the material underlying the bridge site using the Erosion Function Chart (Figure 3-4 and Figure 3-5). The erosion function is the left boundary curve of the erosion category that best fits the material. • Get the erosion rate corresponding to the maximum hydrograph velocity, V_{appr}, (or V_{max}) on the selected erosion function. This erosion rate is the initial scour rate, \dot{Z}_i.
3-16	<p>Computation of the equivalent time for contraction scour ($t_{e,c}$) using Equation (2.8). The equivalent time is defined as the time required for the maximum velocity of the hydrograph, V_{max}, to create the same scour depth as the one created by the complete hydrograph (Briaud et al. 2004).</p>
3-17	<p>Determination of the final contraction scour depth using the hyperbolic model (Equation [2.6]).</p>
3-18	<p>The determination of the total final scour depth, $Z_{fin,t}$. The total final scour depth is the summation of the final scour depths of the three components of time-dependent scour and is given by Equation (7.1).</p>
3-19	<p>Input of allowable scour depth, Z_{thresh}. This is based on the foundation element being considered.</p>

Table 7-1. Step-by-Step Procedure for BSA 3 (Time Analysis) (Continued).

Box No.	Description
3-20	The decision box that determines if the bridge is deemed to have low scour risk or requires action against scour damage. This is done by comparing the values of the total final local scour depth, $Z_{fin,l}$, against the allowable scour depth, Z_{thresh} . If $Z_{fin,l}$ is greater than Z_{thresh} , the bridge is deemed “action required.” Otherwise, the bridge is deemed “minimal risk” and should undergo regular monitoring.
3-21	Indication that the bridge is susceptible to scour-related damage and requires immediate action.
3-22	Indicates that the bridge is deemed as having low scour risk and should undergo regular bridge scour monitoring.

7.4. EXAMPLE OF BSA 3 ANALYSIS

Problem: Determine the maximum scour depth corresponding to the following information that characterizes the bridge scour problem:

- The geomaterial type is uniform medium erodibility material (Category III).
- Contraction ratio $R_c = 0.85$.
- Upstream water depth $H_1 = 32.8$ ft (10 m).
- Pier diameter $D = 3.28$ ft (1.0 m).
- Maximum hydrograph velocity $V_{max} = 6.56$ ft/s (2.0 m/s).
- Kinematic viscosity of water at 68°F (20°C), $\nu = 1.1 \times 10^{-5}$ ft²/s (10^{-6} m²/s).
- Allowable scour depth $Z_{thresh} = 19.7$ ft (6.0 m).
- Age of the bridge $t_{hyd} = 25$ years.

The following is the solution according to BSA 3 flowchart box numbers:

- [Box 3-1](#): Start of BSA 3. Proceed to [Box 3-2](#).

- [Box 3-2](#): Pier scour parameters.

- $D = 3.28 \text{ ft (1.0 m)}$, $V_{\text{appr}} = 6.56 \text{ ft/s (2.0 m/s)}$, $\nu = 1.1 \times 10^{-5} \text{ ft}^2/\text{s} \text{ (} 10^{-6} \text{ m}^2/\text{s)}$.

Proceed to [Box 3-3](#).

- [Box 3-3](#):

$$Z_{\text{max,p}} \text{ (mm)} = 0.18 \left(\frac{V_{\text{appr}} D}{\nu} \right)^{0.635}$$

$$= 1804.8$$

$$Z_{\text{max,p}} = 5.91 \text{ ft (1.8 m)}$$

Proceed to [Box 3-4](#).

- [Box 3-4](#): Contraction scour parameters.

$$R_c = 0.85, H_1 = 32.8 \text{ ft (10.0 m)}, V_{\text{appr}} = 6.56 \text{ ft/s (2.0 m/s)}, V_c = 1.64 \text{ ft/s (0.5 m/s)}.$$

Proceed to [Box 3-5](#).

- [Box 3-5](#):
$$Z_{\text{max,c}} = 1.9H_1 \left[\frac{1.38V_{\text{appr}}}{R_c \sqrt{gH_1}} - \frac{V_c}{\sqrt{gH_1}} \right]$$

$$= 1.9(10.0) \left[\frac{1.38(2.0)}{0.85 \sqrt{9.81 \times 10.0}} - \frac{0.5}{\sqrt{9.81 \times 10.0}} \right]$$

$$= 17.4 \text{ ft (5.3 m)}$$

Proceed to [Box 3-6](#).

- [Box 3-6](#): The bridge is founded on a uniform profile. Proceed to [Box 3-10](#).

- [Box 3-10](#): Hydrograph parameters.

$$V_{\text{max}} = V_{\text{appr}} = 6.56 \text{ ft/s (2 m/s)}, t_{\text{hyd}} = 25 \text{ years}.$$

Proceed to [Box 3-11](#).

- [Box 3-11](#): From [Figure 3-4](#), \dot{Z} corresponding to $V_{\max} = 6.56$ ft/s (2.0 m/s) is 5.91 in/hr (150 mm/hr). Proceed to [Box 3-12](#).
- [Box 3-12](#): $t_{\text{eq,p}}(\text{hr}) = 73[t_{\text{hyd}}(\text{yrs})]^{0.126}[V_{\max}(\text{m/s})]^{1.706}[\dot{Z}_i(\text{mm/hr})]^{-0.20}$

$$= 73[25]^{0.126}[2.0]^{1.706}[150]^{-0.20}$$

$$= 131.16 \text{ hr}$$

Proceed to [Box 3-13](#).

- [Box 3-13](#): $Z_{\text{fin,p}} = \frac{t_{\text{eq,p}}}{\frac{1}{Z_i} + \frac{t_{\text{eq,p}}}{Z_{\text{max,p}}}}$

$$= \frac{131.16}{\frac{1}{(150/1000)} + \frac{131.16}{1.8}}$$

$$= 5.25 \text{ ft (1.6 m)}$$

Proceed to [Box 3-14](#).

- [Box 3-14](#): Same as [Box 3-10](#). Proceed to [Box 3-15](#).
- [Box 3-15](#): Same as [Box 3-11](#). Proceed to [Box 3-16](#).
- [Box 3-16](#): $t_{\text{eq,c}}(\text{hr}) = 644.32[t_{\text{hyd}}(\text{yrs})]^{0.4242}[V_{\max}(\text{m/s})]^{1.648}[\dot{Z}_i(\text{mm/hr})]^{-0.605}$

$$= 644.32[25]^{0.4242}[2.0]^{1.648}[150]^{-0.605}$$

$$= 381.7 \text{ hr}$$

Proceed to [Box 3-17](#).

$$Z_{\text{fin,c}} = \frac{t_{\text{eq,c}}}{\frac{1}{Z_i} + \frac{t_{\text{eq,c}}}{Z_{\text{max,c}}}}$$

- **Box 3-17:**

$$= \frac{381.7}{\frac{1}{(150/1000)} + \frac{381.7}{5.3}}$$

$$= 16.1 \text{ ft (4.9 m)}$$

Proceed to **Box 3-18**.

- **Box 3-18:** $Z_{\text{fin,l}} = Z_{\text{fin,p}} + Z_{\text{fin,c}}$

$$= 1.6 + 4.9$$

$$= 6.5 \text{ m} = 21.3 \text{ ft.}$$

Proceed to **Box 3-19**.

- **Box 3-19:** $Z_{\text{thresh}} = 6.0 \text{ m} = 19.7 \text{ ft}$. Proceed to **Box 3-20**.
- **Box 3-20:** $Z_{\text{fin,l}}$ is greater than Z_{thresh} . Proceed to **Box 3-21**.
- **Box 3-21:** Immediate action is required at this bridge to mitigate scour-related failure.

8. CASE HISTORIES AND VALIDATION

8.1. INTRODUCTION

In order to develop and validate the simplified method for estimating scour, 11 case histories in Texas were chosen. These cases were used to develop and validate the procedures in BSA 1, 2, and 3. The collection of the data for the case histories was carried out by contacting the relevant TxDOT district offices to obtain copies of the bridge folders maintained by TxDOT. These bridge folders contain bridge foundation information, scour measurements, and soil information. However, the extent of the information and its clarity vary from folder to folder due to the fact that the bridges can be quite old (up to approximately 80 years old) and that the practice of performing bridge scour measurements was not routine before the early 1990s.

8.2. CRITERIA FOR SELECTION

There are several criteria that were identified to make a bridge suitable as a case history for the validation process. In order to develop a set of case histories that was suitable, it was essential to obtain cases that covered the widest variety of conditions, i.e., soil types, foundation types, location within the state of Texas, and scour status. However, there were limitations in some of the cases where there was inadequate availability of data. The general criteria for selection are based on the following items:

1. channel profile measurement records,
2. flow data,
3. soil information,
4. foundation information, and
5. current scour status.

8.3. THE BRIDGES SELECTED AS CASE HISTORIES

8.3.1. Overview and Location

Table 8-1 summarizes the 11 bridges selected for validation. Figure 8-1 shows the locations of these bridges on the map of Texas. Out of the 11 bridges selected for validation, 10 are scour critical, and the remaining 1 is stable for calculated scour conditions. Data on the 11 case histories are presented in detail in Appendix C, which also includes cross-section drawings of the bridges.

Table 8-1. Summary of the 11 Case Histories Selected for Validation.

No.	Latitude	Longitude	Waterway	Highway	Scour Status	EFA Test Data Status	Flow Data Status
1	31.47056308000	-96.29239209000	Sanders Creek	FM 39	Critical	Available*	Not Available
2	31.97030066000	-96.08752535000	Alligator Creek	US 287	Critical	Available [§]	Not Available
3	29.47641599000	-95.81304823000	Big Creek	SH 36	Critical	Not Available	Available
4	29.59232540000	-97.58796201000	San Marcos River	FM 2091	Critical	Not Available	Available
5	29.86972042000	-96.15511481000	Mill Creek	FM 331	Critical	Not Available	Available
6	29.96498001000	-98.89669924000	Guadalupe River	US 87	Critical	Not Available	Available
7	30.02640843000	-95.25897002000	San Jacinto River	US 59 SB	Critical	Not Available	Available
8	30.13653693000	-99.31566628000	Dry Branch Creek	SH 27	Critical	Not Available	Available
9	30.20833445000	-95.18168475000	Peach Creek	US 59 @ Creekwood Drive	Critical	Not Available	Available
10	29.58279722000	-95.75768056000	Brazos River	US 90A WB	Critical	Available ⁺	Available
11	31.25425278000	-96.33052778000	Navasota River	SH 7	Stable	Available [#]	Available

Note: * EFA Sample Nos. 1464, 1465, and 1466

§ EFA Sample Nos. 1459, 1460, and 1462

+ EFA Sample Nos. Brazos Layer 1 and Brazos Layer 2

EFA Sample Nos. Navasota Layer 1 and Navasota Layer 2

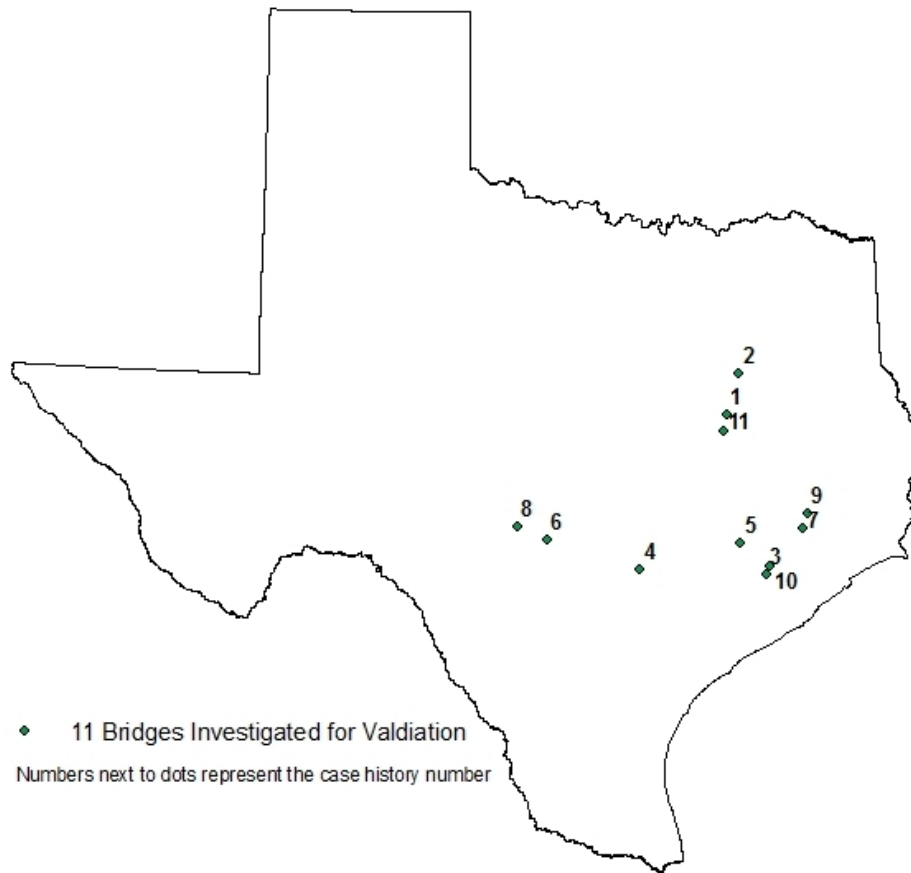


Figure 8-1. Location of the 11 Case Histories Selected for Validation.

8.3.2. Case-by-Case Description of Bridges

The general description of the bridges, such as the number of spans, foundation type, and geomaterials underlying the bridge site, are given in this section. As mentioned above, more detailed information on the bridges is given in [Appendix C](#).

8.3.2.1. Case History No. 1: Bridge on FM 39 Crossing Sanders Creek

This bridge is located in Limestone County within the Waco District in Texas. The TxDOT structure number for this bridge is 09-147-0643-02-038. The bridge is on FM 39 and crosses Sanders Creek. The bridge was built in 1977 and has a length of 316 ft. It has six spans and is

founded on 2.5-ft diameter drilled shafts that vary between 15 ft and 22.5 ft in length. The drilled shafts are embedded mainly in sand and silty sand. This bridge has been deemed scour critical by a concise analysis. This case history does not have flow records but does have site-specific EFA test data.

8.3.2.2. Case History No. 2: Bridge on US 287 Crossing Alligator Creek

This bridge is located in Freestone County within the Bryan District in Texas. The TxDOT structure number for this bridge is 17-082-0122-03-036. The bridge is on US 287 and crosses Alligator Creek. The bridge was built in 1984 and has a length of 292 ft. It has seven spans and is founded on 2-ft diameter drilled shafts that have a minimum length of 24 ft. The soil at the site is clay and sand. This bridge has been deemed scour critical by a concise analysis. This case history does not have flow records but does have site-specific EFA test data.

8.3.2.3. Case History No. 3: Bridge on SH 36 Crossing Big Creek

This bridge is located in Fort Bend County within the Houston District in Texas. The TxDOT structure number for this bridge is 12-080-0188-02-023. The bridge is on SH 36 and crosses Big Creek. The bridge was built in 1932 and has a length of 257 ft. It has nine spans and is founded on 14-inch concrete piles that vary between 25 ft and 35 ft in length. The soil at the site is a deep sand deposit, extending more than 40 ft below the channel bottom. This bridge is stable in terms of scour. This case history has flow records but does not have site-specific EFA test data.

8.3.2.4. Case History No. 4: Bridge on FM 2091 Crossing San Marcos River

This bridge is located in Gonzales County within the Yoakum District in Texas. The TxDOT structure number for this bridge is 13-090-2080-01-005. The bridge is on FM 2091 and crosses the San Marcos River. The bridge was built in 1960 and has a length of 382 ft. It has six spans and is founded on 15-inch wide, 32-ft long precast concrete piles and 14-inch wide, 33-ft long steel H-piles. The soil at the site is clay and sand. This bridge is on the scour-critical list. This case history has flow records but does not have site-specific EFA test data.

8.3.2.5. Case History No. 5: Bridge on FM 331 Crossing Mill Creek

This bridge is located in Austin County within the Austin District in Texas. The TxDOT structure number for this bridge is 13-008-0408-05-019. The bridge is on FM 331 and crosses

Mill Creek. The bridge was built in 1951 and has a length of 271 ft. It has six spans and is founded on 18-inch wide precast concrete piles with a minimum length of 20 ft. The soil at the site is clay and silty sand. This bridge has been deemed scour critical by a concise analysis. This case history has flow records but does not have site-specific EFA test data.

8.3.2.6. Case History No. 6: Bridge on US 87 Crossing Guadalupe River

This bridge is located in Kendall County within the San Antonio District in Texas. The TxDOT structure number for this bridge is 15-131-0072-04-020. The bridge is on US 87 and crosses the Guadalupe River. The bridge was built in 1932 and has a length of 1434 ft. It has 34 spans and is founded on 16-inch wide concrete square piles that are between 36 ft and 50 ft in length. The bridge was widened in 1984; the widened section is on 6-ft diameter drilled shafts that are approximately 17 ft long. The soil at the site is clay and sandy gravel. This bridge has been deemed scour critical by a concise analysis. This case history has flow records but does not have site-specific EFA test data.

8.3.2.7. Case History No. 7: Bridge on US 59 SB Crossing West Fork San Jacinto River

This bridge is located in Harris County within the Houston District in Texas. The TxDOT structure number for this bridge is 12-102-0177-06-081. The bridge is on US 59 SB and crosses the West Fork San Jacinto River. The bridge was built in 1961 and has a length of 1645 ft. It is founded on 16-inch square concrete piles with a minimum length of 10 ft. The soil at the site is sand. This bridge has been deemed scour critical by a concise analysis. This case history has flow records but does not have site-specific EFA test data.

8.3.2.8. Case History No. 8: Bridge on SH 27 Crossing Dry Branch Creek

This bridge is located in Kerr County within the San Antonio District in Texas. The TxDOT structure number for this bridge is 15-133-0142-03-008. The bridge is on SH 27 and crosses Dry Branch Creek. The bridge was built in 1935 and has a length of 142 ft. It has five spans and is founded on spread footings that are embedded approximately between 10 ft and 15 ft below the channel bottom. The bridge was widened in 1963; the widened section is on 2-ft diameter drilled shafts that are approximately 15 ft long. The soil at the site is clay, shale, and limestone. This bridge has been deemed scour critical by a concise analysis. This case history has flow records but does not have site-specific EFA test data.

8.3.2.9. Case History No. 9: Bridge on US 59 at Creekwood Drive Crossing Peach Creek

This bridge is located in Montgomery County within the Houston District in Texas. The TxDOT structure number for this bridge is 12-170-0177-05-119. The bridge is on US 59 at Creekwood Drive and crosses Peach Creek. The bridge was built in 1970 and has a length of 120 ft. It has three spans and is founded on 16-inch wide, approximately 35-ft long square piles. The soil at the site is sand. This bridge has been deemed scour critical by a concise analysis. This case history has flow records but does not have site-specific EFA test data.

8.3.2.10. Case History No. 10: Bridge on US 90A WB Crossing Brazos River

This bridge is located in the Houston District in Texas. The TxDOT structure number for this bridge is 12-080-0027-08-092. The bridge is on US 90A WB and crosses the Brazos River. The bridge was built in 1965 and has a length of 942 ft. It has 10 spans and is founded on 16-inch to 20-inch square piles. The pile lengths vary between 70 ft and 78 ft. The soil at the site is silty sand and clayey sand. This bridge has been deemed scour critical by a concise analysis. This case history has both flow records and site-specific EFA test data.

8.3.2.11. Case History No. 11: Bridge on SH 7 Crossing Navasota River

This bridge is located in Leon County within the Bryan District in Texas. The TxDOT structure number for this bridge is 17-145-0382-05-021. The bridge is on SH 7 and crosses the Navasota River. The bridge was built in 1956 and has a length of 271 ft. It has seven spans and is founded on 14-inch wide concrete piles that vary between 28 ft and 50 ft in length. The soil at the site is sand. This bridge has been deemed stable by a concise analysis. This case history has both flow records and site-specific EFA test data.

8.4. VALIDATION OF THE SIMPLIFIED METHOD

8.4.1. Validation of BSA 1

The validation of BSA 1 is aimed at evaluating how well results of the proposed BSA 1 method match actual field measurements. This is carried out by using both flow records and scour measurements at a particular case history bridge. In this investigation, nine bridge case histories were selected for validation. These are the case histories that have flow records. In order to carry

out a meaningful validation, actual flow records recorded by a suitable flow gage were used. The validation process is summarized as follows:

1. The validation procedure starts at the time the first scour measurement was taken at a particular case history bridge. This time is called T_1 and could represent a particular date, e.g., August 21, 1952, or even a year, say 1952.
2. From the measured velocity time history, the maximum flow velocity experienced by the bridge until T_1 , termed V_{mo1} , is obtained. The scour depth measured at the bridge, Z_{mo1} , at time T_1 is obtained from bridge inspection records.
3. A “mock” scour prediction is made at T_1 for a future flood event with velocity V_{fut1} over the next scour measurement interval time, t_{meas1} . It is required that there be actual scour measurements taken at the bridge site at time $T_1 + t_{meas1}$. V_{fut1} is the maximum velocity obtained between T_1 and $T_1 + t_{meas1}$.
4. The Z-Future Chart is then used to obtain the scour depth ratio Z_{fut}/Z_{mo} by using the velocity ratio V_{fut}/V_{mo} . In this case, Z_{mo} is Z_{mo1} , V_{fut} is V_{fut1} , and V_{mo} is V_{mo1} . Z_{fut} is obtained using Equation (5.1). This Z_{fut} is termed $Z_{fut,predict1}$. Then, $Z_{fut,predict1}$ is compared with the actual measured scour depth, $Z_{fut,meas1}$.
5. The process is continued by replacing T_1 with $T_2 = T_1 + t_{meas1}$. T_2 is the time when the next scour measurement was taken at the bridge.
6. From the measured velocity time history, the maximum flow velocity experienced by the bridge until T_2 , V_{mo2} , is obtained. The scour depth measured at the bridge, Z_{mo2} , at time T_2 is obtained from bridge inspection records.
7. A “mock” scour prediction is made at T_2 for a future flood event with velocity V_{fut2} over the next scour measurement interval time, t_{meas2} . It is required that there be actual scour measurements taken at the bridge site at time $T_2 + t_{meas2}$. V_{fut2} is the maximum velocity obtained between T_2 and $T_2 + t_{meas2}$.
8. The Z-Future Chart is then used to obtain the scour depth ratio Z_{fut}/Z_{mo} by plugging in the velocity ratio V_{fut}/V_{mo} . In this case, Z_{mo} is Z_{mo2} , V_{fut} is V_{fut2} , and V_{mo} is V_{mo2} . Z_{fut} is obtained using Equation (5.1). This Z_{fut} is now termed $Z_{fut,predict2}$. Then, $Z_{fut,predict2}$ is compared with the actual measured scour depth, $Z_{fut,meas2}$.

9. Steps 1 through 4 are repeated for the remaining bridge inspection records.

The validation process might yield one or more sets of predicted and measured scour depth for each of the selected bridge case histories. The bridge records had limited bridge scour measurements. In fact, there were no bridge scour measurements taken before the year 1991. Since most of the bridges were reasonably old, they had experienced the largest flow velocity prior to the first bridge scour measurement. This resulted in all the cases having a V_{fut}/V_{mo} ratio of equal to or less than unity. Results of the validation are shown in Figure 8-2 where they are plotted against the equal value line. Figure 8-2 shows a good agreement between the two values. However, it should be noted that this validation is only for V_{fut}/V_{mo} ratios equal to or less than unity.

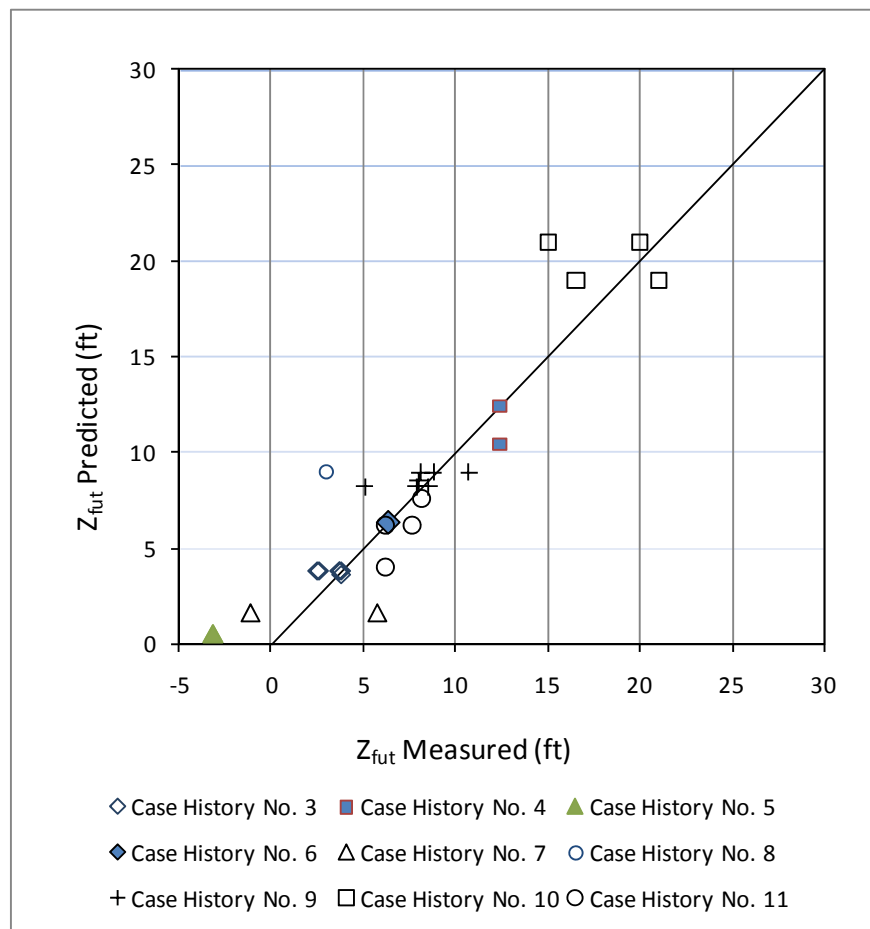


Figure 8-2. Comparison between Z_{fut} Values Predicted by BSA 1 and Corresponding Field Measurements.

8.4.2. Validation of BSA 2

The validation of BSA 2 is aimed at comparing the maximum scour depth predicted by this method and maximum scour depths obtained by the SRICOS-EFA Method. For validating BSA 2, three case histories were selected. The flow velocity corresponding to the 100-year flood was used as the input velocity to obtain the maximum scour depth. The 100-year flood is obtained based on flow records until the most recent scour depth measurements carried out and recorded in the case history bridge folders. The three case histories are ones that have EFA test data.

First, the maximum pier and contraction scour depths are computed using [Equation \(2.2\)](#) and [Equation \(2.4\)](#). The EFA data are used to obtain the critical velocity of the geomaterial underlying the bridge site. The critical velocity is a required input in [Equation \(2.4\)](#). The total maximum scour depth is the sum of the maximum pier and contraction scour. The total maximum scour depth using the EFA data is termed $Z_{\max,I-EFA}$.

Subsequently, the maximum scour depth is obtained using BSA 2. In this case, the only difference is the critical velocity used in [Equation \(2.4\)](#), which instead is obtained from the Erosion Function Charts for the material concerned. The critical velocities are obtained from the mean of the EFA test data on CL, CH, and SC soils ([Figure 3-6](#), [Figure 3-7](#), and [Figure 3-11](#), respectively). The maximum scour depth using BSA 2 is termed $Z_{\max,I-BSA2}$. The values of $Z_{\max,I-EFA}$ and $Z_{\max,I-BSA2}$ were then compared with each other for the three case histories. To investigate the outcome of both methods, the input parameters for the calculations of maximum scour depth were varied as indicated below, resulting in 144 data sets:

1. approach velocity, $V_{\text{appr}} = 1.64 \text{ ft (0.5 m/s)}$ and $11.5 \text{ ft/s (3.5 m/s)}$;
2. upstream water depth, $H_1 = 32.8 \text{ ft (10 m)}$ and 65.6 ft (20 m) ;
3. pier diameter, $D = 0.33 \text{ ft (0.1 m)}$, 3.28 ft (1.0 m) , and 32.8 ft (10 m) ; and
4. contraction ratio, $R_c = 0.5$ and 0.9 .

[Figure 8-3](#) shows the comparison between $Z_{\max,I-EFA}$ and $Z_{\max,I-BSA2}$ against the equal value line. The calculation results are presented in [Appendix C](#). This validation exercise shows a good agreement between both methods.

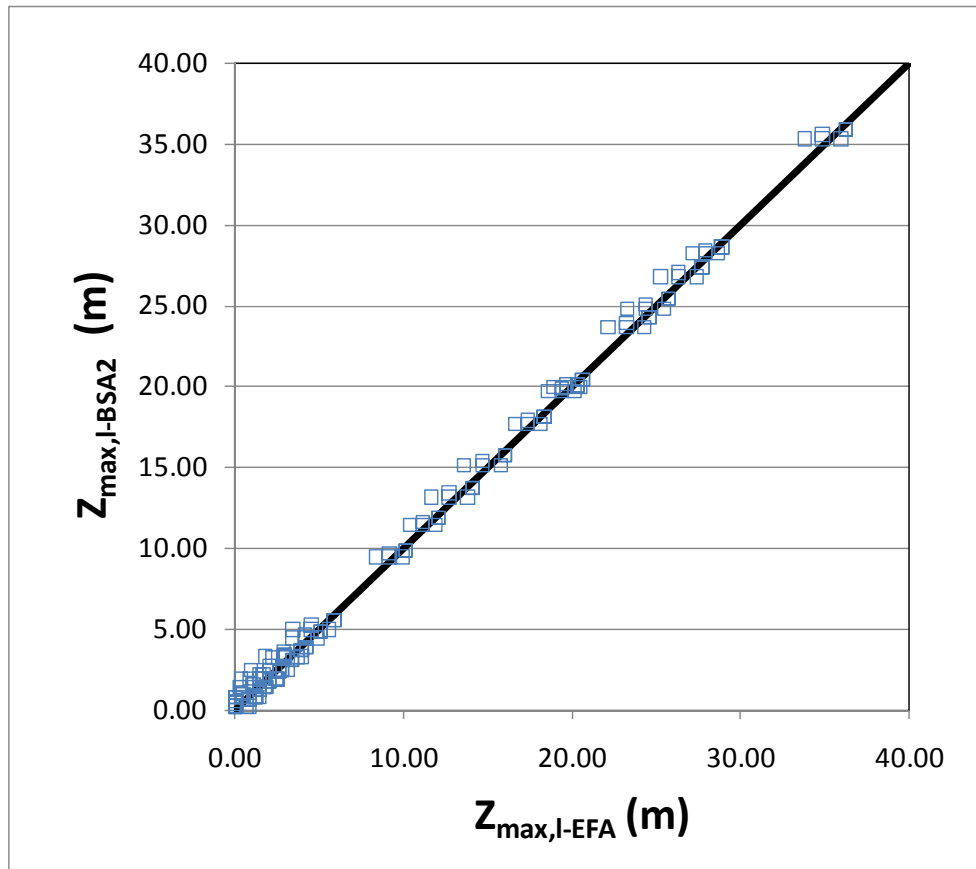


Figure 8-3. Comparison of Maximum Scour Depth Obtained Using EFA Test Data and the Erosion Function Chart.

8.4.3. Validation of BSA 3

The validation of BSA 3 is aimed at comparing the time-dependent scour depth, Z_{fin} , predicted by this method and bridge scour measurements. Only three case histories were validated for BSA 3. This was because out of the 11 case histories, only three cases had flow data and all the available parameters for BSA 3 analysis. [Table 8-2](#) shows the results of the BSA 3 validation.

Table 8-2. Results of BSA 3 Validation.

Case History No.	Z_{max} (ft) (from BSA 2)	Z_{BSA3} (ft) (Final Scour Depth)	$Z_{measured}$ (ft)
3	12.7	11.0	3.6
7	30.7	29.0	5.7
11	24.5	20.5	13.6

The validation results show that BSA 3 tends to overestimate the scour depth. This could be due to the fact that there are only three data points (three cases). In addition to this, the poor agreement between the predicted and measured values could be due to some unknown conditions in the field. However, BSA 3 produces scour depths that are approximately 2 ft to 4 ft lower than the maximum scour depth, Z_{max} . For the sake of this report, the addition of all scour components has been adopted. TxDOT however, does not include abutment scour because of riprap placed at the abutments to counter the effects of scour. Refer to the SRICOS Method (Briaud et al. 1999, 2005) which does something different.

8.5. SCHOHARIE CREEK REVISITED

As a supplement to the 11 case histories, the Schoharie Creek Bridge failure in 1987 was investigated (Figure 8-4). The bridge was a five-span, 540-ft long highway bridge over the Schoharie Creek in Montgomery County near Amsterdam, New York (National Transportation Safety Board 1987). The bridge was built in 1954 and was founded on spread footings that were approximately 19 ft wide and 5 ft thick. On April 5, 1987, one of the piers of the bridge (Pier 3) collapsed, causing two spans of the bridge to plunge into the creek (Figure 8-5). This was followed by the collapse of an adjacent pier (Pier 2). The failure of this bridge caused the deaths of 10 people. The cause of the failure was attributed to scour (National Transportation Safety Board 1987; Resource Consultants, Inc., and Colorado State University 1987; Wiss, Janney, Elstner Associates, Inc., and Mueser Rutledge Consulting Engineers 1987).

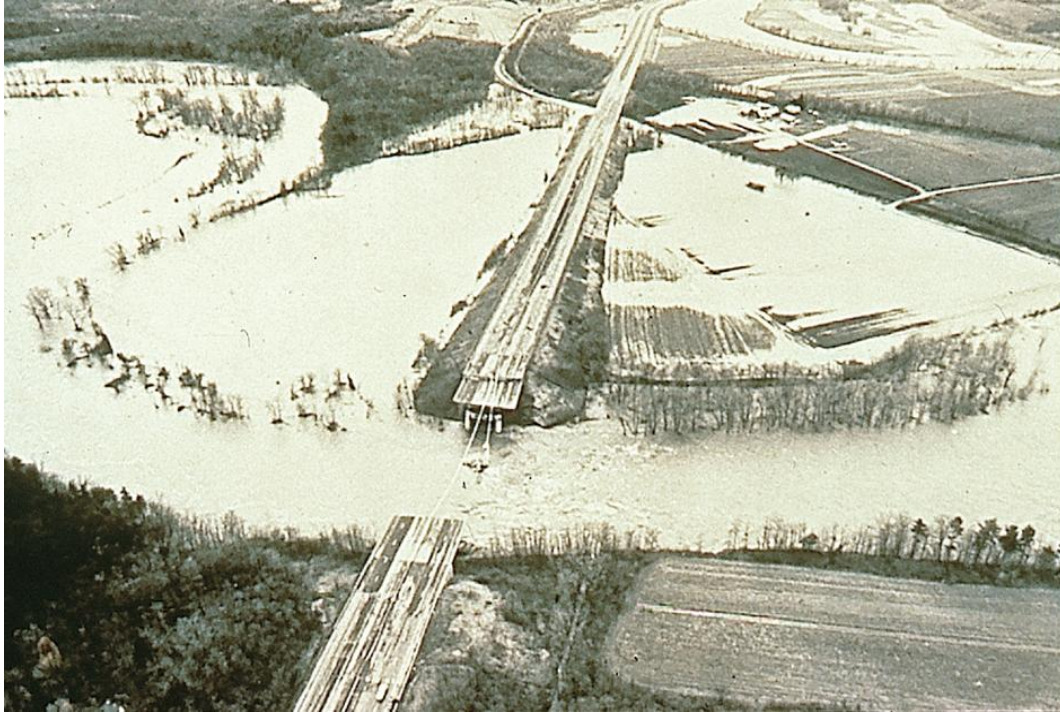


Figure 8-4. The 1987 Schoharie Creek Bridge Failure.

The bridge experienced its largest flood in 1955. The second largest flood was the flood that took place in 1987 during the failure of the bridge. According to the [National Transportation Safety Board \(NTSB\) \(1987\)](#), the magnitudes of both floods (peak) were $Q_{\text{peak},1955} = 73,600$ cfs and $Q_{\text{peak},1987} = 62,100$ cfs, respectively. The flow velocities at Pier 3 were obtained from the one-dimensional flow computer model, Water-Surface Profile Computations (WSPRO) developed by USGS. The computer simulations were carried out by Resource Consultants, Inc., and presented by [NTSB \(1987\)](#) ([Table 8-3](#)).



Figure 8-5. One of the Schoharie Creek Bridge Spans Plunging into the River.

Table 8-3. Peak Discharge versus WSPRO Mean Velocity at Schoharie Creek Pier 3 (after NTSB 1987).

Peak Discharge (cfs)	WSPRO Mean Velocity (ft/s)
10,000	3.6
20,000	5.5
30,000	7.0
40,000	8.2
50,000	9.4
60,000	10.3

The flow-velocity data shown in [Table 8-3](#) were plotted and shown in [Figure 8-6](#). A regression was performed on the data to obtain the flow-velocity relationship. The regression produced an R^2 value of 0.99. Using the relationship shown in [Figure 8-6](#), the flow values $Q_{\text{peak},1955} = 73,600$ cfs and $Q_{\text{peak},1987} = 62,100$ cfs translate into velocities $V_{\text{peak},1955} = 3.6$ m/s and $V_{\text{peak},1987} = 3.2$ m/s, respectively.

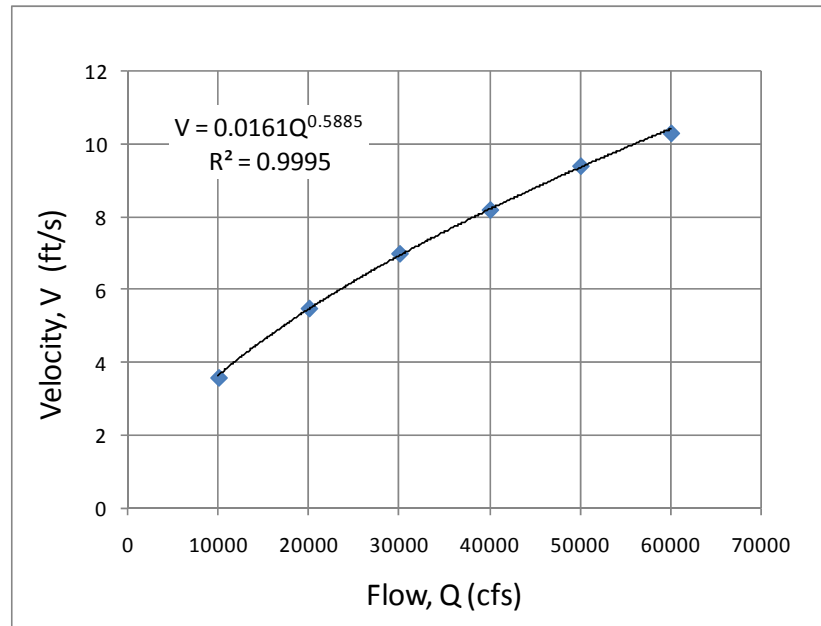


Figure 8-6. Flow-Velocity Relationship for Schoharie Creek Pier 3.

Prior investigations into the failure revealed that riprap was placed at the bridge piers prior to 1955 as protection against scour. [NTSB \(1987\)](#) states, “At Piers 2 and 3, riprap was installed from bottom of footing (elevation 270 ft) sloping to elevation 279.5 ft prior to the 1955 flood. Therefore, at Pier 3 the thickness of the riprap was approximately 9.5 ft [[Figure 8-7](#)]. Photos taken on October 30, 1956, showed riprap movement at Piers 2 and 3. Various photographs taken from 1954 to 1977 during low water showed that some of the rocks had moved northward (downstream) during that time. Photographic analysis of Pier 2 (aided by computers) confirms the downstream movement of rock at Pier 2 from 1954 to 1977.”

Figure 8-7, Figure 8-8, Figure 8-9, and Figure 8-10 show photos of Pier 2 taken in 1956, 1977, and 1987, respectively. Figure 8-11 shows a photo of Pier 3 taken in 1987 after the failure of the bridge.

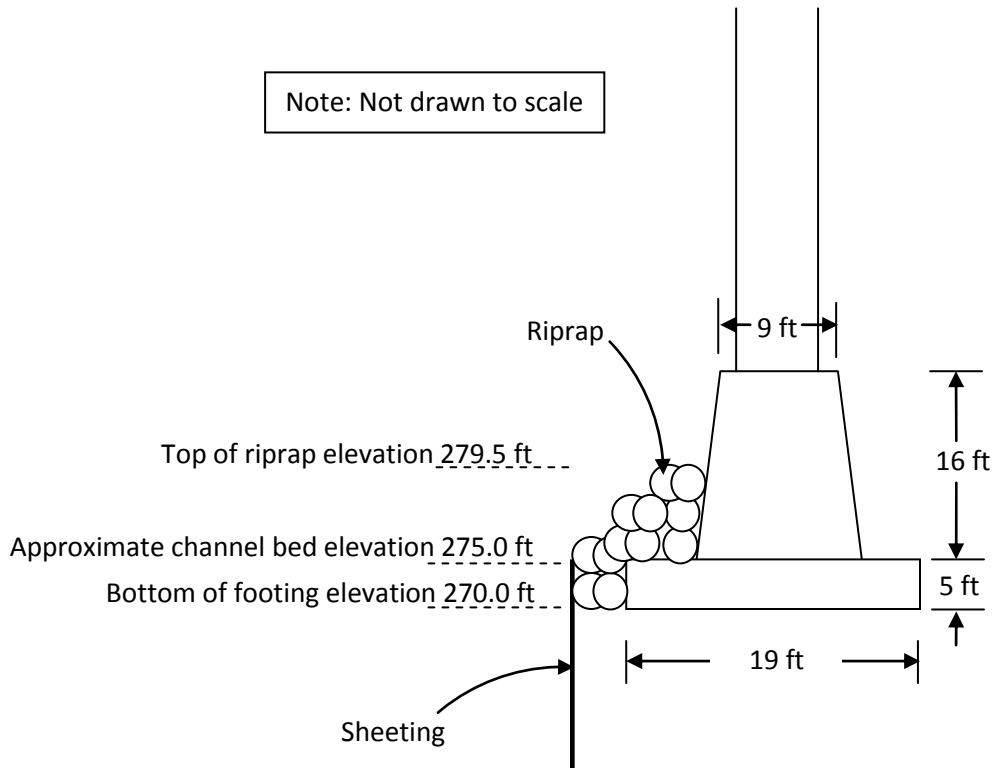


Figure 8-7. Schoharie Creek Pier 3 (after NTSB 1987).

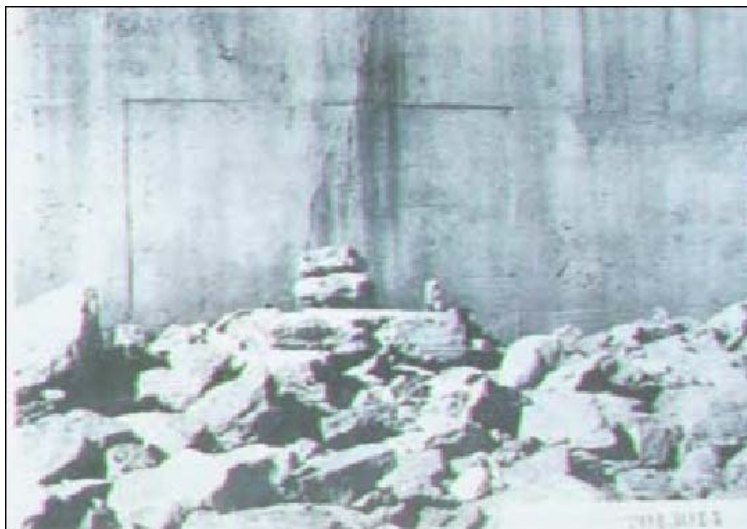


Figure 8-8. Photo of Pier 2 Taken in 1956.



Figure 8-9. Photo of Pier 2 Taken in 1977.



Figure 8-10. Photo of Pier 2 Taken in 1987 after the Failure.



Figure 8-11. Photo of Pier 3 Taken in 1987 after the Failure.

Regarding the riprap placed at the bridge prior to the 1955 flood, [NTSB \(1987\)](#) states, “The only riprap dimensions specified in the bridge plans should be a minimum thickness of 8 inches and a maximum thickness of 15 inches. The plans also call for the riprap to be an Item 80 riprap according to the New York Department of Public Works (DPW) specifications. An Item 80 riprap should have at least 50% of the stones weighing in excess of 300 lbs each.”

According to the Erosion Threshold Chart ([Figure 3-18](#)), for $D_{50} = 8 \text{ inches} = 203 \text{ mm}$:

$$\begin{aligned} V_c(\text{m/s}) &= 0.35[D_{50}(\text{mm})]^{0.45} \\ &= 0.35(203)^{0.45} \\ &= 12.5 \text{ ft/s (3.8 m/s)} \end{aligned}$$

For a DPW Item 80 riprap, assuming the weight of a spherical piece of riprap with a diameter $D_{50} = 300 \text{ lb}$ and its specific gravity $S_g = 2.65$:

$$\text{Weight (lb)} = \text{Density (lb/ft}^3) \times \text{Volume (ft}^3)$$

$$300 \text{ lb} = 2.65 \times 62.4 \text{ (lb/ft}^3) \times \frac{4}{3} \pi \left(\frac{D_{50}}{2} \right)^3$$

$$D_{50} = 2.4 \text{ ft} = 731 \text{ mm}$$

Again from the Erosion Threshold Chart:

$$\begin{aligned} V_c \text{ (m/s)} &= 0.35 [D_{50} \text{ (mm)}]^{0.45} \\ &= 0.35 (731)^{0.45} \\ &= 22.3 \text{ ft/s (6.8 m/s)} \end{aligned}$$

However, [NTSB \(1987\)](#) states, “field observations and photographs indeed showed movement of riprap between 1954 and 1977, the critical velocity, V_c of the riprap should be less than 3.6 m/s, which is the largest flood velocity experienced at the Schoharie Creek bridge.” It goes on to state, “it is evident that there was riprap movement between 1956 and 1977.” The maximum flow between 1956 and 1977 was 40,400 cfs ([National Transportation Safety Board 1987](#)), which corresponds to an approach velocity of 8.3 ft/s or 2.5 m/s. Therefore, it is reasonable to assume that the critical velocity of the riprap should be below 1.5 times the approach velocity, 12.3 ft/s (3.75 m/s). This is the local velocity at the pier and is given by [Equation \(6.1\)](#). Taking V_c of the riprap as 11.5 ft/s (3.5 m/s) (below 12.3 ft/s or 3.75 m/s), the upper boundary of a Category V material can be taken as the erosion function of the riprap. This is shown in [Figure 8-12](#). According to [Resource Consultants, Inc., and Colorado State University \(1987\)](#), V_c of the glacial till = 4.9 f/s = 1.5 m/s. The upper boundary of a Category IV material is translated to the right so that the critical velocity corresponds to the critical velocity of the glacial till ([Figure 8-12](#)).

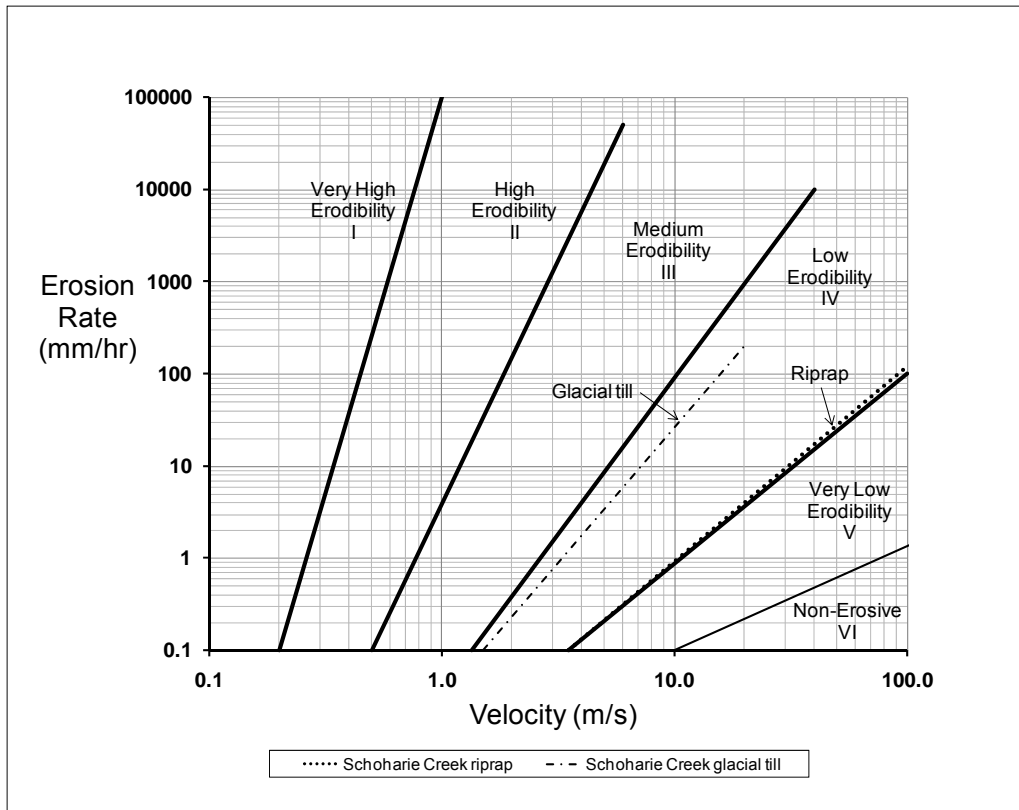


Figure 8-12. Estimated Erosion Functions for the Schoharie Creek Riprap and Glacial Till.

Through prior investigations into the Schoharie Creek bridge failure, it was found that the 1955 flood and following smaller floods caused the riprap to move between 1955 and prior to the 1987 collapse. Since the riprap was placed down to the bottom level of the footing, it is believed that there was still some remaining riprap just prior to the 1987 flood. Otherwise, the erosion would have undermined the footing before the 1987 flood. Since the velocity of the 1987 flood was greater than V_c of the riprap, it is highly likely that the 1987 flood moved the remaining riprap, thus exposing the more erodible glacial till beneath. As shown in [Figure 8-12](#), the till was more erodible than the riprap. Therefore, once the till was exposed, the footing was undermined, very rapidly causing the bridge to fail.

Therefore, the reason for the Schoharie Creek Bridge failure under a lesser flood in 1987 than the flood of 1955 is a multilayer deposit response and not a uniform deposit response. Indeed, during the 1955 event, the scour hole remained in the riprap, while in 1987 it eroded

what was left of the riprap (strong layer) and rapidly advanced in the glacial till below (weak layer). If the bridge scour assessment procedure presented in this report was used to evaluate the Schoharie Creek bridge prior to its collapse, it would have identified the bridge as requiring immediate attention. This is because Z_{thresh} would have been exceeded (for footings, Z_{thresh} is normally taken as the length between the original as-built channel level and the top of the footing). In the case of the Schoharie Creek bridge, the riprap below the top of footing level had moved prior to the 1987 collapse.

9. APPLICATION TO SCOUR-CRITICAL BRIDGES

9.1. INTRODUCTION

A total number of 16 bridges were selected as an example of the proposed bridge scour assessment method in this report. Out of these 16 bridges, 11 were the same bridges selected as case histories for validation, and 5 are additional bridges selected solely for the purpose of evaluating the proposed bridge scour assessment method. Of the 16 bridges, TxDOT characterized 12 as scour critical and 4 as stable. Both stable and scour critical bridges were selected to test the proposed bridge scour assessment method and to compare it against TxDOT's scour designation. For all cases evaluated, the future flow was taken as the 100-year flood with a corresponding velocity, V_{100} . A summary of the information on the 16 bridges is provided in [Table 9-1](#). The results of the application of BSA 1 are compared with the current TxDOT scour designation of the bridges later in this chapter.

9.1.1. Case-by-Case Description of Bridges

The general description of the bridges, such as the type of bridge, foundation type, and geomaterials underlying the bridge site are given in this section. As mentioned above, detailed information on the bridges is given in [Appendix C](#).

Table 9-1. Bridges Selected for Application Using the Proposed Bridge Scour Assessment Method.

Application No.	Latitude	Longitude	Waterway	Highway	Scour Status	EFA Test Data Status	Flow Data Status
1	31.47056308000	-96.29239209000	Sanders Creek	FM 39	Critical	Available	Not Available
2	31.97030066000	-96.08752535000	Alligator Creek	US 287	Critical	Available	Not Available
3	29.47641599000	-95.81304823000	Big Creek	SH 36	Critical	Not Available	Available
4	29.59232540000	-97.58796201000	San Marcos River	FM 2091	Critical	Not Available	Available
5	29.86972042000	-96.15511481000	Mill Creek	FM 331	Critical	Not Available	Available
6	29.96498001000	-98.89669924000	Guadalupe River	US 87	Critical	Not Available	Available
7	30.02640843000	-95.25897002000	San Jacinto River	US 59 SB	Critical	Not Available	Available
8	30.13653693000	-99.31566628000	Dry Branch Creek	SH 27	Critical	Not Available	Available
9	30.20833445000	-95.18168475000	Peach Creek	US 59 @ Creekwood Drive	Critical	Not Available	Available
10	29.58279722000	-95.75768056000	Brazos River	US 90A WB	Critical	Available	Available
11	31.25425278000	-96.33052778000	Navasota River	SH 7	Stable	Available	Available
12	31.91973292000	-97.66186263000	North Bosque River	SH 22	Critical	Available	Not Available
13	29.59945278000	-97.65082500000	San Marcos River	SH 80	Stable	Available	Not Available
14	29.82402778000	-95.28920000000	Sims Bayou	SH 35 NB	Stable	Available	Not Available
15	30.90126667000	-95.77777500000	Bedias Creek	SH 75	Critical	Available	Available
16	30.91262222000	-95.91015278000	Bedias Creek	SH 90	Stable	Available	Not Available

9.1.1.1. Application No. 1: Bridge on FM 39 Crossing Sanders Creek

This bridge is located in Limestone County within the Waco District in Texas. The TxDOT structure number for this bridge is 09-147-0643-02-038. The bridge is on FM 39 and crosses Sanders Creek. The bridge was built in 1977 and has a length of 316 ft. It has six spans and is founded on 2.5-ft diameter drilled shafts that vary between 15 ft and 22.5 ft in length. The drilled shafts are embedded mainly in sand and silty sand. This bridge has been deemed scour critical by a concise analysis. This case history does not have flow records but does have site-specific EFA test data.

9.1.1.2. Application No. 2: Bridge on US 287 Crossing Alligator Creek

This bridge is located in Freestone County within the Bryan District in Texas. The TxDOT structure number for this bridge is 17-082-0122-03-036. The bridge is on US 287 and crosses Alligator Creek. The bridge was built in 1984 and has a length of 292 ft. It has seven spans and is founded on 2-ft diameter drilled shafts that have a minimum length of 24 ft. The soil at the site is clay and sand. This bridge has been deemed scour critical by a concise analysis. This case history does not have flow records but does have site-specific EFA test data.

9.1.1.3. Application No. 3: Bridge on SH 36 Crossing Big Creek

This bridge is located in Fort Bend County within the Houston District in Texas. The TxDOT structure number for this bridge is 12-080-0188-02-023. The bridge is on SH 36 and crosses Big Creek. The bridge was built in 1932 and has a length of 257 ft. It has nine spans and is founded on 14-inch concrete piles that vary between 25 ft and 35 ft in length. The soil at the site is a deep sand deposit, extending more than 40 ft below the channel bottom. This bridge is stable in terms of scour. This case history has flow records but does not have site-specific EFA test data.

9.1.1.4. Application No. 4: Bridge on FM 2091 Crossing San Marcos River

This bridge is located in Gonzales County within the Yoakum District in Texas. The TxDOT structure number for this bridge is 13-090-2080-01-005. The bridge is on FM 2091 and crosses the San Marcos River. The bridge was built in 1960 and has a length of 382 ft. It has six spans and is founded on 15-inch wide, 32-ft long precast concrete piles and 14-inch wide, 33-ft long

steel H-piles. The soil at the site is clay and sand. This bridge is on the scour-critical list. This case history has flow records but does not have site-specific EFA test data.

9.1.1.5. Application No. 5: Bridge on FM 331 Crossing Mill Creek

This bridge is located in Austin County within the Yoakum District in Texas. The TxDOT structure number for this bridge is 13-008-0408-05-019. The bridge is on FM 331 and crosses Mill Creek. The bridge was built in 1951 and has a length of 271 ft. It has six spans and is founded on 18-inch wide precast concrete piles with a minimum length of 20 ft. The soil at the site is clay and silty sand. This bridge has been deemed scour critical by a concise analysis. This case history has flow records but does not have site-specific EFA test data.

9.1.1.6. Application No. 6: Bridge on US 87 Crossing Guadalupe River

This bridge is located in Kendall County within the San Antonio District in Texas. The TxDOT structure number for this bridge is 15-131-0072-04-020. The bridge is on US 87 and crosses the Guadalupe River. The bridge was built in 1932 and has a length of 1434 ft. It has 34 spans and is founded on 16-inch wide concrete square piles that vary between 36 ft and 50 ft in length. The bridge was widened in 1984; the widened section is on 6-ft diameter drilled shafts that are approximately 17 ft long. The soil at the site is clay and sandy gravel. This bridge has been deemed scour critical by a concise analysis. This case history has flow records but does not have site-specific EFA test data.

9.1.1.7. Application No. 7: Bridge on US 59 SBML Crossing West Fork San Jacinto River

This bridge is located in Harris County within the Houston District in Texas. The TxDOT structure number for this bridge is 12-102-0177-06-081. The bridge is on US 59 SB and crosses the West Fork San Jacinto River. The bridge was built in 1961 and has a length of 1645 ft. It is founded on 16-inch square concrete piles with a minimum length of 10 ft. The soil at the site is sand. This bridge has been deemed scour critical by a concise analysis. This case history has flow records but does not have site-specific EFA test data.

9.1.1.8. Application No. 8: Bridge on SH 27 Crossing Dry Branch Creek

This bridge is located in Kerr County within the San Antonio District in Texas. The TxDOT structure number for this bridge is 15-133-0142-03-008. The bridge is on SH 27 and crosses Dry

Branch Creek. The bridge was built in 1935 and has a length of 142 ft. It has five spans and is founded on spread footings that are embedded approximately between 10 ft and 15 ft below the channel bottom. The bridge was widened in 1963; the widened section is on 2-ft diameter drilled shafts that are approximately 15 ft long. The soil at the site is clay, shale, and limestone. This bridge has been deemed scour critical by a concise analysis. This case history has flow records but does not have site-specific EFA test data.

9.1.1.9. Application No. 9: Bridge on US 59 at Creekwood Drive Crossing Peach Creek

This bridge is located in Montgomery County within the Houston District in Texas. The TxDOT structure number for this bridge is 12-170-0177-05-119. The bridge is on US 59 at Creekwood Drive and crosses Peach Creek. The bridge was built in 1970 and has a length of 120 ft. It has three spans and is founded on 16-inch wide, approximately 35-ft long square piles. The soil at the site is sand. This bridge has been deemed scour critical by a concise analysis. This case history has flow records but does not have site-specific EFA test data.

9.1.1.10. Application No. 10: Bridge on US 90A WB Crossing Brazos River

This bridge is located the Houston District in Texas. The TxDOT structure number for this bridge is 12-080-0027-08-092. The bridge is on US 90A WB and crosses the Brazos River. The bridge was built in 1965 and has a length of 942 ft. It has 10 spans and is founded on 16-inch to 20-inch square piles. The pile lengths vary between 70 ft and 78 ft. The soil at the site is silty sand and clayey sand. This bridge has been deemed scour critical by a concise analysis. This case history has both flow records and site-specific EFA test data.

9.1.1.11. Application No. 11: Bridge on SH 7 Crossing Navasota River

This bridge is located in Leon County within the Bryan District in Texas. The TxDOT structure number for this bridge is 17-145-0382-05-021. The bridge is on SH 7 and crosses the Navasota River. The bridge was built in 1956 and has a length of 271 ft. It has seven spans and is founded on 14-inch wide concrete piles that vary between 28 ft and 50 ft in length. The soil at the site is sand. This bridge has been deemed stable by a concise analysis. This case history has both flow records and site-specific EFA test data.

9.1.1.12. Application No. 12: Bridge on SH 22 Crossing North Bosque River

This bridge is located in Bosque County within the Waco District in Texas. The TxDOT structure number for this bridge is 09-018-0121-01-038. The bridge is on SH 22 and crosses the North Bosque River. The bridge was built in 1940 and has a length of 566 ft. It has 12 spans and is founded on 4-ft thick footings embedded 15 ft to 35 ft below the channel bottom. The footings for 9 of the 11 piers are supported by steel piling that is set into shale and soft sandstone. The remaining 2 piers are on footings embedded approximately 1 ft into shale and soft sandstone. Generally, the geomaterial at the site is sand, gravel, soft sandstone, and shale. The material within the depth of interest, however, is the sand and gravel, which extend approximately 3 ft below the top of footing level. This bridge is on the scour-critical list.

9.1.1.13. Application No. 13: Bridge on SH 80 Crossing San Marcos River

This bridge is located in the Austin District in Texas. The TxDOT structure number for this bridge is 14-028-0287-01-014. The bridge is on SH 80 and crosses the San Marcos River. The bridge was built in 1939 and has a length of 579 ft. It has 11 spans and is founded on 16-inch wide concrete piles that vary between 20 ft and 50 ft in length. The soil in the site is silty sand and sand. This bridge is not on the scour-critical list.

9.1.1.14. Application No. 14: Bridge on SH 35 NB Crossing Sims Bayou

This bridge is located in the Houston District in Texas. The TxDOT structure number for this bridge is 12-102-0178-01-060. The bridge is on SH 35 NB and crosses Sims Bayou. The bridge was built in 1948 and has a length of 200 ft. It has five spans and is founded on 30-inch diameter drilled shafts that vary between 35 ft and 55 ft in length. The soil at the site is clay and sand. This bridge is not on the scour-critical list.

9.1.1.15. Application No. 15: Bridge on SH 75 Crossing Bedias Creek

This bridge is located in the Bryan District in Texas. The TxDOT structure number for this bridge is 17-154-0166-07-047. The bridge is on SH 75 and crosses Bedias Creek. The bridge was built in 1947 and has a length of 892 ft. It has 29 spans and is founded on precast concrete piles and spread footings. The piles are 16 inches wide and embedded a minimum 30 ft below ground

level. The spread footings are embedded 15 ft to 24 ft below the channel bed. The soil at the site is sand and sandy clay. This bridge is on the scour-critical list.

9.1.1.16. Application No. 16: Bridge on SH 90 Crossing Bedias Creek

This bridge is located in the Bryan District in Texas. The TxDOT structure number for this bridge is 17-154-0315-01-070. The bridge is on SH 90 and crosses Bedias Creek. The bridge was built in 1976 and has a length of 200 ft. It has five spans and is founded on 28-inch to 32-inch treated timber piles that vary between 30 ft and 35 ft in length. The site is underlain by sandy clay and silt. This bridge is not on the scour-critical list.

9.1.2. Results of Application

9.1.2.1. Results of Application

The results of the application of BSA 1 on scour-critical bridges are shown in [Table 9-2](#). Out of the 16 bridges, 6 bridges that were designated as scour critical by TxDOT were found to be stable by BSA 1. Of the 16, 3 bridges could not be evaluated for BSA 1 due to reasons explained in the footnotes of [Table 9-2](#). The remaining 7 bridges had outcomes similar to the TxDOT designation. Out of the 7 bridges that had similar outcomes for both BSA 1 and the TxDOT designation, 3 were stable and 4 were scour critical. So, 6 of the 10 bridges that were originally scour critical and had sufficient information were found to be stable after BSA 1 according to the stability criterion.

Out of the 4 bridges that remained scour critical after BSA 1, 2 bridges did not have sufficient information for BSA 2 or BSA 3 to be carried out. The remaining 2 having sufficient information are Application No. 7 and Application No. 12. BSA 2 and BSA 3 were applied to these 2 cases, resulting in the bridges remaining as scour critical. The BSA 2 and BSA 3 calculations for Application No. 7 and Application No. 12 are shown in the next [sections 9.1.2.2](#) and [9.1.2.3](#).

9.1.2.2. BSA 2 on Application No. 7 and Application No. 12

Application No. 7

- From flow records, Q_{100} is 64,600 cfs.
- $B_2/B_1 = 0.69$.
- $V_{100} = 20$ ft/s (6.1 m/s) in the main channel. $V_{100} = 11$ ft/s (3.4 m/s) in the left and right overbanks.
- $H_1 = 47$ ft (14.3 m). The water level in this case is above the low chord of the bridge, creating pressure flow under the bridge.
- $D = 16$ inches (0.4 m).
- The soil underlying the site is a silty sand. V_c is taken as 0.06 ft/s (0.2 m/s).
- Kinematic viscosity of water at 68°F (20°C), $\nu = 1.1 \times 10^{-5}$ ft²/s (10^{-6} m²/s).
- Allowable scour depth $Z_{\text{thresh}} = 16.0$ ft (4.9 m).
- Age of the bridge $t_{\text{hyd}} = 46$ years.
- Maximum pier scour

$$Z_{\text{max,p}}(\text{mm}) = 0.18 \left(\frac{V_{\text{appro}} D}{\nu} \right)^{0.635}$$

$$Z_{\text{max,p}}(\text{mm}) = 0.18 \left(\frac{6.1 \times 0.4}{10^{-6}} \right)^{0.635}$$

$$= 2047.7$$

$$Z_{\text{max,p}} = 6.71 \text{ ft (2.05 m)}$$

- Maximum contraction scour

$$\begin{aligned}
 Z_{\max,c} &= 1.9H_1 \left[\frac{1.38V_{\text{appr}}}{R_c\sqrt{gH_1}} - \frac{V_c}{\sqrt{gH_1}} \right] \\
 &= 1.9(14.3) \left[\frac{1.38(6.1)}{0.69\sqrt{9.81 \times 14.3}} - \frac{0.2}{\sqrt{9.81 \times 14.3}} \right] \\
 &= 90.9 \text{ ft (27.7 m)}
 \end{aligned}$$

Total maximum scour depth = 6.71 ft + 90.9 ft = 97.6 ft (29.8 m). The maximum scour depth from BSA 2 for Application No. 7 exceeds Z_{thresh} . Therefore, under BSA 2, the bridge remains scour critical.

Application No. 12

- From the 2009 USGS Regional Regression Equation, Q_{100} is 101,000 cfs.
- $B_2/B_1 = 0.91$.
- $V_{100} = 14$ ft/s (4.3 m/s) in the main channel. $V_{100} = 3$ ft/s (0.9 m/s) in the left and right overbanks.
- $H_1 = 41$ ft (12.5 m). The water level in this case is above the low chord of the bridge, creating pressure flow under the bridge.
- $D = 3.28$ ft (1.0 m).
- The soil underlying the site is gravel and sand. V_c is taken as 2.3 ft/s (0.7 m/s).
- Kinematic viscosity of water at 68°F (20°C), $\nu = 1.1 \times 10^{-5}$ ft²/s (10^{-6} m²/s).
- Allowable scour depth Z_{thresh} is 16.0 ft (4.9 m) at Bent 8 and 12.0 feet (3.7 m) at Bent 9.
- Age of the bridge $t_{\text{hyd}} = 75$ years.

- Maximum pier scour

$$Z_{\max,p}(\text{mm}) = 0.18 \left(\frac{V_{\text{appro}} D}{v} \right)^{0.635}$$

$$Z_{\max,p}(\text{mm}) = 0.18 \left(\frac{4.3 \times 1.0}{10^{-6}} \right)^{0.635}$$

$$= 2934$$

$$Z_{\max,p} = 9.6 \text{ ft (2.9 m)}$$

- Maximum contraction scour

$$Z_{\max,c} = 1.9H_1 \left[\frac{1.38V_{\text{appr}}}{R_c\sqrt{gH_1}} - \frac{V_c}{\sqrt{gH_1}} \right]$$

$$= 1.9(12.5) \left[\frac{1.38(4.3)}{0.91\sqrt{9.81 \times 12.5}} - \frac{0.7}{\sqrt{9.81 \times 12.5}} \right]$$

$$= 41.2 \text{ ft (12.6 m)}$$

Total maximum scour depth = 9.6 ft + 41.2 ft = 50.8 ft (15.5 m). The maximum scour depth from BSA 2 for Application No. 12 exceeds Z_{thresh} . Therefore, under BSA 2, the bridge remains scour critical.

9.1.2.3. BSA 3 on Application No. 7 and Application No. 12

Application No. 7

- Since the maximum total scour depth is very much larger than Z_{thresh} , a simpler and more optimistic approach was taken to assess the time dependent scour depth for Application No. 7.
- In 2007, the measured scour depth was 5.7 ft. The bridge was built in 1961. As a simple and optimistic approach, the erosion rate is estimated as the measured scour depth over the age of the bridge when the measurement was made:

$$\dot{Z} = \left(\frac{5.7 \text{ ft}}{46 \text{ yrs}} \right) = 0.00016 \text{ inch/hr} = 0.0043 \text{ mm/hr}$$

- The equivalent time

$$\begin{aligned} t_{eq,p}(\text{hr}) &= 73[t_{hyd}(\text{yrs})]^{0.126}[V_{max}(\text{m/s})]^{1.706}[\dot{Z}_i(\text{mm/hr})]^{-0.20} \\ &= 73[46]^{0.126}[6.1]^{1.706}[0.0043]^{-0.20} \\ &= 7690 \text{ hrs} \end{aligned}$$

$$\begin{aligned} t_{eq,c}(\text{hr}) &= 644.32[t_{hyd}(\text{yrs})]^{0.4242}[V_{max}(\text{m/s})]^{1.648}[\dot{Z}_i(\text{mm/hr})]^{-0.605} \\ &= 644.32[46]^{0.4242}[6.1]^{1.648}[0.0043]^{-0.605} \\ &= 1,739,477 \text{ hrs} \end{aligned}$$

- Final scour depth

$$\begin{aligned} Z_{fin,p} &= \frac{t_{eq,p}}{\frac{1}{Z_i} + \frac{t_{eq,p}}{Z_{max,p}}} \\ &= \frac{7690}{\frac{1}{(0.0043/1000)} + \frac{7690}{2.05}} \\ &= 0.11 \text{ ft (0.03 m)} \end{aligned}$$

$$\begin{aligned} Z_{fin,c} &= \frac{t_{eq,c}}{\frac{1}{Z_i} + \frac{t_{eq,c}}{Z_{max,c}}} \\ &= \frac{1,739,477}{\frac{1}{(0.0043/1000)} + \frac{1,739,477}{27.7}} \\ &= 19.3 \text{ ft (5.9 m)} \end{aligned}$$

Even with the use of a very optimistically low erosion rate, the scour depth still exceeds Z_{thresh} . Therefore, more refined calculations are unnecessary. Furthermore, pressure flow,

which would lead to larger scour depth, was not considered in the analysis. The bridge remains scour critical.

Application No. 12

- The equivalent time,

\dot{Z} is taken as 39.4 inch/hr (1000 mm/hr) under a velocity of 14.1 ft/s (4.3 m/s)

$$\begin{aligned} t_{eq,p}(\text{hr}) &= 73[t_{hyd}(\text{yrs})]^{0.126}[V_{max}(\text{m/s})]^{1.706}[\dot{Z}_i(\text{mm/hr})]^{-0.20} \\ &= 73[75]^{0.126}[4.3]^{1.706}[1000]^{-0.20} \\ &= 380 \text{ hrs} \end{aligned}$$

$$\begin{aligned} t_{eq,c}(\text{hr}) &= 644.32[t_{hyd}(\text{yrs})]^{0.4242}[V_{max}(\text{m/s})]^{1.648}[\dot{Z}_i(\text{mm/hr})]^{-0.605} \\ &= 644.32[75]^{0.4242}[4.3]^{1.648}[1000]^{-0.605} \\ &= 681 \text{ hrs} \end{aligned}$$

- Final scour depth

$$\begin{aligned} Z_{fin,p} &= \frac{t_{eq,p}}{\frac{1}{Z_i} + \frac{t_{eq,p}}{Z_{max,p}}} \\ &= \frac{380}{\frac{1}{(1000/1000)} + \frac{380}{2.9}} \\ &= 9.5 \text{ ft (2.9 m)} \end{aligned}$$

$$\begin{aligned}
Z_{\text{fin,c}} &= \frac{t_{\text{eq,c}}}{\frac{1}{Z_i} + \frac{t_{\text{eq,c}}}{Z_{\text{max,c}}}} \\
&= \frac{681}{\frac{1}{(1000/1000)} + \frac{681}{12.6}} \\
&= 41.3 \text{ ft (12.55 m)}
\end{aligned}$$

$$\begin{aligned}
Z_{\text{fin,l}} &= Z_{\text{fin,p}} + Z_{\text{fin,c}} \\
&= 9.5 \text{ ft} + 41.3 \text{ ft} \\
&= 50.8 \text{ ft (15.5 m)}
\end{aligned}$$

The bridge still remains scour critical because $Z_{\text{fin,l}}$ from BSA 3 exceeds Z_{thresh} .

Table 9-2. Comparison between BSA 1 Outcome and the Current TxDOT Scour Designation for the 18 Bridges.

Application No.	Waterway	Highway	Scour Location	Z _{mo} (ft)	Z _{thresh} (ft)	V ₁₀₀ /V _{mo}	Z ₁₀₀ /Z _{mo} (from Chart)	Z ₁₀₀ (ft)	Outcome of BSA 1 (BSA 3 if specifically indicated)	TxDOT Current Scour Status
1	Sanders Creek	FM 39	Bent 5	1.5	11.3	1.05	1.10	1.7	Stable	Critical
2 ^s	Alligator Creek	US 287	Bent 3	13.1	16.0	1.04	1.20	15.7	Stable	Critical
3	Big Creek	SH 36	Bent 5	3.8	13.0	1.00	1.00	3.8	Stable	Critical
4	San Marcos River ^s	FM 2091	Bent 5	12.4	16.0	0.95	§	§	§	Critical
5 ^s	Mill Creek	FM 331	Bent 4	0.8	1.5	1.33	1.50	1.2	Stable	Critical
6 ^s	Guadalupe River	US 87	Bent 27	6.3	8.5	1.11	1.20	7.6	Stable	Critical
7	San Jacinto River	US 59 SB	Bent 15	5.7	16.0	1.11	1.20	19.4 [£]	Critical [£]	Critical
8	Dry Branch Creek	SH 27	Bent 4	9	13.0	1.11	†	†	†	Critical
9	Peach Creek	US 59 @ Creekwood Drive	Bent 2	8.5	21.0	1.20	1.35	11.5	Stable	Critical
			Bent 3	12.1	22.0			16.3		
10	Brazos River	US 90A WB	Bent 3	21	26.0	1.67	2.10	45.1	Critical [@]	Critical
11	Navasota River	SH7	Bent 5	8.1	13.0	1.17	1.35	11.0	Stable	Stable
12	North Bosque River	SH 22	Bent 8	5	16.0	1.43	1.55	50.0 [¥]	Critical [¥]	Critical
			Bent 9	8	12.0			50.0 [¥]		
13 ^s	San Marcos River	SH 80	Bent 8	7.5	12.0	0.95	1.00	7.5	Stable	Stable
			Bent 9	10	12.5			10		
14	Sims Bayou	SH 35 NB	Bent 4	4	20.0	1.11	1.20	4.8	Stable	Stable
15	Bedias Creek	SH 75	Bent 26	8	8.0	1.18	1.30	10.4	Critical [@]	Critical
16	Bedias Creek*	SH 90	*	*	*	*	*	*	*	Stable

Notes:

[§] A large caisson was added in 1995 at the scour-critical pier. It was not possible to extrapolate Z_{mo} that corresponds to a smaller pier size to obtain Z_{fit} for a larger pier size.

[†] Soil information unclear. Assessment could not be carried out.

* Channel excavation was carried out, and no corresponding date was indicated in the bridge folder.

^s Although the evaluation of these bridges indicates that they are stable with respect to scour, TxDOT's practice would be to carefully monitor these bridges and to visit them either during or immediately after a high flow event due to Z₁₀₀ being nearly equal to Z_{thresh}.

[@] BSA 2 or BSA 3 could not be carried out due to insufficient information.

[£] Outcome of BSA 3 using optimistic erosion rate.

[¥] Outcome of BSA 3.

10. CONCLUSIONS

10.1. GENERAL

The topic addressed is the assessment of bridges for scour. The scour components included in BSA 1 are pier and contraction scour. Abutment scour was not included because the Texas Department of Transportation recommends not including abutment scour in their bridge scour assessment ([Texas Department of Transportation 2006](#)). However, for BSA 2, the option of including the maximum abutment scour was included in the procedure for completeness. In BSA 3, the time dependent abutment scour was not included as this work is ongoing at Texas A&M University. The proposed method eliminates site-specific erosion testing and uses actual measured scour data. It is economical, relatively simple, and improves on the over-conservative nature of previous bridge scour assessment procedures especially in erosion-resistant soils.

10.2. ERODIBILITY OF GEOMATERIALS

The erodibility of soil or rock is defined as the relationship between the erosion rate, \dot{Z} , and the velocity of water, V , at the soil/rock-water interface. This definition, however, is not very satisfactory because the velocity varies in direction and intensity in the flow field ([Briaud 2008](#)). To be exact, the velocity of water is zero at the soil/rock interface. A more adequate definition is the relationship between the erosion rate \dot{Z} and the shear stress τ at the soil/rock interface. However, the velocity is often used because it is easier to gauge an erosion problem from a velocity standpoint.

One of the most important material parameters in soil erosion is the threshold of erosion ([Briaud 2008](#)). Below the threshold value, erosion does not take place. Once the applied hydraulic shear stress (or more simply the velocity) exceeds the threshold value, erosion is initiated until the equilibrium scour depth is obtained. The threshold values for erosion in terms of shear stress are the critical shear stress τ_c and in terms of velocity the critical velocity V_c . Important parameters that assist in describing the erosion function include the threshold value, the initial rate of scour, and the equilibrium scour depth. The erosion rate in clays and rocks can be many times smaller than the erosion rate in sands.

From the erodibility standpoint, the main contributions of this report are the erosion threshold charts and erosion function charts. These charts can be used in BSA 2 and BSA 3 to obtain the critical velocity and erosion rates when EFA data is not available.

10.3. BRIDGE SCOUR ASSESSMENT 1

Bridge Scour Assessment 1 is a bridge scour assessment procedure that makes use of existing data collected either from bridge records maintained by the authorities or by site visit (Govindasamy et al. 2008). It is the first level of bridge scour assessment within the bridge scour assessment framework proposed in this report. The main idea behind the BSA 1 procedure is that the scour depth corresponding to a specified future flood event is obtained from historical and site-specific scour depth observations (Z_{mo}), from historical and site-specific maximum flood observations (V_{mo}), and extrapolation charts that relate the future scour depth ratio (Z_{fut}/Z_{mo}) to the future velocity ratio (V_{fut}/V_{mo}). Here, Z_{fut} is the scour depth corresponding to a specified future flood, Z_{mo} is the maximum observed scour at the bridge, V_{fut} is the velocity corresponding to the specified future flood, and V_{mo} is the maximum velocity ever observed at the bridge until the time Z_{mo} is measured. The extrapolation charts are termed the Z-Future Charts. The vulnerability associated with scour depends on the comparison between Z_{fut} and the allowable scour depth of the foundation, Z_{thresh} . BSA 1 is summarized in two flowcharts that are presented in a decision tree format: BSA 1 (Uniform Deposit) and BSA 1 (Multilayer Analysis).

10.4. BRIDGE SCOUR ASSESSMENT 2

Bridge Scour Assessment 2 is the assessment procedure that has to be carried out if BSA 1 did not conclude with a specific plan of action for the bridge. The plan of action could be in the form of a recommendation for regular monitoring if the bridge is found to have minimal risk, special action such as specialized scour monitoring, or immediate action to prevent scour-induced failure. BSA 2 is a process that determines the scour vulnerability by first calculating the maximum scour depth. The maximum bridge scour depth concept is based on the assumption that the bridge will experience the maximum possible scour depth (equilibrium scour depth) within its lifetime. This might not be the case for some more erosion-resistant materials such as

clays and some rocks. In BSA 2, the maximum scour at the bridge, termed maximum total local scour ($Z_{\max,l}$), is the arithmetic sum of the three components of scour, i.e., maximum pier scour ($Z_{\max,p}$), maximum contraction scour ($Z_{\max,c}$), and maximum abutment scour ($Z_{\max,a}$). The vulnerability associated with scour depends on the comparison between the maximum total local scour depth and the allowable scour depth of the bridge. BSA 2 is represented by a flowchart presented in decision tree format.

10.5. BRIDGE SCOUR ASSESSMENT 3

Bridge Scour Assessment 3 is the assessment procedure that has to be carried out if BSA 2 did not conclude with a specific plan of action for the bridge. The plan of action could be in the form of recommendations for regular monitoring if the bridge is found to have minimal risk, special action such as specialized scour monitoring, or immediate action to prevent scour-induced failure. BSA 3 analysis also has to be carried out if the maximum calculated scour depth in BSA 2 extends beyond the topmost layer in the presence of a layered geologic profile. BSA 3 involves the calculation of time-dependent scour depth, which is the scour depth after a specified time, rather than simply using the maximum scour depth. This method is valuable in the case of clays and some rocks that have high erosion resistance (low erosion rate) and do not achieve the maximum scour depth as computed in BSA 2 within the lifetime of the bridge. The time-dependent scour depth is termed the final scour depth, Z_{fin} . In BSA 3, the total final local scour depth at the bridge, termed the final local scour ($Z_{\text{fin},l}$), is the arithmetic sum of the three components of scour, i.e., final pier scour ($Z_{\text{fin},p}$), final contraction scour ($Z_{\text{fin},c}$), and final abutment scour ($Z_{\text{fin},a}$). Similar to BSA 2, the vulnerability associated with scour depends on the comparison between the total final scour depth, $Z_{\text{fin},l}$, and the allowable scour depth of the bridge, Z_{thresh} . BSA 3 is represented by two flowcharts that are presented in decision tree format: BSA 3 (Time Analysis) and BSA 3 (Multilayer Time Analysis). The outcome of BSA 3 is a conclusive plan of action for the bridge.

10.6. HYDRAULIC PARAMETER FOR BSA 1 FROM HYDROLOGIC ANALYSIS

The hydraulic parameter required for BSA 1 is the velocity ratio $V_{\text{fut}}/V_{\text{mo}}$, where V_{fut} is the flow velocity corresponding to a specified future flow Q_{fut} and V_{mo} is the flow velocity corresponding to the maximum flow Q_{mo} experienced by the bridge during its life. The hydraulic and hydrologic analysis in this report refers to V_{100} and Q_{100} as normalizing values. The 100-year flood is the flood that has a 1 percent chance of being exceeded in any one year. In order to know the flow history at a bridge, a flow gage should be installed at that location to collect data during floods. However, most bridges do not have pre-installed flow gages. Indeed, in the state of Texas, there are approximately 900 flow gages compared to 42,208 bridges over waterways (Olona 1992).

For bridges being assessed for scour that have gages and flow history, the determination of the velocity ratio V_{100}/V_{mo} can be done by estimating $Q_{\text{fut}} = Q_{100}$ through flood frequency analysis and determining Q_{mo} directly from the flow history. These values are then converted into explicit values of V_{100} and V_{mo} using a simplified hydraulic analysis program developed specifically for this project (TAMU-FLOW).

For ungaged bridges, the velocity ratio V_{100}/V_{mo} is determined without estimating the explicit values of V_{100} and V_{mo} . To obtain the velocity ratio, the recurrence interval of Q_{mo} , termed $RI_{Q_{\text{mo}}}$, is determined by using the $RI_{Q_{\text{mo}}}$ of nearby gages. This process calls for engineering judgment and local experience and information and is aided by an interpolation technique provided by the program TAMU-FLOOD. Subsequently, $RI_{Q_{\text{mo}}}$ is converted into the flow ratio (Q_{mo}/Q_{100}) using a relationship between this ratio and $RI_{Q_{\text{mo}}}$ developed in this project. Finally, the velocity ratio V_{100}/V_{mo} is obtained from the flow ratio Q_{100}/Q_{mo} using Manning's equation. This process is incorporated into the computer program TAMU-FLOOD, which was also developed specifically for this project. This computer program ultimately generates a map of recurrence intervals of flows for the state of Texas.

10.7. HYDRAULIC PARAMETERS FOR BSA 2 AND BSA 3 FROM HYDROLOGIC ANALYSIS

In the case of BSA 2 and BSA 3, the explicit value of V_{100} is required. V_{100} is required to estimate the scour depth corresponding to the 100-year flood. For BSA 2, this would be the maximum scour depth corresponding to the 100-year flood. For BSA 3, this would be the time-dependent scour depth corresponding to the 100-year flood. In the case of BSA 3, V_{mo} could be required to determine the scour depth at the bridge site due to its flow history. This value is then compared against the measured value in the field to give the inspecting engineer an idea of how calculated values using BSA 3 compare with measured scour depths.

For gaged bridges, V_{100} and V_{mo} can be determined by applying exactly the same methodology used in BSA 1. For ungaged basins, $RI_{Q_{mo}}$ at the bridge is determined using TAMU-FLOOD and then converted into Q_{mo} using the USGS regional regression equations for Texas. Subsequently, Q_{mo} is converted into V_{mo} using TAMU-FLOW. In a similar manner, Q_{100} can be determined using the regional regression equations, from which V_{100} is estimated using TAMU-FLOW.

10.8. VALIDATION OF THE PROPOSED ASSESSMENT METHOD

Several full case histories were selected for the validation of the proposed bridge scour assessment procedure. The required information was soil data, flow data, age of the bridge, foundation type and dimensions, and scour depths. There were 11 cases that were considered adequate and suitable and were used in the validation process.

The bridge records for the case histories had limited bridge scour measurements. In fact, there were no bridge scour measurements taken before the year 1991. Since most of the bridges were reasonably old (up to approximately 80 years old), they had experienced the largest flow velocity prior to the first bridge scour measurement. This resulted in all the cases having a V_{fut}/V_{mo} ratio equal to or less than unity for the BSA 1 validation. Results of the BSA 1 validation, shown in [Figure 8-2](#), show good agreement between predicted and measured values. However, this validation is only for V_{fut}/V_{mo} ratios equal to or less than unity. [Figure 8-3](#) shows that the results of the validation of BSA 2 show good agreement between the BSA 2 method and

the SRICOS-EFA Method. The validation of BSA 3 indicates that BSA 3 tends to overestimate the scour depth when compared to field measurements. This could be due to the fact that the selection of erosion categories on the basis of soil type is very conservative (by design). However, BSA 3 does improve on the over-estimation of scour depth by 2 ft to 4 ft when compared to maximum scour depths.

10.9. APPLICATION TO SCOUR-CRITICAL BRIDGES

BSA 1 was applied to 10 scour critical and 3 non scour critical bridges. Results of the application of BSA 1 on scour-critical bridges are shown in [Table 9-2](#). In this process, 6 of the 10 scour critical bridges were found to be stable and could be removed from the scour critical list and the 3 non scour critical bridges were confirmed as non scour critical. Out of the 4 bridges that remained scour critical after BSA 1, 2 bridges did not have sufficient information for BSA 2 or BSA 3 to be carried out. The remaining 2 having sufficient information remained scour critical after BSA 2 and BSA 3 were carried out.

10.10. RECOMMENDATIONS

The following are the researchers' recommendations:

- Studies should be carried out to quantify the amount of infilling that takes place in live-bed scour conditions. This could be in the form of scour-monitoring methods or sediment transport analysis.
- The level of risk associated with employing BSA 1 should be studied and addressed. It would be meaningful to determine the probability of the $Z_{\text{fut}}/Z_{\text{mo}}$ ratios predicted using BSA 1 exceeding field values.
- The time-dependent abutment scour depth should be addressed and included in BSA 1 and BSA 3.

11. REFERENCES

- Adams, L., R.N. Palmer, and G. Turkiyyah (1995). "An expert system for evaluating scour potential and stream stability at bridges." Proceedings of the 22nd Annual National Conference, Water Resources Planning and Management Division, ASCE, Cambridge, Massachusetts, May, pp. 786-789.
- Aranda, D.F.C. (2001). "Contrast of five fitting methods of the general extreme values distribution from 31 historical records of annual maximum events." *Ingenieria Hidraulica En Mexico*, Vol. 16, No. 2, pp. 77-92.
- Asquith, W.H. and R.M. Slade, Jr. 1995a, "Documented and potential extreme peak discharges and relation between potential extreme peak discharges and probable maximum flood peak discharges in Texas: U.S. Geological Survey Water-Resources Investigations Report"
- Asquith, W.H. and R.M. Slade, Jr. (1996). "Water Resources Investigation Report 96-4307: Regional equations for estimation of peak-streamflow frequency for natural basins in Texas."
- Asquith, W. H., and Thompson, B. D (2008). "Scientific Investigation Report 2008-5084: Alternative Regression Equations for Estimation of Annual Peak-Streamflow Frequency for Undeveloped Watersheds in Texas using PRESS Minimization"
- Asquith, W. H. and Roussel, M. C. (2009). "Regression Equations for Estimation of Annual Peak-Streamflow Frequency for Undeveloped Watersheds in Texas Using an L-moment-Based, PRESS-Minimized, Residual-Adjusted Approach", Scientific Investigation Report 2009-5087, USGS.
- Ayres Associates (2004). "Plans of action for scour critical bridges." Office Manual, Idaho Transportation Department, Boise, Idaho.
- Briaud, J.-L. (2008). "Case histories in soil and rock erosion: Woodrow Wilson Bridge, Brazos River meander, Normandy Cliffs, and New Orleans levees." 2007 Ralph B. Peck Lecture, *Journal of Geotechnical and Geoenvironmental Engineering*, ASCE, Vol. 134, No. 10, pp. 1425-1447.
- Briaud, J.-L., F.C.K. Ting, H.-C. Chen, R. Gudavalli, S. Perugu, and G. Wei (1999). "SRICOS: Prediction of scour rate in cohesive soils at bridge piers." *Journal of Geotechnical and Geoenvironmental Engineering*, ASCE, Vol. 125, No. 4, pp. 237-246.
- Briaud, J.-L., F.C.K. Ting, H.-C. Chen, Y. Cao, S.W. Han, and K.W. Kwak (2001a). "Erosion Function Apparatus for scour rate predictions." *Journal of Geotechnical and Geoenvironmental Engineering*, ASCE, Vol. 127, No. 2, pp. 105-113.
- Briaud, J.-L., H.-C. Chen, K.W. Kwak, S.W. Han, and F.C.K. Ting (2001b). "Multiflood and multilayer method for scour rate prediction at bridge piers." *Journal of Geotechnical and Geoenvironmental Engineering*, ASCE, Vol. 127, No. 2, pp. 114-125.

- Briaud, J.-L., H.-C. Chen, Y. Li, P. Nurtjahyo, and J. Wang (2004). "Pier and contraction scour in cohesive soils." National Cooperative Highway Research Program Report 516, Transportation Research Board, Washington, D.C.
- Briaud, J.-L., H.-C. Chen, Y. Li, P. Nurtjahyo, and J. Wang (2005). "SRICOS-EFA method for contraction scour in cohesive soils." *Journal of Geotechnical and Geoenvironmental Engineering*, ASCE, Vol. 131, No. 10, pp. 1283-1294.
- Briaud J.-L., H.-C. Chen, K.-A. Chang, S. Oh, and X. Chen (2009). "Abutment scour in cohesive materials." NCHRP Report 24-15(2), Transportation Research Board, National Academy of Sciences, Washington, D.C. (upcoming report)
- California Department of Transportation (2007). "Scour plan of action." Division of Maintenance, <http://www.dot.ca.gov/hq/structur/strmaint/scour.htm#SamplePOA>. Accessed on November 4, 2008.
- Cao, Y., J. Wang, J.-L. Briaud, H.-C. Chen, Y. Li, and P. Nurtjahyo (2002). "EFA tests and the influence of various factors on the erodibility of cohesive soils." Proceedings of the First International Conference on Scour of Foundations, Texas A&M University, College Station, Texas.
- Cato, K.D. (1991). "Performance of geologic materials under hydraulic stress." PhD Dissertation, Department of Geology, Texas A&M University, College Station, Texas, 272 p.
- Colorado Highway Department (1990). "Colorado bridge safety assurance procedure for Colorado Highway Department." Report Ref. 1514, Denver, Colorado.
- Cunnane, C. (1978) "Unbiased plotting positions – A review." *Journal of Hydrology*, Volume 37, Issues 3-4, May 1978, Pages 205-222.
- Delphia, J. (2008). Written communication, e-mail to Anand V. Govindasamy on May 6, 2008.
- Dingman, S.L. (2001). "Physical hydrology." Prentice Hall, New York, NY.
- Farquharson, F.A.K., J.R. Meigh, and J.V. Sutcliffe (1992). "Regional flood frequency analysis in arid and semiarid areas." *Journal of Hydrology*, Vol. 138, No. 3-4, pp. 487-501.
- Federal Highway Administration (1991). "Evaluating scour at bridges." Technical Advisory T 5140.23, Washington, D.C.
- Federal Highway Administration (2004). "National bridge inspection standards." Washington, D.C.
- Froehlich, D.C. (1989a). "Abutment scour prediction." Presentation, Transportation Research Board, Washington, D.C. Froehlich, D.C. (1989b). "Local scour at bridge abutments." Proceedings of the 1989 National Conference on Hydraulic Engineering, New Orleans, Louisiana.

- Govindasamy, A.V., J.-L. Briaud, H.-C. Chen, J. Delphia, K. Elsbury, P. Gardoni, G. Herrman, D. Kim, C.C. Mathewson, M. McClelland, and F. Olivera (2008). "Simplified method for estimating scour at bridges." GeoCongress 2008, New Orleans, Louisiana.
- Gudavalli, R., F. Ting, H.-C. Chen, S. Perugu, and G. Wei (1997). "Flume tests to study scour rate of cohesive soils." Research Report prepared for Texas Department of Transportation, Department of Civil Engineering, Texas A&M University, College Station, Texas.
- Haas, C., J. Weissmann, and T. Groll (1999). "Remote bridge scour monitoring: A prioritization and implementation guideline." Report No. TX-00/0-3970-1, Texas Department of Transportation Research and Technology Transfer Section/Construction Division Austin, May, p. 194.
- Harmsen, P., R. Palmer, and G. Turkiyyah (2001). "Development and application of an expert system for evaluation of scour and stream stability." Civil and Environmental Systems, Overseas Publishers Association, Vol. 18, No. 3, pp. 171-192.
- Hjulström, F. (1935). "The morphological activity of rivers as illustrated by river Fyris." Bulletin of the Geological Institute, Uppsala No. 25, Chapter 3, p. 221.
- Holnbeck, S.R., and C. Parrett (1997). "Method for rapid estimation of scour at highway bridges based on limited site data." Water-Resources Investigations Report 96-4310, United States Geological Survey, Helena, Montana, p. 79.
- Hosking, J.R.M. (1985). "Maximum-likelihood estimation of the parameters of the Generalized Extreme Value distribution." Applied Statistics, Vol. 34, pp. 3001-3010.
- Hosking, J.R.M., and J.R. Wallis (1996). "Regional frequency analysis of floods in central Appalachia." Research Report RC20349, IBM Research, Yorktown Heights, New York.
- Huizinga, R.J., and P.H. Rydlund (2004). "Potential-scour assessments and estimates of scour depth using different techniques at selected bridge sites in Missouri." Scientific Investigations Report 2004-5213, United States Geological Survey, p. 41.
- Johnson, P.A. (2005). "Preliminary assessment and rating of stream channel stability near bridges." Journal of Hydraulic Engineering, Vol. 131, No. 10, pp. 845-852.
- Jones, J.S., and J.E.P. Ortiz (2002). "Approach to developing a plan of action for scour critical bridges." Presentation, Transportation Research Board Annual Meeting, Washington, D.C.
- Kattell, J., and M. Eriksson (1998). "Bridge scour evaluation: Screening, analysis & countermeasures." United States Department of Agriculture Forest Service, San Dimas, California.
- Kumar, R., and C. Chatterjee (2005). "Regional flood frequency analysis using L-moments for North Brahmaputra region of India." Journal of Hydrologic Engineering, Vol. 10, No. 1, pp. 1-7.

- Lagasse, P.F., J.D. Schall, F. Johnson, E.V. Richardson, and F. Chang (1995). "Stream stability at highway structures." Federal Highway Administration Report No. FHWA-IP-90-014 (HEC-20), Washington, D.C., p. 144.
- Leung A. (1996). "Perfecting bridge inspecting (use of multimedia technology for data acquisition and storage)." *Civil Engineering*, Vol. 66, No. 3, p. 59-60.
- National Climate Data Center (2008), <http://www.ncdc.noaa.gov/oa/about/about.html#dataprod>, Accessed on 6/1/2008.
- National Transportation Safety Board (1987). "Collapse of the New York Thruway (I-90) Bridge over the Schoharie Creek, near Amsterdam, New York, April 5, 1987." Highway Accident Reports, NTSB/HAR-88/02, United States Government, Washington, D.C.
- Olona, S.B. (1992). "Texas Bridge Scour Evaluation Program." *Hydraulic Engineering: Saving a Threatened Resource—In Search of Solutions*, Proceedings of the Hydraulic Engineering sessions at Water Forum '92, ASCE, New York, New York, pp. 70-75.
- Palmer, R., G. Turkiyyah, and P. Harmsen. (1999). "CAESAR: An expert system for evaluation of scour and stream stability." National Cooperative Highway Research Program Report 426, Transportation Research Board, National Research Council, National Academy Press, Washington, D.C., p. 54.
- Palmer, R., G. Turkiyyah, P. Harmsen, D. Owens, S. Quan, L. Adams, S. Pollen, J. Shepard, and D. Landrum (1997). "CAESAR, an expert system for cataloging and expert evaluation of scour risk and river stability at bridge sites user's guide (draft)." Department of Civil Engineering, University of Washington, Seattle, Washington, p. 51.
- Pearson, D., S. Stein, and J.S. Jones (2002). "HYRISK methodology and users guide." Report FHWA-RD-02-XXX, Federal Highway Administration, Washington, D.C.
- Resource Consultants, Inc., and Colorado State University (1987). "Hydraulic, erosion, and channel stability analysis of the Schoharie Creek Bridge failure, New York." Report for the National Transportation Safety Board, Washington, D.C., and the New York State Thruway Authority, Albany, New York.
- Richardson, E.V., and S.M. Davis (2001). "Evaluating scour at bridges." Publication No. FHWA NHI 01-001, HEC No. 18, U.S. Dept. of Transportation, Washington, D.C.
- Richardson, E.V., D.B. Simons, and P.F. Lagasse (2001). "River engineering for highway encroachments—Highways in the river environment." FHWA NHI 01-004, Federal Highway Administration, Hydraulic Series No. 6, Washington, D.C.
- Rosbjerg, D., and H. Madsen (1995). "Uncertainty measures of regional flood frequency estimators." *Journal of Hydrology*, Vol. 167, pp. 209-224.

- Shields, A. (1936). "Anwendung der aehnlichkeitsmechanik und der turbulenzforschung auf die geschiebbewegung." Doktor-Ingenieurs dissertation, Technischen Hochschule, Berlin (in German).
- Simon, A., G.S. Outlaw, and R. Thoman (1989). "Evaluation, modeling and mapping of potential bridge scour, West Tennessee." Proceedings of the Bridge Scour Symposium, Subcommittee on Sedimentation, Interagency Advisory Committee on Water Data, co-sponsored by Federal Highway Administration and United States Geological Survey, pp. 112-139.
- Smith, J.A. (1987). "Estimating the upper tail of flood frequency distributions." Water Resources Research Vol. 23, No. 8, pp. 1657-1666.
- Stedinger, J.R., and L.-H. Lu (1995). "Appraisal of regional and index flood quantile estimators." Stochastic Hydrology and Hydraulics, Vol. 9, No. 1, pp. 49-75.
- Texas Department of Transportation (1993). "Texas secondary evaluation and analysis for scour (TSEAS)." Texas Bridge Scour Program, Division of Bridges and Structures, Austin, Texas, p. 12.
- Texas Department of Transportation (2006). "Geotechnical Manual." Manual Notice 2006-1, Austin, Texas.
- United States Army Corps of Engineers (1995). "Constructing quality management." Engineering Regulation No. 1180-1-6, Washington, D.C.
- United States Army Corps of Engineers (2008), HEC-RAS (2008).
<http://www.hec.usace.army.mil/software/hec-ras/>. Accessed on 6/1/2008.
- United States Department of the Interior Geological Survey (1982), "Bulletin 17B of the Hydrology Subcommittee – Guidelines For Determining Flood Frequency."
- United States Geological Survey (1993). "Aspects of the Tennessee level 1 bridge-scour assessment methodology applicable to the Texas secondary evaluation and analysis for scour." Prepared in cooperation with Design Division, Texas Department of Transportation, Austin, Texas.
- United States Geological Survey (1996). "Water-Resources Investigations Report 96-4307, Regional Equations for Estimation of Peak-Streamflow Frequency for Natural Basins in Texas."
- United States Geological Survey (2008). "USGS surface water for USA: Peak stream flow."
<http://nwis.waterdata.usgs.gov/usa/nwis/peak>. Accessed on 6/1/2008.
- Vogel, R.M., W.O. Thomas, and T.A. McMahon (1993). "Flood-flow frequency model selection in southwestern United States." Journal of Water Resources Planning and Management-ASCE, Vol. 119, No. 3, pp. 353-366.

- Wang, J. (2004). "The SRICOS-EFA Method for complex pier and contraction scour." Ph.D. Dissertation, Civil Engineering, Texas A&M University, College Station, Texas.
- Wang, Q.J. (1997). "LH moments for statistical analysis of extreme events." *Water Resources Research*, Vol. 33, No. 12, pp. 2841-2848.
- Wei, G., H.-C. Chen, F. Ting, J.-L. Briaud, R. Gudavalli, and S. Perugu (1997). "Numerical simulation to study scour rate in cohesive soils." Research report to the Texas Department of Transportation, Department of Civil Engineering, Texas A&M University, College Station, Texas.
- Wiss, Janney, Elstner Associates, Inc., and Mueser Rutledge Consulting Engineers (1987). "Collapse of the Thruway Bridge at Schoharie Creek for New York State Thruway Authority, Albany, NY."
- Wurbs, R.A., and W.P. James (2001), "Water resources engineering." Princeton Hall, New York, NY.
- Zaidman, M.D., V. Keller, A.R. Young, and D. Cadman (2003). "Flow-duration-frequency behaviour of British rivers based on annual minima data." *Journal of Hydrology*, Vol. 277, No. 3-4, pp. 195-213.

**APPENDIX A:
DATA ON Z-FUTURE CHARTS**

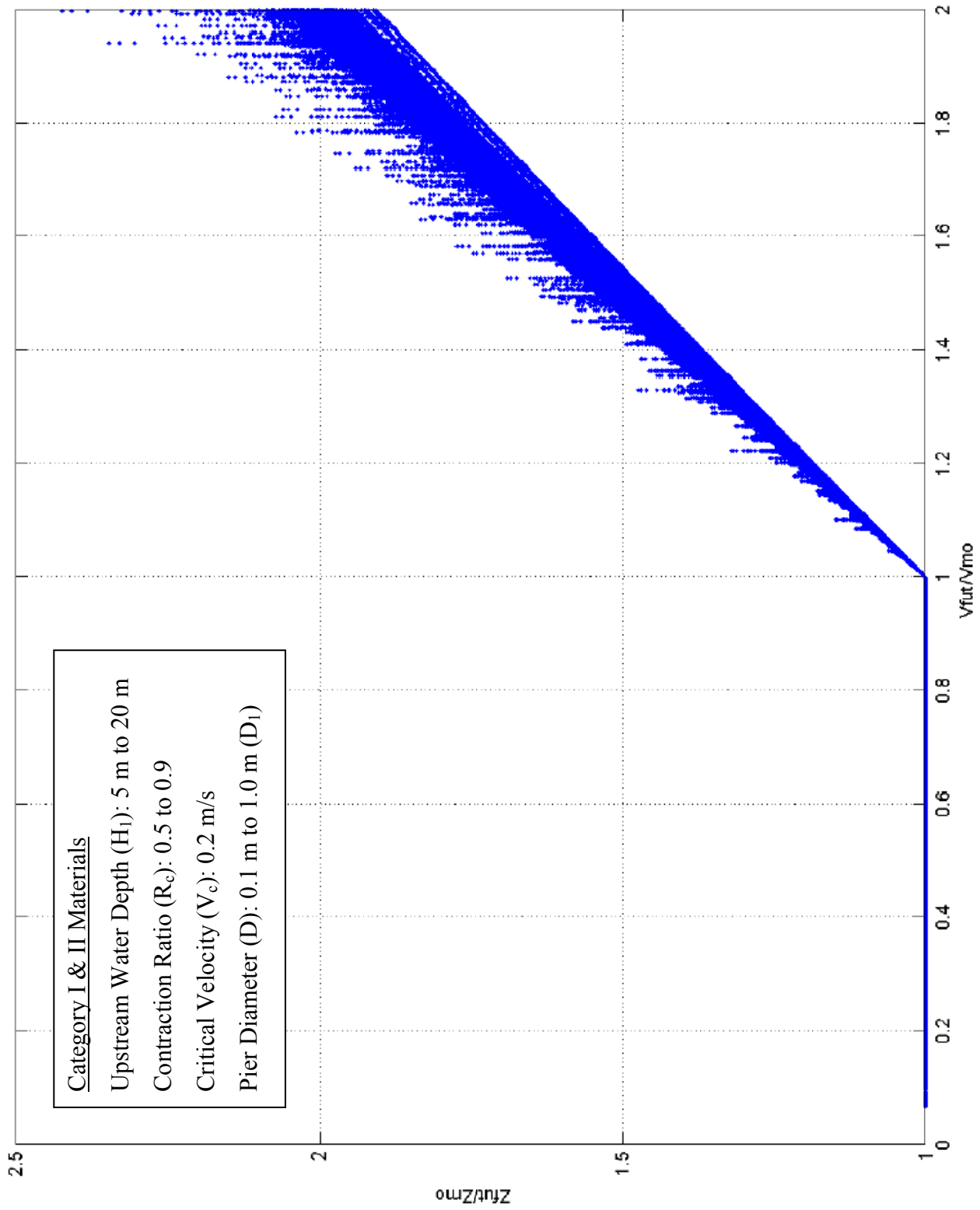


Figure A-1. Z-Future Chart Simulation Data for Category I and II Materials ($0.1 \text{ m} \leq D \leq 1.0 \text{ m}$).

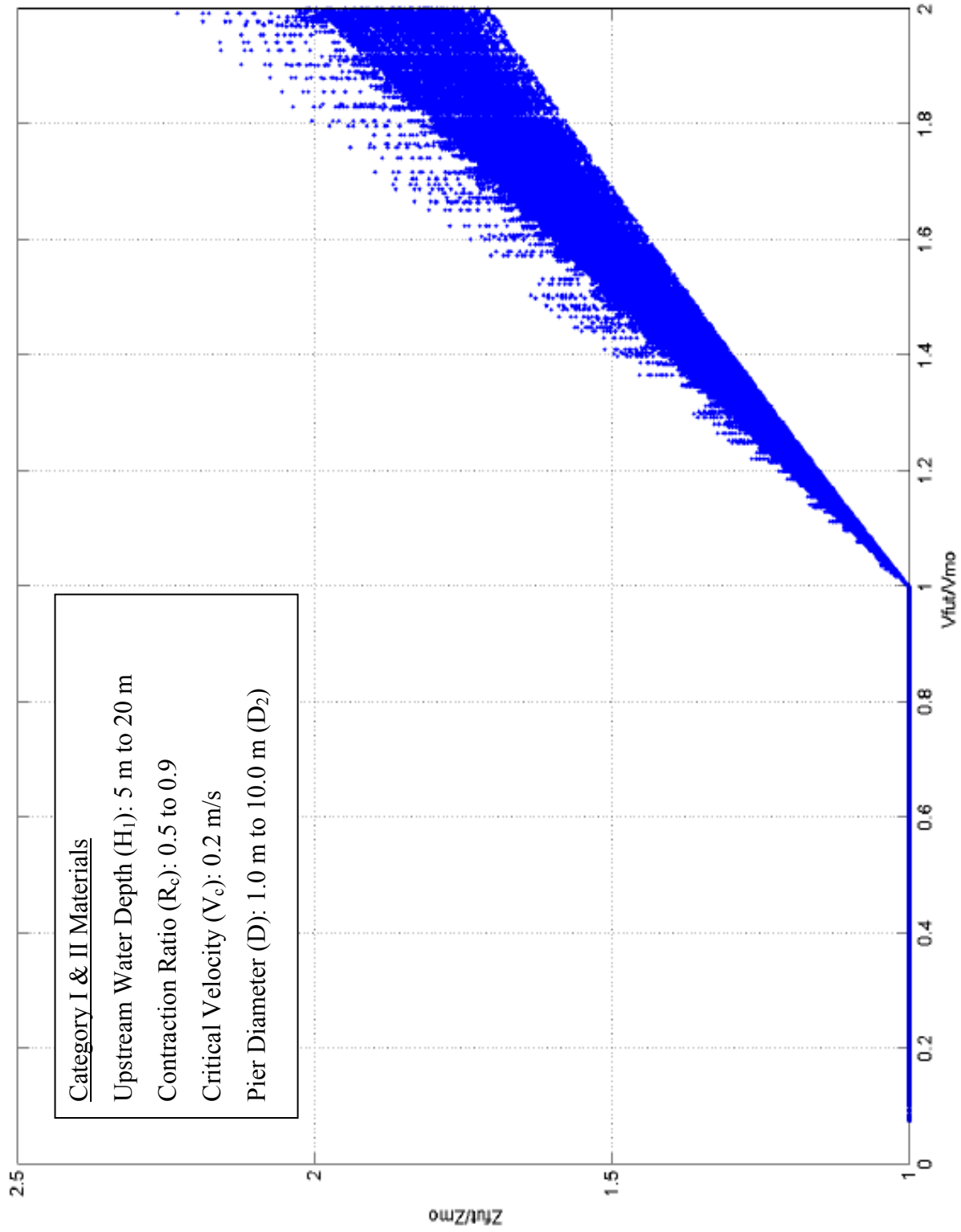


Figure A-2. Z-Future Chart Simulation Data for Category I and II Materials ($1.0 \text{ m} \leq D \leq 10.0 \text{ m}$).

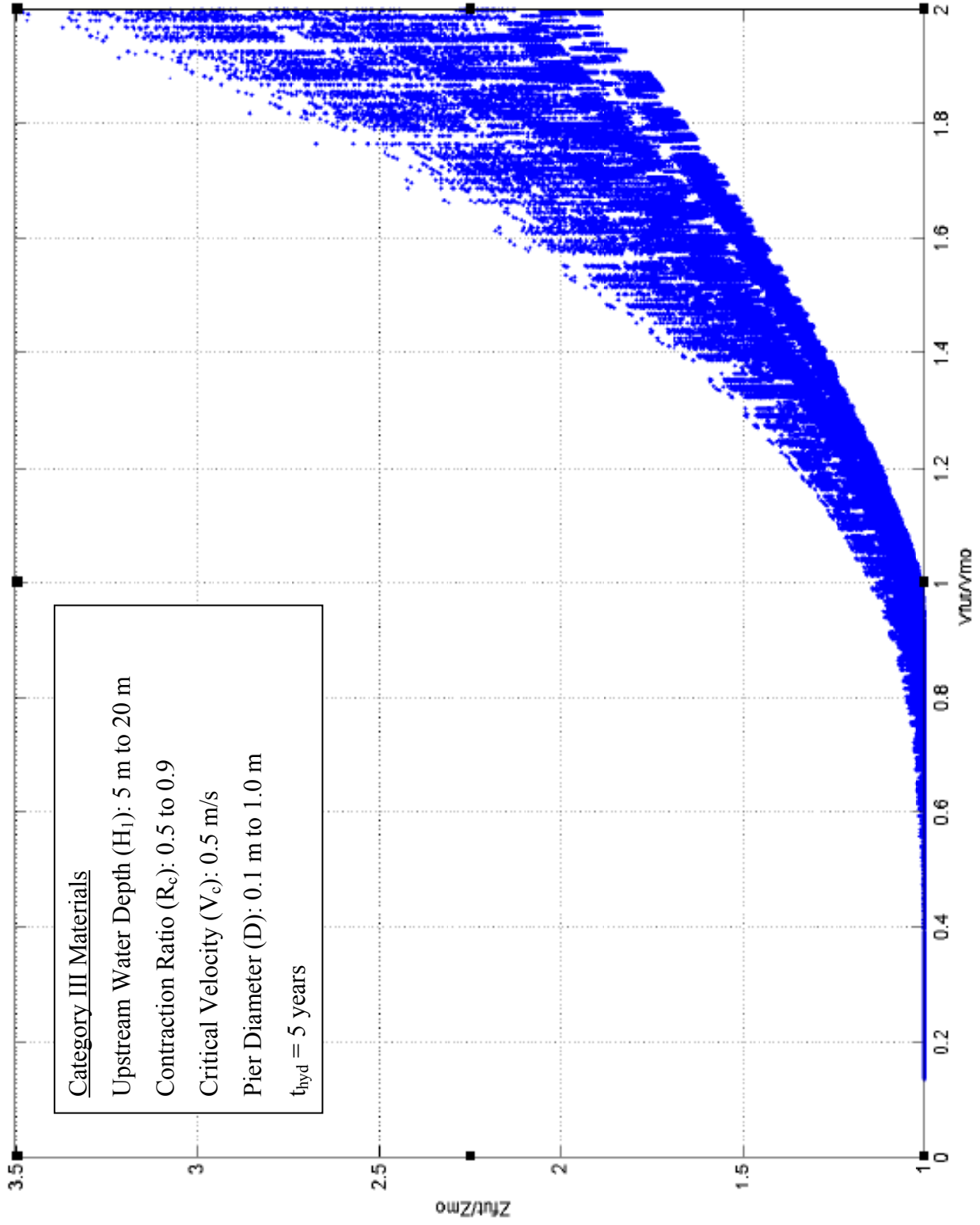


Figure A-3. Z-Future Chart Simulation Data for Category III Materials ($0.1 \text{ m} \leq D \leq 1.0 \text{ m}$).

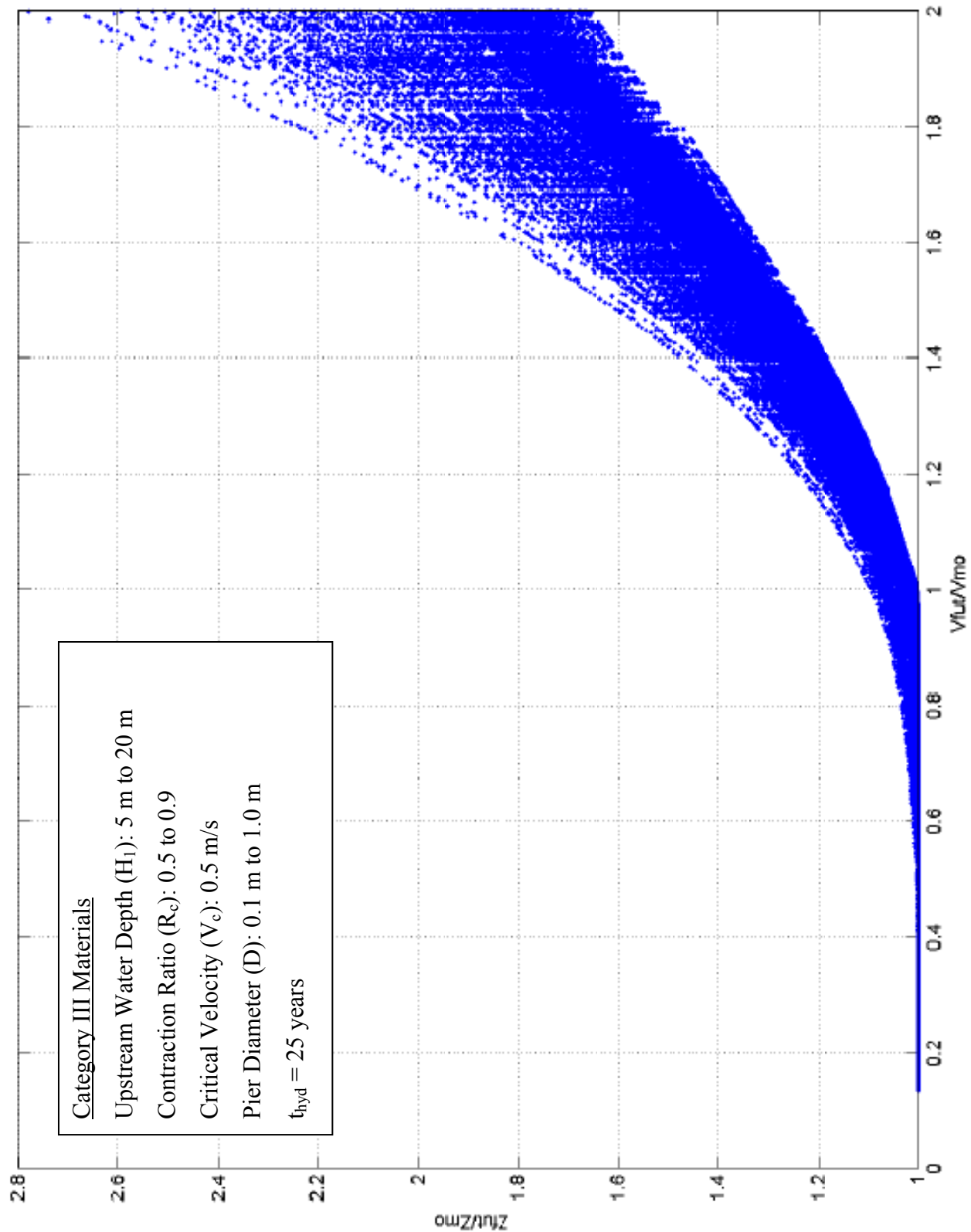


Figure A-4. Z-Future Chart Simulation Data for Category III Materials ($0.1 \text{ m} \leq D \leq 1.0 \text{ m}$).

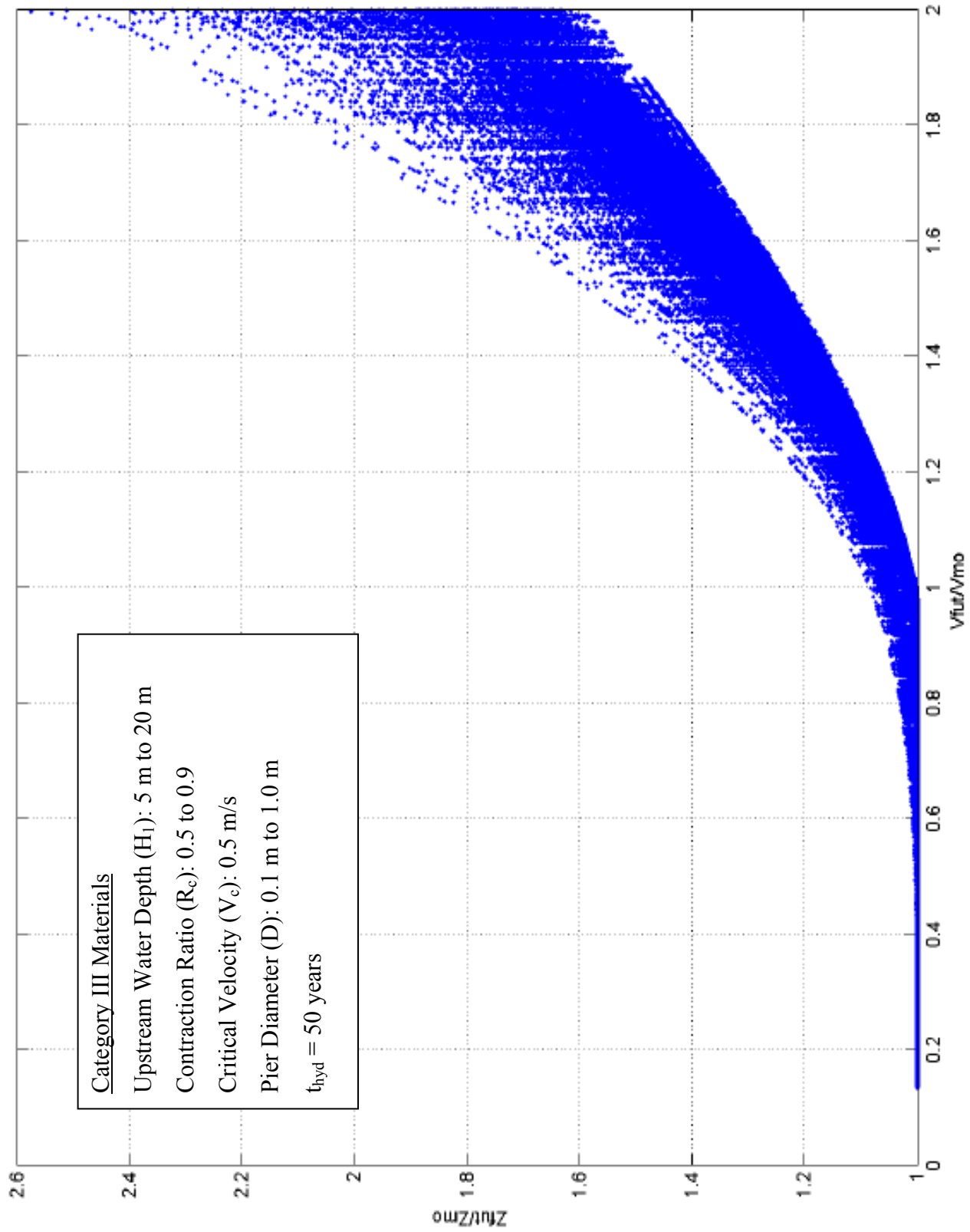


Figure A-5. Z-Future Chart Simulation Data for Category III Materials ($0.1 \text{ m} \leq D \leq 1.0 \text{ m}$).

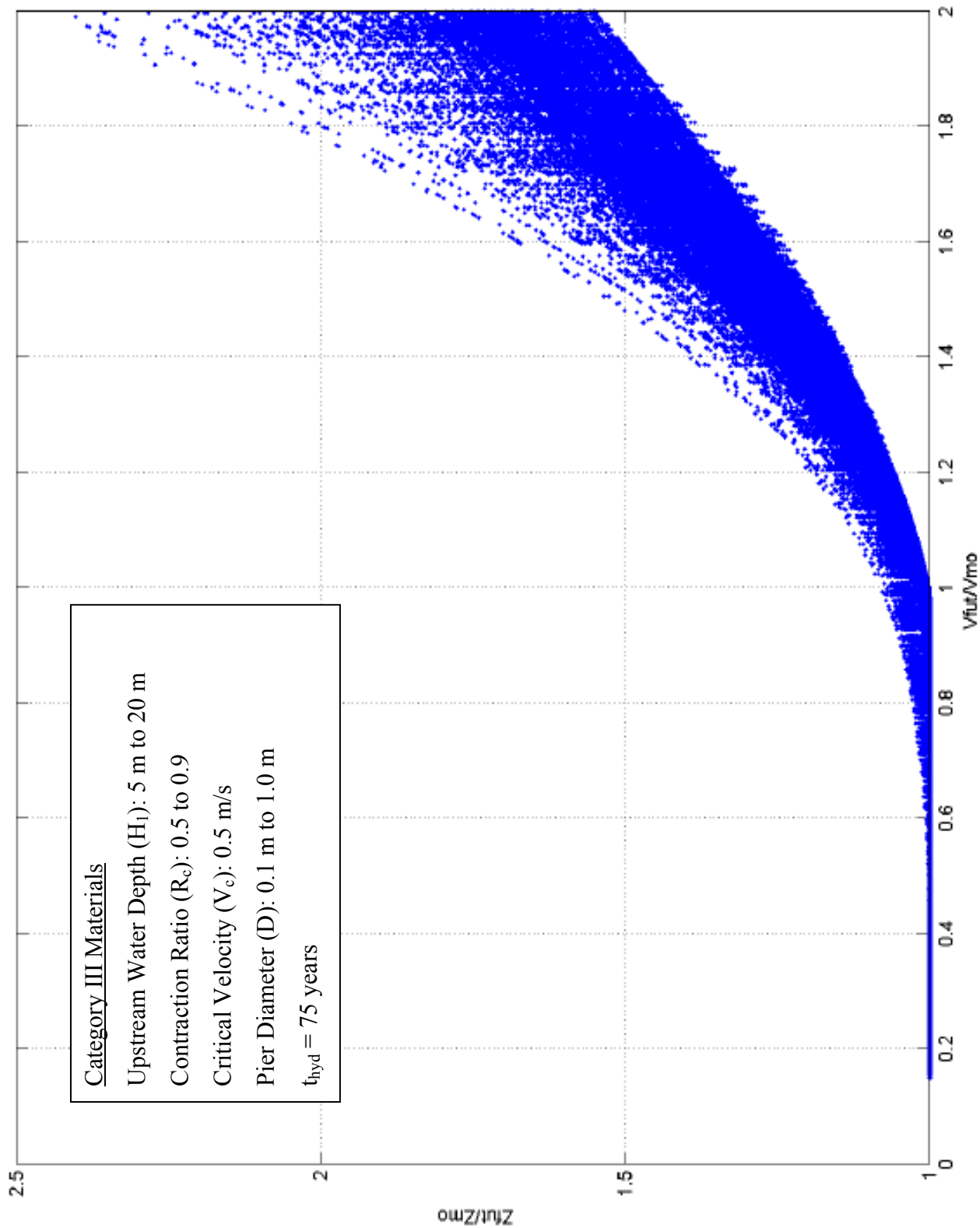


Figure A-6. Z-Future Chart Simulation Data for Category III Materials ($0.1 \text{ m} \leq D \leq 1.0 \text{ m}$).

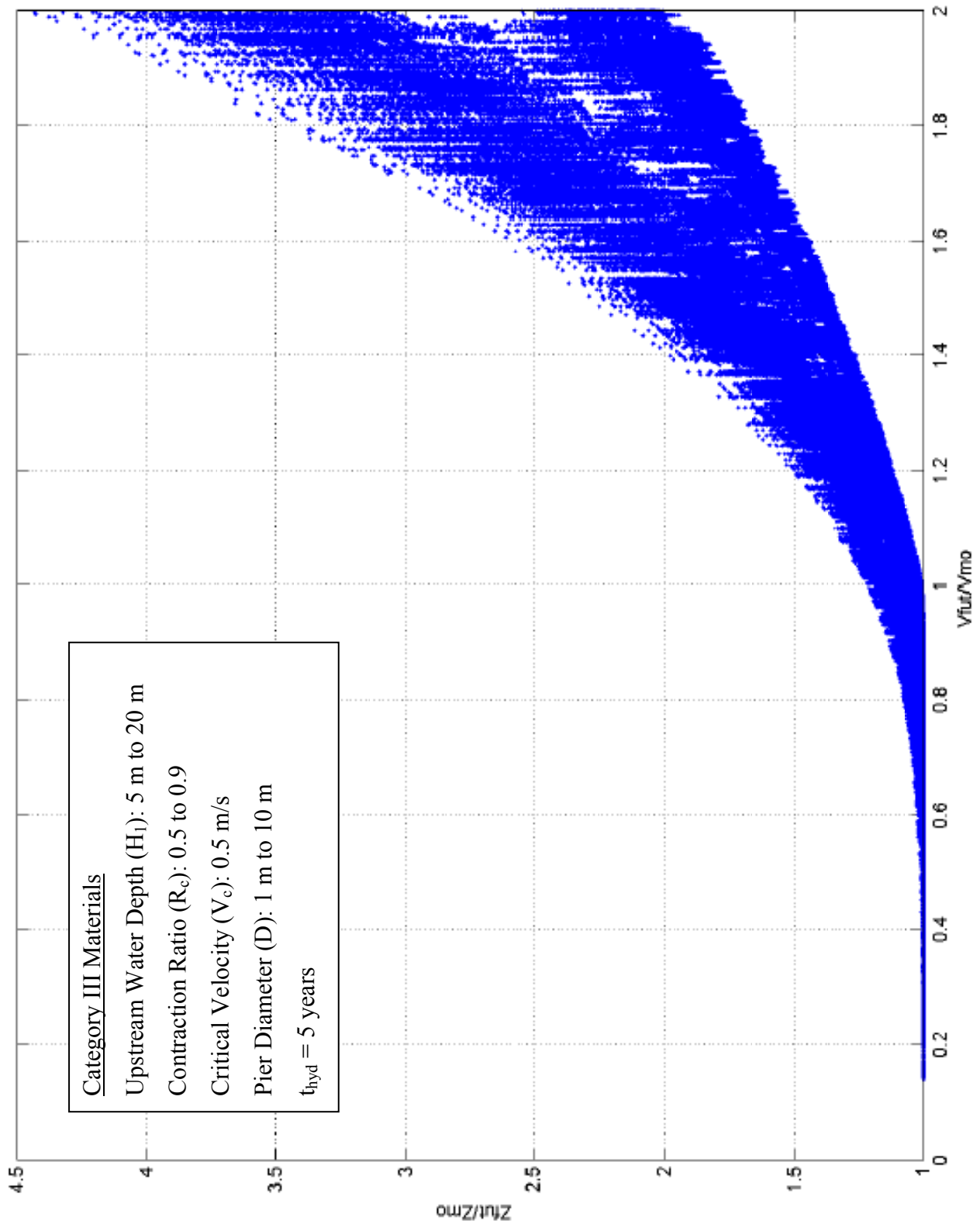


Figure A-7. Z-Future Chart Simulation Data for Category III Materials ($1.0 \text{ m} \leq D \leq 10.0 \text{ m}$).

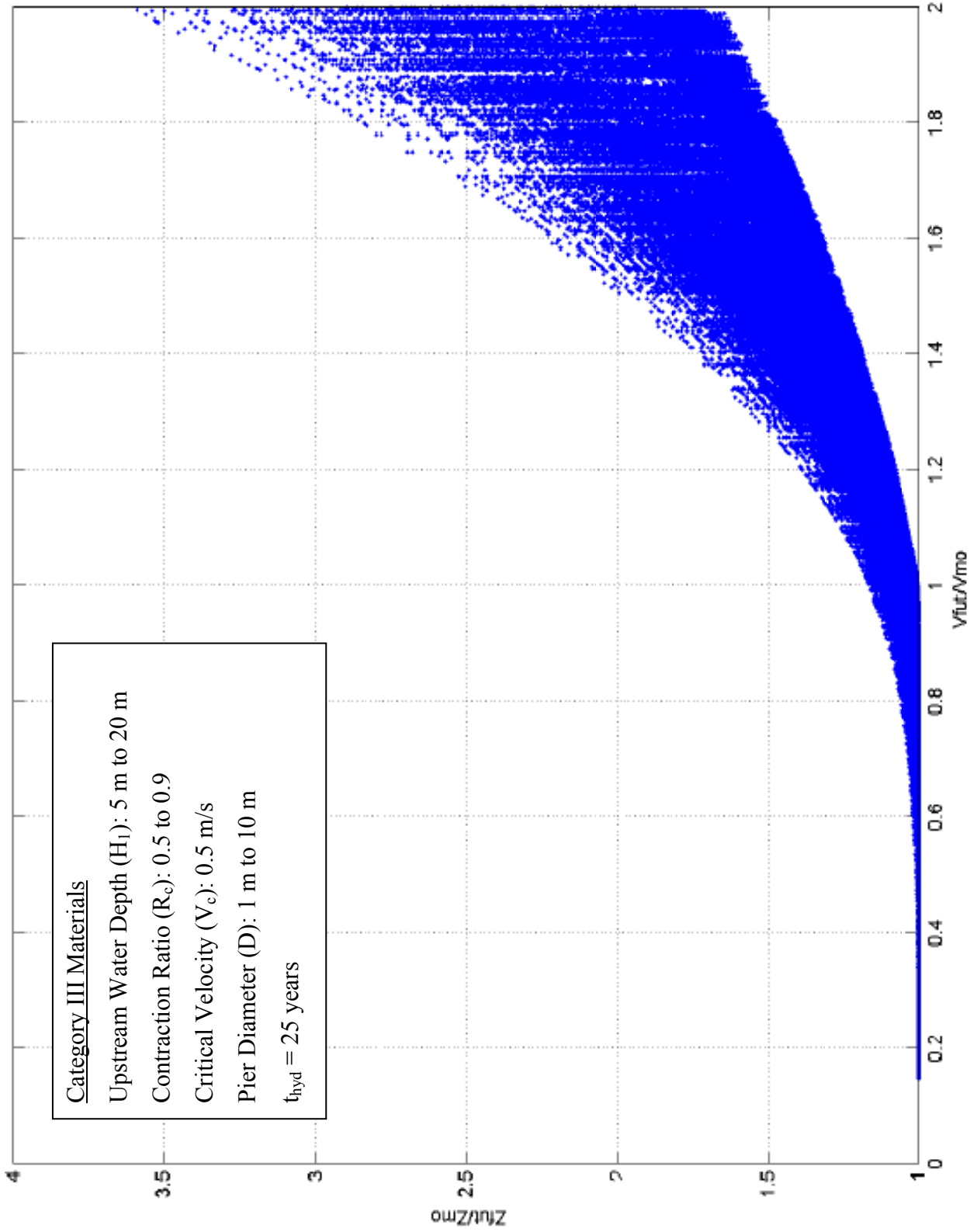


Figure A-8. Z-Future Chart Simulation Data for Category III Materials ($1.0 \text{ m} \leq D \leq 10.0 \text{ m}$).

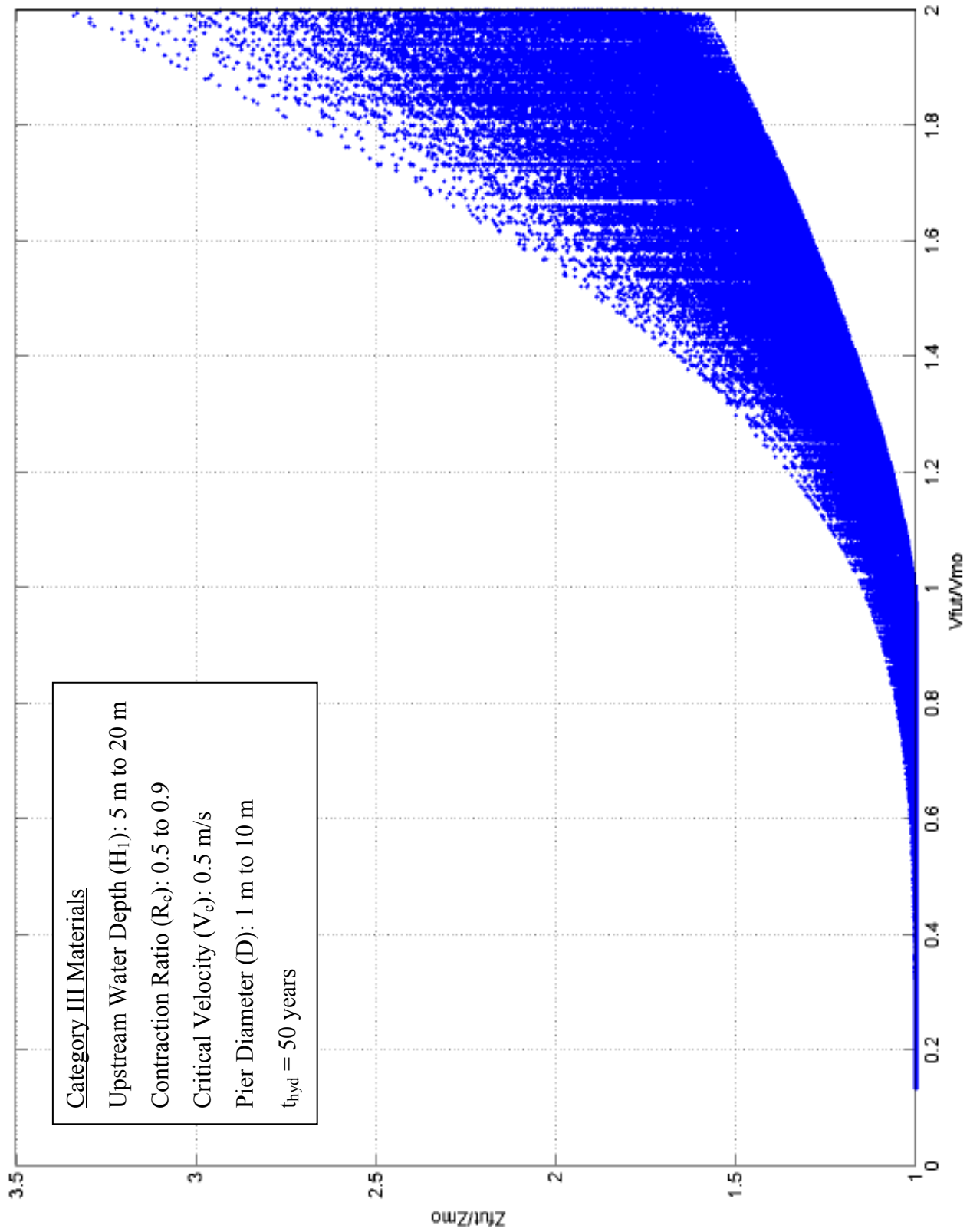


Figure A-9. Z-Future Chart Simulation Data for Category III Materials ($1.0 \text{ m} \leq D \leq 10.0 \text{ m}$).

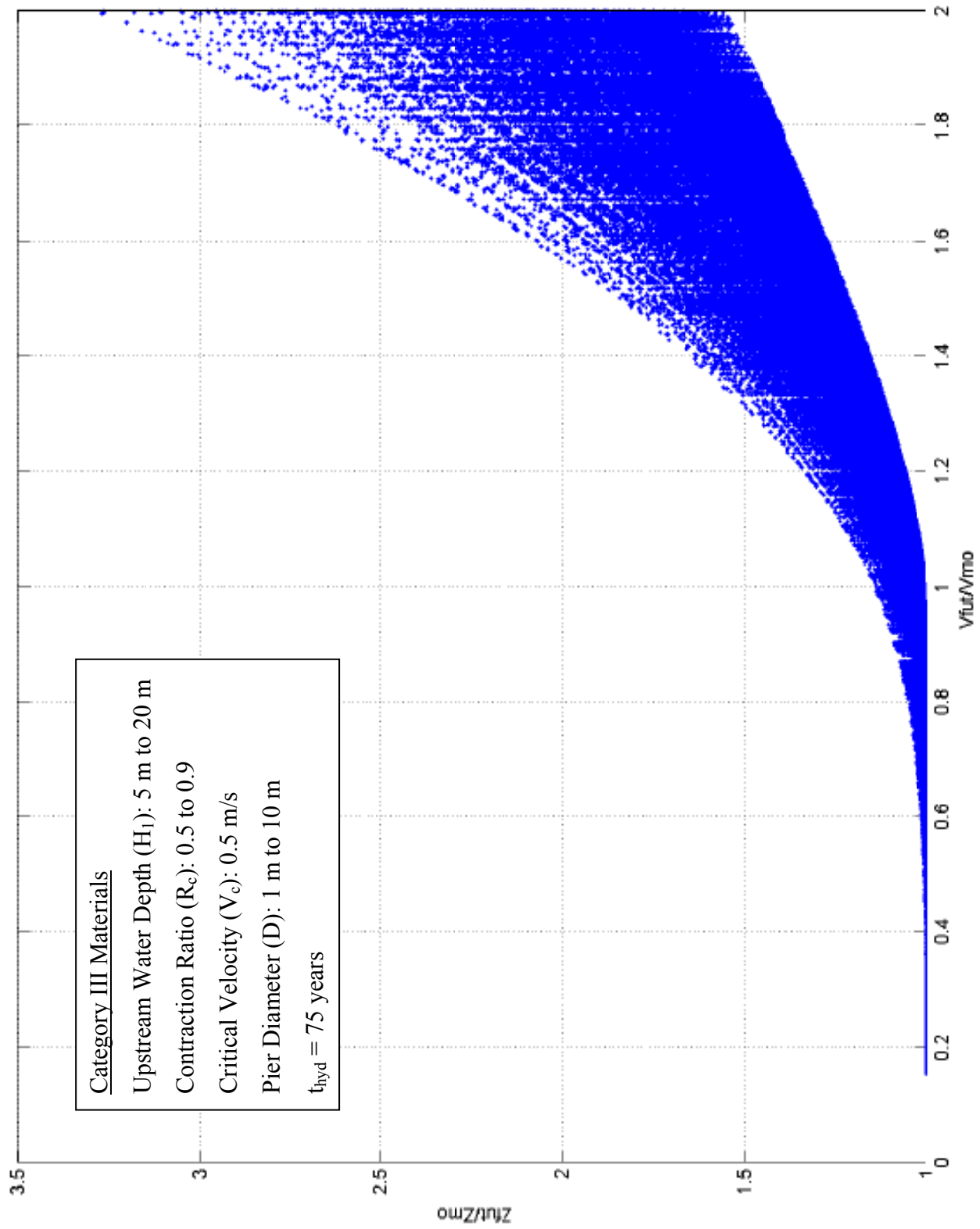


Figure A-10. Z-Future Chart Simulation Data for Category III Materials ($1.0 \text{ m} \leq D \leq 10.0 \text{ m}$).

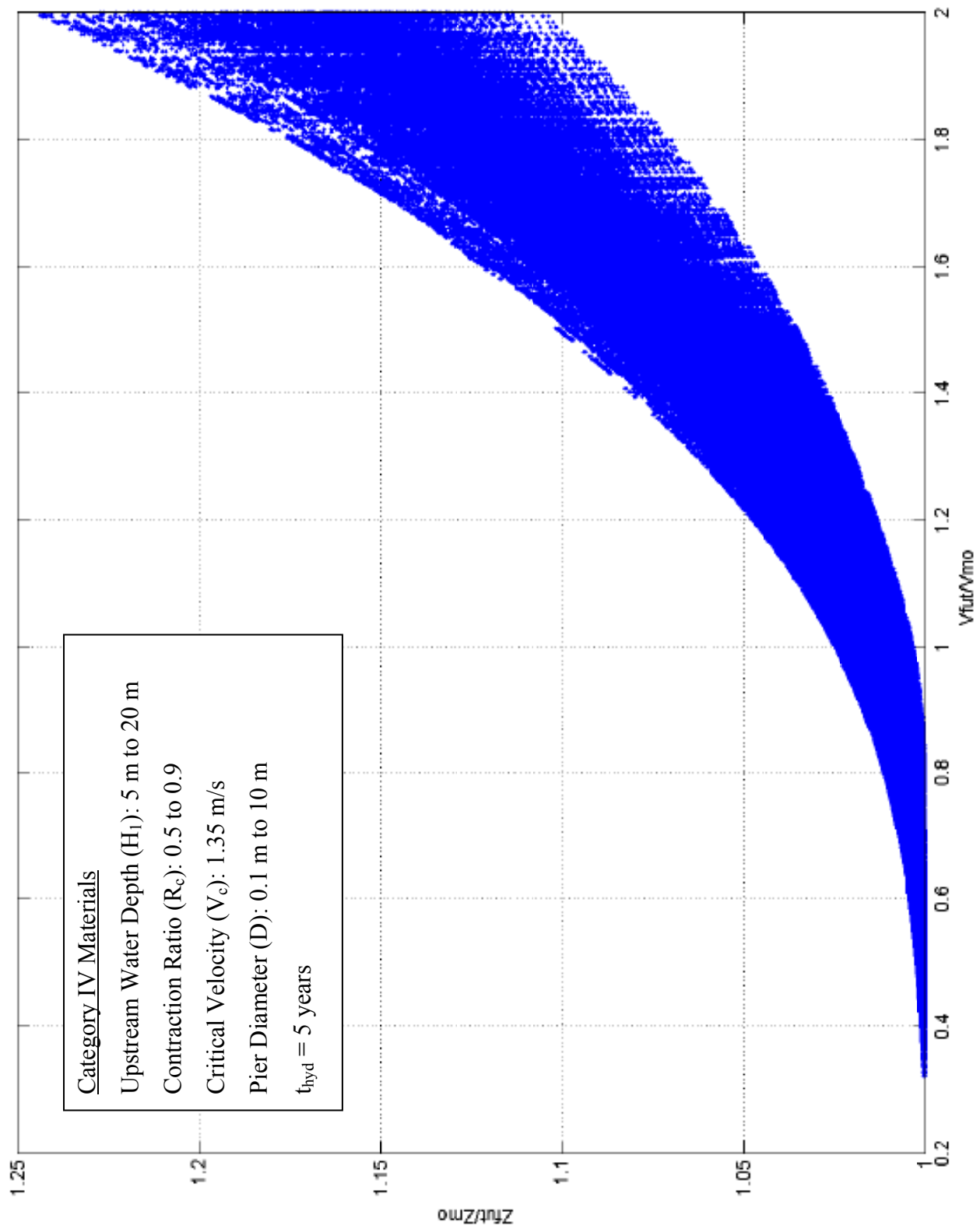


Figure A-11. Z-Future Chart Simulation Data for Category IV Materials ($0.1 \text{ m} \leq D \leq 10.0 \text{ m}$).

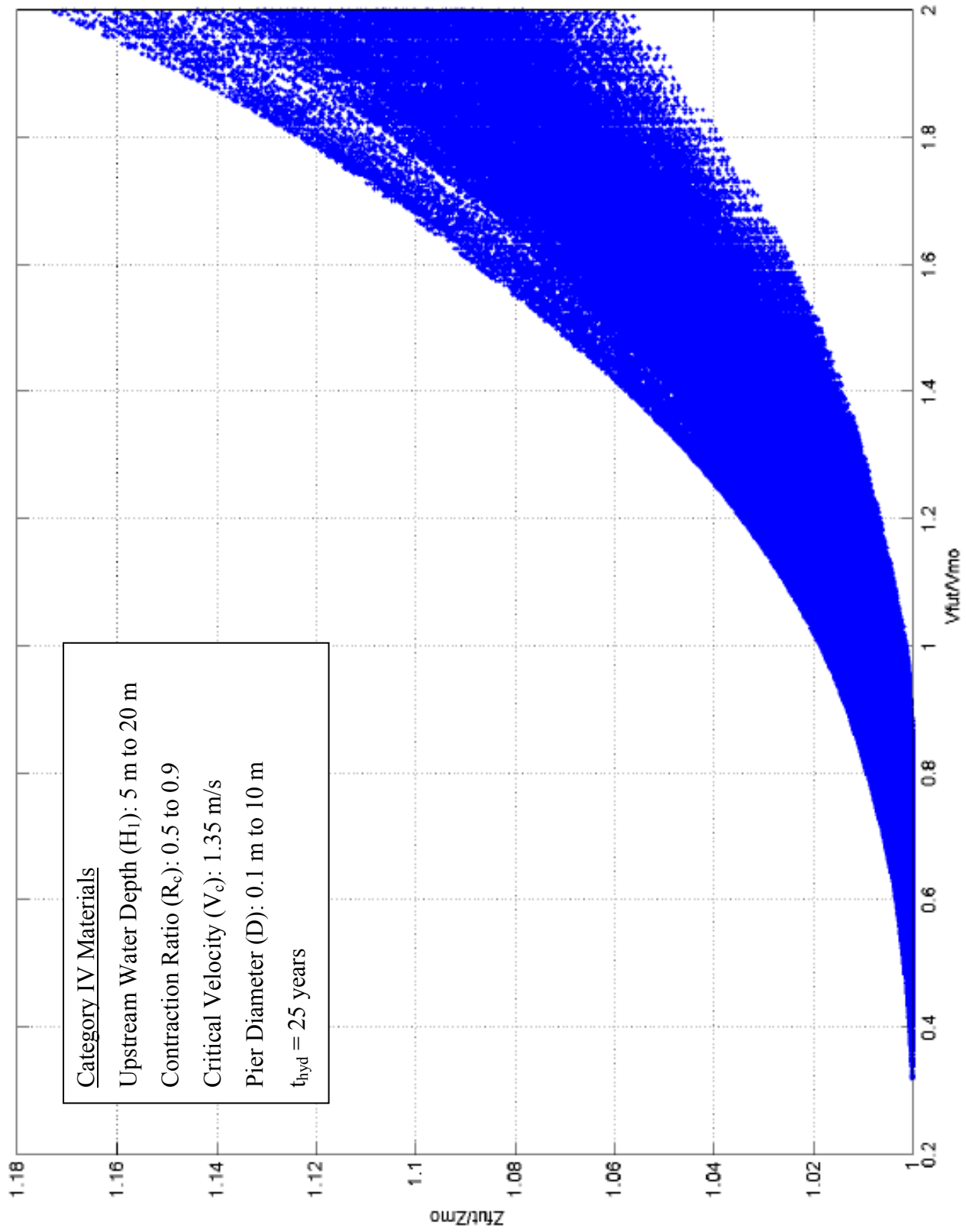


Figure A-12. Z-Future Chart Simulation Data for Category IV Materials ($0.1 \text{ m} \leq D \leq 10.0 \text{ m}$).

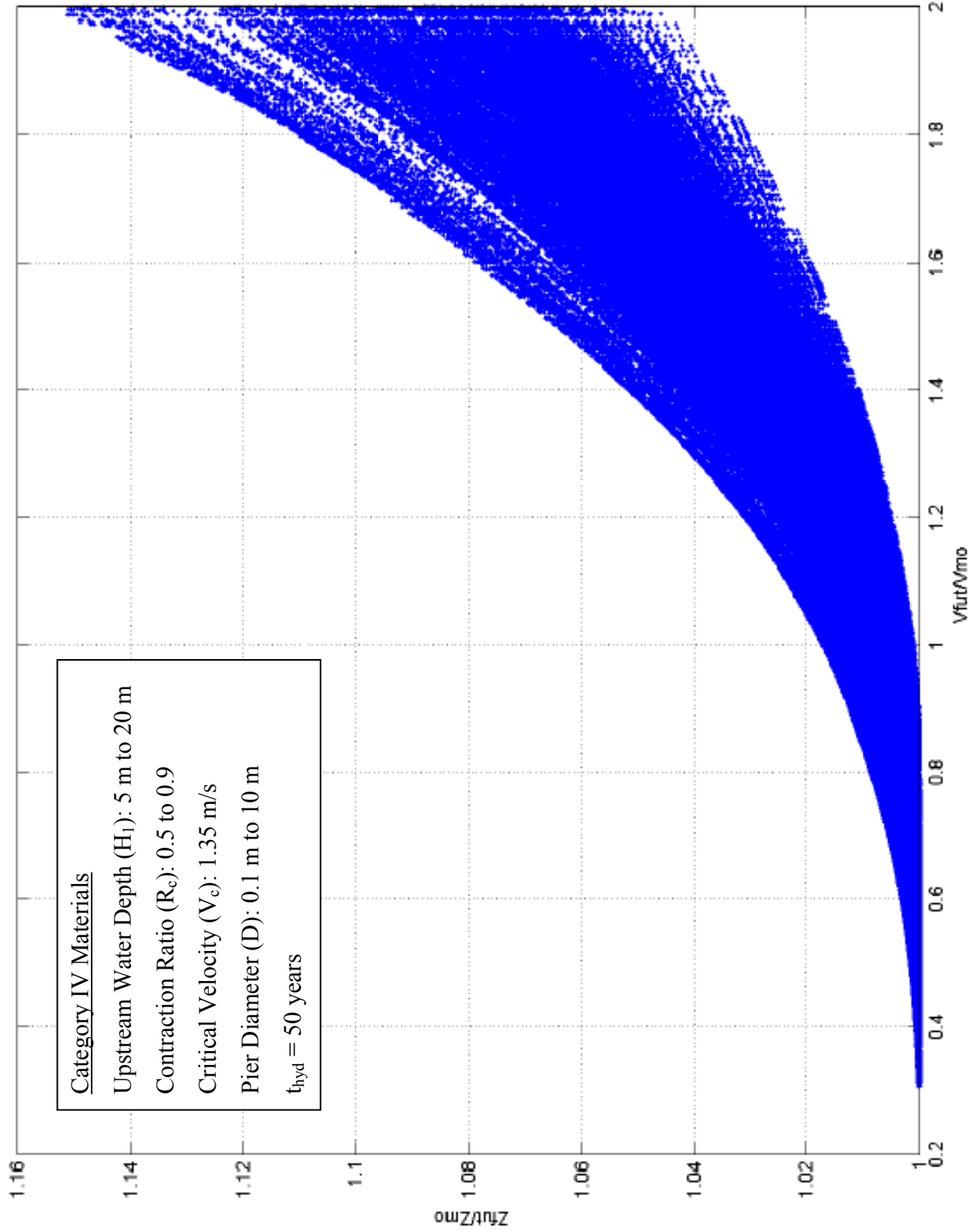


Figure A-13. Z-Future Chart Simulation Data for Category IV Materials ($0.1 \text{ m} \leq D \leq 10.0 \text{ m}$).

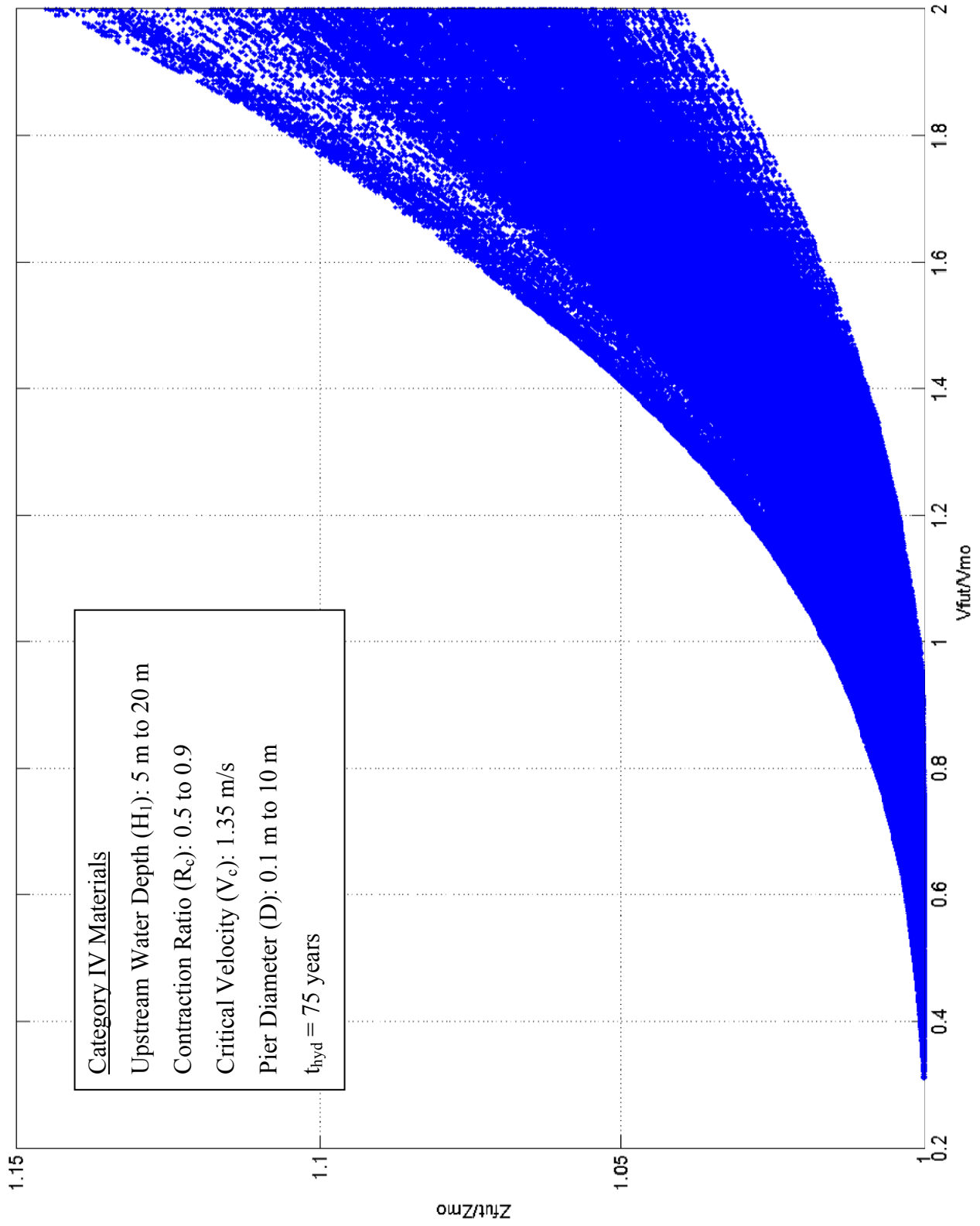


Figure A-14. Z-Future Chart Simulation Data for Category IV Materials ($0.1 \text{ m} \leq D \leq 10.0 \text{ m}$).

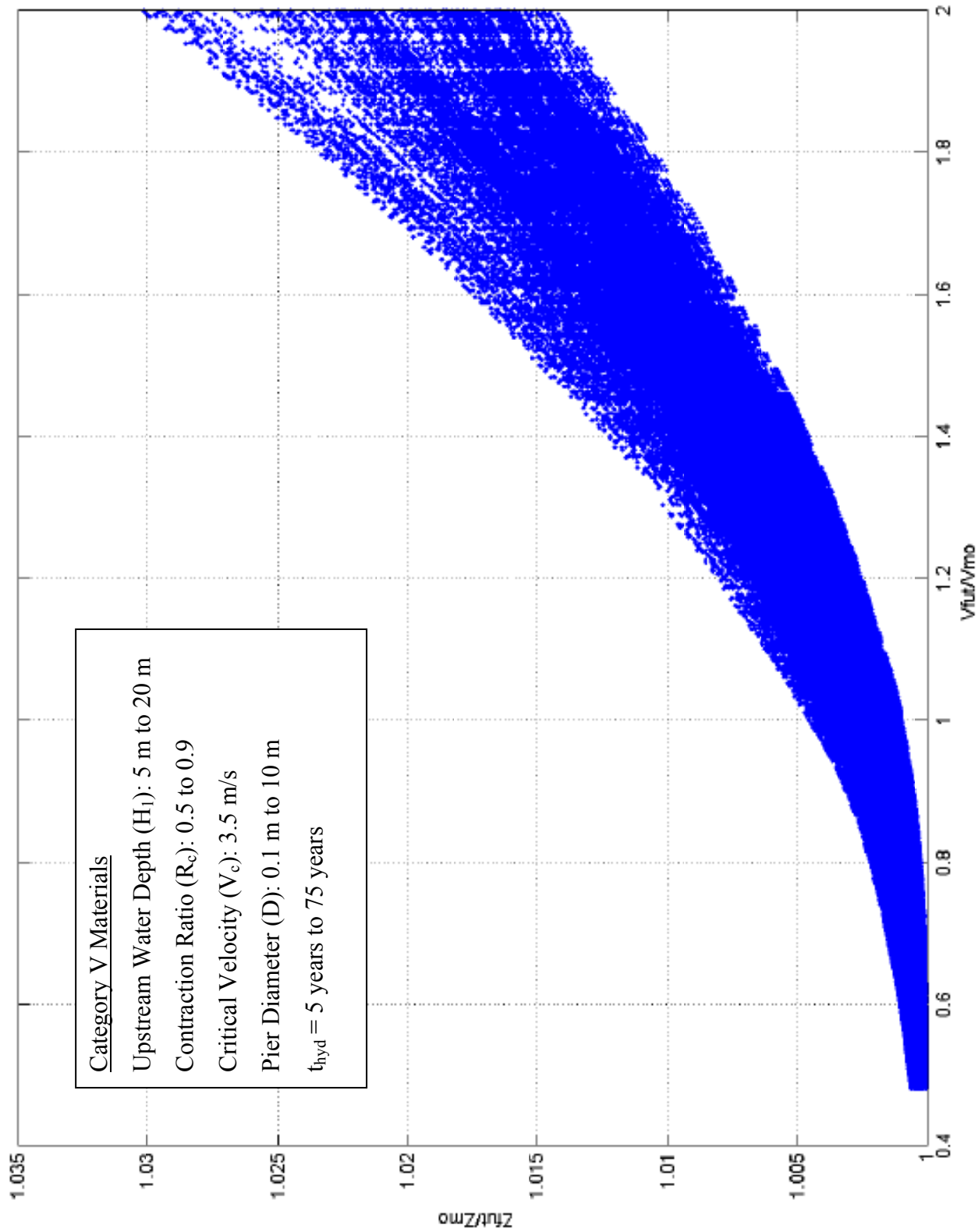


Figure A-15. Z-Future Chart Simulation Data for Category V Materials ($0.1 \text{ m} \leq D \leq 10.0 \text{ m}$).

**APPENDIX B:
BSA 1 (MULTILAYER ANALYSIS)
CALCULATION FLOWCHART**

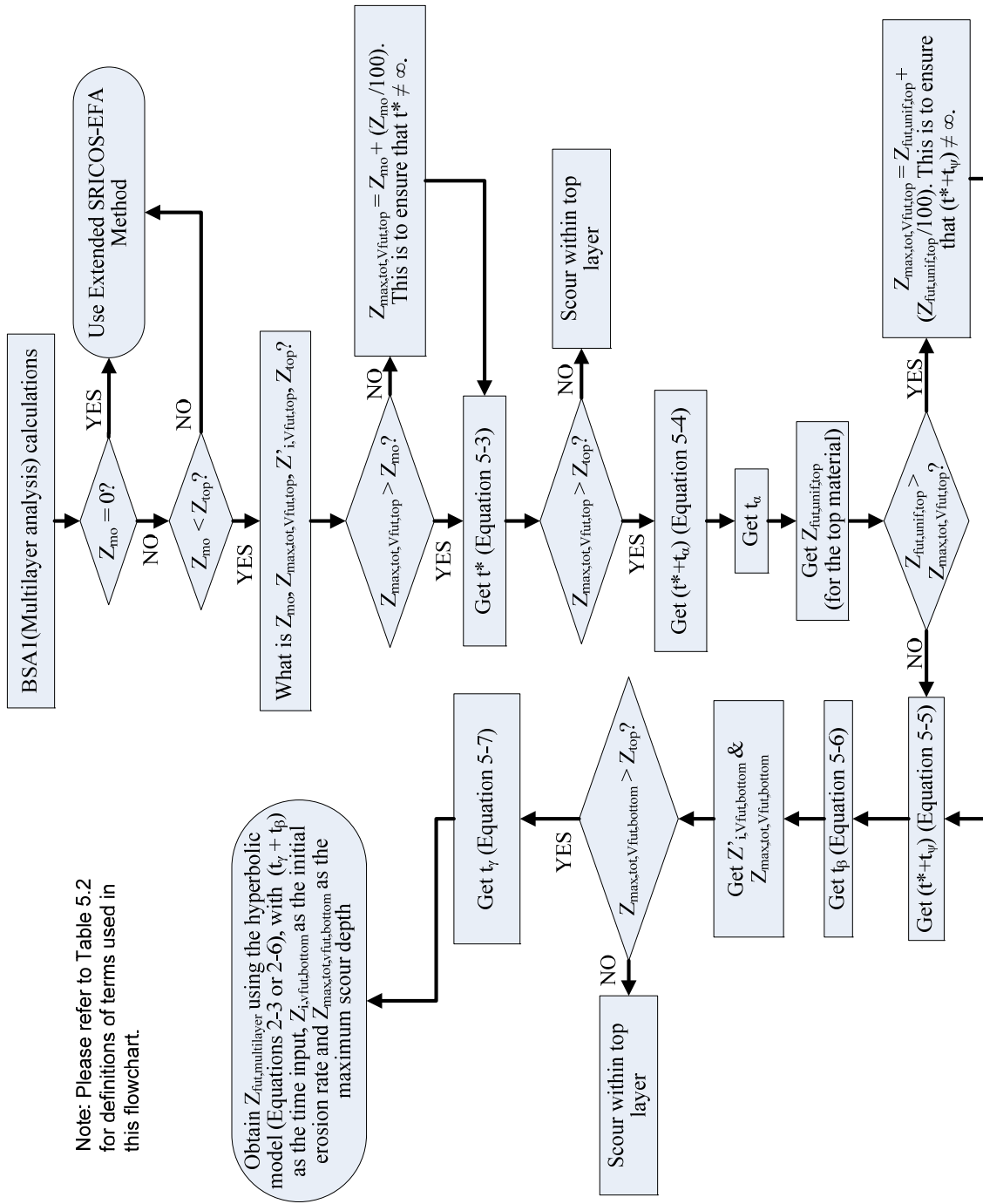


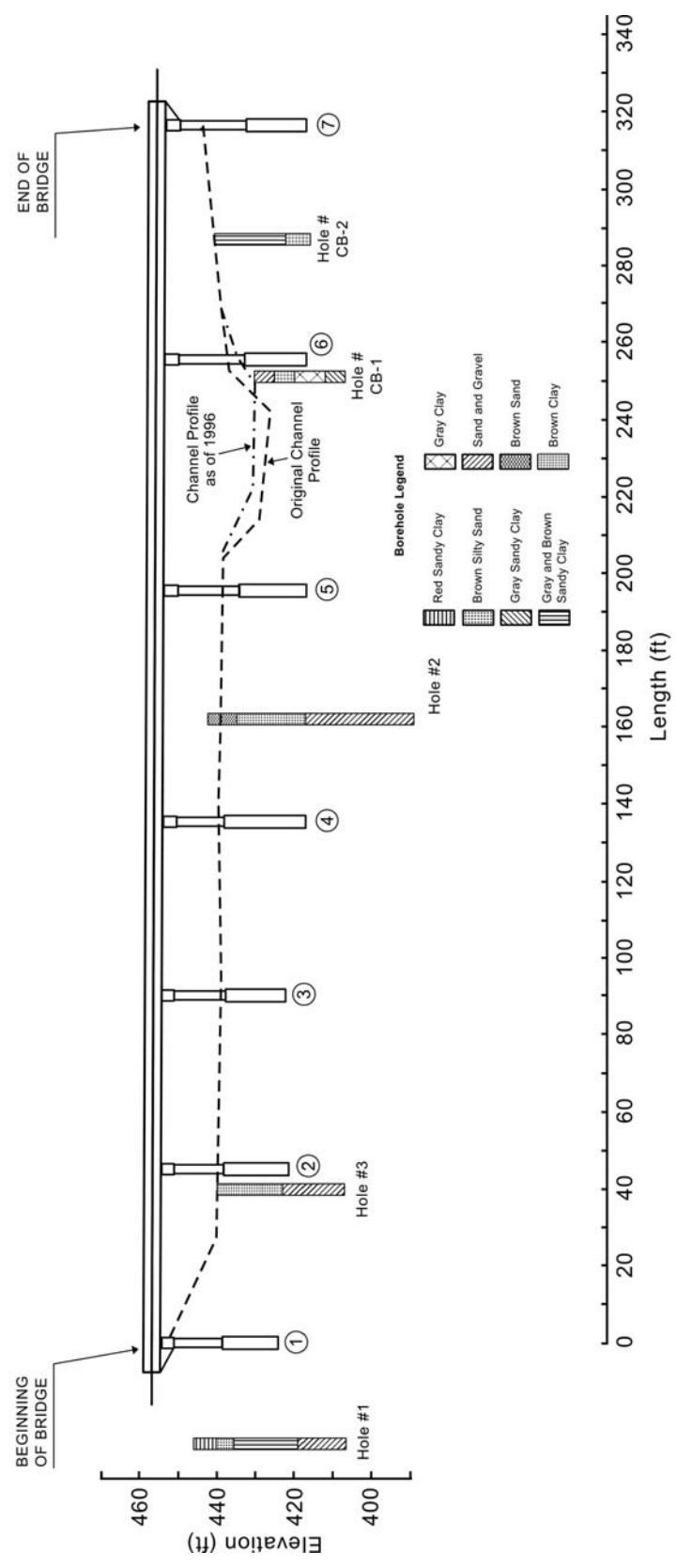
Figure B-1. BSA 1 (Multilayer Analysis) Calculation Flowchart.

**APPENDIX C:
DATA ON CASE HISTORIES**

Table C-1. Case History No. 1.

District:	Waco (9)
County:	Limestone
Structure No.:	09-147-0643-02-038
Source:	Anand4
Highway:	FM 39
River:	Sanders Creek
Status:	Unstable by Concise Analysis
Foundation:	Drilled shafts
Pier/Foundation Dimensions:	2.5-ft diameter drilled shaft with approximately 22.5-ft embedment at Bents 5 and 6 (Secondary Scour Evaluation Sheet, Nov. 25, 1996 and Channel Profile Drawing).
Upstream Channel Width:	Not available
Channel Width at Bridge:	Main channel width is approximately 60 ft, and total channel width (including left and right overbank) is approximately 315 ft (Channel Profile Drawing).
Material:	Dense sand begins approximately 20 ft below channel bottom. The overlying material is loose, silty sand. (Bridge Scour Action Plan, Nov 25, 1996) and clay (soil boring carried out for the present research).
Year Built:	1977
Length:	316 ft
No. of Spans	6-span prestressed concrete box beam superstructure
Z _{fresh 1} :	11.3 ft based on bearing stability at Bent 5 (Bridge Scour Action Plan, Nov. 25, 1996).
Z _{fresh 2} :	N/A
Critical Scour Location:	Bent 5 (Channel Profile Drawing)

Case History No. 1
 Highway: FM 39
 Waterway: Sanders Creek
 District: Waco



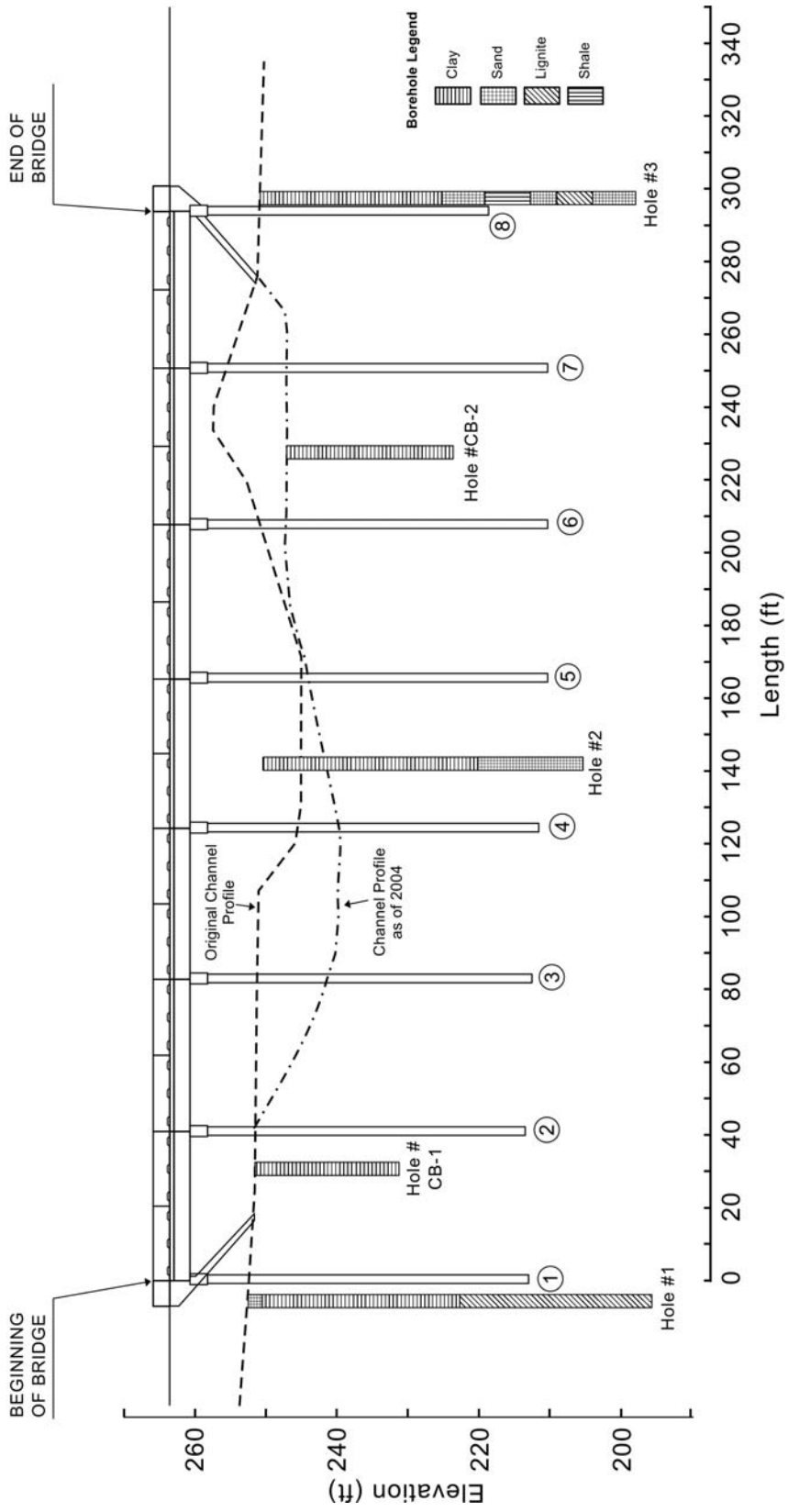
Note: The accuracy of the drawing presented above is dependent upon the accuracy of the data provided.

Figure C-1. Case History No. 1—Bridge Cross Section.

Table C-2. Case History No. 2.

District:	Bryan (17)
County:	Freestone (082)
Structure No.:	17-082-0122-03-036
Source:	Anand4
Highway:	US 287
River:	Alligator Creek (Trinity River Relief)
Status:	Unstable by Concise Analysis
Foundation:	Drilled shafts (Bridge Scour Action Plan 8/6/96)
Pier/Foundation Dimensions:	Drilled shafts that extend a minimum 24 ft below the 8/6/96 channel bed elevation (Bridge Scour Action Plan 8/6/96). The drilled shaft diameter is 2 ft (TSEAS Scour Evaluation Form pg. B-1).
Upstream Channel Width:	36 ft (Live Bed Contraction Scour Calculation Sheet)
Channel Width at Bridge:	32 ft (Live Bed Contraction Scour Calculation Sheet)
Material:	14 ft of clay underlain by thick sand layer (Bridge Scour Action Plan 8/6/96)
Year Built:	1984
Length:	292 ft
No. of Spans:	7-span girder superstructure.
Z _{fresh 1} :	16 ft based on bearing stability (Bridge Scour Action Plan 8/6/96).
Z _{fresh 2} :	-
Critical Scour Location:	None (Bridge Scour Action Plan 8/6/96)

Case History No. 2
 Highway: US 287
 Waterway: Alligator Creek
 District: Bryan



Note: The accuracy of the drawing presented above is dependent upon the accuracy of the data provided.

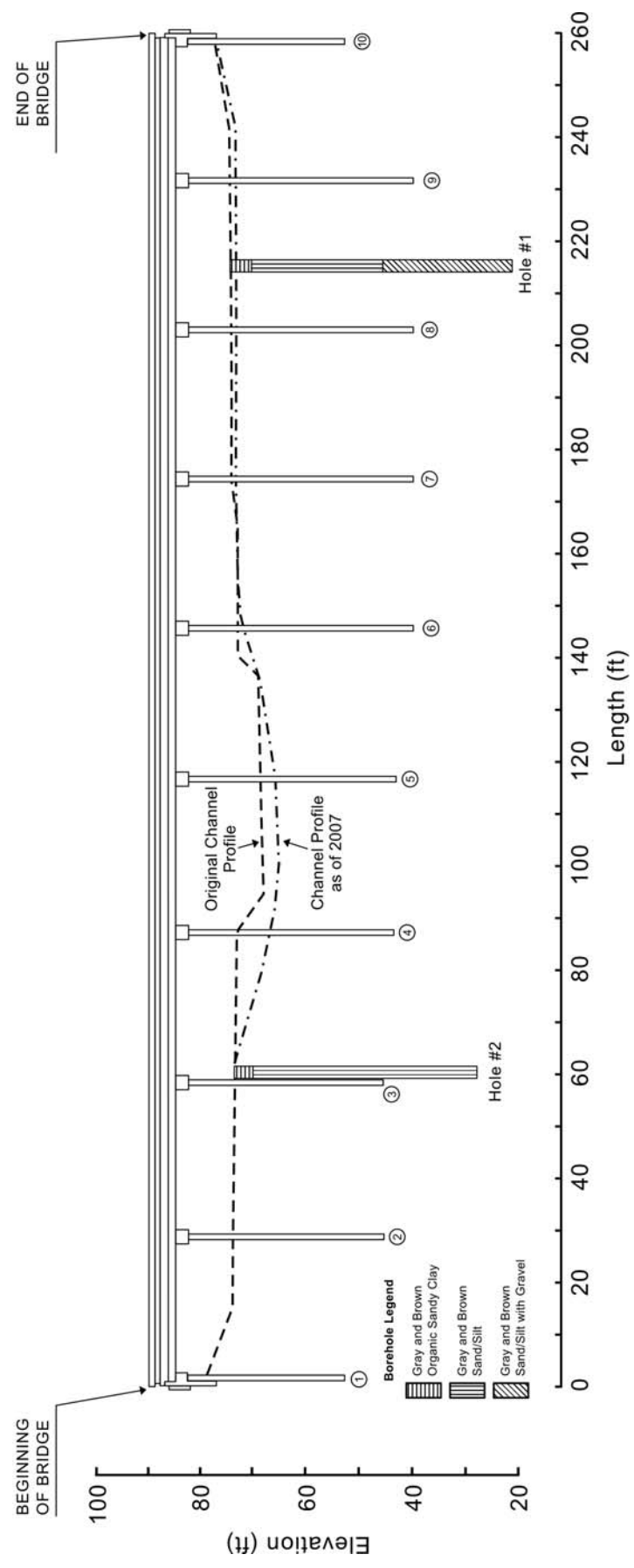
Figure C-2. Case History No. 2—Bridge Cross Section.

Table C-3. Case History No. 3.

District:	Houston (12)												
County:	Fort Bend (80)												
Structure No.:	12-080-0188-02-023												
Source:	DK20												
Highway:	SH 36												
River:	Big Creek												
Status:	Unstable by Concise Analysis												
Foundation:	Concrete piles (Secondary Scour Evaluation, 5/16/94)												
Pier/Foundation Dimensions:	14-inch wide concrete piles at Bent 5 (Secondary Scour Evaluation Notes). The concrete piles are approximately 25 ft to 35 ft long (Channel Profile Drawing).												
Upstream Channel Width:	40.0 ft (Secondary Scour Evaluation Worksheet 4, 5/10/94)												
Channel Width at Bridge:	37.6 ft (Secondary Scour Evaluation Worksheet 4, 5/10/94)												
Material:	Deep sand deposit extending 40 ft below the channel bottom (Secondary Scour Evaluation, 5/16/94)												
Year Built:	1932 (Form 113.2 — Bridge Scour Survey, 6/18/91)												
Length:	257 (Form 113.2 — Bridge Scour Survey, 6/18/91)												
No. of Spans:	9 ft (Secondary Scour Evaluation, 5/16/94)												
Z _{fresh 1} :	13 ft at Bent 5 (Secondary Scour Evaluation Notes 1, 5/10/94)												
Z _{fresh 2} :	N/A												
Critical Scour Location:	Bents 4, 5, and 6 (Secondary Scour Evaluation, 5/16/94)												
Ref. No. (for Z _{fresh})	Measurement Date	Source	Scour Depth (ft)	Location	V _{fit} (ft/s)	V _{mo} (ft/s)	V _{fit} /V _{mo}	Z _{mo} (ft)	Z _{fit} /Z _{mo}		Z _{fit,model} (ft)	Z _{fit,field} (ft)	Z _{fit,model} /Z _{fit,field}
									Ratio	Notes			
1	1994	CPDM	3.6	Bent 5	-	-	-	-	-	-	-	-	-
1	1995	CPDM	3.8	Bent 5	5.7	6.9	0.83	3.6	1	-	3.6	3.8	0.95
1	1997	CPDM	3.8	Bent 5	4.2	6.9	0.61	3.8	1	-	3.8	3.8	1.0
1	1998	CPDM	3.7	Bent 5	5.1	6.9	0.74	3.8	1	-	3.8	3.7	1.03
1	2001	CPDM	3.5	Bent 5	4.6	6.9	0.66	3.8	1	-	3.8	3.5	1.09
1	1/9/2005	CPDM	2.6	Bent 5	5	6.9	0.72	3.8	1	-	3.8	2.6	1.46
1	1/21/2007	CPDM	2.5	Bent 5	5	6.9	0.72	3.8	1	-	3.8	2.5	1.52

Note: CPDM = Channel Profile Drawings and Channel Profile Measurements

Case History No. 3
 Highway: SH 36
 Waterway: Big Creek
 District: Houston



Note: The accuracy of the drawing presented above is dependent upon the accuracy of the data provided.

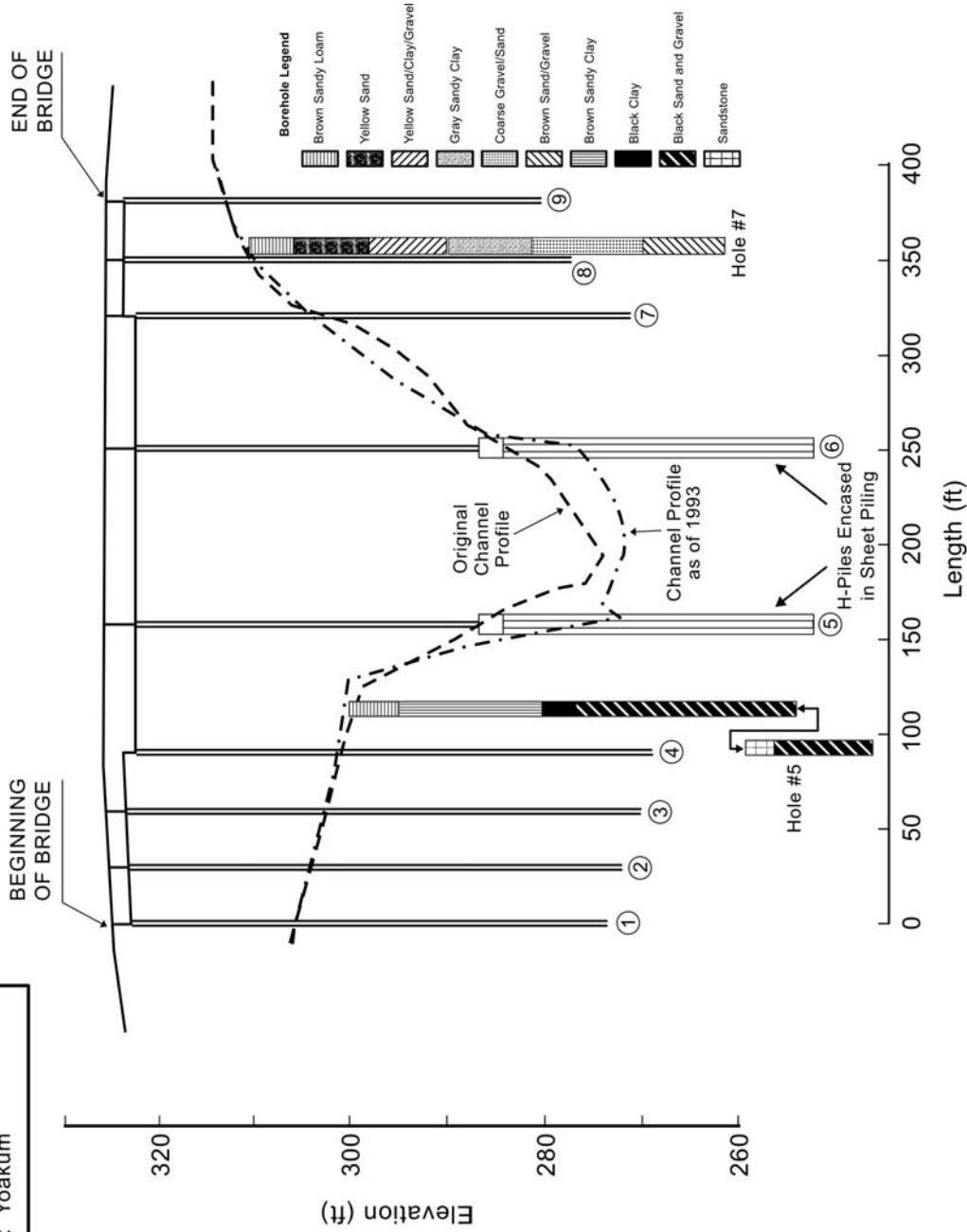
Figure C-3. Case History No. 3—Bridge Cross Section.

Table C-4. Case History No. 4.

District:	Yoakum (13)												
County:	Gonzales												
Structure No.:	13-090-2080-01-005												
Source:	DK20												
Highway:	FM 2091												
River:	San Marcos River												
Status:	On the scour critical list												
Foundation:	Precast concrete square piles, steel H-piles, and caisson												
Pier/Foundation Dimensions:	Bents 2, 3, 4, 7, and 8 consist of concrete caps founded on three 15-inch wide square precast concrete piles that are 32 ft long. Bents 5 & 6 consist of concrete caps, each on two circular columns that are founded on four 14 inch steel H-piles that are 33 ft long. Caisson was added at Bent 5 in 1995.												
Upstream Channel Width:	Not available												
Channel Width at Bridge:	40 ft (Computer-Generated Channel Profile Drawing on 3/23/94)												
Material:	Clay and sand												
Year Built:	1960												
Length:	381.5 ft												
No. of Spans:	5 simple spans, 1 continuous span												
Z _{dresh} 1:	16.5 ft (33 ft pile length x 0.5, assumed)												
Z _{dresh} 2:	15 ft (30 ft caisson length x 0.5, assumed)												
Critical Scour Location:	Bents 5 and 6 (Underwater Inspection Report)												
Ref. No. (for Z _{dresh})	Measurement Date	Source	Scour Depth (ft)	Location	V _{fit} (ft/s)	V _{mo} (ft/s)	V _{fit} /V _{mo}	Z _{mo} (ft)	Z _{fit} /Z _{mo} Ratio	Z _{fit} /Z _{mo} Notes	Z _{fit,model} (ft)	Z _{fit,field} (ft)	Z _{fit,model} /Z _{fit,field}
1	8/2/91	CPD	9 ft	Bent 5	-	-	-	-	-	-	-	-	-
1	1/9/92	CPD	12.4 ft	Bent 5	11.3	12.0	0.94	9	1.15		10.4	12.4	0.84
1	1993	CPD	12.4 ft	Bent 5	7.3	12.0	0.61	12.4	1.00		12.4	12.4	1.00
Caisson added at Bent 5 in 1995.													
2	1997	CPD	-5 ft (deposition)	Bent 5	9.6	12.0	0.80	-	-	-	-	-	-
2	1999	CPD	-1 ft (4 ft of scour compared to 1997)	Bent 6	8.0	12.0	0.66	-	-	-	-	-	-

Note: CPD = Channel Profile Drawings

Case History No. 4
 Highway: FM 2091
 Waterway: San Marcos River
 District: Yoakum



Note: The accuracy of the drawing presented above is dependent upon the accuracy of the data provided.

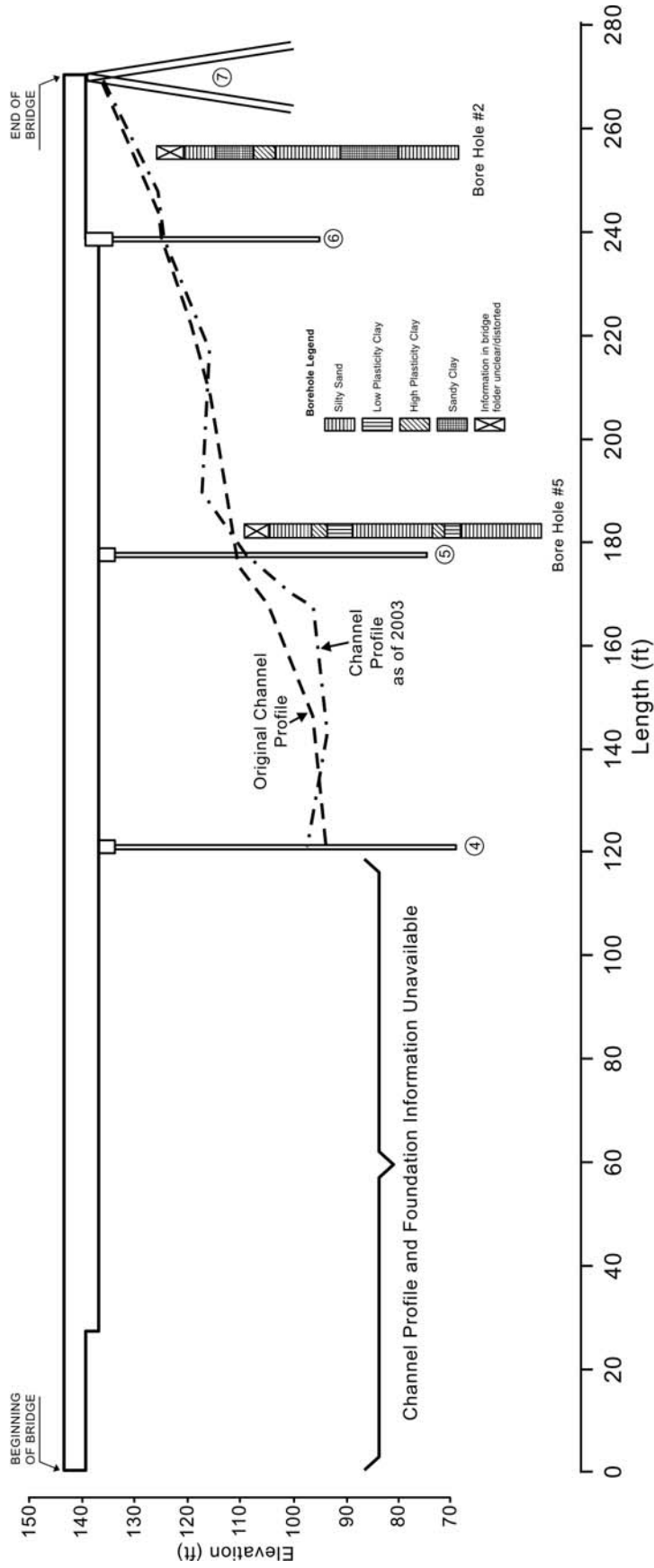
Figure C-4. Case History No. 4—Bridge Cross Section.

Table C-5. Case History No. 5.

District:	Austin (13)											
County:	Austin (08)											
Structure No.:	13-008-0408-05-019											
Source:	DK20											
Highway:	FM 331											
River:	Mill Creek											
Status:	Unstable by Concise Analysis											
Foundation:	Precast concrete piles											
Pier/Foundation Dimensions:	18-inch wide precast concrete piles that are embedded a minimum 20 ft into the channel bed (Secondary Scour Evaluation - Allowable Scour Depth Worksheet for Bent 4)											
Upstream Channel Width:	Not available											
Channel Width at Bridge:	210 ft (HEC-RAS figure)											
Material:	Silty sand and clay. It is assumed that at Bent 4, all scour took place in the sand.											
Year Built:	1951											
Length:	271 ft											
No. of Spans:	3 simple prestressed concrete beam main spans and 3 pan girder approach spans on concrete pile bents.											
Z _{thresh 1} :	1.46 ft (allowable scour depth based on lateral stability at Bent 4, Secondary Scour Evaluation Worksheet 1 Notes, Landtech Consultants)											
Z _{thresh 2} :	N/A											
Critical Scour Location:	Bent 4 (Secondary Scour Evaluation - Allowable Scour Depth Worksheet 1)											
Ref. No. (for Z _{thresh})	Measurement Date	Source	Scour Depth (ft)	Location	V _{fur} (ft/s)	V _{no} (ft/s)	V _{fur} /V _{no}	Z _{no} (ft)	Z _{fur} /Z _{no} Ratio	Z _{fur,model} (ft)	Z _{fur,field} (ft)	Z _{fur,model} /Z _{fur,field}
1	6/10/93	CPD	0.5	Bent 4	-	-	-	-	-	-	-	-
1	6/95	CPD	-3.2 (deposition)	Bent 4	-	-	-	-	-	-	-	-
1	4/20/2001	CPD	-3.2 (deposition)	Bent 4	9.43	9.6	0.98	0.5	1.0	0.5	-3.2	-0.16
1	7/18/2003	CPD	-3.2 (deposition)	Bent 4	4.69	9.6	0.49	0.5	1.0	0.5	-3.2	-0.16

Note: CPD = Channel Profile Drawings

Case History No. 5
 Highway: FM 331
 Waterway: Mill Creek
 District: Austin



Note: The accuracy of the drawing presented above is dependent upon the accuracy of the data provided.

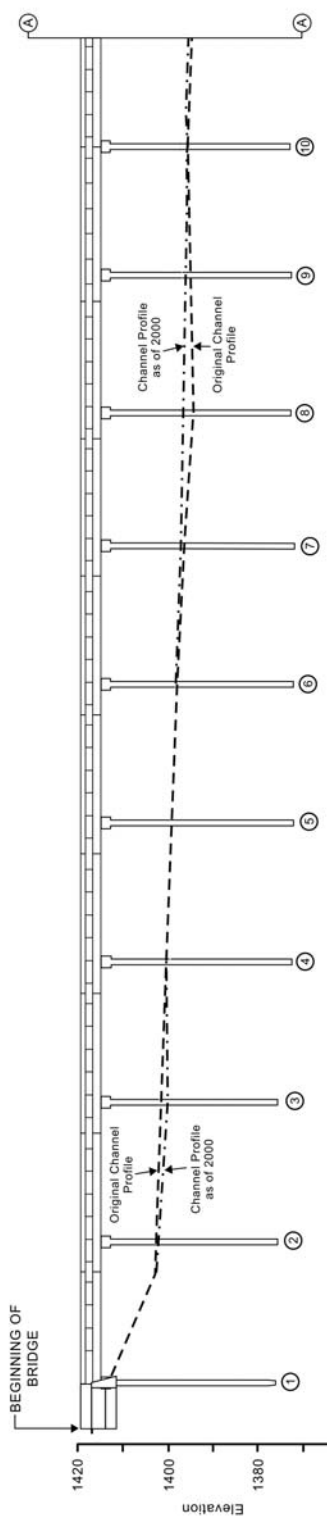
Figure C-5. Case History No. 5—Bridge Cross Section.

Table C-6. Case History No. 6.

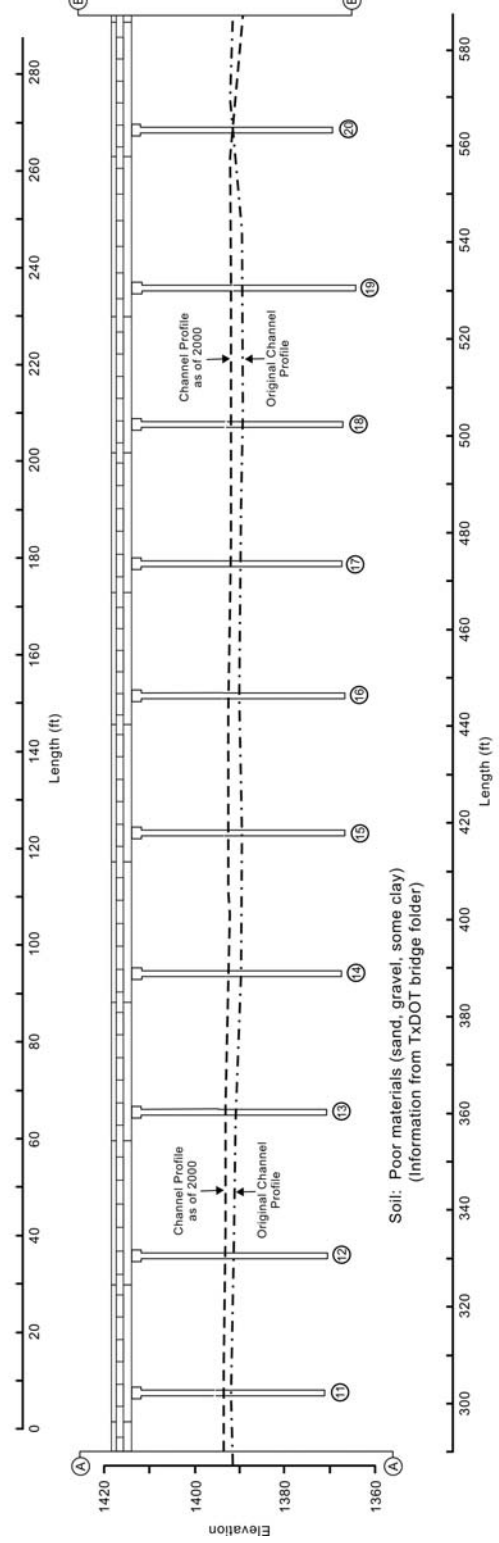
District:	San Antonio											
County:	Kendall (131)											
Structure No.:	15-131-0072-04-020											
Source:	DK20											
Highway:	US 87											
River:	Guadalupe River											
Status:	Unstable by Concise Analysis											
Foundation:	Square piles. Drilled shaft at Bent 27.											
Foundation Dimensions :	16-inch wide, 36-ft to 50-ft long concrete square piles (Channel Profile Drawing). 6-ft diameter, 17-ft long drilled shaft at Bent 27 (Secondary Scour Evaluation Worksheet 1).											
Channel Upstream Width (ft):	1616.3 (HEC-RAS Output, p. A2)											
Channel Width at Bridge (ft):	1199.5 (HEC-RAS Output, p. A2)											
Material:	Poor materials, i.e., clay and sandy gravel (Bridge Scour Action Plan 11/30/99).											
Year Built:	1932. Widened in 1984 (Bridge Scour Action Plan 11/30/99).											
Length (ft):	1434 (Channel Profile Drawing)											
No. of Spans:	29 concrete slab and girder spans, 2 steel stringer spans, 3-span continuous steel plate girder (Bridge Scour Action Plan 11/30/99)											
Z _{fresh 1} (ft)	8.5 (Bridge Scour Action Plan 11/30/99)											
Z _{fresh 2} (ft)	N/A											
Critical Scour Location:	Bent 27 (Bridge Scour Action Plan 11/30/99)											
Ref. No. (for Z _{fresh})	Measurement Date	Source	Scour depth (ft)	Location	V _{out} (ft/s)	V _{ms} (ft/s)	V _{dir} /V _{ms}	Z _{ms} (ft)	Z _{dir} /Z _{ms}	Z _{dir,model} (ft)	Z _{dir,field} (ft)	Z _{dir,model} /Z _{dir,field}
1	1998	CPD	6.3	Bent 27	-	-	-	-	-	-	-	-
1	2000	CPD	6.3	Bent 27	6.82	25.83	0.26	6.3	1	6.3	6.3	1.00

Note: CPD = Channel Profile Drawings

Case History No. 6
 Highway: US 87
 Waterway: Guadalupe River
 District: San Antonio



Soil: Poor materials (sand, gravel, some clay)
 (Information from TxDOT bridge folder)

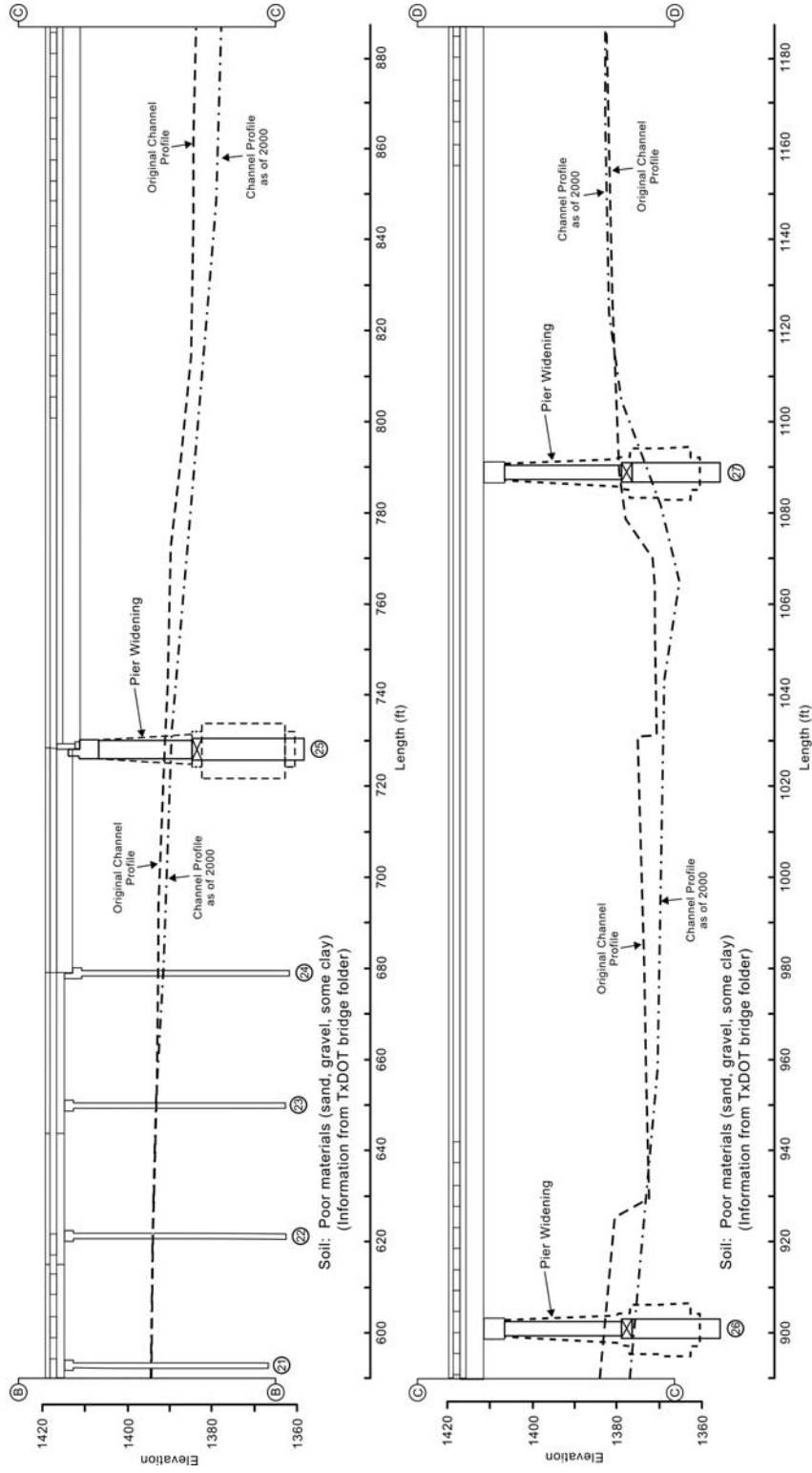


Soil: Poor materials (sand, gravel, some clay)
 (Information from TxDOT bridge folder)

Note: The accuracy of the drawing presented above is dependent upon the accuracy of the data provided.

Figure C-6. Case History No. 6—Bridge Cross Section Part 1.

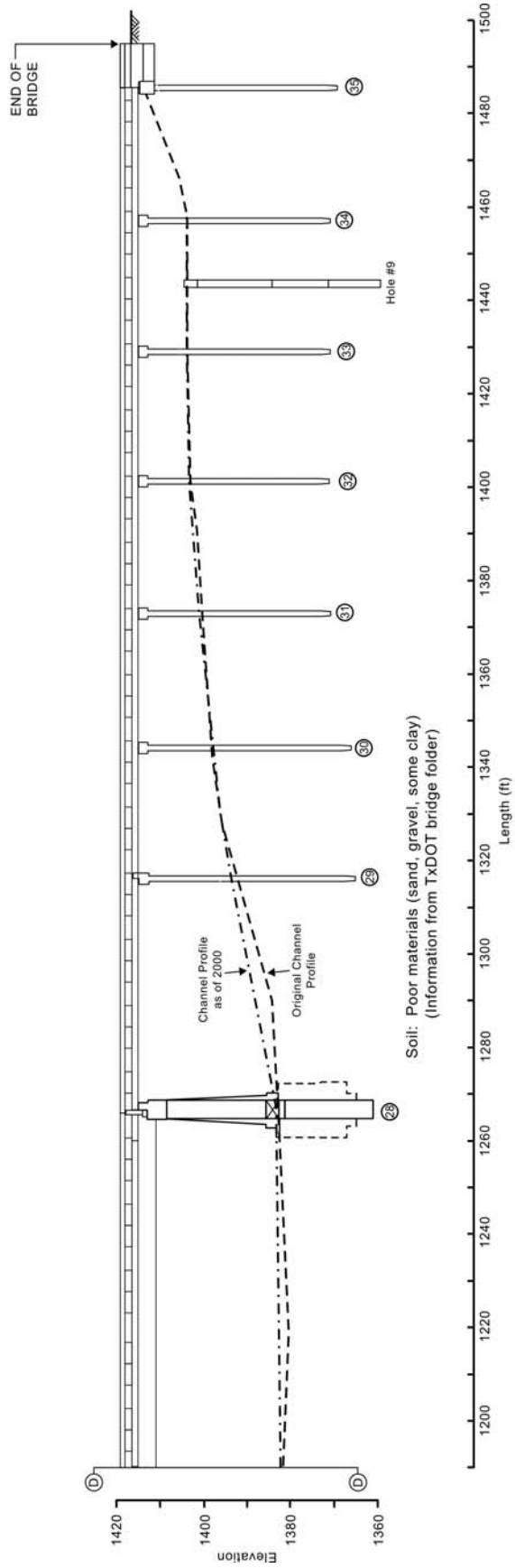
Case History No. 6
 Highway: US 87
 Waterway: Guadalupe River
 District: San Antonio



Note: The accuracy of the drawing presented above is dependent upon the accuracy of the data provided.

Figure C-7. Case History No. 6—Bridge Cross Section Part 2.

Case History No. 6
 Highway: US 87
 Waterway: Guadalupe River
 District: San Antonio



Note: The accuracy of the drawing presented above is dependent upon the accuracy of the data provided.

Figure C-8. Case History No. 6—Bridge Cross Section Part 3.

Table C-7. Case History No. 7.

District:	Houston (12)											
County:	Harris											
Structure No.:	12-102-0177-06-081											
Source:	DK20											
Highway:	US 59 South Bound											
River:	West Fork San Jacinto River											
Status:	Unstable by Concise Analysis											
Foundation:	Concrete square piles (Summary of Concise Analysis Results, 5/27/94)											
Pier/Foundation Dimensions:	16-inch wide concrete square piles with a minimum length of 10 ft (Summary of Concise Analysis Results, 5/27/94)											
Upstream Channel Width:	270 ft (Secondary Scour Evaluation Worksheet 4)											
Channel Width at Bridge:	187 ft (Secondary Scour Evaluation Worksheet 4)											
Material:	Foundation is embedded in more than 10 ft of sand (Summary of Results of Secondary Screening and Field Visit, 3/30/94)											
Year Built:	1961 (Form 113.2 — Bridge scour survey, 6/12/91)											
Length:	1645 (Form 113.2 — Bridge scour survey, 6/12/91)											
No. of Spans:	26											
Z _{dresh,1} :	16 ft (Summary of Concise Analysis Results, 5/27/94)											
Z _{dresh,2} :	N/A											
Critical Scour Location:	Bent 15 (TSEAS Secondary Scour Evaluation Worksheet 1)											
Ref No. (for Z _{dresh})	Measurement Date	Source	Scour Depth (ft)	Location	V _{fit} (ft/s)	V _{mo} (ft/s)	V _{fit} /V _{mo}	Z _{mo} (ft)	Z _{fit} /Z _{mo} Ratio	Z _{fit,model} (ft)	Z _{fit,field} (ft)	Z _{fit,model} /Z _{fit,field}
1	2/10/95	CCMR	0	Bent 15	-	-	-	-	-	-	-	-
1	1/29/97	CCMR	-0.3	Bent 15	11.1	9.8	1.13	0	1.5	-	-	-
1	1999	CCMR	1.6	Bent 15	7.4	11.1	0.67	0	1	-	-	-
1	1/2003	CCMR	-1.1	Bent 15	9	11.1	0.81	1.6	1	1.6	-1.1	-1.45
1	2/28/2007	CPD	5.7	Bent 15	7.8	11.1	0.70	1.6	1	1.6	5.7	0.28

Note: CCMR = Channel Cross-section Measurement Records; CPD = Channel Profile Drawing

Case History No. 7
 Highway: US 59 (SB)
 Waterway: San Jacinto River
 District: Houston

Note: The accuracy of the drawing presented below is dependent upon the accuracy of the data provided.

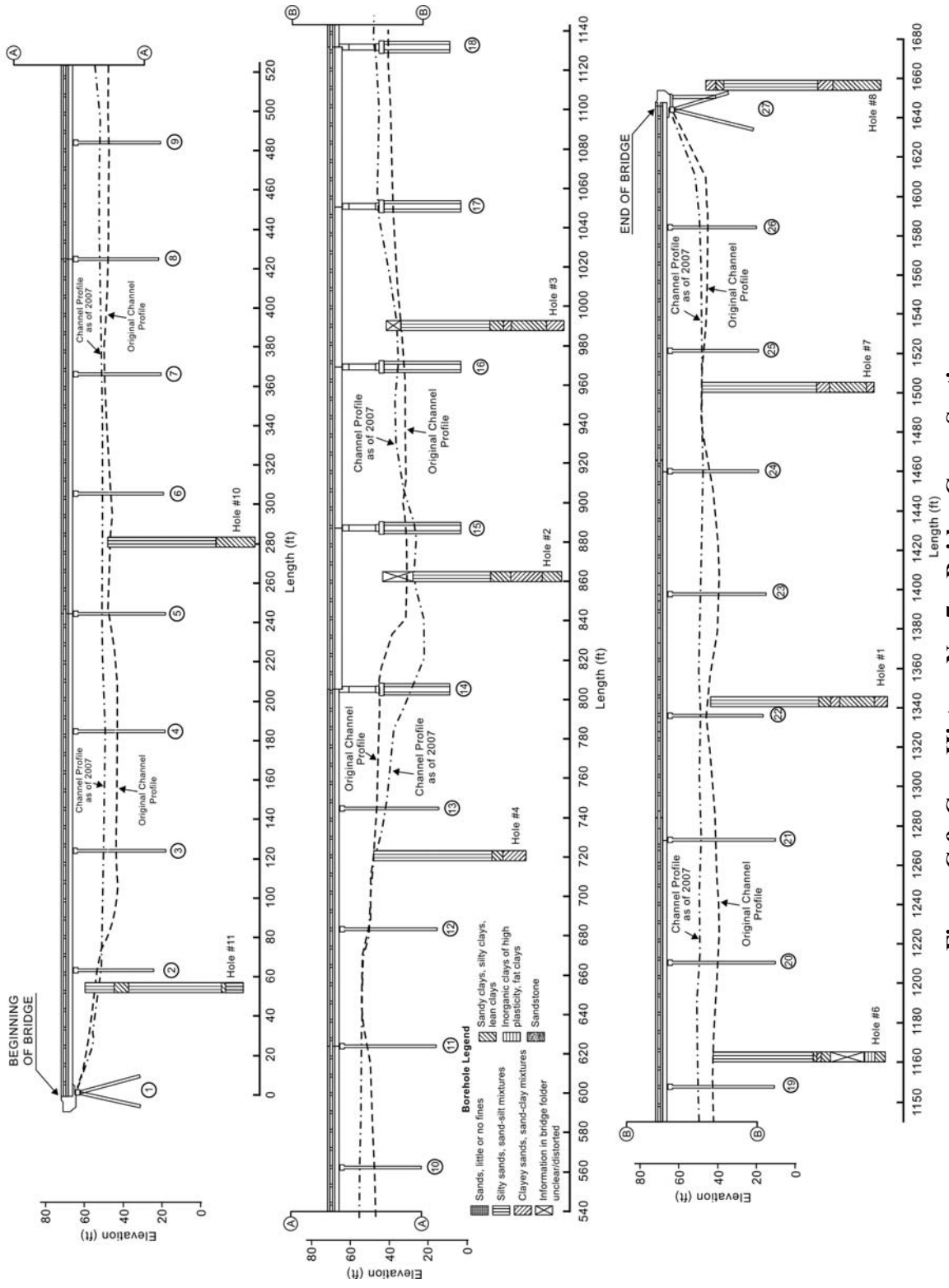


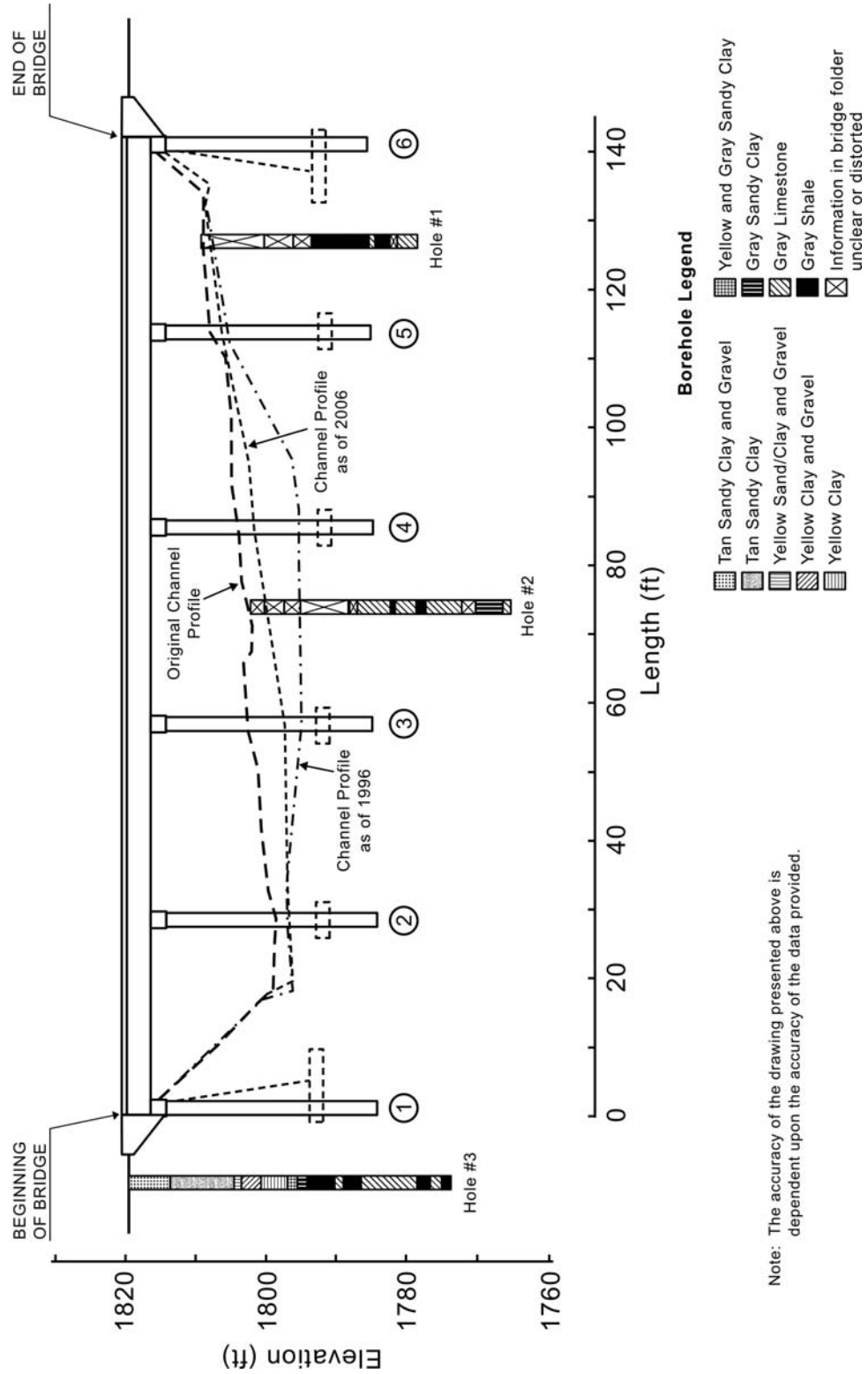
Figure C-9. Case History No. 7—Bridge Cross Section.

Table C-8. Case History No. 8.

District:	San Antonio (15)												
County:	Kerr (133)												
Structure No.:	15-133-0142-03-008												
Source:	DK20												
Highway:	SH 27												
River:	Dry Branch Creek												
Status:	Unstable by Concise Analysis												
Foundation:	Original bridge is on spread footings in shale clay. Widened portion of the bridge is on drilled shafts embedded in limestone or shale (Bridge Scour Action Plan, 11/15/99)												
Pier/Foundation Dimensions:	2-ft diameter drilled shafts (Secondary Scour Evaluation Worksheet 2 (A6) at Bent 4). The length of the drilled shafts is approximately 15 ft. The spread footings are embedded approximately 10 ft to 15 ft below the channel bottom (Channel Profile Drawing).												
Upstream Channel Width:	84.11 ft (Secondary Scour Evaluation Worksheet 4)												
Channel Width at Bridge:	78.11 ft (Secondary Scour Evaluation Worksheet 4)												
Material:	Clay, shale, limestone (Bridge Scour Action Plan, 11/15/99)												
Year Built:	1935, widened in 1963												
Length:	142 ft (Bridge Scour Action Plan)												
No. of Spans:	5-span concrete slab												
Z _{dresh 1} :	13 ft at Bent 4 (Bridge Scour Action Plan, 11/15/99)												
Z _{dresh 2} :	N/A												
Critical Scour Location:	Bent 4 (Bridge Scour Action Plan, 11/15/99)												
Ref. No. (for Z _{dresh})	Measurement Date	Source	Scour Depth (ft)	Location	V _{fit} (ft/s)	V _{ms} (ft/s)	V _{fit} /V _{ms}	Z _{mo} (ft)	Z _{fit} /Z _{mo}		Z _{fit,model} (ft)	Z _{fit,field} (ft)	Z _{fit,model} /Z _{fit,field}
1	1996	CPD	9	Bent 4	Data missing between 1994 and 1999	-	-	-	-	Ratio	Notes	-	-
1	1998	CPD	3	Bent 4	-	-	-	-	-	-	-	-	-
1	2000	CPD	3	Bent 4	-	-	-	-	-	-	-	-	-
1	2003	CPD	3	Bent 4	11.6	16.9	0.69	9	1	-	9	3	3
1	2004	CPD	3	Bent 4	10.4	16.9	0.62	9	1	-	9	3	3
1	2006	CPD	3	Bent 4	2.87	16.9	0.17	9	1	-	9	3	3

Note: CPD = Channel Profile Drawings

Case History No. 8
 Highway: SH 27
 Waterway: Dry Branch Creek
 District: San Antonio



Note: The accuracy of the drawing presented above is dependent upon the accuracy of the data provided.

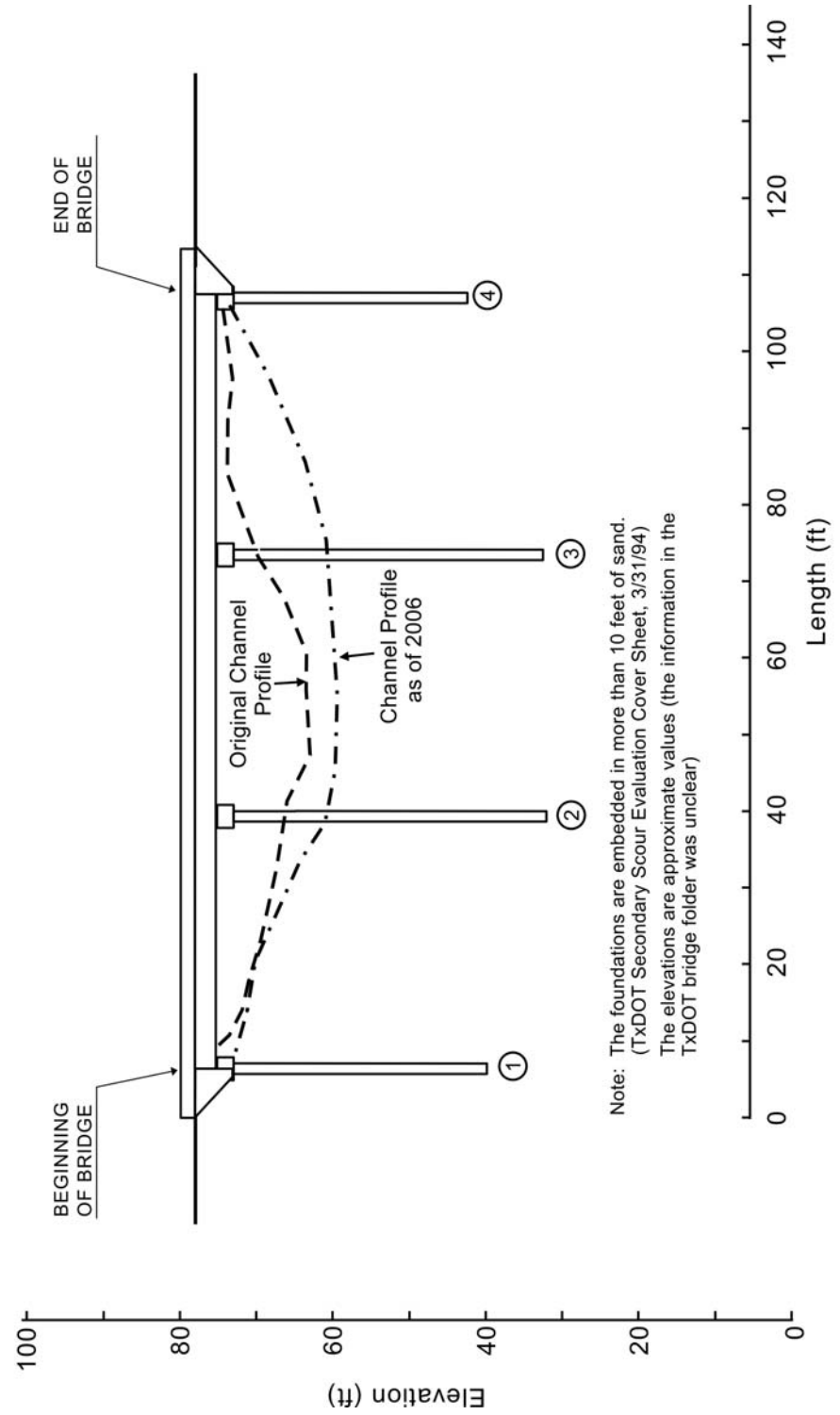
Figure C-10. Case History No. 8—Bridge Cross Section.

Table C-9. Case History No. 9.

District:	Houston (12)											
County:	Montgomery											
Structure No.:	12-170-0177-05-119											
Source:	DK20											
Highway:	US 59 @ Creekwood Drive											
River:	Peach Creek											
Status:	Unstable by Concise Analysis											
Foundation:	Concrete square piles (Form 113.2 — Bridge Scour Survey)											
Pier/Foundation Dimensions:	16 inch wide concrete square piles that are approximately 35 ft long (Secondary Scour Evaluation Sheet, 5/25/94 and Channel Profile Drawing)											
Upstream Channel Width:	650 ft (Secondary Scour Evaluation Worksheet s 4, 5/25/1994)											
Channel Width at Bridge:	Information unclear											
Material:	10 ft of sand (Secondary Scour Evaluation Cover Sheet, 3/31/94)											
Year Built:	1970 (Form 113.2 — Bridge Scour Survey)											
Length:	120 ft (Form 113.2 — Bridge Scour Survey)											
No. of Spans:	3 (Channel Profile Dwg.)											
Z _{fresh 1} :	21 ft at Bent 2 and 22 ft at Bent 3 (Secondary Scour Evaluation Sheet, 5/25/94)											
Z _{fresh 2} :	N/A											
Critical Scour Location:	Bents 2 and 3 (Secondary Scour Evaluation Sheet, 5/25/94 & Channel Profile Drawing)											
Ref. No. (for Z _{fresh})	Measurement Date	Source	Scour Depth (ft)	Location	V _{fit} (ft/s)	V _{mo} (ft/s)	V _{fit} /V _{mo}	Z _{mo} (ft)	Z _{fit} /Z _{mo}	Z _{fit,model} (ft)	Z _{fit,field} (ft)	Z _{fit,model} /Z _{fit,field}
1	1/7/1999	CPDM	8.2	Bent 2	-	-	-	-	-	-	-	-
1	1/19/2001	CPDM	5.1	Bent 2	4.5	13.7	0.33	8.2	1	8.2	5.1	1.6
1	1/2/2003	CPDM	7.9	Bent 2	8.6	13.7	0.63	8.2	1	8.2	7.9	1.0
1	1/21/2005	CPDM	8.5	Bent 2	8.1	13.7	0.60	8.2	1	8.2	8.5	1.0
1	12/4/2006	CPD	8	Bent 2	6.5	13.7	0.47	8.5	1	8.5	8	1.1
1	1/19/2001	CPDM	9	Bent 3	-	-	-	-	-	-	-	-
1	1/2/2003	CPDM	8.8	Bent 3	8.6	13.7	0.63	9	1	9	8.8	1.0
1	1/21/2005	CPDM	8.1	Bent 3	8.1	13.7	0.59	9	1	9	8.1	1.1
1	12/4/2006	CPD	10.7	Bent 3	6.5	13.7	0.47	9	1	9	10.7	0.8

Note: CPDM = Channel Profile Drawings and Channel Profile Measurements; CPD = Channel Profile Drawings

Case History No. 9
 Highway: US 59 @ Creekwood Drive
 Waterway: Peach Creek
 District: Houston



Note: The accuracy of the drawing presented above is dependent upon the accuracy of the data provided.

Figure C-11. Case History No. 9—Bridge Cross Section.

Table C-10. Case History No. 10.

District:	Houston (12)												
County:	80												
Structure No.:	12-080-0027-08-092												
Source:	DK20												
Highway:	US 90A (WB)												
River:	Brazos River												
Status:	On the scour critical list												
Foundation:	Square piles (Channel Profile Drawing, Russell -Veteto Engineering)												
Pier/Foundation Dimensions:	16-inch to-20 inch wide square piles that are approximately 70 ft to 78 ft long (Channel Profile Drawing, Russell-Veteto Engineering)												
Upstream Channel Width:	Not available												
Channel Width at Bridge:	Not available												
Material:	Silty sand, clayey sand (Channel Profile Drawing)												
Year Built:	1965 (Form 113.2 — Bridge Scour Survey, 6/17/91)												
Length:	942 ft (Form 113.2 — Bridge Scour Survey, 6/17/91)												
No. of Spans:	10 (Bridge Inspection Record, 2/4/07)												
Z _{fresh,1} :	26 ft at Bent 3 (Lateral stability controls)												
Z _{fresh,2} :	N/A												
Critical Scour Location:	Not specified												
Ref. No. (for Z _{fresh})	Measurement Date	Source	Scour Depth (ft)	Location	V _{fur} (ft/s)	V _{mo} (ft/s)	V _{fur} /V _{mo}	Z _{mo} (ft)	Z _{fur} /Z _{mo} Ratio	Notes	Z _{fur,model} (ft)	Z _{fur,field} (ft)	Z _{fur,model} /Z _{fur,field}
1	1992	CPD	19	Bent 3	-	-	-	-	-	-	-	-	-
1	3/28/1997	CPD	16.5	Bent 3	13.5	13.9	0.97	19	1	-	19	16.5	1.2
1	1999	CPD	21	Bent 3	11.9	13.9	0.86	19	1	-	19	21	0.9
1	2000	CPD	15	Bent 3	13.2	13.9	0.95	21	1	-	21	15	1.4
1	2002	CPD	15	Bent 3	11.5	13.9	0.83	21	1	-	21	15	1.4
1	2/4/07	CPD	20	Bent 3	13.1	13.9	0.94	21	1	-	21	20	1.05

Note: CPD = Channel Profile Drawings

Case History No. 10
 Highway: US 90A (WB)
 Waterway: Brazos River
 District: Houston

Note: The accuracy of the drawing presented below is dependent upon the accuracy of the data provided.

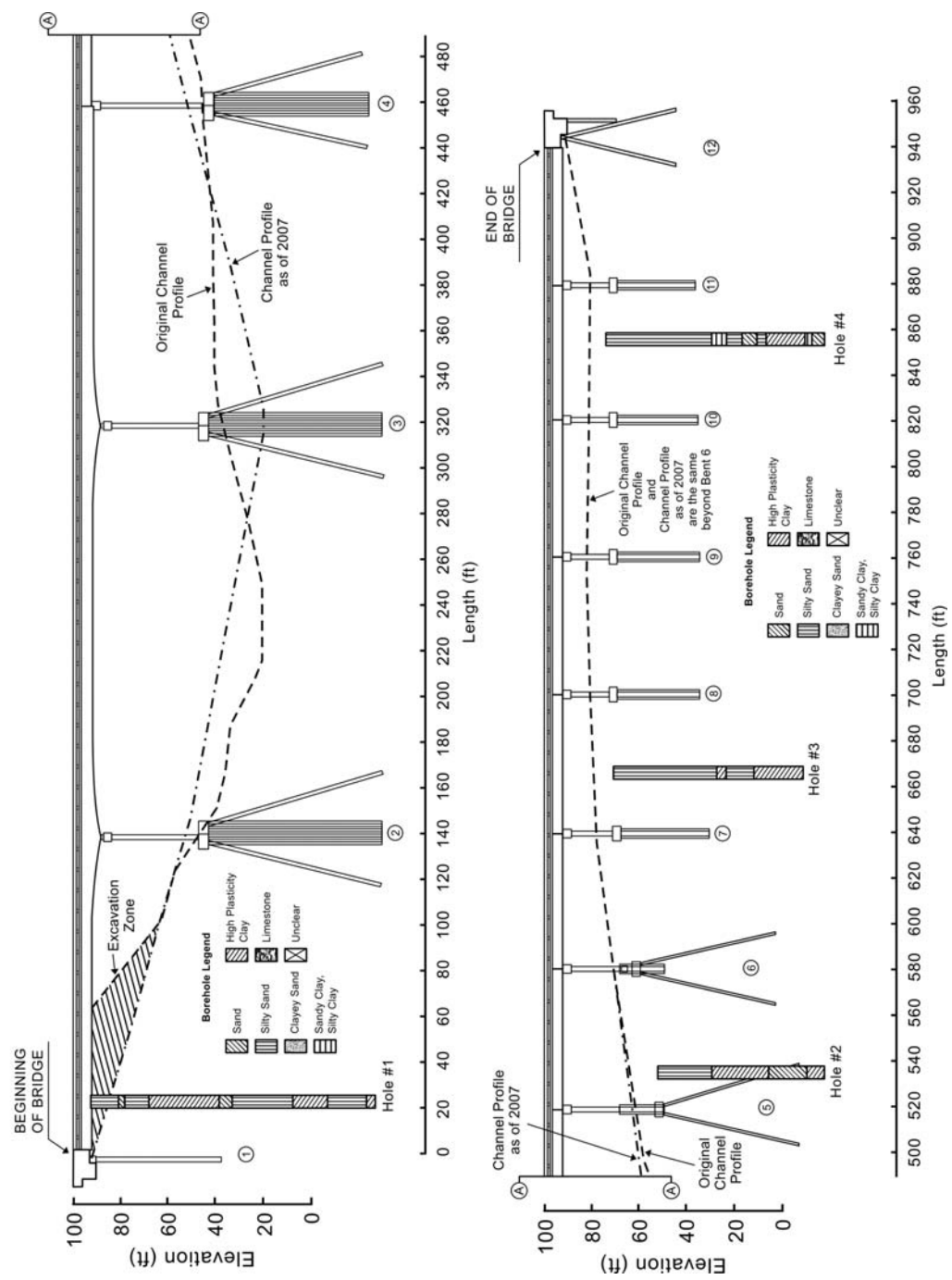


Figure C-12. Case History No. 10—Bridge Cross Section.

Table C-11. Case History No. 11.

District:	Bryan (17)											
County:	Leon (145)											
Structure No.:	17-145-0382-05-021											
Source:	Kiscok8											
Highway:	SH 7 (8 miles downstream of Lake Limestone dam and reservoir - Bridge Scour Action Plan)											
River:	Navasota River											
Status:	Stable by Concise Analysis											
Foundation:	Concrete piles (Bridge Inventory Record, 1/18/99)											
Pier/Foundation Dimensions :	14-inch diameter concrete piles that are approximately 28 ft to 50 ft long (Pier Scour Calculation Sheet, 8/1/96 and Channel Profile Drawing)											
Upstream Channel Width:	70 ft (Contraction Scour Calculation Sheet, 8/1/96)											
Channel Width at Bridge:	50 ft (Contraction Scour Calculation Sheet, 8/1/96)											
Material:	Sand (Bridge Scour Action Plan, 8/6/96)											
Year Built:	1956 (Bridge Scour Action Plan, 8/6/96)											
Length:	271 ft (Bridge Scour Action Plan, 8/6/96)											
No. of Spans:	7 (Bridge Scour Action Plan, 8/6/96)											
Z _{fresh 1} :	13 ft (lateral stability controls)											
Z _{fresh 2} :	N/A											
Critical Scour Location:	Bent 5 (Bridge Scour Action Plan, 8/6/96)											
Ref. No. (for Z _{fresh})	Measurement Date	Source	Scour Depth (ft)	Location	V _{fit} (ft/s)	V _{no} (ft/s)	V _{fit} /V _{no}	Z _{no} (ft)	Z _{fit} /Z _{no} Ratio	Z _{fit,model} (ft)	Z _{fit,field} (ft)	Z _{fit,model} /Z _{fit,field}
1	11/1994	CPD	4.0	Bent 5	-	-	-	-	-	-	-	-
1	1996	CPDM	6.2	Bent 5	3.7	5.9	0.63	4.0	1	4.0	6.2	0.7
1	12/14/1998	CPDM	6.2	Bent 5	4.6	5.9	0.78	6.2	1	6.2	12.5	0.9
1	4/16/01	CPDM	6.2	Bent 5	5	5.9	0.85	6.2	1	6.2	6.2	1
1	3/13/2003	CPDM	7.6	Bent 5	4.5	5.9	0.76	6.2	1	6.2	7.6	0.8
1	3/17/05	CPDM	8.1	Bent 5	3.4	5.9	0.58	7.6	1	7.6	8.1	0.9

Note: CPDM = Channel Profile Drawings and Channel Profile Measurements; CPD = Channel Profile Drawings

Case History No. 11
 Highway: SH 7
 Waterway: Navasota River
 District: Bryan

Note: The accuracy of the drawing presented below is dependent upon the accuracy of the data provided.

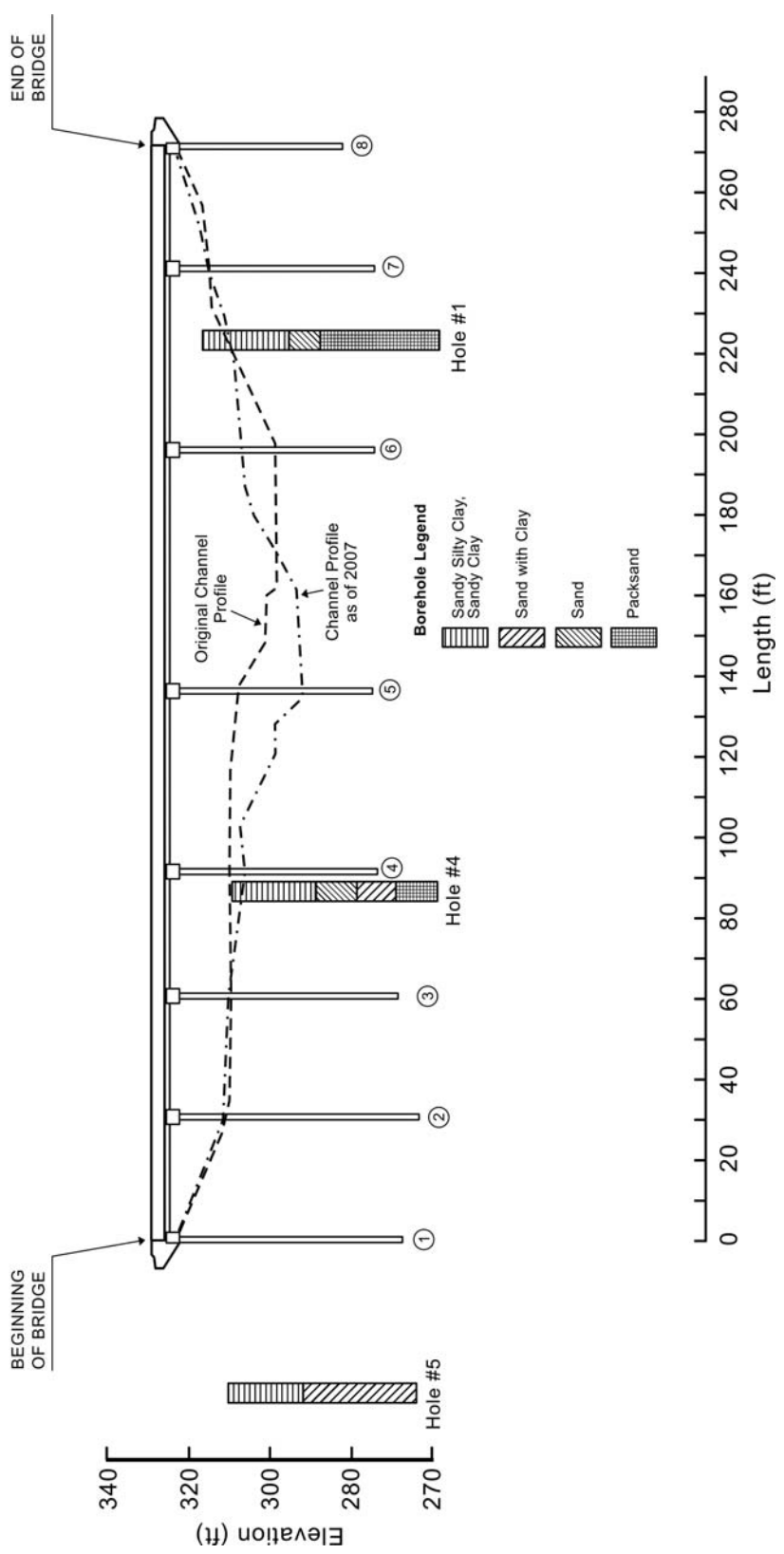


Figure C-13. Case History No. 11—Bridge Cross Section.

Table C-12. Results of Validation of BSA 2 for Case History No. 1.

Case History No.	Waterway	Highway	Sample No.	Sample Type	$V_{c,test}$ (m/s)	$V_{c,chart}$ (m/s)	V_{appr} (m/s)	Pier Diameter (m)	Water Upstream Depth (m)	Contraction Ratio	$Z_{max,I-EFA}$ (m)	$Z_{max,I-BSA2}$ (m)	$Z_{max,I-BSA2} / Z_{max,I-EFA}$
1	Sanders Creek	FM 39	1464	CL	0.4	0.51	0.5	0.1	10	0.5	2.05	1.84	0.90
							3.5	0.1	10	0.5	18.36	18.15	0.99
							0.5	1	10	0.5	2.63	2.42	0.92
							3.5	1	10	0.5	20.34	20.13	0.99
							0.5	10	10	0.5	5.11	4.90	0.96
							3.5	10	10	0.5	28.87	28.66	0.99
							0.5	0.1	20	0.5	2.83	2.53	0.89
							3.5	0.1	20	0.5	25.72	25.42	0.99
							0.5	1	20	0.5	3.41	3.11	0.91
							3.5	1	20	0.5	27.70	27.40	0.99
							0.5	10	20	0.5	5.89	5.59	0.95
							3.5	10	20	0.5	36.23	35.93	0.99
							0.5	0.1	10	0.9	0.88	0.67	0.76
							3.5	0.1	10	0.9	10.12	9.91	0.98
							0.5	1	10	0.9	1.45	1.24	0.85
							3.5	1	10	0.9	12.10	11.89	0.98
							0.5	10	10	0.9	3.93	3.72	0.95
							3.5	10	10	0.9	20.64	20.43	0.99
							0.5	0.1	20	0.9	1.17	0.87	0.74
							3.5	0.1	20	0.9	14.07	13.77	0.98
							0.5	1	20	0.9	1.74	1.44	0.83
							3.5	1	20	0.9	16.05	15.75	0.98
							0.5	10	20	0.9	4.22	3.93	0.93
							3.5	10	20	0.9	24.59	24.29	0.99
1	Sanders Creek	FM 39	1466	CH	0.9	0.73	0.5	0.1	10	0.5	1.09	1.42	1.30
							3.5	0.1	10	0.5	17.40	17.73	1.02
							0.5	1	10	0.5	1.67	2.00	1.20
							3.5	1	10	0.5	19.38	19.71	1.02
							0.5	10	10	0.5	4.15	4.48	1.08
							3.5	10	10	0.5	27.92	28.24	1.01
							0.5	0.1	20	0.5	1.48	1.94	1.31
							3.5	0.1	20	0.5	24.36	24.82	1.02
							0.5	1	20	0.5	2.05	2.51	1.22
							3.5	1	20	0.5	26.34	26.80	1.02
							0.5	10	20	0.5	4.53	4.99	1.10
							3.5	10	20	0.5	34.88	35.34	1.01
							0.5	0.1	10	0.9	0.00	0.24	243.77
							3.5	0.1	10	0.9	9.17	9.49	1.04
							0.5	1	10	0.9	0.49	0.82	1.66
							3.5	1	10	0.9	11.14	11.47	1.03
							0.5	10	10	0.9	2.97	3.30	1.11
							3.5	10	10	0.9	19.68	20.01	1.02
							0.5	0.1	20	0.9	0.00	0.27	272.90
							3.5	0.1	20	0.9	12.71	13.18	1.04
							0.5	1	20	0.9	0.39	0.85	2.19
							3.5	1	20	0.9	14.69	15.15	1.03
							0.5	10	20	0.9	2.87	3.33	1.16
							3.5	10	20	0.9	23.23	23.69	1.02

Table C-13. Results of Validation of BSA 2 for Case History No. 2.

Case History No.	Waterway	Highway	Sample No.	Sample Type	$V_{c,test}$ (m/s)	$V_{c,chart}$ (m/s)	V_{appr} (m/s)	Pier Diameter (m)	Water Upstream Depth (m)	Contraction Ratio	$Z_{max,I-EFA}$ (m)	$Z_{max,I-BSA2}$ (m)	$Z_{max,I-BSA2} / Z_{max,I-EFA}$
2	Alligator Creek	US 287	1460	CH	1.3	0.73	0.5	0.1	10	0.5	0.33	1.42	4.34
							3.5	0.1	10	0.5	16.63	17.73	1.07
							0.5	1	10	0.5	0.90	2.00	2.21
							3.5	1	10	0.5	18.61	19.71	1.06
							0.5	10	10	0.5	3.38	4.48	1.32
							3.5	10	10	0.5	27.15	28.24	1.04
							0.5	0.1	20	0.5	0.39	1.94	4.96
							3.5	0.1	20	0.5	23.28	24.82	1.07
							0.5	1	20	0.5	0.97	2.51	2.60
							3.5	1	20	0.5	25.25	26.80	1.06
							0.5	10	20	0.5	3.45	4.99	1.45
							3.5	10	20	0.5	33.79	35.34	1.05
							0.5	0.1	10	0.9	0.00	0.24	243.77
							3.5	0.1	10	0.9	8.40	9.49	1.13
							0.5	1	10	0.9	0.00	0.82	818.71
							3.5	1	10	0.9	10.38	11.47	1.11
							0.5	10	10	0.9	2.21	3.30	1.50
							3.5	10	10	0.9	18.91	20.01	1.06
							0.5	0.1	20	0.9	0.00	0.27	272.90
							3.5	0.1	20	0.9	11.63	13.18	1.13
0.5	1	20	0.9	0.00	0.85	847.85							
3.5	1	20	0.9	13.61	15.15	1.11							
0.5	10	20	0.9	1.78	3.33	1.87							
3.5	10	20	0.9	22.14	23.69	1.07							
2	Alligator Creek	US 287	1462	CH	0.5	0.73	0.5	0.1	10	0.5	1.86	1.42	0.76
							3.5	0.1	10	0.5	18.17	17.73	0.98
							0.5	1	10	0.5	2.44	2.00	0.82
							3.5	1	10	0.5	20.15	19.71	0.98
							0.5	10	10	0.5	4.92	4.48	0.91
							3.5	10	10	0.5	28.68	28.24	0.98
							0.5	0.1	20	0.5	2.56	1.94	0.76
							3.5	0.1	20	0.5	25.45	24.82	0.98
							0.5	1	20	0.5	3.14	2.51	0.80
							3.5	1	20	0.5	27.43	26.80	0.98
							0.5	10	20	0.5	5.62	4.99	0.89
							3.5	10	20	0.5	35.96	35.34	0.98
							0.5	0.1	10	0.9	0.68	0.24	0.36
							3.5	0.1	10	0.9	9.93	9.49	0.96
							0.5	1	10	0.9	1.26	0.82	0.65
							3.5	1	10	0.9	11.91	11.47	0.96
							0.5	10	10	0.9	3.74	3.30	0.88
							3.5	10	10	0.9	20.45	20.01	0.98
							0.5	0.1	20	0.9	0.90	0.27	0.30
							3.5	0.1	20	0.9	13.80	13.18	0.95
0.5	1	20	0.9	1.47	0.85	0.58							
3.5	1	20	0.9	15.78	15.15	0.96							
0.5	10	20	0.9	3.95	3.33	0.84							
3.5	10	20	0.9	24.31	23.69	0.97							

Table C-14. Results of Validation of BSA 2 for Case History No. 11.

Case History No.	Waterway	Highway	Sample No.	Sample Type	$V_{c,test}$ (m/s)	$V_{c,chart}$ (m/s)	V_{appr} (m/s)	Pier Diameter (m)	Water Upstream Depth (m)	Contraction Ratio	$Z_{max,I-EFA}$ (m)	$Z_{max,I-BSA2}$ (m)	$Z_{max,I-BSA2} / Z_{max,I-EFA}$
11	Navasota River	SH 7	Navasota Layer 1	SC	0.9	0.63	0.5	0.1	10	0.5	1.09	1.61	1.47
							3.5	0.1	10	0.5	17.40	17.92	1.03
							0.5	1	10	0.5	1.67	2.19	1.31
							3.5	1	10	0.5	19.38	19.90	1.03
							0.5	10	10	0.5	4.15	4.67	1.12
							3.5	10	10	0.5	27.92	28.43	1.02
							0.5	0.1	20	0.5	1.48	2.21	1.50
							3.5	0.1	20	0.5	24.36	25.09	1.03
							0.5	1	20	0.5	2.05	2.78	1.36
							3.5	1	20	0.5	26.34	27.07	1.03
							0.5	10	20	0.5	4.53	5.26	1.16
							3.5	10	20	0.5	34.88	35.61	1.02
							0.5	0.1	10	0.9	0.00	0.44	435.60
							3.5	0.1	10	0.9	9.17	9.68	1.06
							0.5	1	10	0.9	0.49	1.01	2.05
							3.5	1	10	0.9	11.14	11.66	1.05
							0.5	10	10	0.9	2.97	3.49	1.17
							3.5	10	10	0.9	19.68	20.20	1.03
							0.5	0.1	20	0.9	0.00	0.54	544.19
							3.5	0.1	20	0.9	12.71	13.45	1.06
0.5	1	20	0.9	0.39	1.12	2.89							
3.5	1	20	0.9	14.69	15.42	1.05							
0.5	10	20	0.9	2.87	3.60	1.26							
3.5	10	20	0.9	23.23	23.96	1.03							
11	Navasota River	SH 7	Navasota Layer 2	CL	0.4	0.51	0.5	0.1	10	0.5	2.05	1.84	0.90
							3.5	0.1	10	0.5	18.36	18.15	0.99
							0.5	1	10	0.5	2.63	2.42	0.92
							3.5	1	10	0.5	20.34	20.13	0.99
							0.5	10	10	0.5	5.11	4.90	0.96
							3.5	10	10	0.5	28.87	28.66	0.99
							0.5	0.1	20	0.5	2.83	2.53	0.89
							3.5	0.1	20	0.5	25.72	25.42	0.99
							0.5	1	20	0.5	3.41	3.11	0.91
							3.5	1	20	0.5	27.70	27.40	0.99
							0.5	10	20	0.5	5.89	5.59	0.95
							3.5	10	20	0.5	36.23	35.93	0.99
							0.5	0.1	10	0.9	0.88	0.67	0.76
							3.5	0.1	10	0.9	10.12	9.91	0.98
							0.5	1	10	0.9	1.45	1.24	0.85
							3.5	1	10	0.9	12.10	11.89	0.98
							0.5	10	10	0.9	3.93	3.72	0.95
							3.5	10	10	0.9	20.64	20.43	0.99
							0.5	0.1	20	0.9	1.17	0.87	0.74
							3.5	0.1	20	0.9	14.07	13.77	0.98
0.5	1	20	0.9	1.74	1.44	0.83							
3.5	1	20	0.9	16.05	15.75	0.98							
0.5	10	20	0.9	4.22	3.93	0.93							
3.5	10	20	0.9	24.59	24.29	0.99							

**APPENDIX D:
DATA ON EFA CURVES**

Table D-1. Summary of EFA Test Data and Associated Soil Classification Tests.

No.	Soil Classification	Sample No.	Data Source	Liquid Limit (%)	Plastic Limit (%)	Plasticity Index (%)	Unit Weight, γ (kN/m ³)	Water Content (%)	Undrained Shear Strength (kPa)	% Passing #200 Sieve	Mean Particle Diameter, D ₅₀ (mm)	Critical Shear Stress, τ_c (Pa)	Critical Velocity, V_c (m/s)
1	CH	S1-B1-(0-2ft)-TW	ILJT 2006 (Katrina)	65	22	43	20.2	31.7	-	89.9	-	12.0	1.5
2	CH	S2-B1-(0-2ft)-TW	ILJT 2006 (Katrina)	49	17	32	19.7	16.1	-	67.2	-	11.3	1.5
3	CH	S7-B1-(0-2ft)-TW	ILJT 2006 (Katrina)	78	32	46	17.4	26.7	-	90.1	-	4.7	1.0
4	CH	S8-B1-(0-2ft)-TW	ILJT 2006 (Katrina)	85	36	49	17.7	32.3	-	97.3	-	5.0	1.0
5	SP	S11-(0-0.5ft)-LC-TW	ILJT 2006 (Katrina)	-	-	-	12.3	1.0	-	-	-	0.2	0.2
6	SP	S11-(0-0.5ft)-HC-TW	ILJT 2006 (Katrina)	-	-	-	13.3	1.0	-	-	-	0.6	0.3
7	CH	S12-B1-(0-2ft)-TW	ILJT 2006 (Katrina)	67	21	46	14.8	44.9	-	92.0	-	0.7	0.4
8	SC	Navasota Layer 1	Kwak, K. 2000, p. 81 & 82	28	14	14	18.0	28.5	-	26.2	0.125	4.0	0.9
9	CL	Navasota River Layer 2	Kwak, K. 2000, p. 81 & 83	26	6	20	18.8	26.6	32.1	57.7	-	0.7	0.4
10	SC	Brazos Layer 1	Kwak, K. 2000, p. 81 & 83	24	9	15	20.2	17.3	-	30.0	0.265	0.4	0.3
11	SC	Brazos Layer 2	Kwak, K. 2000, p. 81 & 84	24	9	15	20.2	17.3	-	30.0	0.265	0.7	0.4
12	CL	San Jacinto Layer 1	Kwak, K. 2000, p. 81 & 84	22	9	13	19.6	151.6	23.9	50.4	-	1.0	0.5
13	CL	San Jacinto Layer 2	Kwak, K. 2000, p. 81 & 85	22	9	13	19.6	151.6	23.9	50.4	-	0.2	0.2
14	Clay/Silt	San Jacinto Layer 3	Kwak, K. 2000, p. 81 & 85	-	-	-	16.7	26.9	4.8	60.7	-	1.0	0.4
15	CL	San Jacinto Layer 4	Kwak, K. 2000, p. 81 & 86	38	13	25	20.8	27.8	21.5	94.5	-	4.3	0.9
16	CH	Sims	Kwak, K. 2000, p. 81 & 88	84	16	68	19.6	25.3	23.0	99.1	0.0012	2.9	0.8
17	Fine Gravel	Trinity Layer 1	Kwak, K. 2000, p. 81 & 86	-	-	-	22.0	7.7	-	11.5	6	1.0	0.5
18	CL	Trinity Layer 2	Kwak, K. 2000, p. 81 & 87	42	9	33	22.1	22.2	11.5	68.4	-	4.2	0.9
19	CL	San Marcos Layer 1	Kwak, K. 2000, p. 81 & 87	41	17	24	19.6	22.0	27.3	78.3	-	0.3	0.2
20	CL	San Marcos Layer 2	Kwak, K. 2000, p. 81 & 88	40	19	21	20.2	24.4	29.7	73.4	-	1.1	0.5
21	CL	Bedias (75) Layer 1	Kwak, K. 2000, p. 81 & 89	48	14	34	20.0	18.1	10.0	86.8	0.048	1.7	0.6
22	Fine Sand with Clay/Silt	Bedias (75) Layer 2	Kwak, K. 2000, p. 81 & 89	-	-	-	21.3	17.5	-	35.1	0.13	0.3	0.2
23	CH	Bedias (90)	Kwak, K. 2000, p. 81 & 90	55	16	39	19.6	23.6	62.0	91.3	0.04	0.2	0.3
24	ML	LAR 1F-08-01-PT2	Sacramento - Ayres	49	35	14	113.5	37.7	-	97.6	0.018	6.0	1.2
25	ML	LAR 1F-08-02-PT1	Sacramento - Ayres	42	37	5	117.2	31.4	-	97.0	0.03	8.0	1.2
26	MH	LAR 1F-08-03-PT2	Sacramento - Ayres	51	45	6	109.7	44.4	-	91.4	0.044	88.3	4.5
27	ML	LAR 1F-08-04-PT2	Sacramento - Ayres	39	35	4	98.8	36.2	-	88.4	0.06	31.4	1.8
28	CL	Porcelain Clay	(TTI Rpt 2937-1, 1999, p. 21, 79)	34	20	14	18.0	28.5	12.5	100.0	0.0062	0.9	0.4
29	SP	Coarse Sand	(TTI Rpt 2937-1, 1999, p. 11 & 58)	-	-	-	13.8	-	-	-	3.375	2.2	0.6
30	CL	1454	SSSRICOS	35	14	21	19.2	20.0	-	76.0	0.028	0.4	0.4
31	CL	1456	SSSRICOS	39	13	26	19.7	21.8	-	60.2	0.046	1.6	0.7
32	CH	1459	SSSRICOS	57	15	42	18.5	28.8	-	83.2	0.004	0.6	0.5
33	CH	1460	SSSRICOS	70	20	50	17.0	36.0	-	94.8	0.001	9.4	1.3
34	CH	1462	SSSRICOS	64	17	47	17.9	29.1	-	87.2	0.004	2.2	0.5
35	CL	1464	SSSRICOS	42	25	17	19.1	26.7	-	96.4	0.011	2.0	0.4
36	ML	1465	SSSRICOS	47	29	18	19.3	28.7	-	99.4	0.01	0.4	0.3
37	CH	1466	SSSRICOS	54	25	29	19.3	22.4	-	99.4	0.009	3.7	0.9
38	CL-ML	1467	SSSRICOS	20	13	7	22.1	11.4	-	50.2	0.073	0.2	0.2
39	SC	1468	SSSRICOS	15	13	2	20.4	17.3	-	33.6	0.13	0.3	0.2
40	CH	EFA-1	TXDOT	99	77	22	18.0	32.6	-	98.3	-	0.4	0.3
41	CL	EFA-2	TXDOT	32	21	11	19.9	30.3	20.9	64.7	-	4.9	1.0

No.	Soil Classification	Sample No.	Data Source	Liquid Limit (%)	Plastic Limit (%)	Plasticity Index (%)	Unit Weight, γ (kN/m ³)	Water Content (%)	Undrained Shear Strength (kPa)	% Passing #200 Sieve	Mean Particle Diameter, D ₅₀ (mm)	Critical Shear Stress, τ_c (Pa)	Critical Velocity, V _c (m/s)
42	CL	EFA-3	TxDOT	47	34	13	19.5	28.1	13.6	100.0	-	0.5	0.3
43	CL	EFA-4	TxDOT	47	35	12	17.8	25.4	-	94.3	-	2.6	0.6
44	CL	EFA-5	TxDOT	35	24	11	21.1	16.5	54.4	75.9	-	0.4	0.3
45	CH	EFA-6	TxDOT	88	70	18	17.0	32.9	51.3	97.4	-	5.0	1.1
46	CH	EFA-7	TxDOT	74	58	16	17.5	37.8	49.2	86.9	-	3.4	0.8
47	CH	EFA-8	TxDOT	74	58	16	18.5	20.4	17.8	86.9	-	0.3	0.3
48	CL	EFA-9	TxDOT	37	24	13	19.8	23.7	57.6	83.7	-	0.5	0.3
49	CL	EFA-10	TxDOT	35	25	10	19.8	18.8	28.3	84.6	-	1.6	0.6
50	SC	EFA-11	TxDOT	43	30	13	18.5	42.1	6.3	11.6	-	0.2	0.2
51	CL	EFA-12	TxDOT	36	25	11	20.8	21.6	30.3	38.7	-	0.3	0.2
52	CH	EFA-13	TxDOT	69	53	16	18.2	13.9	0.7	93.3	-	5.5	1.0
53	CL	EFA-14	TxDOT	49	30	19	18.9	31.8	13.6	96.5	-	0.4	0.3
54	CH	EFA-15	TxDOT	80	48	32	17.5	39.1	44.5	94.4	-	0.5	0.3
55	CH	EFA-17	TxDOT	59	37	22	19.1	24.9	38.7	90.7	-	9.9	1.5
56	CL	EFA-18	TxDOT	47	32	15	19.8	24.2	6.3	90.7	-	2.0	0.6
57	CH	EFA-19	TxDOT	74	55	19	17.8	44.5	31.4	93.7	-	1.0	0.4
58	SC	EFA-20	TxDOT	27	16	11	19.6	17.8	15.7	15.4	-	1.6	0.6
59	SM-SC	EFA-21	TxDOT	23	18	5	18.0	20.5	37.2	43.9	-	1.9	0.7
60	CH	EFA-22	TxDOT	81	25	56	18.8	30.4	26.2	85.3	-	2.8	0.8
61	CL	EFA-23	TxDOT	38	14	24	19.9	20.0	62.3	82.7	-	1.6	0.6
62	SM-SC	EFA-24	TxDOT	19	13	6	19.0	21.7	22.0	32.3	-	4.0	0.9
63	CL	EFA-25	TxDOT	45	12	33	19.1	24.0	6.3	77.9	-	1.6	0.6
64	CL	EFA-26	TxDOT	28	12	16	15.6	35.9	8.9	58.7	-	1.6	0.6
65	CH	EFA-27	TxDOT	54	18	36	16.7	28.5	21.5	81.2	-	1.6	0.6
66	SC	EFA-28	TxDOT	38	16	22	22.0	9.5	32.4	43.1	-	9.9	1.5
67	CL	EFA-29	TxDOT	38	16	22	19.2	19.0	32.4	56.9	-	2.1	0.7
68	SC	EFA-30	TxDOT	38	15	23	21.5	12.8	44.0	39.9	-	4.4	1.0
69	CL=ML	EFA-35	TxDOT	22	16	6	19.6	20.7	22.0	68.7	-	4.4	1.0
70	CL	EFA-36	TxDOT	26	17	9	20.4	16.2	-	77.1	-	4.4	1.0
71	CL	EFA-37	TxDOT	26	19	7	17.7	21.8	70.1	94.4	-	4.4	1.0
72	CH	EFA-38	TxDOT	66	19	47	24.3	35.4	-	77.8	-	4.4	1.0
73	CH	B1-(30-32)	Meander Migration	66	20	46	20.5	28.2	83.0	-	-	0.4	0.3
74	CL	B1-(40-42)	Meander Migration	32	13	19	20.3	30.0	34.0	-	-	0.1	0.1
75	CL	B2-(30-32)	Meander Migration	39	15	23	20.8	21.7	43.0	-	-	0.4	0.4
76	SP	B2-(48-50)	Meander Migration	-	-	-	20.6	19.6	-	-	-	0.3	0.2
77	SC	B3-(10-12)	Meander Migration	-	-	-	23.3	12.1	-	-	-	0.2	0.2
78	CL	B3-(20-22)	Meander Migration	47	13	34	20.4	23.3	92.0	-	-	0.5	0.3
79	CH	B3-(30-32)	Meander Migration	64	24	40	21.2	25.5	140.0	-	-	0.5	0.3
80	CH	B3-(38-40)	Meander Migration	82	26	56	19.3	29.9	140.0	-	-	0.3	0.3
81	CH	B3-(48-50)	Meander Migration	85	29	56	20.1	31.6	140.0	-	-	0.2	0.3

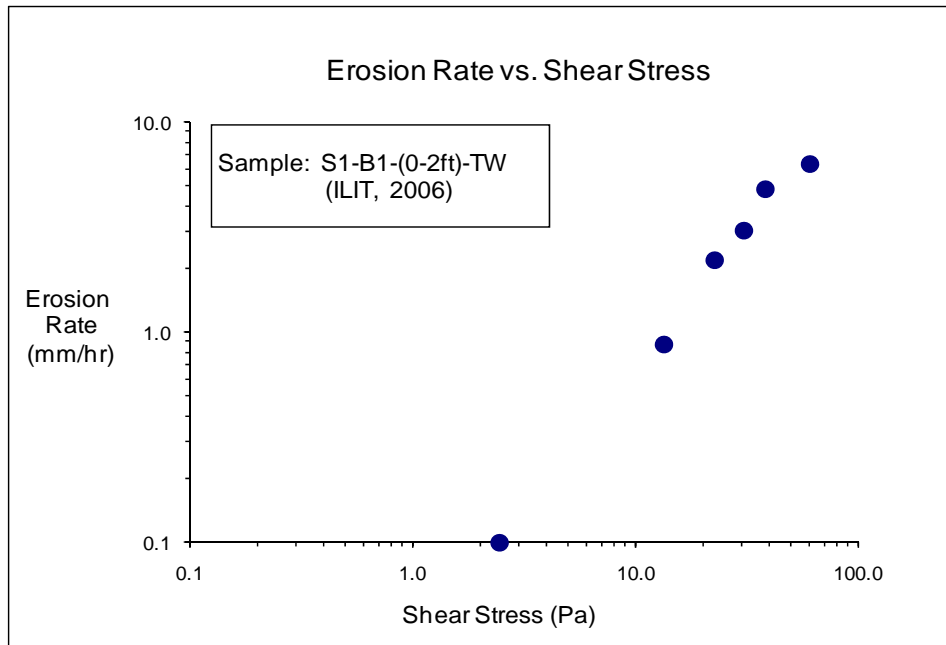


Figure D-1(a). EFA Test Results for Soil Sample S1-B1-(0-2ft)-TW (Shear Stress).

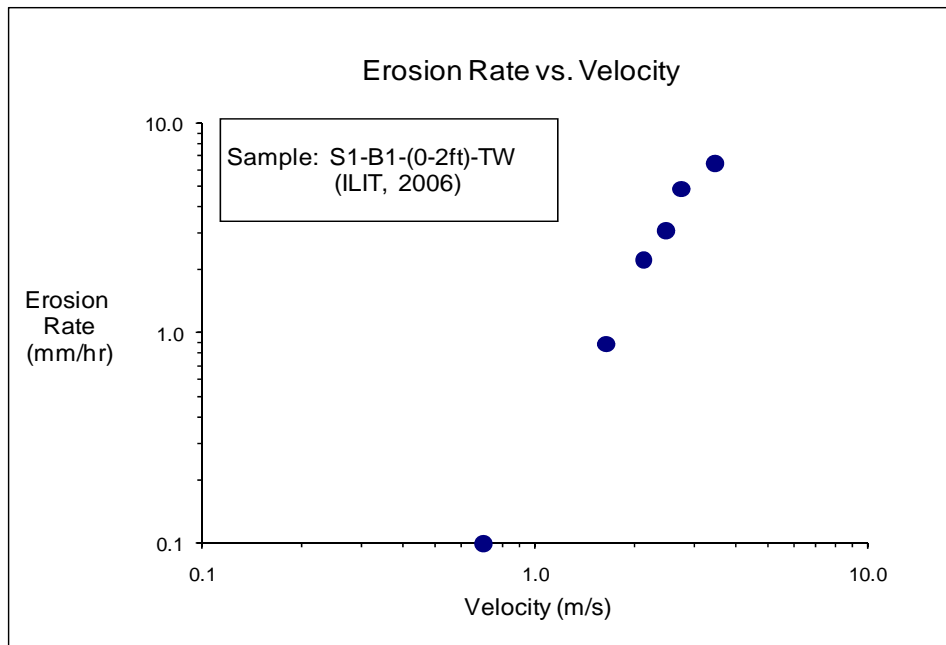


Figure D-1(b). EFA Test Results for Soil Sample S1-B1-(0-2ft)-TW (Velocity).

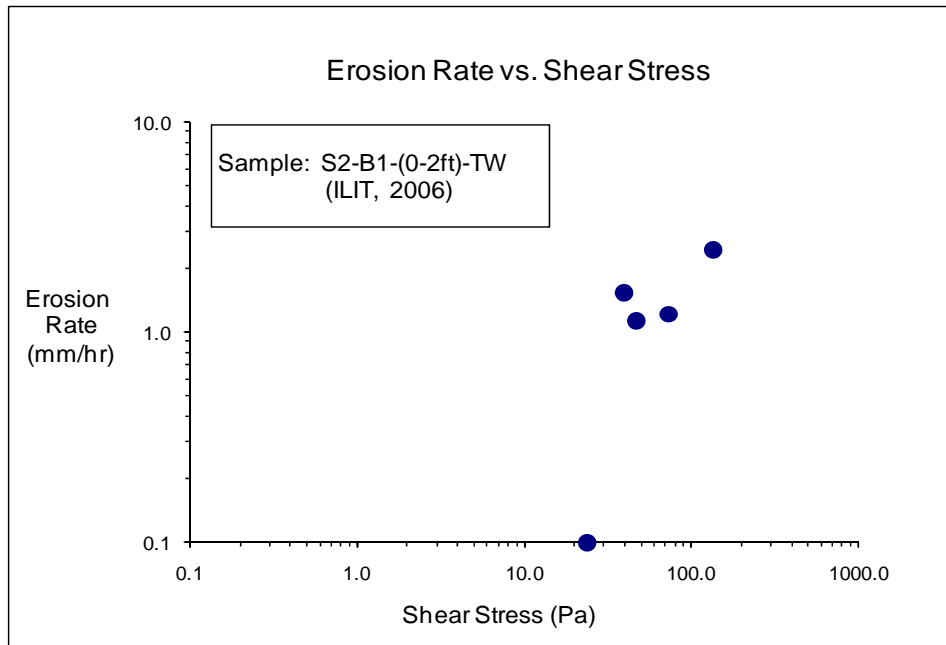


Figure D-2(a). EFA Test Results for Soil Sample S2-B1-(0-2ft)-TW (Shear Stress).

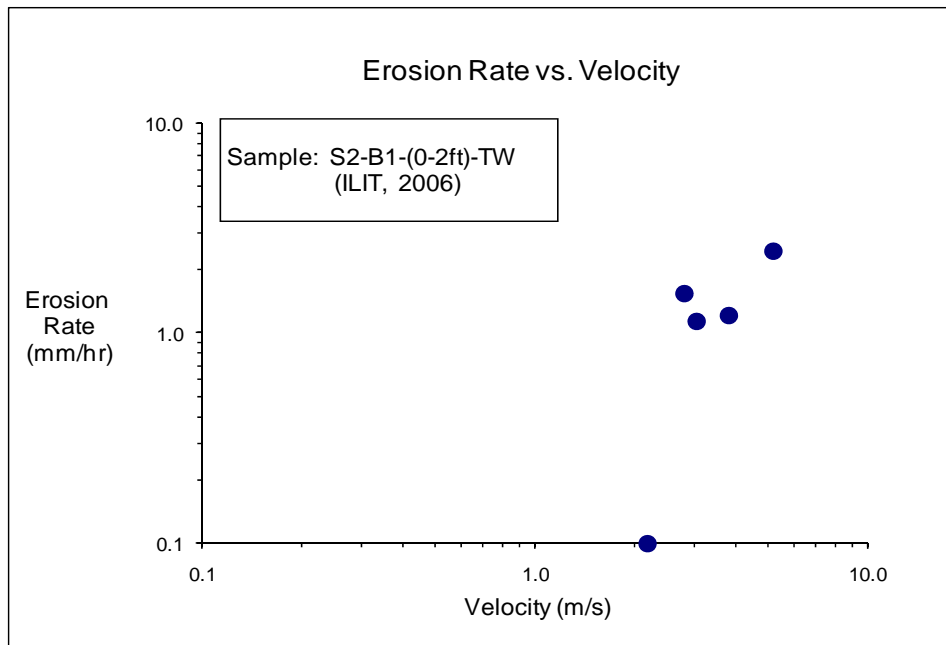


Figure D-2(b). EFA Test Results for Soil Sample S2-B1-(0-2ft)-TW (Velocity).

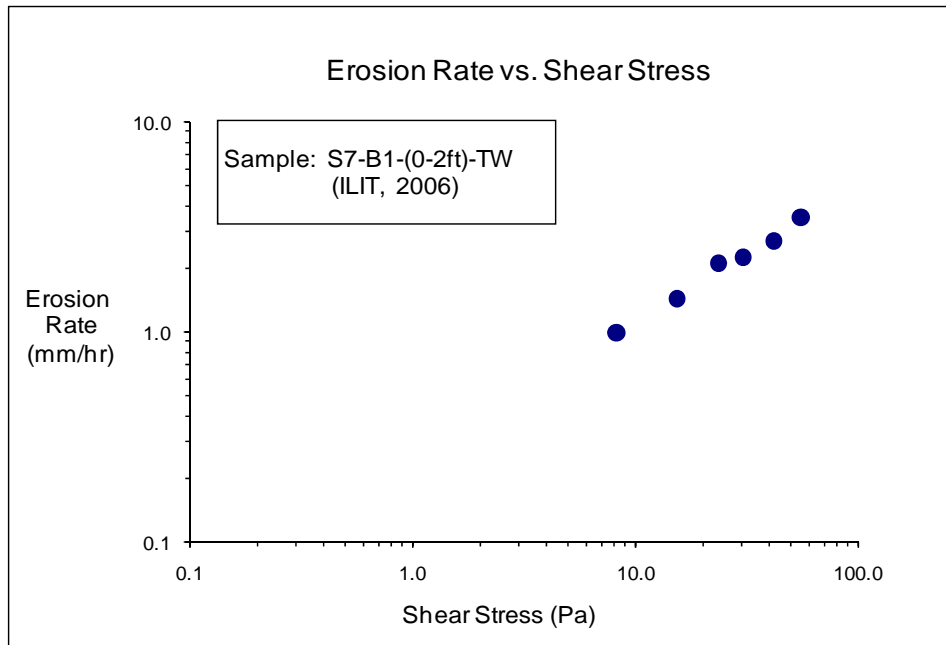


Figure D-3(a). EFA Test Results for Soil Sample S7-B1-(0-2ft)-TW (Shear Stress).

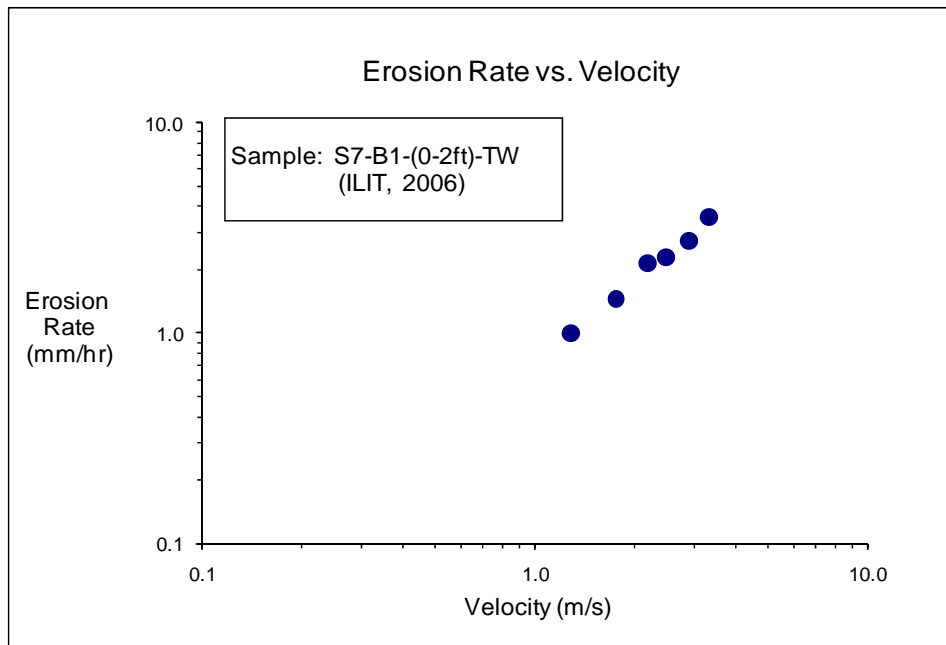


Figure D-3(b). EFA Test Results for Soil Sample S7-B1-(0-2ft)-TW (Velocity).

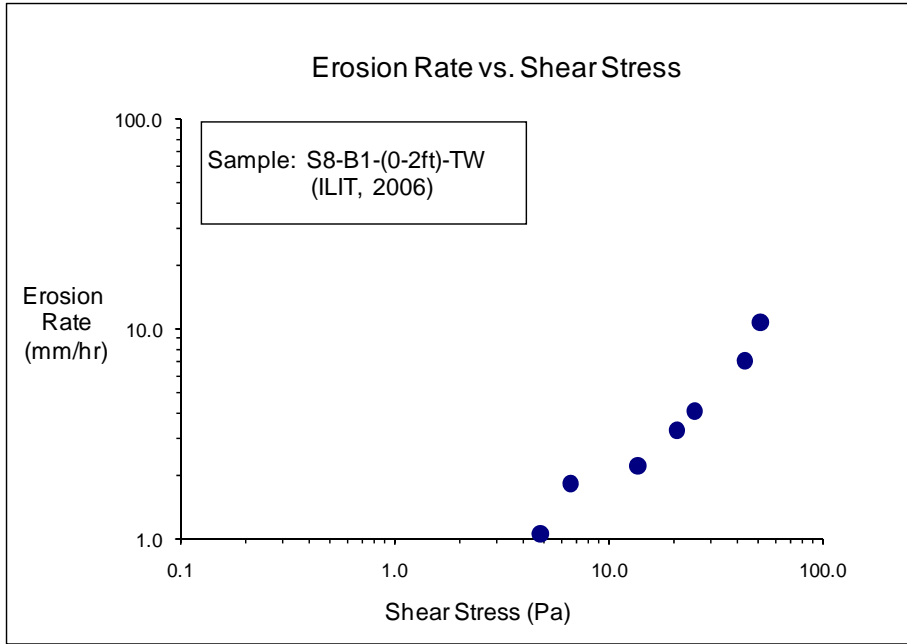


Figure D-4(a). EFA Test Results for Soil Sample S8-B1-(0-2ft)-TW (Shear Stress).

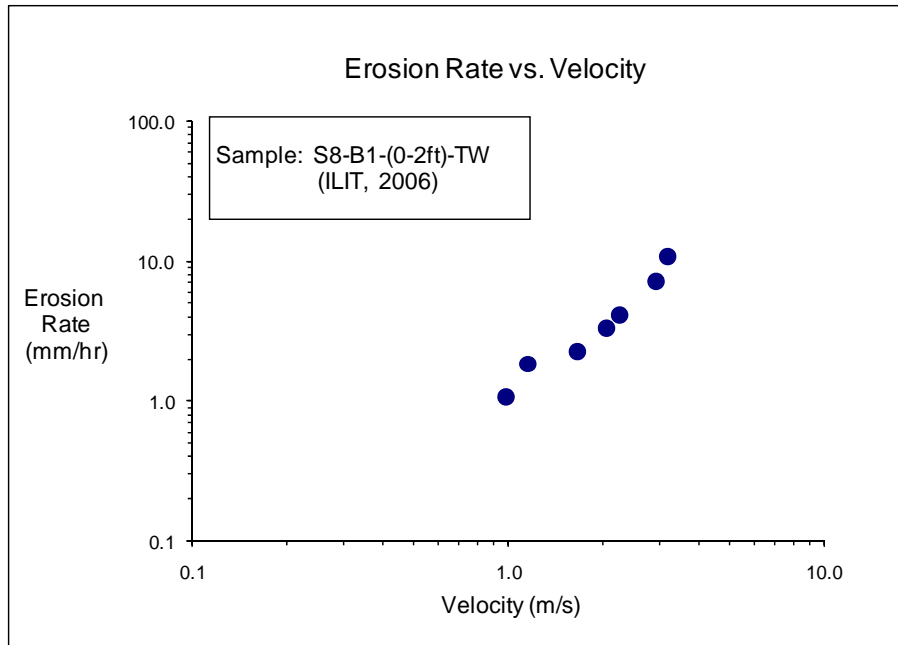


Figure D-4(b). EFA Test Results for Soil Sample S8-B1-(0-2ft)-TW (Velocity).

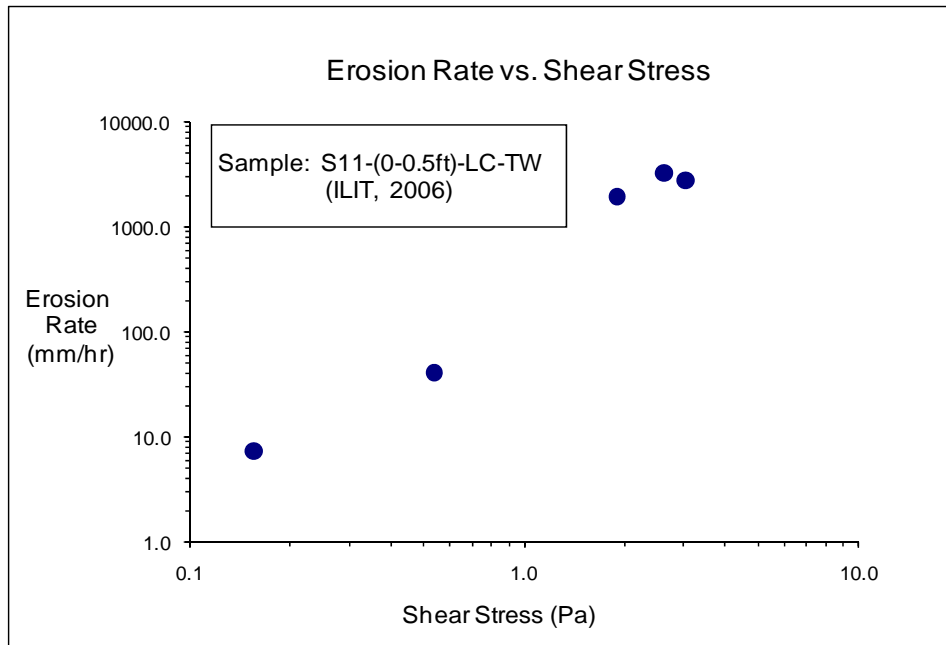


Figure D-5(a). EFA Test Results for Soil Sample S11-(0-0.5ft)-LC-TW (Shear Stress).

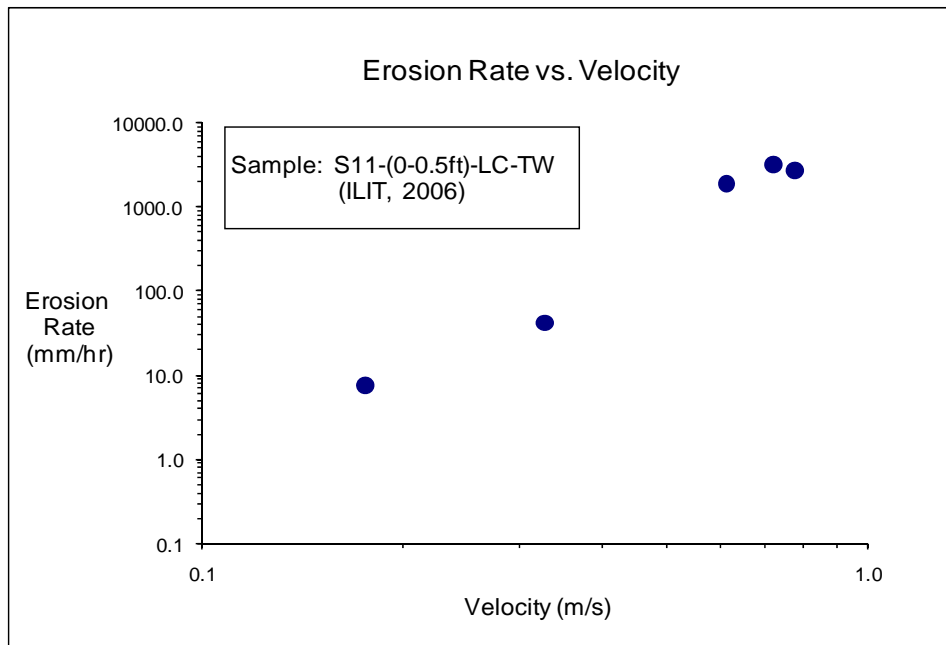


Figure D-5(b). EFA Test Results for Soil Sample S11-(0-0.5ft)-LC-TW (Velocity).

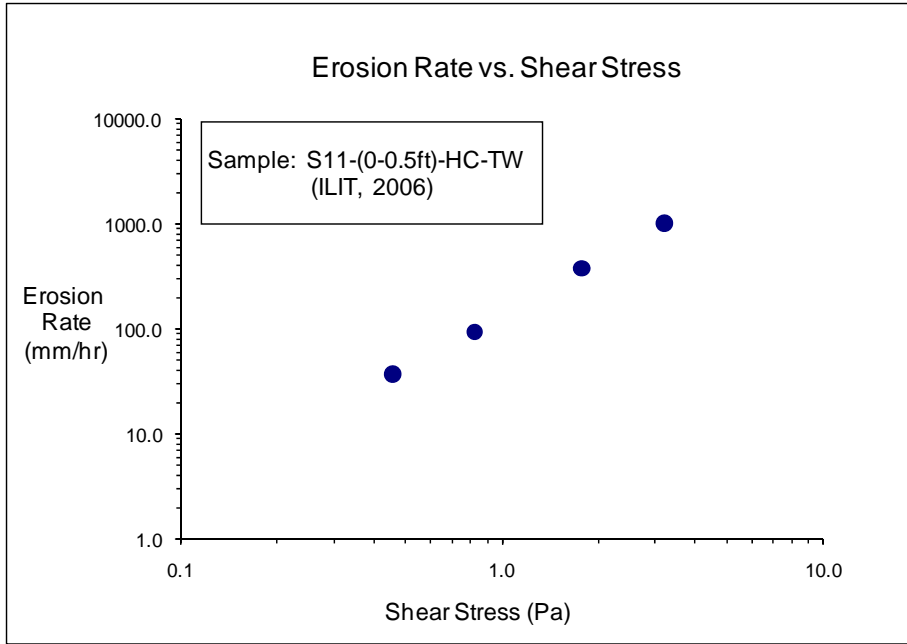


Figure D-6(a). EFA Test Results for Soil Sample S11-(0-0.5ft)-HC-TW (Shear Stress).

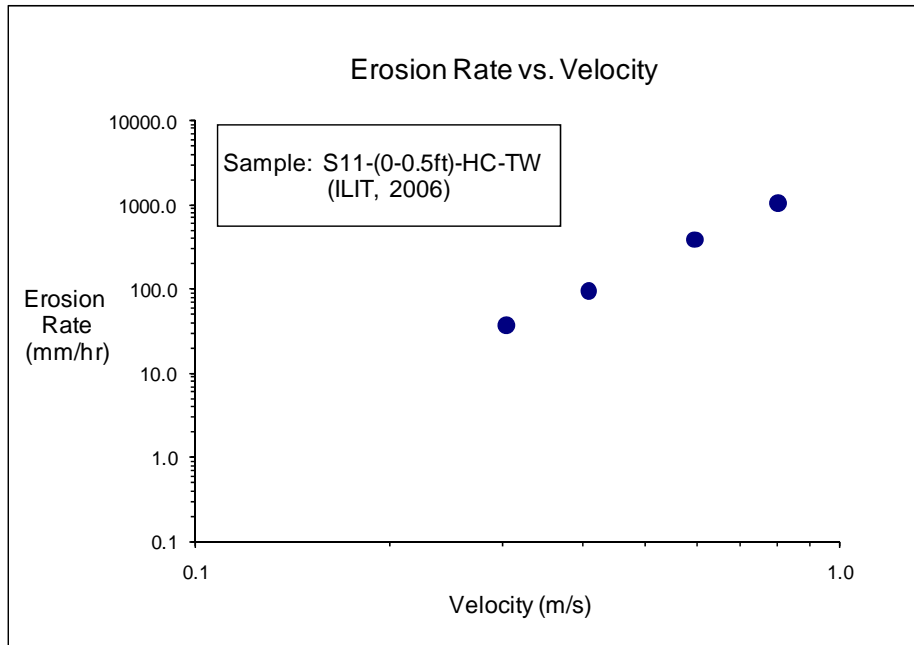


Figure D-6(b). EFA Test Results for Soil Sample S11-(0-0.5ft)-HC-TW (Velocity).

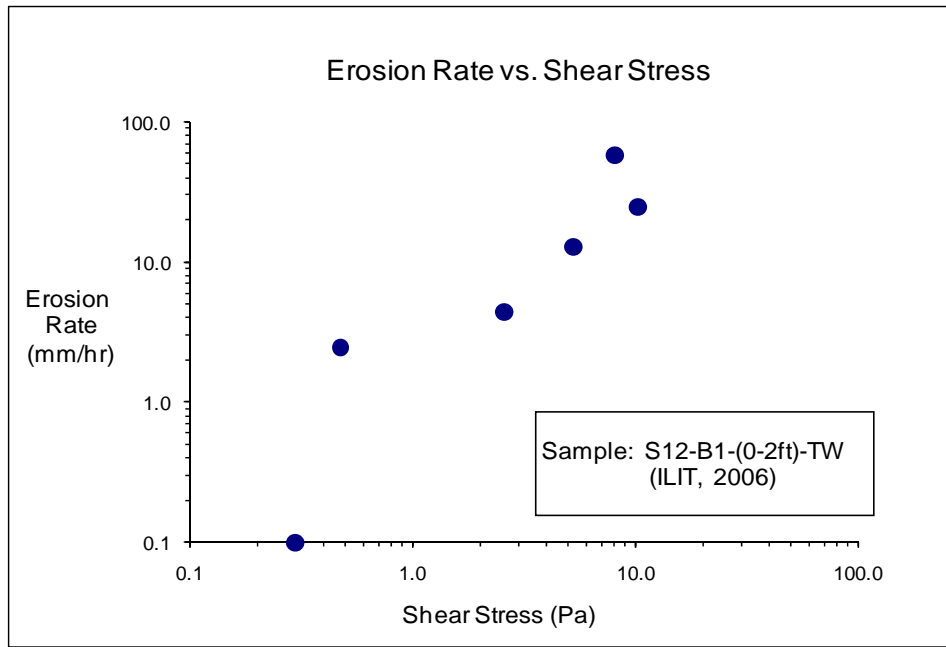


Figure D-7(a). EFA Test Results for Soil Sample S12-B1-(0-2ft)-TW (Shear Stress).

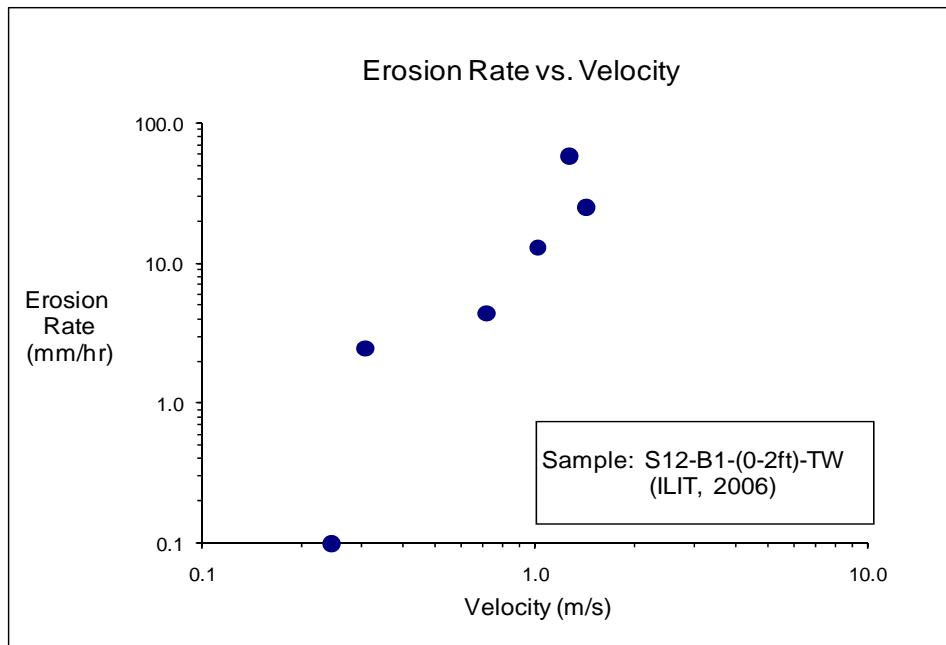


Figure D-7(b). EFA Test Results for Soil Sample S12-B1-(0-2ft)-TW (Velocity).

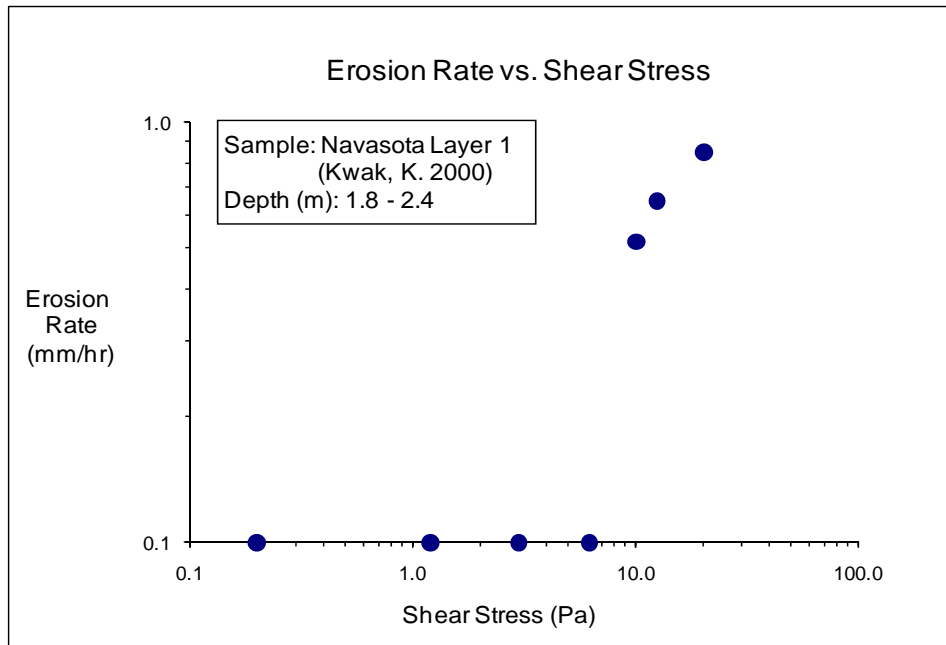


Figure D-8(a). EFA Test Results for Soil Sample Navasota Layer 1 (Shear Stress).

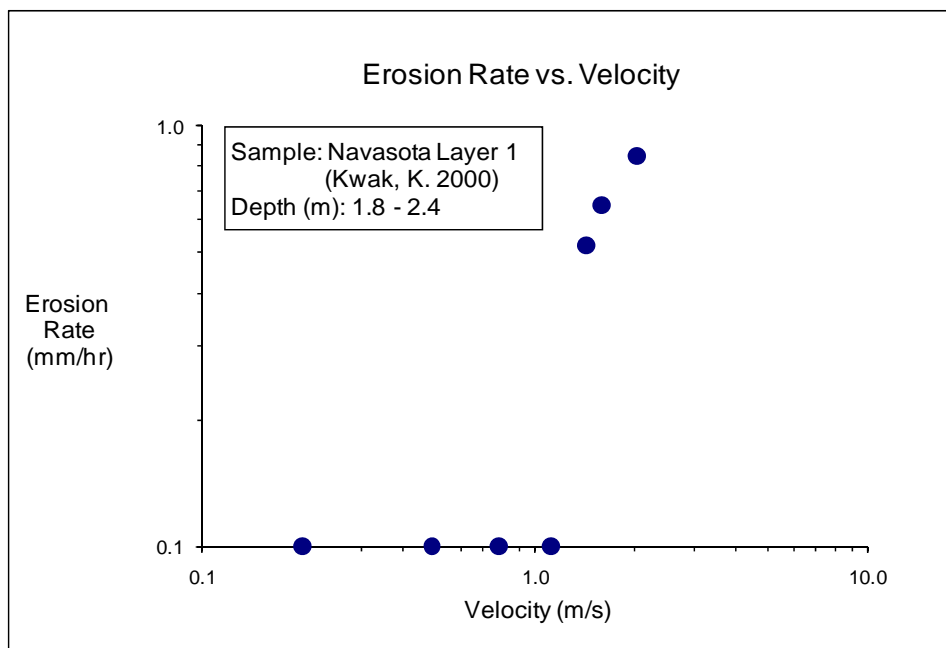


Figure D-8(b). EFA Test Results for Soil Sample Navasota Layer 1 (Velocity).

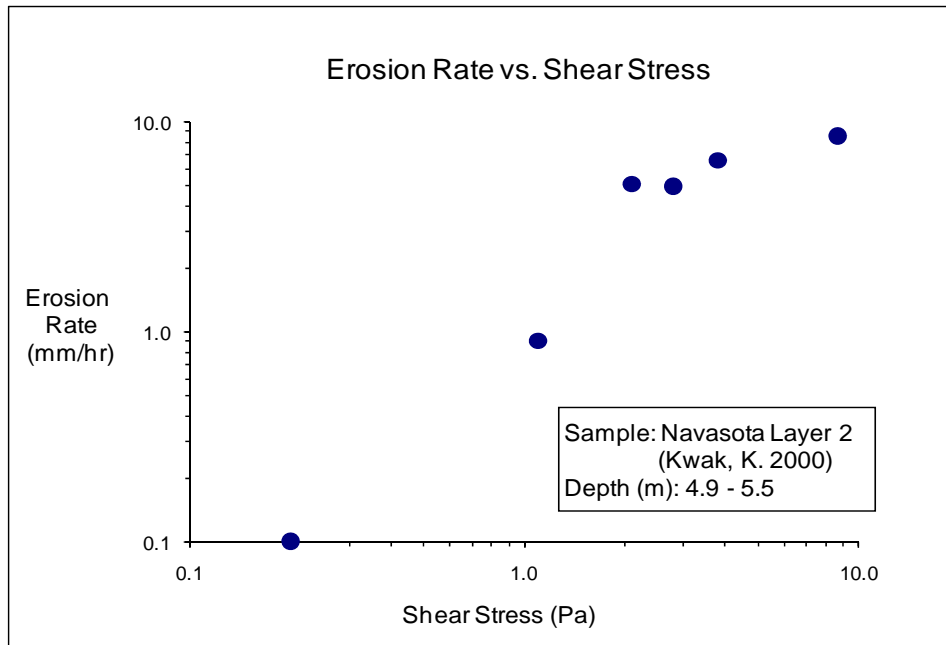


Figure D-9(a). EFA Test Results for Soil Sample Navasota Layer 2 (Shear Stress).

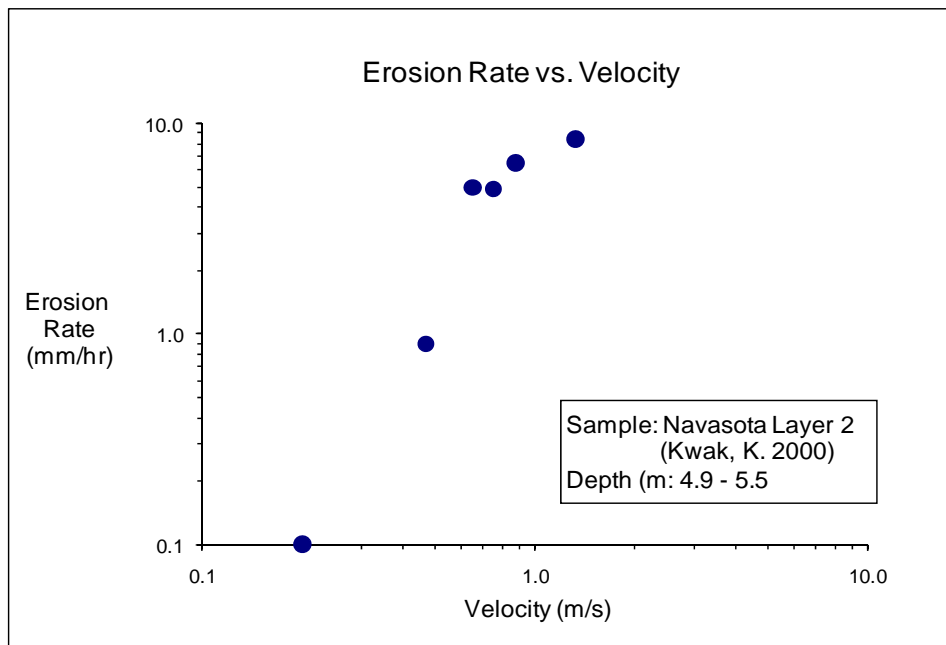


Figure D-9(b). EFA Test Results for Soil Sample Navasota Layer 2 (Velocity).

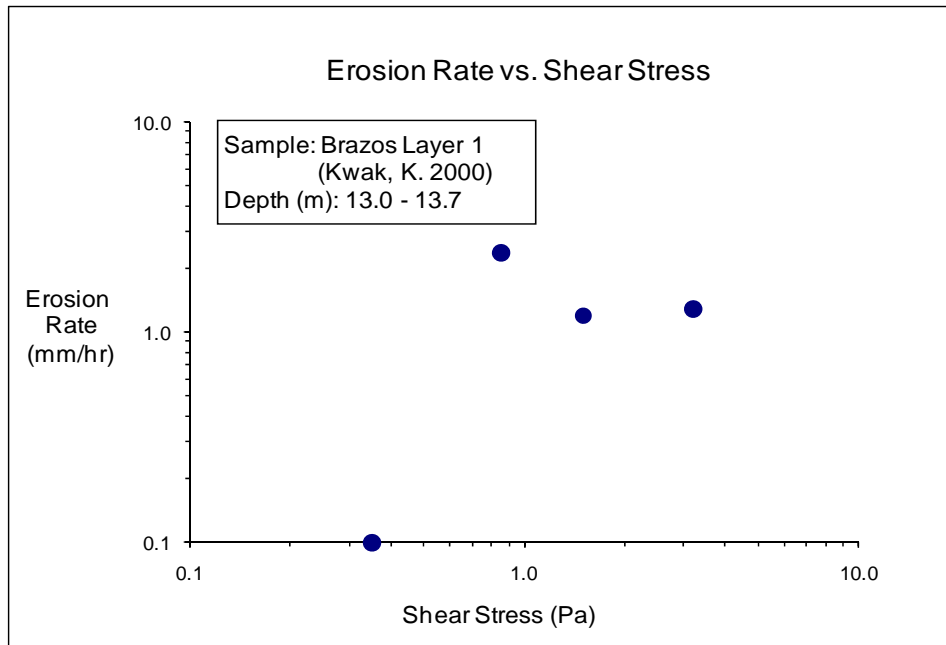


Figure D-10(a). EFA Test Results for Soil Sample Brazos Layer 1 (Shear Stress).

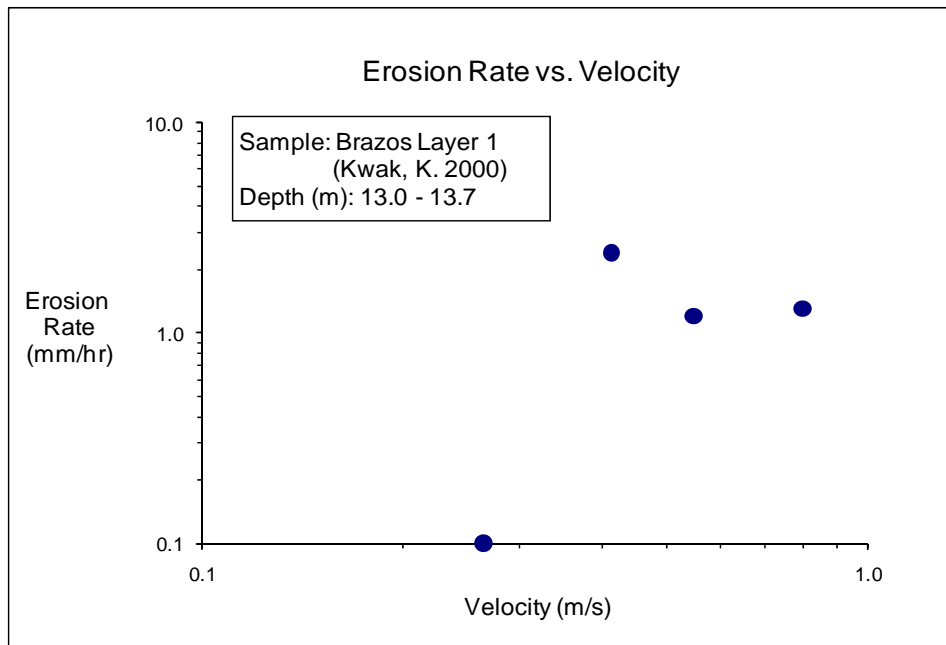


Figure D-10(b). EFA Test Results for Soil Sample Brazos Layer 1 (Velocity).

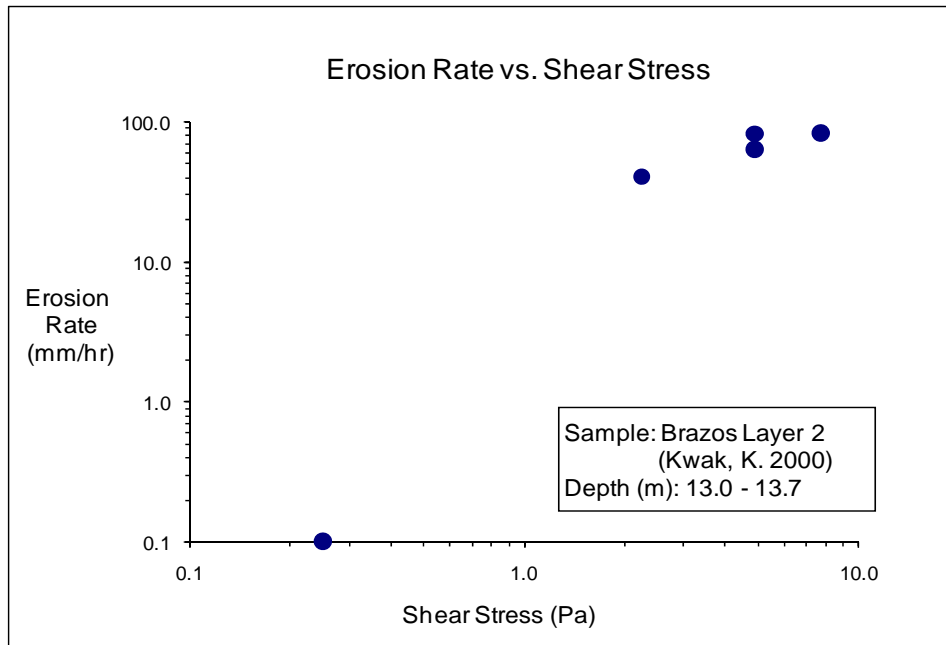


Figure D-11(a). EFA Test Results for Soil Sample Brazos Layer 2 (Shear Stress).

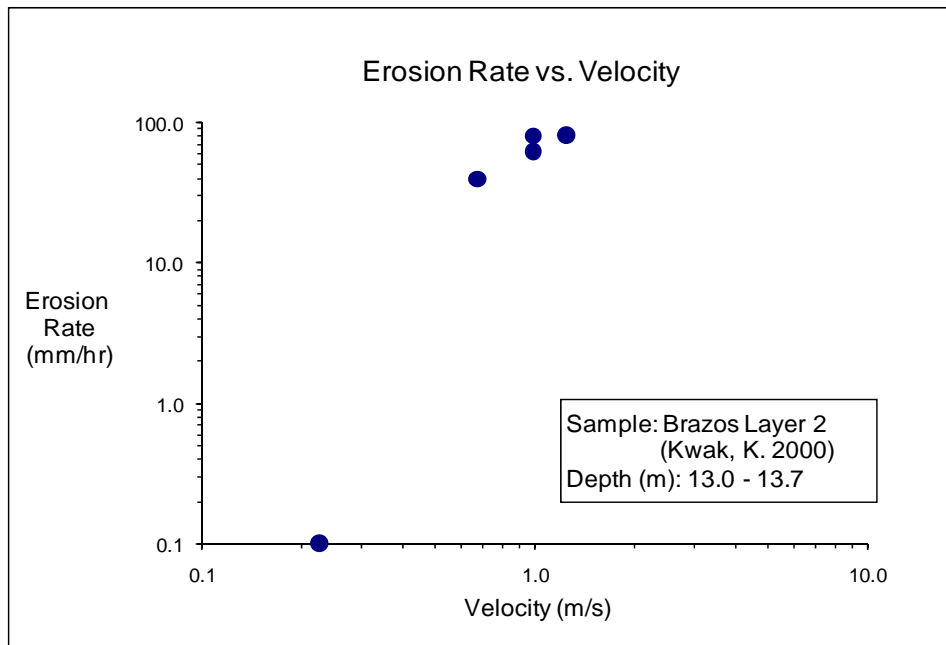


Figure D-11(b). EFA Test Results for Soil Sample Brazos Layer 2 (Velocity).

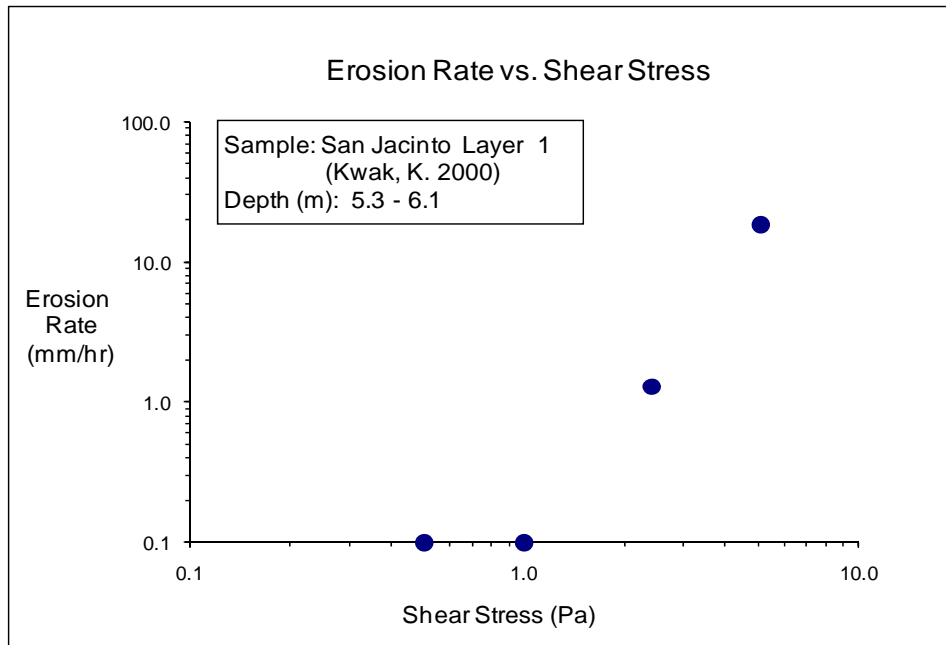


Figure D-12(a). EFA Test Results for Soil Sample San Jacinto Layer 1 (Shear Stress).

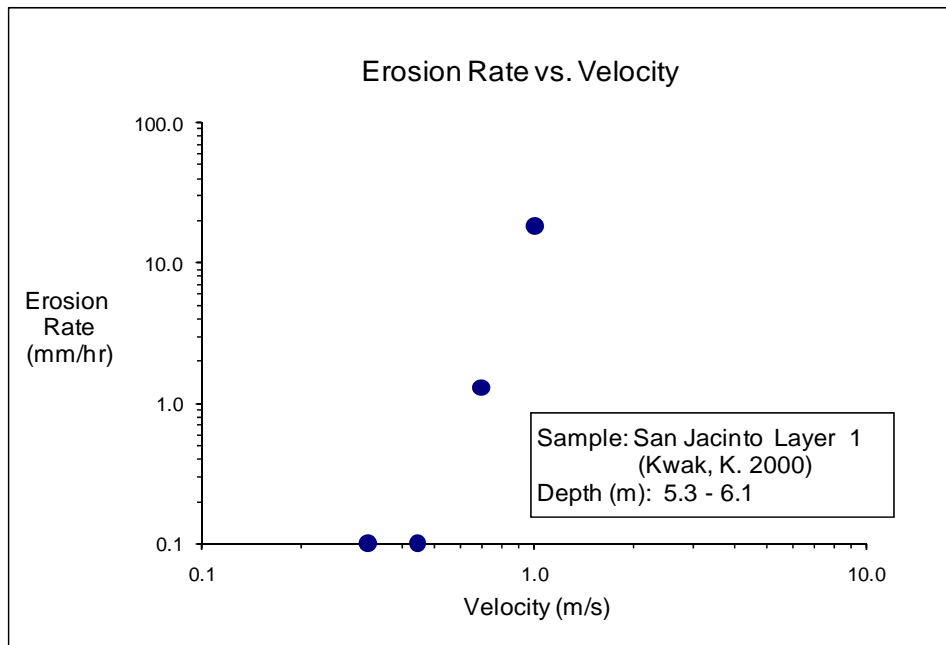


Figure D-12(b). EFA Test Results for Soil Sample San Jacinto Layer 1 (Velocity).

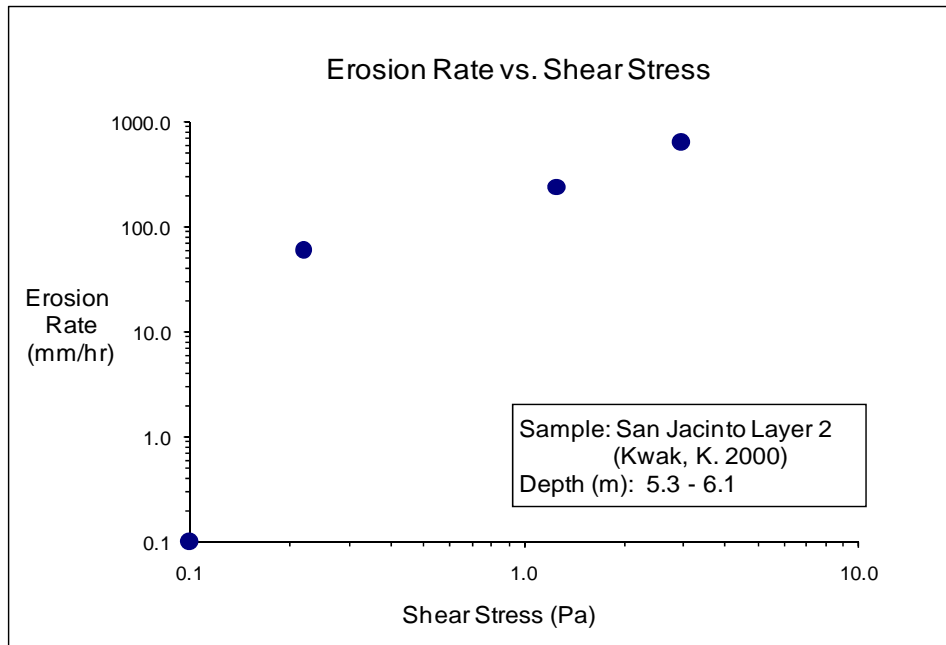


Figure D-13(a). EFA Test Results for Soil Sample San Jacinto Layer 2 (Shear Stress).

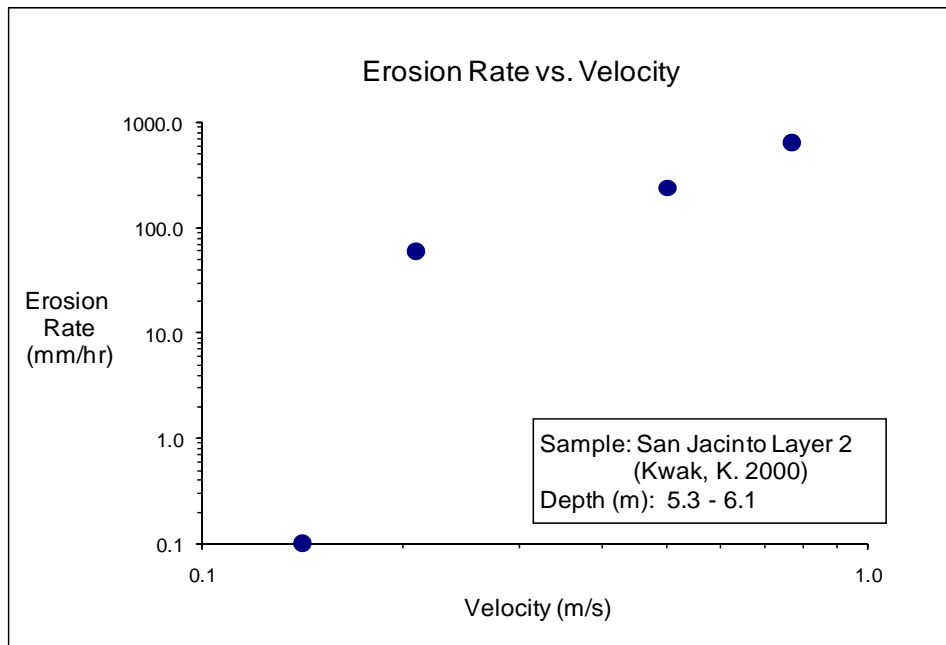


Figure D-13(b). EFA Test Results for Soil Sample San Jacinto Layer 2 (Velocity).

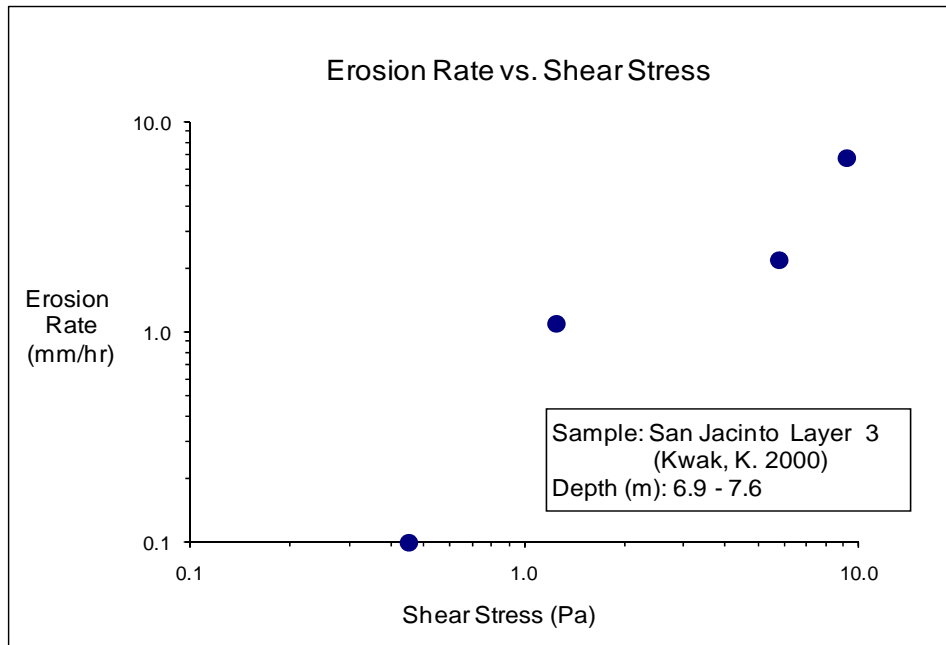


Figure D-14(a). EFA Test Results for Soil Sample San Jacinto Layer 3 (Shear Stress).

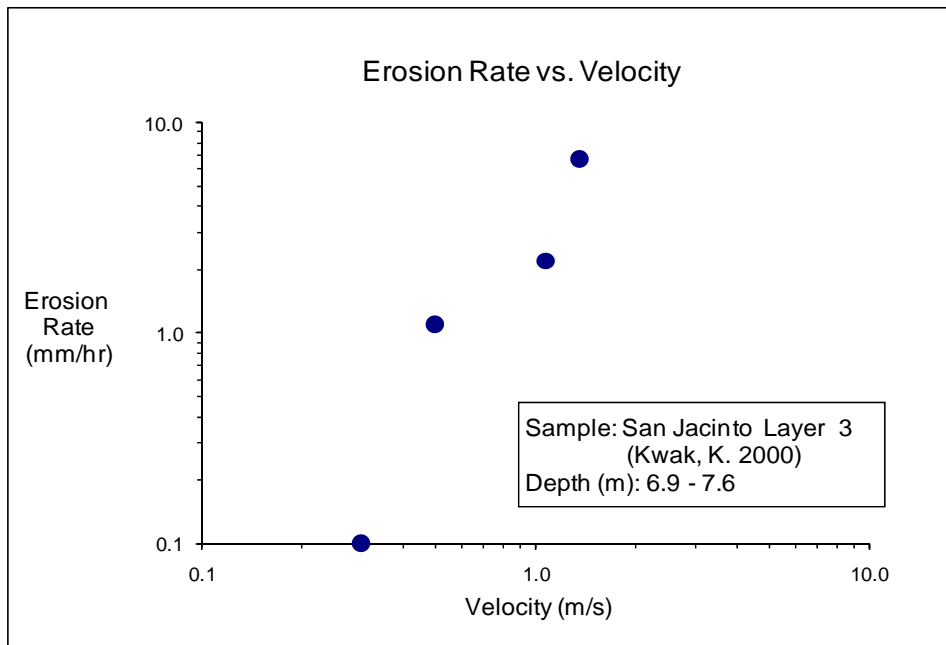


Figure D-14(b). EFA Test Results for Soil Sample San Jacinto Layer 3 (Velocity).

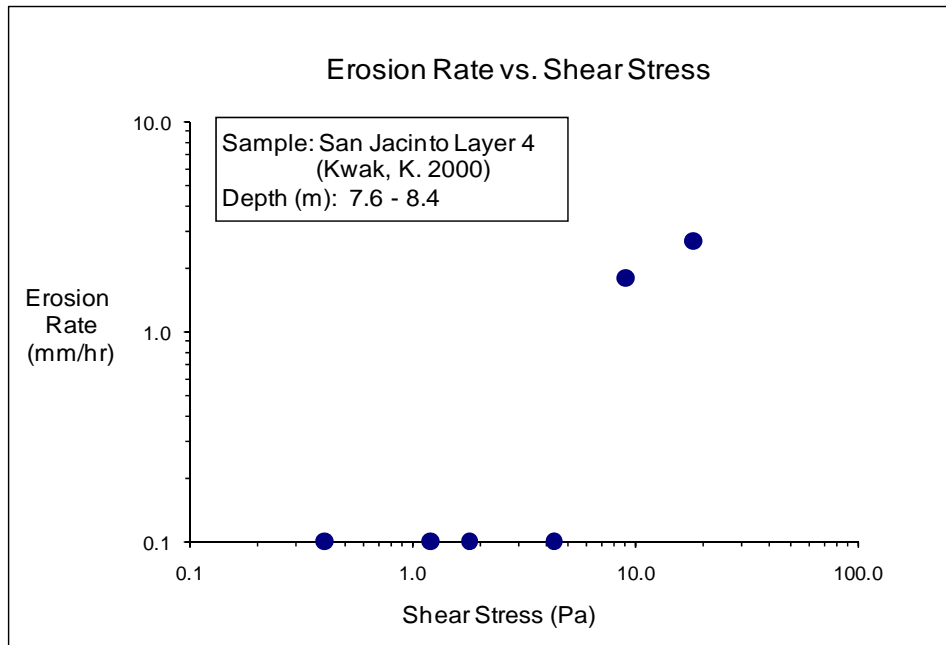


Figure D-15(a). EFA Test Results for Soil Sample San Jacinto Layer 4 (Shear Stress).

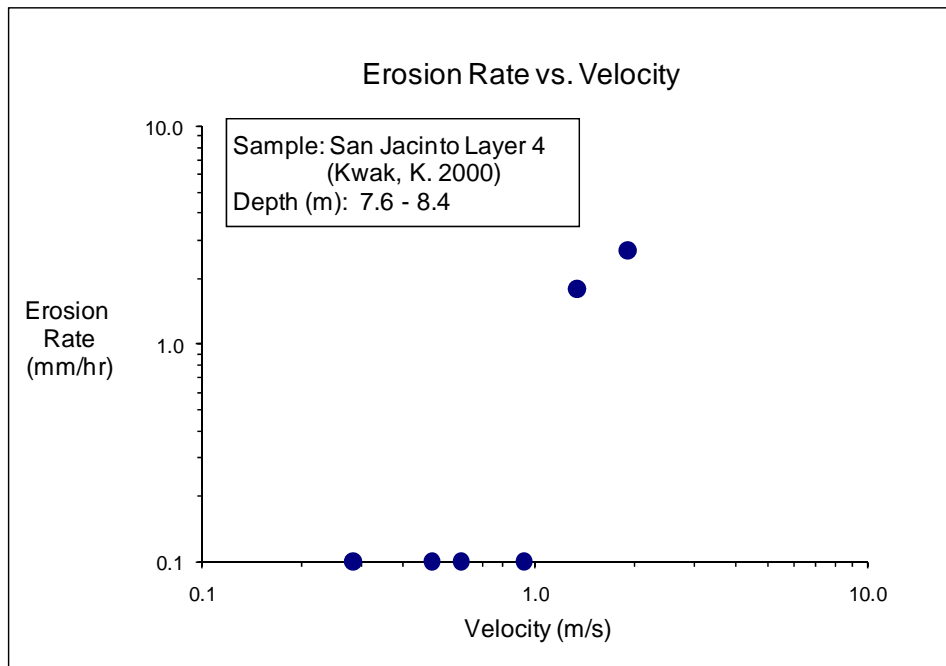


Figure D-15(b). EFA Test Results for Soil Sample San Jacinto Layer 4 (Velocity).

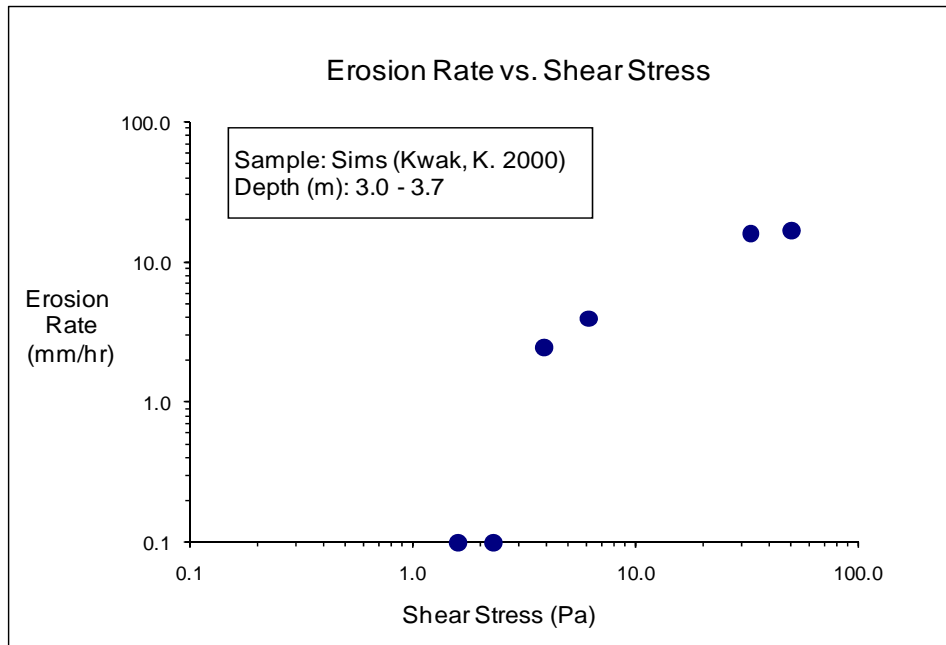


Figure D-16(a). EFA Test Results for Soil Sample Sims (Shear Stress).

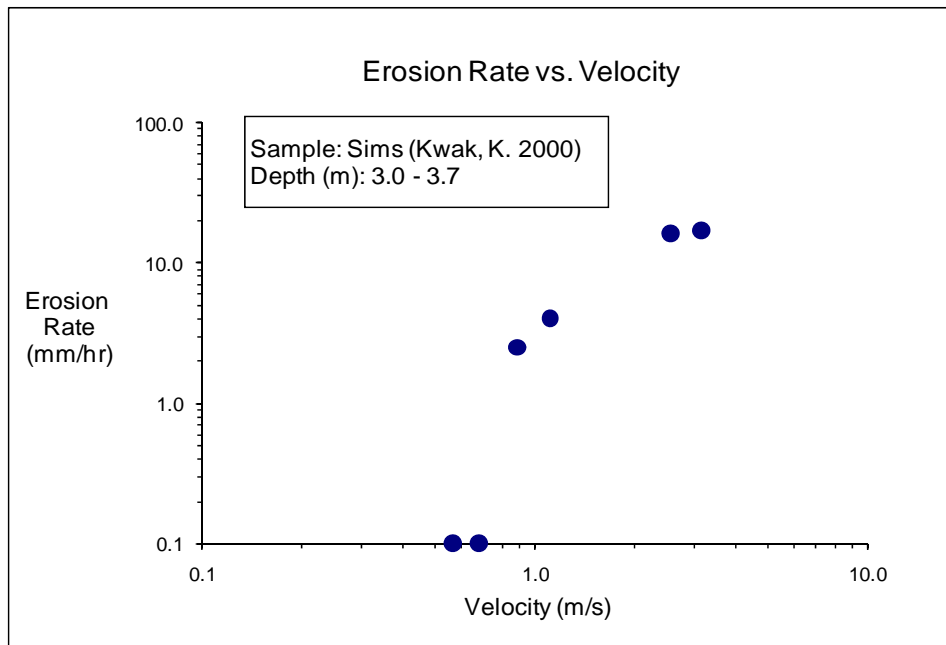


Figure D-16(b). EFA Test Results for Soil Sample Sims (Velocity).

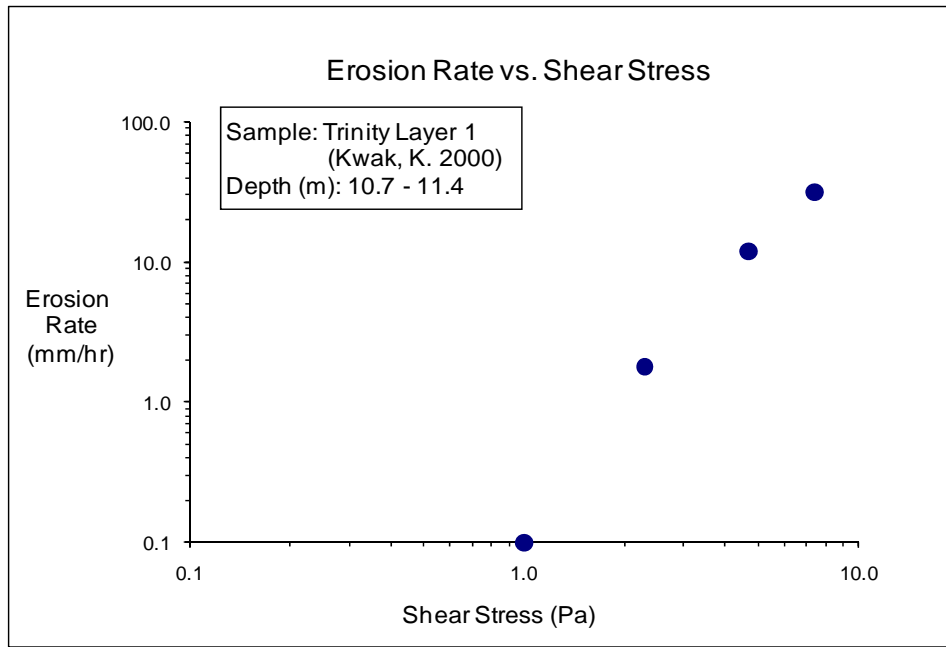


Figure D-17(a). EFA Test Results for Soil Sample Trinity Layer 1 (Shear Stress).

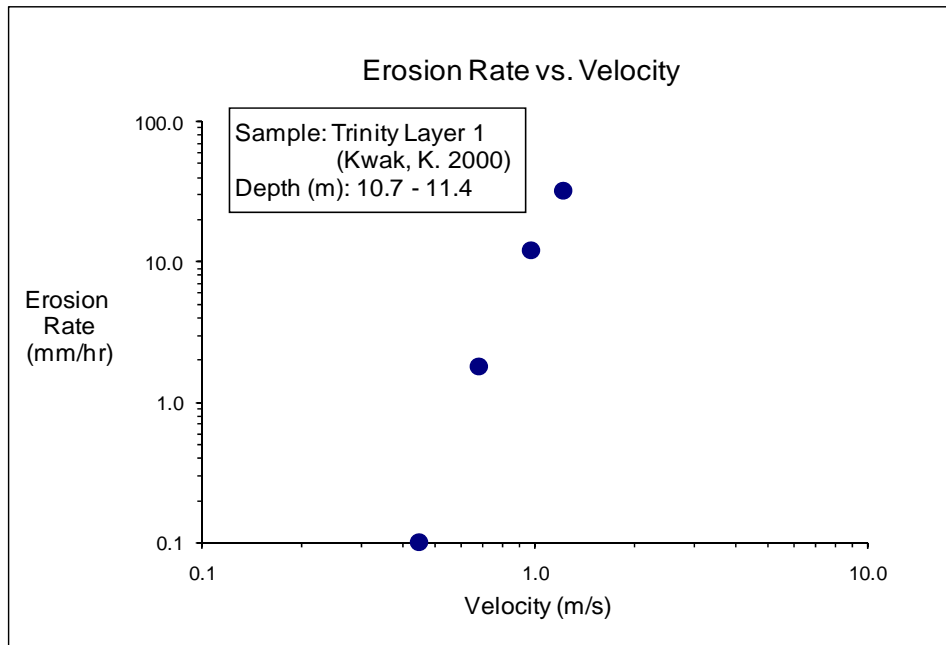


Figure D-17(b). EFA Test Results for Soil Sample Trinity Layer 1 (Velocity).

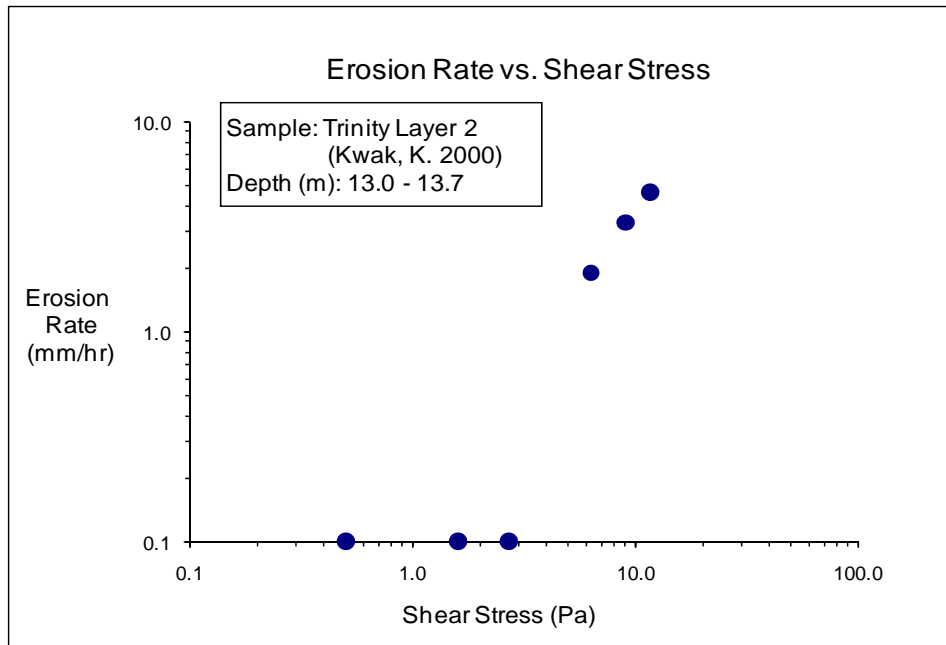


Figure D-18(a). EFA Test Results for Soil Sample Trinity Layer 2 (Shear Stress).

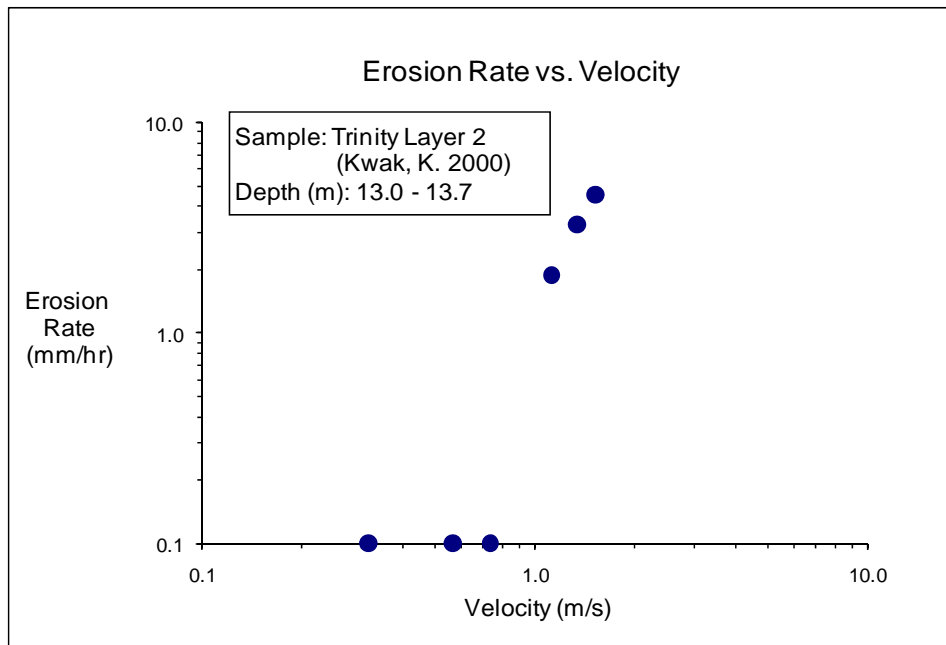


Figure D-18(b). EFA Test Results for Soil Sample Trinity Layer 2 (Velocity).

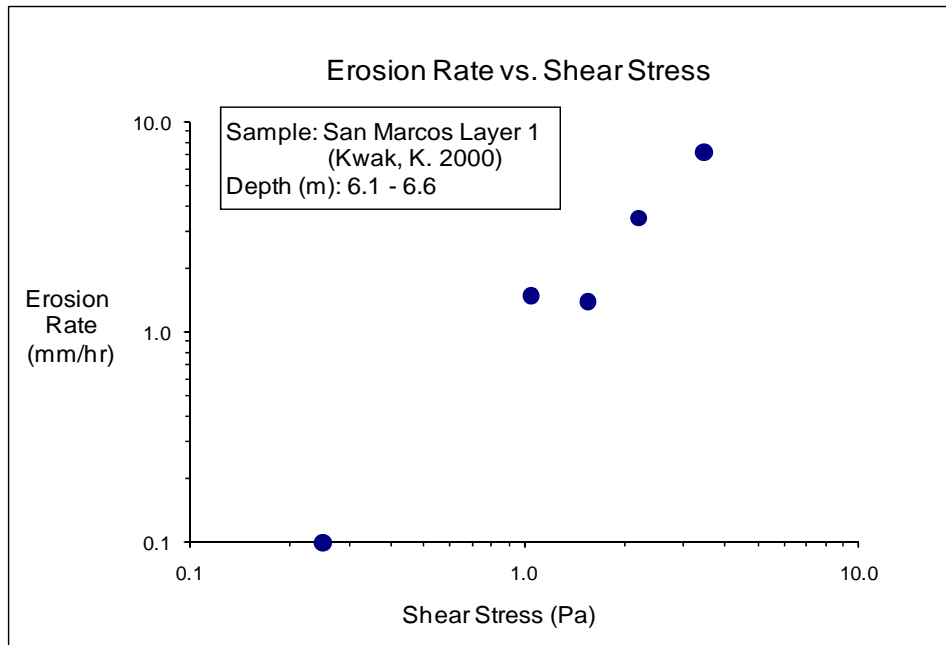


Figure D-19(a). EFA Test Results for Soil Sample San Marcos Layer 1 (Shear Stress).

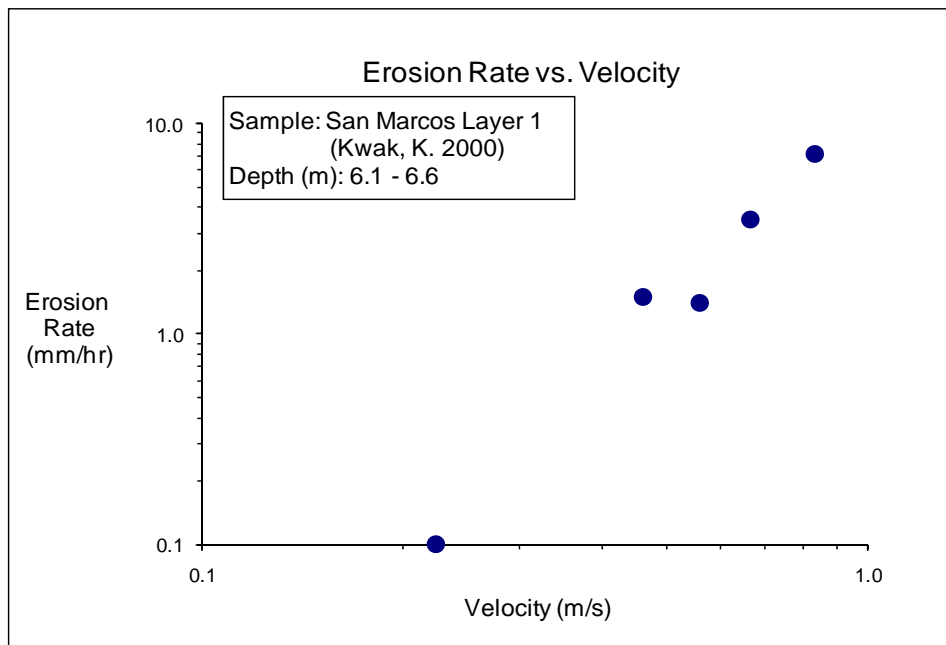


Figure D-19(b). EFA Test Results for Soil Sample San Marcos Layer 1 (Velocity).

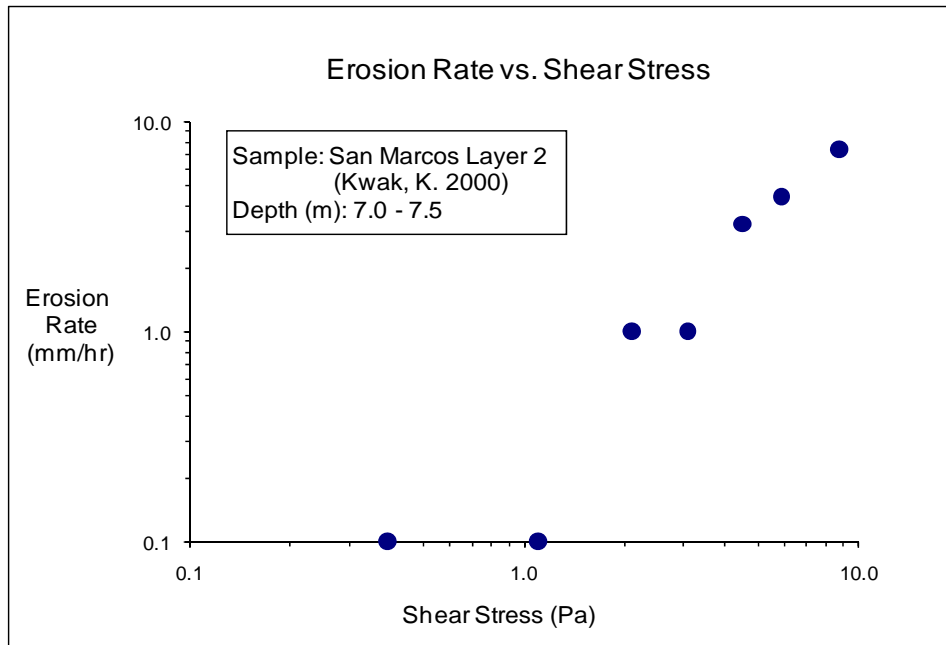


Figure D-20(a). EFA Test Results for Soil Sample San Marcos Layer 2 (Shear Stress).

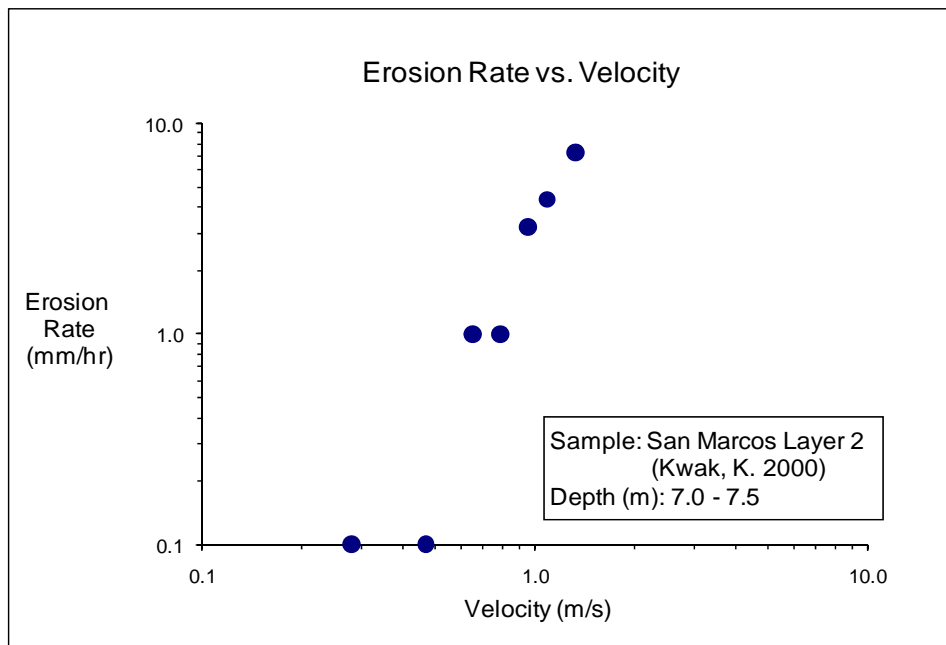


Figure D-20(b). EFA Test Results for Soil Sample San Marcos Layer 2 (Velocity).

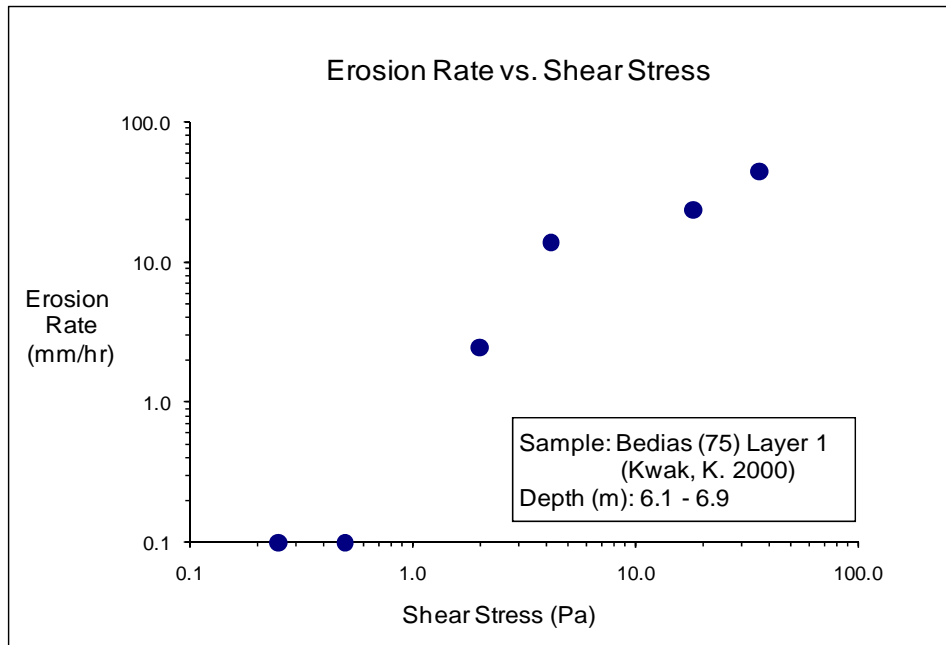


Figure D-21(a). EFA Test Results for Soil Sample Bedias (75) Layer 1 (Shear Stress).

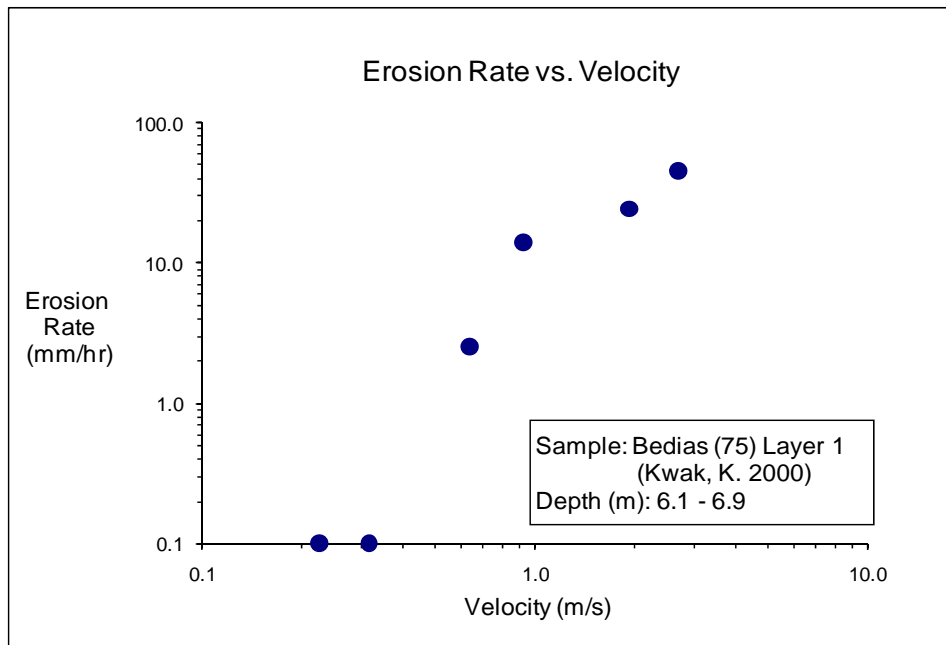


Figure D-21(b). EFA Test Results for Soil Sample Bedias (75) Layer 1 (Velocity).

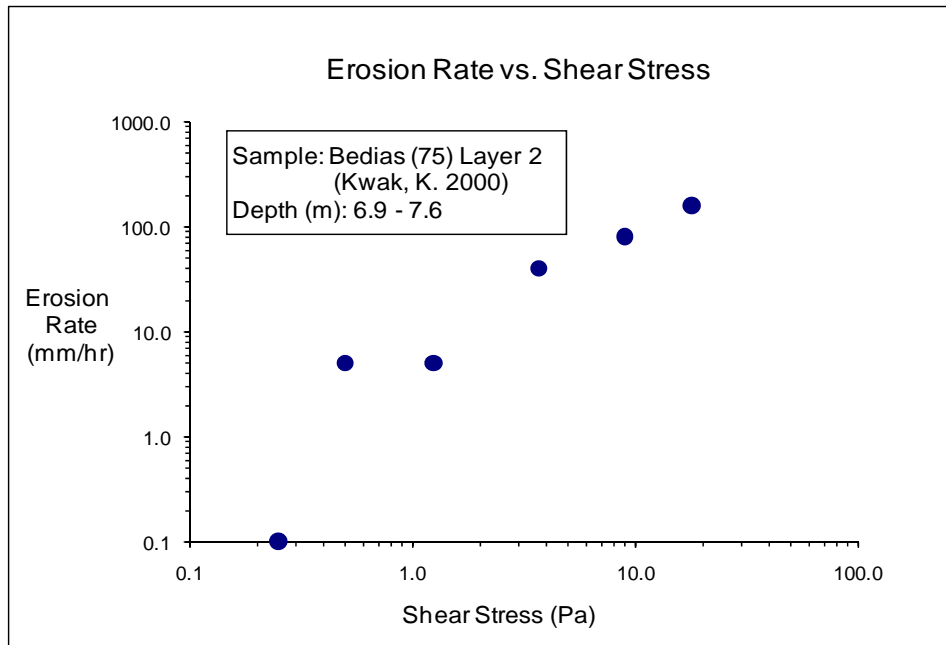


Figure D-22(a). EFA Test Results for Soil Sample Bedias (75) Layer 2 (Shear Stress).

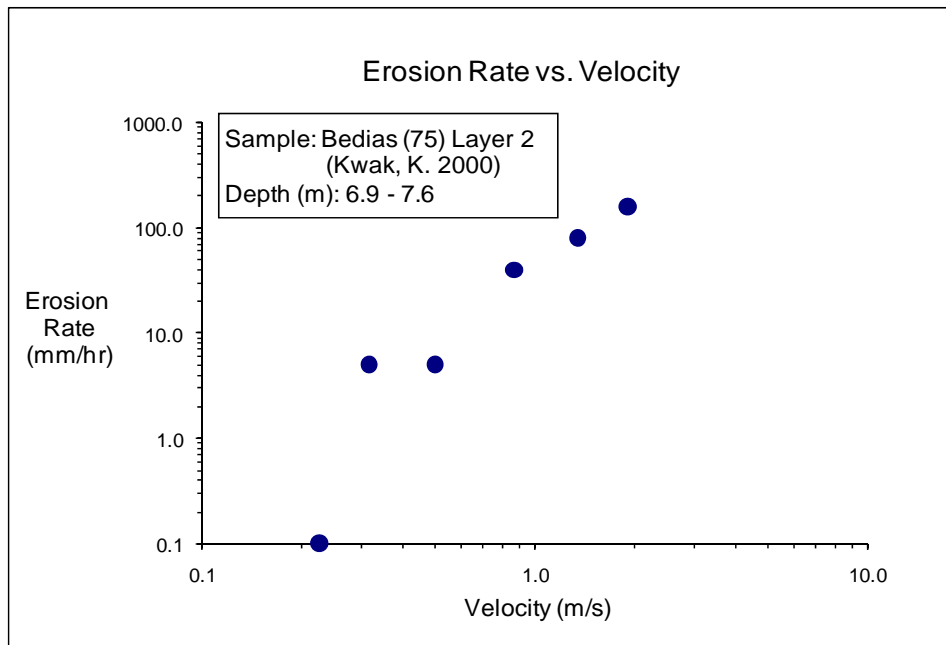


Figure D-22(b). EFA Test Results for Soil Sample Bedias (75) Layer 2 (Velocity).

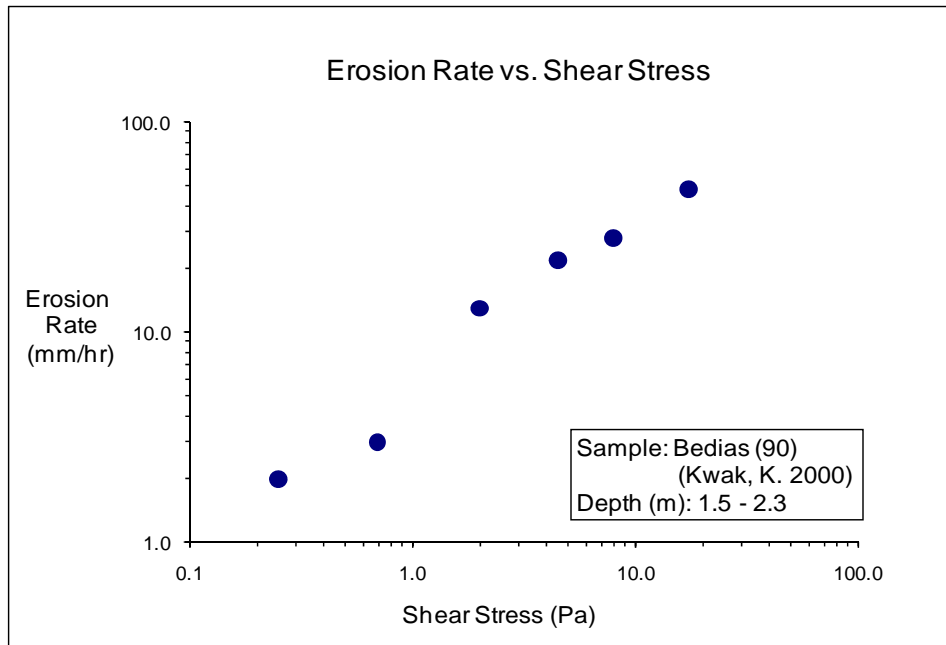


Figure D-23(a). EFA Test Results for Soil Sample Bedias (90) (Shear Stress).

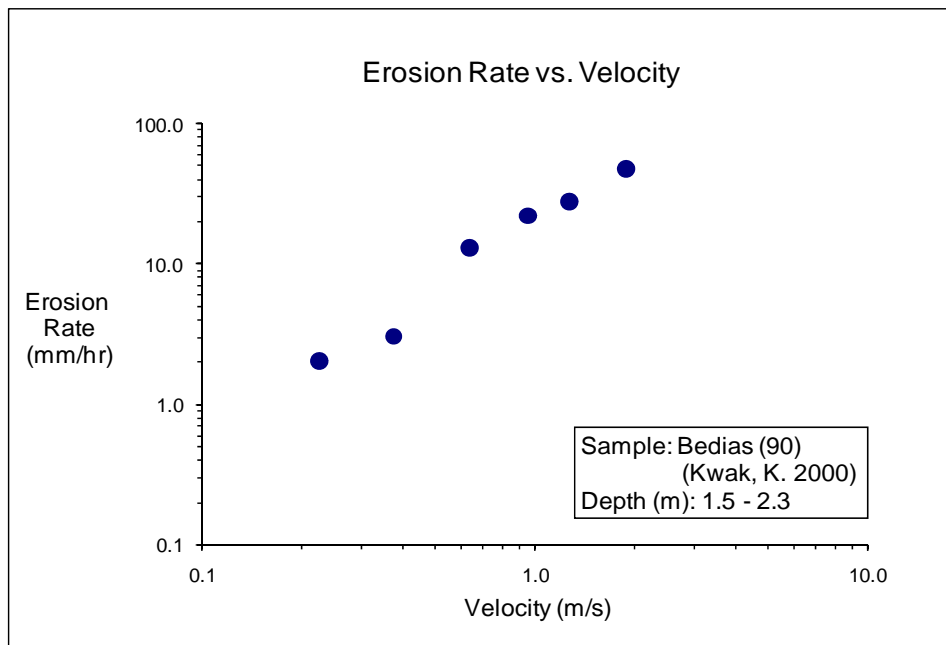


Figure D-23(b). EFA Test Results for Soil Sample Bedias (90) (Velocity).

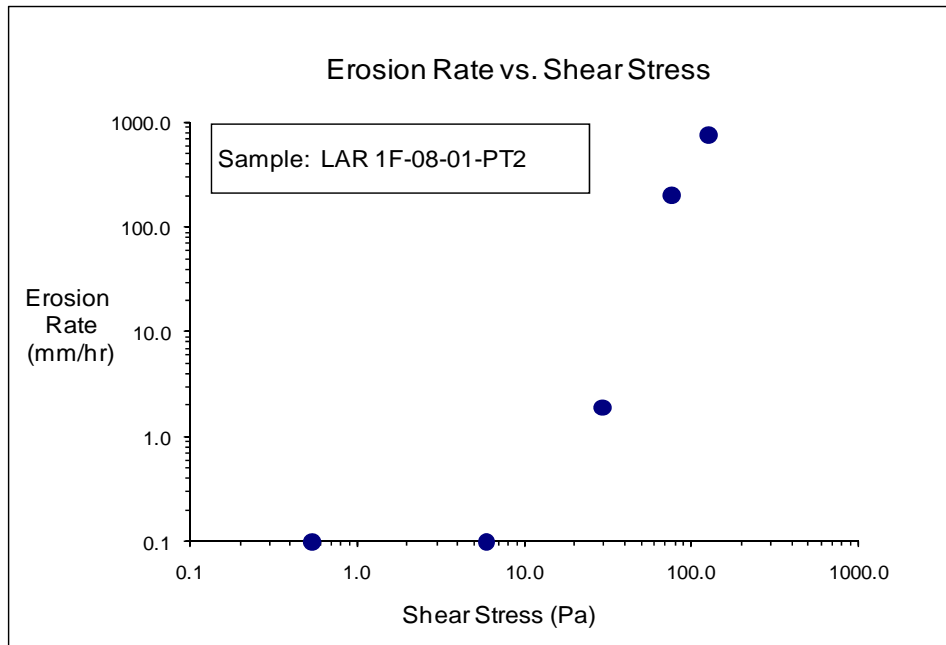


Figure D-24(a). EFA Test Results for Soil Sample LAR 1F-08-01-PT2 (Shear Stress).

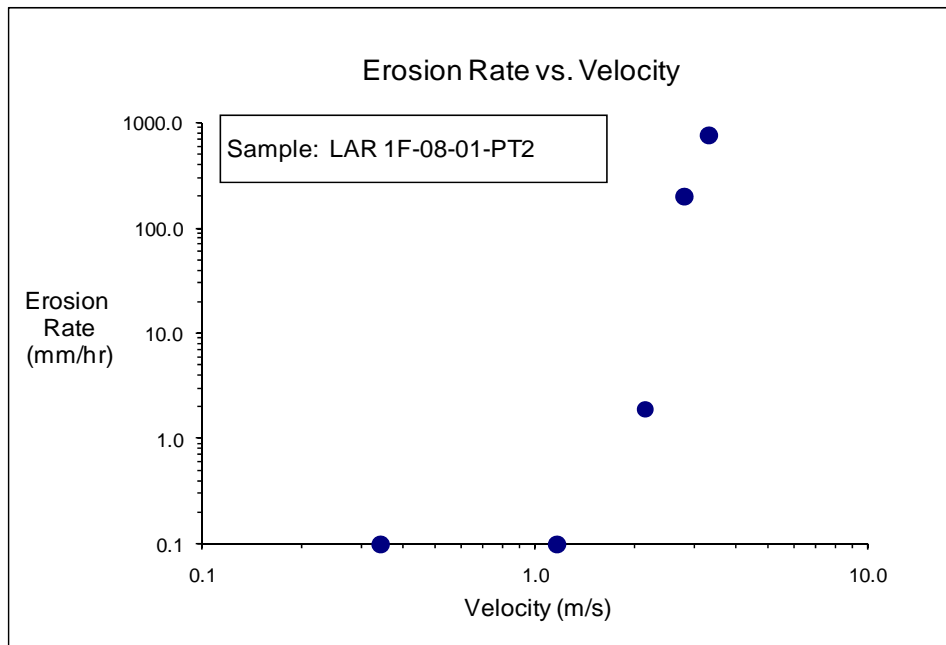


Figure D-24(b). EFA Test Results for Soil Sample LAR 1F-08-01-PT2 (Velocity).

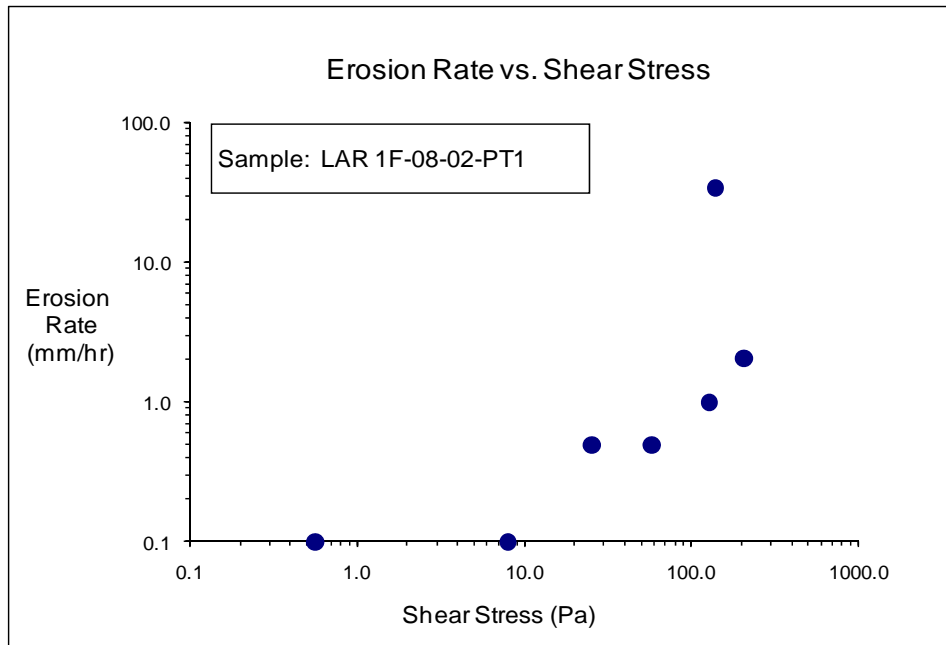


Figure D-25(a). EFA Test Results for Soil Sample LAR 1F-08-01-PT1 (Shear Stress).

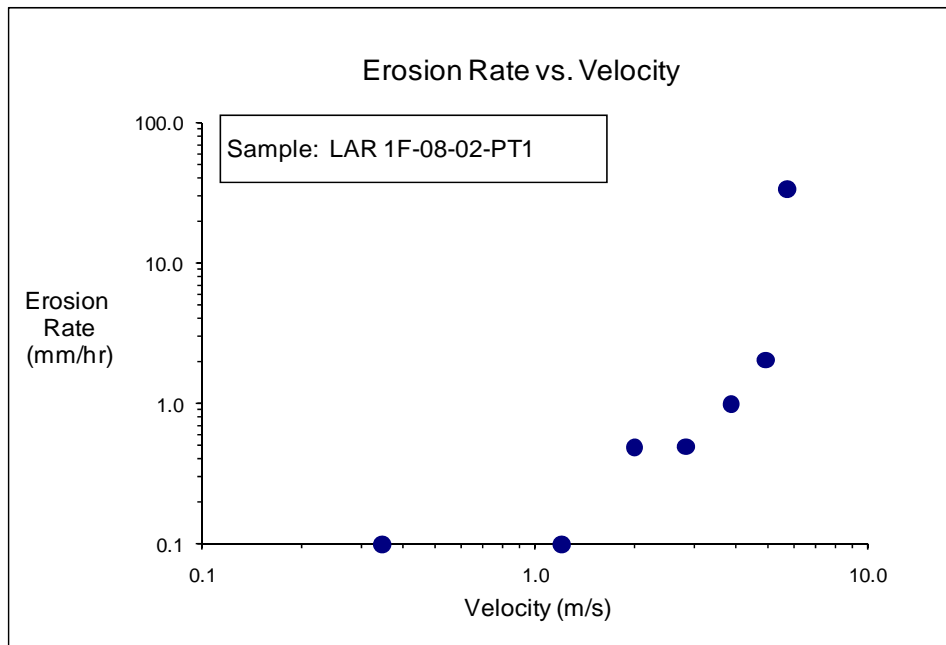


Figure D-25(b). EFA Test Results for Soil Sample LAR 1F-08-01-PT1 (Velocity).

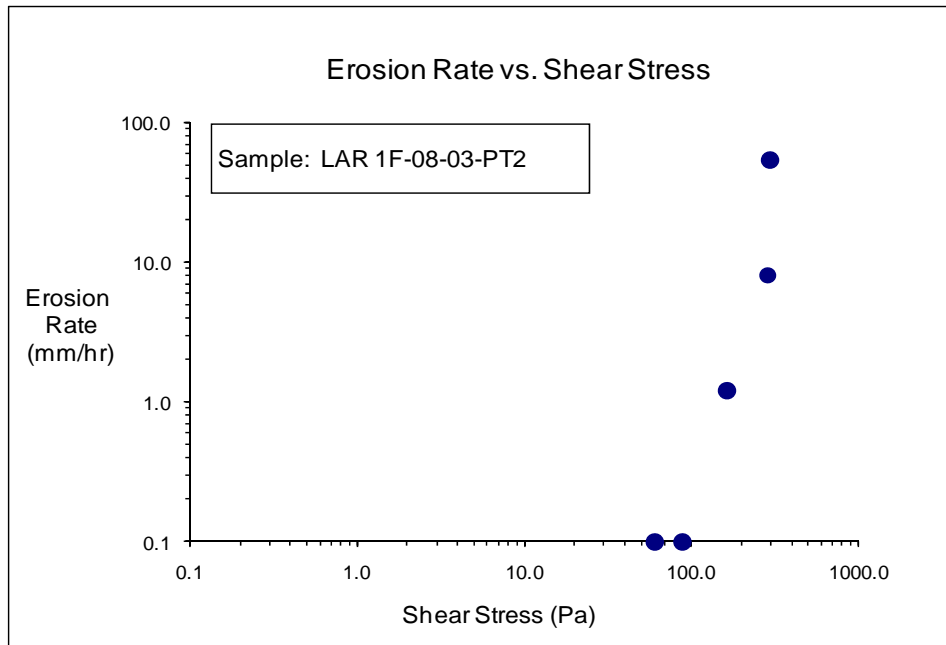


Figure D-26(a). EFA Test Results for Soil Sample LAR 1F-08-03-PT2 (Shear Stress).

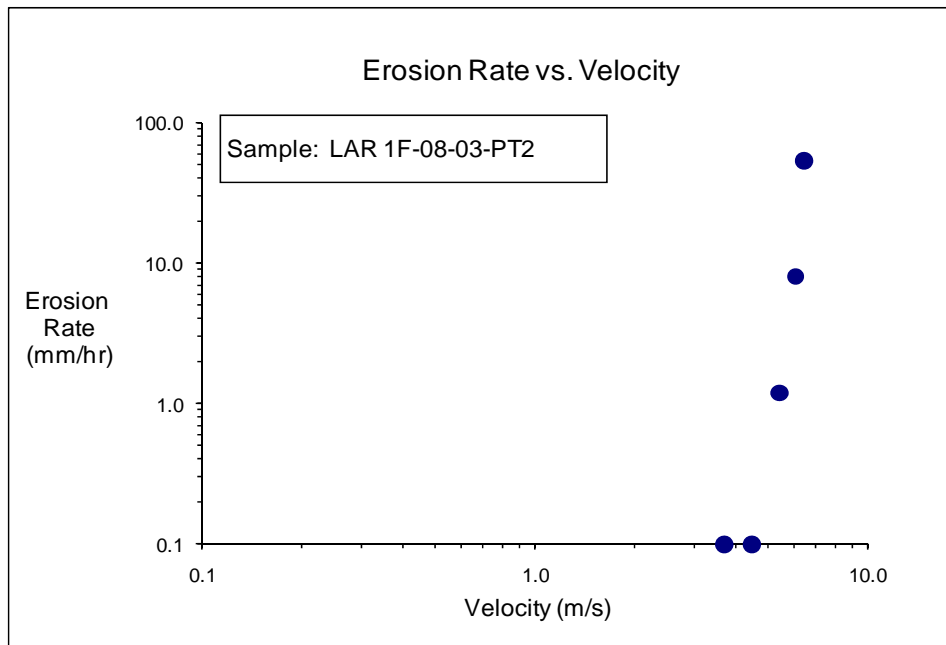


Figure D-26(b). EFA Test Results for Soil Sample LAR 1F-08-03-PT2 (Velocity).

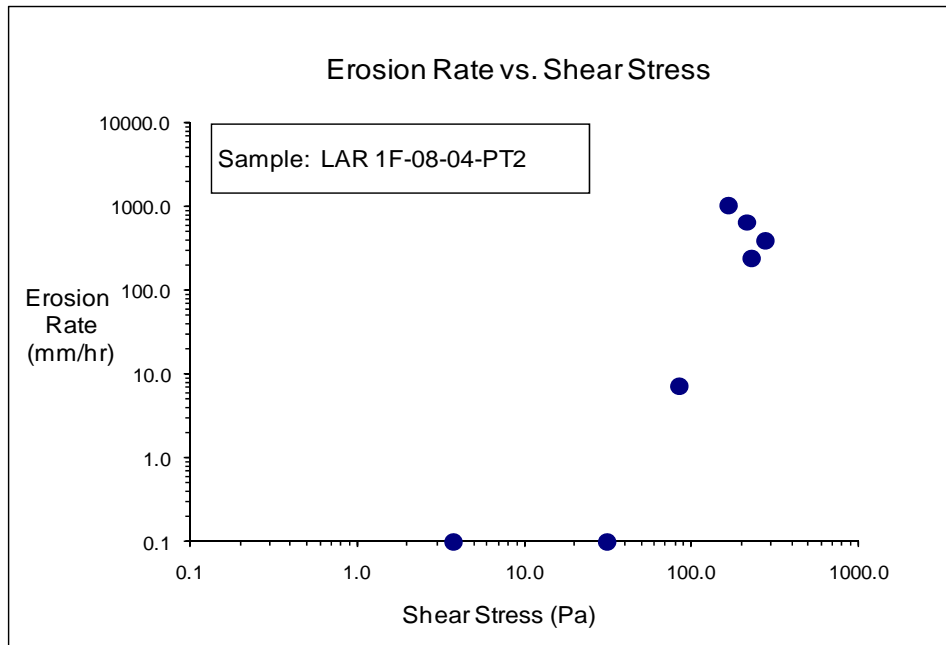


Figure D-27(a). EFA Test Results for Soil Sample LAR 1F-08-04-PT2 (Shear Stress).

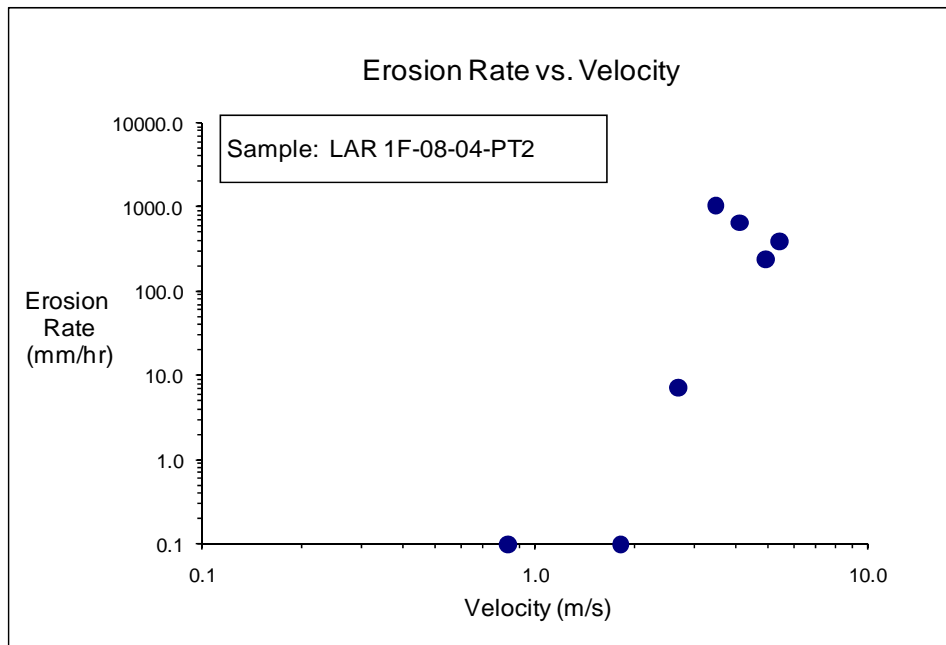


Figure D-27(b). EFA Test Results for Soil Sample LAR 1F-08-04-PT2 (Velocity).

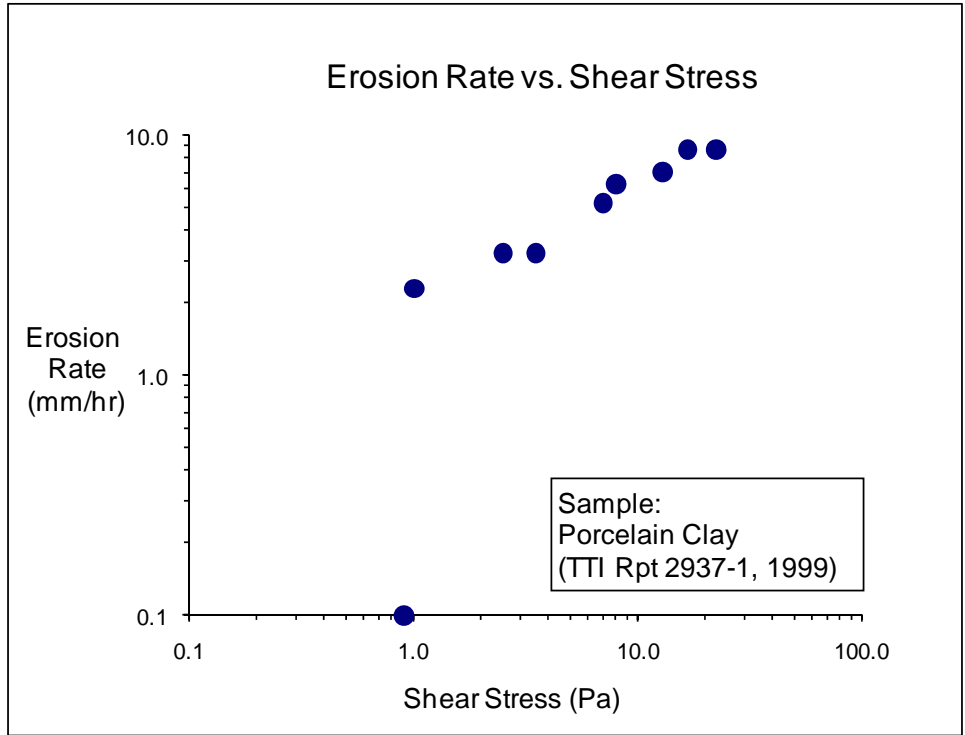


Figure D-28(a). EFA Test Results for Soil Sample Porcelain Clay (Shear Stress).

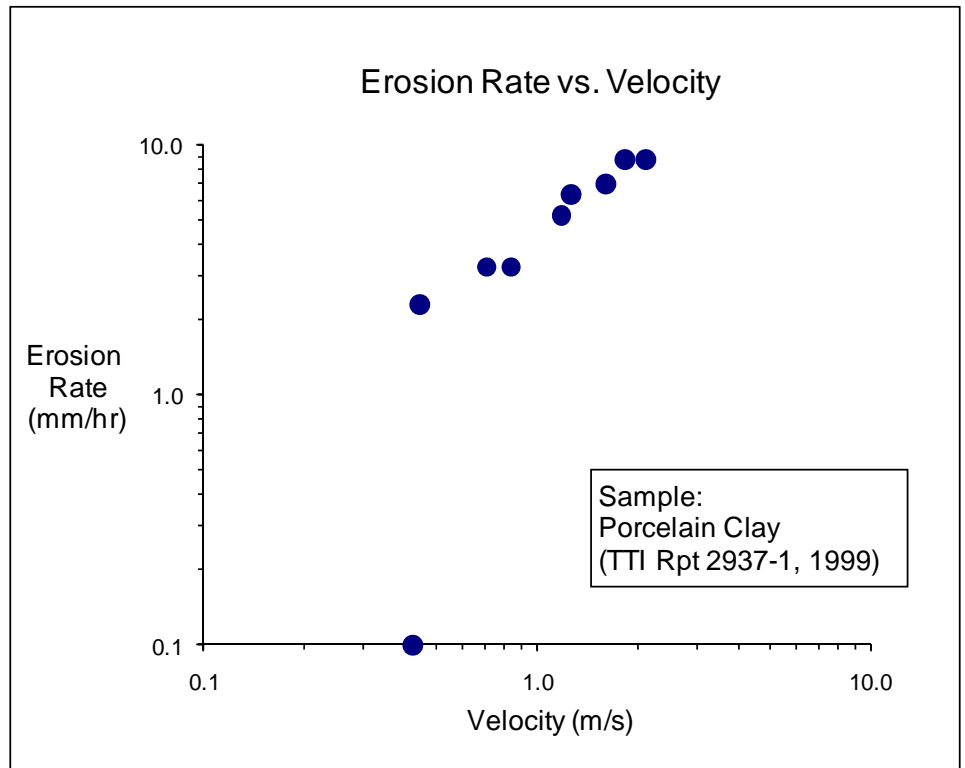


Figure D-28(b). EFA Test Results for Soil Sample Porcelain Clay (Velocity).

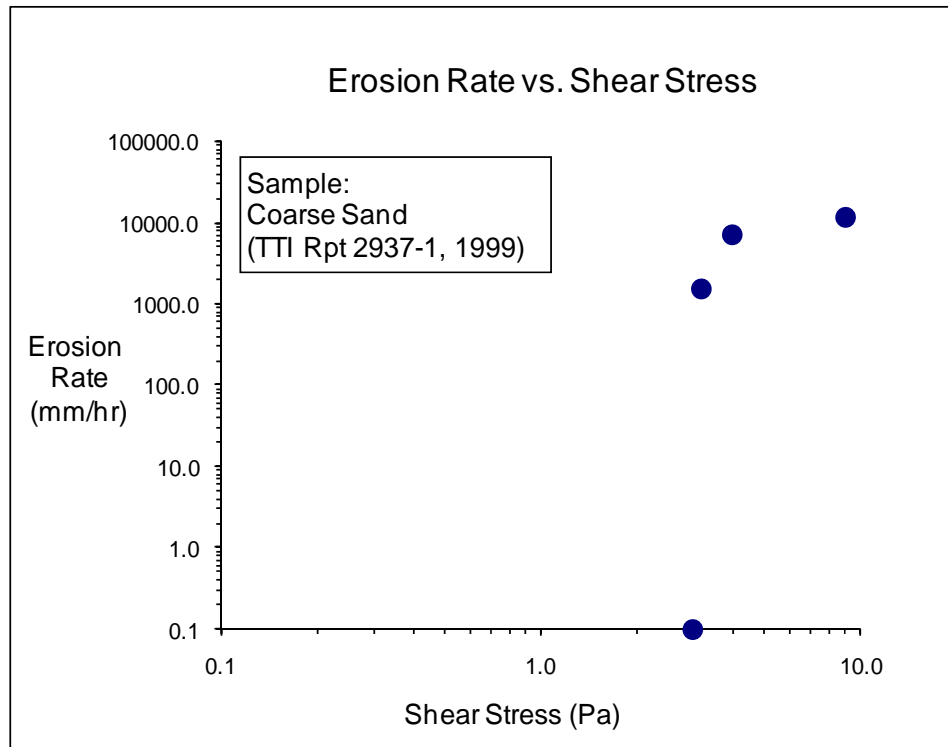


Figure D-29(a). EFA Test Results for Soil Sample Coarse Sand (Shear Stress).

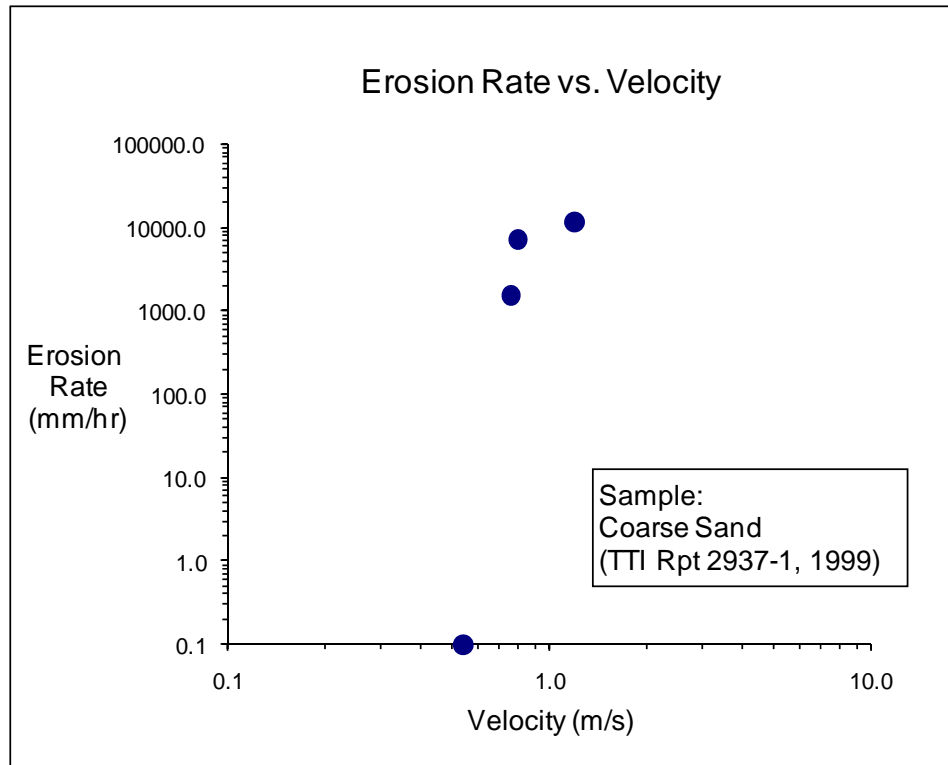


Figure D-29(b). EFA Test Results for Soil Sample Coarse Sand (Velocity).

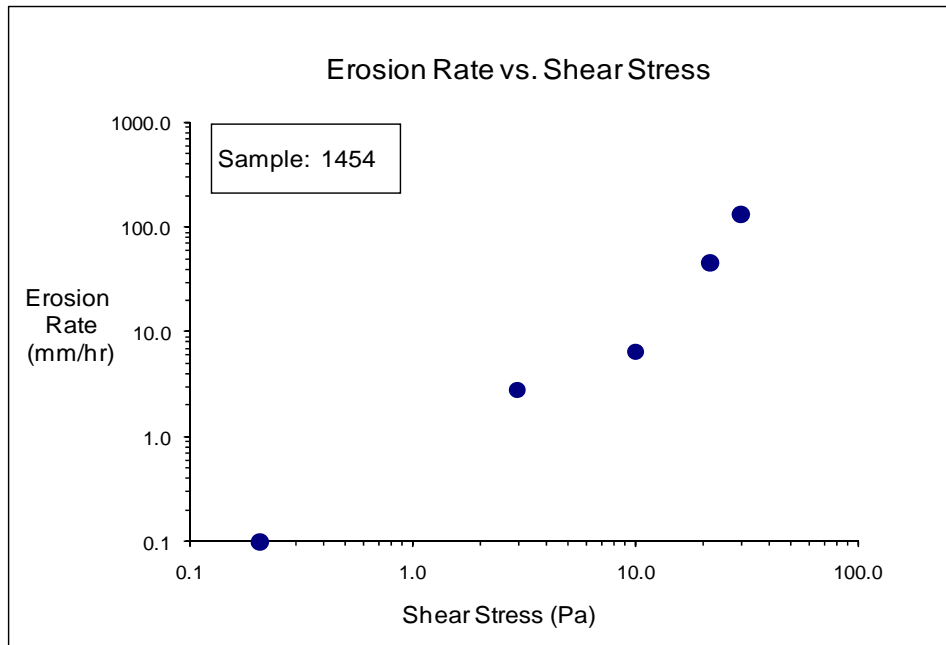


Figure D-30(a). EFA Test Results for Soil Sample 1454 (Shear Stress).

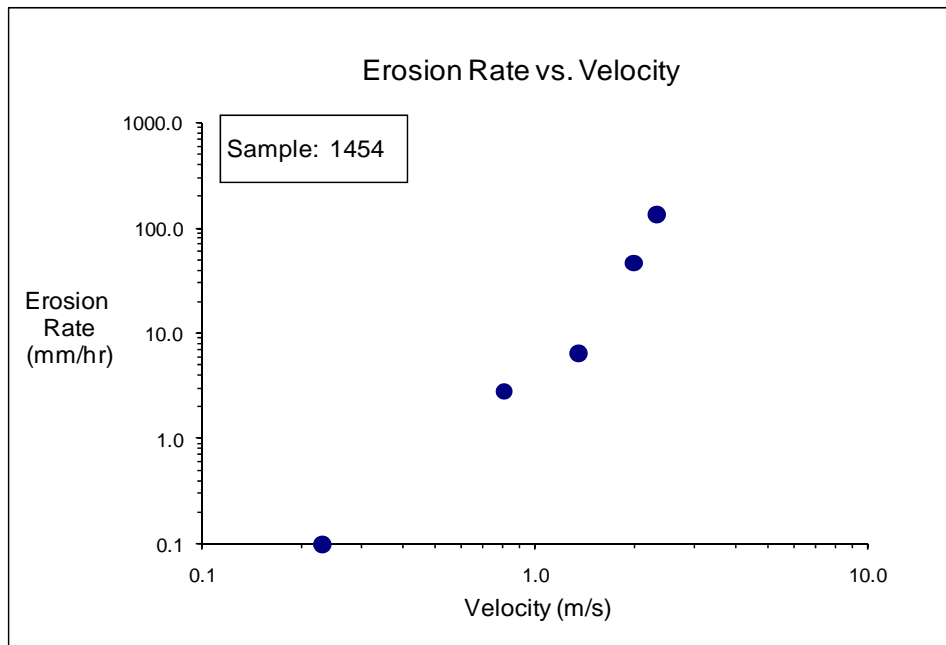


Figure D-30(b). EFA Test Results for Soil Sample 1454 (Velocity).

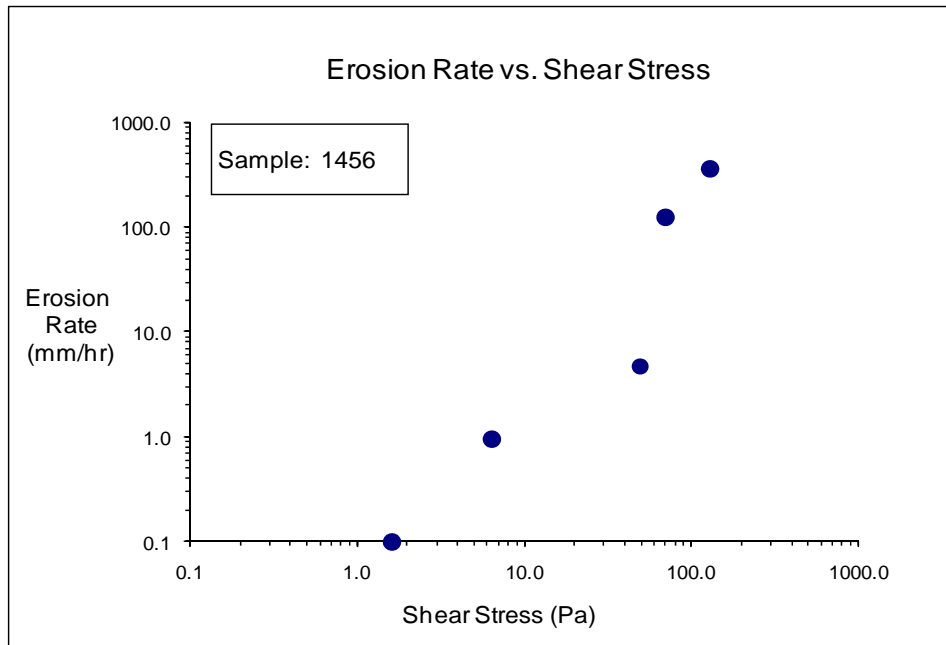


Figure D-31(a). EFA Test Results for Soil Sample 1456 (Shear Stress).

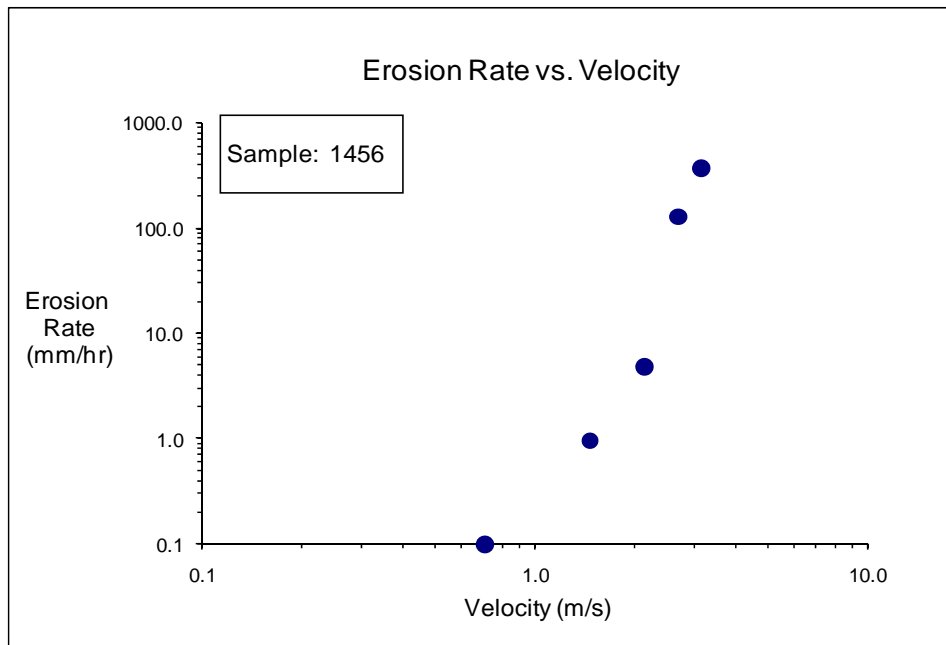


Figure D-31(b). EFA Test Results for Soil Sample 1456 (Velocity).

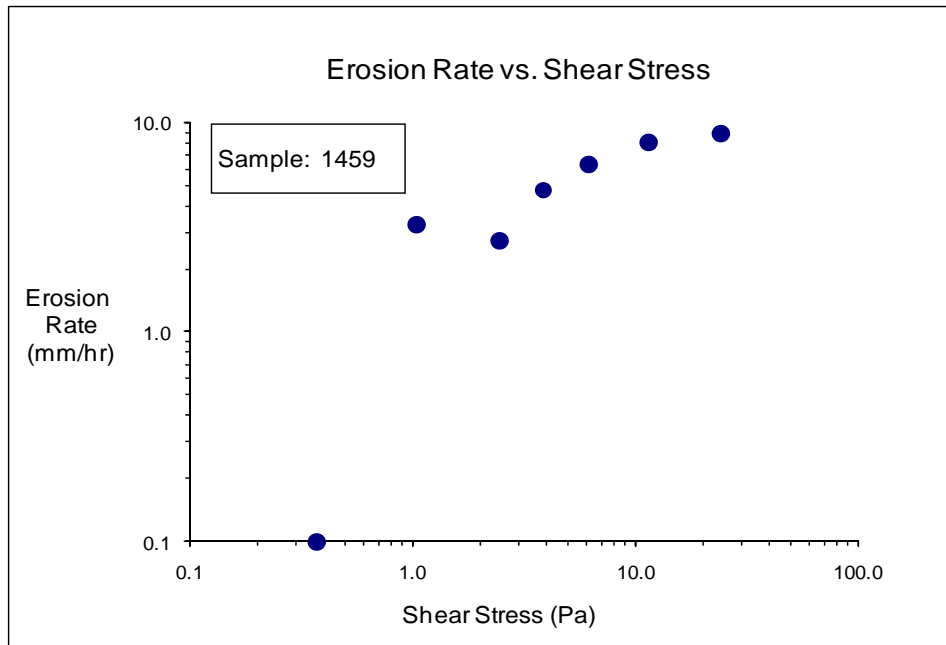


Figure D-32(a). EFA Test Results for Soil Sample 1459 (Shear Stress).

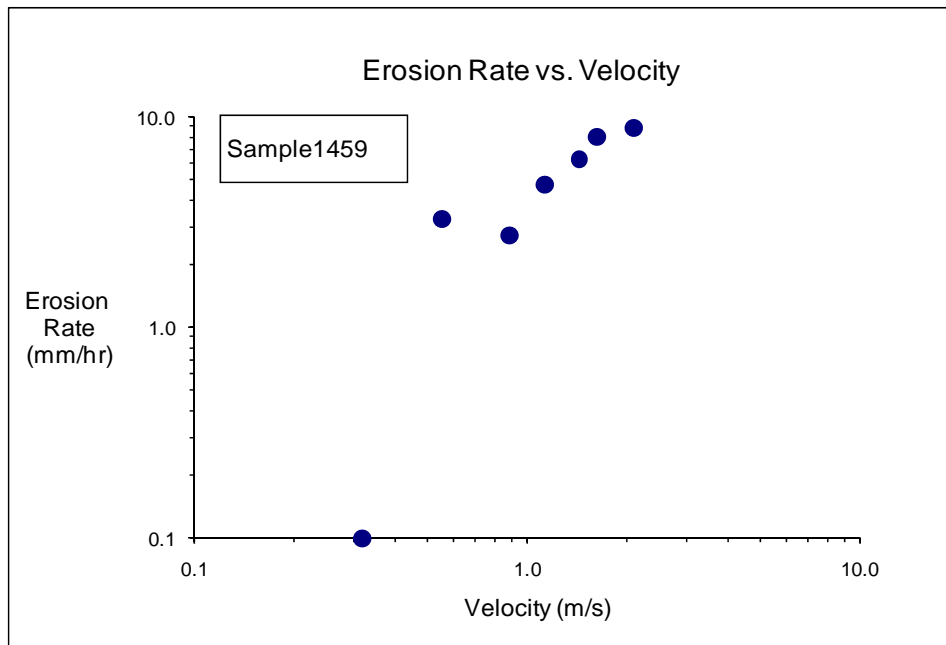


Figure D-32(b). EFA Test Results for Soil Sample 1459 (Velocity).

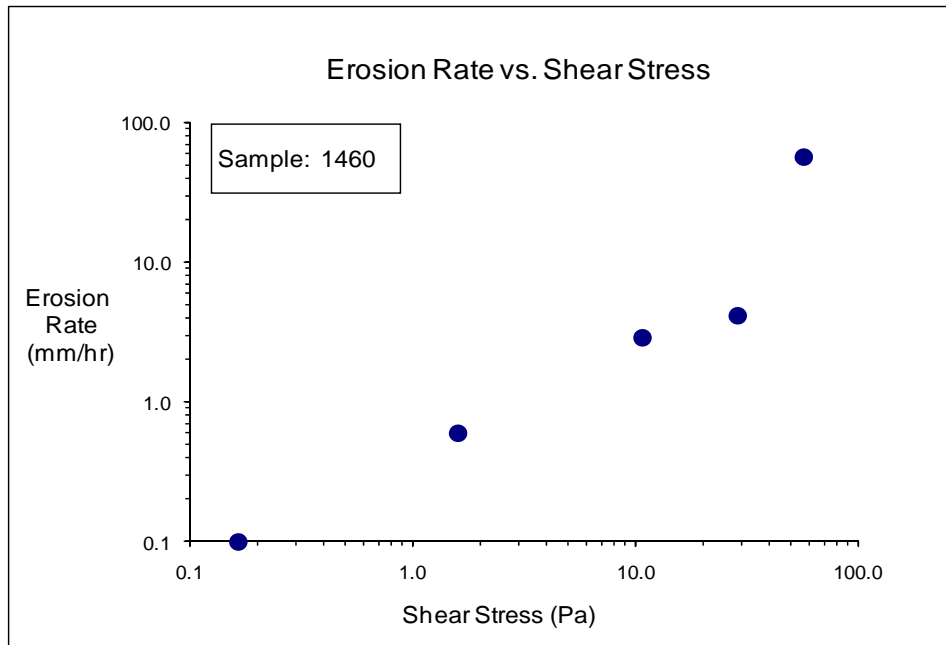


Figure D-33(a). EFA Test Results for Soil Sample 1460 (Shear Stress).

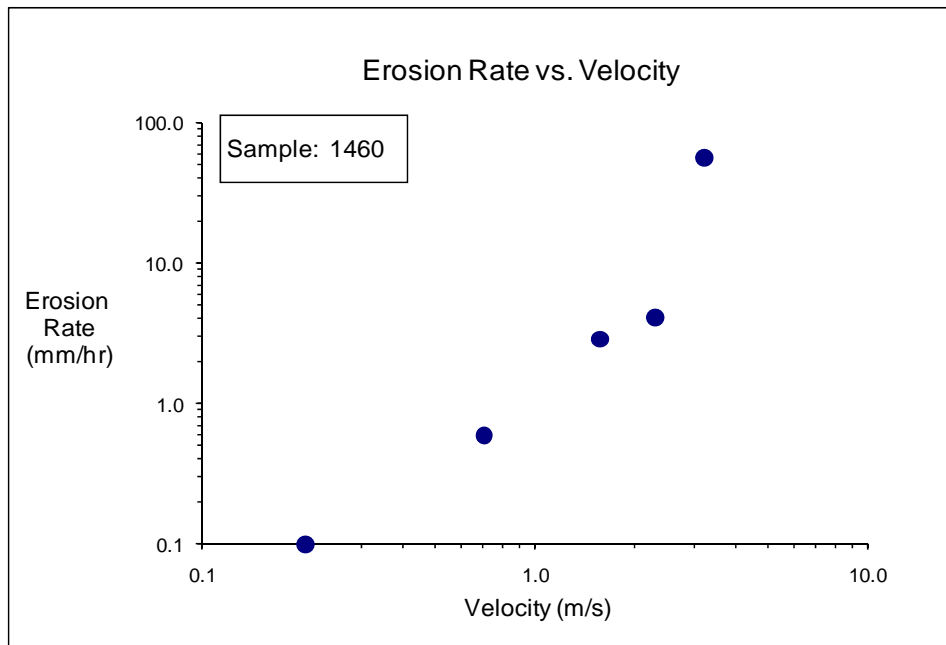


Figure D-33(b). EFA Test Results for Soil Sample 1460 (Velocity).

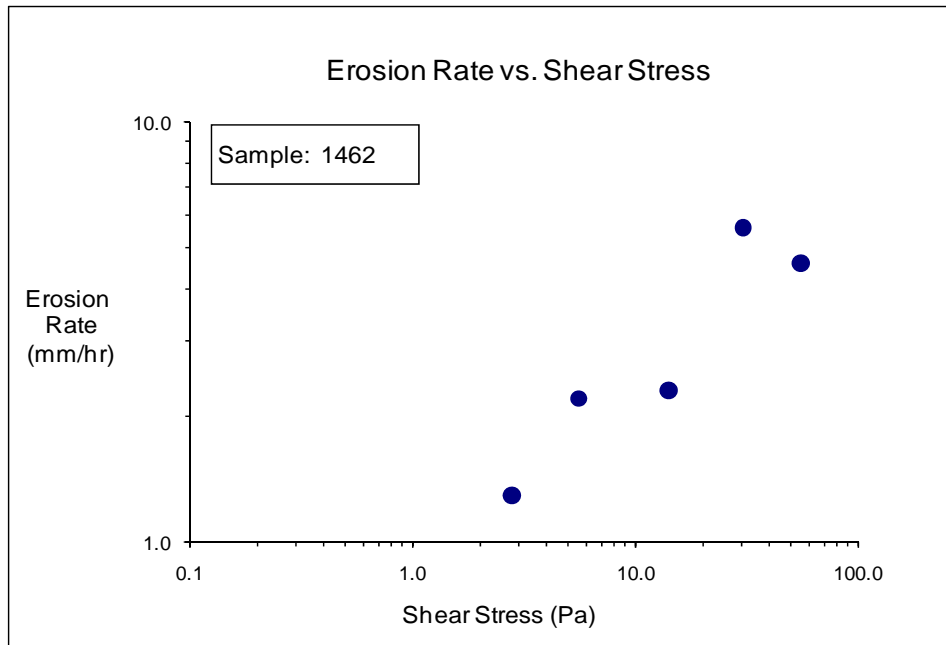


Figure D-34(a). EFA Test Results for Soil Sample 1462 (Shear Stress).

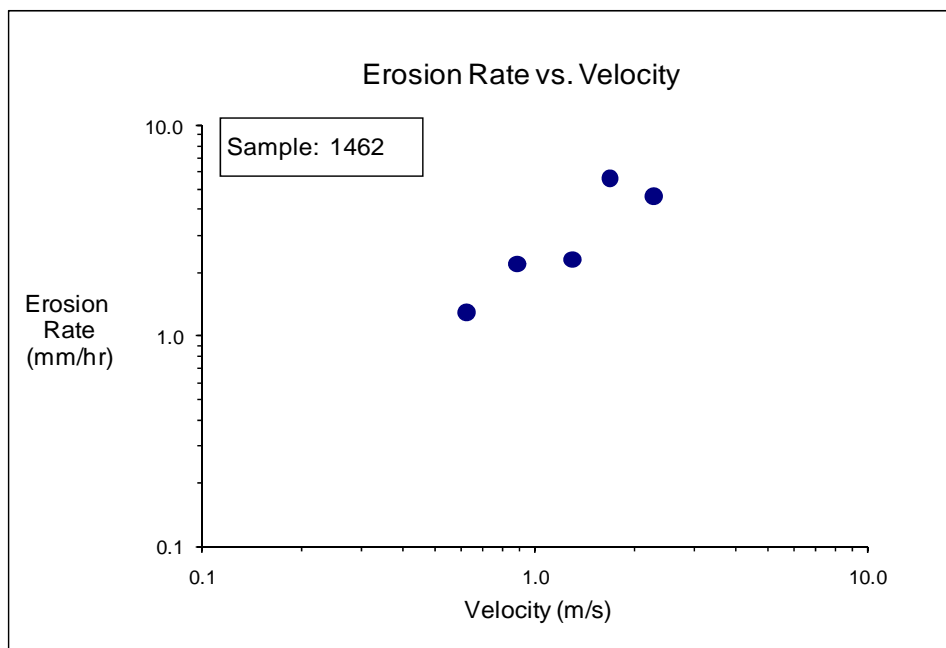


Figure D-34(b). EFA Test Results for Soil Sample 1462 (Velocity).

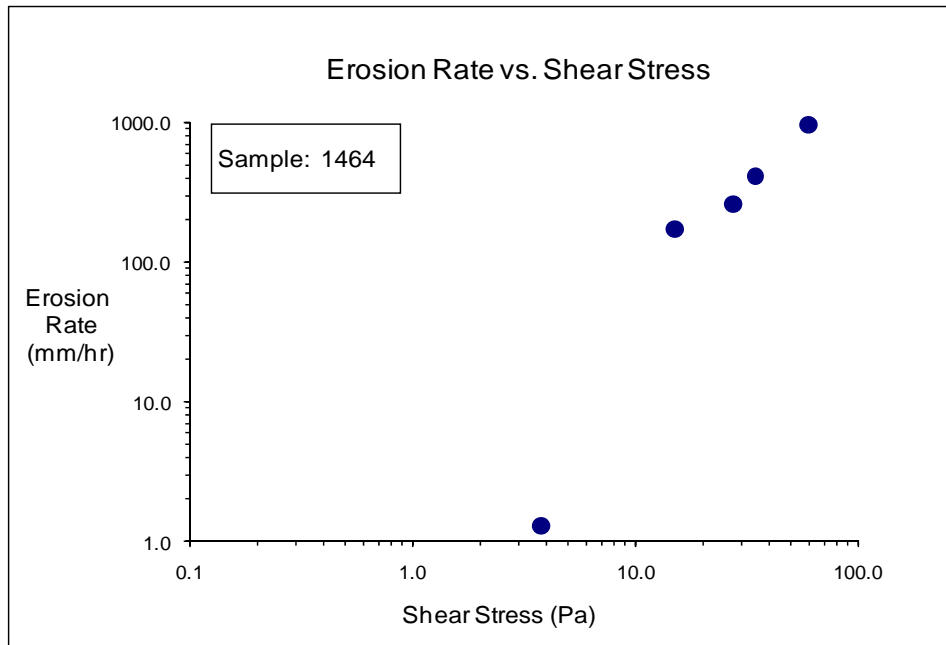


Figure D-35(a). EFA Test Results for Soil Sample 1464 (Shear Stress).

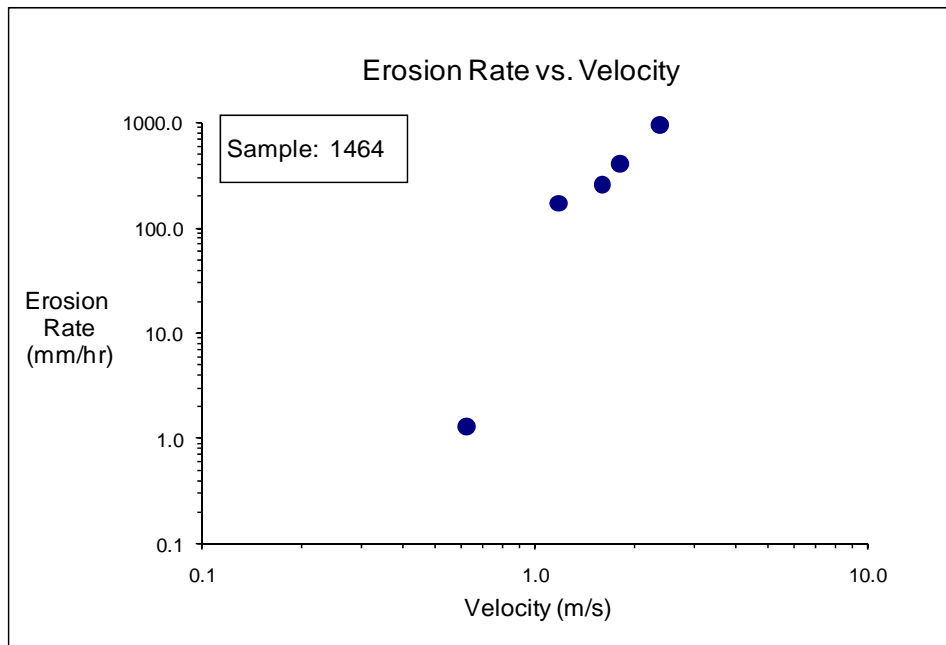


Figure D-35(b). EFA Test Results for Soil Sample 1464 (Velocity).

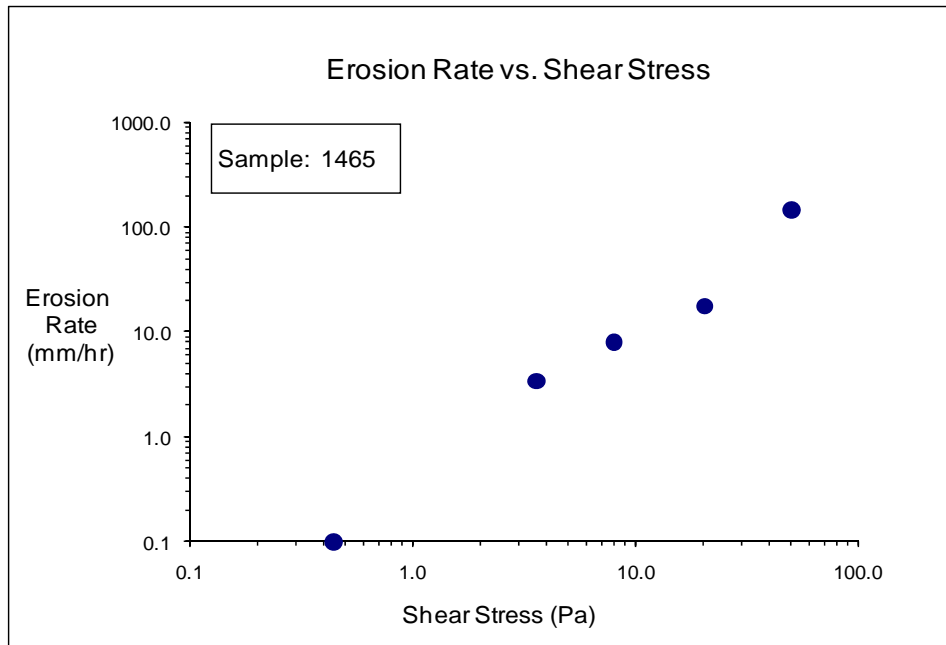


Figure D-36(a). EFA Test Results for Soil Sample 1456 (Shear Stress).

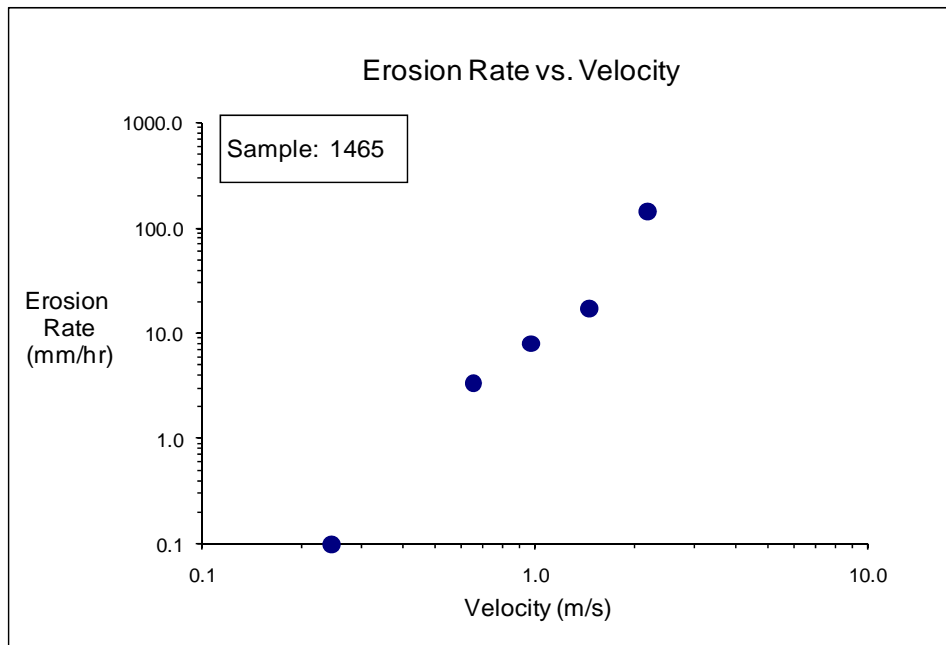


Figure D-36(b). EFA Test Results for Soil Sample 1456 (Velocity).

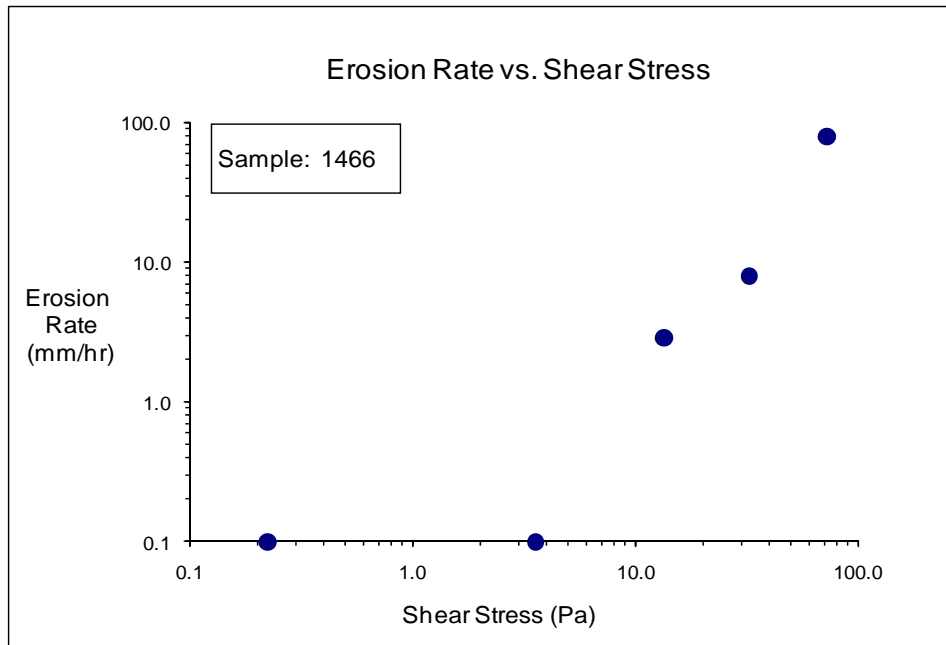


Figure D-37(a). EFA Test Results for Soil Sample 1466 (Shear Stress).

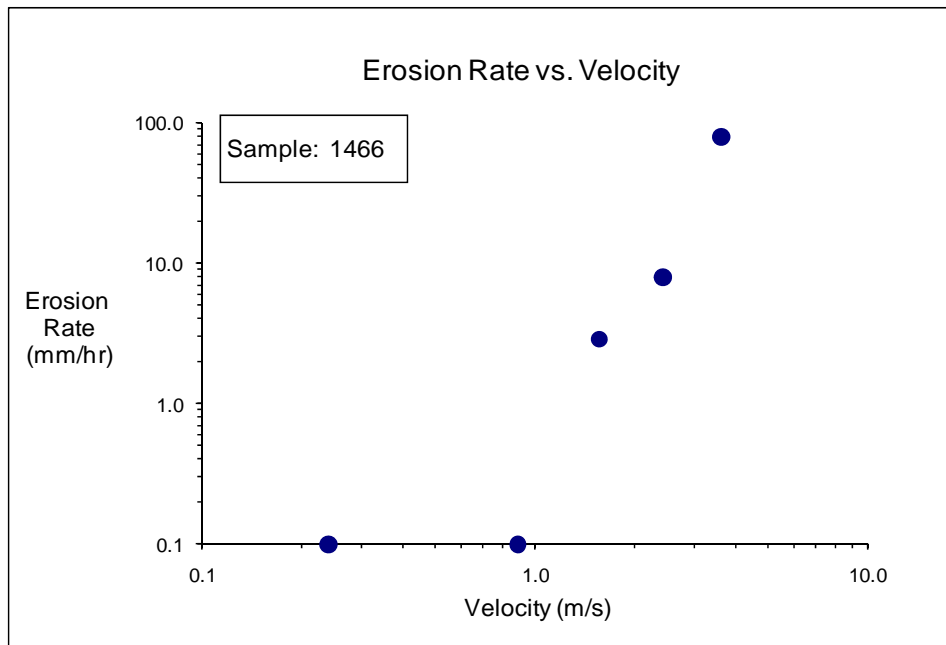


Figure D-37(b). EFA Test Results for Soil Sample 1466 (Velocity).

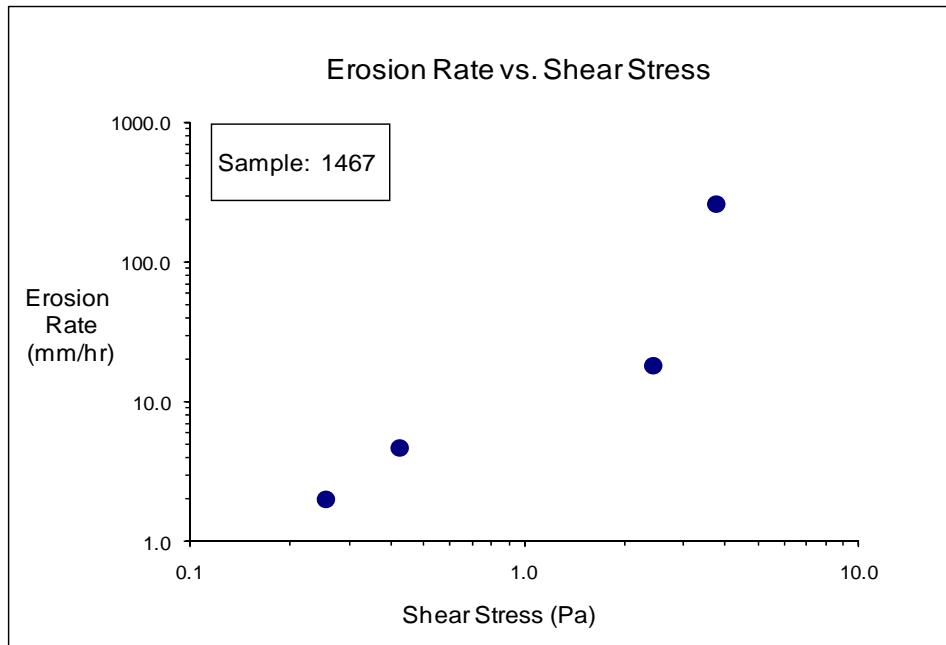


Figure D-38(a). EFA Test Results for Soil Sample 1467 (Shear Stress).

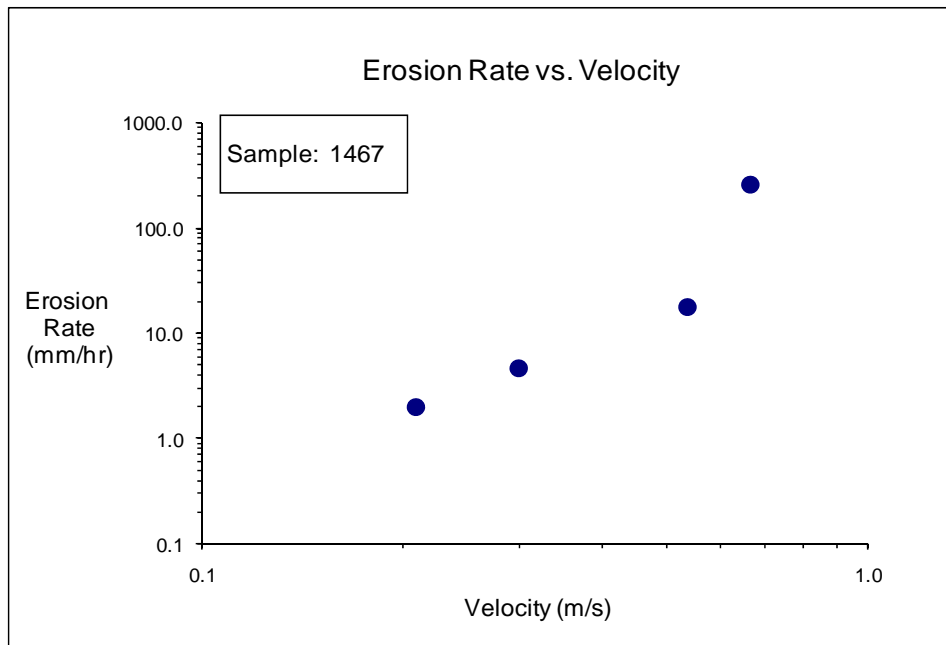


Figure D-38(b). EFA Test Results for Soil Sample 1467 (Velocity).

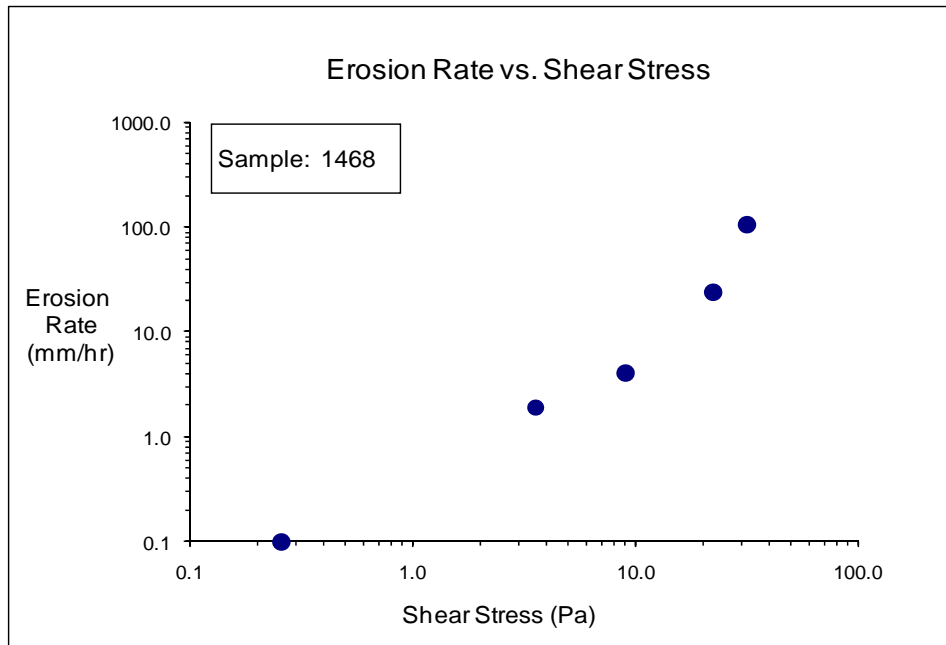


Figure D-39(a). EFA Test Results for Soil Sample 1468 (Shear Stress).

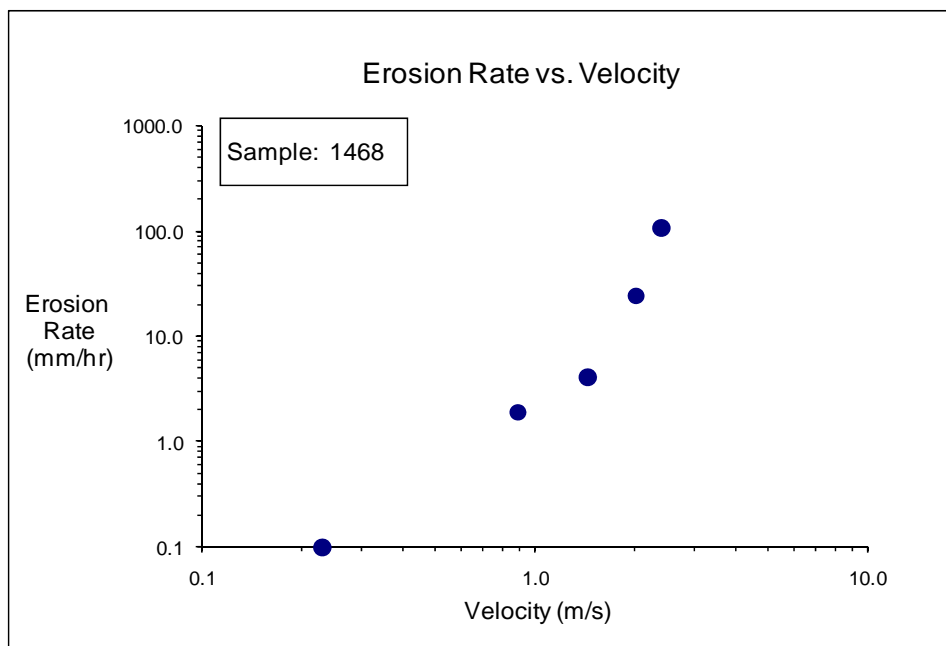


Figure D-39(b). EFA Test Results for Soil Sample 1468 (Velocity).

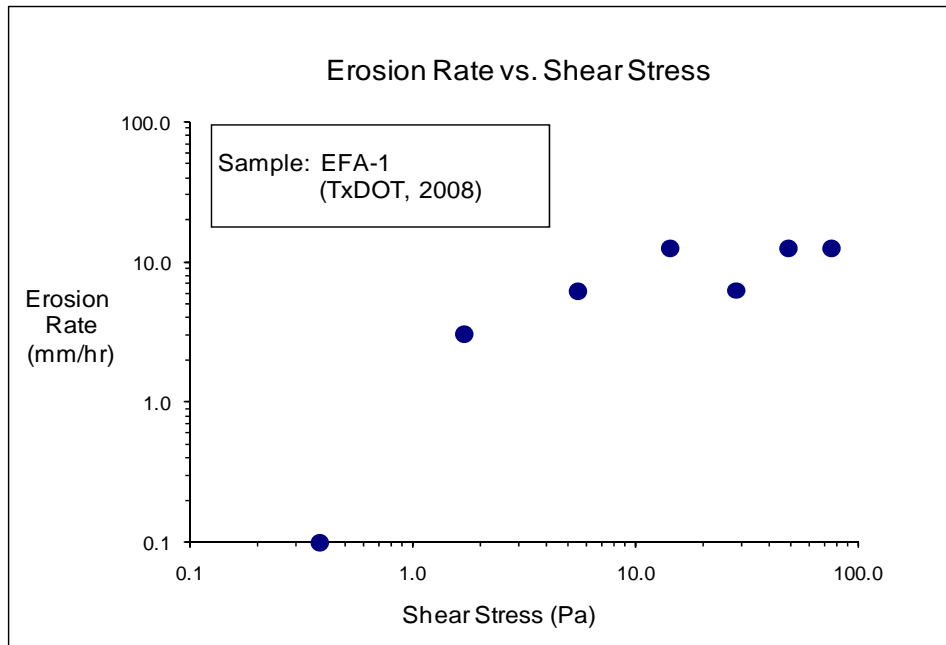


Figure D-40(a). EFA Test Results for Soil Sample EFA-1 (Shear Stress).

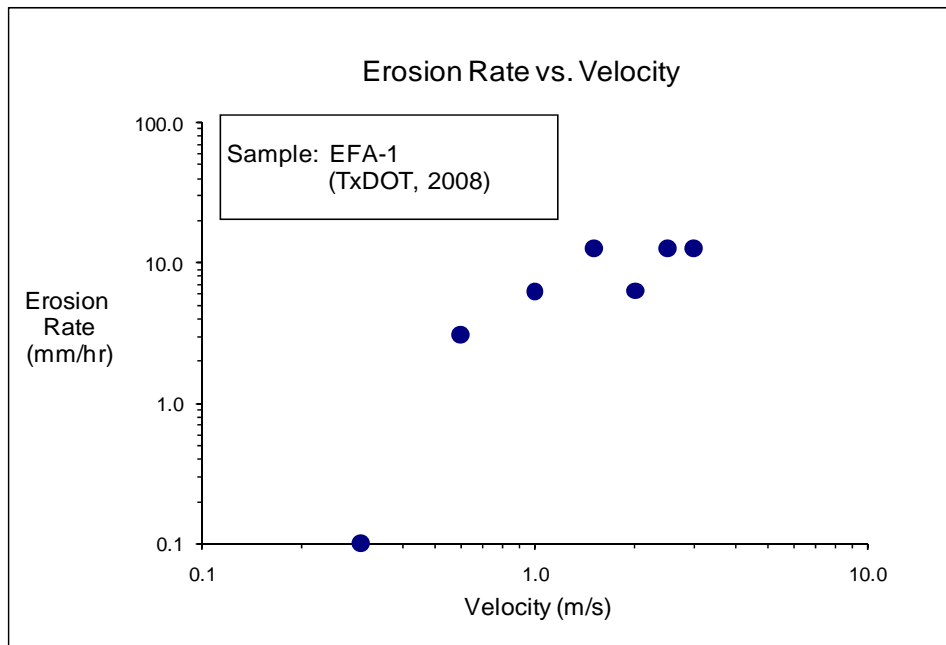


Figure D-40(b). EFA Test Results for Soil Sample EFA-1 (Velocity).

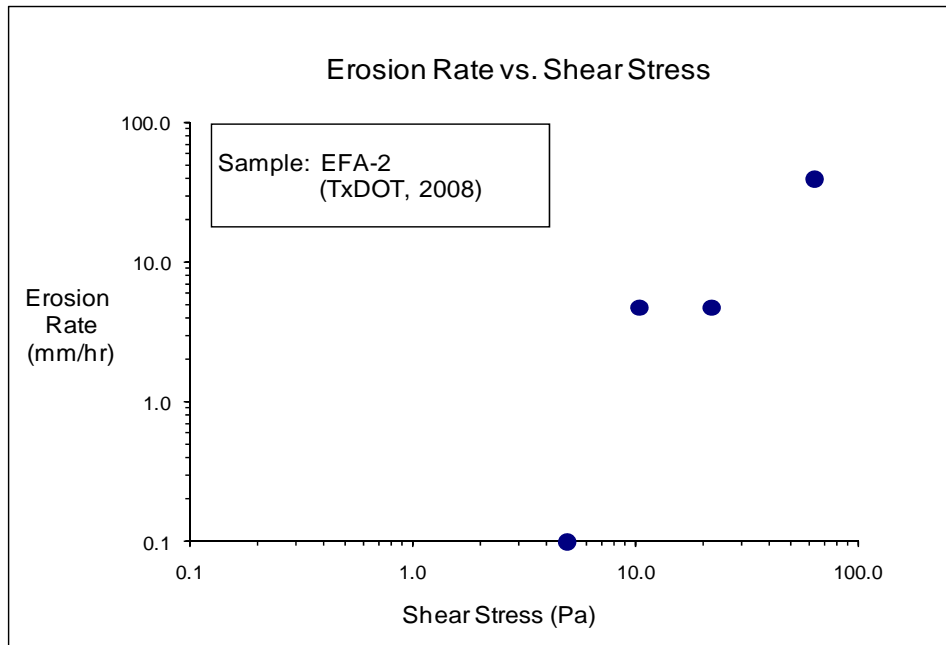


Figure D-41(a). EFA Test Results for Soil Sample EFA-2 (Shear Stress).

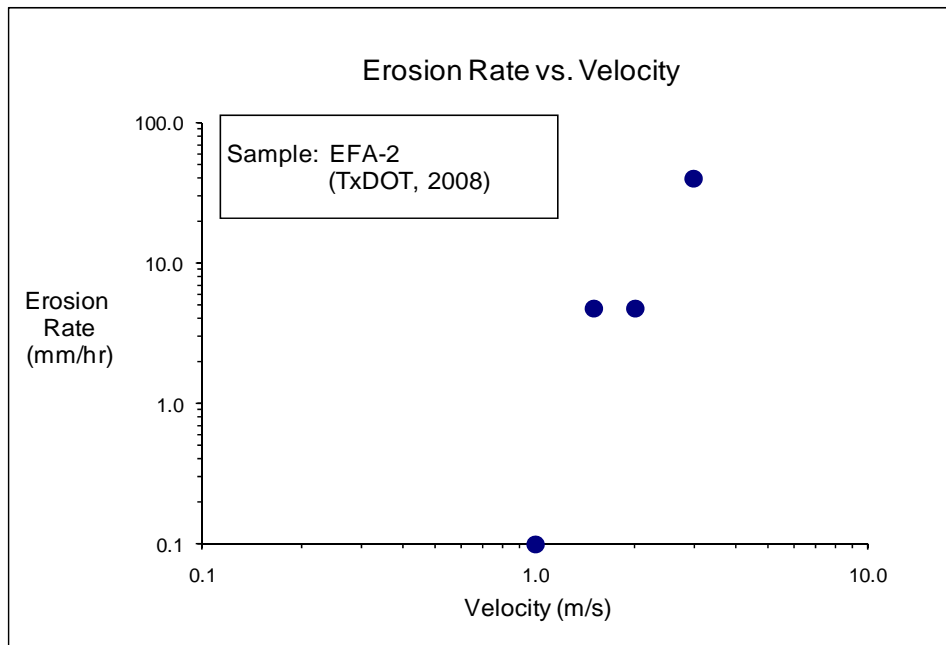


Figure D-41(b). EFA Test Results for Soil Sample EFA-2 (Velocity).

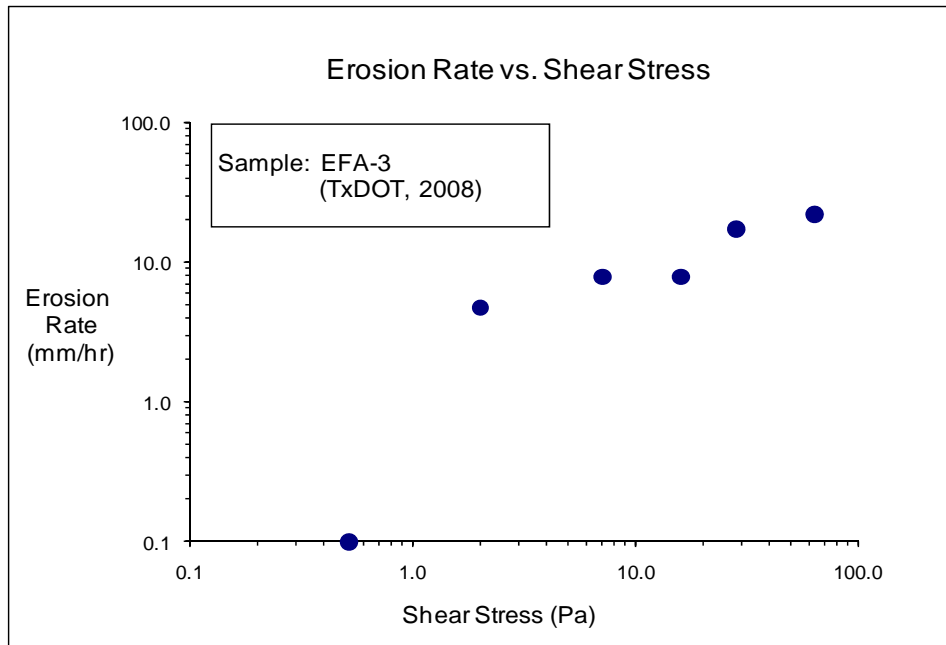


Figure D-42(a). EFA Test Results for Soil Sample EFA-3 (Shear Stress).

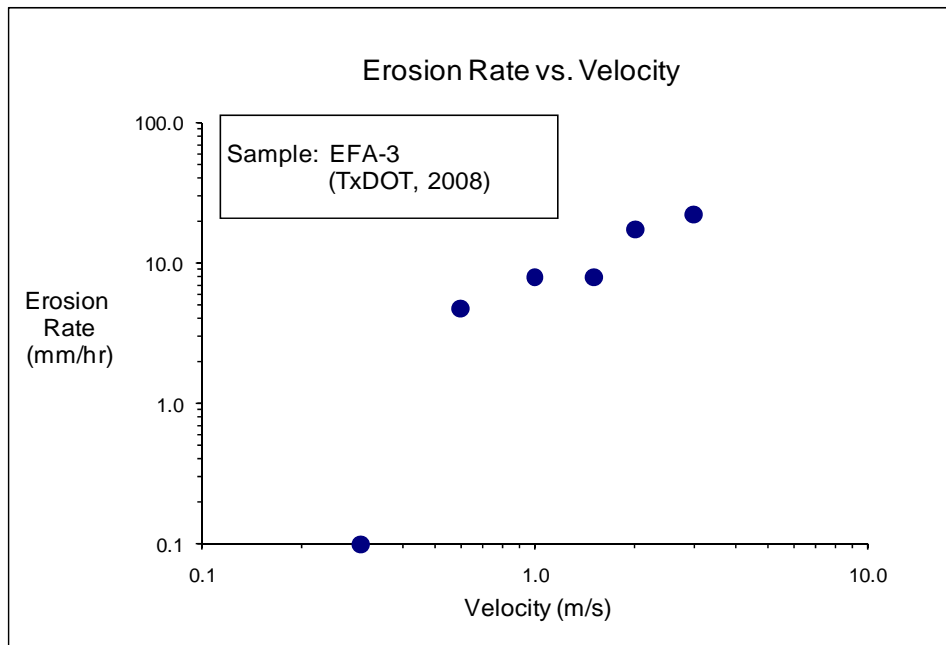


Figure D-42(b). EFA Test Results for Soil Sample EFA-3 (Velocity).

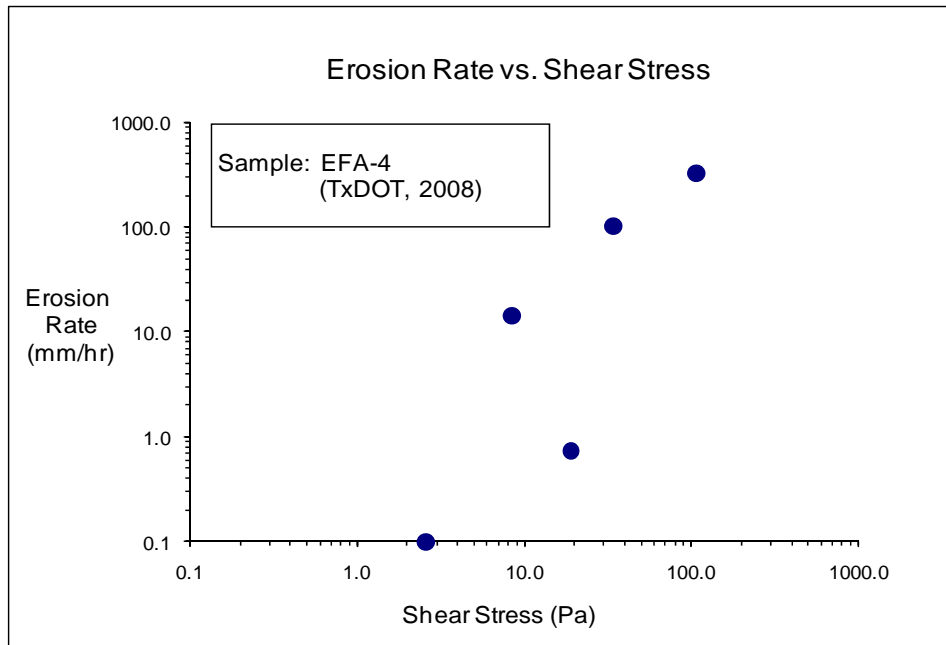


Figure D-43(a). EFA Test Results for Soil Sample EFA-4 (Shear Stress).

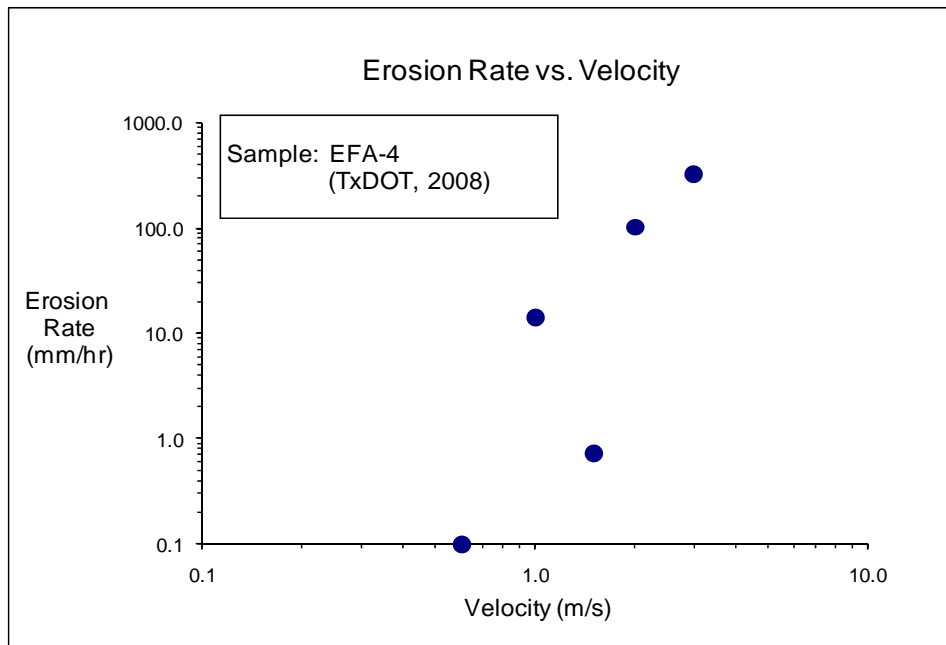


Figure D-43(b). EFA Test Results for Soil Sample EFA-4 (Velocity).

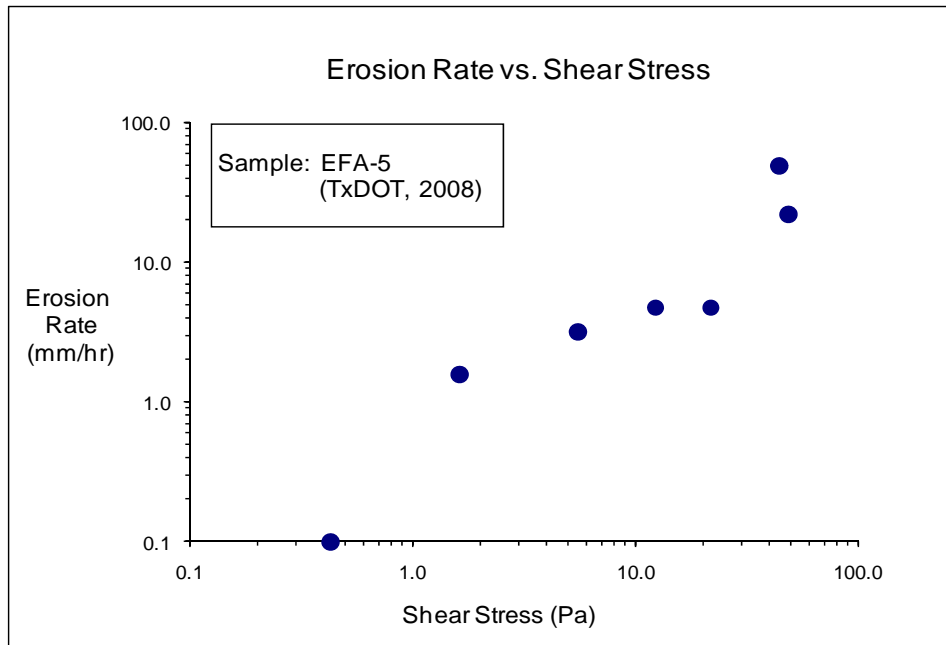


Figure D-44(a). EFA Test Results for Soil Sample EFA-5 (Shear Stress).

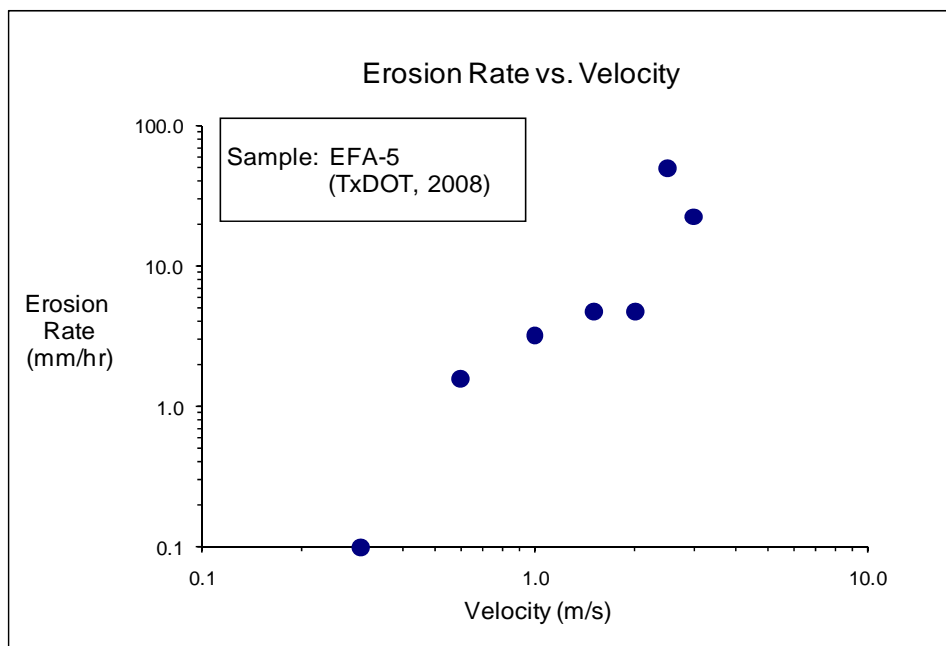


Figure D-44(b). EFA Test Results for Soil Sample EFA-5 (Velocity).

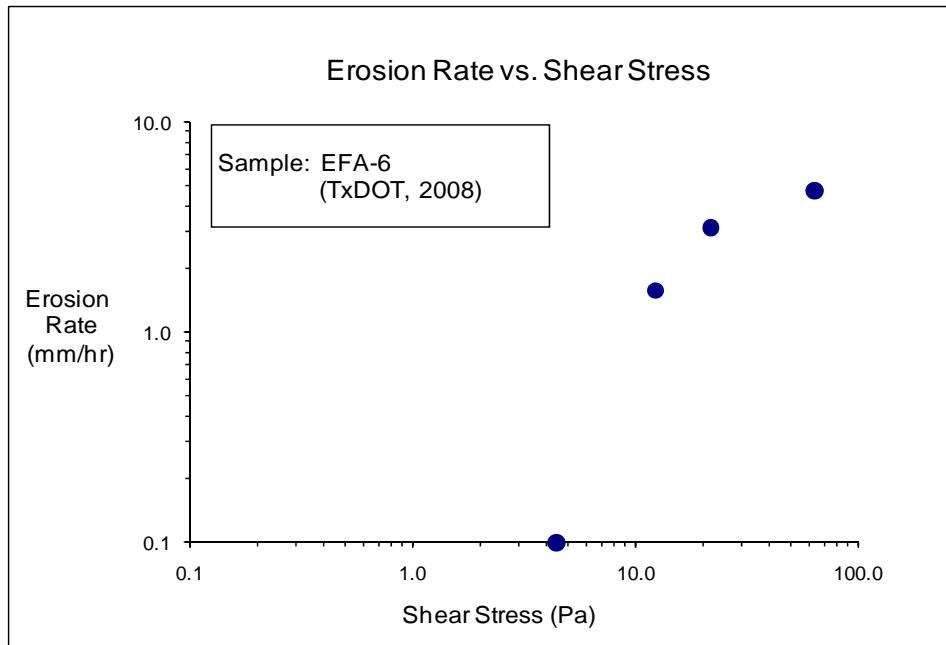


Figure D-45(a). EFA Test Results for Soil Sample EFA-6 (Shear Stress).

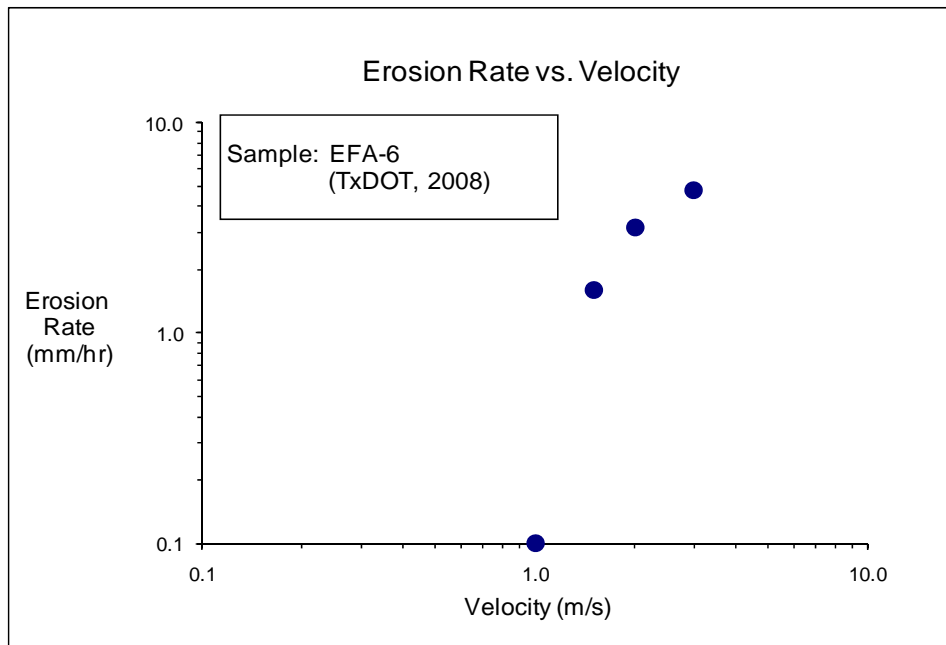


Figure D-45(b). EFA Test Results for Soil Sample EFA-6 (Velocity).

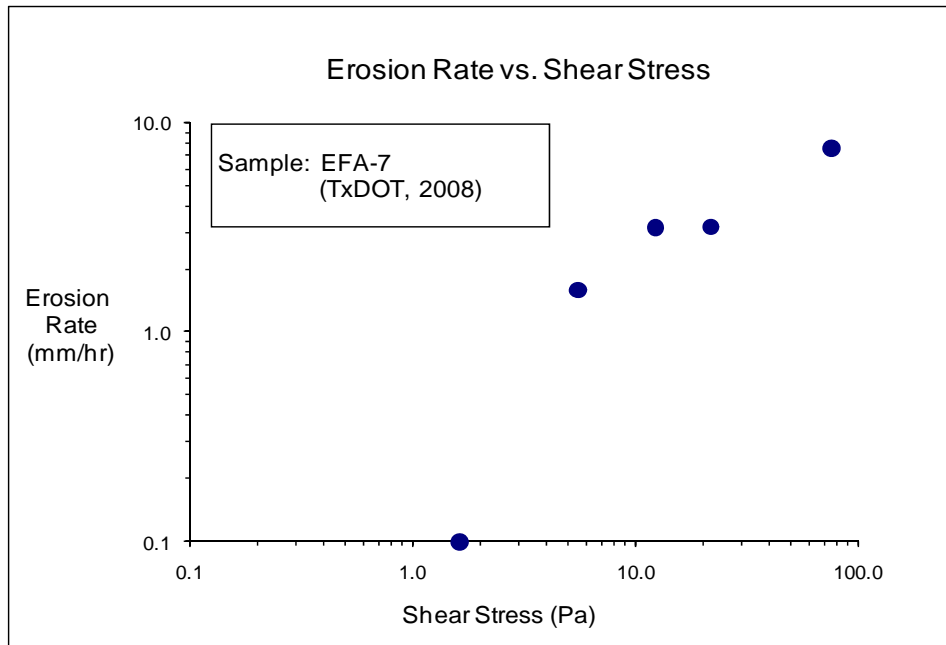


Figure D-46(a). EFA Test Results for Soil Sample EFA-7 (Shear Stress).

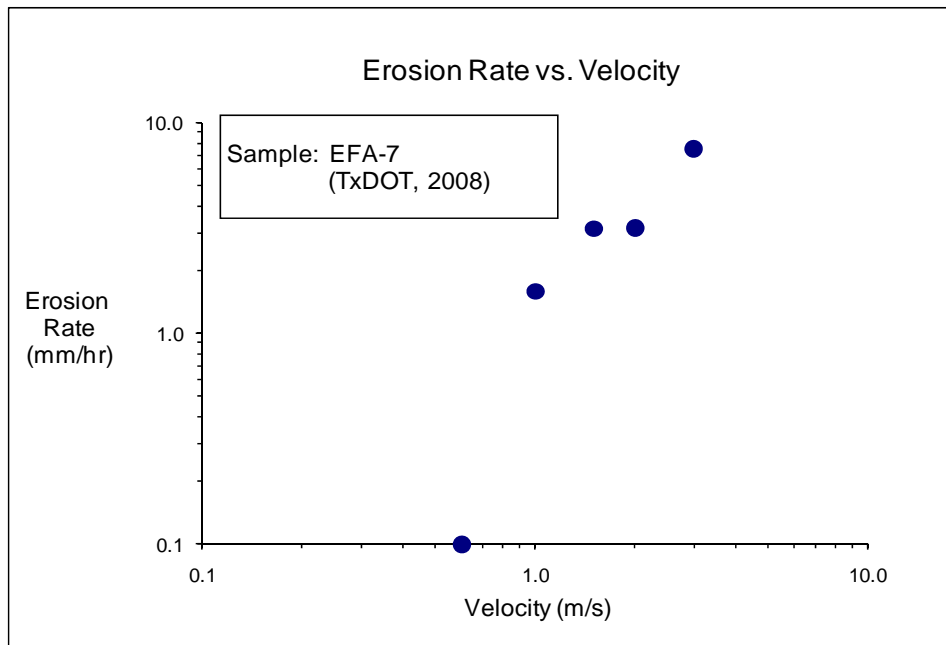


Figure D-46(b). EFA Test Results for Soil Sample EFA-7 (Velocity).

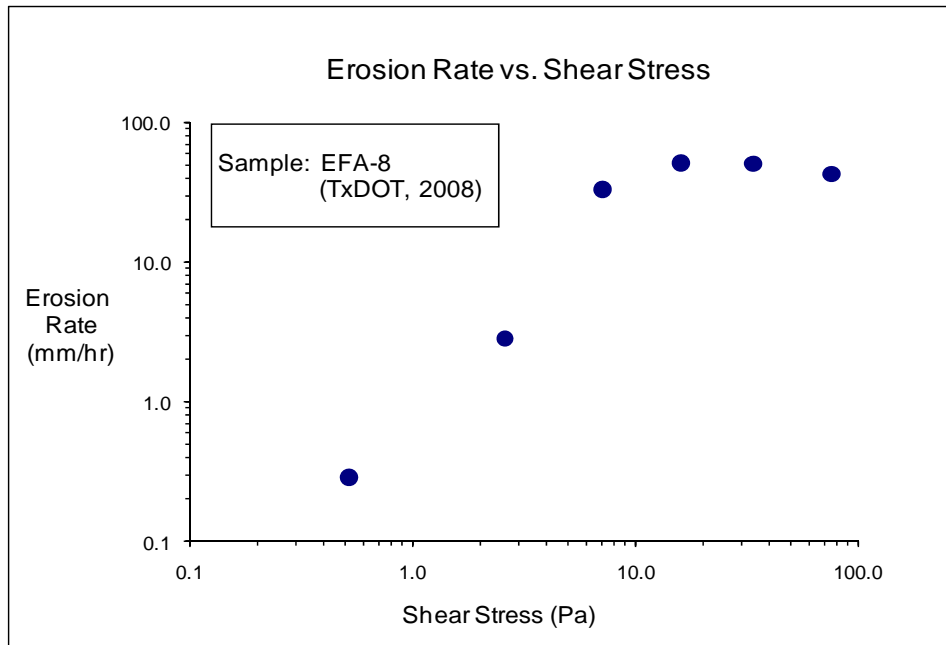


Figure D-47(a). EFA Test Results for Soil Sample EFA-8 (Shear Stress).

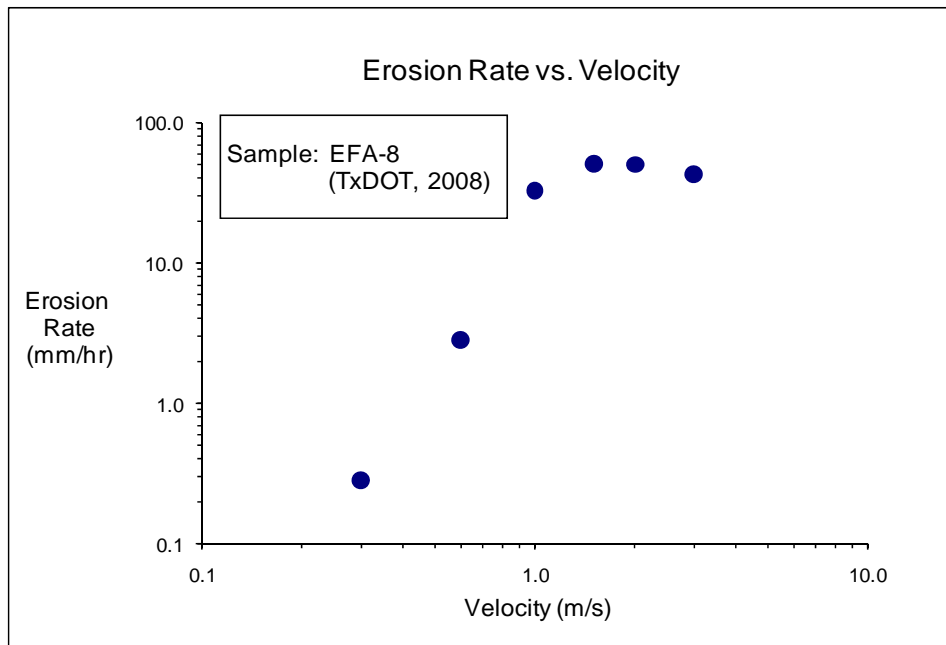


Figure D-47(b). EFA Test Results for Soil Sample EFA-8 (Velocity).

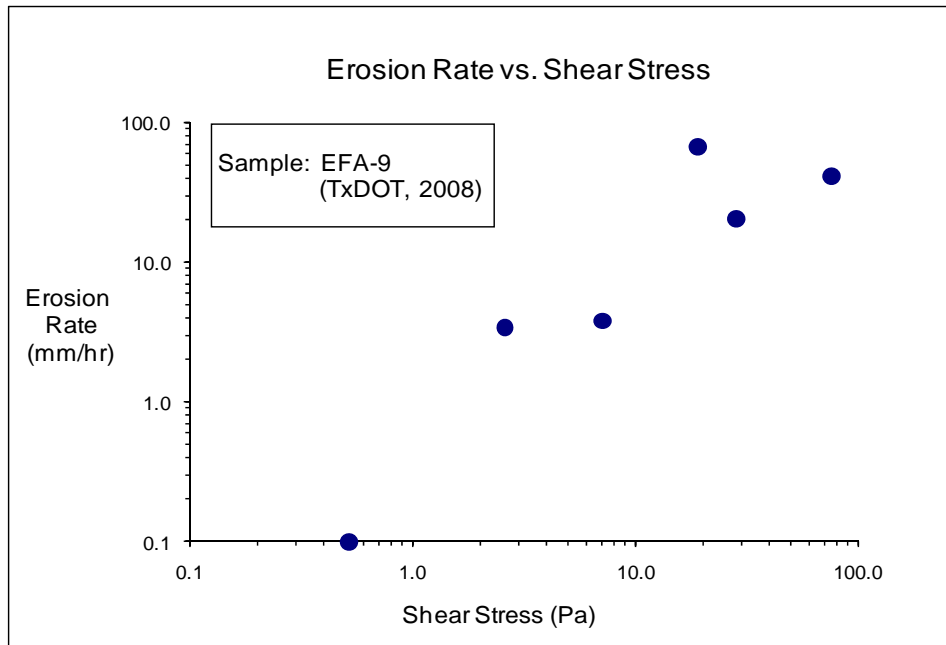


Figure D-48(a). EFA Test Results for Soil Sample EFA-9 (Shear Stress).

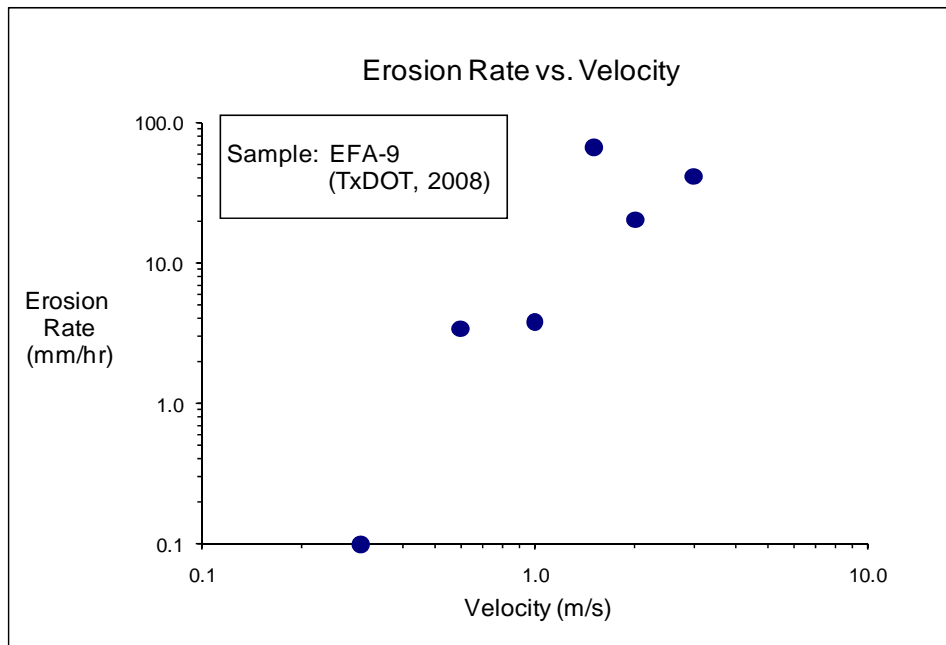


Figure D-48(b). EFA Test Results for Soil Sample EFA-9 (Velocity).

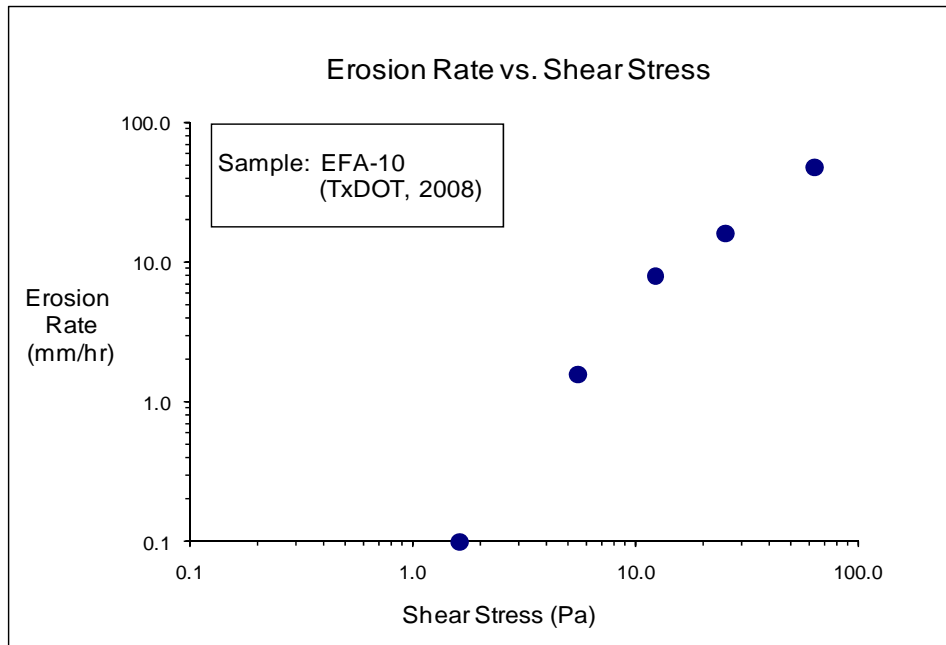


Figure D-49(a). EFA Test Results for Soil Sample EFA-10 (Shear Stress).

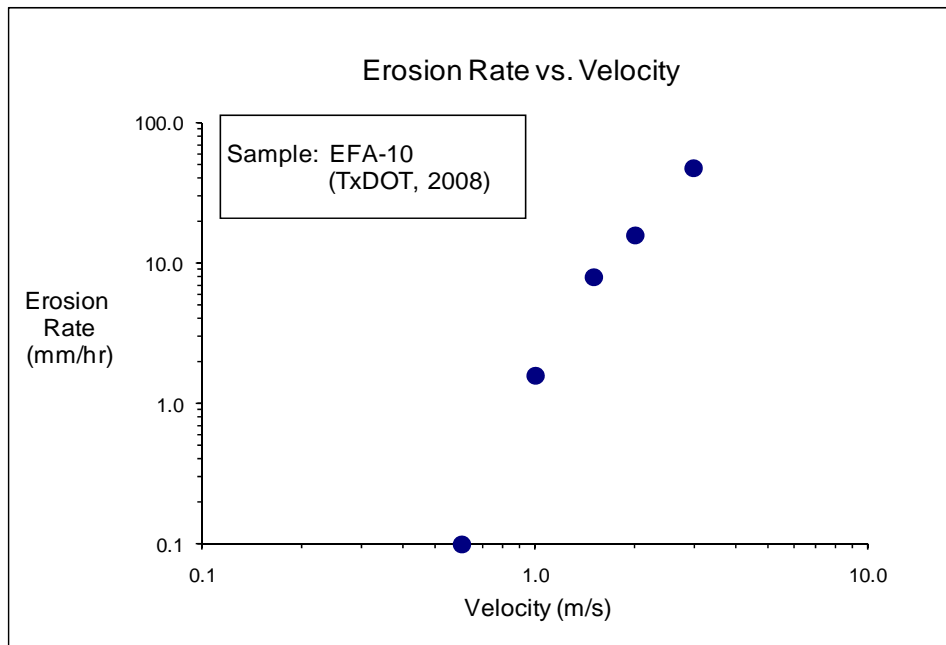


Figure D-49(b). EFA Test Results for Soil Sample EFA-10 (Velocity).

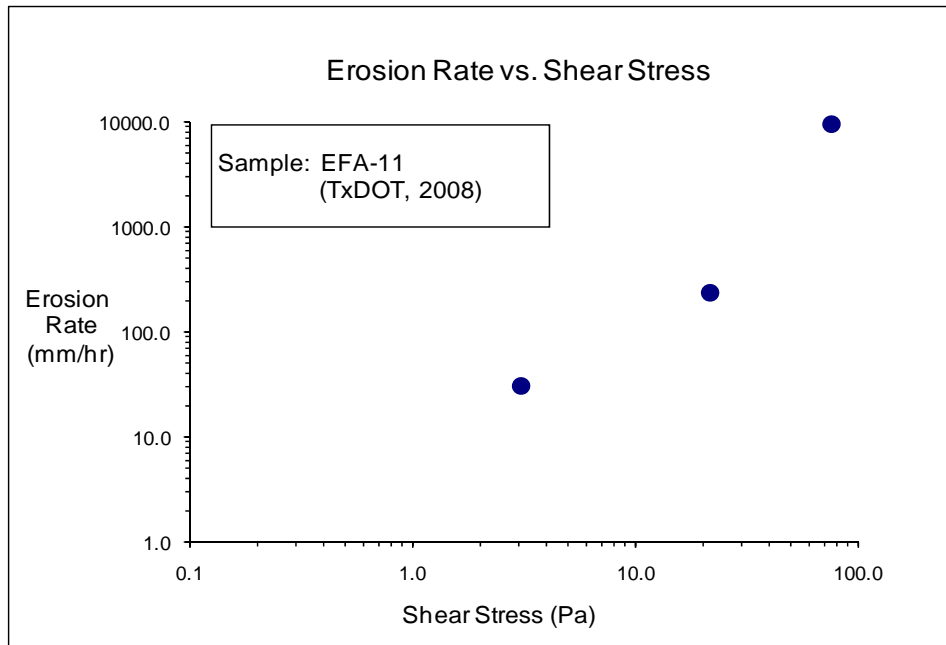


Figure D-50(a). EFA Test Results for Soil Sample EFA-11 (Shear Stress).

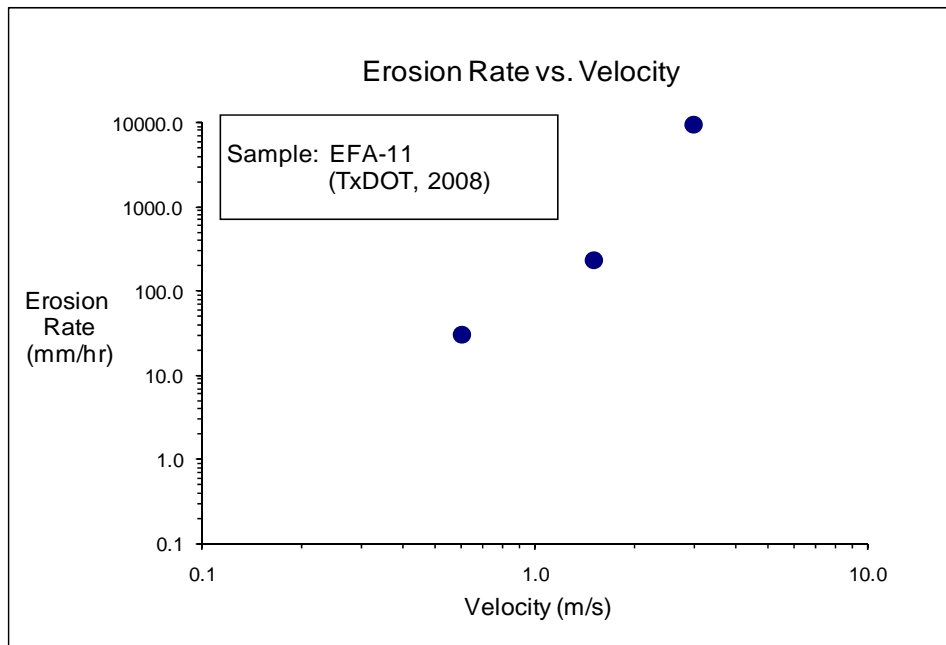


Figure D-50(b). EFA Test Results for Soil Sample EFA-11 (Velocity).

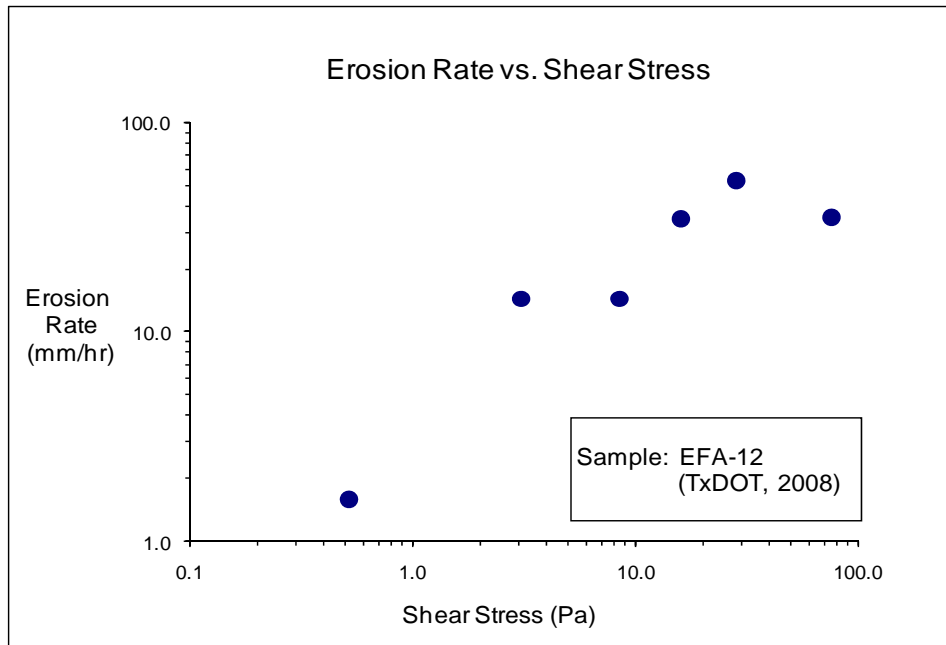


Figure D-51(a). EFA Test Results for Soil Sample EFA-12 (Shear Stress).

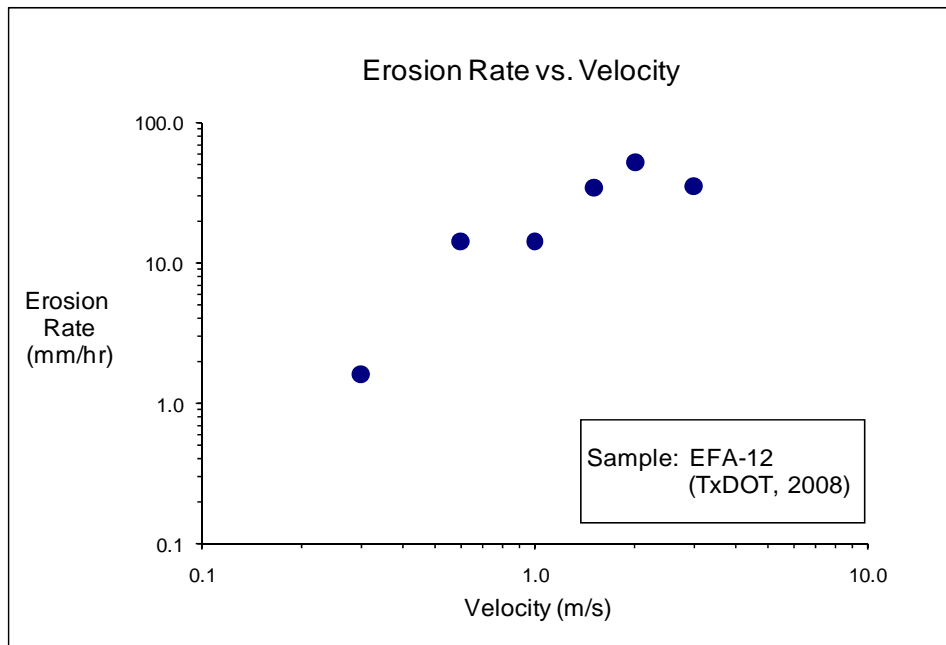


Figure D-51(b). EFA Test Results for Soil Sample EFA-12 (Velocity).

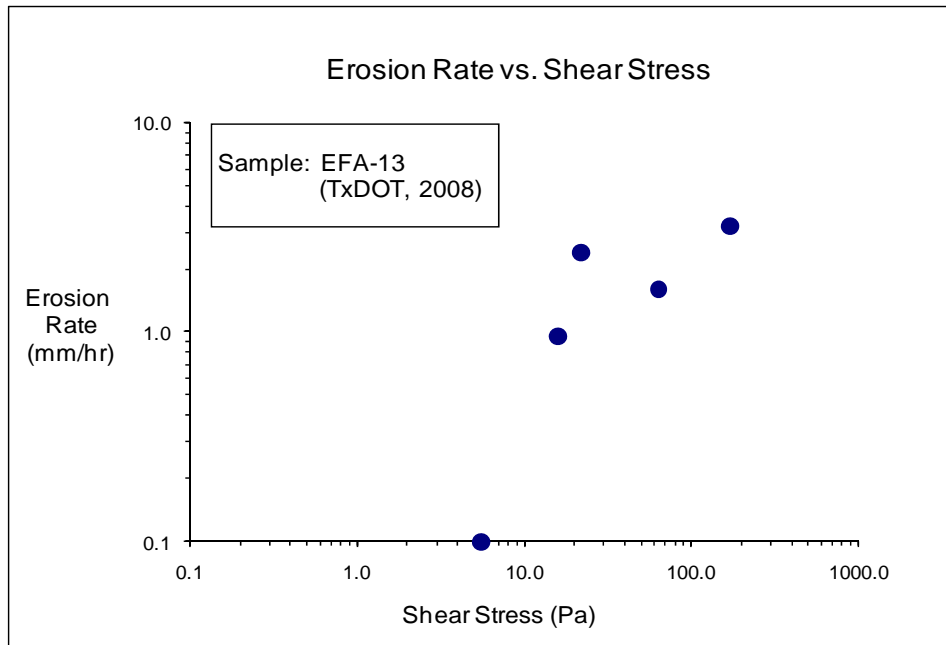


Figure D-52(a). EFA Test Results for Soil Sample EFA-13 (Shear Stress).

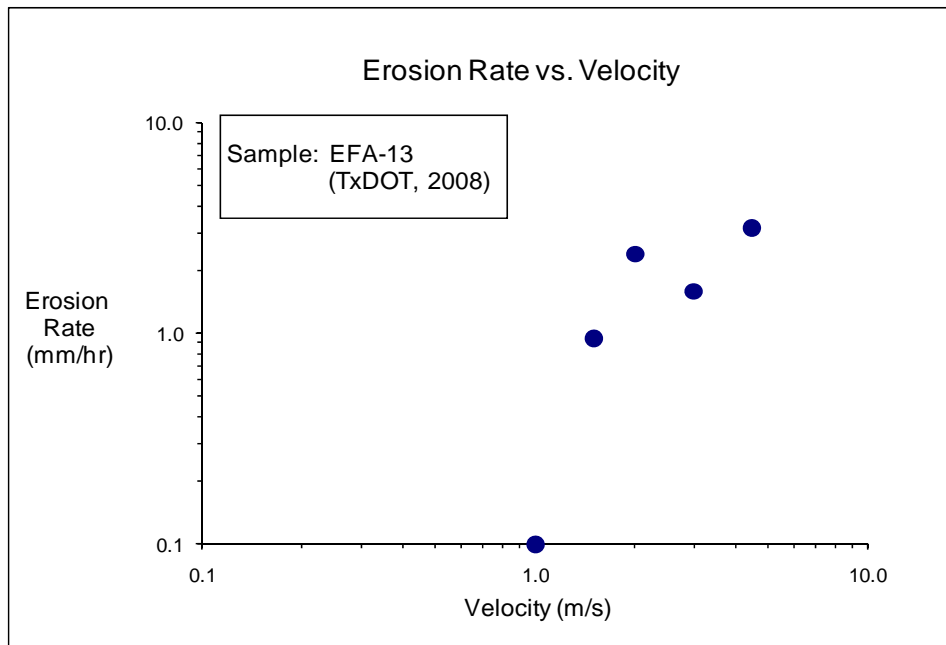


Figure D-52(b). EFA Test Results for Soil Sample EFA-13 (Velocity).

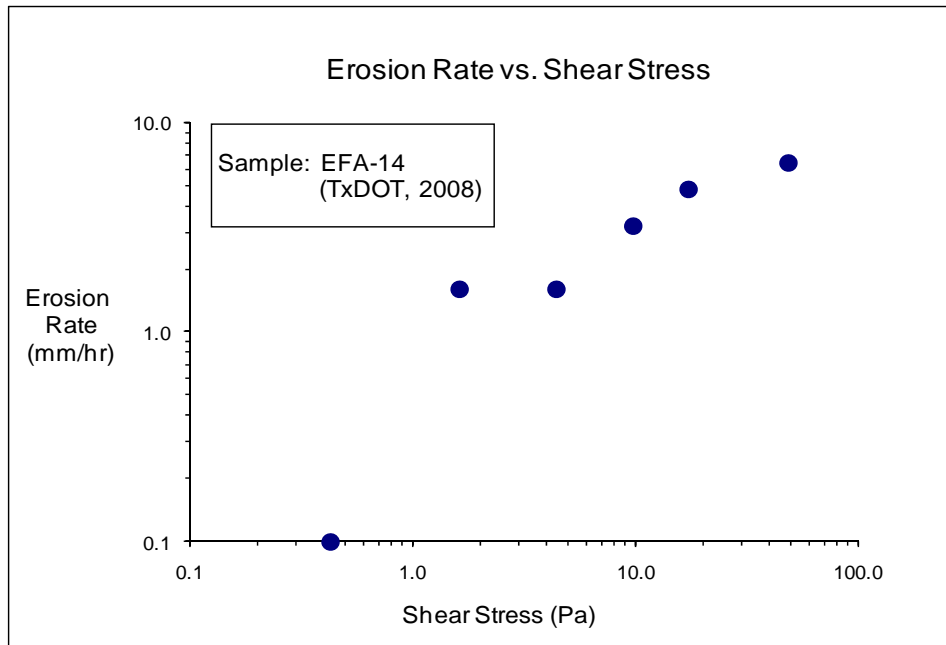


Figure D-53(a). EFA Test Results for Soil Sample EFA-14 (Shear Stress).

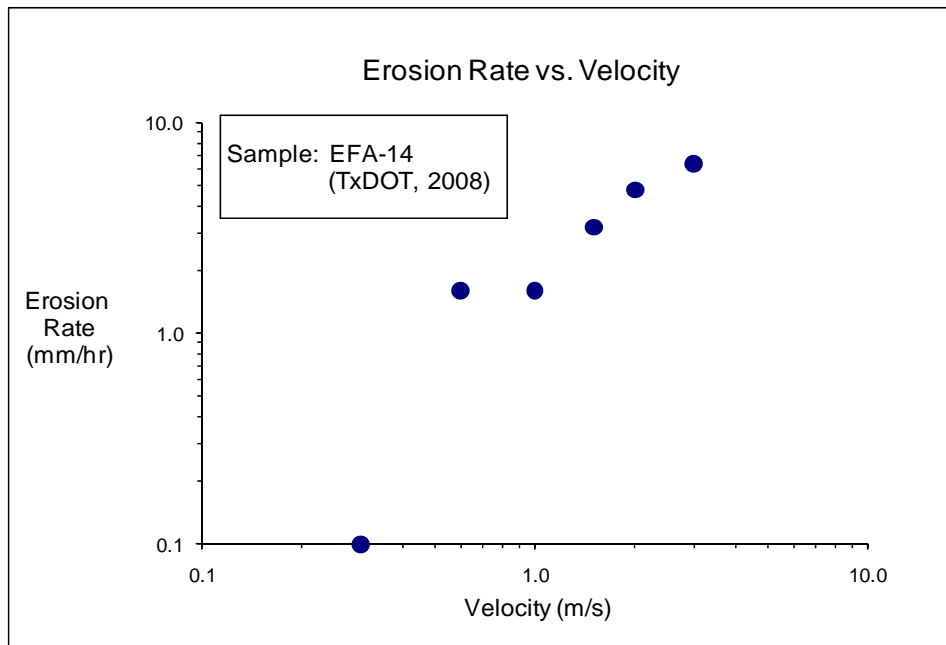


Figure D-53(b). EFA Test Results for Soil Sample EFA-14 (Velocity).

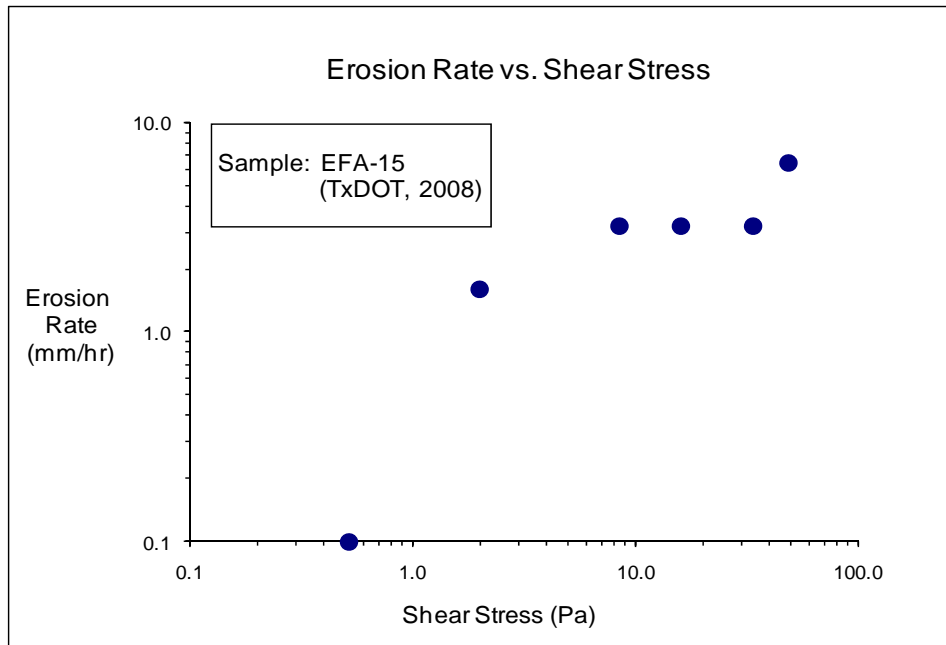


Figure D-54(a). EFA Test Results for Soil Sample EFA-15 (Shear Stress).

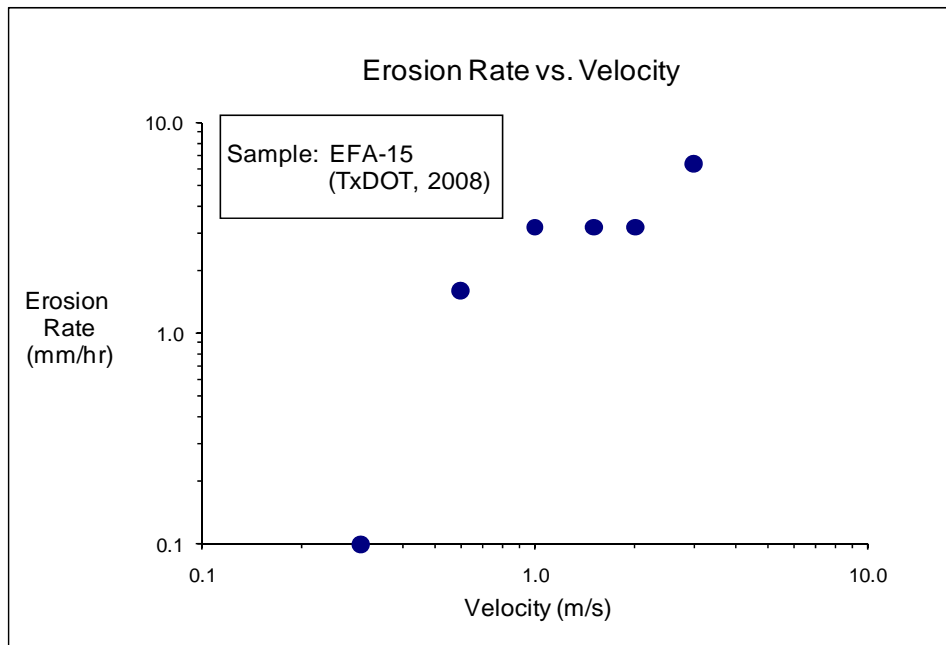


Figure D-54(b). EFA Test Results for Soil Sample EFA-15 (Velocity).

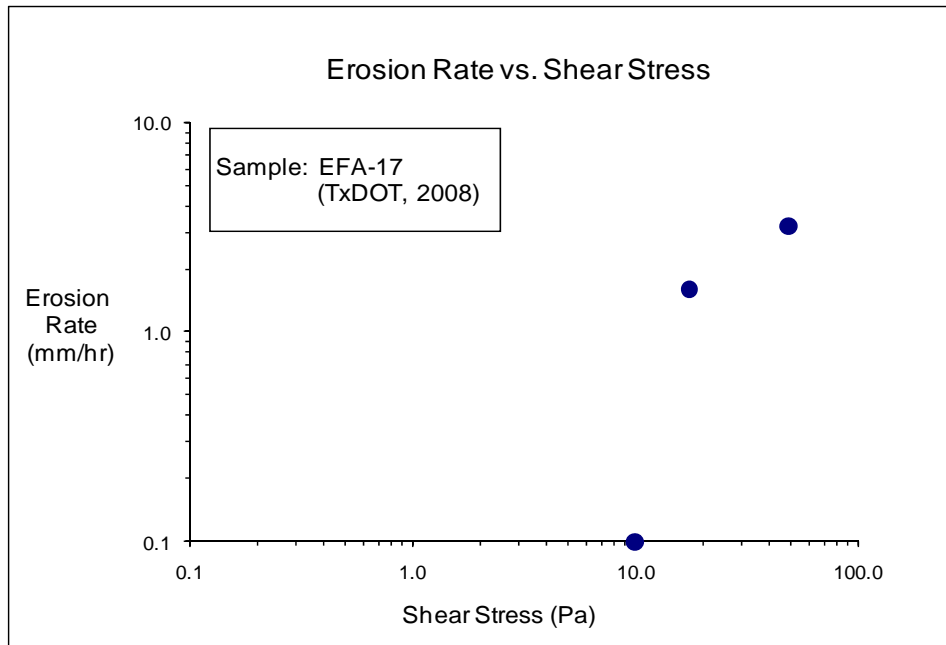


Figure D-55(a). EFA Test Results for Soil Sample EFA-17 (Shear Stress).

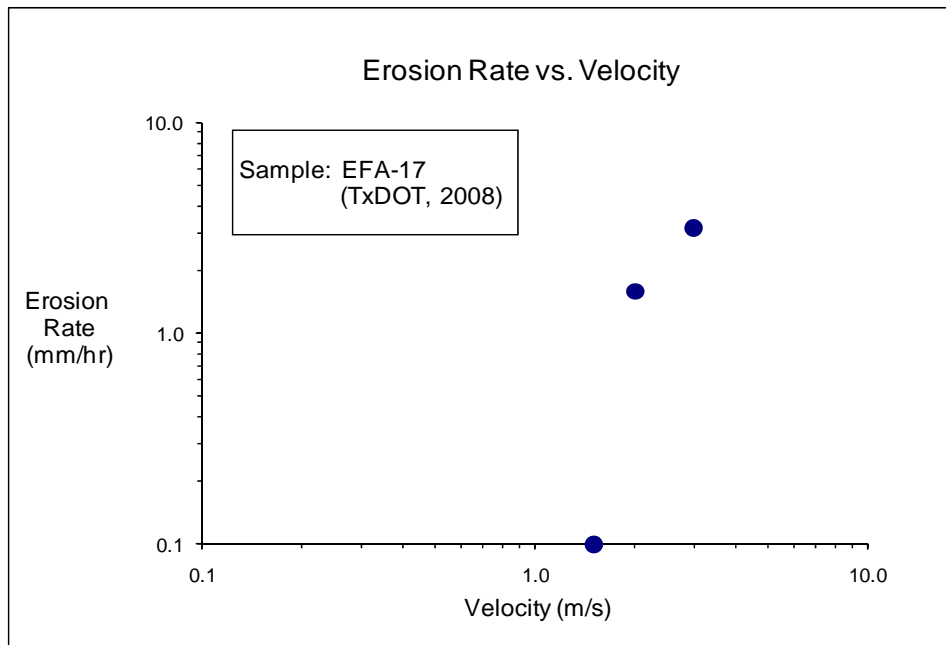


Figure D-55(b). EFA Test Results for Soil Sample EFA-17 (Velocity).

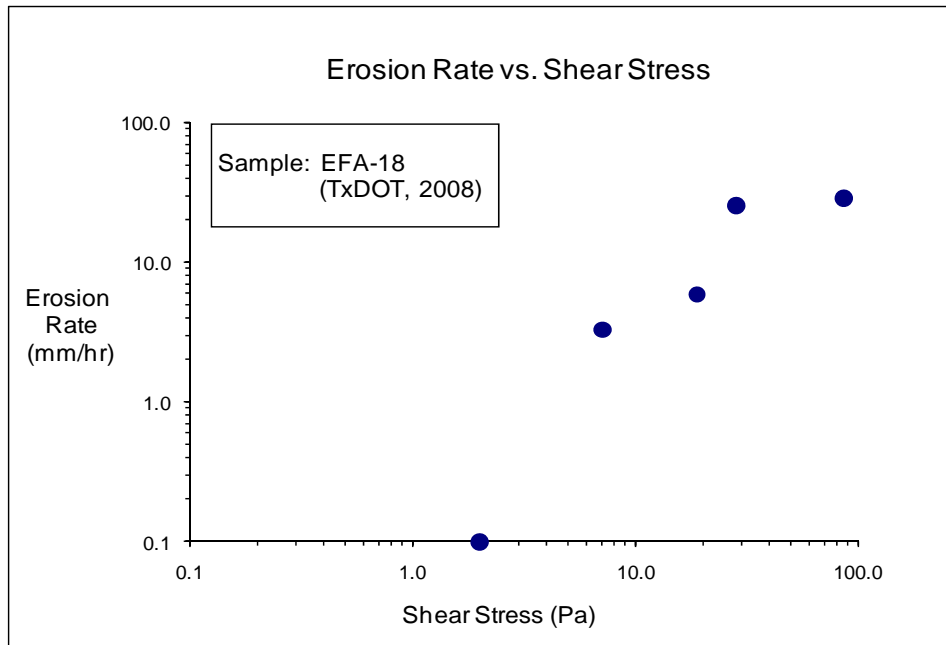


Figure D-56(a). EFA Test Results for Soil Sample EFA-18 (Shear Stress).

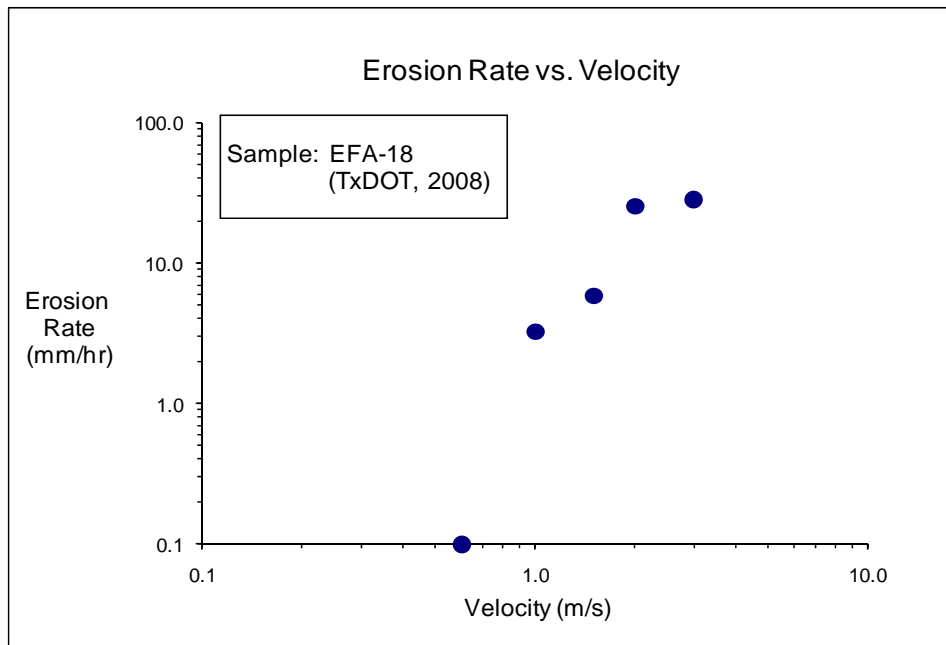


Figure D-56(b). EFA Test Results for Soil Sample EFA-18 (Velocity).

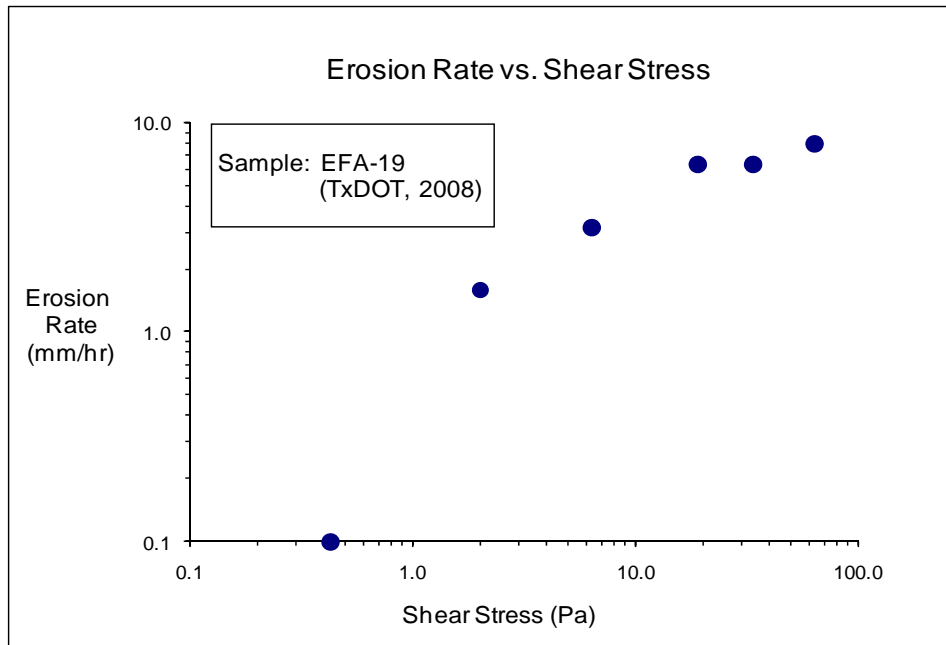


Figure D-57(a). EFA Test Results for Soil Sample EFA-19 (Shear Stress).

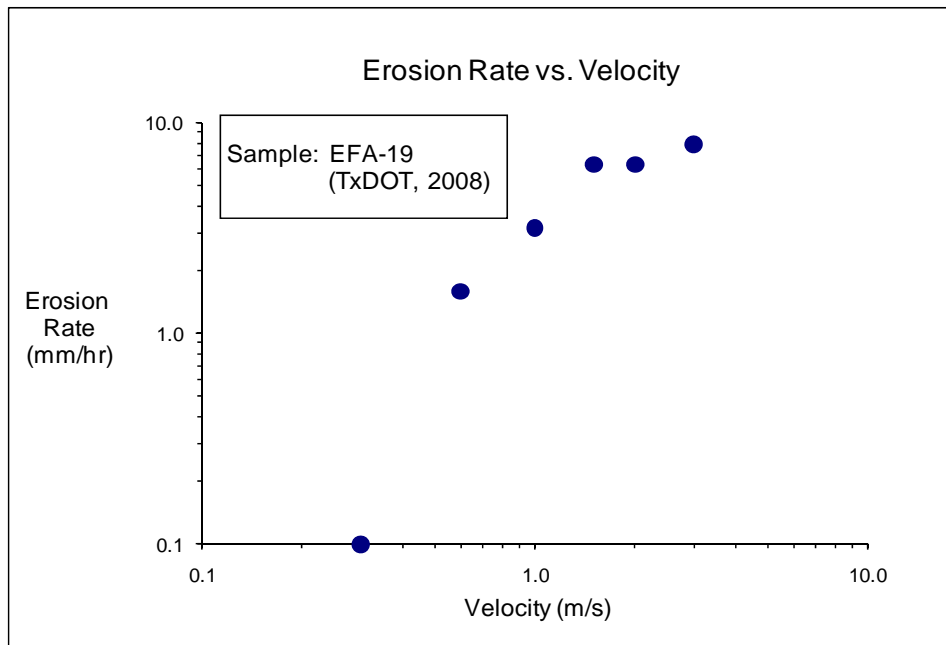


Figure D-57(b). EFA Test Results for Soil Sample EFA-19 (Velocity).

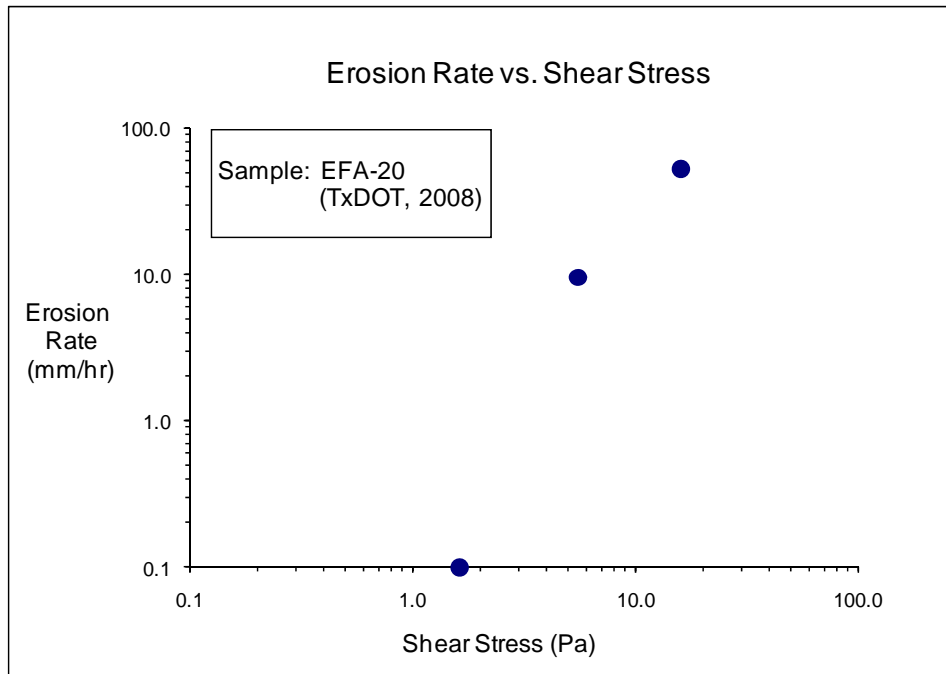


Figure D-58(a). EFA Test Results for Soil Sample EFA-20 (Shear Stress).

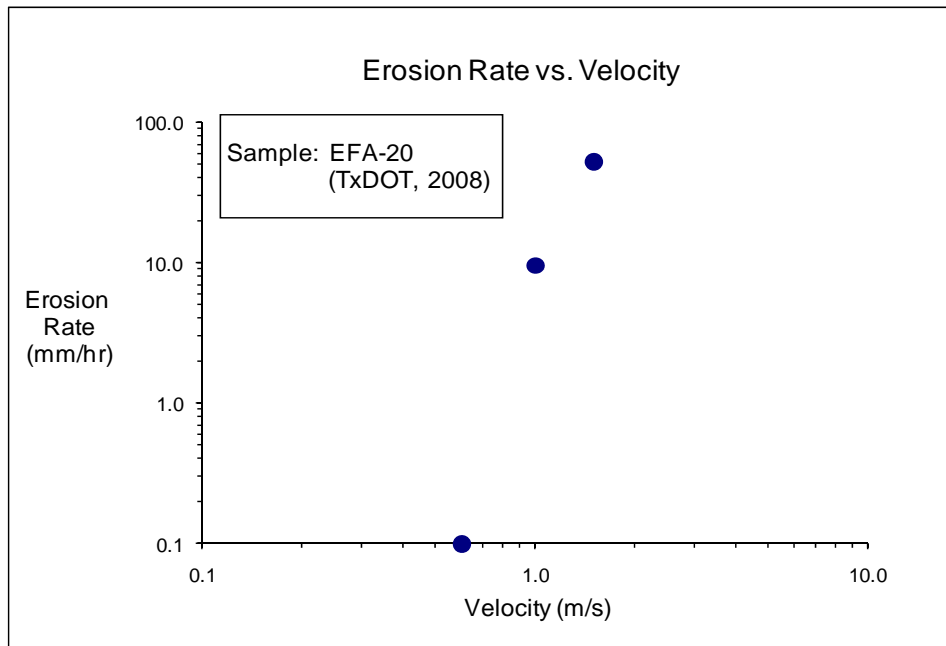


Figure D-58(b). EFA Test Results for Soil Sample EFA-20 (Velocity).

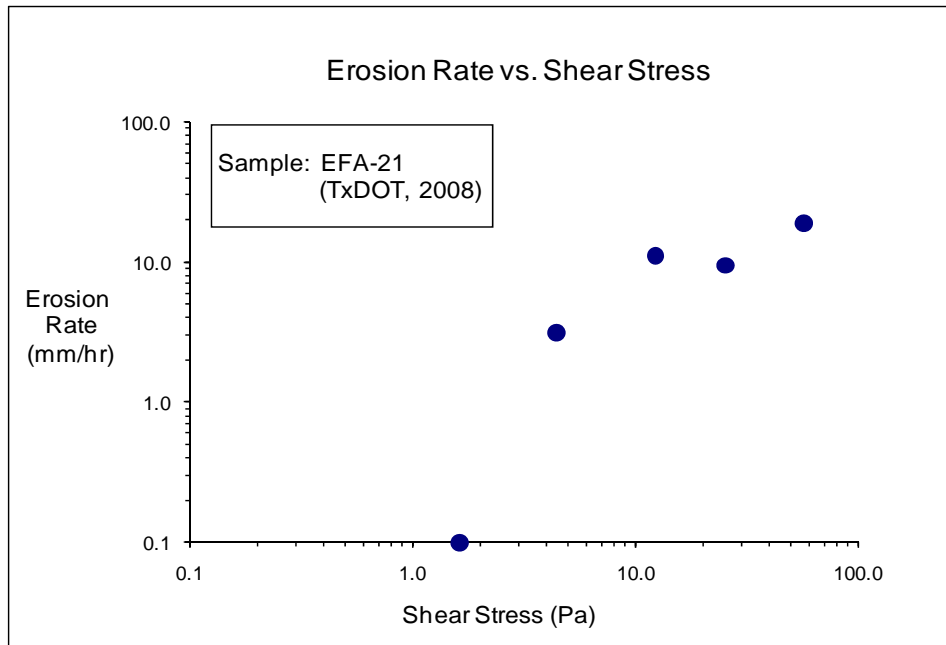


Figure D-59(a). EFA Test Results for Soil Sample EFA-21 (Shear Stress).

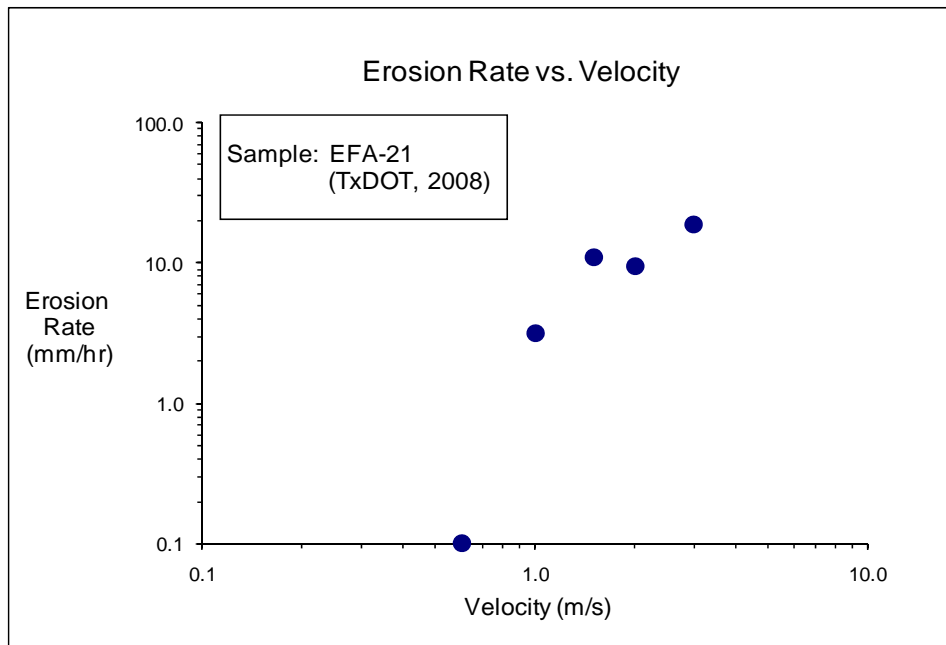


Figure D-59(b). EFA Test Results for Soil Sample EFA-21 (Velocity).

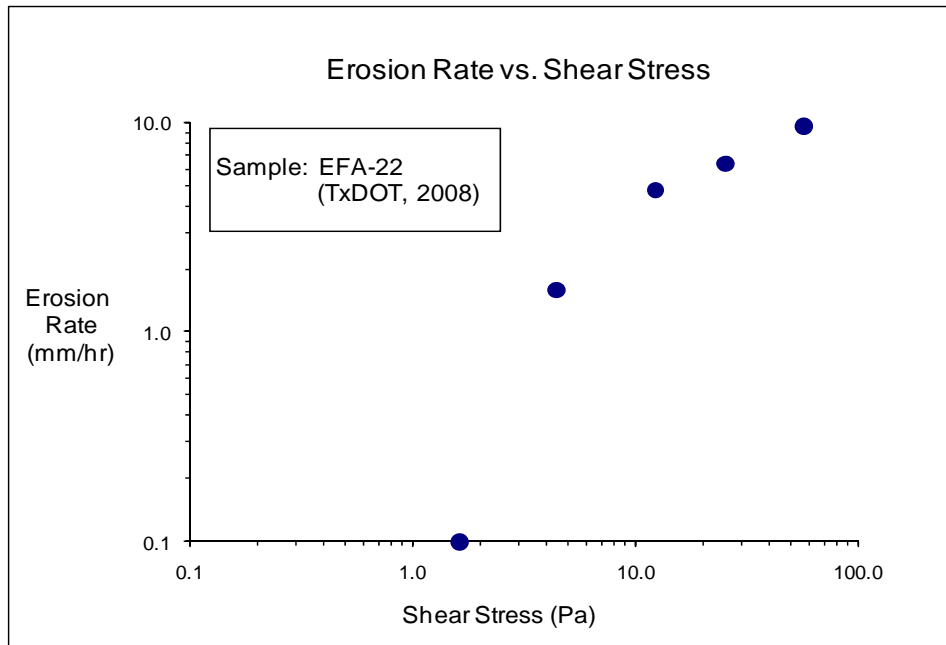


Figure D-60(a). EFA Test Results for Soil Sample EFA-22 (Shear Stress).

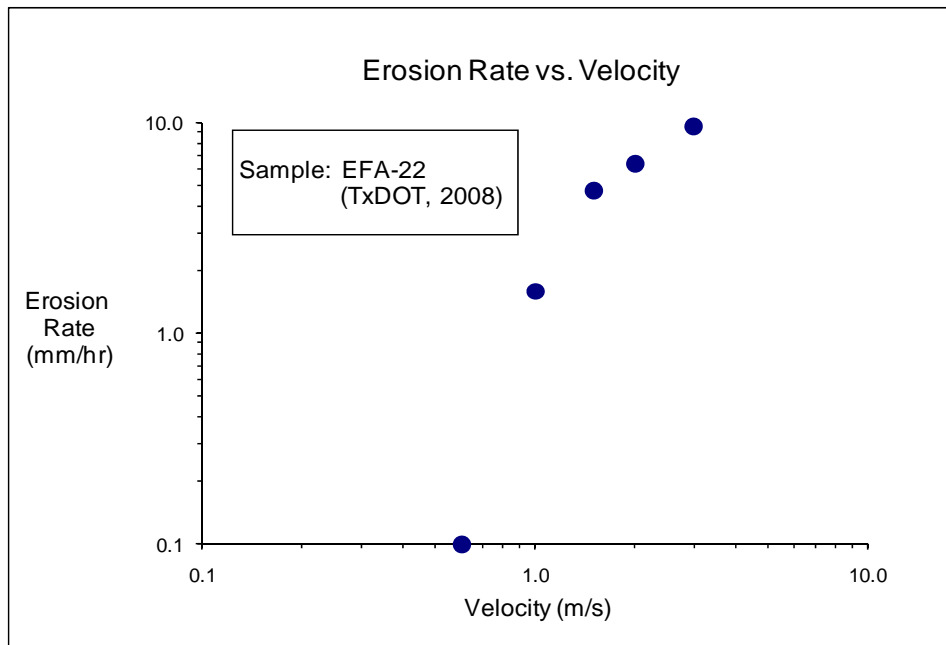


Figure D-60(b). EFA Test Results for Soil Sample EFA-22 (Velocity).

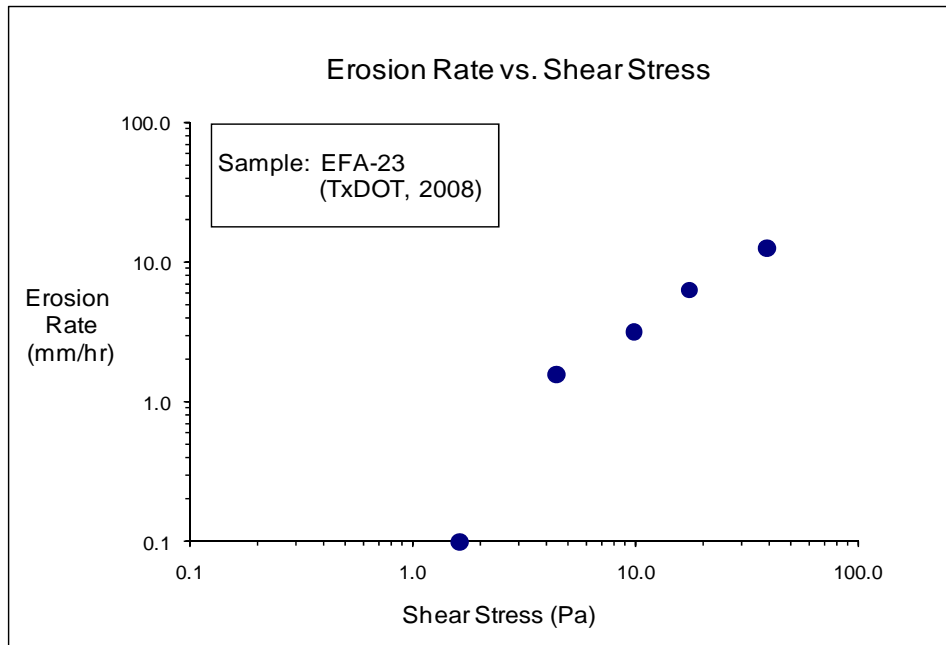


Figure D-61(a). EFA Test Results for Soil Sample EFA-23 (Shear Stress).

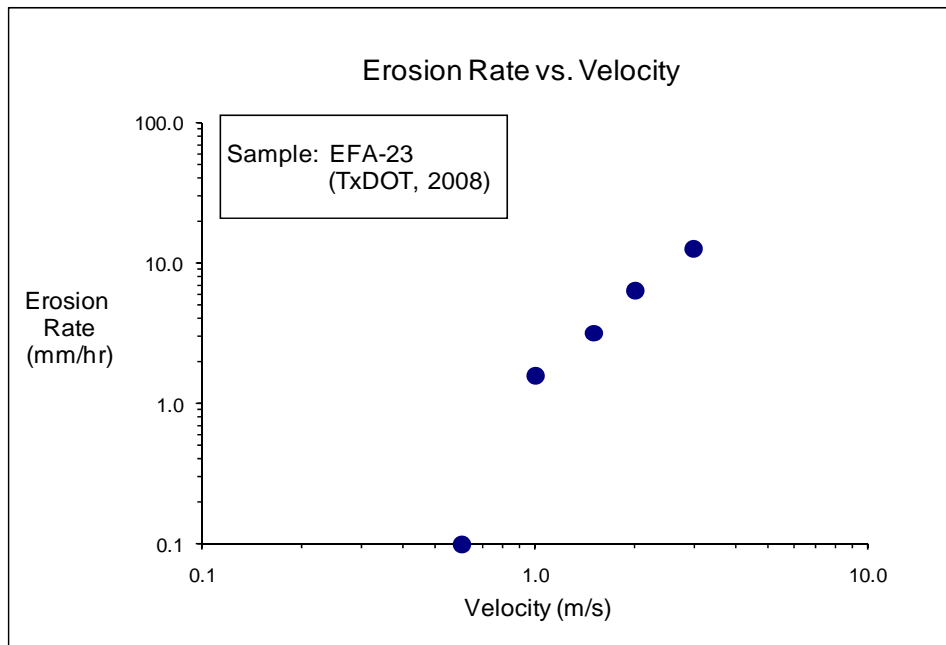


Figure D-61(b). EFA Test Results for Soil Sample EFA-23 (Velocity).

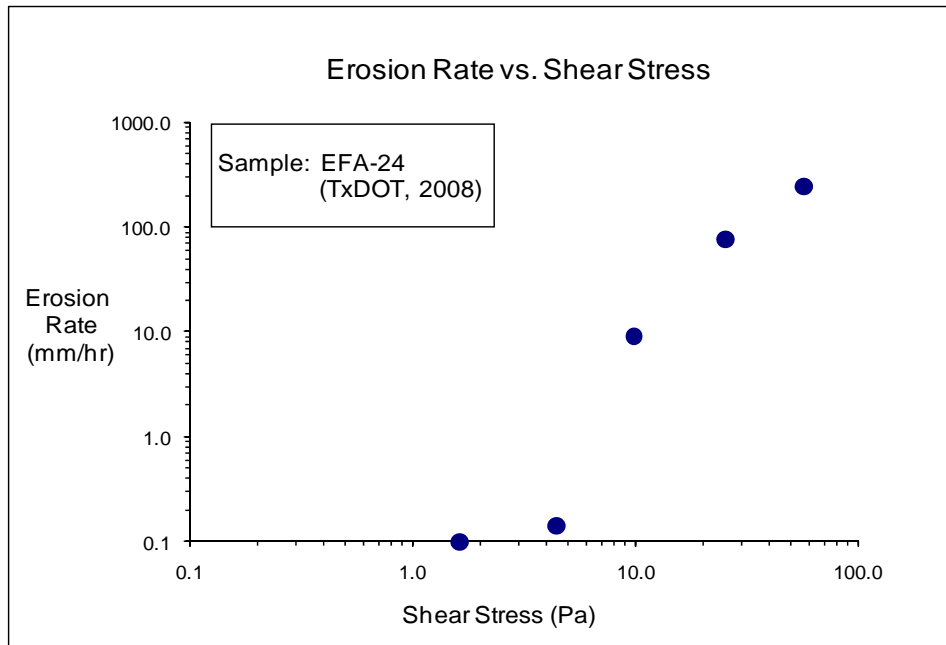


Figure D-62(a). EFA Test Results for Soil Sample EFA-24 (Shear Stress).

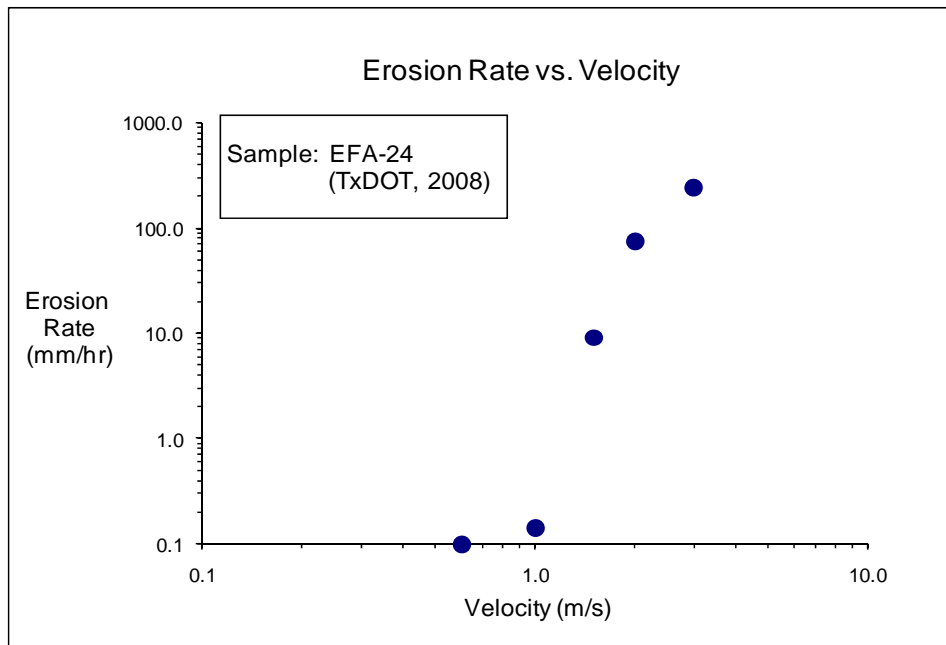


Figure D-62(b). EFA Test Results for Soil Sample EFA-24 (Velocity).

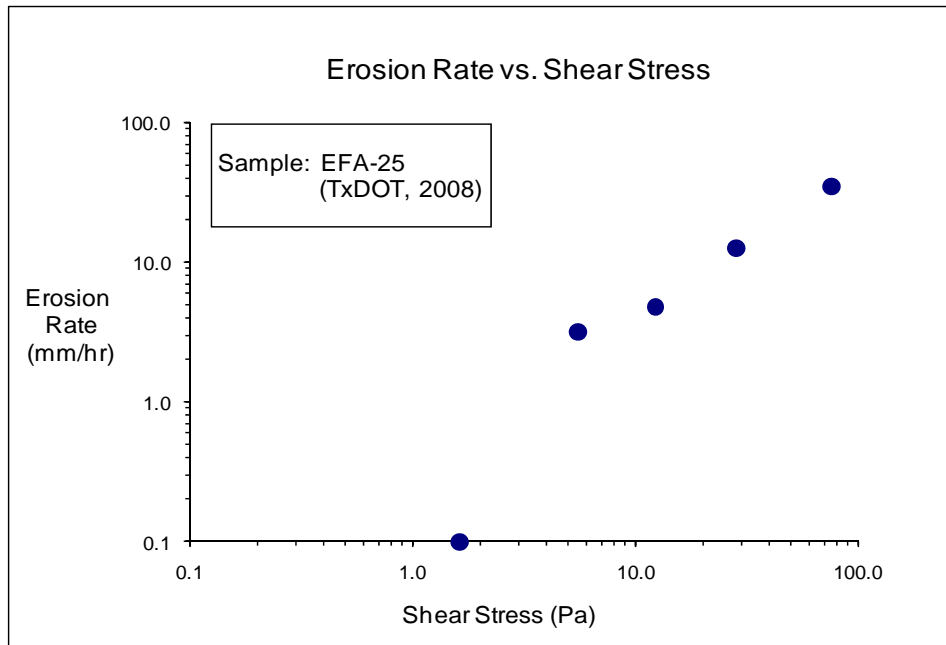


Figure D-63(a). EFA Test Results for Soil Sample EFA-25 (Shear Stress).

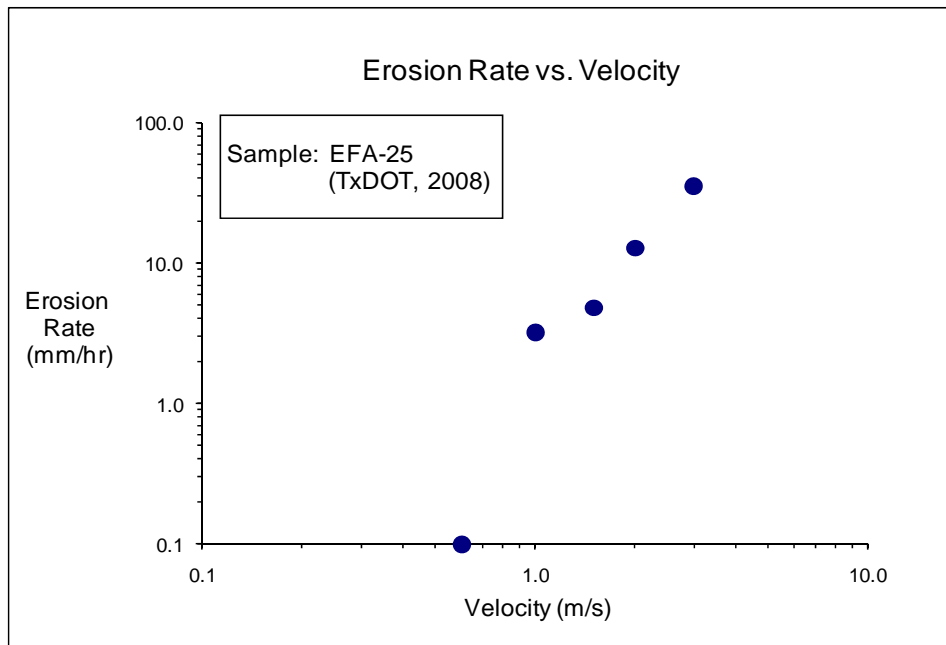


Figure D-63(b). EFA Test Results for Soil Sample EFA-25 (Velocity).

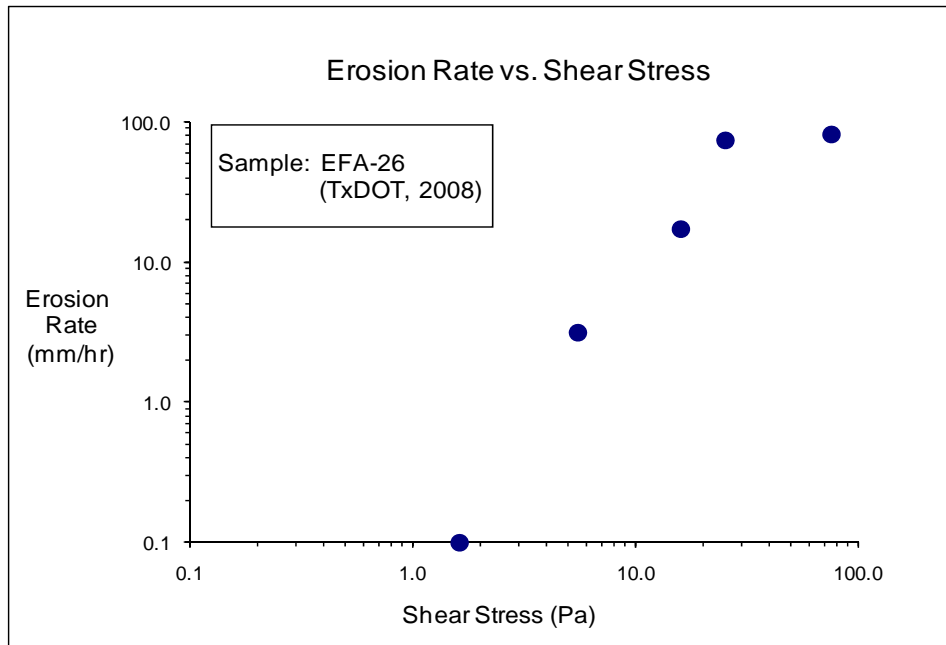


Figure D-64(a). EFA Test Results for Soil Sample EFA-26 (Shear Stress).

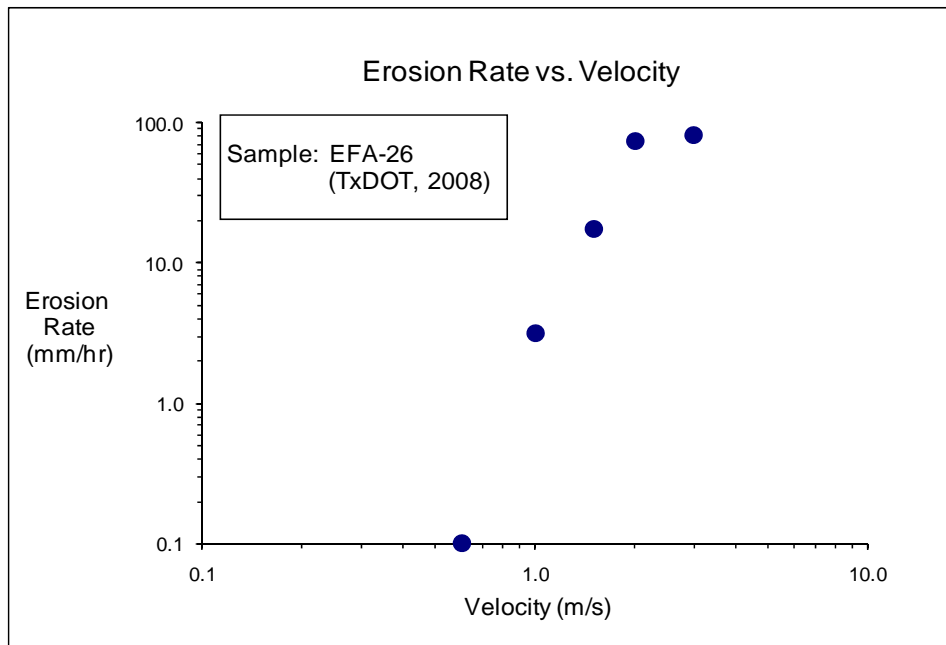


Figure D-64(b). EFA Test Results for Soil Sample EFA-26 (Velocity).

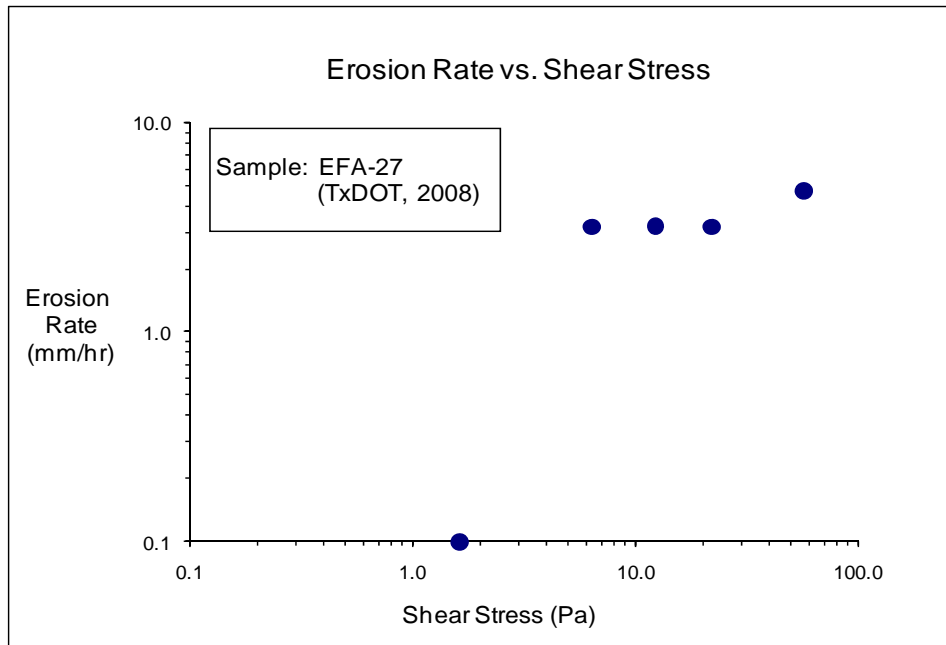


Figure D-65(a). EFA Test Results for Soil Sample EFA-27 (Shear Stress).

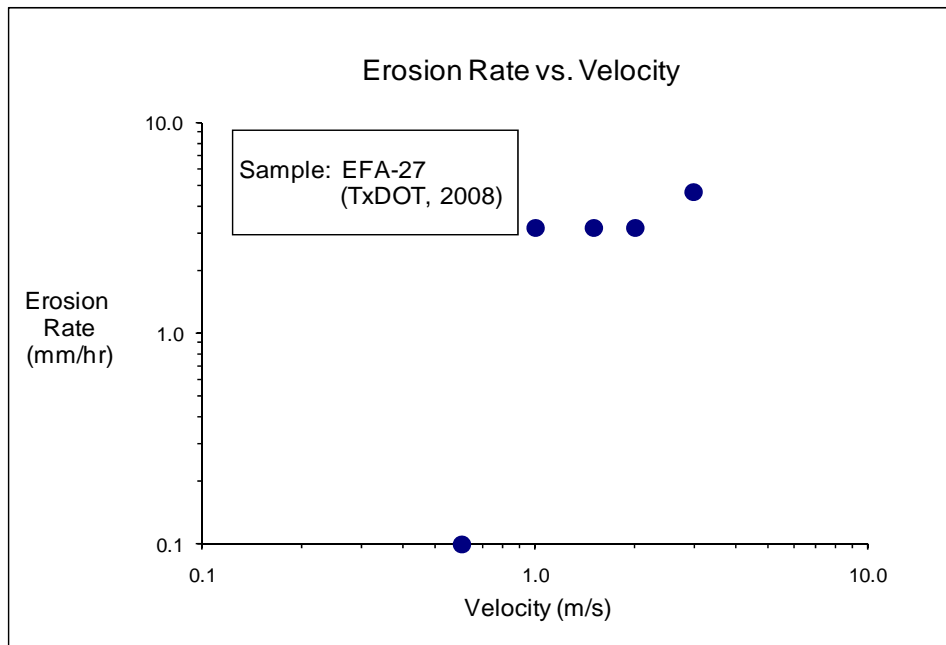


Figure D-65(b). EFA Test Results for Soil Sample EFA-27 (Velocity).

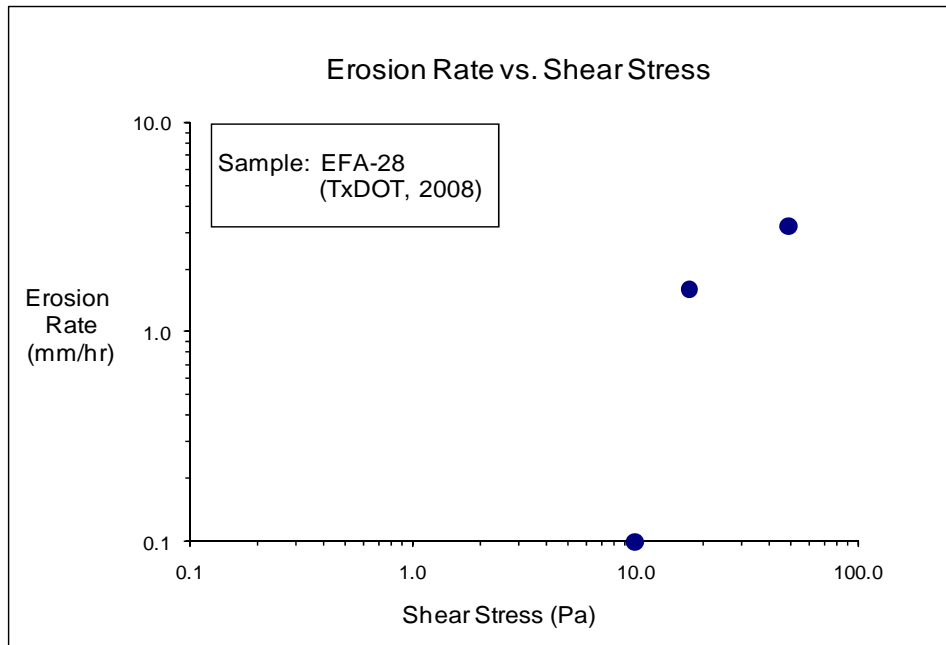


Figure D-66(a). EFA Test Results for Soil Sample EFA-28 (Shear Stress).

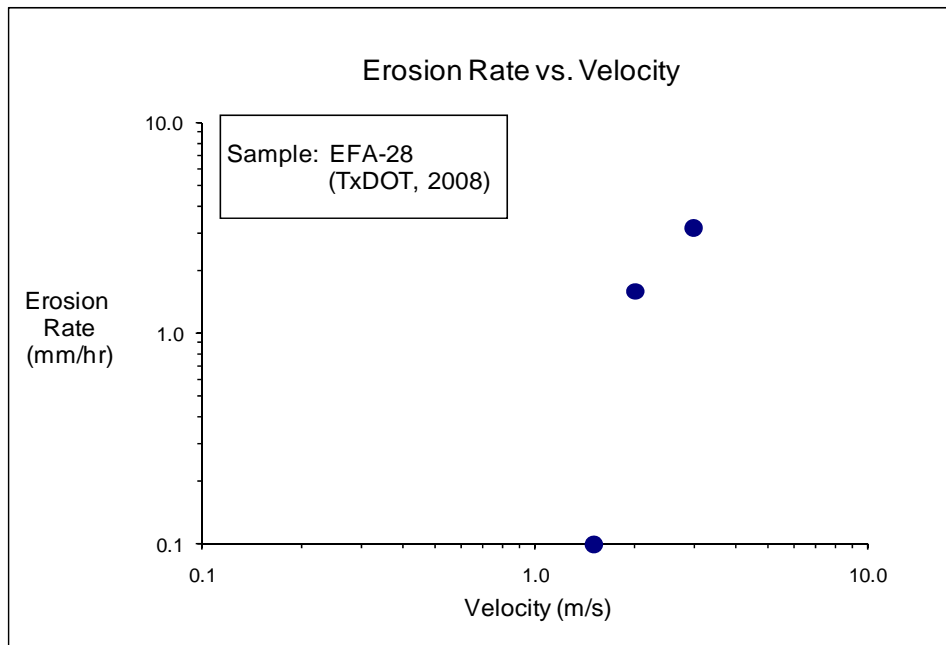


Figure D-66(b). EFA Test Results for Soil Sample EFA-28 (Velocity).

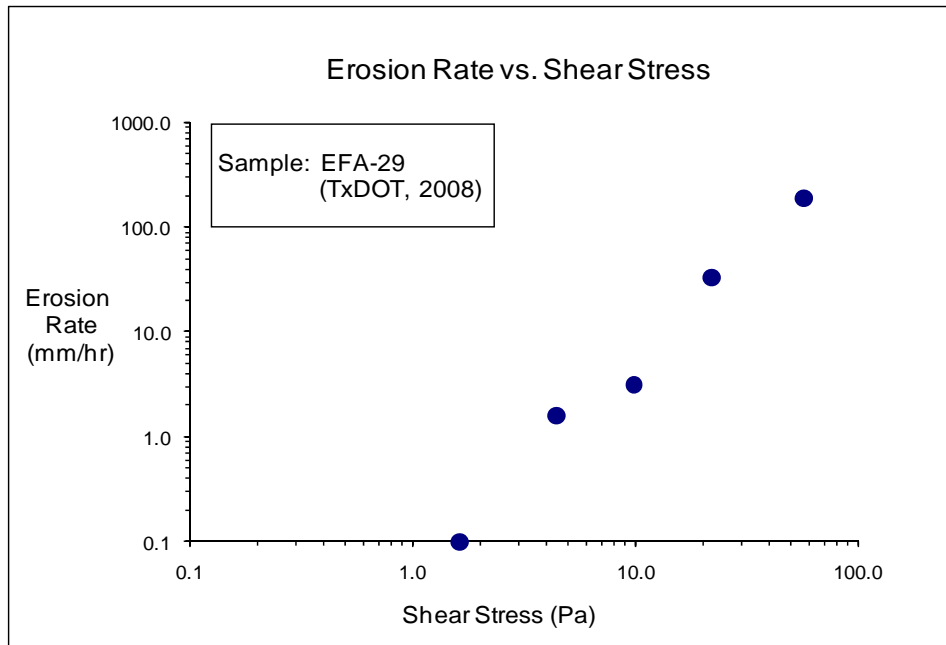


Figure D-67(a). EFA Test Results for Soil Sample EFA-29 (Shear Stress).

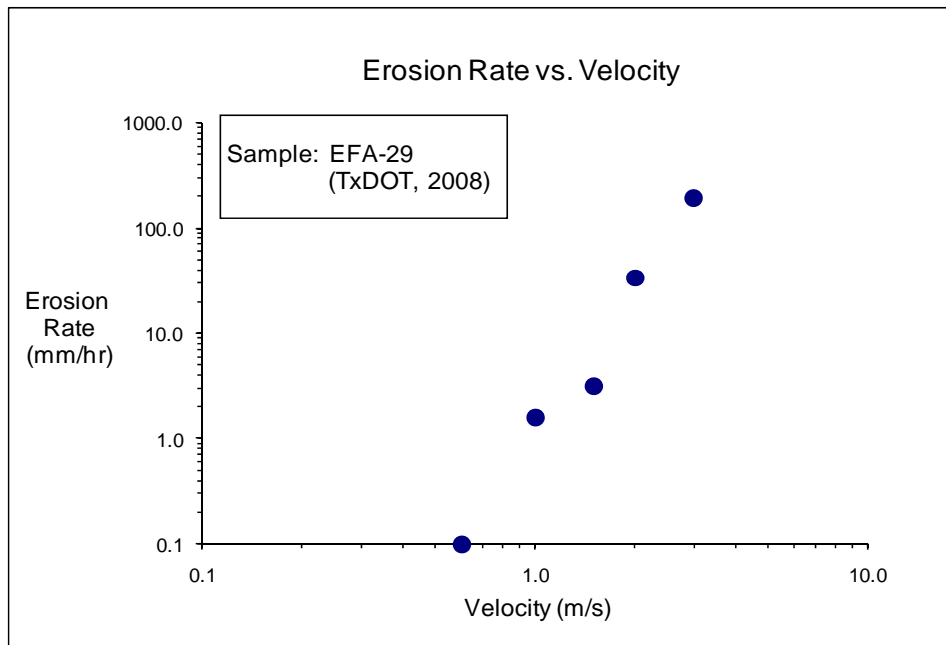


Figure D-67(b). EFA Test Results for Soil Sample EFA-29 (Velocity).

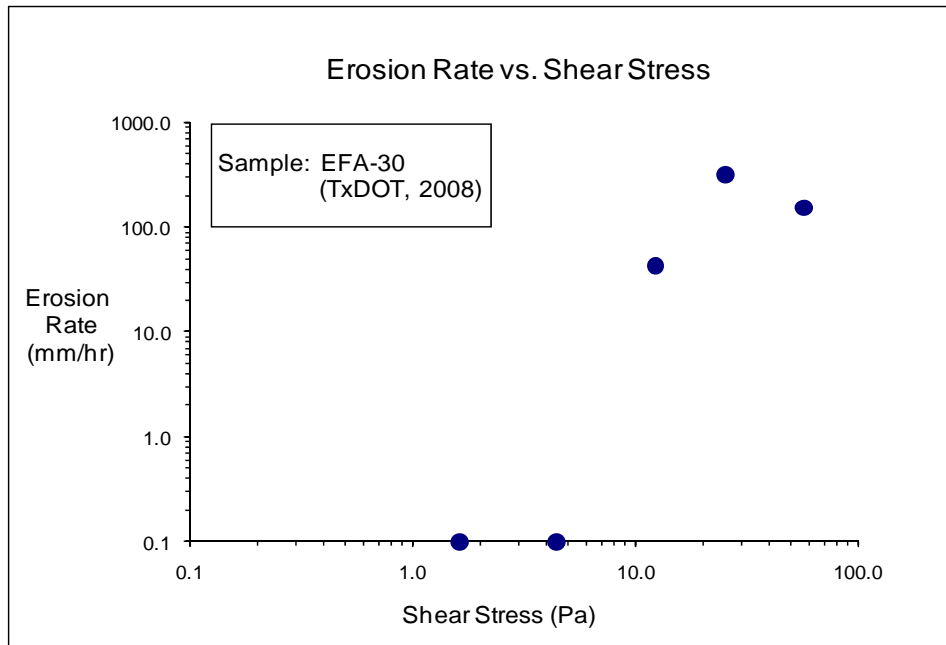


Figure D-68(a). EFA Test Results for Soil Sample EFA-30 (Shear Stress).

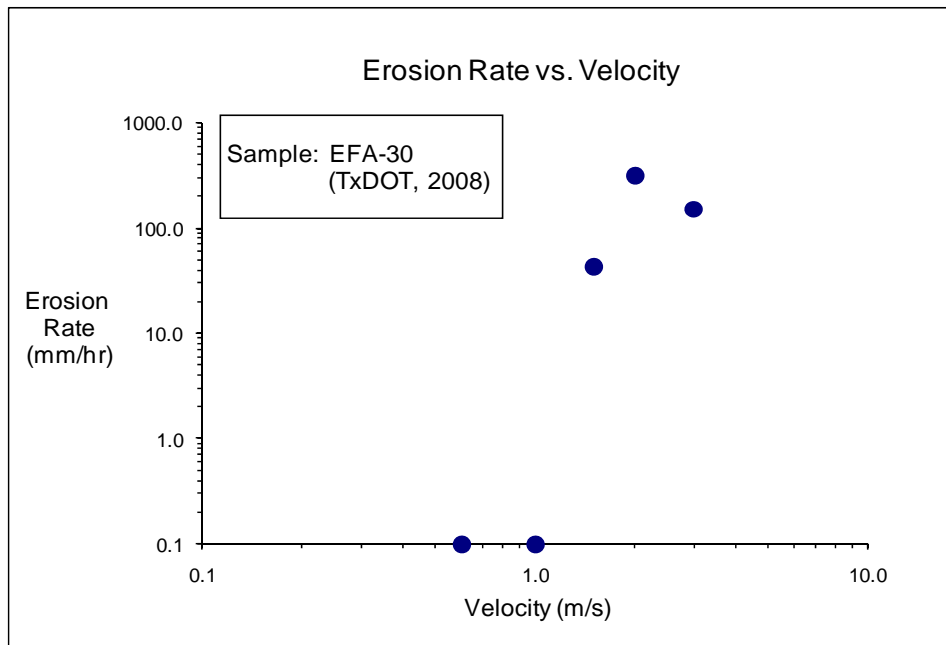


Figure D-68(b). EFA Test Results for Soil Sample EFA-30 (Velocity).

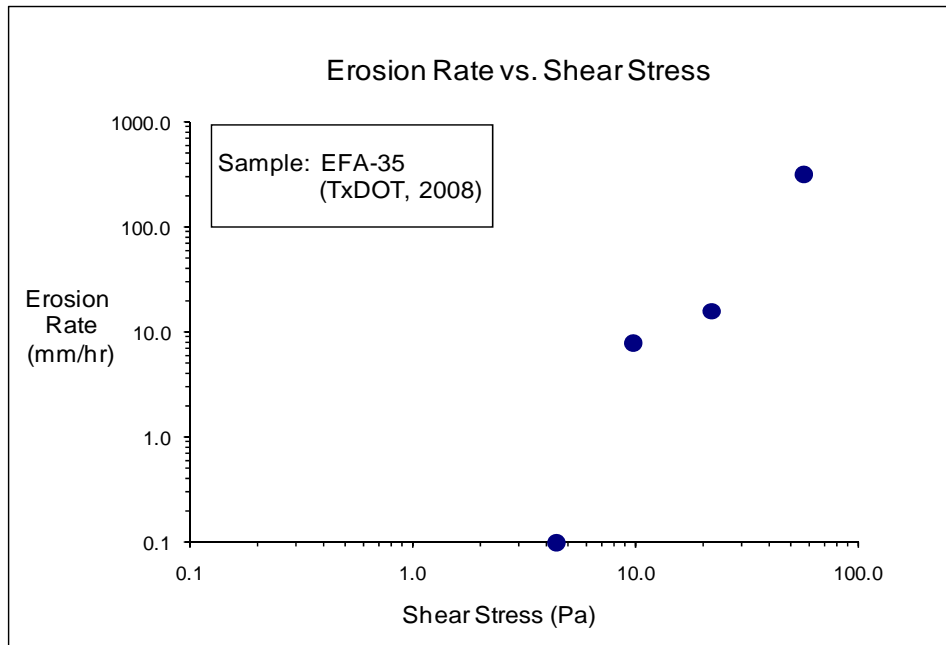


Figure D-69(a). EFA Test Results for Soil Sample EFA-35 (Shear Stress).

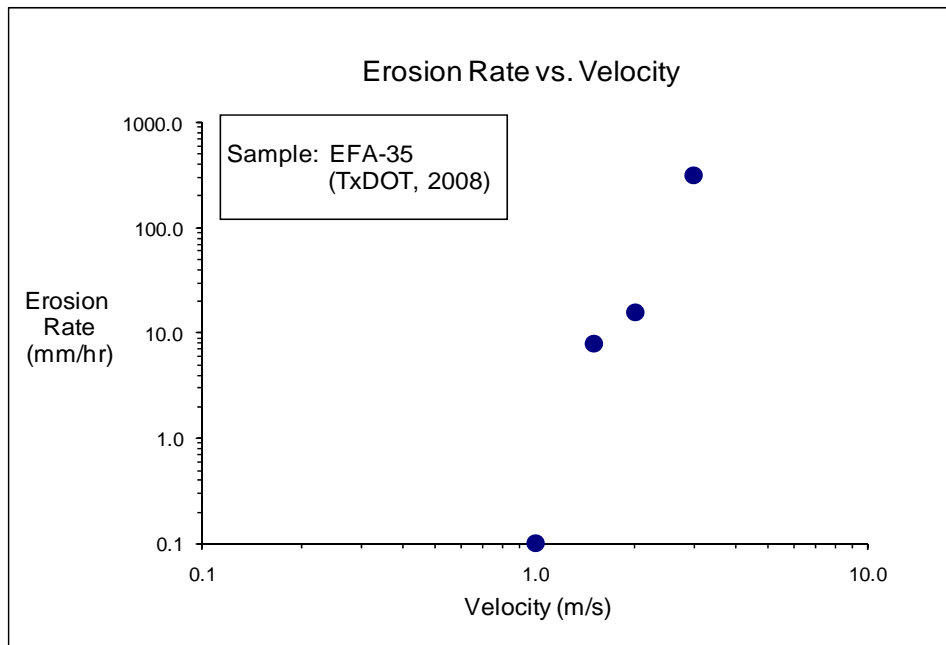


Figure D-69(b). EFA Test Results for Soil Sample EFA-35 (Velocity).

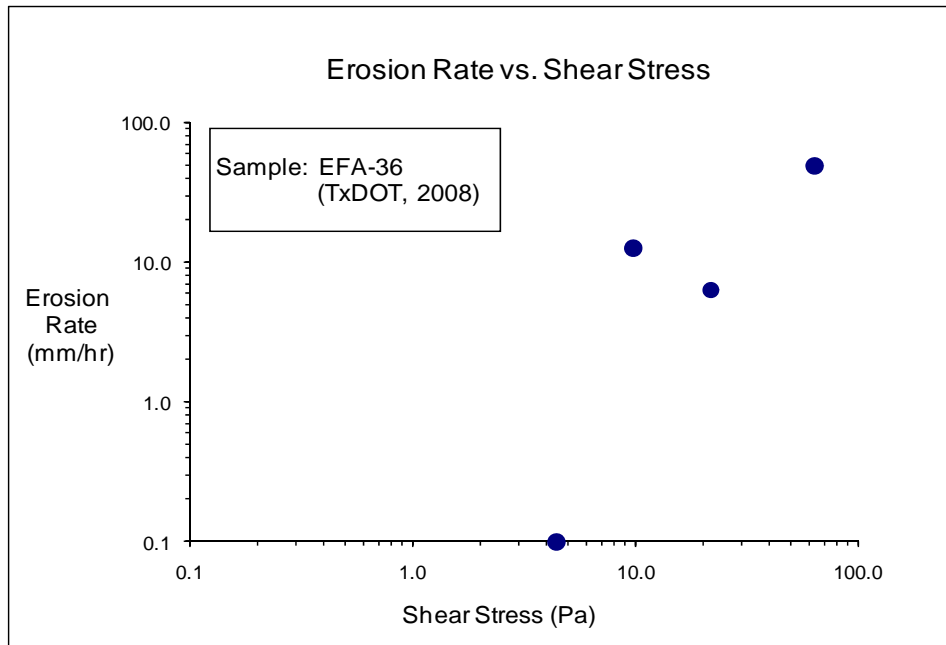


Figure D-70(a). EFA Test Results for Soil Sample EFA-36 (Shear Stress).

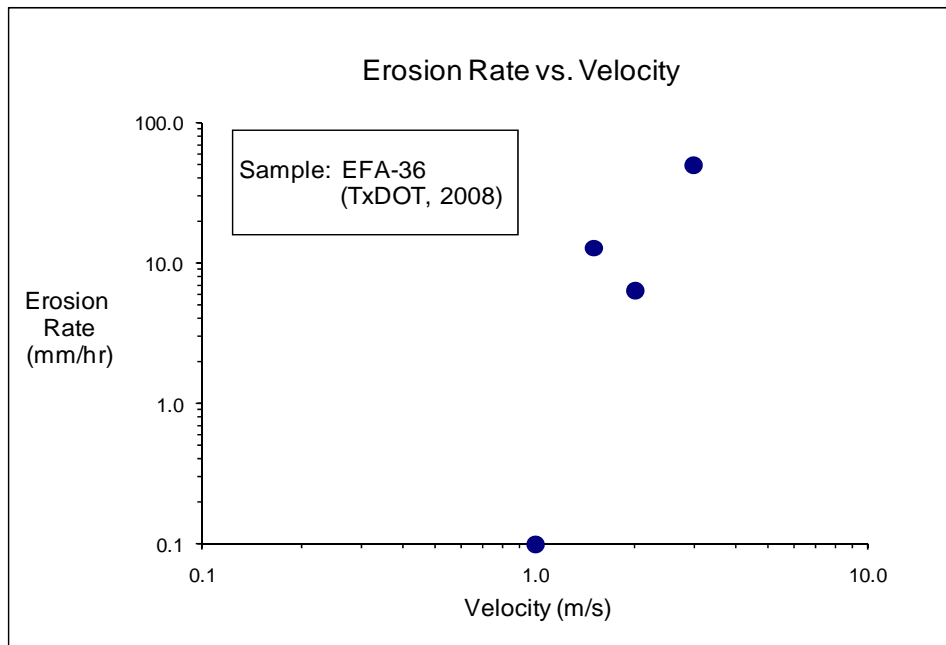


Figure D-70(b). EFA Test Results for Soil Sample EFA-36 (Velocity).

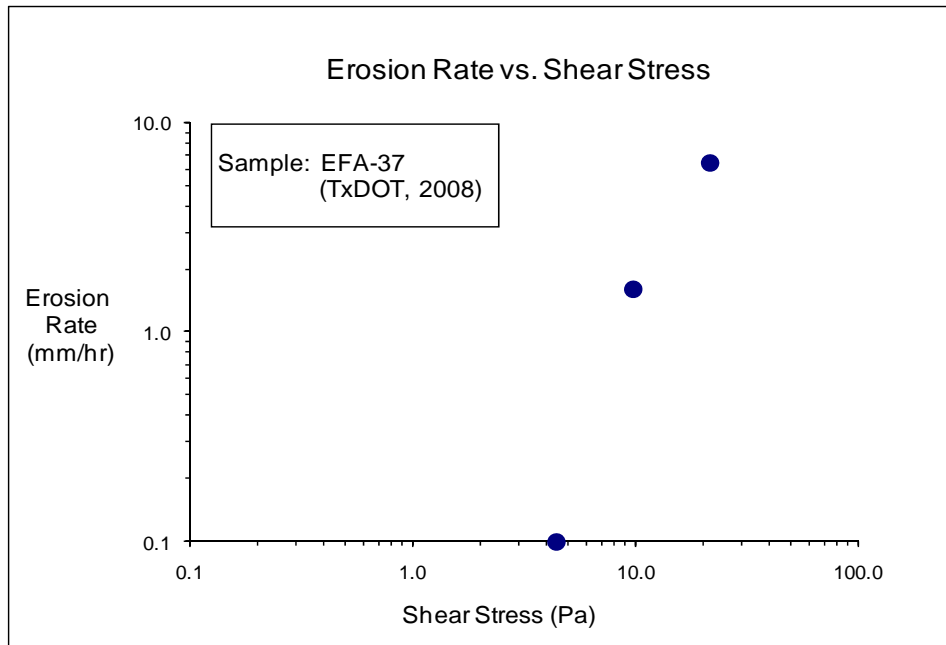


Figure D-71(a). EFA Test Results for Soil Sample EFA-37 (Shear Stress).

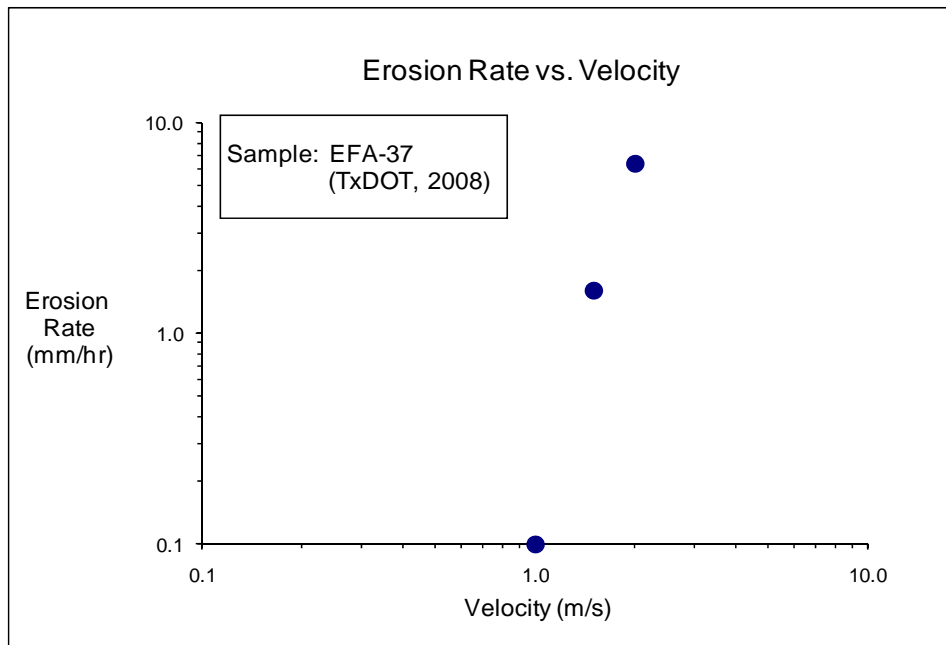


Figure D-71(b). EFA Test Results for Soil Sample EFA-37 (Velocity).

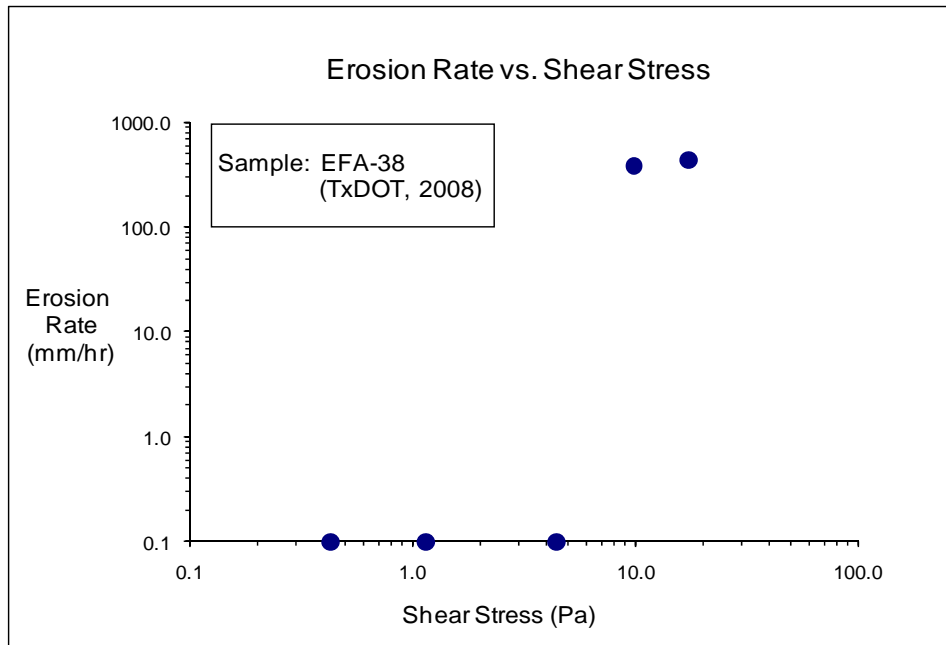


Figure D-72(a). EFA Test Results for Soil Sample EFA-38 (Shear Stress).

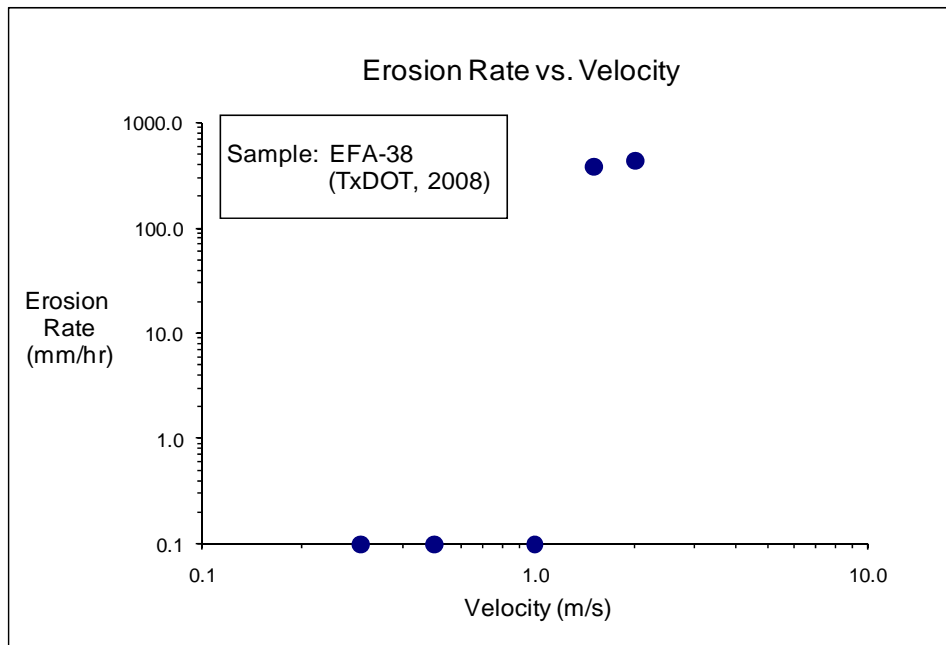


Figure D-72(b). EFA Test Results for Soil Sample EFA-38 (Velocity).

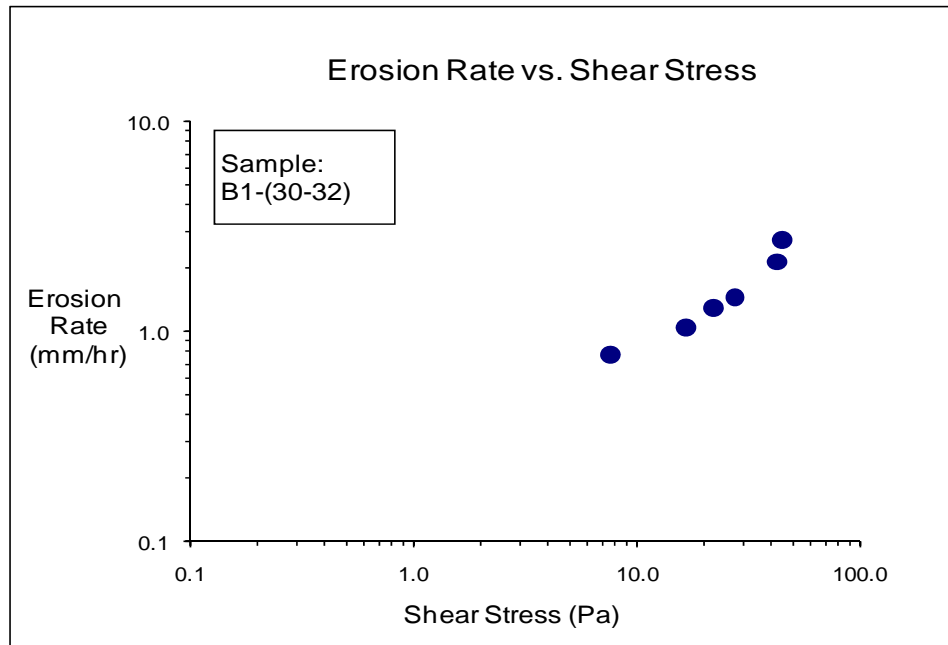


Figure D-73(a). EFA Test Results for Soil Sample B1-(30-32) (Shear Stress).

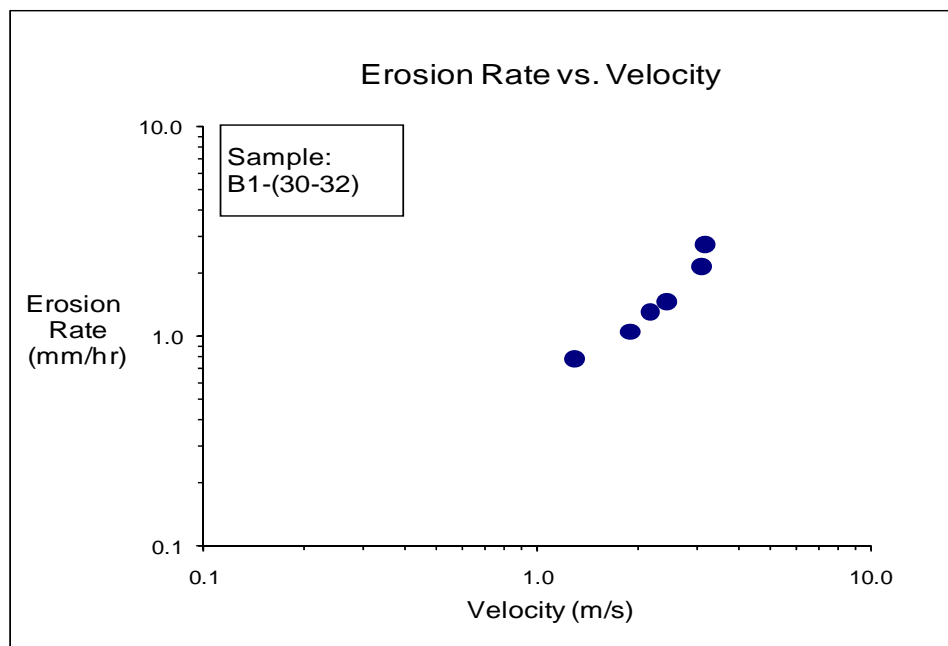


Figure D-73(b). EFA Test Results for Soil Sample B1-(30-32) (Velocity).

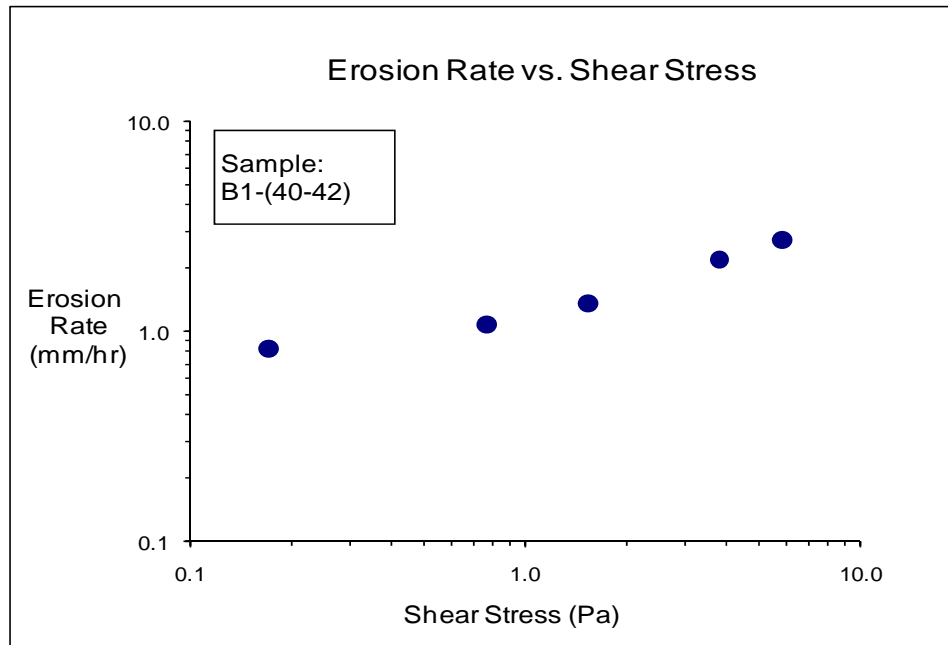


Figure D-74(a). EFA Test Results for Soil Sample B1-(40-42) (Shear Stress).

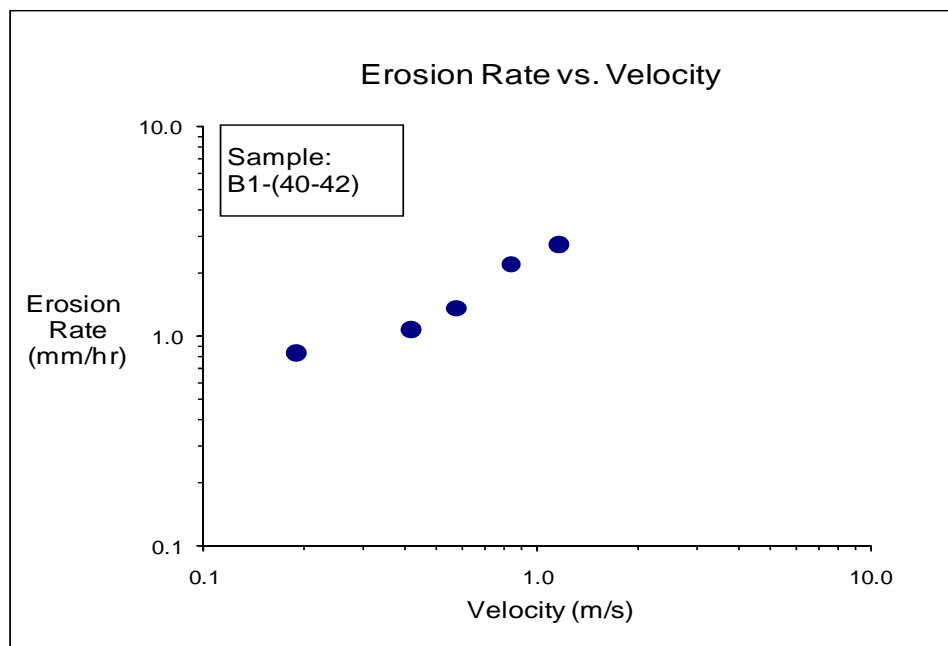


Figure D-74(b). EFA Test Results for Soil Sample B1-(40-42) (Velocity).

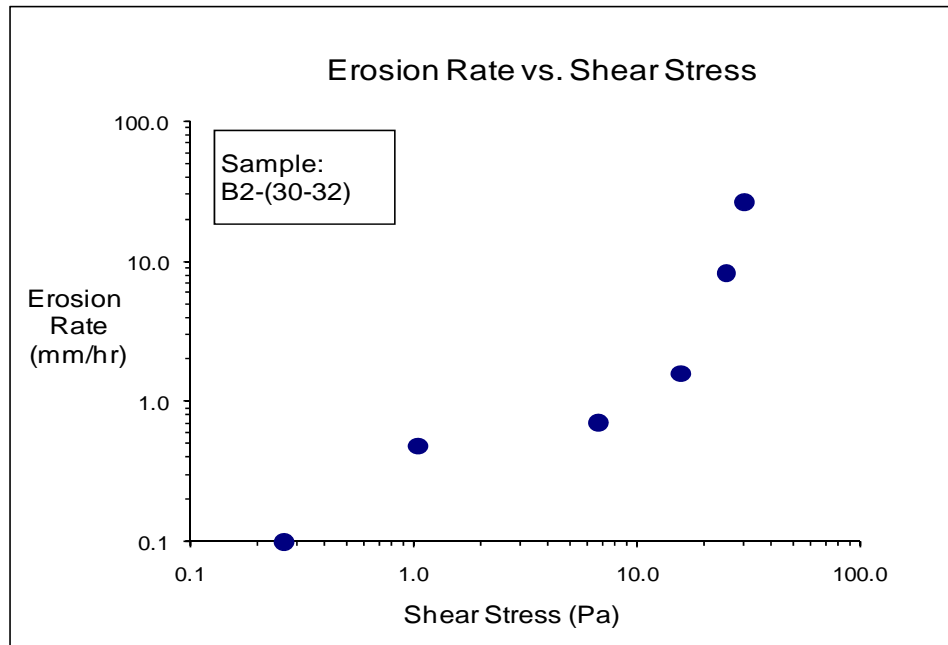


Figure D-75(a). EFA Test Results for Soil Sample B2-(30-32) (Shear Stress).

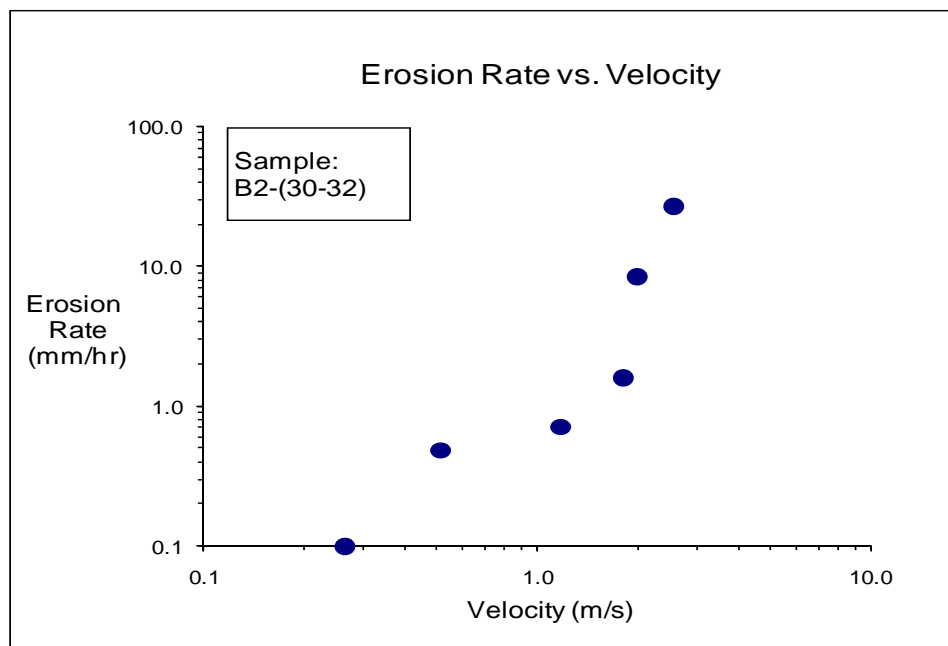


Figure D-75(b). EFA Test Results for Soil Sample B2-(30-32) (Velocity).

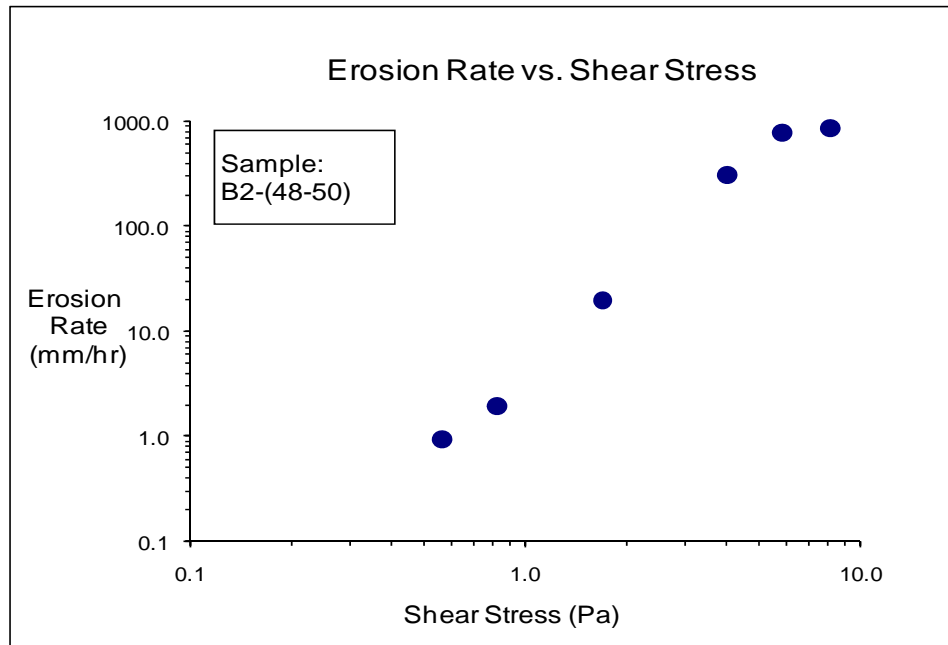


Figure D-76(a). EFA Test Results for Soil Sample B2-(48-50) (Shear Stress).

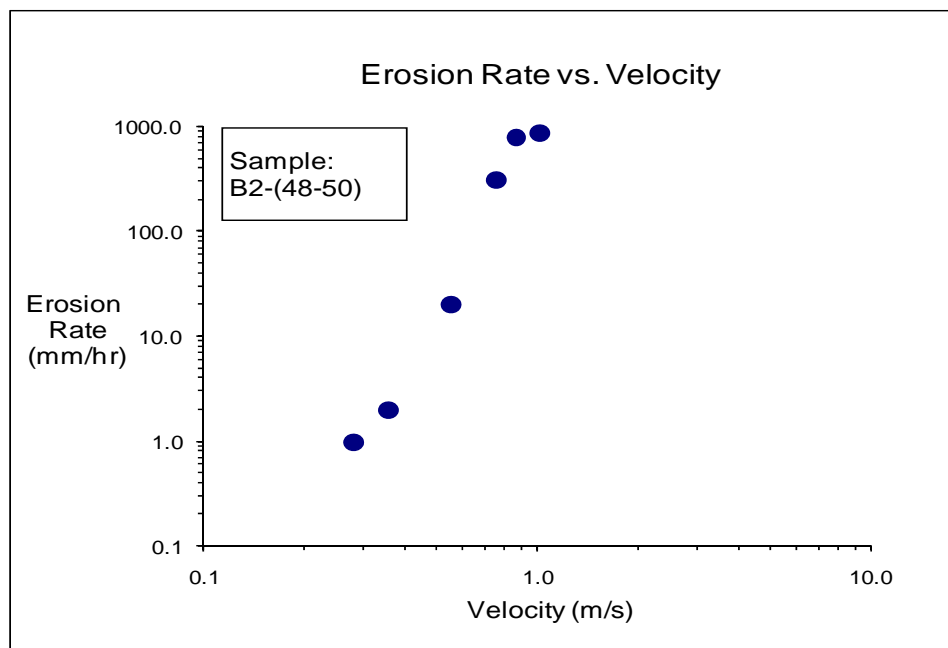


Figure D-76(b). EFA Test Results for Soil Sample B2-(48-50) (Velocity).

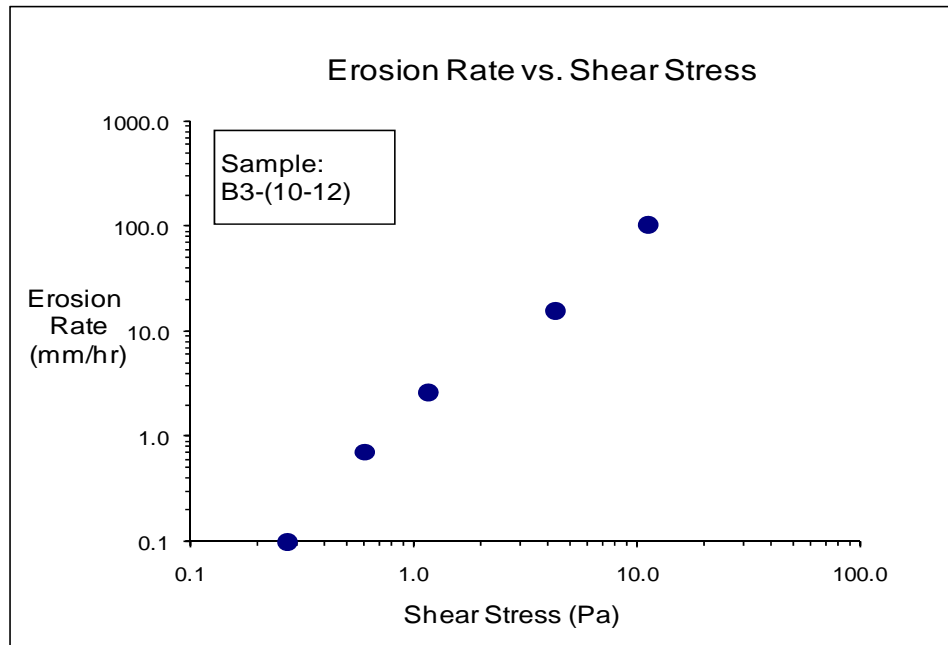


Figure D-77(a). EFA Test Results for Soil Sample B3-(10-12) (Shear Stress).

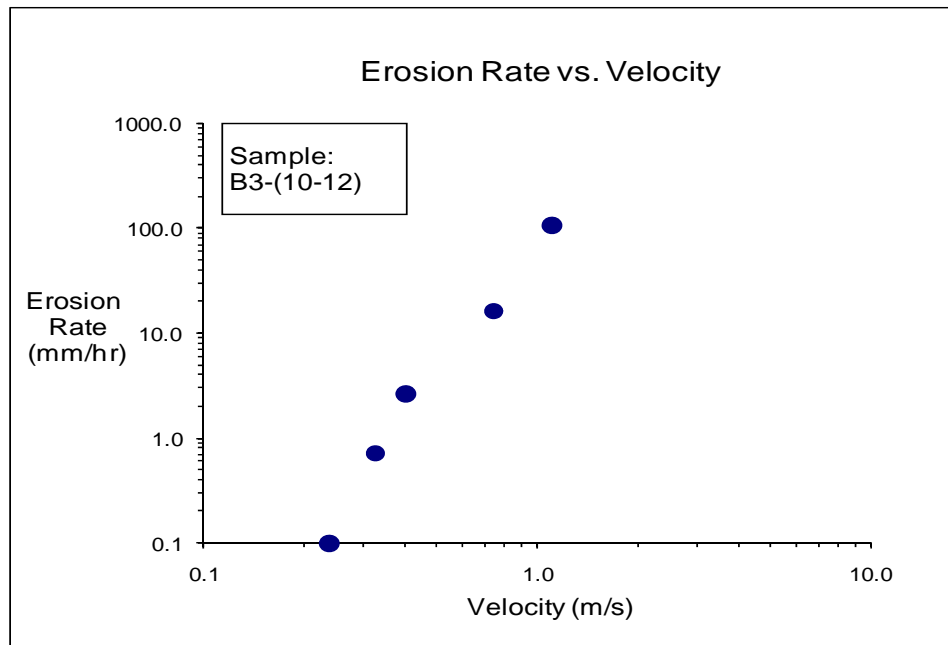


Figure D-77(b). EFA Test Results for Soil Sample B3-(10-12) (Velocity).

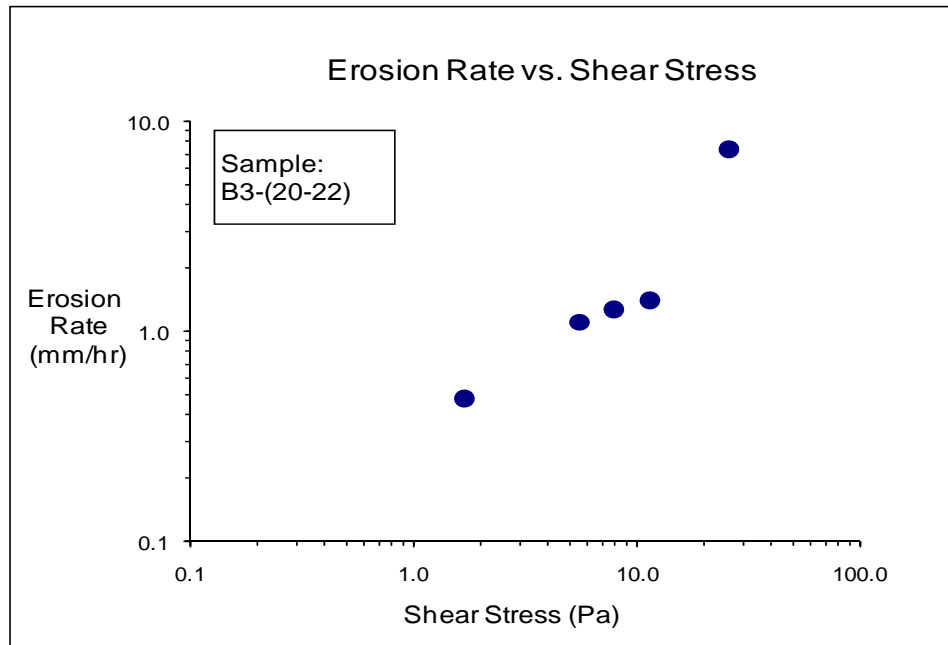


Figure D-78(a). EFA Test Results for Soil Sample B3-(20-22) (Shear Stress).

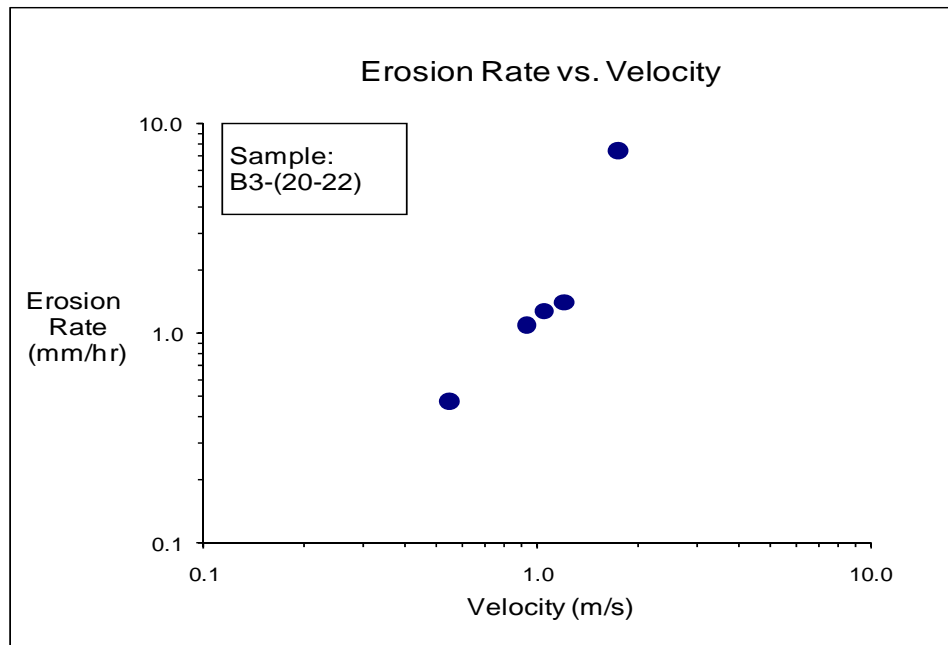


Figure D-78(b). EFA Test Results for Soil Sample B3-(20-22) (Velocity).

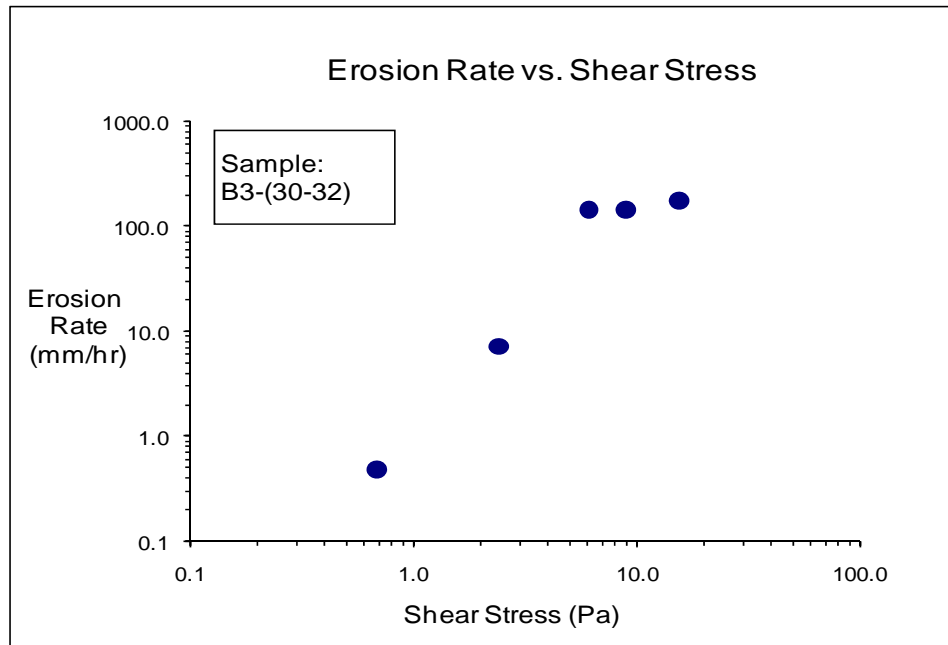


Figure D-79(a). EFA Test Results for Soil Sample B3-(30-32) (Shear Stress).

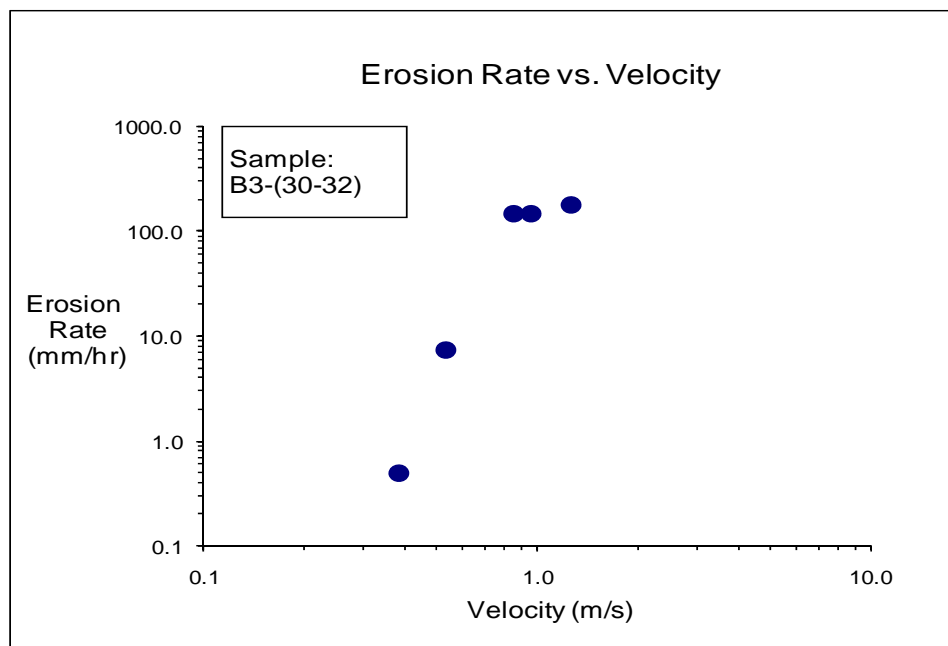


Figure D-79(b). EFA Test Results for Soil Sample B3-(30-32) (Velocity).

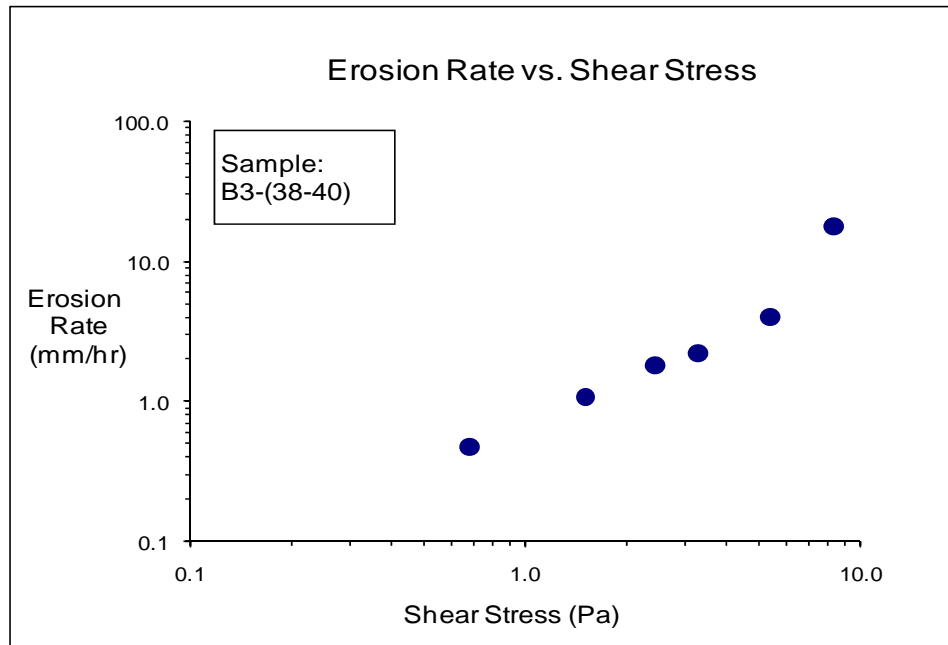


Figure D-80(a). EFA Test Results for Soil Sample B3-(38-40) (Shear Stress).

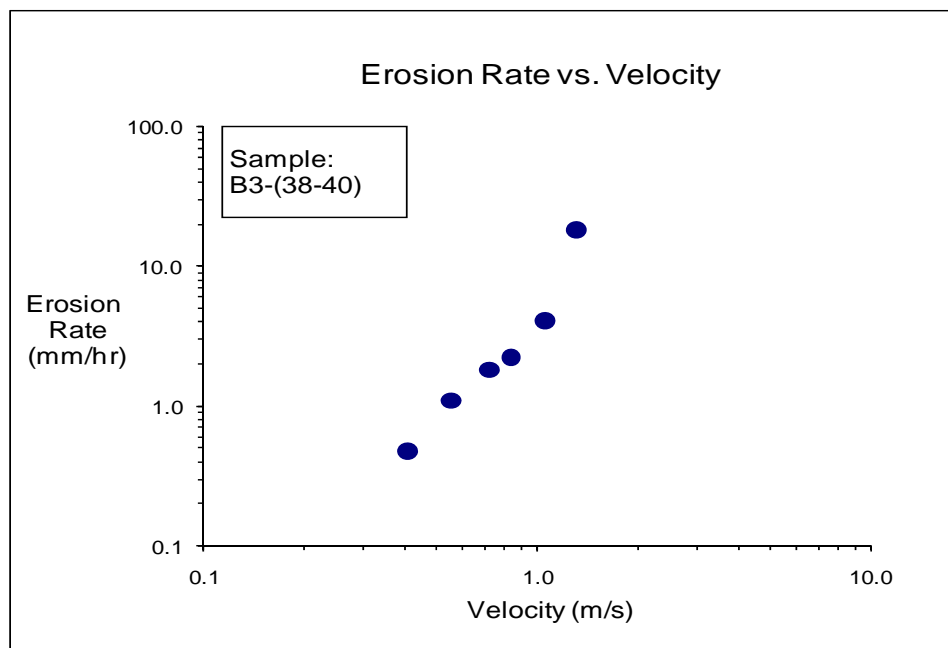


Figure D-80(b). EFA Test Results for Soil Sample B3-(38-40) (Velocity).

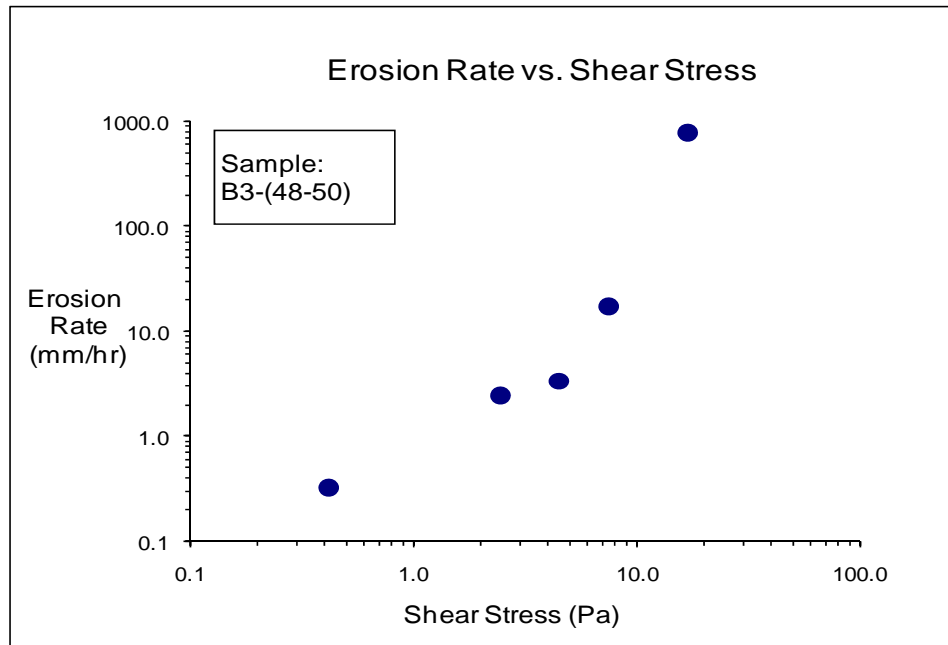


Figure D-81(a). EFA Test Results for Soil Sample B3-(48-50) (Shear Stress).

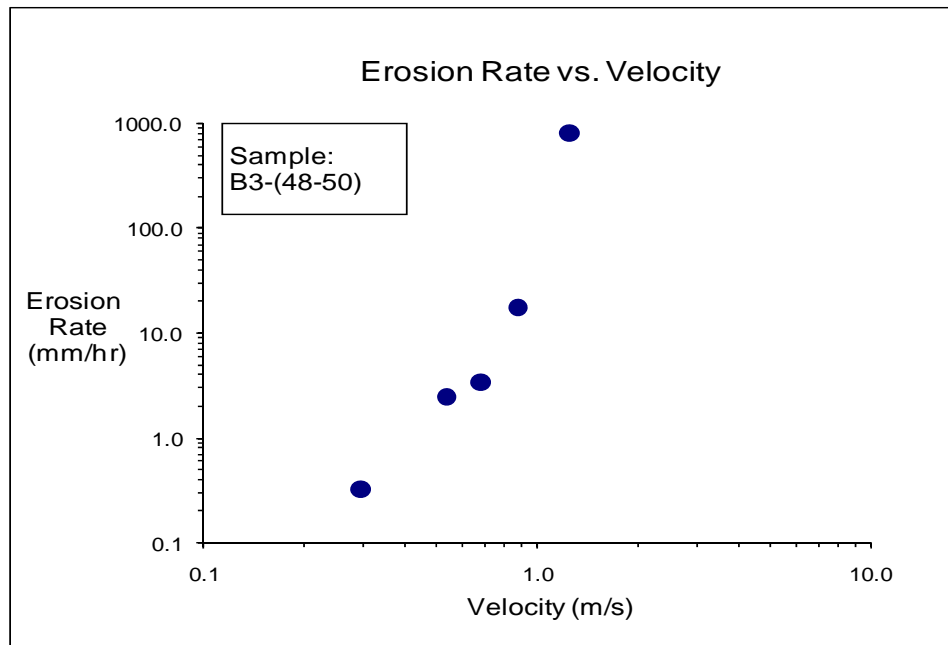


Figure D-81(b). EFA Test Results for Soil Sample B3-(48-50) (Velocity).

**APPENDIX E:
TAMU-FLOW USER'S MANUAL**



TAMU-FLOW Ver. 1.00

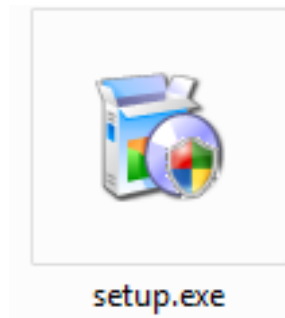
User's Guide

BEFORE YOU GO AHEAD, PLEASE NOTE...

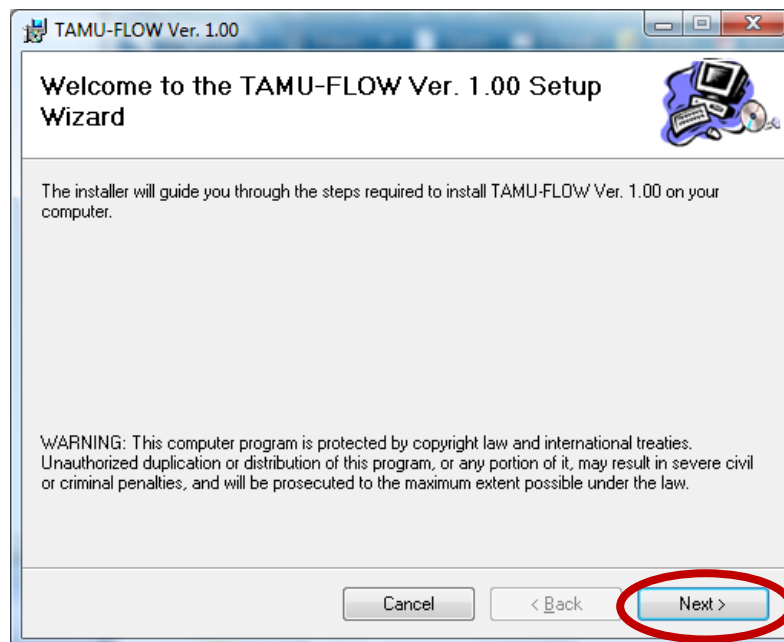
TAMU-FLOW is a software tool that calculates the relationship between discharge and velocity at a given river cross section. TAMU-FLOW assumes uniform flow, which means that **TAMU-FLOW can assure the accuracy of its result only if the cross section of the channel does not vary much with regard to the flow path.** If the cross section varies significantly along with the flow path, the use of other river analysis software that can model non-uniform flow is strongly recommended. HEC-RAS is the most widely used river analysis tool to model non-uniform flow.

INSTALLATION

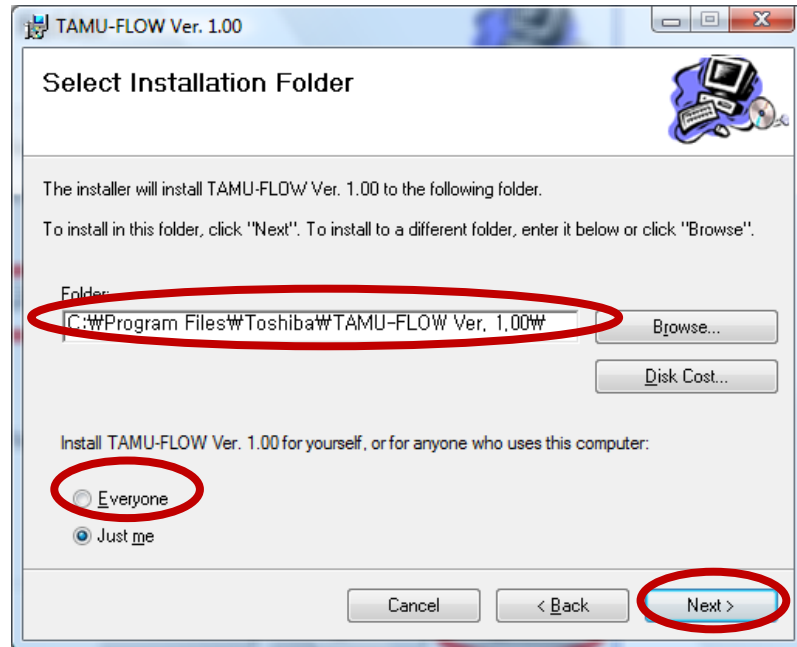
1. Insert the provided CD in the CD drive or the flash drive in the flash drive slot of your computer. The setup should automatically start. If it does not start automatically, manually browse the CD or flash drive and double click on the file "setup.exe."



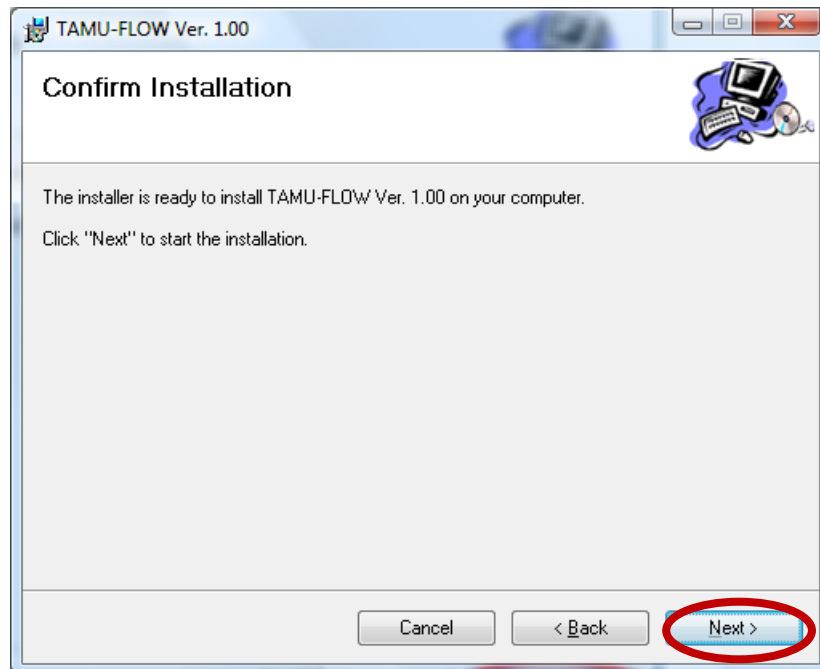
2. Setup wizard notifies you that it will install TAMU-FLOW on your computer. Click "Next" to proceed.



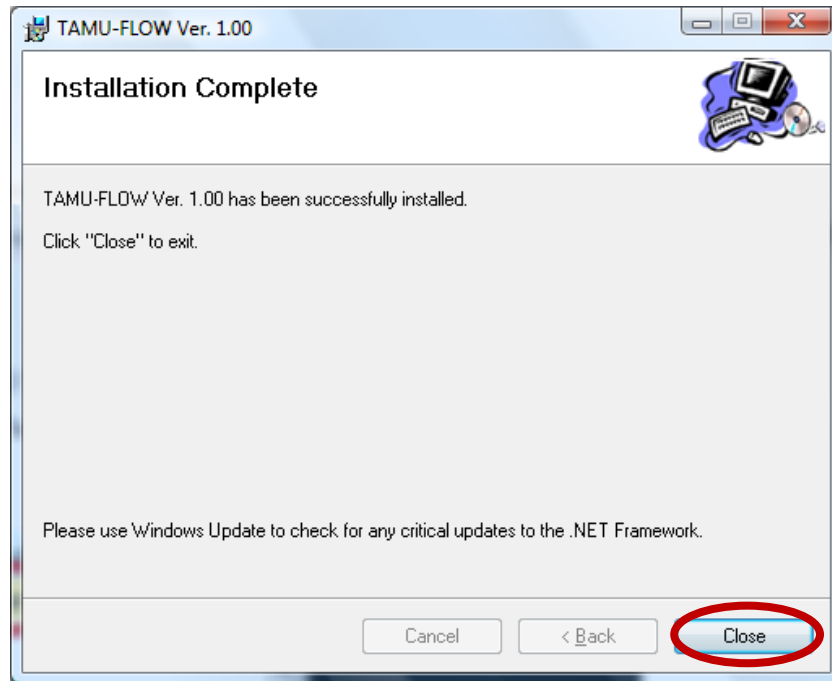
3. Setup wizard asks you in which folder you want to install TAMU-FLOW. It also asks whether you want TAMU-FLOW to become available only for you or for anybody that uses the computer. Choose the appropriate radio button, specify the folder you want, and click "Next."



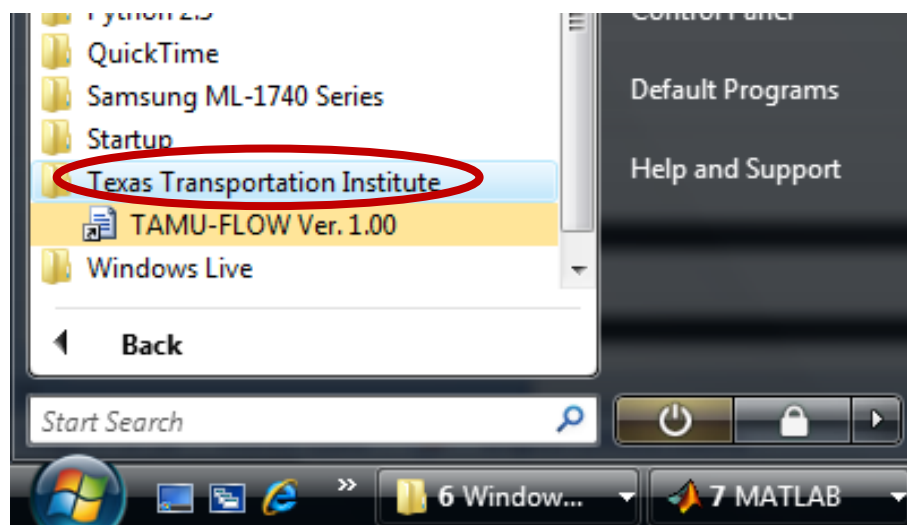
4. Setup wizard asks for your confirmation before the installation. Click "Next."



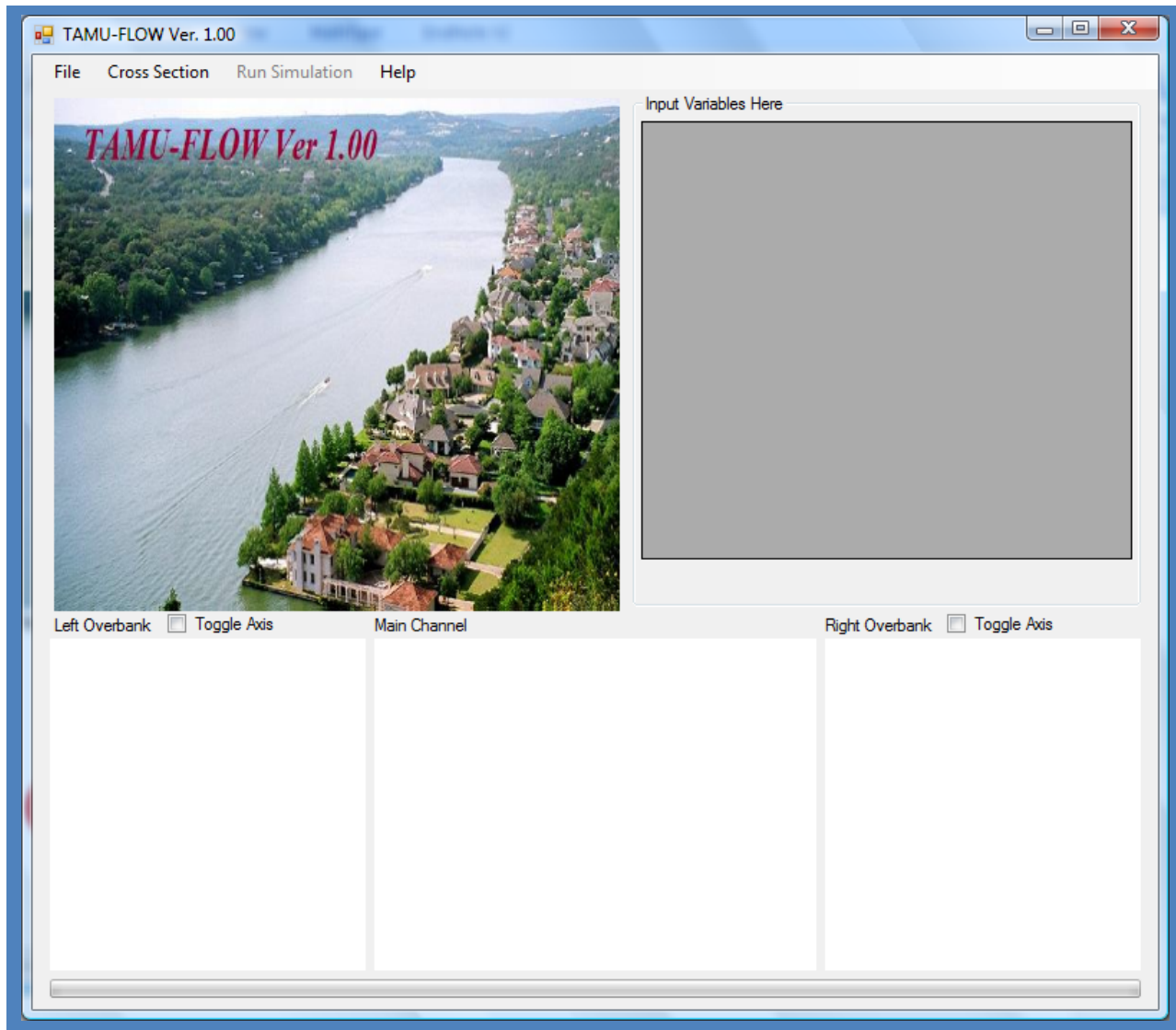
- Installation proceeds and finishes with the following dialog box. Click "Close" to close the window.



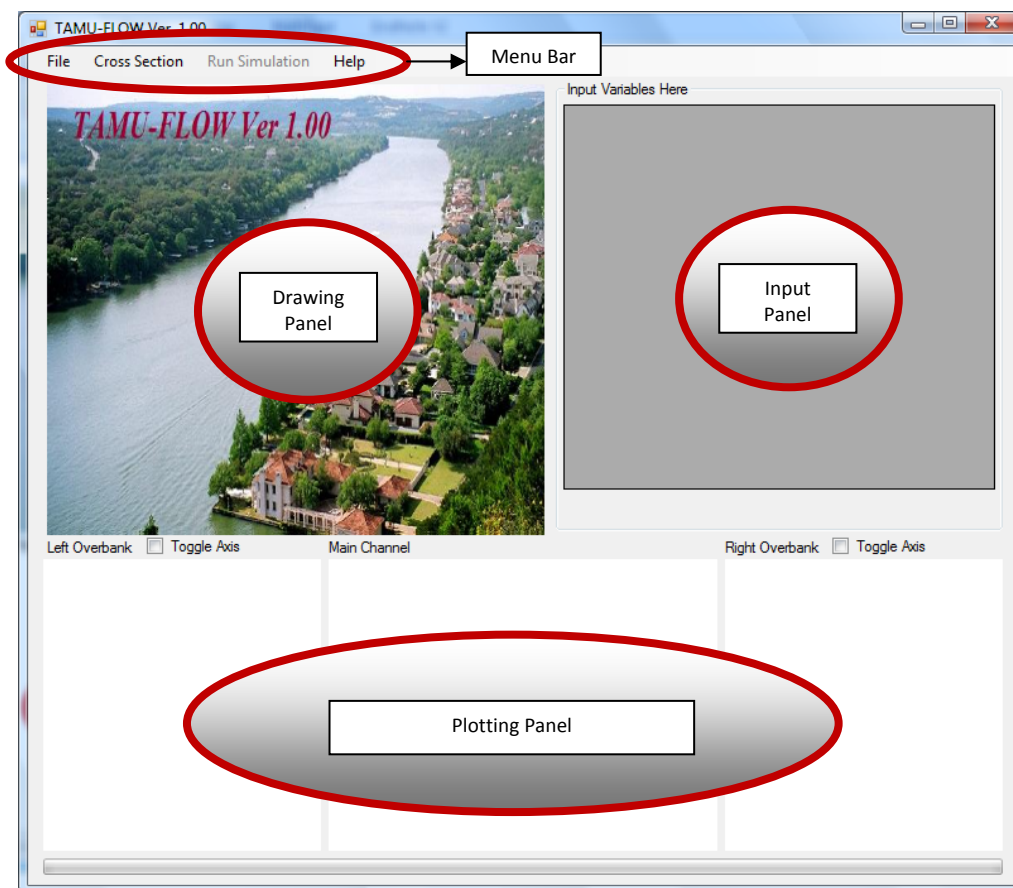
- TAMU-FLOW appears in the start-up menu of Windows. Go to the start-up menu and find the folder "Texas Transportation Institute." Make sure the file "TAMU-FLOW Ver. 1.00" is in the folder. Click on the file to start TAMU-FLOW.



7. TAMU-FLOW launches and is ready to go.



COMPONENTS OF TAMU-FLOW



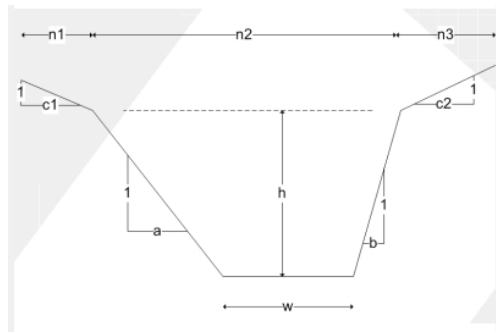
TAMU-FLOW has the following components in its graphical user interface (GUI):

- (1) Menu Bar
You can communicate with TAMU-FLOW by using the menu bar. You can start and run a new project, load the saved project, and save the current project. You can also save the analysis result here.
- (2) Drawing Panel
During the input stage of the analysis, the cross section of the river is shown here. After the analysis, water depth at a given discharge is shown along with the river cross section.
- (3) Input Panel
The dimensions of the channel cross section are input here.
- (4) Plotting Panel
After the analysis is performed, the relationship between discharge and velocity is shown in the plotting channel. The relationship of discharge and velocity at the left overbank, main channel, and right overbank is shown.

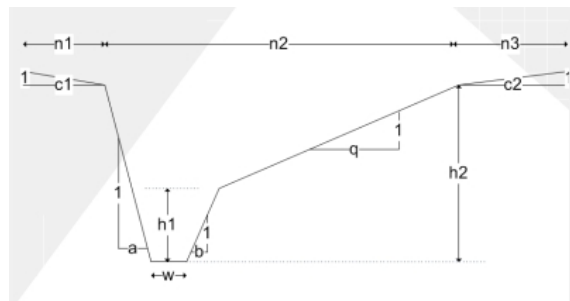
RUNNING TAMU-FLOW

TYPES OF CROSS SECTION

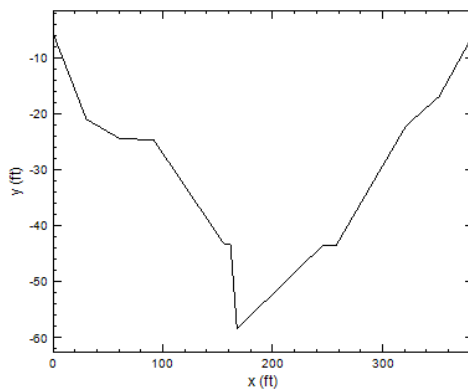
Three different types of cross section are available in TAMU-FLOW. The first one is a trapezoidal channel and looks as follows.



The second type of cross section is called a trapezoid with triangle and looks as follows.

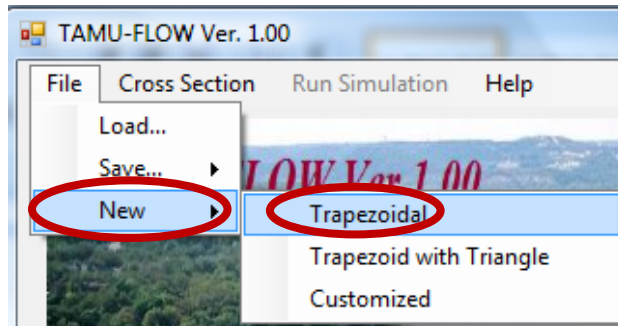


The last type of cross section does not have any predefined dimension for the channel. The channel cross section can be defined by entering the x and y coordinates of the river bottom. One example is shown in the following figure.

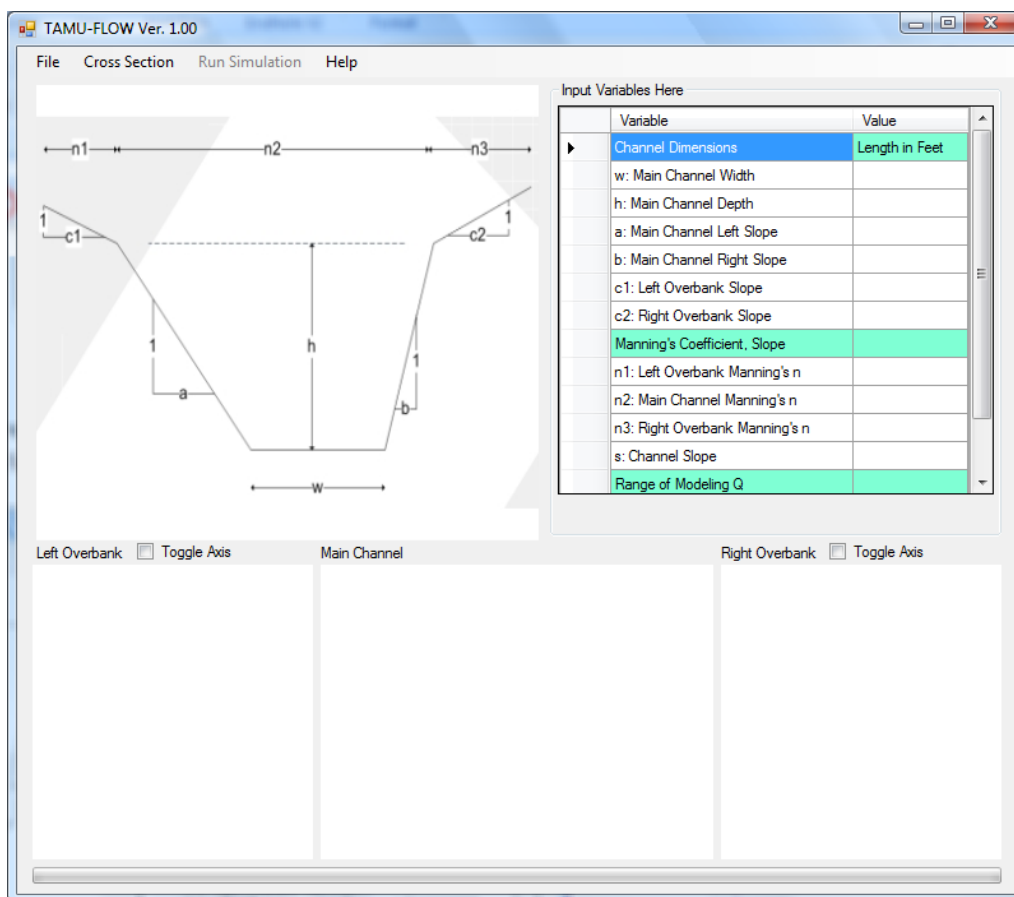


TRAPEZOIDAL CROSS SECTION

The first cross section is a trapezoidal cross section. On the menu bar at the top of the application, choose “File” – “New” – “Trapezoidal.”



TAMU-FLOW shows the default dimensions of the trapezoidal cross section in the plotting panel on the left and the input variables in the input panel on the right as follows.

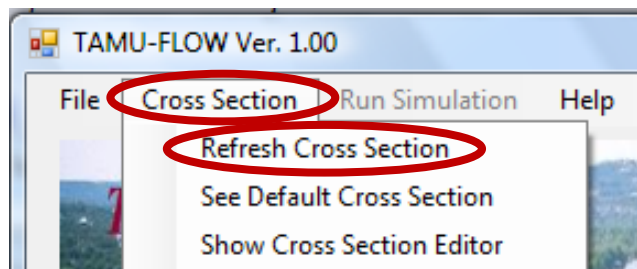


Now, enter each entry of the channel cross section to draw it. In the input panel, enter the following values.

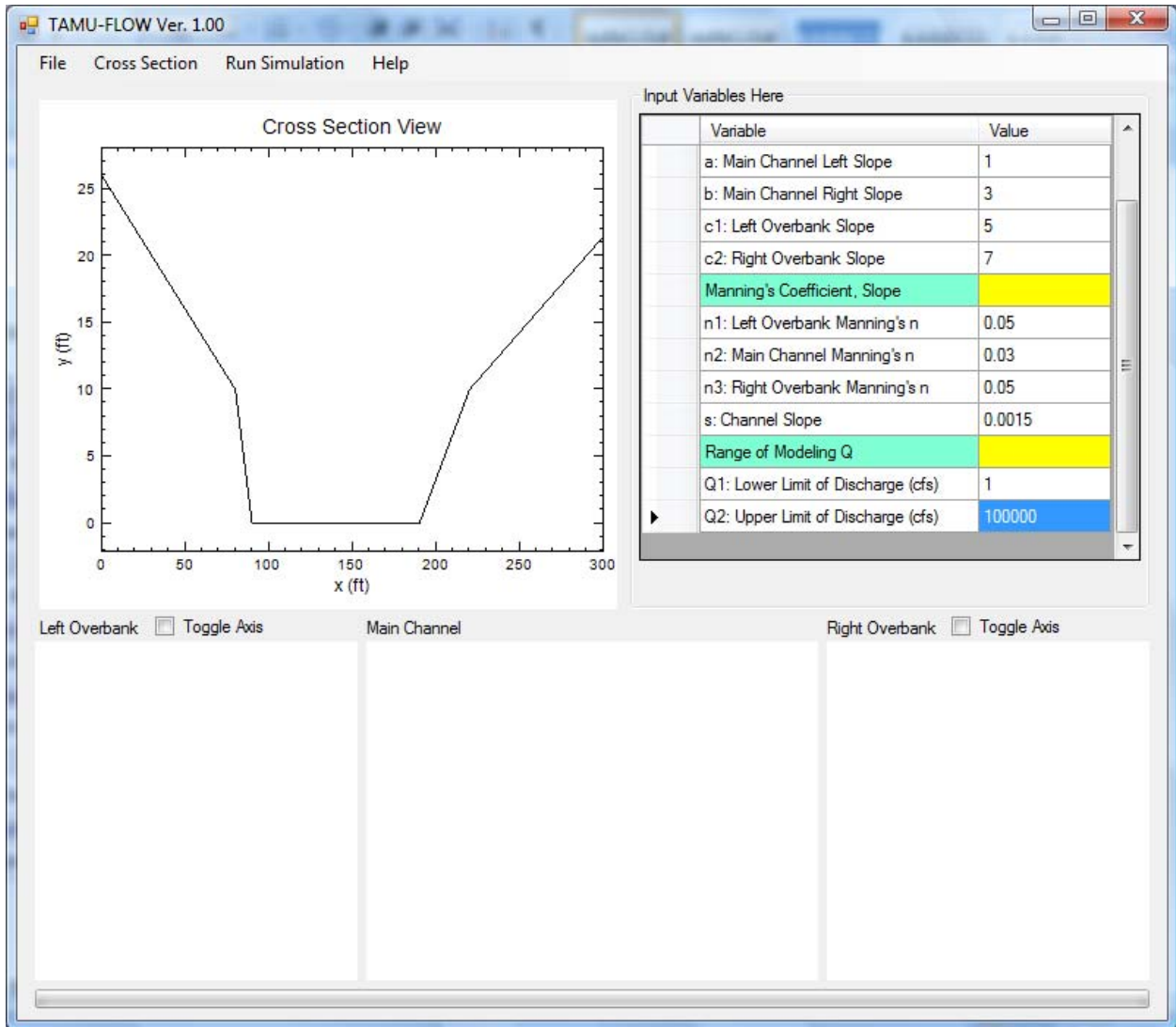
Channel Dimension	Length in Feet
w: Main Channel Width	100
h: Main Channel Depth	10
a: Main Channel Left Slope	1
b: Main Channel Right Slope	3
c1: Left Overbank Slope	5
c2: Right Overbank Slope	7
Manning's Coefficient, Slope	
n1: Left Overbank Manning's n	0.05
n2: Main Channel Manning's n	0.03
n3: Right Overbank Manning's n	0.05
s: Channel Slope	0.0015
Range of Modeling Q	
Q1: Lower Limit of Discharge (cfs)	1
Q2: Upper Limit of Discharge (cfs)	100000

Note that lengths should be entered in the unit of feet, and the discharge should be entered in the unit of cubic-feet per second. Each entry has its counterpart in the default trapezoidal cross section drawn in the plotting panel.

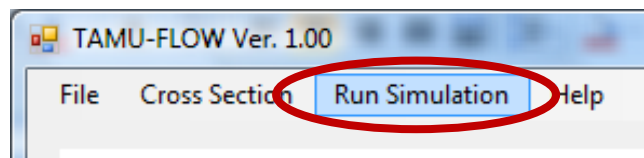
Next, on the menu bar, go to "Cross Section" – "Refresh Cross Section." This will let the computer recognize the input channel variables and draw the cross section in the drawing panel on the left.



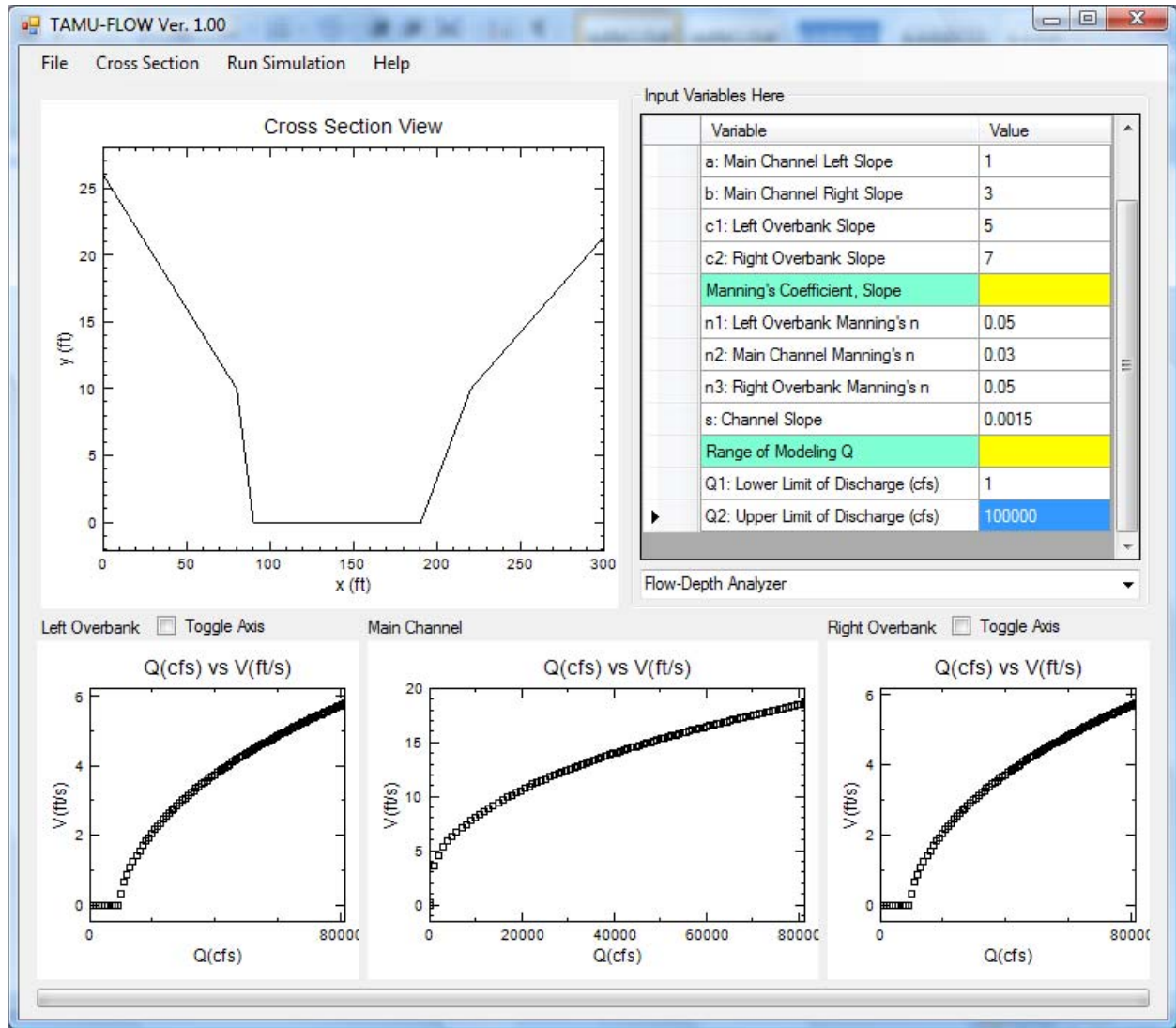
The following cross section is drawn in the drawing panel.



Now, the program is ready to run the analysis. On the menu bar, click on "Run Simulation."

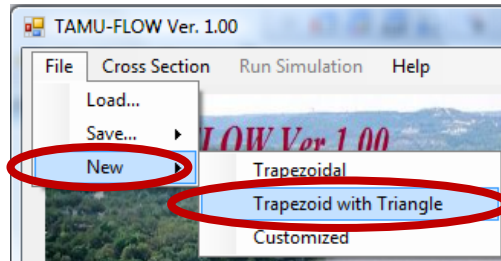


After the simulation is run, the relationship between discharge and flow velocity is shown in the plotting panel.

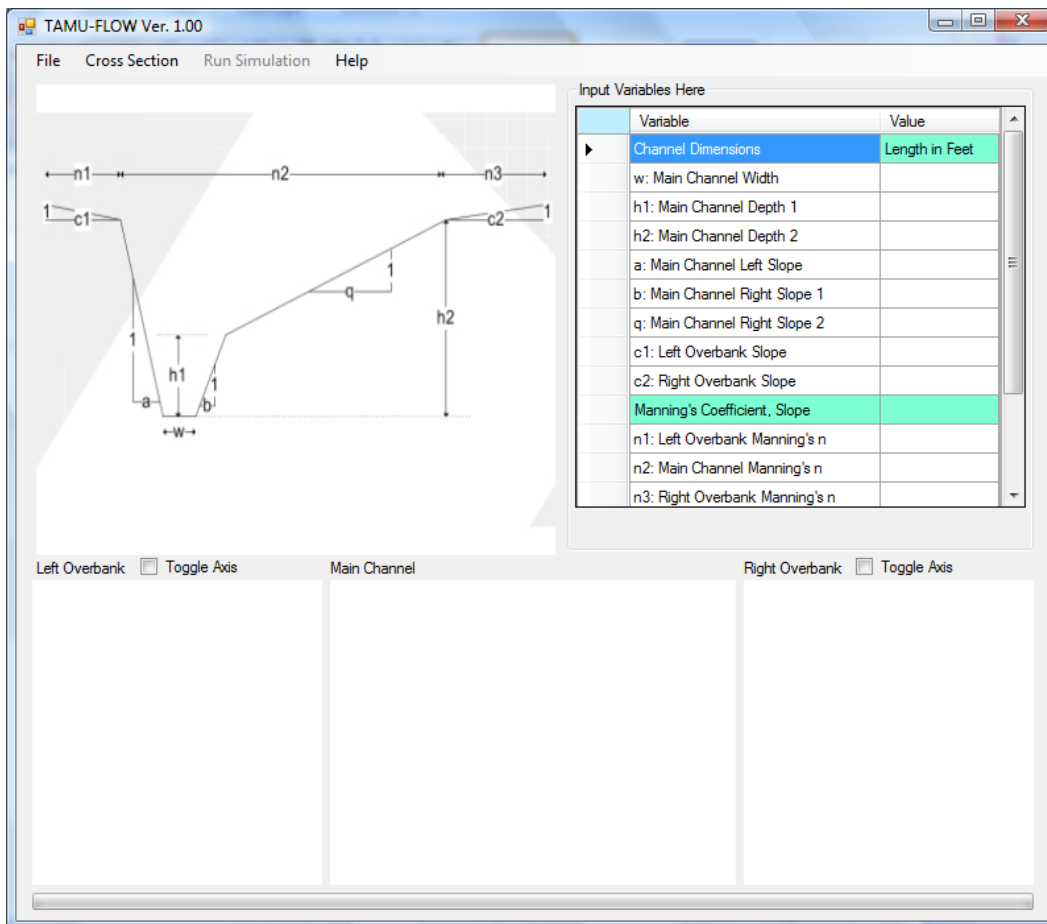


TRAPEZOID WITH TRIANGLE CROSS SECTION

Oftentimes, the cross section is not simple enough to be characterized by a trapezoid. This cross section deals with a trapezoidal cross section with a varying slope on one side. To open the default cross section for this case, go to “File” – “New” – “Trapezoid with Triangle.”



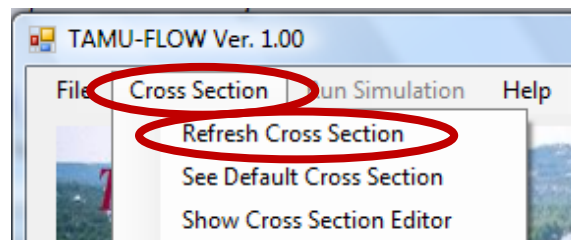
The dimensions of the cross section are drawn in the drawing panel. In the input panel, the table for inputting each entry of the cross-section dimension is prepared.



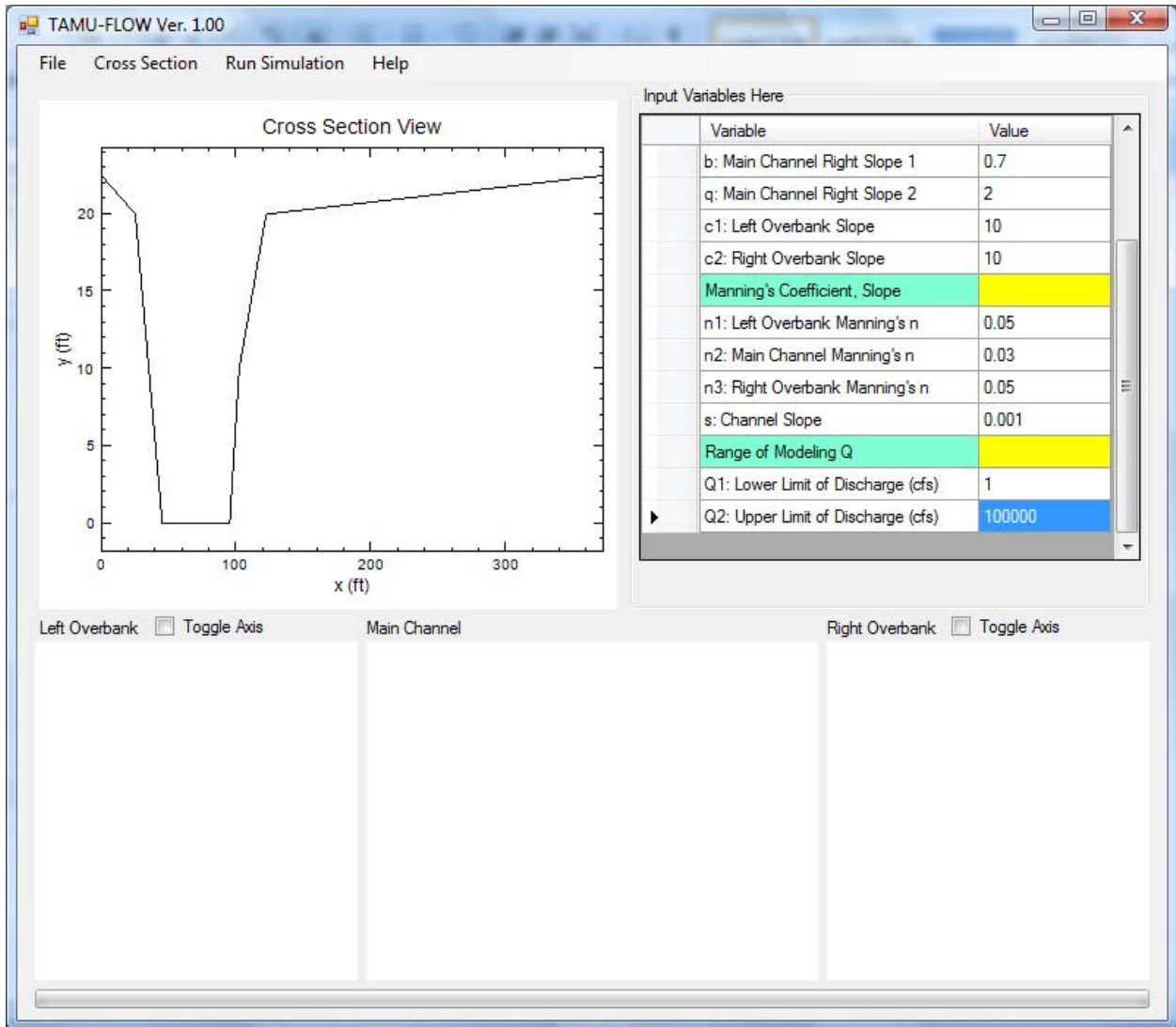
Enter each entry of the channel cross section to draw it. In the input panel, enter the following values.

Channel Dimension	Length in Feet
w: Main Channel Width	50
h1: Main Channel Depth 1	10
h2: Main Channel Depth 2	20
a: Main Channel Left Slope	1
b: Main Channel Right Slope 1	0.7
q: Main Channel Right Slope 2	2
c1: Left Overbank Slope	10
c2: Right Overbank Slope	10
Manning's Coefficient, Slope	
n1: Left Overbank Manning's n	0.05
n2: Main Channel Manning's n	0.03
n3: Right Overbank Manning's n	0.05
s: Channel Slope	0.001
Range of Modeling Q	
Q1: Lower Limit of Discharge (cfs)	1
Q2: Upper Limit of Discharge (cfs)	100000

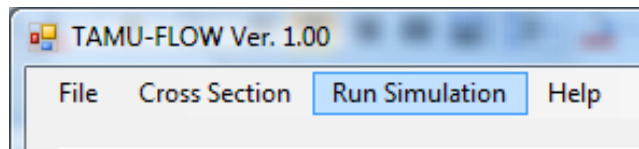
Then, on the menu bar, go to "Cross section" – "Refresh Cross Section." This will let the computer recognize the input channel variables and draw the cross section in the drawing panel on the left.



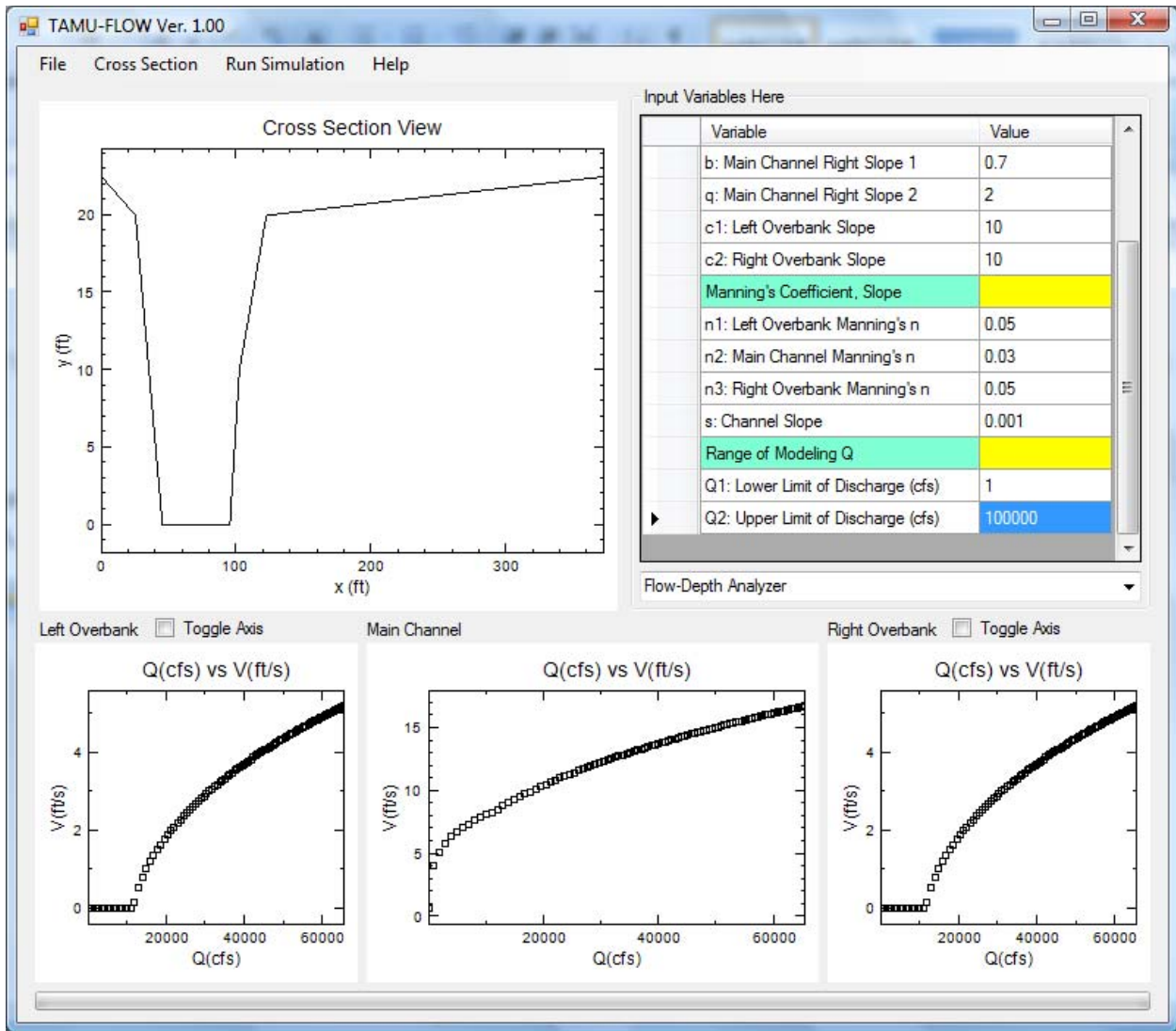
The channel cross section is drawn as follows.



TAMU-FLOW is ready to run the analysis. On the menu bar, click on "Run Simulation."



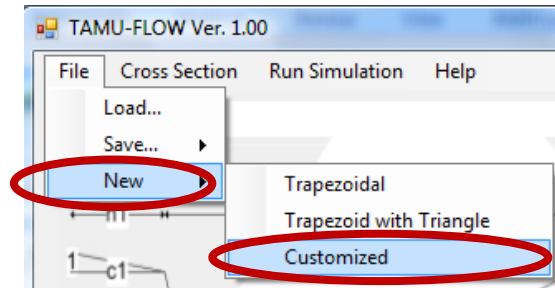
The analysis result is shown in the plotting panel. The relationship between the discharge and velocity for the left overbank, main channel, and right overbank is plotted in each of the plots.



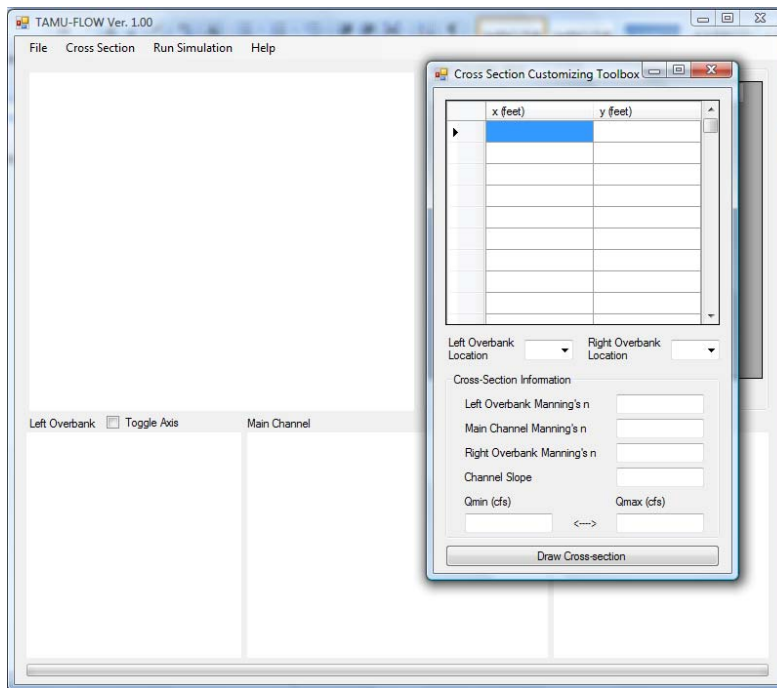
CUSTOMIZED CROSS SECTION

Oftentimes, it is impossible to characterize the channel cross section with the two default cross sections presented previously. The relationship between the discharge and flow for the channels with complicated geometry can be modeled using the customized cross section option of TAMU-FLOW.

First, open the Cross Section Customizing Toolbox by going to “File” – “New” – “Customized.”



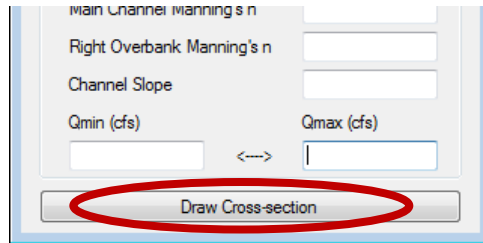
The project is reset, and the Cross Section Customizing Toolbox appears.



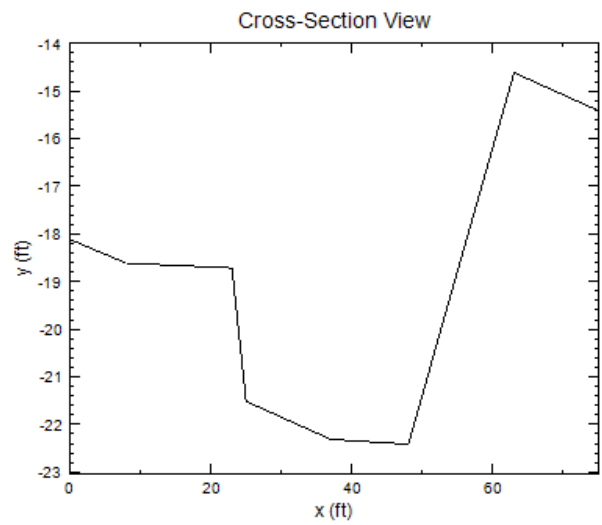
Input the x and y coordinates of the channel cross section in the data grid. This example uses the cross section measured in a local stream in Texas. Use the keyboard to input the x and y coordinates of the river cross section as shown in the following figure.

	x (feet)	y (feet)
	0	-18.1
	8	-18.6
	23	-18.7
	25	-21.5
	37	-22.3
	48	-22.4
	63	-14.6
	75	-15.4

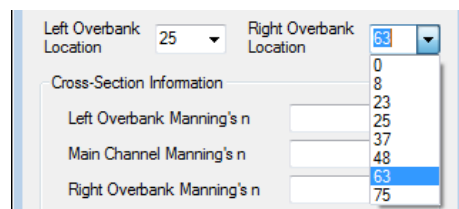
These entries need to be verified. To draw the cross section based on the input data in the data grid, click the "Draw Cross Section" button located at the bottom the Cross Section Customizing Toolbox.



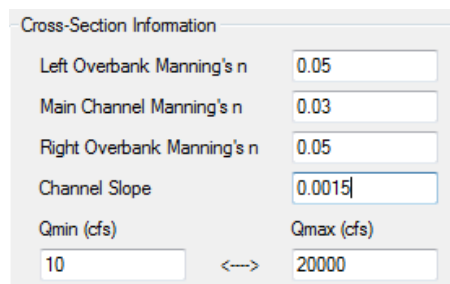
The channel cross section is drawn in the drawing panel as follows.



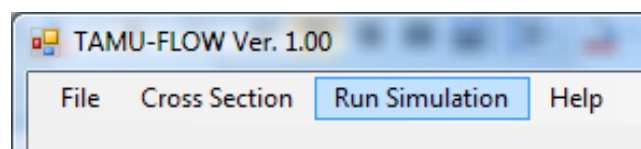
Now, choose the boundary between the overbanks and main channel by clicking on the drop-down menu “Left-Overbank Location” and “Right-Overbank Location.” In this example, input 25 and 63, respectively.



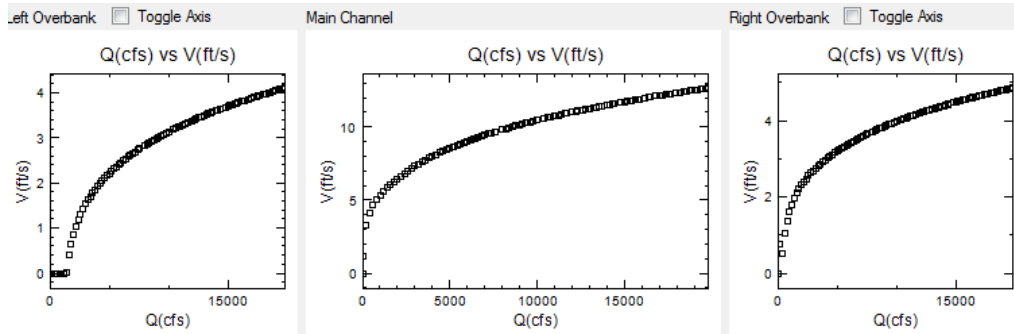
Then, input the rest of the parameters such as Manning’s coefficient for the left overbank, main channel, and right overbank; the channel slope; and the range of the discharge within which you want to analyze the relationship between the discharge and velocity.



TAMU-FLOW is ready to analyze. Click the button on the menu bar that says “Run Simulation.”

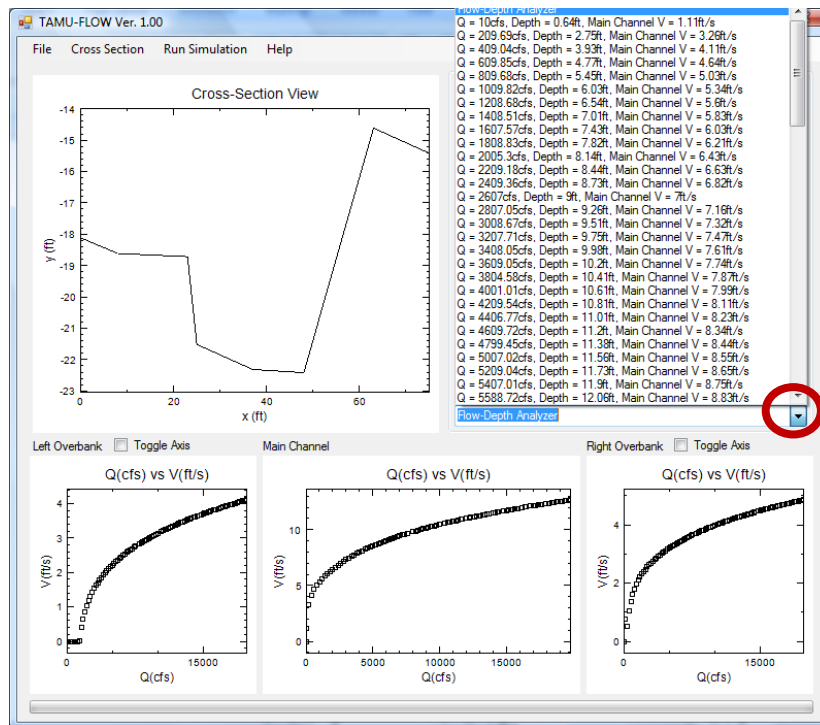


The relationship between the flow and velocity at each part of the channel is shown in the plotting panel.



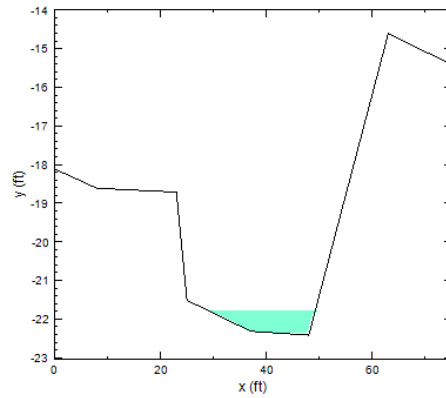
VISUALIZING THE ANALYSIS RESULTS

Once the analysis is performed for a cross section, the relationship between the discharge and flow depth can be visualized. Click on the “Flow-Depth Analyzer” drop-down menu located below the input panel.



Note: the Flow-Depth Analyzer will not be activated before running the analysis.

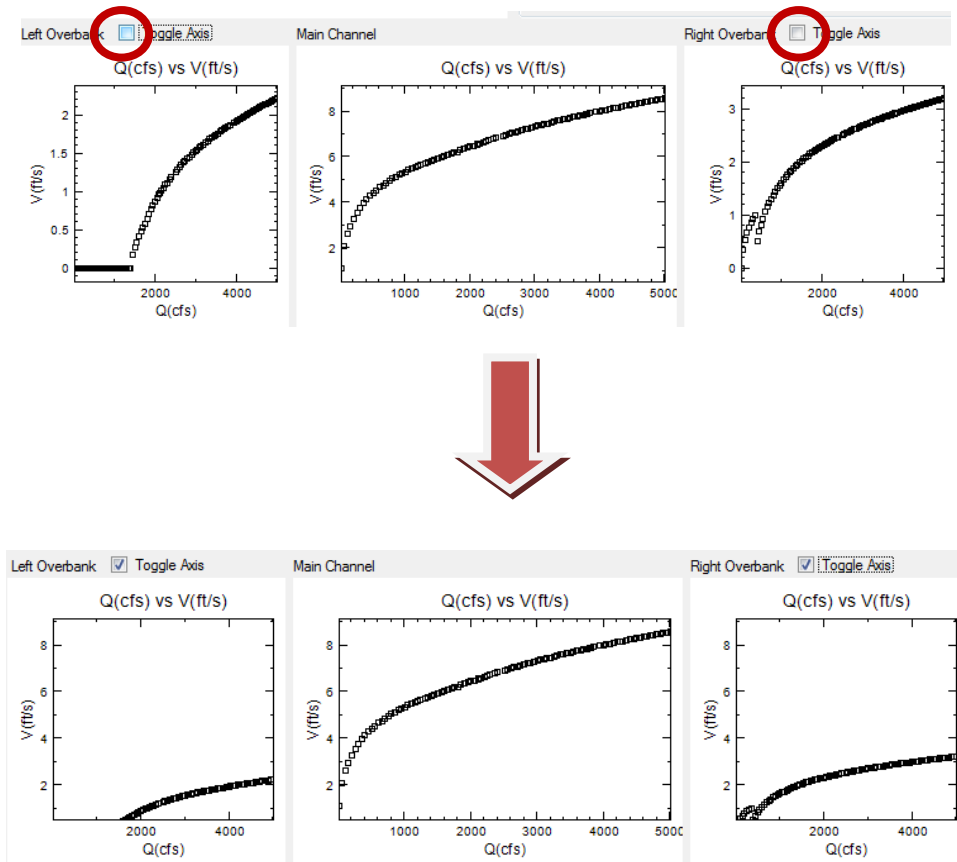
From the entries listed in the drop-down menu, choose the one that is closest to the discharge value for which you want to know the relationship between the flow and water depth. This example uses the one that starts with "Q = 10 cfs...." In the drawing panel, the location of the water table when the discharge is 10 cfs is drawn.



The water table of the flow at the other values of discharge can be also drawn by choosing the other values in the drop-down menu.

TOGGLING THE AXIS IN THE PLOTTING PANEL

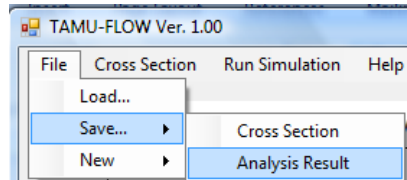
After the analysis is performed, you can see the relationship between the discharge and velocity in the plotting channel. The ranges of the y-axis of each plot are different, making it difficult to compare the plots. You can toggle the range of the y-axis of the plots for the left overbank and right overbank so that they can fit the y-axis of the main channel. To do this, click on the check box located right above the plotting panel.



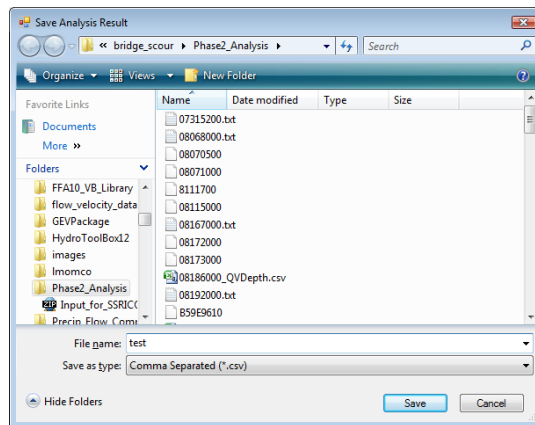
SAVING THE ANALYSIS RESULT

Oftentimes, it is not enough just to see the visualized result on the relationship between discharge, velocity, and water table. The result of the analysis can be saved in a comma-delimited format (*.csv).

After the analysis is performed, go to “File” – “Save” – “Analysis Result” on the menu bar.



The file save dialog box appears. Specify the folder and the name of the file where you want to save the result.



Open the saved file using any text editor to make sure everything was saved correctly.

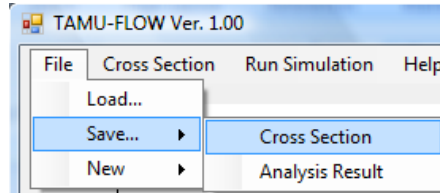
	A	B	C	D	E	F	G	H
1	Q_sum(cfs)	LOBQ(cfs)	MCQ(cfs)	ROBQ(cfs)	LOBV(ft/s)	MCV(ft/s)	ROBV(ft/s)	Depth(ft)
2	10.00185	0	10.00185	0	0	1.112582	0	-21.7641
3	59.91888	0.038326	59.88056	0	0.343574	2.061254	0	-20.9412
4	109.7187	0.215229	109.5034	0	0.5289	2.581225	0	-20.4321
5	159.544	0.518736	159.0253	0	0.658999	2.95787	0	-20.0144
6	209.547	0.933066	208.6139	0	0.763178	3.260729	0	-19.6493

The following is the description of each column in the saved file.

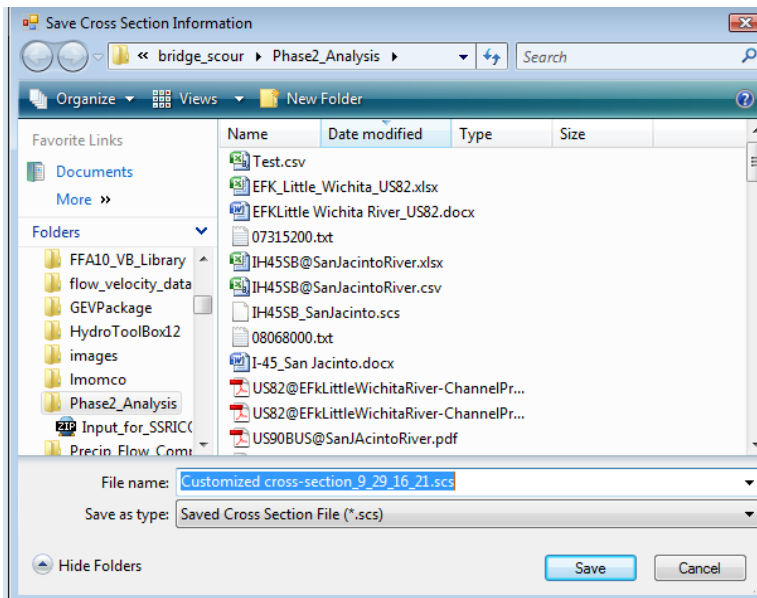
Column #	Column Name	Description
1	SumQ(cfs)	Sum of the discharge of the main channel and overbanks
2, 3, 4	LOBQ(cfs), MCQ(cfs), and ROBQ(cfs)	Discharge at the left overbank, main channel, and right overbank
5, 6, 7	LOBV(ft/s), MCV(ft/s), and ROBV(ft/s)	Flow velocity at the left overbank, main channel, and right overbank
8	Depth(ft)	y coordinate of the water table

SAVING THE CROSS SECTION

The input cross-section data can be saved and loaded. After completing the input, go to “File” – “Save” – “Cross Section.”

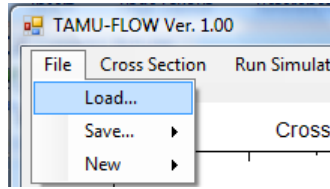


The file save dialog box appears. Specify the folder and the name of the file where you want to save the cross section.

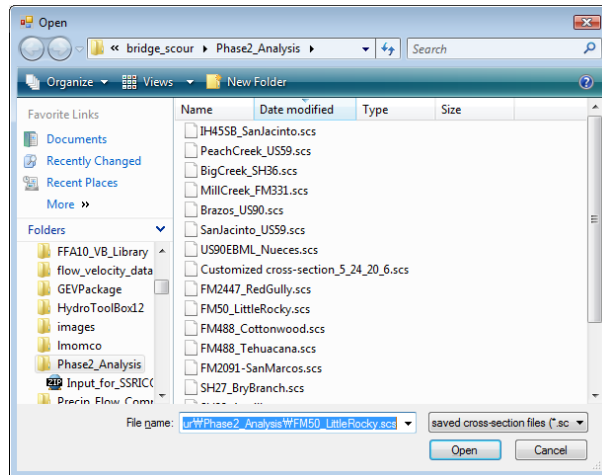


LOADING THE CROSS SECTION

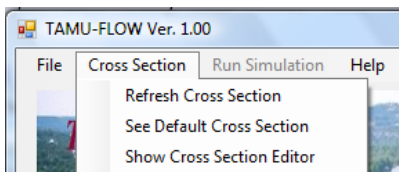
Saved cross sections can be loaded onto the system. Go to “File” – “Load.”



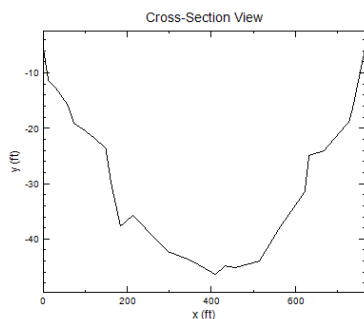
The file load dialog box appears. Specify the folder and the name of the file you want to load. Some of the saved cross-section files are saved in the folder where the program was installed. This folder is usually “C:\Program Files\TAMU Flow Ver. 1.00\Data.” Browse to the folder and open any of the files that have the “scs” extension.



The saved cross section is loaded into TAMU-FLOW. To draw the cross section of the loaded channel cross section, go to “Cross section” – “Refresh Cross Section.”

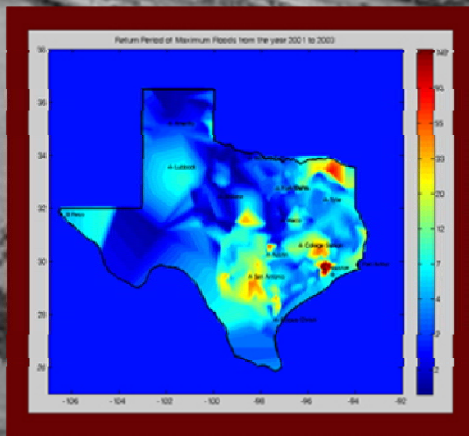


The loaded cross section is drawn in the drawing panel.



**APPENDIX F:
TAMU-FLOOD USER'S MANUAL**

TAMU- FLOOD



User's Manual

Contents

What Is TAMU-FLOOD? What Can I Do with It?	425
Installation	426
Running TAMU-FLOOD.....	430
Understanding the Output Maps and Charts of TAMU-FLOOD.....	439
Notes	464

What Is TAMU-FLOOD? What Can I Do with It?

TAMU-FLOOD is a software tool developed for bridge scour analysis. Most bridge scour happens during flood events, and TAMU-FLOOD enables users to determine the recurrence interval of floods that the bridge has experienced since its construction.

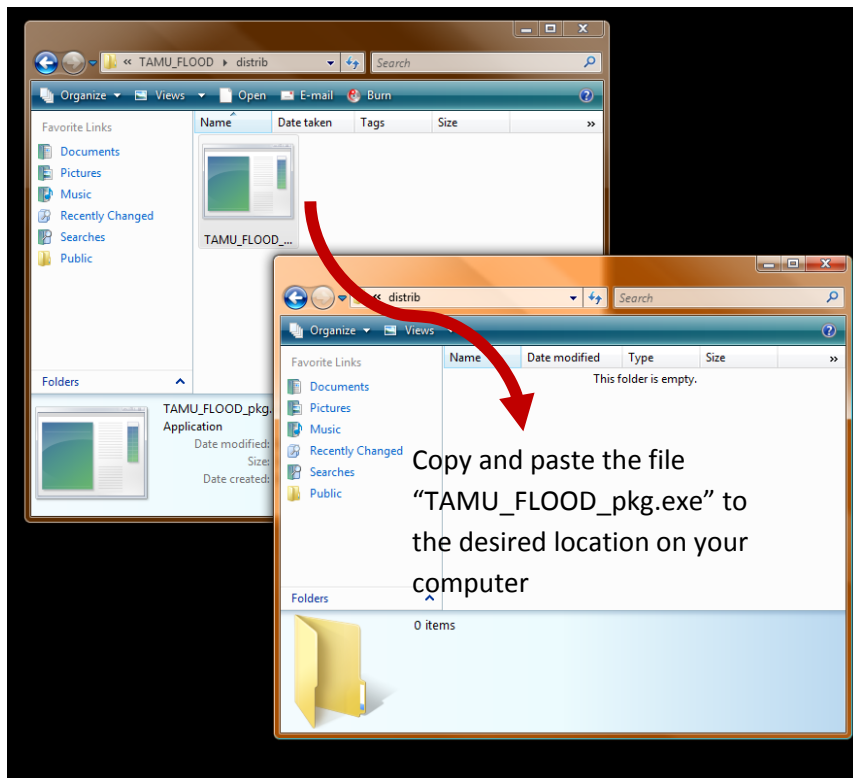
TAMU-FLOOD provides a map of Texas color coded to show the recurrence interval of floods that occurred in a given year or a given time period. By looking at the colors in the map, one can see graphically what kind of storm occurred at that bridge.

Installation

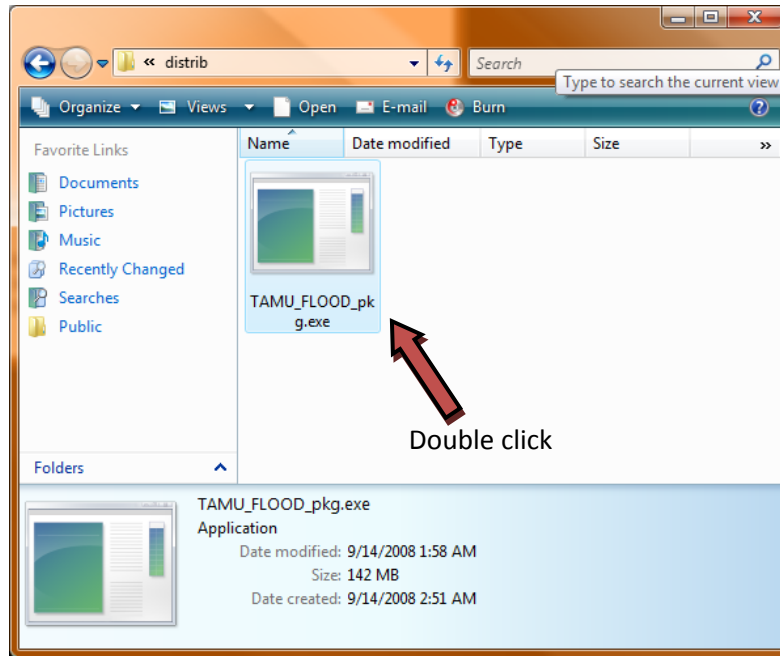
1. Insert the CD-ROM into the CD-ROM drive.



2. Copy and paste the file "TAMU_FLOOD_pkg.exe" to the location on your computer where you want to install TAMU-FLOOD.



3. Double click the file "TAMU_FLOOD_pkg.exe."



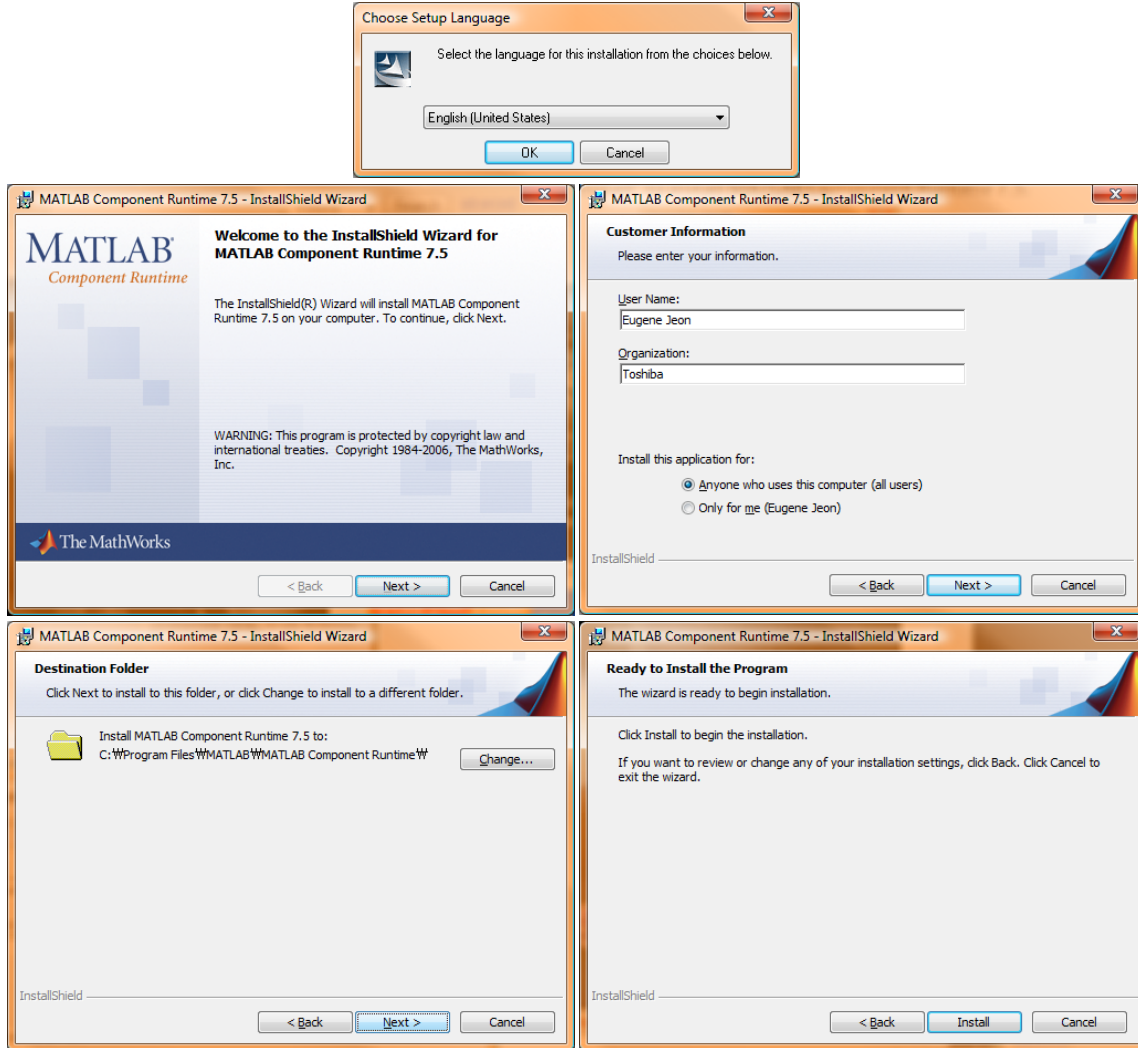
4. The files for the installation are extracted in the directory. The following dialog box is displayed.

```
D:\Softwares\TAMU_FLOOD\distrib\TAMU_FLOOD_pkg.exe
MWUnZipSFX 5.41 of 16 April 2000, by Info-ZIP. Modified by The MathWorks, Inc.
Send bug reports to support@mathworks.com.
  inflating: _install.bat
  inflating: MCRInstaller.exe
  inflating: TAMU_FLOOD.exe
  inflating: TAMU_FLOOD.ctf

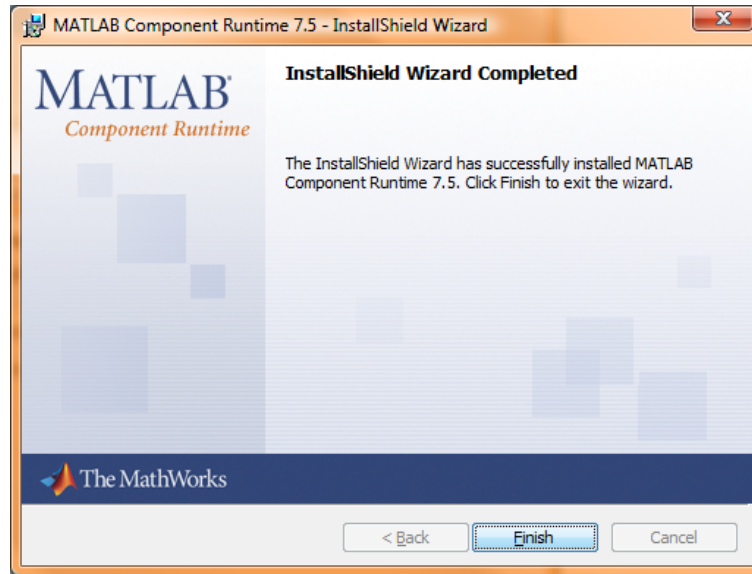
D:\Softwares\TAMU_FLOOD\distrib>echo off
Deploying project TAMU_FLOOD.
Running MCRInstaller
```

5. If the computer asks if you will allow it to run "MCR_installer.exe," click "Allow."

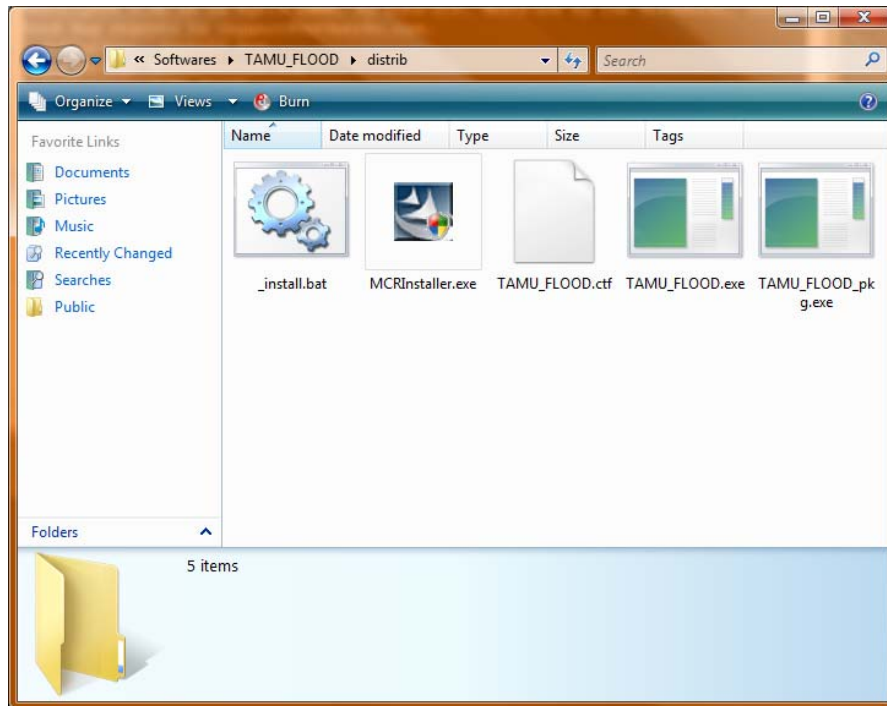
- MATLAB Component Runtime 7.5 will be installed on your computer and will show you the following dialog boxes. If you are asked any questions, click "Next," "OK," or "Install" to install MATLAB Component Runtime 7.5.



- Once MATLAB Component Runtime 7.5 is installed successfully on your machine, you should see the following dialog box. Click "Finish."



- After the installation is finished, you should see the following files in the directory.

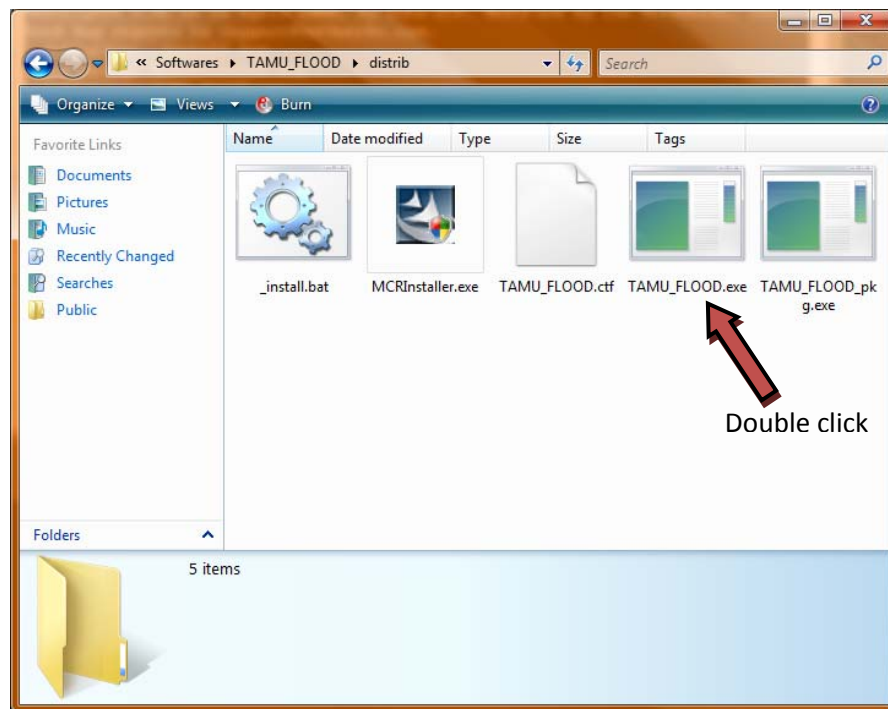


Running TAMU-FLOOD

The best way to learn how to use TAMU-FLOOD is simply to try it. The following step-by-step procedure will help you understand the user interface of TAMU-FLOOD.

1. Start TAMU-FLOOD.

To start TAMU-FLOOD, click on “TAMU_FLOOD.exe” in the directory where you installed TAMU-FLOOD.



You should see the following user interface for TAMU-FLOOD.

TAMU-FLOOD Ver. 1.00

Help

Input Panel

Select the unit of coordinate

Decimals (i.e. -97.3456)

Longitude (Decimals) Latitude (Decimals)

Longitude (DMS) W Latitude (DMS) N

Year Bridge Built 1920 Year Last Inspected

Flood Frequency Analysis Methods

Choose a method Log-Pearson Type III - MOM (USGS Custom)

Output Format

I want flow map for each year - using only unregulated gages

I want flow map for each year - using all available gages

I want rainfall map for each year

Rainfall Duration Selector

Generate Maps

Output

Maximum RI of the bridge(Year) N/A

N/A < Vmo/V100 < N/A

2. Input the location of the bridge.

You need to input the location of the bridge (or any location you want to know the flood information for) in the format of longitude and latitude. The longitude and latitude can either be a decimal unit or degree, minute, and second (DMS) unit.

Here, input a location in Houston with a longitude and latitude of -95.3 and 29.75 . First, let the computer know that you are using the decimal unit system. To do this, push the arrow shape next to the drop-down menu that says "Select the unit of coordinate." Select "Decimals (i.e., -97.3456)."

The screenshot shows the TAMU-FLOOD Ver. 1.00 software interface. The 'Input Panel' section is active, showing the 'Select the unit of coordinate' dropdown menu set to 'Decimals (i.e. -97.3456)'. Below this are text boxes for 'Longitude (Decimals)' and 'Latitude (Decimals)'. There are also fields for 'Longitude (DMS)' and 'Latitude (DMS)'. The 'Year Bridge Built' is set to 1920. The 'Flood Frequency Analysis Methods' dropdown is set to 'Log-Pearson Type III - MOM (USGS Custom)'. The 'Output Format' section has three unchecked checkboxes and a 'Rainfall Duration Selector' dropdown. A 'Generate Maps' button is visible. The 'Output' section shows 'Maximum RI of the bridge(Year) N/A' and 'N/A < Vmo/V100 < N/A'.

After the unit is chosen, "Longitude (Decimals)" and "Latitude (Decimals)" text boxes are activated. Input the longitude (-95.3) and latitude (29.75) of

the location of the bridge in the boxes. Keep in mind that the longitude of Texas in decimal units is always negative, which means that it is in the Western Hemisphere.

TAMU-FLOOD Ver. 1.00

Help

Input Panel

Select the unit of coordinate

Decimals (i.e. -97.3456)

Longitude (Decimals) -95.3 Latitude (Decimals) 29.75

Longitude (DMS) W Latitude (DMS) N

Year Bridge Built 1920 Year Last Inspected

Flood Frequency Analysis Methods

Choose a method Log-Pearson Type III - MOM (USGS Custom)

Output Format

I want flow map for each year - using only unregulated gages

I want flow map for each year - using all available gages

I want rainfall map for each year

Rainfall Duration Selector

Generate Maps

Output

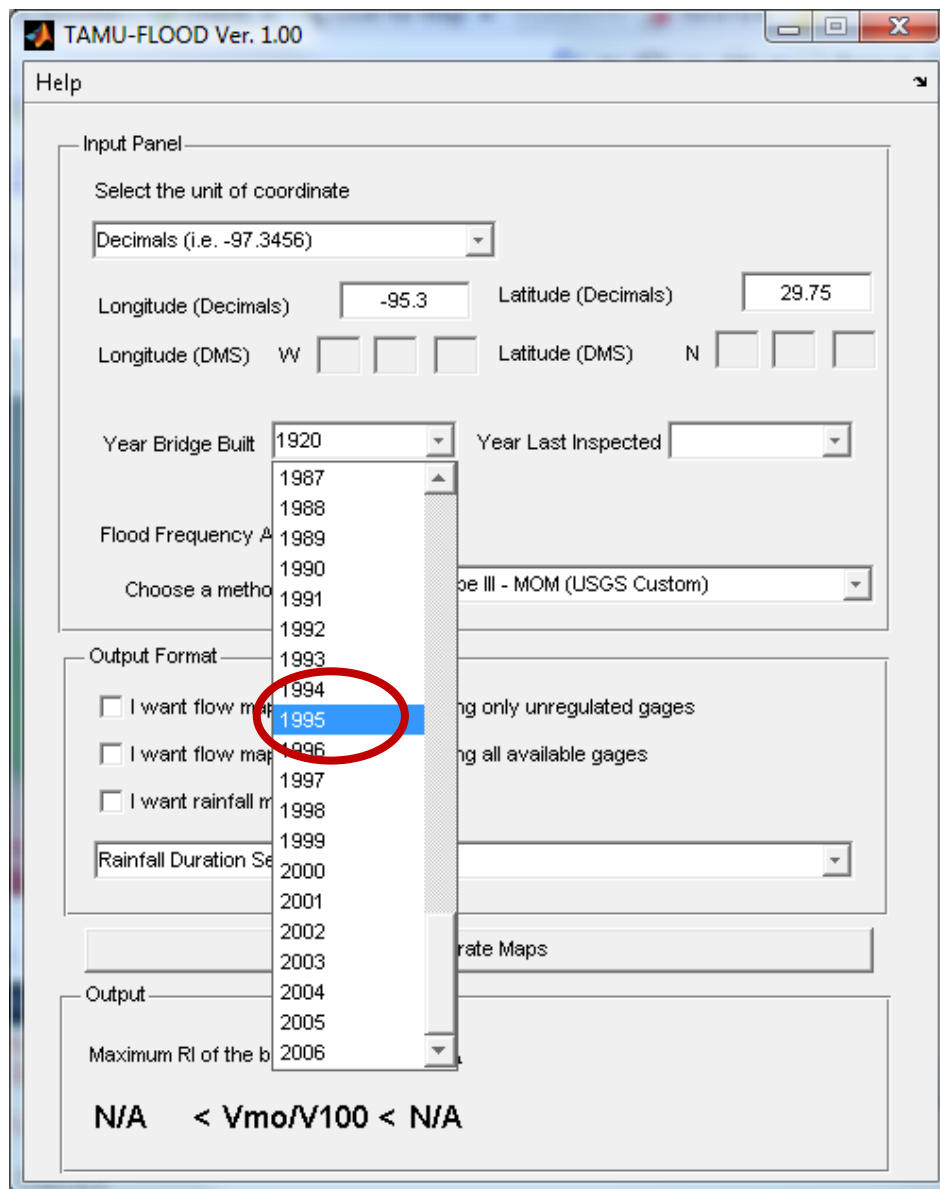
Maximum RI of the bridge(Year) N/A

N/A < V_{mo}/V_{100} < N/A

3. Input the time period.

Next, input the time period for which you want the flood information for the bridge. Say that the bridge was built in 1995 and you want to know the flood information for the bridge since then.

Click on the drop-down menu that says “Year Bridge Built” and choose 1995.



Then, input the ending year of the period, which is, in this example, the latest available year in the software—2006. Click the drop-down menu that says “Year Last Inspected” and choose 2006.

4. Select a flood frequency analysis method.

Four different types of flood frequency analysis methods are available in TAMU-FLOOD, which are as follows:

- a. Log-Pearson Type III—method of moments
- b. Generalized extreme value—method of L-moments
- c. Generalized extreme value—method of maximum likelihood
- d. Generalized extreme value—a mixture of the method of L-moments and the method of maximum likelihood

A detailed description of these methods is given in the technical report. Here, choose the method Log-Pearson Type III—method of moments.

The screenshot shows the TAMU-FLOOD Ver. 1.00 software interface. The window title is "TAMU-FLOOD Ver. 1.00". The interface is divided into several sections:

- Input Panel:**
 - Select the unit of coordinate: Decimals (i.e. -97.3456)
 - Longitude (Decimals): -95.3; Latitude (Decimals): 29.75
 - Longitude (DMS): W; Latitude (DMS): N
 - Year Bridge Built: 1995; Year Last Inspected: 2006
- Flood Frequency Analysis Methods:**
 - Choose a method: Log-Pearson Type III - MOM (USGS Custom) (highlighted in blue and circled in red)
 - Other options in the dropdown: GEV - LMOM and MLE mixed, GEV - Method of L-Moment, GEV - Method of Maximum Likelihood
- Output Format:**
 - I want flow map for
 - I want flow map for
 - I want rainfall map for each year
 - Rainfall Duration Selector
- Buttons:** Generate Maps
- Output:**
 - Maximum RI of the bridge(Year) N/A
 - N/A < V_{mo}/V_{100} < N/A

5. Output the format selection.

Three types of output maps are available:

- a. Map of the recurrence interval of the observed flow peaks using only unregulated flow data (most accurate)
- b. Map of the recurrence interval of the observed flow peaks using all available flow data (less accurate yet more useful in the southwestern area of Texas where there are few USGS gages)
- c. Map of the recurrence interval of the observed rainfall from NCDRC hourly precipitation gages

Here, choose to see all three available maps. Check all three check boxes in the output format.

The screenshot shows the TAMU-FLOOD Ver. 1.00 software interface. The window title is "TAMU-FLOOD Ver. 1.00". The interface is divided into several sections:

- Input Panel:**
 - Select the unit of coordinate: Decimals (i.e. -97.3456)
 - Longitude (Decimals): -95.3; Latitude (Decimals): 29.75
 - Longitude (DMS): W; Latitude (DMS): N
 - Year Bridge Built: 1995; Year Last Inspected: 2006
 - Flood Frequency Analysis Methods: Choose a method: Log-Pearson Type III - MOM (USGS Custom)
- Output Format:**
 - want flow map for each year - using only unregulated gages
 - want flow map for each year - using all available gages
 - want rainfall map for each year
 - Rainfall Duration Selector: [Dropdown menu]
- Buttons:**
 - Generate Maps
- Output:**
 - Maximum RI of the bridge(Year): N/A
 - N/A < Vmo/V100 < N/A

When TAMU-FLOOD draws the recurrence interval of the rainfall map, it requires the duration of the rainfall. In this example, choose 6 hours. If you choose 6 hours, TAMU-FLOOD will draw the recurrence interval map of the 6-hour duration rainfall. Click on the “Rainfall Duration Selector” drop-down menu and choose 6 hours.

TAMU-FLOOD Ver. 1.00

Help

Input Panel

Select the unit of coordinate

Decimals (i.e. -97.3456)

Longitude (Decimals) -95.3 Latitude (Decimals) 29.75

Longitude (DMS) W Latitude (DMS) N

Year Bridge Built 1995 Year Last Inspected 2006

Flood Frequency Analysis Methods

Choose a method Log-Pearson Type III - MOM (USGS Custom)

Output Format

I want flow map for each year - using only unregulated gages

I want flow map for each year - using all available gages

I want rainfall map for each year

Rainfall Duration Selector

1 hour

3 hours

6 hours

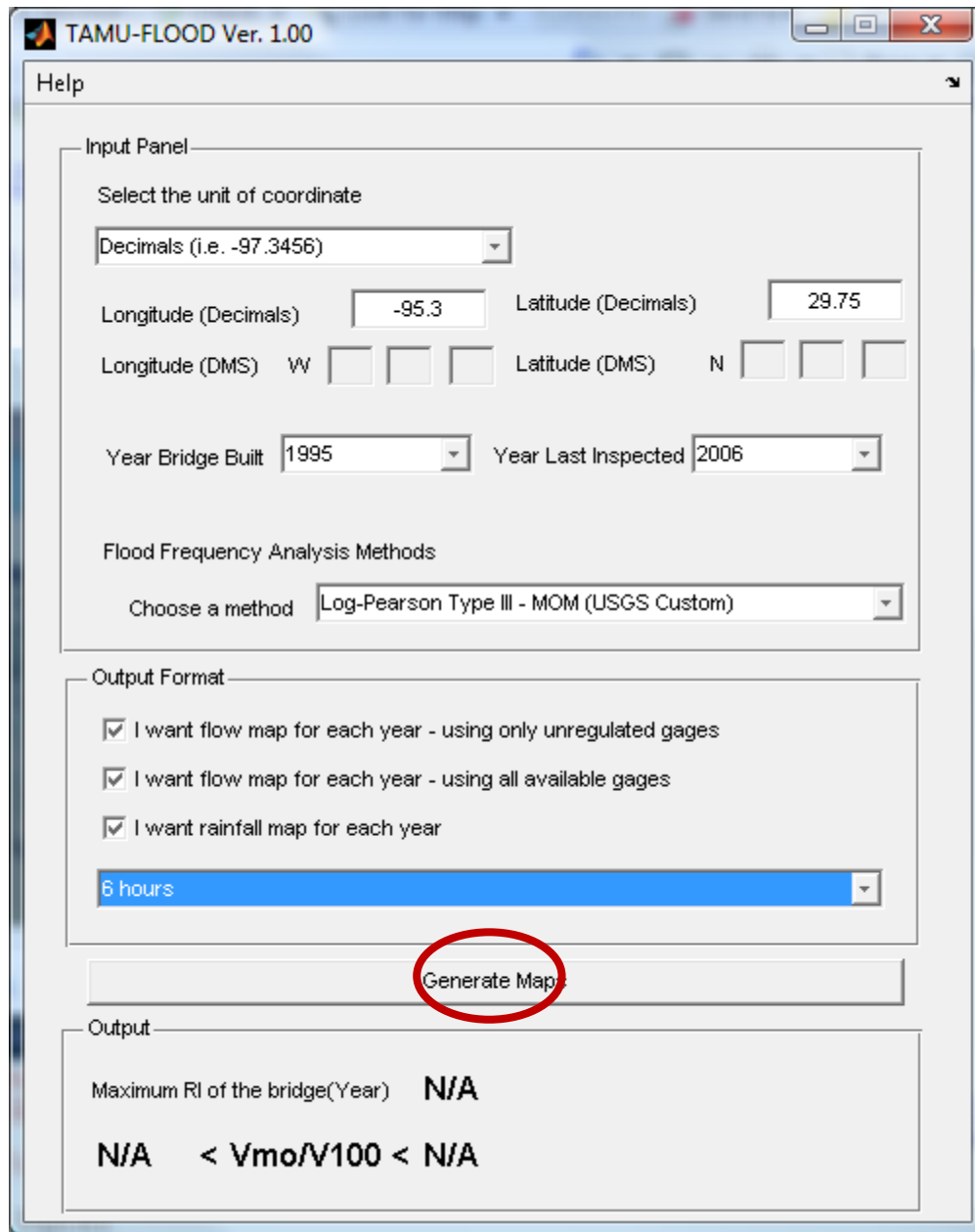
12 hours

24 hours

N/A < Vmo/V100 < N/A

6. Generate the maps of flow and rainfall recurrence intervals.

Now, you are finished with inputting all required information and can start generating the maps of recurrence intervals. Simply click the button “Generate Maps.”



Understanding the Output Maps and Charts of TAMU-FLOOD

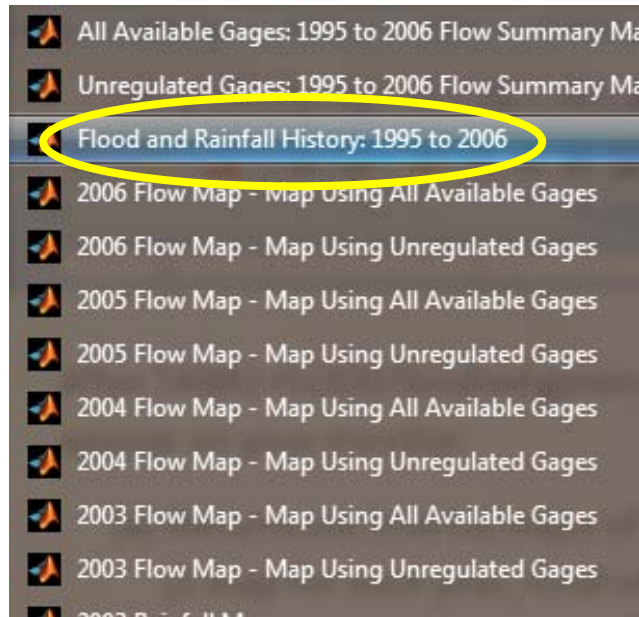
After TAMU-FLOOD finishes generating the maps, the following windows should appear on your screen:

1. Recurrence interval maps of yearly flow peaks using unregulated flow data (1 map for each year, total of 12 maps)
2. Recurrence interval maps of yearly flow peaks using all flow data (1 map for each year, total of 12 maps)
3. Recurrence interval maps of yearly 6-hour rainfall (1 map for each year, total of 12 maps)
4. Recurrence interval map of the maximum flow peaks that happened between 1995 and 2006 (1 map using unregulated flow data and 1 map using all available flow data)
5. Flood and rainfall history chart
6. TAMU-FLOOD Figure Layer Controller

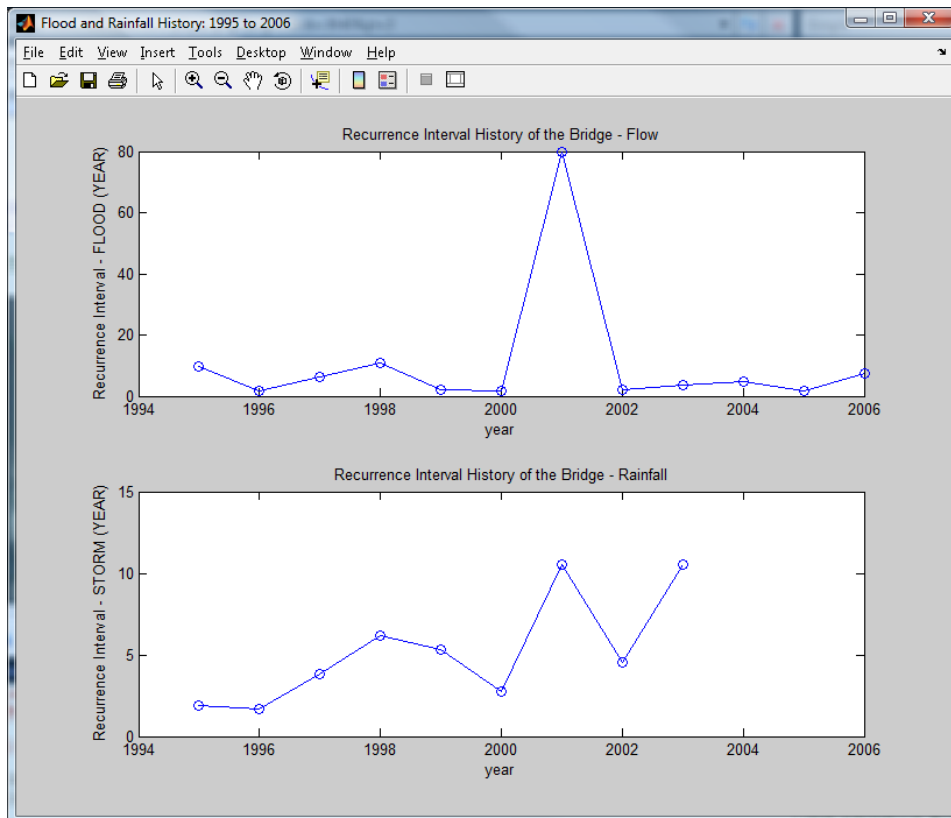
Detailed description of these windows is given as follow:

1. Flood and Rainfall History Chart

To open the Flood and Rainfall History Chart, go to the bottom menu bar of Windows Explorer and choose "Flood and Rainfall History: 1995-2006."



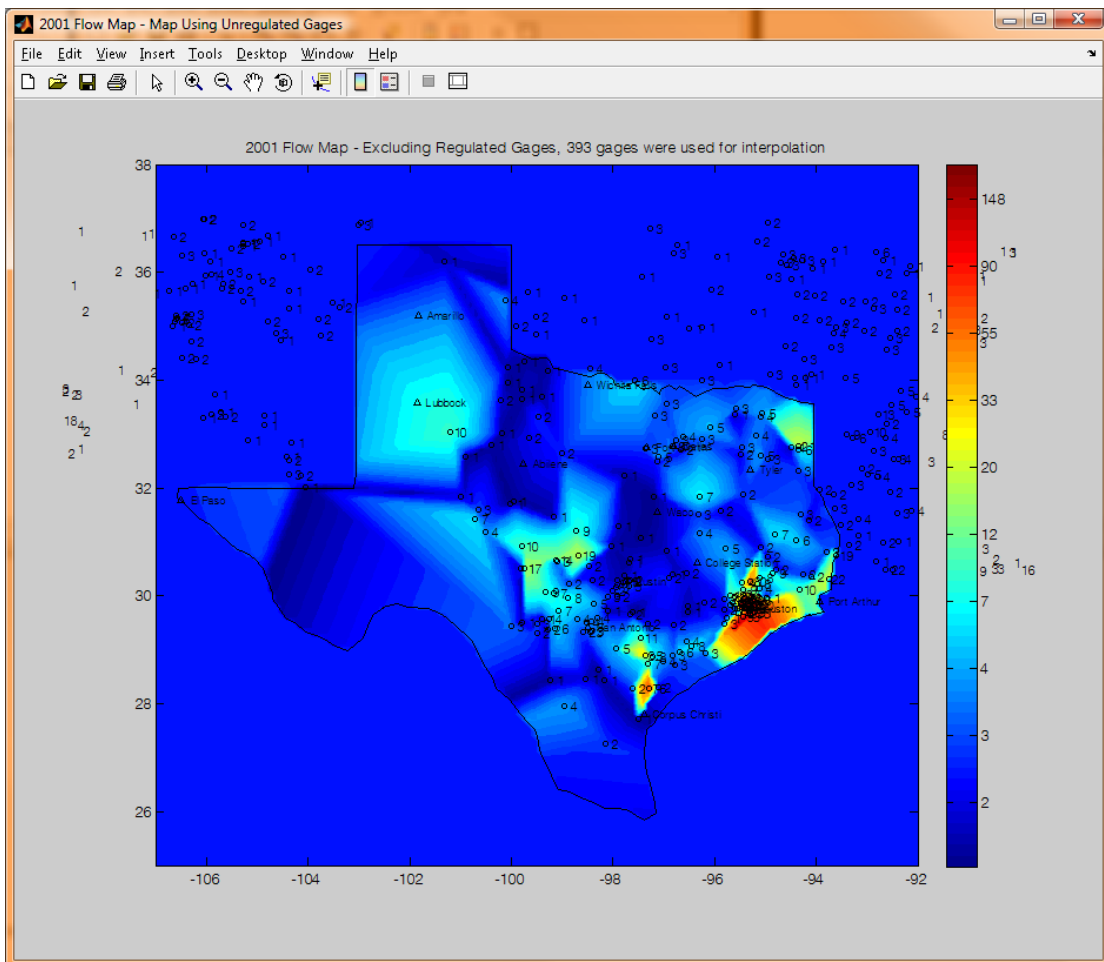
The following window pops up.



The chart shows the history of the recurrence interval of the maximum observed flow peaks and rainfall peaks at the location entered in the previous chapter (longitude -95.3 and latitude 29.75). From this chart, you can see that the location experienced a major flood in the year 2001. What happened in the year 2001? Go to the recurrence interval map of the year 2001.


2. Recurrence Interval Maps of Each Year

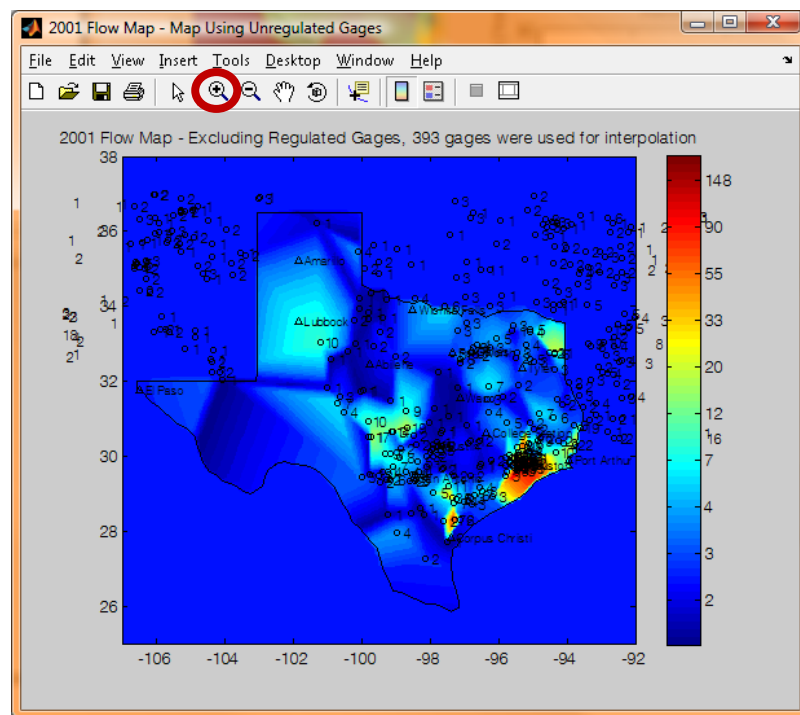
To open the recurrence interval map of the year 2001, go to the bottom menu bar of Windows Explorer and choose "2001 Flow Map—Map Using Unregulated Gages." The following window pops up.




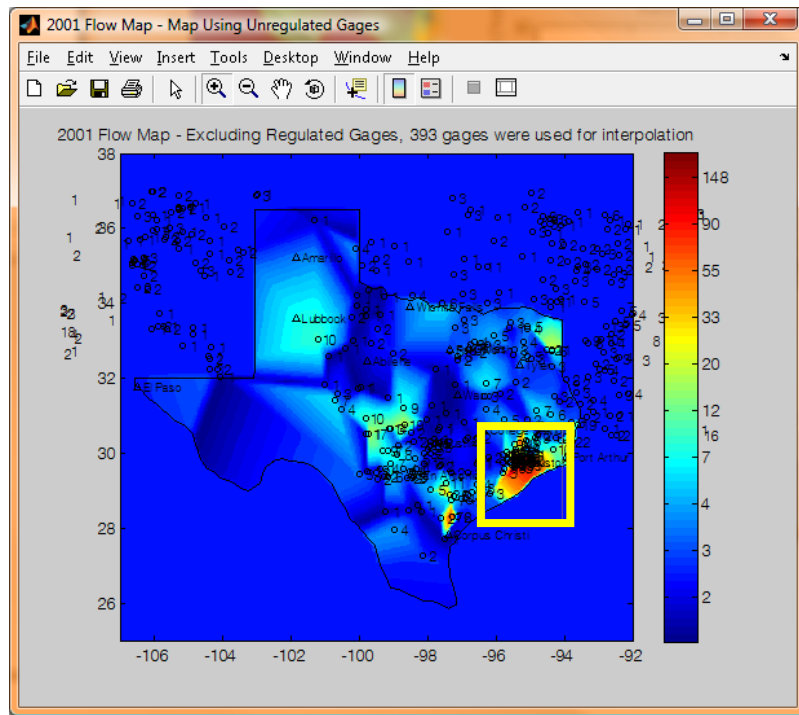
The color shadings in the map represent the recurrence interval of the maximum flow that happened in the year 2001. The color bar at the right of the figure gives you an idea of the magnitude of the flood experienced by the location. In this map, the Houston area is in red to yellow shading, which means that the area experienced floods with a recurrence interval between 30 and 150 years. Small circles on the map indicate the location of the USGS gages used for the generation of the map. The number beside each circle represents the recurrence interval of the maximum flow that happened in the year 2001.

a. Zoom In

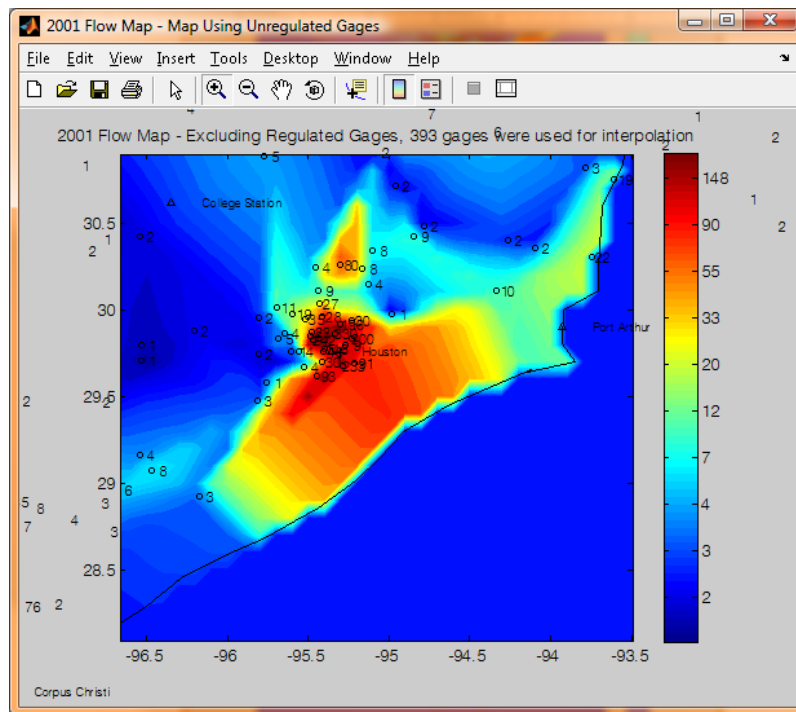
We want to zoom in on the Houston area of the map. To do this, click on the  icon on the menu bar.



The cursor changes from the arrow shape to the  shape. Click and drag through the area you want to zoom in on.

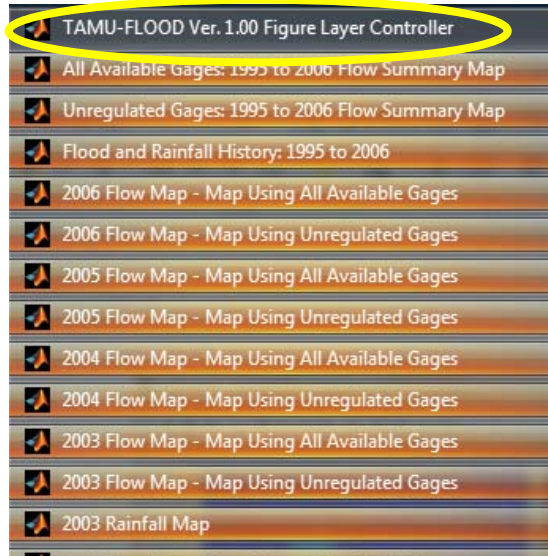


The area within the square is zoomed in as follows.

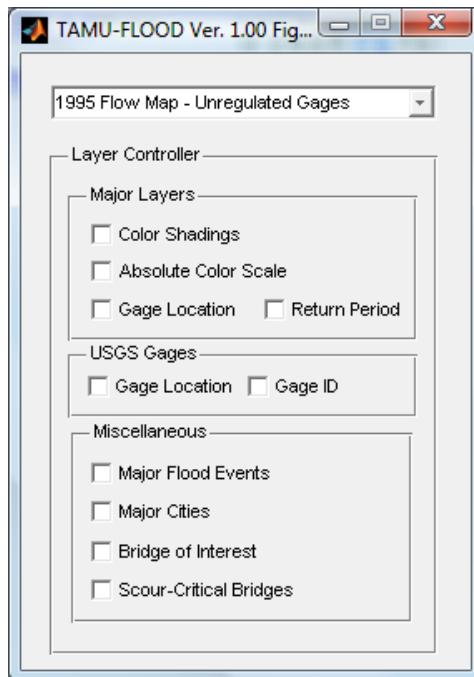


b. Figure Layer Controlling

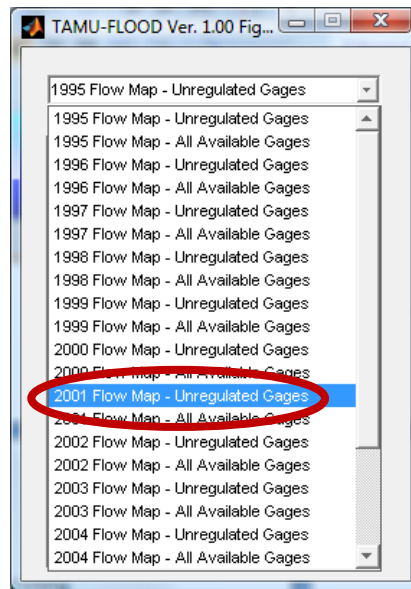
The map still looks complicated. To see the color shadings without the circles and numbers, first activate the Figure Layer Controller in Windows Explorer.



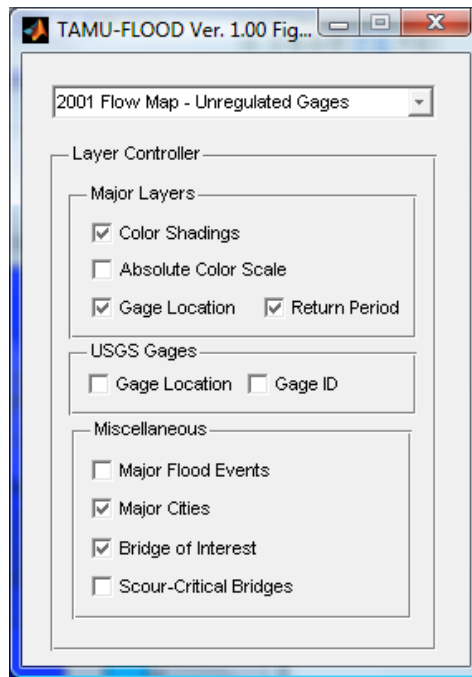
The following window pops up.



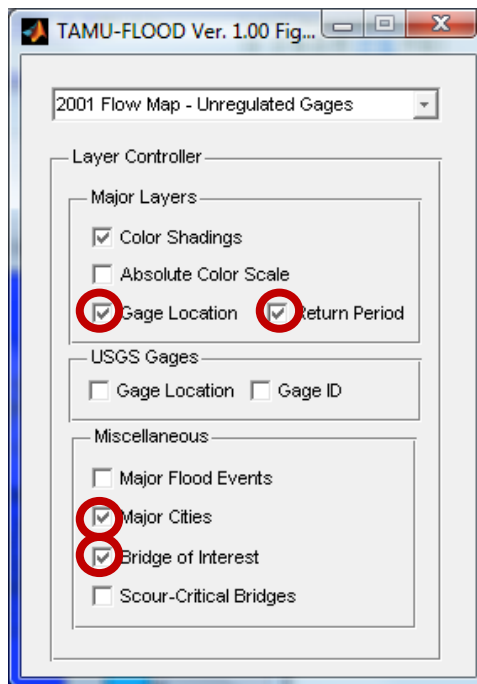
First, we want to control the map “2001 Flow Map—Map Using Unregulated Gages.” To do this, go to the drop-down menu at the top and choose “2001 Flow Map—Unregulated Gages.”



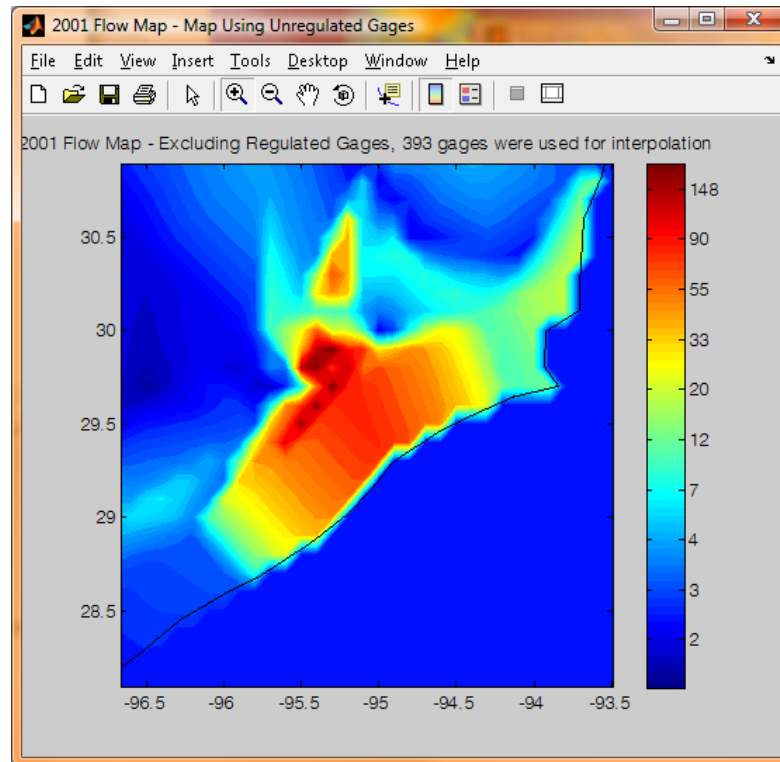
Then, the map “2001 Flow Map—Map Using Unregulated Gages” is activated, with the check boxes filled or blank according to the currently shown layers on the map.



To see just the color shadings, uncheck all layers except the layer “Color Shadings.”



Then, the map shows only the color shadings as follows.



In a similar manner, you can turn on or off the layers in the figure. The following layers are available for the figures:

(1) Major Layers

- (a) Color Shadings: Represent the recurrence interval of the maximum flow or rain
- (b) Gage Location: Location of the USGS gages used for the generation of the map
- (c) Return Period: Recurrence interval (return period) of the maximum flow that was observed in the gage

(2) USGS Gages

- (a) Gage Location: Location of all available USGS gages in Texas
- (b) Gage ID: Gage ID of the USGS gages

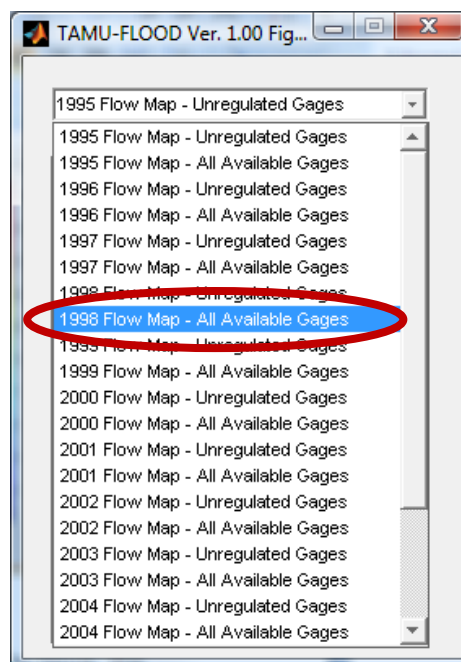
(3) Miscellaneous

- (a) Major Flood Events: Major flood events reported by USGS
- (c) Major Cities: Location of major cities in Texas
- (d) Bridge of Interest: Location of the bridge that was entered in the input window
- (e) Scour-Critical Bridges: Location of all bridges indexed as “scour critical” by TxDOT

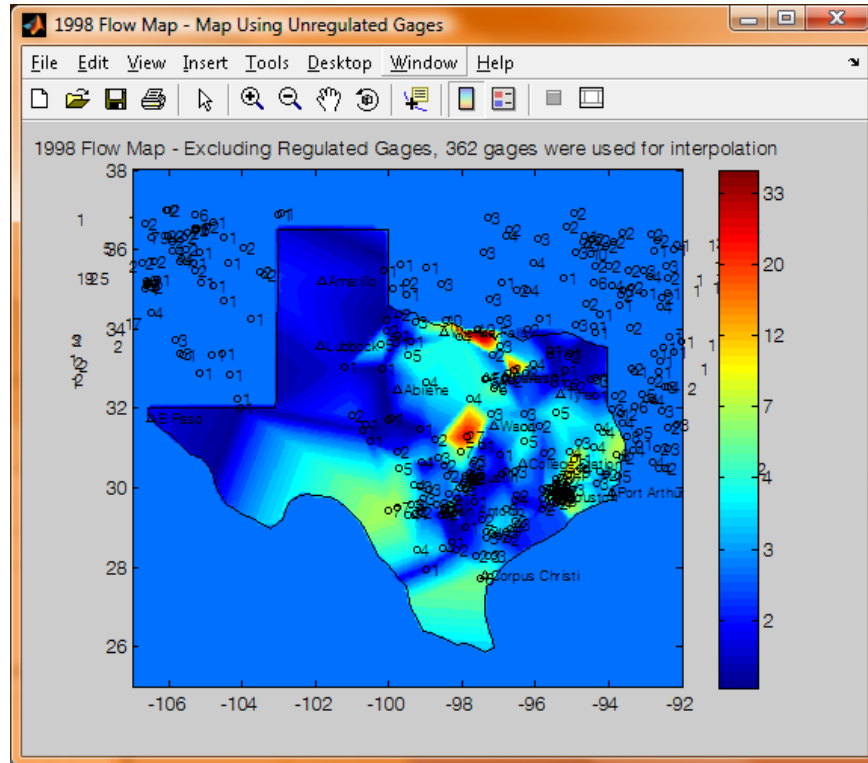
c. Changing Color Shading Scale

You may want to know whether the red section on the map actually represents a large flood in the region. TAMU-FLOOD provides an option to change the color scale in maps such that they vary from a 1-year recurrence interval to a 172-year recurrence interval. Because red always represents catastrophic events in this color scale, TAMU-FLOOD calls this color scale the “absolute color scale.”

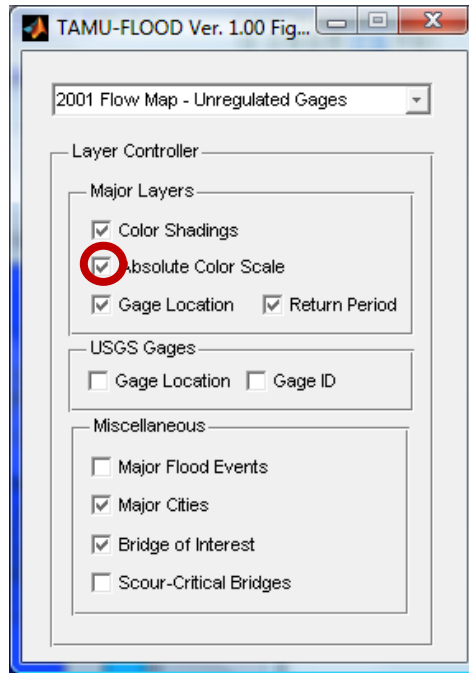
We will explore this using the flow map for 1998. First, choose the 1998 flow recurrence interval map from the Figure Layer Controller.



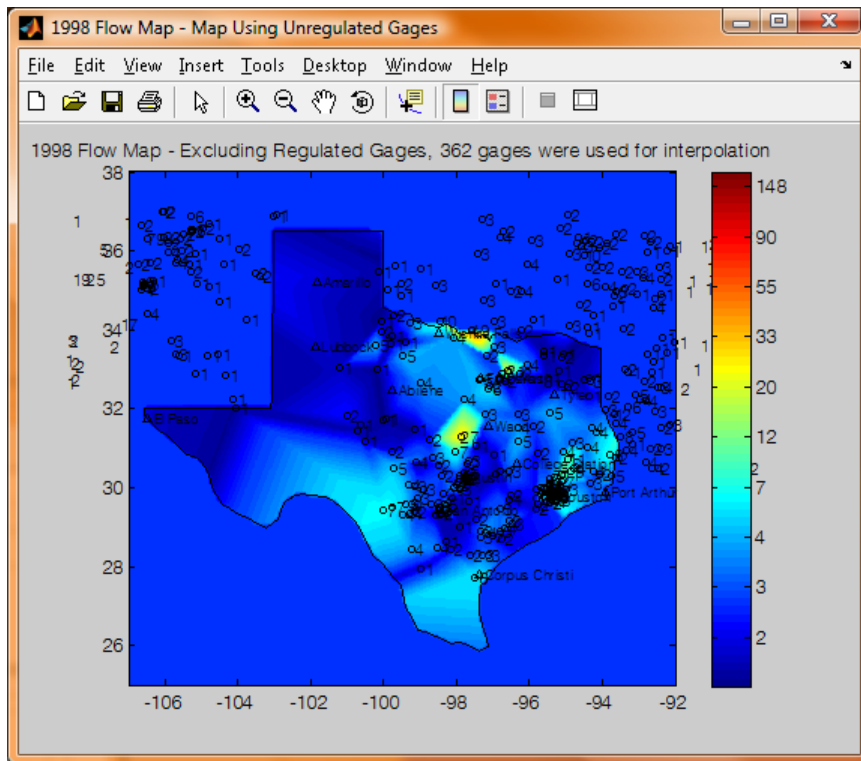
The 1998 flow map is retrieved.



The map seems to indicate that the central portion of Texas experienced a large flood. Is it very large? To figure this out, go to the Figure Layer Controller again, and check the check box that says “Absolute Color Scale.”



The color scale of the 1998 flow recurrence interval map was changed into a 1- to 175-year recurrence interval range as follows.

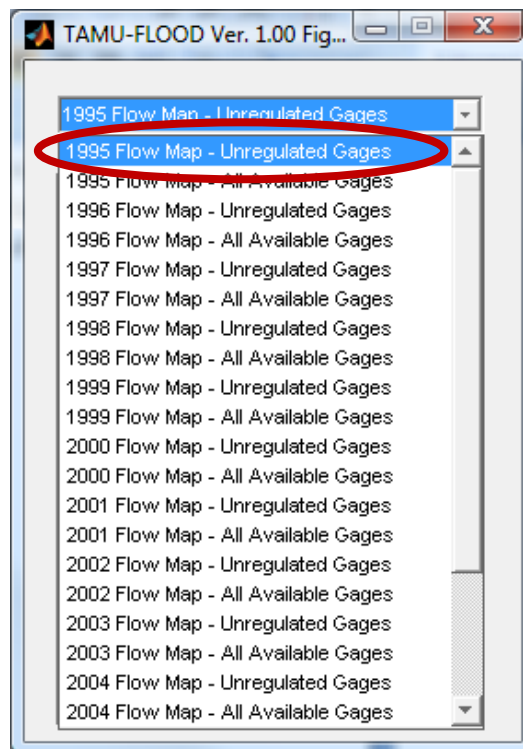


The color in the central portion of Texas changed from red to yellow. From this color scale, we can figure that the flood in the region was severe but not as severe as the other historical catastrophic events such as Tropical Storm Allison in 2001, which had an approximately 180-year recurrence interval.

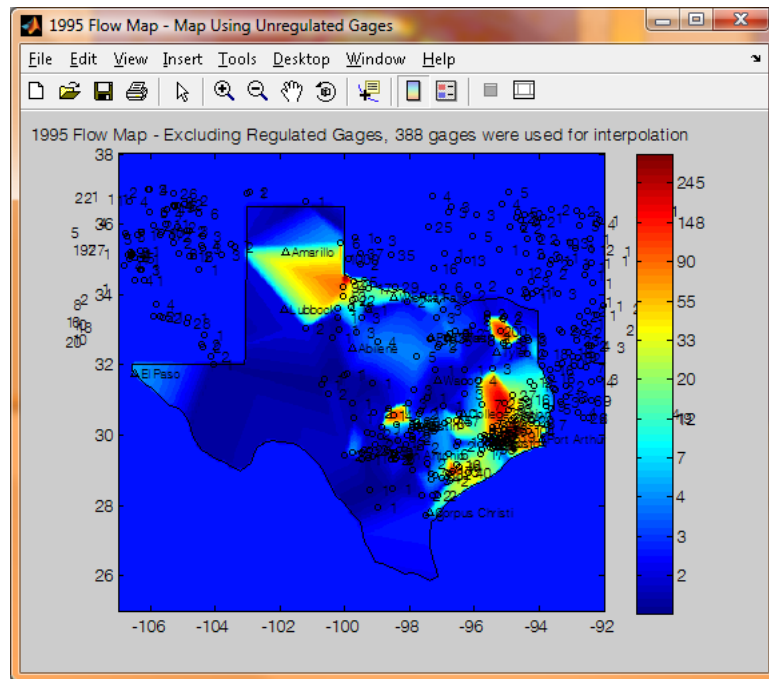
d. Acquiring an Exact Color Value at a Given Location on the Map

You may want to acquire the exact value of the color at a precise location on the map.

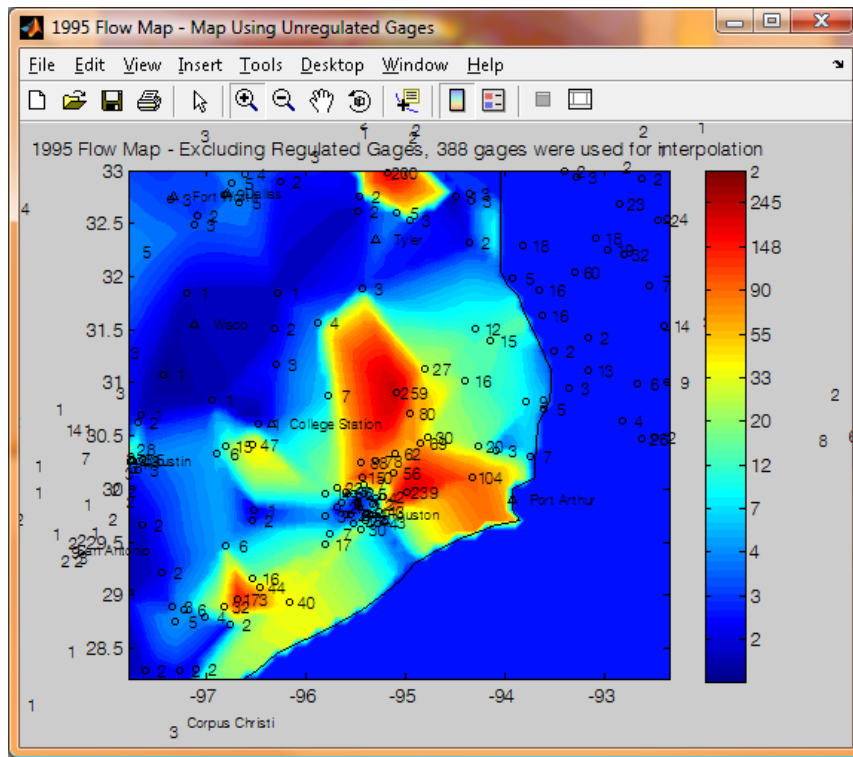
To do this, use the flow recurrence interval map of the year 1995. First, retrieve the map from the Figure Layer Controller.



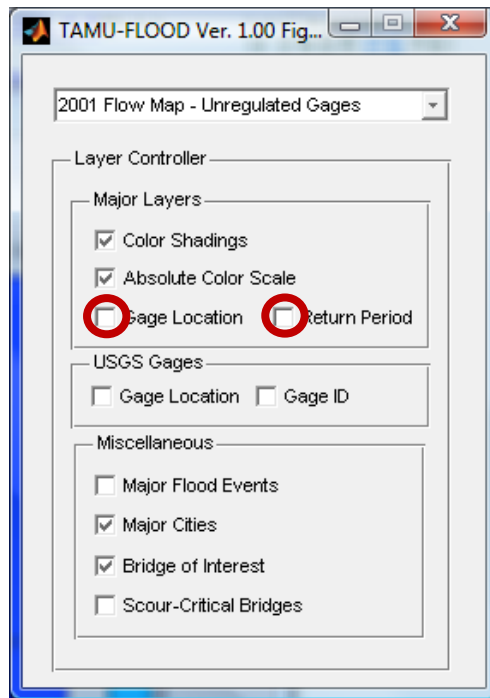
The 1995 flow recurrence interval map is retrieved.



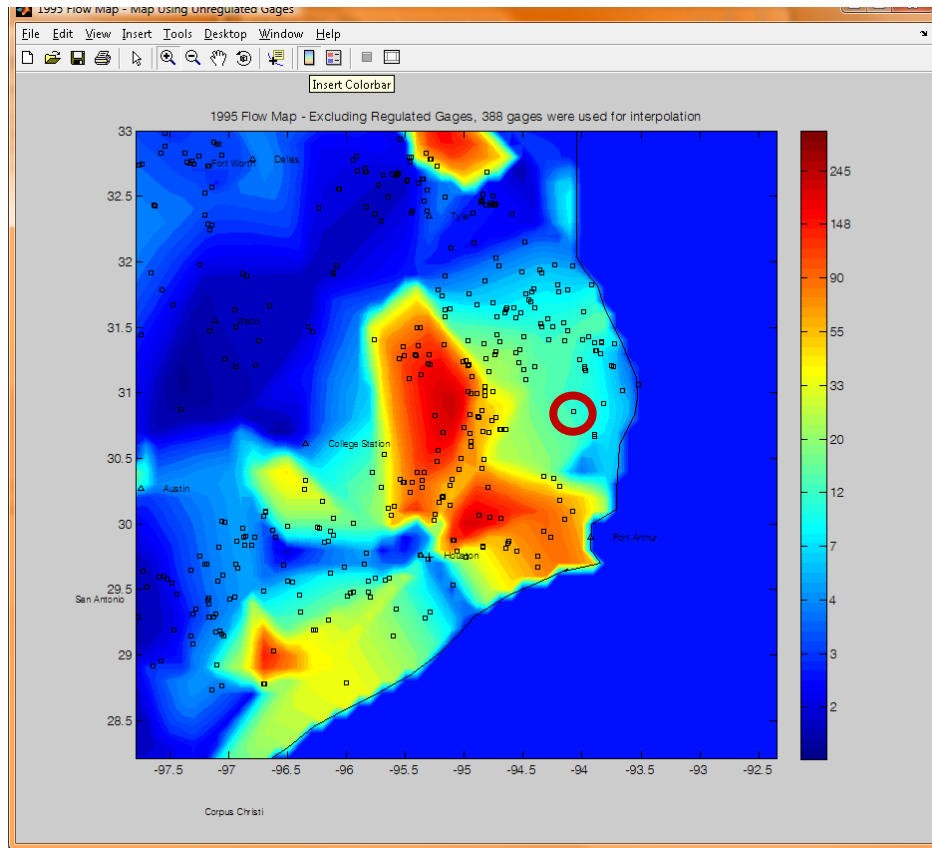
There was a big flood event in the southeastern part of Texas. Zoom in to the location as described in the previous section. After zooming in, you should see a map that looks like the following.




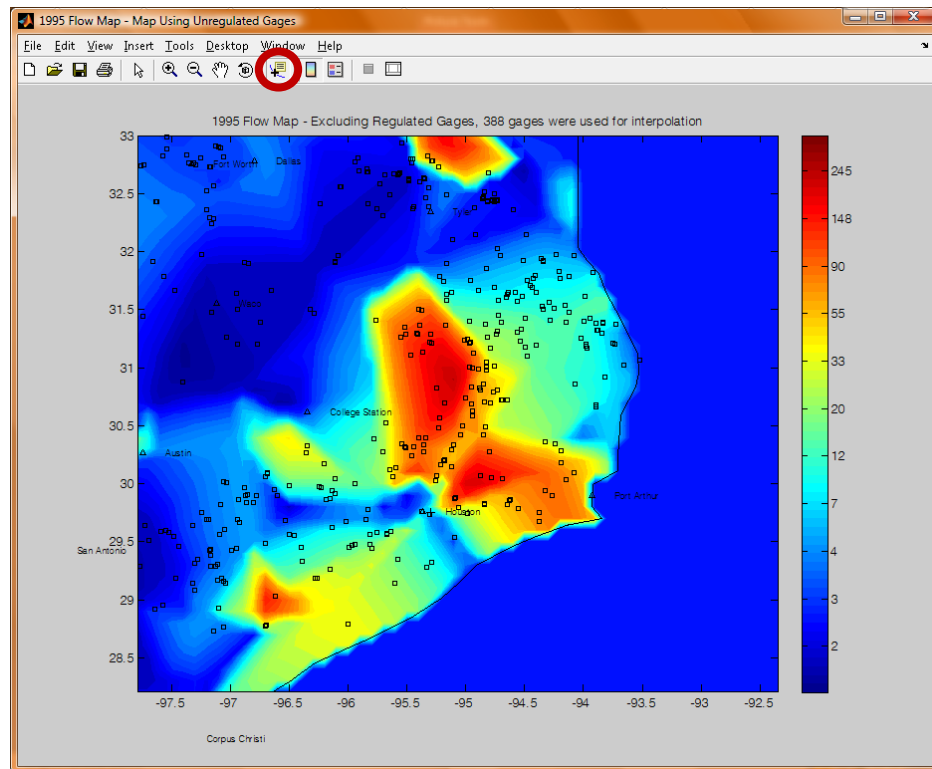
The map still looks complicated. Turn off the gages and recurrence interval layers from the Figure Layer Controller, and turn on the layer of Scour-Critical Bridges.



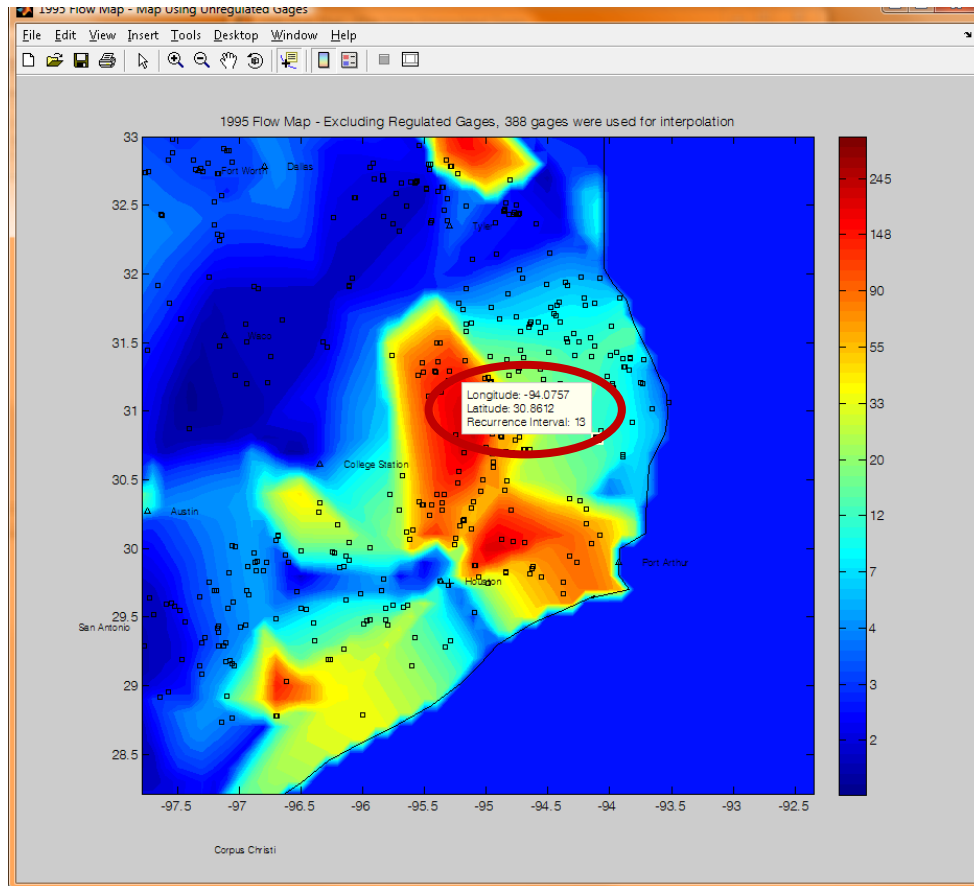
The map now looks like the following.



Here, you want to know the recurrence interval of a scour-critical bridge circled in red. To do this, click on the data cursor button  in the menu bar of the figure.



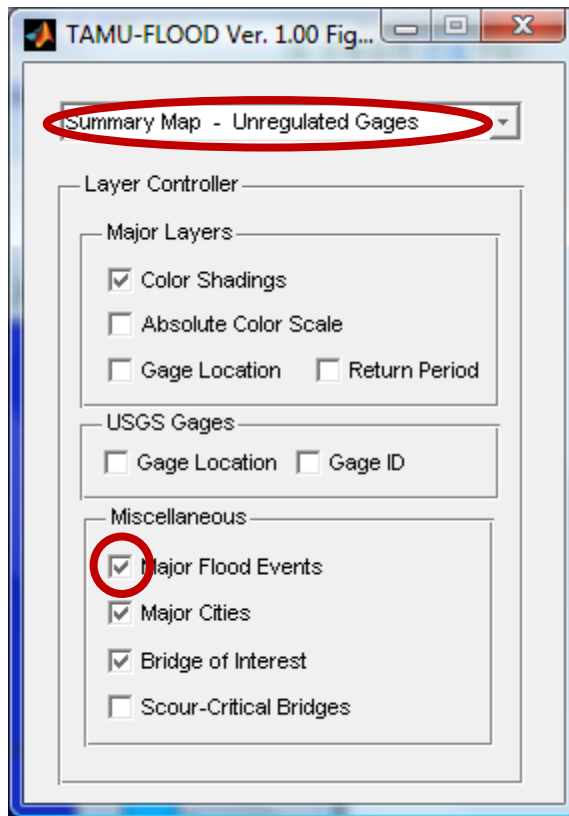
The cursor changes from the arrow shape into a cross shape. With the cross-shaped cursor, click on the location on the map where the bridge is. The longitude, latitude, and recurrence interval of the flow peak of the location you just clicked pops up as follows.



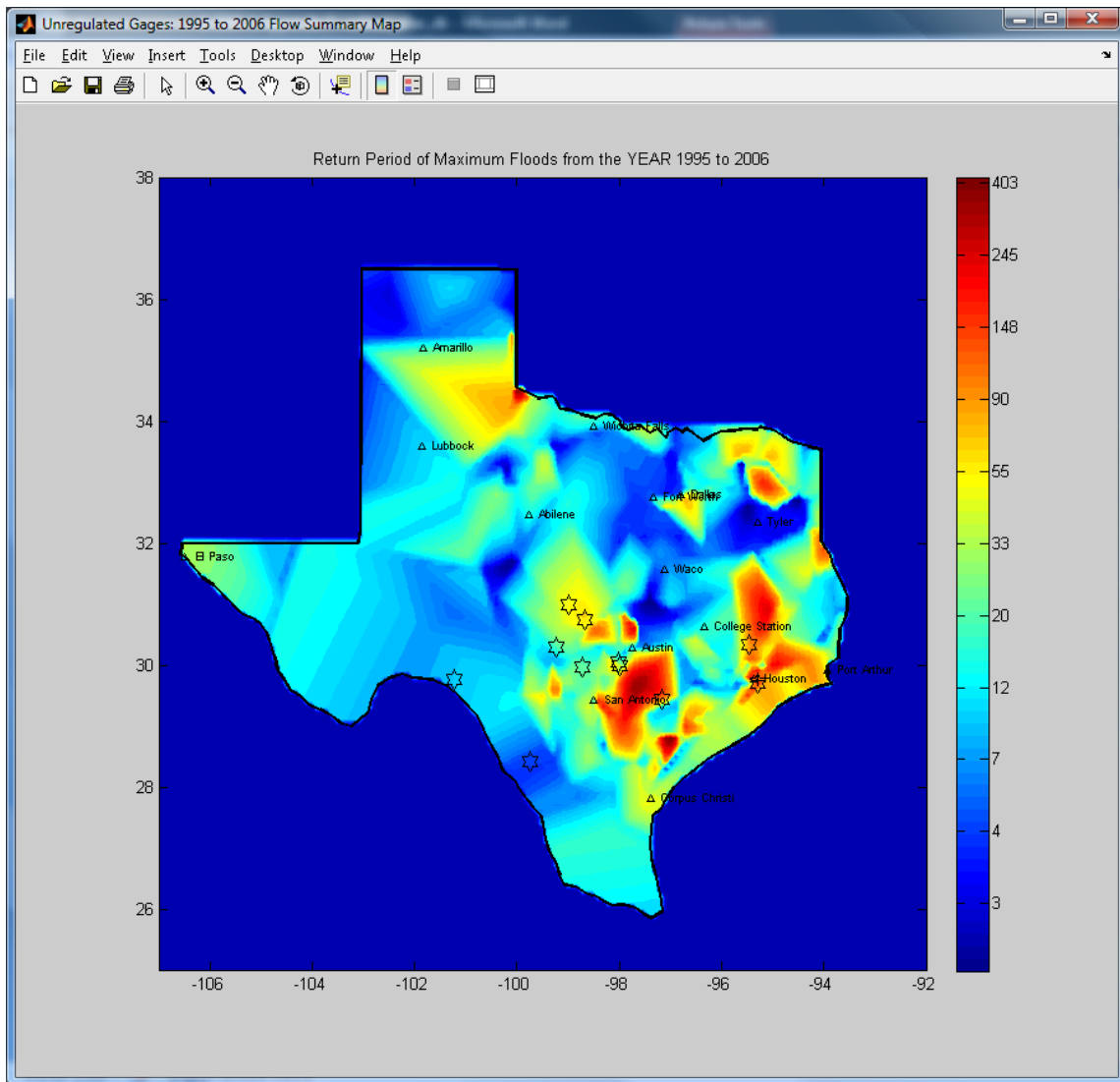
e. Checking Major Flood Events

TAMU-FLOOD contains the database of major flood events that occurred in Texas from the year 1920 to 2003. These data can be read interactively using TAMU-FLOOD.

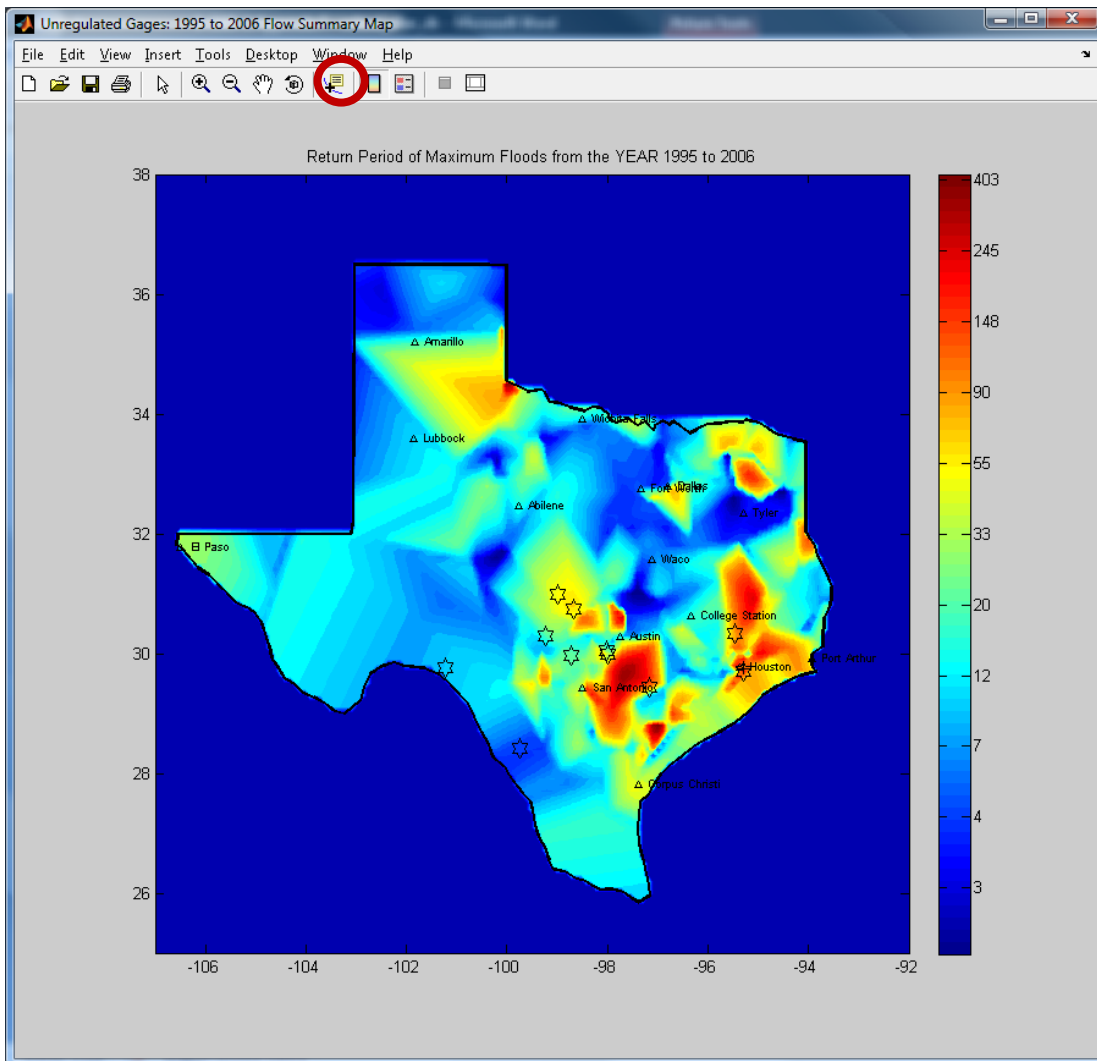
The layer of major flood events only appears on one of the summary maps. Choose one of the summary maps (Summary Map—Unregulated Gages, Summary Map—All Available Gages) from the TAMU-FLOOD Figure Layer Controller. Also, turn on the Major Flood Events layer from the TAMU-FLOOD Figure Layer Controller if the layer is not turned on.



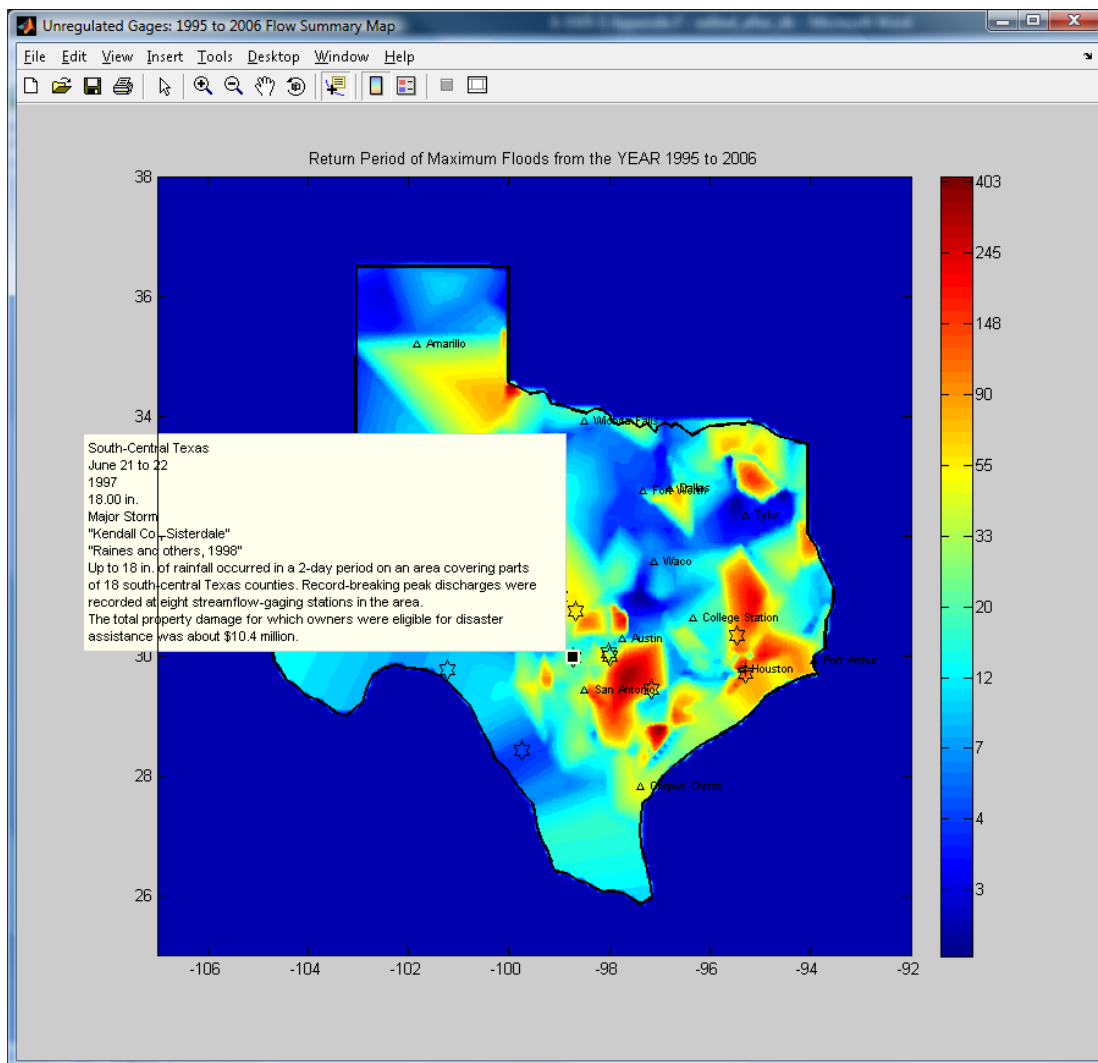
The Major Flood Events layer is turned on and is shown as a hexagram (a star with six points). Each star on the map represents the location of the flood that occurred during the time period specified by the user.



To see a description of each flood, click the data cursor button.



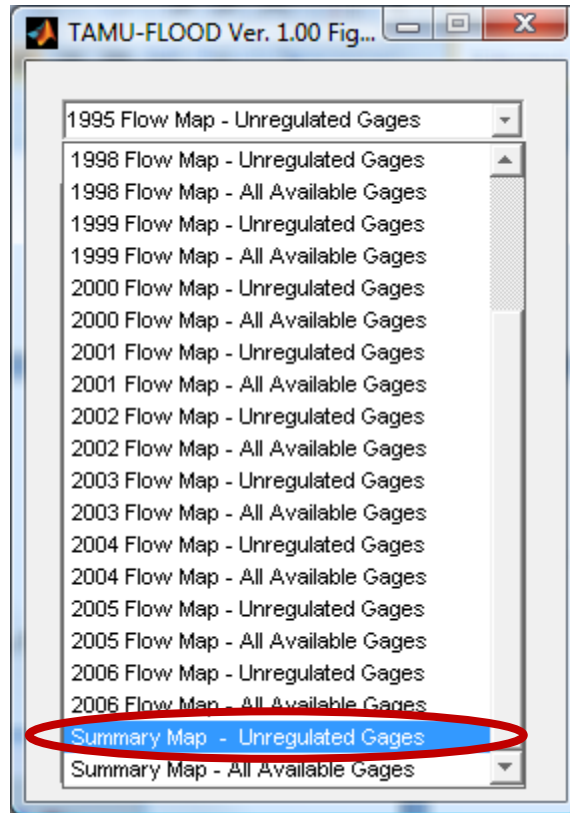
Then, click on one of the hexagrams. A description of the flood is shown in the dialog box.



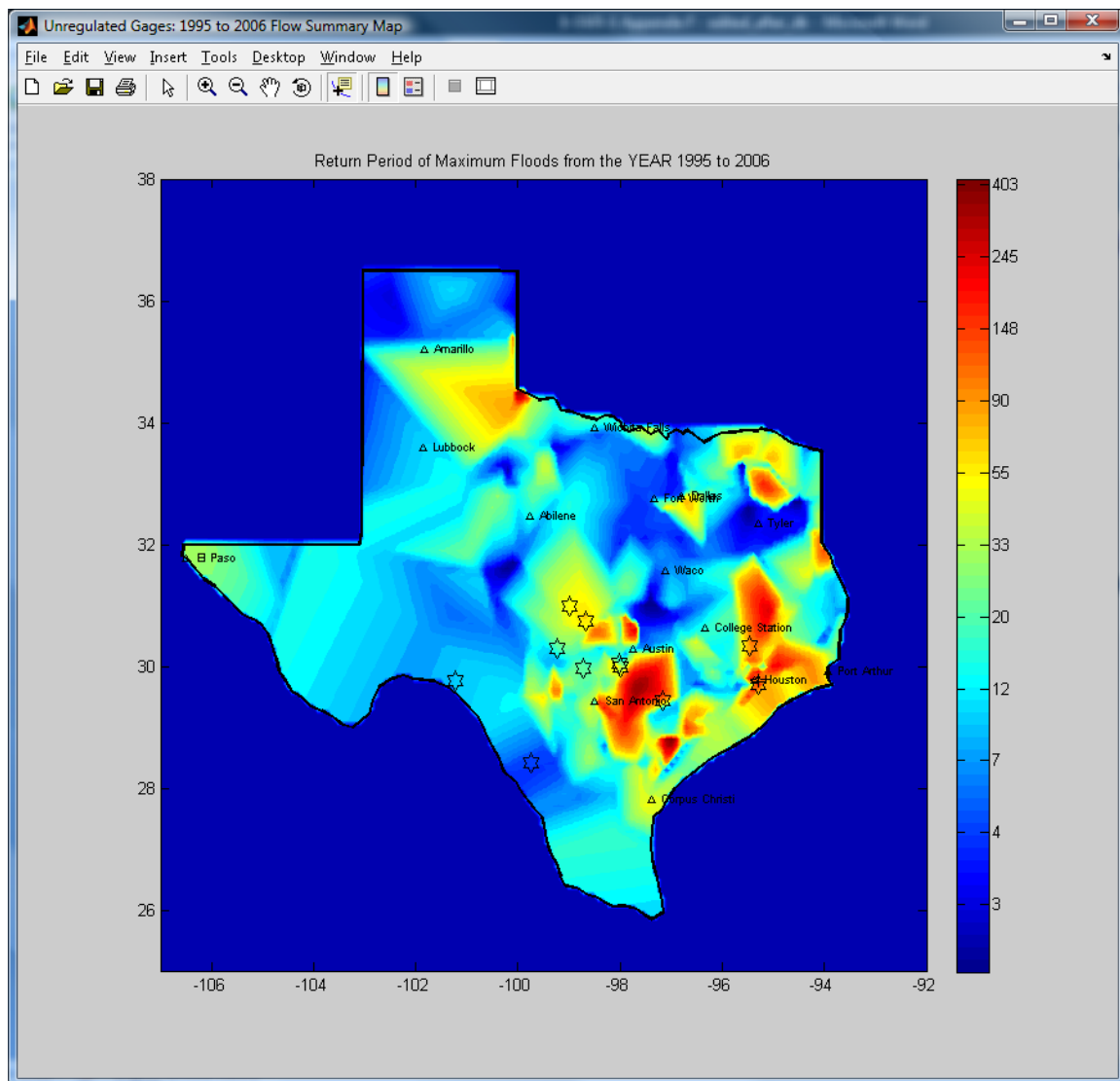
3. Summary Maps

You may want to know the maximum flood that the bridge has experienced since its construction. This can be observed from the summary maps. Summary maps show the color shadings of the recurrence interval of the maximum flood event that occurred during the period that was defined in the input section (in this example, 1995-2006). Two different types of summary maps are available: one based only on unregulated flow peaks and one based on all available flow peaks regardless of regulation. The second type of map is useful in regions with few USGS gages. Because the area that is dealt with in

this study contains many USGS gages around it, we will look at one based only on unregulated flow peaks. Go to the Figure Layer Controller and activate the map “Summary Map—Unregulated Gages.”



The summary map appears as follows.



The layers in the summary map can be turned on or off in a similar manner to the other maps. The summary map does not have the layers representing the locations of the gages and the corresponding recurrence intervals. The data cursor, which enables the reading of the color value, can also be used in the summary maps.

Notes

1. Water Year

The flow recurrence interval map of TAMU-FLOOD is based on water year. This means that any flow peak that happened in the month of October and November of a given year will be found on the map of the next year. For example, a catastrophic flood event that happened in October 1998 in south central Texas appears on the flow recurrence interval map of 1999. This may cause mismatches in the flow-rainfall history comparison chart.

2. Regions with Few USGS Flow Gages

The southwestern part of Texas does not have enough USGS gages to produce reliable estimates of the recurrence interval. Thus, the color shadings in this region can be inaccurate. One way to reduce the uncertainty is to look at the recurrence interval map based on all available gages. While the recurrence interval estimates based on all available gages are less accurate than ones based on unregulated gages, it will help you to capture the past occurrences of the major flood events that otherwise would be missed. Another way to avoid this issue is to look through the flood events that occurred during the specified time period. The step-by-step procedure for this is described in this manual.